Identification of potential regulators of PIK3CA promoter in chemoresistant ovarian cancer cells

By

Bhushan Laxman Thakur

LIFE09201204010

**Tata Memorial Centre,
Navi-Mumbai**

A thesis submitted to the
Board of Studies in Life Sciences
In partial fulfillment of requirements
for the Degree of

DOCTOR OF PHILOSOPHY

of

HOMI BHABHA NATIONAL INSTITUTE

December, 2017

Homi Bhabha National Institute

Recommendations of the Viva Voce Committee

As members of the Viva Voce Committee, we certify that we have read the dissertation prepared by Mr. Bhushan Laxman Thakur entitled **"Identification of potential regulators of PIK3CA promoter in chemoresistant ovarian cancer cells"** and recommend that it may be accepted as fulfilling the thesis requirement for the award of Degree of Doctor of Philosophy.

Chairman – Prof. Shubhada V. Chiplunkar   Date: 28/12/17

Guide/Convener – Dr. Pritha Ray   Date: 28/12/2017

External Examiner – Dr. Sharmila A Bapat   Date: 28th Dec. 2017

Member – Dr. Neelam Shirsat   Date: 28.12.2017

Member - Dr. Sanjay Gupta   Date: 28/12/17

Technical Advisor – Prof. Samit Chattopadhyay   Date: 3/1/18

Final approval and acceptance of this thesis is contingent upon the candidate's submission of the final copies of the thesis to HBNI.

I hereby certify that I have read this thesis prepared under my direction and recommend that it may be accepted as fulfilling the thesis requirement.
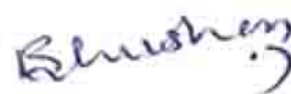
Date: 28/12/2017
Place: Navi Mumbai

Dr. Pritha Ray
Guide

STATEMENT BY AUTHOR

This dissertation has been submitted in partial fulfillment of requirements for an advanced degree at Homi Bhabha National Institute (HBNI) and is deposited in the Library to be made available to borrowers under rules of the HBNI.
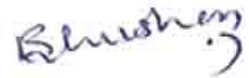
Brief quotations from this dissertation are allowable without special permission, provided that accurate acknowledgement of source is made. Requests for permission for extended quotation from or reproduction of this manuscript in whole or in part may be granted by the Competent Authority of HBNI when in his or her judgment the proposed use of the material is in the interests of scholarship. In all other instances, however, permission must be obtained from the author.

Bhushan Laxman Thakur

DECLARATION

I, hereby declare that the investigation presented in the thesis has been carried out by me. The work is original and has not been submitted earlier as a whole or in part for a degree / diploma at this or any other Institution / University.

Bhushan Laxman Thakur

List of Publications arising from the thesis

Journal

1. "Cisplatin triggers cancer stem cell enrichment in platinum-resistant cells through NF-κB-TNFα-PIK3CA loop", Bhushan Thakur and Pritha Ray, *Journal of Experimental & Clinical Cancer Reseach*, **2017,** *Vol. 36:164*, 1-14.

2. "p53 Loses grip on PIK3CA expression leading to enhanced cell survival during platinum resistance", Bhushan Thakur and Pritha Ray, *Molecular Oncology*, **2016**, *Vol. 10(8),* 1283-1295.

Chapters in books and lectures notes: None

Conferences:

A. **Oral Presentations:**

Bhushan Thakur and Pritha Ray, 2014. Monitoring drug responsive dynamics of p53-PIK3CA promoter modulation. XXXVIII All India Cell Biology Conference, CSIR – CDRI, Jankipuram Extension, Lucknow, India. (Platform presentation)
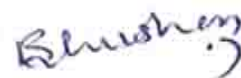
B. **Poster presentations:**

1. **Bhushan Thakur,** Pritha Ray, 2016, Systematic halt and release in proliferation by drug resistant ovarian cancer cells: a mechanism for continuance of resistance, XXX All India Cell Biology Conference, Jiwaji University, Gwalior.

2. **Bhushan Thakur,** Pritha Ray. 2015. p53 dependent PIK3CA promoter modulation in chemoresistance: Mechanism beyond genomic alterations. Platinum Jubilee TMC Conference, Mumbai.

3. **Bhushan Thakur,** S M Gaikwad and Pritha Ray, 2013, Modulation in PIK3CA signaling during acquired chemoresistance: p53 ordinance insufficiency. XXXVII All India Cell Biology Conference, in Stem, JN Tata Auditorium ,IISC, Bangalore, India.

C. **Award:** Directors prize for best participant among the Ph.D. student in Oral presentation. XXXVIII All India Cell Biology Conference, CSIR – CDRI, Jankipuram Extension, Lucknow, India

Others:

1. Aastha Kapoor, Amlan Barai, **Bhushan Thakur**, Alakesh Das, Sejal R Patwardhan, Melissa Monteiro, Snehal Gaikwad, Amirali B Bukhari, Pankaj Mogha, Abhijit Majumder, Abhijit De, Pritha Ray, Shamik Sen. "Soft drug-resistant ovarian cancer cells migrate via two distinct mechanisms utilizing myosin II-based contractility". Biochimica et Biophysica Acta (BBA)-Molecular Cell Research, 2017. (Accepted)

2. Kelkar MG, **Thakur B**, Derle A, *et al.* Tumor suppressor protein p53 exerts negative transcriptional regulation on human sodium iodide symporter gene expression in breast cancer. Breast Cancer Res Treat. 2017;164(3):603-15.

3. Pradhan L#, **Thakur B#**, Srivastava R, Ray P*, Bahadur D*. "Assessing Therapeutic Potential of Magnetic Mesoporous Nanoassemblies for Chemo-Resistant Tumors". Theranostics. 2016. (# These authors have equally contributed to the work)

3. Gaikwad SM#, **Thakur B#,** Sakpal A, Ray P. "Differential activation of NF-κB signaling is associated with Platinum and Taxane resistance in MyD88 deficient epithelial ovarian cancer cells". Int J Biochem Cell Biol. Apr;61:90-102, 2015. (# These authors have equally contributed to the work)

4. Singh M, Singh SK, **Thakur B**, Ray P, Singh SK. Design and Synthesis of Novel Schiff base-benzothiazole hybrids as potential Epidermal Growth Factor Receptor (EGFR) Inhibitors. Anticancer Agents Med Chem. 2015 Oct 7.

5. **Thakur B**, Chatterjee S, Chaudhury S, Ray P. Molecular Imaging of Therapeutic Potential of Reporter Probes. Curr Drug Targets. 2015;16(6):645-57

6. Chaudhury S, **Thakur B**, Chatterjee S, Ray P. Molecular imaging aided improvement in drug discovery and development. Curr Biotech. 3(3): 218-237, 2014.

Bhushan Laxman Thakur

Dedicated to my Mom, Dad and Brother...

ACKNOWLEDGEMENTS

First and foremost I would like to extend my eternal gratitude to my supervisor, Dr. Pritha Ray, for her resounding advice and valuable input throughout my PhD tenure, which enabled me to develop the knowledge and skills I have in this subject. Furthermore, I would also like to thank her for believing in me and knowing the best way to bring out my full potential. Despite her busy schedule, she managed to set time aside to assist me in improving my skills on scientific writing and presentation, and for that, I am very grateful. Lastly, if it was not for her patience, there is no doubt that this PhD would have been possible. It is a real honor to be a part of her lab. Thank you.

Secondly, I thank Dr. Shubhada Chiplunkar (Director, ACTREC), for providing me with an excellent research atmosphere and infrastructure. I am thankful to my doctoral committee members, Dr. Shubhada Chiplunkar, Dr. Neelam Shirsat, Dr. Sanjay Gupta, and Dr. Samit Chattopadhyay for their timely and valuable suggestions for improving my doctoral research. I am grateful to Dr. Abhijit De for his expert comments and critical analysis of my work during lab meetings. I also would like to thank him for establishing wonderful Molecular Imaging Facility, which was a bliss for my animal imaging experiments. I extend my gratitude to the staff at the Common Instrument Facility (CIR), Animal House Facility, ACTREC Digital Imaging Facility, Flow Cytometry Facility, Mass-spectrometry facility, Real-time facility, Library and Administration for their constant help and support. I also thank The Council of Scientific and Industrial Research (CSIR, Gov. of India) for providing fellowship support.
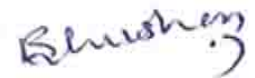
Additionally, I would like to thank Mrs. Asmita Sakpal (Lata di) for always ensuring that cells for tissue culture were readily available, and for placing the necessary orders. Thank you for Lunchtime Company and always putting a smile on my face.

Additionally, to all the previous and current members of the Imaging Cell Signaling and

CONTENTS

Homi Bhabha National Institute

Ph. D. PROGRAMME

1. Name of the Student: Bhushan Laxman Thakur

2. Name of the Constituent Institution: Tata Memorial Centre**,** Advanced Centre for Treatment Research and Education in Cancer

3. Enrolment No. : LIFE09201204010

4. Title of the Thesis: Identification of potential regulators of PIK3CA promoter in chemoresistant ovarian cancer cells

5. Board of study: Life Science

SYNOPSIS REPORT

Introduction:

Cancer is a heterogeneous disease that continues to increase global burden of mortality.[1] Current clinical strategies for cancer management include surgery, radiation therapy, chemotherapy, hormone therapy, immunotherapy and molecular targeted therapy.[2] However, these therapies are only successful in early stages while resistance developed against these therapeutics limits its efficacy. Chemotherapy is one of the prevailing methods used to treat malignant tumors as they are effective against multiple tumor types.[3, 4] Though chemothrapeutic agents such as cisplatin, 5-fluorouracil, doxorubicin, camptothecin and paclitaxel differ in their mode of action, they target rapidly dividing tumor cells and kill tumor cells by inhibiting proliferation and/or inducing apoptosis. However, Chemoresistance, either intrinsic or acquired, substantially handicaps the efficacy of chemotherapy and results in significant mortality in cancer patients. Chemo resistance is majorly caused and sustained by reduced drug accumulation, alterations in drug targets, enhanced DNA-damage repair and evasion of apoptosis via deregulation of signal transduction molecules.[5-8] Other mechanisms and factors include tumour microenvironment, epigenetics, tumor stroma and a small fraction of inherently resistant cancer stem cells.[9, 10] The essence of therapeutic success lies in the understanding how chemotherapeutics dictate cellular fate and translating this knowledge into development of innovative cancer therapeutics to overcome resistance.

Based on the biochemical and molecular composition of cellular milieu, signaling pathways drive cells towards either pro- or anti- apoptotic fate when treated with the same drug. The advent of high-throughput technologies has accelerated our current knowledge of cell-intrinsic and cell-extrinsic pathways that aids resistant tumor cells to escape therapeutic action. Deregulation of oncogenic signaling like MAPK/JNK/ERK, PI3K/AKT, NF-κB signalling, focal adhesion kinases and WNT signalling are the major cell-intrinsic molecular

determinants that control and govern resistance.[11, 12] Among these, PI3K /AKT signalling cascade endows survival advantage against various therapeutics such as Adriamycin, paclitaxel, cisplatin, 5-fluorouracil, etoposide and camptothecin in multiple cancers including ovarian, breast and colon cancer.[13] Moreover, hyper activation of PI3K/AKT aids in maintenance of cell-extrinsic factors including quiescence and resistance in CSC's via NF-κB and BCl2.[10] Since activation of PI3K/AKT signalling is involved in cellular survival, proliferation and in other hallmarks of cancer, it could be a vital target for developing therapeutics to overcome chemoresistance.[14] Phosphatidylinositol-4,5-bisphosphate 3-kinase catalytic subunit alpha (PIK3CA) gene codes for P110α protein which phosphorylates AKT and is frequently altered in breast, ovarian, colon, lung and ovarian cancer. PI3K/AKT cascade is found to be upregulated in 50% of cancer cases due to gain-in function mutation (~ 23%) and amplification (~11%) in PIK3CA gene, loss of function mutations in PTEN (~11%) gene and amplification in AKT gene (~20%).[15] Gain-in-function mutation and amplification in PIK3CA gene alone escalate downstream PI3K-AKT-mTOR pathway within cancer cells. In ovarian cancer, copy number amplification of PIK3CA gene locus has been reported in 17-35% of ovarian carcinomas and it is implicated to be an oncogene. [16-18]

Ovarian cancer is the leading cause of mortality among patients suffering from gynaecological malignancies with high grade serous ovarian carcinoma (HGSOC) being the most frequent subtype. Due to its asymptomatic nature, only 15% of the patients are diagnosed in early stages, while most women remain undiagnosed until the cancer metastasizes resulting in poor prognosis and death.[19] Current clinical strategy for HGSOC management includes cytoreductive surgery followed by combination of platinum-taxol based therapeutics for advanced stage disease. In spite of promising initial response of platinum based adjuvant therapy, most women succumb to the disease due to recurrence and chemoresistance. Moreover, success rate of alternative treatment against cisplatin resistant

tumor is very poor.[20] Even targeted therapeutics, Bevacizumab[21] and olaparib[22] are promising only in combination with carboplatin and paclitaxel. Thus, failure in early diagnosis and platinum resistance are the two major obstacles towards management of the epithelial ovarian cancer.

Platinum based drugs, cisplatin and carboplatin are alkylating agents which play a central role in management of testicular, ovarian, cervical, head and neck and non-small cell lung cancer. They are alkylating agents which crosslink with adenine or guanine base resulting in DNA double strand breaks and DNA damage and repair.[12] Other than the classical mode of DNA damaging stress, cisplatin is known to induce oxidative and endoplasmic stress. Thus cisplatin induced stresses activate several signalling cascade including c-ABL, p53 signaling, MAPK/JNK/ERK and suppresses PI3K/AKT, NF-κB signalling, focal adhesion kinases and WNT signalling. Apart from 18% PIK3CA amplification, 7% PTEN mutations and 3% AKT amplification, genetic alterations in components of PI3K/AKT signalling are rare in HGSOC.[23] Yet therapy resistant ovarian cancer displays 50% escalated AKT activity.[24] The TCGA data for HGSOC provisional set (n=316) revealed a total of 9% cases associated with PIK3CA transcript upregulation without any change in the gene copy number. Such incidences indicate alteration in levels of specific regulators and subsequent promoter regulation in the cancer cells. Little is known about these mediators of upregulated PIK3CA transcription and their role during acquirement of chemoresistance in ovarian carcinoma. Astanahe et al (2008) reported negative regulation of PIK3CA transcription via direct binding of p53 to its promoter in ovarian surface epithelial cells.[25] This study corroborates with clinical observations of association of p53 mutations and PI3K/AKT activation in ovarian carcinoma made by Kolasa et al (2009).[24] Other reports also showed that transcriptional activation of PIK3CA promoter by FOXO3A [26], NF-κB[27] and YB-1[25] transcription factor escalates AKT activation. Previously our lab has shown that chemotherapeutic drugs

such as cisplatin and paclitaxel negatively modulate PIK3CA promoter in chemosensitive ovarian cancer cells as well as in tumor xenografts.[28] The repressing activities of these drugs are probably mediated via p53 and mutation at three of the four p53 binding sites relieved such promoter attenuation. However, mutations at all the four binding sites surprisingly decreased the activity indicating a complex regulation of the PIK3CA promoter by p53.[28] Inhibition of PI3K/AKT pathway often sensitizes the cancer cells to cisplatin.[13] Interestingly, cisplatin could up-regulate PIK3CA transcription in cisplatin-resistant OVCAR3 cells but not in sensitive cells[29] indicating presence of a differential regulation of PIK3CA promoter in resistant scenario. The molecular mechanism is yet to be deciphered.

Rationale:

Constitutively active AKT has been found in chemoresistant lung, glioma and ovarian cancer cell lines, compared to their sensitive parental counterparts.[30-32] Lee et al, (2008) observed cisplatin escalated PIK3CA expression in OVCAR-3/CDDP cells which inhibit BAX translocation via activated PI3K/AKT conforming platinum resistance.[29] However, the molecular mechanism of this effect of cisplatin remained unexplored. With the help of our isogenic A2780 chemoresistant model, we also observed that drug mediated repression of PIK3CA promoter activity gradually diminished with increased resistance towards cisplatin.[33] Interestingly, cisplatin induced PIK3CA expression in resistant A2780-CisR cells along with decreased p53 stabilization and increased phosphorylation of AKT. However, the molecular mechanism behind this contrasting effect of cisplatin between sensitive and acquired resistant cells and biological consequence was not examined. Also, whether and how cisplatin induced PI3CKA expression aid in maintenance of cancer stem cells has not been investigated.

Hypothesis:

Since cisplatin treatment induces distinct modulation of PIK3CA promoter activity and expression in sensitive and resistant cells, we hypothesise that the same drug would trigger differential transcriptional regulation of PIK3CA in both these cells. We also assume that negative regulation of PIK3CA by p53 might be governed by its post translational modifications which are known to critically determine transcriptional activity of p53. In absence of this p53 ordinance in resistant cells, cisplatin might induce other transcription factors that upregulate PIK3CA expression and may favour cancer stem cell like features.

Based on this hypothesis, we designed following **key questions:**

1. Out of four p53 binding sites, which is/are the most crucial site(s) in PIK3CA promoter modulation?

2. How does p53 interact with PIK3CA promoter during acquired chemoresistance?

3. Which are the other regulators of PIK3CA promoter in chemoresistant ovarian cancer cells?

To address these key questions following objectives were designed

Objective 1: To study p53 mediated modulation of PIK3CA promoter in cisplatin chemoresistant ovarian cancer cells.

Chemotherapeutic agents like cisplatin and paclitaxel actives p53 which represses PIK3CA promoter in chemosensitive ovarian cancer cells.[28] Since little is understood about the overall mechanism of p53-PIK3CA interaction and influence of p53 upon transcriptional status of PIK3CA during cisplatin resistance, we attempted to explore the mechanism using different cell lines and acquired cisplatin resistant model developed indigenously in A2780 cells. Similar to PIK3CA promoter attenuation, we found that cisplatin treatment to platinum-sensitive ovarian cancer cells (A2780 and OAW42) reduced level of PIK3CA expression and

p110α, while it induced PIK3CA expression in acquired resistant A2780-CisR cells and naturally resistant TOV21G, and SKOV3 cells. Here, cisplatin induced p53 activation which negatively regulates PIK3CA expression in sensitive cells. Hence we hypothesized that, in cisplatin resistant cells, p53 probably losses inhibitory effect on PIK3CA promoter and may undergo complex regulation by other unidentified regulatory proteins. To investigate whether resistant cells lacks p53 ordinance, we overexpressed p53 in A2780-CisR cells which restored p53 mediated attenuation of PIK3CA promoter activity. Next to investigate causality for the decreased ordinance of p53 over PIK3CA promoter during Chemoresistance, we monitored dynamics of p53 activation and PIK3CA promoter modulation via live cell imaging. Here p53-protein fused with nanoluc reporter serves as a promising reporter for quantitative measurement of p53 stabilization as a function of nanoluc activity. Live cell imaging of resistant cells exhibited 8hr delay and 5 fold reduced level of p53 induction after cisplatin treatment. Though our dynamic imaging of p53 demonstrated activation of p53 in both sensitive and resistant cells under cisplatin treatment, time dependent PIK3CA promoter attenuation was observed only in sensitive cells but not in resistant cells. In concordance with this data, sensitive and resistant tumor xenograft also demonstrated ~5 fold and ~3 fold increase in p53 stabilization post cisplatin treatment respectively. Decreased PIK3CA promoter activity (5 folds) was observed in sensitive tumor xenograft but not in resistant tumor xenograft post cisplatin treatment.

Levels of stabilization, differential affinity towards specific DNA sequences and various post translational modifications (PTM) dictates transcriptional activity of p53. Hence, interaction of p53 with its response element (RE) on PIK3CA promoter in sensitive and resistant stages was critically analysed. For this we generated single site mutation constructs having at mutant p53-RE and deletion constructs containing single p53-RE in PIK3CA promoter. Mutations at site 3 or site 4 p53-RE relieved cisplatin dependent promoter attenuation in sensitive (A2780

and OAW42) cells but not in A2780-CisR, TOV21G and SKOV3 cells. Next we performed site-specific chromatin immune-precipitation with p53 antibody to check site-specific physical interaction of p53 protein within PIK3CA promoter. In sensitive cells, p53 remained bound to site 1 in unstressed condition and moved to site 3 and 4 following cisplatin treatment. On the contrary, unstressed resistant cells exhibited absence of p53 binding at site 1, 3 and 4. Cisplatin treatment to resistant cells enhanced p53 occupancy only at site 1. Both mutant PIK3CA promoter activity and p53-ChIP indicate the importance of site 3 and 4 for p53 dependent PIK3CA attenuation. Cisplatin induces 'relocation' of p53 between its RE on PIK3CA promoter during stress in both sensitive and resistant cells. This differential binding could be due to differential affinity of p53 to its RE and might be dictated by PTMs of p53. As expected, high phosphorylation of serine 15, 20 and 46 were observed in cisplatin treated sensitive cells which were either low (serine 15 and serine 20) or absent (serine 46) in resistant cells. Under stress condition, phosphorylation of serine 46 escalates differential binding of p53 to apoptosis-related genes (BAX, PIG3, and p53AIP1).[34-36]We hypothesize that absence of serine 46 phosphorylation in resistant cells hinders recruitment of p53 on PIK3CA promoter. To investigate the critical role of serine 46 phosphorylation in PIK3CA promoter attenuation, we developed two p53 mutations as phosphorylation-mimicking mutant S46D (serine to aspartate) and phosphorylation-deficient mutant S46A (serine to alanine). The phosphorylation-deficient S46A mutant did not show any repressive effect on PIK3CA promoter in SKOV3 (p53 deficient) cells while S46D attenuated PIK3CA promoter activity. To investigate causality of loss of serine 46 phosphorylation in resistant cells, we studied levels and nuclear localization of its kinases HIPK2 and DYRK2. As expected both kinases HIPK2 and DYR2 showed reduced levels and cytoplasmic retention which hinders p53 serine 46 phosphorylation in resistant cells after cisplatin treatment. Cisplatin treatment to resistant cells augmented expression of Bcl2 and cFLIP, absence of

PARP cleavage indicate an apoptosis resistant phase in these cells. Hence though cisplatin decreases protein synthesis and favors growth arrested state in sensitive as well as resistant cells, it activated apoptotic machinery in the sensitive cells while static PI3K/AKT signaling adapted a pro-survival fate in resistant cells.

Mutation in p53 gene is a hallmark of 50% human malignancies including high grade serous ovarian carcinoma. Though wild type p53 is a negative regulator of PI3K/AKT pathway, different mutant p53 may exerts an unequal oncogenic activity on PI3K/AKT pathway. To understand oncogenic activity of mutant p53, we categorised p53 missense mutations from ovarian cancer TCGA data based on its co-relation with PIK3CA transcript and phosphorylated AKT as 'PIK3CA regulators' and 'PIK3CA non-regulators'. We generated two representative mutations from each group as R248Q, R273H (PIK3CA non-regulators category) and C176Y and Y220C (PIK3CA regulators). Stable expression of R248Q and R273C in p53-defecient SKOV3 cells did not reduce PIK3CA expression activity while expression of C176Y and Y220C attenuated PIK3CA expression under cisplatin treatment. Though R248Q and R273H belong to PIK3CA non regulator category, cisplatin treatment induced PIK3CA expression only in SKOV3 cells expressing R248Q p53 mutation while it remain unchanged in R273H expressing cells. Interestingly, only C176Y and Y220C mutants underwent p53 serine 46 phosphorylation after cisplatin treatment, which was absent in R248Q and R273C expressing SKOV3 cells. However cisplatin treatment induced phosphorylation of p53 at serine 15 and 20 in all four p53 mutations. Hence different p53 missense mutations exert differential regulatory effect on the PI3K/AKT signalling based on their serine 46 phosphorylation status.

Objective 2: To identify novel interacting partners for PIK3CA promoter in acquired chemoresistance

Since we observed increased PIK3CA expression in three different platinum resistant cells (A2780-CisR, TOV21G and SKOV3) under cisplatin treatment and loss of p53 binding at vital p53-RE in PIK3CA promoter, we hypothesized that other unidentified regulator/s might play role escalating PIK3CA expression as a response towards cisplatin. To understand this complex PIK3CA regulation in cisplatin resistant cells, we adopted promoter (DNA)-binder (protein) pull down strategy for identification of novel regulators. A short (OS4) PIK3CA promoter fragment (~340bp containing the fourth p53-RE) was used for two major reasons: A) site 4 was found to be the most critical regulatory site (for p53 as well as presence of other transcription factor binding sites as found by JASPER analysis) & B) to avoid non-specific binding of protein complexes to the full length promoter. PIK3CA binding partners from nuclear fraction of A2780-CisR cells were pulled down using biotinylated OS4-PIK3CA fragment. Nano-LC-MS analysis of these bound fraction revealed 1331, 451 and 362, 256 proteins in two independent biological replicates of pre and post cisplatin treated A2780-CisR cells. Further, these protein signatures were analysed with Reactome pathway analysis software. Transcription factors and their associated partners were identified using GSEA server via molecular and biological functional categorisation.

We identified 53 differential binders of PIK3CA promoter in cisplatin treated cells. From these protein signatures, NF-κB, β-catenin and CREB were selected based on the presence of putative binding sites on OS4 as well as full length PIK3CA promoter. Further these factors were validated using PIK3CA promoter luciferase sensor and with and without TNFα, Lithium chloride (LiCl) and forskolin as inducer for NF-κB, β-catenin and CREB respectively. Both TNFα and LiCl induced 2-3 fold increase in PIK3CA promoter activity only in cisplatin resistant cell line but not in sensitive cells. However, forskolin treatment induced PIK3CA promoter activity by 1.4 and 2.4 fold in sensitive and resistant cells respectively. Endogenous PIK3CA expression also corroborated with promoter activity data.

As described earlier, while acquirement of resistance activates PI3K/AKT signalling, fraction of inherently resistant cancer stem cells also increases during resistance development. Recent evidence reveals involvement of activated PI3K/AKT cascade in the maintenance and survival of colon, breast and naopharyngeal cancer stem cells. Tadoro et al (2007) demonstrated that activation of PI3K/AKT/BCl2 signalling enriches CD133+ colon cancer stem cells in response to Adriamycin and 5-FU. Other studies also revealed that CD44+ ovarian CSCs promote resistance against paclitaxel and carboplatin via constitutive activation of NF-κB signalling. Further inhibition of EGFR/AKT/β-catenin pathway via Gefitinib in naopharyngeal carcinoma was shown to repress self-renewal potential of CSC population. Hence to understand the impact of PIK3CA promoter modulation on intrinsically resistant cancer stem cell (CSC) population, we assessed the PIK3CA expression level in these cells. CSC enriched side-population (SP) fraction was isolated from A2780-CisR, TOV21G and SKOV3 cells using DCV-dye exclusion methodology. Both main population (MP) and SP fraction isolated from resistant cells demonstrated increased PIK3CA expression after cisplatin treatment. Intriguingly, SP fraction showed 1.5 fold increase in PIK3CA transcript levels compared to MP fraction. However such modulation was not observed in non-side population (NSP) cells. TNFα, Lithium chloride and forskolin treatment to SP fraction induced PIK3CA promoter activity by 1.9, 1.1 and 0.9 fold as measured by luciferase assay. Cumulative treatment of cisplatin along with TNFα further augmented PIK3CA promoter activity up to 3.1 fold, while cisplatin in combination with lithium chloride or forskolin induced PIK3CA promoter activity up to 1.7 and 2 fold. These results indicated that NF-κB could be one of the major contributor for the PIK3CA promoter activity escalation in SP cells. Interestingly, dual immunostaining with NF-κB and OCT4 antibodies in SP cells revealed that, ~45% of the NF-κB localised to nucleus in the cancer stem cells (nuclear OCT4 +ve) cells. To understand the effect of PIK3CA modulation on the cancer stem cells

phenotype, enrichment in the SP fraction was assessed post TNFα or cisplatin treatment. Cisplatin treatment to MP or SP fraction significantly increased total SP fraction of A2780-CisR, TOV21G and SKOV4 similar to TNFα. Hence, a chemotherapeutic drug, cisplatin is likely to enrich the CSC fraction in resistant cells via escalation of PIK3CA signaling. To assess the effect of PIK3CA induction on differentiation ability of CSC population, SP fraction was acquired from third generation SP fraction pre or post TNFα or cisplatin treatment. SP fraction of the A2780-CisR in untreated condition was found to be around 38.7+3.5% while rest of the fraction differentiated into NSP population. Surprisingly, TNFα or cisplatin treatment led to enhanced SP fraction up to 67.1+7.23% and 59.9+12.2% respectively. This NF-κB mediated PIK3CA escalation persuaded enrichment of SP fraction in MP as well as SP fraction of TOV21G and SKOV3 cells. To ascertain that this enrichment depends on PIK3CA activity, we inhibited PIK3CA activity using a wortmannin, an irreversible inhibitor of p110α□. Inhibition of PIK3CA activity decreased ~30% of SP fraction in MP and SP population of A2780-CisR cells. Other cisplatin resistant cells SKOV3, also demonstrated similar effect where SP fraction was reduced from 4.8+1.7% to 1.9+0.2% post wortmannin treatment. Effect of PIK3CA inhibition was more robust on 3rd generation SP population as SP fraction in these cells decreased upto ~50% post 24hr of wortmannin treatment.

Conclusion:

Differential cellular response towards cisplatin governs fate of a cancer cell. Activation of PI3K/AKT pathway may favour endurance of a cell against stress such as drug treatment. Here, we demonstrated that phosphorylation of p53 at serine 46 accelerates p53-PIK3CA promoter interaction under cisplatin treatment. This interaction attenuated PI3K/AKT survival cascade thereby imposing sensitive cells towards apoptotic fate. Absence of p53 serine 46 phosphorylation in resistant cells hinders recruitment of p53 to site 3 and 4 on

PIK3CA promoter. In absence of p53 losses its ordinance on PIK3CA promoter, cisplatin induced transcription factors NF-κB and β-catenin escalated PIK3CA expression in resistant cells. Upregulated and unaltered PI3K/AKT cascade promotes cell survival as well as self-renewal of cancer stem cells by escalating PIK3CA expression via NF-κB in platinum-resistant cells. Thus, our study signifies that persistent treatment of chemotherapeutic drug/s leads to upregulation of PIK3CA expression via decoupling of p53-PIK3CA interaction which in turn enriches CSC population which is a prime culprit for relapse in EOC patients. Inhibition of PI3K/AKT signaling might provide a therapeutic intervention against cancer stem cells in chemoresistant ovarian carcinoma.

References:

[1]Torre LA, Bray F, Siegel RL, et al. Global cancer statistics, 2012. CA Cancer J Clin. 2015;65(2):87-108.
[2]Gatenby RA. A change of strategy in the war on cancer. Nature. 2009;459(7246):508-9.
[3]Piccolo MT, Menale C, Crispi S. Combined anticancer therapies: an overview of the latest applications. Anticancer Agents Med Chem. 2015;15(4):408-22.
[4]Chabner BA, Roberts TG, Jr. Timeline: Chemotherapy and the war on cancer. Nat Rev Cancer. 2005;5(1):65-72.
[5]Longley DB, Johnston PG. Molecular mechanisms of drug resistance. J Pathol. 2005;205(2):275-92.
[6]Gottesman MM, Fojo T, Bates SE. Multidrug resistance in cancer: role of ATP-dependent transporters. Nat Rev Cancer. 2002;2(1):48-58.
[7]Borst P, Elferink RO. Mammalian ABC transporters in health and disease. Annu Rev Biochem. 2002;71:537-92.
[8]Fojo T, Bates S. Strategies for reversing drug resistance. Oncogene. 2003;22(47):7512-23.
[9]Pan ST, Li ZL, He ZX, Qiu JX, Zhou SF. Molecular mechanisms for tumour resistance to chemotherapy. Clin Exp Pharmacol Physiol. 2016;43(8):723-37.
[10]Abdullah LN, Chow EK. Mechanisms of chemoresistance in cancer stem cells. Clin Transl Med. 2013;2(1):3.

[11]Chao SY, Chiang JH, Huang AM, Chang WS. An integrative approach to identifying cancer chemoresistance-associated pathways. BMC Med Genomics. 2011;4:23.
[12]Wang D, Lippard SJ. Cellular processing of platinum anticancer drugs. Nat Rev Drug Discov. 2005;4(4):307-20.
[13]Cheaib B, Auguste A, Leary A. The PI3K/Akt/mTOR pathway in ovarian cancer: therapeutic opportunities and challenges. Chin J Cancer. 2015;34(1):4-16.
[14]Liu P, Cheng H, Roberts TM, Zhao JJ. Targeting the phosphoinositide 3-kinase pathway in cancer. Nat Rev Drug Discov. 2009;8(8):627-44.
[15]Ciriello G, Miller ML, Aksoy BA, et al. Emerging landscape of oncogenic signatures across human cancers. Nat Genet. 2013;45(10):1127-33.

[16]Zhang W, Ding W, Chen Y, et al. Up-regulation of breast cancer resistance protein plays a role in HER2-mediated chemoresistance through PI3K/Akt and nuclear factor-kappa B signaling pathways in MCF7 breast cancer cells. Acta Biochim Biophys Sin (Shanghai). 2011;43(8):647-53.

[17]Abubaker J, Bavi P, Al-Haqawi W, et al. PIK3CA alterations in Middle Eastern ovarian cancers. Mol Cancer. 2009;8:51.

[18]Liang S, Yang N, Pan Y, et al. Expression of activated PIK3CA in ovarian surface epithelium results in hyperplasia but not tumor formation. PLoS One. 2009;4(1):e4295.

[19]Matulonis UA, Sood AK, Fallowfield L, et al. Ovarian cancer. Nat Rev Dis Primers. 2016;2:16061.

[20]Markman M. Second-line therapy for ovarian cancer. Clin Adv Hematol Oncol. 2008;6(6):421-2.

[21]Burger RA, Brady MF, Bookman MA, et al. Incorporation of bevacizumab in the primary treatment of ovarian cancer. N Engl J Med. 2011;365(26):2473-83.

[22]Oza AM, Cibula D, Benzaquen AO, et al. Olaparib combined with chemotherapy for recurrent platinum-sensitive ovarian cancer: a randomised phase 2 trial. Lancet Oncol. 2015;16(1):87-97.

[23]Cancer Genome Atlas Research N. Integrated genomic analyses of ovarian carcinoma. Nature. 2011;474(7353):609-15.

[24]Kolasa IK, Rembiszewska A, Felisiak A, et al. PIK3CA amplification associates with resistance to chemotherapy in ovarian cancer patients. Cancer Biol Ther. 2009;8(1):21-6.

[25]Astanehe A, Finkbeiner MR, Hojabrpour P, et al. The transcriptional induction of PIK3CA in tumor cells is dependent on the oncoprotein Y-box binding protein-1. Oncogene. 2009;28(25):2406-18.

[26]Hui RC, Gomes AR, Constantinidou D, et al. The forkhead transcription factor FOXO3a increases phosphoinositide-3 kinase/Akt activity in drug-resistant leukemic cells through induction of PIK3CA expression. Mol Cell Biol. 2008;28(19):5886-98.

[27]Yang N, Huang J, Greshock J, et al. Transcriptional regulation of PIK3CA oncogene by NF-kappaB in ovarian cancer microenvironment. PLoS One. 2008;3(3):e1758.

[28]Gaikwad SM, Gunjal L, Junutula AR, et al. Non-Invasive Imaging of Phosphoinositide-3-Kinase-Catalytic-Subunit-Alpha (PIK3CA) Promoter Modulation in Small Animal Models. PLoS One. 2013;8(2):e55971.

[29]Lee S, Choi EJ, Jin C, Kim DH. Activation of PI3K/Akt pathway by PTEN reduction and PIK3CA mRNA amplification contributes to cisplatin resistance in an ovarian cancer cell line. Gynecol Oncol. 2005;97(1):26-34.

[30]Carpten JD, Faber AL, Horn C, et al. A transforming mutation in the pleckstrin homology domain of AKT1 in cancer. Nature. 2007;448(7152):439-44.

[31]Clark AS, West K, Streicher S, Dennis PA. Constitutive and inducible Akt activity promotes resistance to chemotherapy, trastuzumab, or tamoxifen in breast cancer cells. Mol Cancer Ther. 2002;1(9):707-17.

[32]Prasad G, Sottero T, Yang X, et al. Inhibition of PI3K/mTOR pathways in glioblastoma and implications for combination therapy with temozolomide. Neuro Oncol. 2011;13(4):384-92.

[33]Gaikwad SM, Thakur B, Sakpal A, Singh RK, Ray P. Differential activation of NF-kappaB signaling is associated with platinum and taxane resistance in MyD88 deficient epithelial ovarian cancer cells. Int J Biochem Cell Biol. 2015;61:90-102.

[34]Rinn JL, Huarte M. To repress or not to repress: this is the guardian's question. Trends Cell Biol. 2011;21(6):344-53.

[35]Di Stefano V, Soddu S, Sacchi A, D'Orazi G. HIPK2 contributes to PCAF-mediated p53 acetylation and selective transactivation of p21Waf1 after nonapoptotic DNA damage. Oncogene. 2005;24(35):5431-42.

[36]Szak ST, Mays D, Pietenpol JA. Kinetics of p53 binding to promoter sites *in vivo*. Mol Cell Biol. 2001;21(10):3375-86.

Publications:

a. Published articles:

7. **Thakur B** and Ray P. "p53 Loses grip on PIK3CA expression leading to enhanced cell survival during platinum resistance" Molecular Oncology, 1283-1295, June 2016.

8. Pradhan L#, **Thakur B#**, Srivastava R, Ray P*, Bahadur D*. "Assessing Therapeutic Potential of Magnetic Mesoporous Nanoassemblies for Chemo-Resistant Tumors". Theranostics. 2016. (# These authors have equally contributed to the work)

9. Gaikwad SM#, **Thakur B#,** Sakpal A, Ray P. "Differential activation of NF-κB signaling is associated with Platinum and Taxane resistance in MyD88 deficient epithelial ovarian cancer cells". Int J Biochem Cell Biol. Apr;61:90-102, 2015. (# These authors have equally contributed to the work)

10. Singh M, Singh SK, **Thakur B**, Ray P, Singh SK. Design and Synthesis of Novel Schiff base-benzothiazole hybrids as potential Epidermal Growth Factor Receptor (EGFR) Inhibitors. Anticancer Agents Med Chem. 2015 Oct 7.

11. **Thakur B**, Chatterjee S, Chaudhury S, Ray P. Molecular Imaging of Therapeutic Potential of Reporter Probes. Curr Drug Targets. 2015;16(6):645-57

12. Chaudhury S, **Thakur B**, Chatterjee S, Ray P. Molecular imaging aided improvement in drug discovery and development. Curr Biotech. 3(3): 218-237, 2014.

Oral Presentations:

Bhushan Thakur, Pritha Ray. 2014 Monitoring drug responsive dynamics of p53-PIK3CA promoter modulation. XXXVIII All India Cell Biology Conference, CSIR – CDRI, Jankipuram Extension, Lucknow, India. (Platform presentation)

Poster presentations:

1. Bhushan Thakur, Pritha Ray, 2016, Systematic halt and release in proliferation by drug resistant ovarian cancer cells: a mechanism for continuance of resistance, XXX All India Cell Biology Conference, Jiwaji University, Gwalior.

2. Bhushan Thakur, Pritha Ray. 2015. p53 dependent PIK3CA promoter modulation in chemoresistance: Mechanism beyond genomic alterations. Platinum Jubilee TMC Conference, Mumbai.

3. Bhushan Thakur, S M Gaikwad and Pritha Ray, 2013, Modulation in PIK3CA signaling during acquired chemoresistance: p53 ordinance insufficiency. XXXVII All India Cell Biology Conference, in Stem, JN Tata Auditorium ,IISC, Bangalore, India.

b. **Accepted:** Not applicable.

c. **Communicated:** Not applicable.

d. **Other Publications:** Not applicable.

Award: Directors prize for best participant among the Ph.D. student in Oral presentation. AICBC, 2014.

Bhushey

Signature of the student

Date: 11/04/17

Doctoral committee members:

S.	Name	Designation	Signature	Date
1	Dr. Shubhada Chiplunkar	Chairperson	*Chiplunkar*	13.4.17
2	Dr. Pritha Ray	Guide & Convener	*Pritha Ray*	12.4.17
3	Dr. Neelam Shirsat	Member	*Shirsat*	11/4/17
4	Dr. Sanjay Gupta	Member	*sign*	12/4/17
5	Dr. Samit Chattopadhyay	Technical Advisor	*Samit Chattopadhyay*	11/4/17

Forwarded Through:

L. Chiplunkar 13/4/17

Dr. S.V. Chiplunkar

Director, ACTREC

Chairperson,

Academic & training Program, ACTREC

Dr. S. V. Chiplunkar
Director
Advanced Centre for Treatment, Research &
Education in Cancer (ACTREC)
Tata Memorial Centre
Kharghar, Navi Mumbai 410210.

Prof. K. Sharma

Director, Academics

T.M.C.
PROF. K. S. SHARMA
DIRECTOR (ACADEMICS)
TATA MEMORIAL CENTRE,
PAREL, MUMBAI

15

List of Figures

List of Tables

Chapter 1:

Introduction and review of literature

Chapter 1: Introduction and review of literature

The road to understanding the role of PI3K in chemoresistance

---

1.1 Signal transduction in cells: The whole is greater than the sum of its parts

In order to maintain cellular homeostasis and survive under different environmental conditions, constant communication between cells and their environment is essential for multicellular organisms.[1-3] A cell, being functional unit of life, is highly sensitive and receptive to fluctuations in their external environment. Typically, these changes are communicated by various molecules and are acquired through direct communication (cell adhesion molecules (CAMs))[4] or indirect communication (receptor tyrosine kinases (RTKs)[5, 6], G-protein coupled receptors (GPCRs)[7] and non-RTKs[4]). The RTKs, GPCRs and non-RTKs include cellular adhesion, growth factors (GFs), hormones, cytokines, mechanical forces, and neuropeptides, which bind to specific transmembrane receptors and activate secondary messengers within the cell. In turn, with limited repertoire of signaling pathways, cells have evolved to sense, integrate, and amplify external and internal cues to execute appropriate cellular responses [1-3] such as survival, growth, gene expression, differentiation, and other functions.[1] All together, this process is referred to as Signal Transduction.[3]

Various signaling ligands interact with the extracellular domains of the receptor proteins, which prompt conformational change and activation of their intracellular domains. [1-3, 8, 9] Stimuli induced activation of receptor is a short-lived response, hence it is required to transduce the signal into a prolonged cue through secondary messenger/s or signal amplification.[10] The customary secondary messengers include cyclic AMP, inositol 1,4,5-triphosphate (IP3), diacylglycerol (DAG), phosphatidylinositol bisphosphate (PIP2),

and phosphatidylinositol triphosphate (PIP3).[11-13] Activation of these secondary messengers trigger a series of protein recruitment, post translational modifications (PTMs) (acetylation, sumoylation, ubiquitination, phosphorylation or dephosphorylation), allosteric activation or inhibition and protein-protein interaction in the cytoplasm, priming cellular response through transcription of target genes.[14] In contrast to presence of large number and quantity of stimuli, numbers of cell surface receptors are limited. Cells deal with this external complexity by wiring signaling pathways to integrate information from multiple receptors. Thus, a signaling cascade 'crosstalk' with an allied pathway and operates in synergy with each other instead of functioning in solitude.[15] Cellular fate is largely dependent on final outcome of signaling networks than a solitary pathway.[16] Hence, signal transduction appears to embrace Aristotle's view that "the whole is greater than the sum of its parts." Perturbation in one or more components of signaling network severely effects its fine-tuning which eventually leads to multitude of diseases such as hypertension, diabetes, heart disease, and cancer.[17-19] Miscommunication between pathways has severe effects on the cell that eventually lead to the current <u>hallmarks of cancer</u> such as, uncontrolled growth and proliferation, migration and invasion, and evasion of cell death (apoptosis).[20] Understanding the regulation of deregulated pathways is essential for opening of therapeutic avenues against multitude of diseases.

1.2 Cancer: An ever-challenging enigma:

Cancer, as old adage goes, is a collection of hundred diseases masquerading as one. In general, tumors are divided into two broad categories as benign tumors (which do not invade), and malignant tumors (which can metastasise in distant organs). Benign tumors are mostly harmless and under rare circumstances, they pressurise vital organs or develop into dysplasia. Malignant neoplasias are collectively called cancer, that caused approximately 8.7

million deaths in 2015 worldwide making it the third most common killer after cardiovascular disease and infectious or parasitic disease.[21] Depending on the cell origin, solid tumors are categorised into either carcinomas (epithelial origin) or sarcomas (mesenchymal origin) such as osteosarcoma, glioma and neuroectodermal tumors. Current clinical intervention for cancer management includes surgery, radiation therapy, chemotherapy, hormone therapy, immunotherapy, and molecular targeted therapy. [22] Chemotherapy is one of the prevailing methods used to treat cancer, as they are effective against multiple tumor types. [23, 24] They can be used singularly or in combination with other treatments such as hormone therapy and radiotherapy. The benefits of chemotherapy and radiotherapy include: 1) killing cancer cells at the primary site or metastasizing sites (e.g. lymphoma & breast cancer) [25, 26]; 2) Tumor debulking prior to surgical intervention (e.g. esophageal cancer) [27]; 3) Palliative care for shrinking tumor sizes to relieve patients from pain caused by cancer (e.g. bone metastasis). [28]

While chemotherapy and/or radiotherapy remain the standard mode of treatment for cancer patients, the response to treatment varies substantially in different types of cancer, or even among patients with the same type of cancer. For example, chemotherapy is extremely successful in childhood acute lymphocytic leukemia (ALL) treatment; where over 95% of the patients attain remission and 91.7% of them survive over 5 years.[29, 30] On the contrary, despite intensive combinatorial treatment of chemotherapy and radiotherapy, most glioblastoma patients suffer from rapid tumor recurrence, where the median time of tumor progression is only about 6.9 months and the 5-year-survival rate is less than 10%.[31] In ovarian cancer, the clinical response rates to neoadjuvant chemotherapy vary from 72.5% to 11.2% in serous adenocarcinoma and clear cell carcinoma, respectively.[32-34] The variations in treatment response suggest that intrinsic or acquired therapeutic resistance exists in a subset of cancer patients, which leads to treatment failures, disease progression, and

eventually mortality. This pervasive barrier confounds the ultimate goal of curing or managing cancer in long term.

Drugs used for cancer therapy can broadly be classified into two groups:

I.   **Standard chemotherapy:** These drugs comprise of molecules with diverse mode of action, structure, or source (Table 1.1)

Table 1. 1**.** Examples of common chemotherapy drugs by their classification and type [35]

Category	Mechanism of action	Example
Antimetabolites	Interfere with intermediary metabolism of proliferating cells Thymidylate synthase inhibitors ribonucleotide reductase	Methotrexate, 5-fluorouracil 5-Fluorouracil Hydroxycarbamide, Pentostatin
Mitosis inhibitors	Target microtubules and associated proteins required in cell division	Taxol
Steroid hormones	Block steroid- and hormone-dependent growth of certain tumours	Tamoxifen, flutamide
Alkylating/cross-linking agents	Damage DNA and result in death of growing cells Prevent replication and transcription	Endoxan, cisplatin, cyclophosphamide, Mitomycin C, Chlormethine Nitrosoureas
Angiogenesis inhibitors	Block blood-vessel formation to tumour	Avastin (Genentech)
Histone-deacetylase inhibitors	Affect transcription of genes	SAHA (Aton Pharma)
Telomerase inhibitors	Affect telomere maintenance required for tumour growth	BIBR1532 (Boehringer Ingelheim)
Antitumour antibiotics	Bind DNA to prevent DNA and/or RNA synthesis	Etoposide, Doxorubicin

II.   **Targeted therapy:** Targeted therapy employs small molecule inhibitors or monoclonal antibodies against 'oncogenic driver' proteins, thus affecting tumor growth, survival, angiogenesis, and drug resistance.[36] Among the most clinically effective small molecule inhibitors are Gefitinib (EGFR)[37] and Imatinib (ABL1)[38] used in treatment of breast cancer and CML (Philadelphia chromosome positive) patients, respectively. Monoclonal antibodies like trastuzumab (herceptin)[39] and bevacizumab[40] which target HER2/neu, and VEGFR, respectively are used as treatment modality in breast, lung, colon and head &

neck cancer. FDA approved targeted therapeutics (monoclonal antibodies and small molecular inhibitors) are enlisted in Table 1.2 and 1.3.

Table 1. 2: FDA Approved monoclonal antibodies against receptor tyrosine kinase used for treatment of cancer (adapted from Miller et al 2013). [41]

Drug	Trade Name	Target	Cancer Type
Transtuzumab	Herceptin	HER2	Breast, gastric
Pertuzumab	Parjeta	HER2	Breast
Cetuximab	Erbitux	HER1	Squamous cell carcinoma
Panitumumab	vectibix	HER1	Colon
Bevacizumab	Avastin	VEGF	Glioblastoma, NSCLC, colorectal kidney
Rituximab	Rituxan	CD20	B-cell non-Hodgkin lymphoma, chronic lymphocytic leukemia
Alemtuzumab	Campath	CD52	B-cell chronic lymphocytic leukemia
Ofatumumab	Arzerra	CD20	Chronic lymphocutic leukemia
Ipilimumab	Yervoy	CTLA-4	Melanoma
Abbreviations: HER, human epidermal growth factor receptor; VEGF, vascular endothelial growth factor; CD, cluster of differentiation; CTLA, cytotoxic T-lymphocyte antigen			

Table 1. 3: FDA Approved tyrosine kinase inhibitors used for treatment of cancer (adapted from Miller et al 2013)[41].

Inhibitor	Trade Name	Target	Cancer Type
Imatinib mesylate	Gleevec	ABL,c-KIT,PDGFR	Ph+ CML, GISTs,ALL
Dasatinib	Sprycel	SFK,ABL	CML, ALL
Nilotinib	Tasigna	ABL,c-KIT,PDGFR	CML
Bosutinib	Bosulif	SFK,ABL	CML
Gefitinib	Iressa	HER1	NSCLC
Erlotinib	Tarceva	HER1	Lung
Lapatinib	Tykerb	HER1,HER2	Breast, others
Vandetanib	Caprelsa	EGFR,VEGFR,RET	Medullary thyroid
Crizotinib	Xalkori	EML4-ALK	NSCLC
Sunitinib	Sutent	VEGFR,PDGFR,c-KIT,FLT-3	GIST, renal
Sorafenib	Nexavar	B-Raf,VEGFR,PDGFR	Renal, hepatocellular, prostate
Pazopanib	votrient	VEGFR,c-KIT,PDGFR	Renal;soft tissues sarcoma
Regorafenib	Stivarga	VEGFR,TIE2,PDGFR,RET,c-KIT,RAF	Colorectal
Cabozantinib	Cometriq	VEGFR,RET,MET,TRKB,TIE2	Medullary thyroid
Abbreviations: ABL,Abelson kinase; PDGFR,platelet-derived growth factor receptor; SFK, Src family kinases; HER, human epidermal growth factor receptor;VEGFR, vascular endothelial			

III. Radiation Therapy

Radiation therapy is an additional mode of cancer therapy where ionising/high energy particles such as γ-rays, photon beam, α-partials and β-emitters are used for cancer treatment. Radiation can be given as total body irradiation (TBI) or through brachytherapy (radioactive source near tumor tissue). Radiation principally works as direct DNA damaging agents producing double strand breaks, or indirectly through forming free radicals, notably hydroxyl radicals, reactive oxygen species which causes damage the DNA.[42, 43] Isotopes commonly used in the radiotherapy includes Iodine-131-sodium iodide in hyperthyroidism and thyroid cancer, Yttrium-90-ibritumomab tiuxetan (Zevalin) and Iodine-131-tositumomab (Bexxar) in

refractory lymphoma, 131I-MIBG (metaiodobenzylguanidine) in neuroendocrine tumors and Samarium-153 or Strontium-89 in palliative care of bone cancer treatment.[44, 45] The degree of radiosensitivity varies across cancers types. For example, leukaemia, most lymphomas, and germ cell tumors are most radiosensitive while majority of epithelial cancers respond moderately to radiation. Renal cell cancer and melanoma are amongst the most radioresistant cancer types, however radiation therapy is used as a palliative therapy for these tumors.[46] Radiotherapy is used as adjuvant, neoadjuvant therapeutic, or palliative in non-melanoma skin cancer, head and neck cancer, breast cancer, non-small cell lung cancer, cervical cancer, anal cancer, prostate cancer.[47, 48] Metastatic cancers are generally incurable with radiation therapy because of their wide spread throughout the body.

In addition to these therapies, hormone therapy (use of estrogen, testosterone, or progestogens in breast and prostate cancer)[49, 50] and immunotherapy (use of Interferons, interleukins, PD-1 inhibitors and cell-based therapies in bladder carcinoma, melanoma, renal cancer and Hodgkin's lymphoma)[51-53] play a crucial role in cancer treatment. An elaborative description about both the therapies is out of the scope of this thesis.

1.3 Chemoresistance: a major caveat of current cancer therapy:

Chemotherapy is one of the widely used methods to treat malignant tumors due to their wide-spectra of effectiveness against multiple tumor types.[23, 24] Cytotoxic drugs such as ionizing radiation and chemotherapeutic (cisplatin, 5-fluorouracil, doxorubicin, camptothecin and paclitaxel) differ in their mode of actions and they target rapidly dividing tumor cells and kill tumor cells by inhibiting proliferation and/or inducing apoptosis. However, manifestations of acquired or intrinsic chemoresistance impede success of therapeutic intervention.[54-57] Intrinsically resistant tumors display pre-existing resistance-mediating features, making therapy ineffective. Acquired drug resistant tumor can develop from sensitive tumors as they adopt during the course of treatment. This adaptation can be caused

through mutations acquired during drug exposure, other adaptive responses, such as increased expression of the therapeutic target and activation of substitute signalling cues. Moreover, increasing evidence indicates selection of a minor subpopulation from heterogeneous tumor population through the drug treatments. [58-60] Targeted therapies have demonstrated superior efficacy in specifically eliminating cancer cells, thus resulting in less toxicity. Unfortunately, even though in many instances remission is observed, this is frequently followed by the reappearance of drug-resistant tumors.[61, 62] Resistance to chemotherapy and molecularly targeted therapies is an enigma in management of cancer, succumbing patient's survival.

The mechanisms of resistance to 'classical' cytotoxic drugs consist of alterations in the drug target, activation of prosurvival pathways and ineffective induction of cell death. Both acquired and intrinsic drug resistance are multifactorial phenomenon involving multiple interrelated or independent mechanisms. Cellular mechanisms for chemoresistance of tumor cells can be grouped into three groups as: (1) decreased intracellular concentration of active drug (2) alterations in drug–target interactions; (3) factors influencing improved cellular survival. [63-65] Decreased accumulation of intracellular drug concentration may result from active efflux (overexpression of ATP-binding cassette (ABC) superfamily membrane transporters such as P-glycoprotein (P-gp), hMRPs, ABCB1), detoxification of intracellular drug through glutathione and reduced expression of influx transporters (hCTR1) intracellular drug.[66-69] Moreover, alteration in drug-target interaction inhibits normal functioning of chemotherapeutic agent leading to its failure. For example, mutation in β-tubulin at 215, 217, or 228 leucine residue inhibit binding of class I β-tubulin and paclitaxel. [70] Similarly, alteration in dihydropyrimidine dehydrogenase (DPD), which catabolise 5-FU into active cellular metabolites leads to resistance against 5-FU.[71, 72] In addition, other mechanisms that can contribute to cellular resistance include enhanced DNA repair, bypass of DNA repair

(overexpression of polymerase beta and eta which has defective proofreading activity) or/and increased tolerance towards stress conditions.[73, 74]

1.4 Chemoresistance associated signaling pathways:

The multifaceted nature of resistance continues to become more complex as more genes inducing chemoresistance are identified from gene expression profiles. Therapeutic intervention alters genetic and epigenetic functioning of crucial survival or apoptosis related genes in cancer cells which eventually induce resistance.[75] For example, Overexpression of Aurora A, a serine/threonine kinase, which is involved in the centrosome separation and bipolar spindle formation, confers resistance to paclitaxel-mediated apoptosis [76]. Few other genes include tumor suppressor gene (such as p53, RB and PTEN), oncogene (such as PI3K/AKT, RAS/RAF, c-MYC and c-JUN), and components of apoptotic machinery (such as Survivin, XIAP, NF-κB, Bad, Bax and BCl2 family). [77-87] For instance, Resistance against paclitaxel is shown to be associated with overexpression of cytokines like IL6, IL8 and monocyte chemotactic protein-1 (MCP-1), which activates signal transducer and activator of transcription 3 (STAT 3) survival signaling [88, 89]. Resistance to cell death may be caused by the over activation of an anti-apoptotic protein or by inactivation of an apoptotic activator or effector.[86, 87] p53, a stress induced transcription factor, is mutated in over half of human cancers. It switches cellular fate between cell cycle arrest versus apoptosis through upregulation of many pro-apoptotic genes such as PUMA, BAX and NOXA. Therefore, loss of wild type p53 functionality inhibits natural progression of apoptotic signaling and prompt resistance to cell death. [90] In addition, downregulation of BCl2, lack of functional p53 or mutations in p53 contribute to paclitaxel resistance. [91, 92]

The Erb/EGFR family members, HER-2/neu, ERBB2 and EGFRVIII, are amplified and overexpressed in tumors with resistance against cisplatin and paclitaxel treatment [93-95]. Activation of these RTKs promotes therapy resistance by activation of PI3K/AKT signaling

axis. Overexpression of a catalytically active subunit of PI3K in ovarian cancer cells confers taxol resistance, which is reversed upon inhibition of the PI3K pathway utilizing a selective inhibitor [96]. Activation of Notch1 signaling promotes chemoresistance and radioresistance in gliomas, and inhibition of NOTCH through γ-secretase inhibitor sensitise resistant cells to radiation treatment.[97, 98] NOTCH activation induces hypoxia/HIF-1α mediated cell proliferation, invasion, and chemoresistance in T-cell acute lymphoblastic leukemia (T-ALL)[99] In addition, Notch1 or Notch2 signaling promoted survival of CD133 positive cancer stem cells in glioma and ALL upon therapeutic treatment. [100] Overexpression of WNT or mutation in β catenin activates downstream wnt/β catenin signaling conforming chemoresistance in melanoma, MLL and glioma cancer.[101-103] Activation of transcription factors like NF-κB, Interferon regulatory factor 9 (IRF 9), etc. are also responsible for paclitaxel resistance [104]. Dual-specificity Y-phosphorylation regulated kinase 1B (DYRK1B, also known as MIRK) is upregulated in multiple solid tumors and in ovarian cancer cells and its depletion potentiates the cisplatin toxicity by causing lethal oxidative stress [105].

Since multiple mechanisms coexist within a resistant tumor cell, the task of identifying therapeutic approaches that will be effective against therapy resistant disease has become daunting. As cell's fate depends on net balance between pro-survival and pro-apoptosis signals induced by chemotherapeutic agents, challenge remains to identify drugable pro-survival signaling pathways. One of the major signal transduction pathways forming the basis to survival of chemoresistant cell is the PI3K pro-survival signalling pathway.[106-108]

1.5 The PI3K/AKT pathway

The PI3K/AKT signaling cascade controls a number of cellular processes, including metabolism, growth, proliferation, apoptosis and cell migration.[109] PI3Ks are the downstream signaling molecules, activated through receptor tyrosine kinases (RTK),

integrins and G-protein coupled receptors upon ligand binding. In addition, intracellular protein moleculess such as PKC, Rac, Rho and Src also activate PI3Ks.[110] Upon activation, PI3K protein catalyses the phosphorylation of phosphatidylinositols-an inositol-containing lipids embedded in intracellular plasma membrane. Phosphatidylinositol-4, 5-bisphosphate (PIP2) is primary substrate for class I PI3K, which is converted to phosphatidylinositol-3, 4, 5-trisphosphate (PIP3), an important intracellular secondary messenger.[111, 112] This PIP3 signals the recruitment and act as docking site for pleckstrin homology (PH) domains proteins.[113-117]

To date, eight distinct members of mammalian PI3Ks family have been recognised and classified into three classes based on their substrate specificity, sequence homology, and distinct regulation.[109] Class I PI3K is subdivided into two subclass , as Class IA and Class IB (see Figure 1.1). Class IA PI3Ks are heterodimeric complex containing regulatory subunit (p85α) and catalytic subunit (p110α), whereas Class IB PI3Ks are accompanied with p101 or p87 adaptor proteins. (Figure 1.1) Class IB shares structural and sequence homology with Class IA, and consists of p101 subunit instead of p110α and lacks a p85 binding domain., (see Fig. 1.1).[110]

Class II PI3Ks are regulated through insulin signalling and thought to preferentially phosphorylate PtdIns and PtdIns-4-phsphate. However, very little is understood about the upstream regulator of class II PI3K's and their part in cellular homeostasis. Class III PI3Ks can phosphorylates only PtdIns as their substrate. These class III PI3Ks upon stimulation function primarily in membrane trafficking and vacuole sorting. However, exact role of class III PI3Ks in signalling pathways is still unknown. .[118] Among these, class IA PI3Ks are associated with several cancers. [119, 120]
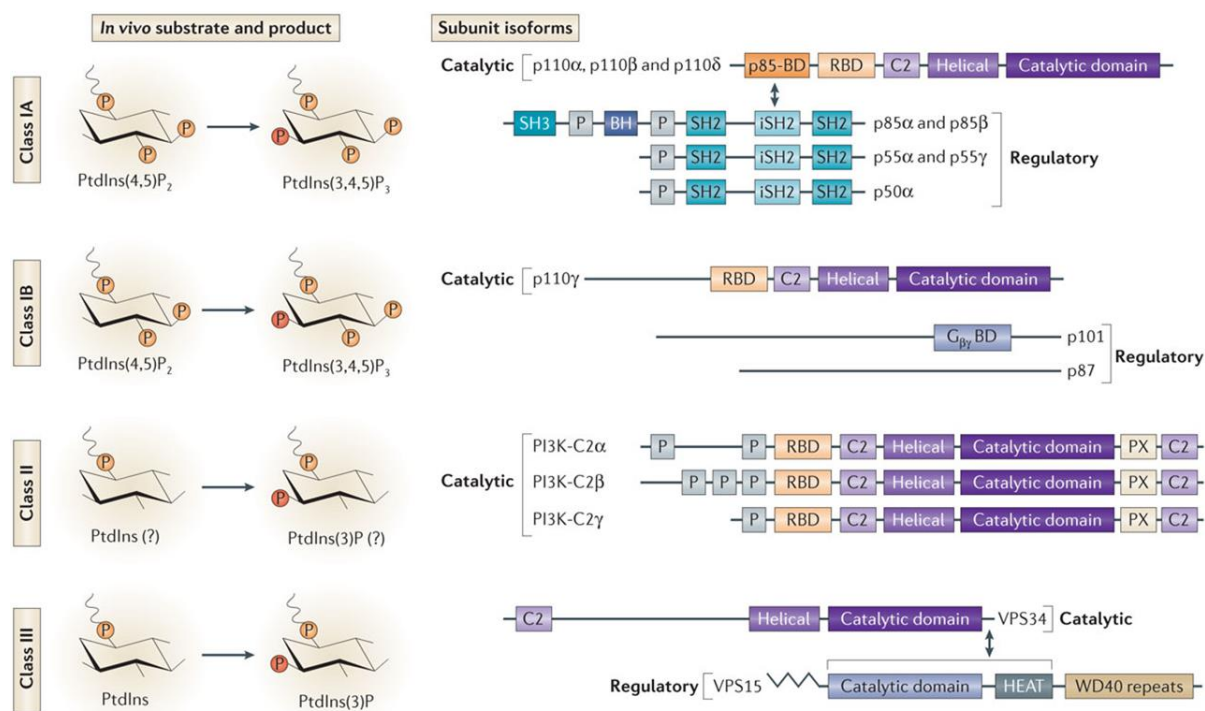
Figure 1. 1:Classification of PI3K family members.

The multiple isoforms of mammalian PI3-Ks divided into three classes, according to their structure similarities, binding specificities and mode of activation in response to different stimuli.[121] In vivo, class IA and IB PI3Ks phosphorylate phosphatidylinositide 4,5-bisphosphate (PtdIns(4,5)P2), and class III PI3Ks phosphorylate PtdIns. Class IA PI3Ks are heterodimers of a p110 (catalytic subunit) and a p85 (regulatory subunit). Class IA catalytic isoforms (p110α, p110β and p110δ) have a p85-binding domain (p85-BD), a RAS-binding domain (RBD), a helical domain and a catalytic domain. (Adapted from Thorpe et al. 2015 [122])

Structure and inter-subunit interactions of p85α and p110α.

The Class IA PI3Kα isoforms are ubiquitously expressed class of PI3K and comprise of heterodimer of a regulatory subunit (p85α) and a catalytic subunit (p110α). Structurally, p85α contains two Src homology 2 (SH2) domains, two proline-rich domains, a single SH3 domain, a breakpoint cluster region (BCR/BH) homology domain, and an inter-SH2 (iSH2)

domain. (Figure 1.1) Alternative splicing of the p85α coding gene-PIK3R1 produces three isoforms, the p85α (85 kDa), p55α (55 kDa), and p50α (50 kDa) proteins. Among these, p85α is the most ubiquitously expressed protein and involved in various growth receptor signaling. The iSH2 domain, along with N-terminal SH2 domain of p85α, interact and binds with p85 adaptor-binding domain (RBD) of the p110α subunit. Structurally, p110α subunit contains a Ras-binding domain, a C2 domain, helical domain and catalytic domain.(Figure 1.1) Along with lipid kinase activity of (conversion of PIP2 to PIP3) p110α, it also contains serine/threonine protein kinase activity. Through serine/threonine kinase activity, p110α phosphorylates p85α and undergoes heterodimerisation with p110α. Hence, this interaction acts as a feedback loop, and exerts overall inhibition of PI3K cascade in the cytoplasm.

Catalytic subunit p110α has a strong dependency on p85α for its intracellular stability. Monomeric p110α is unstable at body temperature (37°C), and requires its interaction with p85α for its stability. [123] However, dimerization of p110α with p85α decreases its lipid kinase activity by 80%. Hence, dimerization of p110α with p85α mediates the delicate balance between stabilization and activation, which determines the overall PI3K activity. [123] In contrast, normal cells possess ample expression of monomeric p85α[124], which compete with the p85α/p110α heterodimer for binding to activated receptor tyrosine kinases, thus act as an antagonist for activation of PI3K signaling.[125] Hence, both monomeric p85α and p110α are unstable in the cytosol, and decrease in level of one protein (eg. p110α levels) concomitantly reduces levels of other (p85α).

Upon ligand binding, receptor tyrosine kinases (RTKs) mediated activation of PI3K kinase convert PIP2 to PIP3. The basic function of PIP_3 is the recruitment of proteins containing pleckstrin homology domain–containing (PH-domain) including AKT. [111, 112]. Translocation of AKT to the membrane brings it close to upstream regulatory kinases such as the phosphoinositide dependent kinase 1 (PDK1) that phosphorylates AKT on Thr 308,

which is necessary for AKT activation. However, maximal activation requires additional phosphorylation at Ser473 either through auto-phosphorylation, through PDK2, integrin-linked kinase (ILK) or through mTOR complex (mTORC2). Activated AKT is known to phosphorylate pro-apoptotic Bad leading to its degradation as well as caspase 9, which inhibits its catalytic activity, thereby protecting the cells from apoptosis. Furthermore, AKT can influence cell survival by indirectly effecting nuclear factor of kappa B (NF-κB), a central regulator of cell death. Activation of AKT promotes multiple effects on cell cycle regulation through phosphorylation and inactivation of the cell cycle regulators, p27(Kip1) and p21(Cip1/WAF1) and by preventing degradation of cyclin D1 through inactivation of glycogen synthase kinase 3β (GSK-3β). In addition, AKT-mediated activation of mammalian target of rapamycin (mTOR) is important in stimulating cell proliferation. mTOR regulates translation in response to nutrients by phosphorylating components of the protein synthesis machinery. Other factors that get activated through AKT are vascular endothelial growth factor (VEGF) transcriptional activation and induced hypoxia inducible factor-1α (HIF1α) expression which are required for cell growth and angiogenesis [106, 126-130].
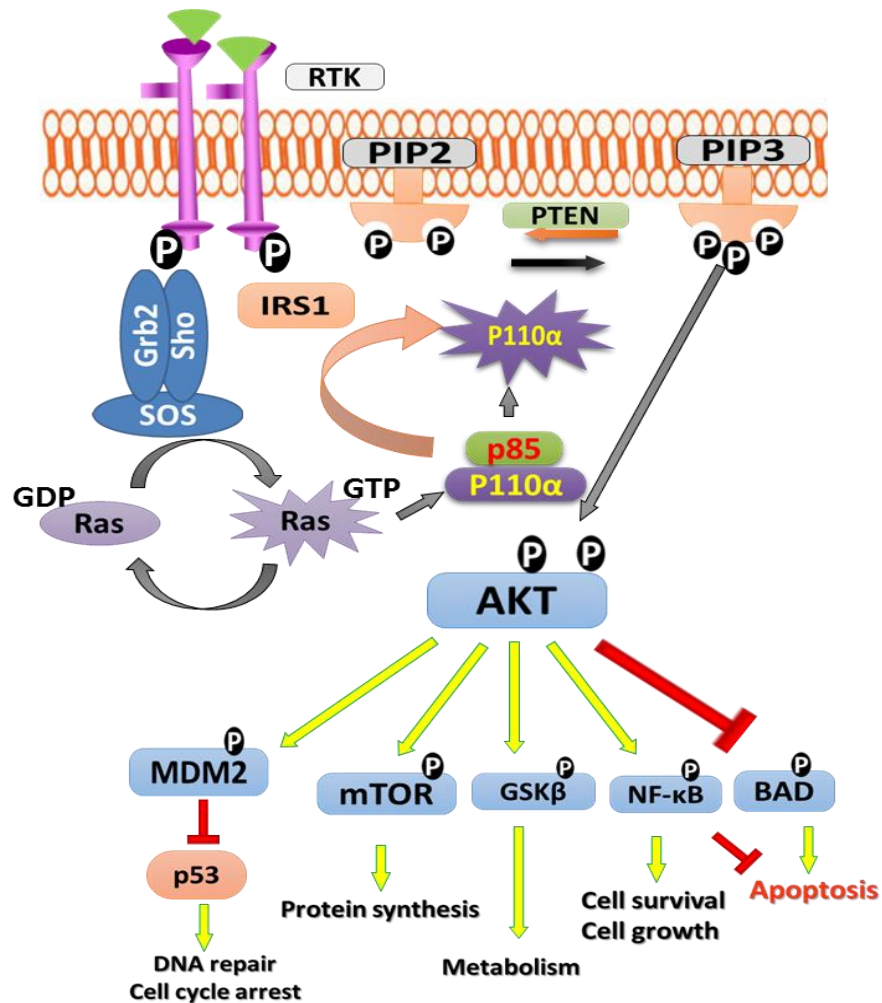
Figure 1. 2 :Navigating downstream of the PI3K/AKT pathway.

Growth factors such as EGF, IGF bind as ligands to the receptor tyrosine kinases (RTK) like EGFR, IGF1R and HER2 and auto-phosphorylate its intracellular phosphorylation, which recruits p110/p85 to membrane. This leads to conformational change and activation of PI3K. PI3K is a heterodimeric protein consisting of a regulatory subunit p85 and a catalytic subunit p110. PI3K initiates activation of AKT through phosphorylation, which further activates its downstream substrates through their phosphorylation. These AKT-substrate moieties participate in various cellular processes such as ribosomal protein synthesis and cell growth, loss of apoptosis, metabolism, cell-cycle arrest and DNA repair mediated.

1.6 Deregulation of PI3K pathway in cancer

The PI3K/PKB pathway is frequently found to be aberrant in various malignancies.[131, 132] There are two widely accepted mechanisms that lead to the constitutive activation of this pathway in cancer: i) Alteration (mutations or amplification) within RTK (receptor tyrosine kinases, and ii) mutations within the major components of the PI3K/PKB pathway.

Influence of the RTK (Receptor tyrosine kinase):

Since membrane localization of PI3K is crucial for its activation and PIP3 production, [132] the membrane localisation of PI3K is commonly allied to RTK deregulation. The amplification or/and overexpression of RTKs such as ERB/EGFR family members, IFG1R, HER-2/neu, ERBB2 and EGFRVIII, activate PI3K/AKT in lung, breast, colon, ovarian and cervix cancer cells. [93-95]

Genetic variations in the PI3K pathways

A number of genetic perturbations exist within PI3K, PKB, and PTEN genes that contribute to the initiation and maintenance of transformation in various tumours (see Table 1.4). The activating hot spot mutations found in the PIK3CA gene are H1047R, E542K and E545K, which escalates its kinase activity. [133, 134] The mutations of p110α triggers constitutive activation of PI3K/AKT pro-survival cue, which has been found in gastric adenocarcinoma, breast, ovarian cancer, head and neck squamous cell carcinoma, and cervical cancer (Table 1.4). In addition to these mutations, PIK3CA is reportedly amplified in certain cancers (Table 1.4).

Table 1. 4: Recent results demonstrating the frequency of genetic variations within the PI3K/PKB pathway found in different tumour types. Adapted from Markman, et al. [135]

Generic Variation	Tumour Type	Frequency (%)
PIK3CA mutations	Breast	21-40
	Colorectal	13-32
	Glioblastoma	5-8%
	Endometrial	24-32
	Hepatocellular	6-36%
PIK3CA amplification	Cervix	69
	Gastric	36
	Lung (squamous)	60
	Head & Neck (H&N)	37
	Ovary	25
p85α mutation	Colorectal	<5
	Ovary	<5
PKB amplification	H&N	30
	Gastric	20
	Pancreas	20
	Ovary	12
PKB1 mutation	Breast	1.8-8
	Colorectal	6
	Ovary	2
PTEN mutation	Glioblastoma	17-44
	Endometrial	36-50
	Colorectal	7
	Prostate	12
	Breast	0-4
	Melanoma	7
PTEN LOH	Glioblastoma	54-74
	Endometrial	32-83
	Gastric	47
	Prostate	29
	Breast	39
	Melanoma	44-37

Along with PIK3CA amplifications, AKT is also found to be amplified in a large variety of tumors. Recently, an activating mutation within the PH domain (G49A/E17K) of AKT gene has been identified in a subset of breast, lung, ovarian and bladder cancers. This mutation at Lys17 in AKT-modifies its interactions with intracellular membrane by forming hydrogen

bonds with membrane phospholipids. This results in recruitment and activation of AKT to the membrane even in the absence of active PI3K.

PI3K/AKT pathway can be triggered perturbation in other components of PI3K/AKT cascade. Inactivation of PTEN-a regulatory protein in PI3K/AKT cascade- is associated with the advanced stages of cancer and metastasis tumors through either mutational inactivation or epigenetic downregulation. Mutations in PTEN gene are confined to its phosphatase domain and frequently found in non-small lung cell cancer and certain colorectal cancers, activation of PI3K/AKT pathway. Moreover, complete loss of PTEN expression has been found in many cancers, more prevalent in prostate cancer. The frequency of loss-of heterozygosity (LOH) in one of the allele of PTEN is more compared to its mutation in its genomic sequence. (Table 1.4). The attenuated PTEN activity leads to constitutive activation of the PI3K/AKTpathway through up-regulated PIP3 levels.

Regulation of class I PI3K gene expression (p110α)

p110α is a lipid kinase, encoded by PIK3CA gene, which shows a ubiquitously distributed in embryonic [136] and adult tissues.[137, 138] Recently, three different studies have characterised the regulators of PIK3CA promoter, where p110α expression is positively regulated by FOXO3a (forkhead box-O3a)[139] and NF-κB (nuclear factor-kappa B)[140] while p53 negatively regulate its expression.[141] The human genomic locus for PIK3CA, transcribe two transcript variants, through alternative splicing of one of two distinct 5' untranslated exons [exon -1a (80bp) or exon -1b (49bp)] onto the ATG-containing exon (defined as exon 1), with the untranslated exons positioned about 50 kb upstream of the translation start site. [139, 141] FOXO3a directly binds to FOXO3a-responsive elements approximately 792 and 225 bp 5' upstream of exon -1b and increments p110α expression.. [139] Given that the PI3K/-AKT cascade inhibits FOXO3a transcriptional activity (by sequestering it to cytoplasm), FOXO3a-PIK3CA promoter interaction has the potential of

negative feedback loop on regulation of its own gene expression. Induction of NF-κB through TNF-α (tumour necrosis factor alpha) triggers its binding to PIK3Ca promoter at approximately 700 bp 5' upstream of exon -1b, and augments PIK3CA mRNA expression in ovarian cancer cells. [140] Astanehe et al, demonstrates that PIK3CA promoter harbours four p53 response elements (RE) in 900bp of 5' exon -1a. p53 binding to these RE leads to transcriptional inhibition of PIK3CA. [141] Indeed, overexpression p53 decreases p110α protein levels and AKT phosphorylation, whereas suppression of p53 protein levels increases p110α mRNA and protein levels. These data corroborates with earlier reports of negative regulation of PIK3CA expression by p53.[142]

Many different stimuli and agonists control transcriptional activation of all three regulators of PIK3CA promoter, NF-κB, FOXO3a and p53. In many cancers, transcriptional activation of PIK3CA is a prevalent alteration along with its copy numbers amplification and/or mutational activation of p110α, which triggers concomitant activation its downstream signaling. [143, 144] In cervical, ovarian, and gastric carcinoma, increased PIK3CA gene copy number is associated with increment in PIK3CA transcript levels, its translation and overall kinase activity.[145, 146] Genetic analysis of high grade serous ovarian carcinoma (HGSOC), prevalent subtype of ovarian cancer, revealed 17-25% alteration in PI3K/AKT pathway in the form of PIK3CA amplification (18%), PTEN mutations (7%) and AKT amplification (3%). Other than these, genetic alterations in other components of PI3K/AKT signalling are negligible in HGSOC.[133] Yet therapy resistant ovarian cancer displays 50% escalated AKT activity.[147] The TCGA data for HGSOC provisional set (n=316) revealed a total of 9% cases associated with PIK3CA transcript upregulation without any change in the gene copy number. Such incidences indicate alteration in levels of specific regulators and subsequent promoter regulation in the cancer cells. Little is known about these mediators of upregulated

PIK3CA transcription and their role during acquirement of chemoresistance in ovarian carcinoma.

Interestingly, immunohistochemistry studies on ovarian cancer sections indicate that p110α levels in the cancer cells are the highest in the non-proliferating regions (as assessed by co-staining with the cell proliferation marker Ki-67), such as in the under-vascularised tumour areas. Interestingly, the proliferating tumor section (Ki-67 positive cells) expressed relatively low amounts of p110α. [140] Astanahe et al (2008) identified a novel PIK3CA promoter from ovarian surface epithelial cells (OSE) containing putative p53.[141] Conditional inactivation of p53 leads to increase in PIK3CA promoter activity and p110 α expression both at transcript and protein levels suggesting that p53 negatively regulates PI3KCA expression through direct binding to the promoter. This study corroborates with clinical observations of association of p53 mutations and PI3K gene amplification in ovarian carcinoma made by Kolasa et al (2009).[147] Inhibition of PI3K/AKT pathway often sensitizes the cancer cells to cisplatin.[148] Interestingly, cisplatin could up-regulate PIK3CA transcription in cisplatin-resistant OVCAR3 cells but not in sensitive cells [149] indicating presence of a differential regulation of PIK3CA promoter in resistant scenario. The molecular mechanism is yet to be deciphered.

In ovarian cancer, PIK3CA amplification has been established as a predictor of chemoresistance acquirement. PIK3CA is expressed in non-proliferating tumor cells in ovarian cancer and is directly upregulated by NF-κB [140]. Overexpression of AKT has been demonstrated in cisplatin resistant ovarian cancer cell lines, compared to the respective cisplatin sensitive cell lines [149-152]. Peng et al., 2010, showed that cisplatin treatment can activate PI3K-AKT pathway along with induction of apoptosis [130]. Many *in vitro* evidences suggest that PI3K activation is associated with decreased sensitivity to several different chemotherapeutic agents, including paclitaxel, doxorubicin and 5-fluorouracil. It

was demonstrated that ovarian cancer cells overexpressing constitutively active AKT or containing AKT gene amplification were highly resistant to paclitaxel as compared to cancer cells expressing low AKT levels. Constitutively active AKT inhibits the release of cytochrome C normally induced by paclitaxel thereby promoting apoptosis resistance [153, 154]. Hence, to understand the transcriptional regulation of PIK3CA promoter, we selected ovarian cancer as our model system.

1.7 Epithelial ovarian cancer (EOC) - The model:

Ovarian cancer is the leading cause of the death in gynaecological malignancy and it is the fifth most common cancer among women worldwide.[155, 156] The cause of ovarian cancer is unknown, however, older age, low parity, and a familial history of ovarian and breast cancer are some of the risk factors associated with ovarian cancer.[156, 157] More than 90% of ovarian cancers are epithelial in origin, and associated with poor survival (5-year overall survival of only 35-40%). This is due to the presence of advanced disease in most patients at initial presentation, and the development of drug resistance. Novel standards for reversal of drug resistance are urgently required to improve the outlook for this disease. [156, 157]

Classification of Ovarian Cancer:

Ovarian cancer is classified according to the cell type of origin into three main groups as epithelial ovarian cancer (EOC), sex cord-stromal tumors and germ cell tumors. [77, 158] More than 90% of ovarian cancers are epithelial in origin, and originated from cells surface epithelium of ovaries or. [156, 157, 159] Based on histopathological analysis, epithelial ovarian cancers (EOC) are further classified as benign, borderline/low malignant potential (LMP) or malignant, depending on the extent of cellular atypia and invasion into basement membrane. EOC are further sub-classified into four main subtypes as serous (60-70%), endometrioid (10-20%), mucinous (5%) and clear cell (5%). These subtypes differ drastically

at genetic alterations, gene expression profiles, IHC markers and their clinical response to chemotherapy and prognosis. [159, 160]

More recently, ovarian cancers have been classified into type I and type II tumors based on their molecular and clinical features. Type I tumors majorly cosnsits of low grade serous, low grade endometrioid, clear cell, mucinous and transitional carcinomas. Type II tumors comprise of high grade serous carcinoma, high grade endometrioid, undifferentiated carcinoma and malignant mixed mesodermal tumors. Type I tumors are less aggressive, lack mutations in p53 and BRCA1/2 genes, harbours activated RAS signaling cascade and areahve high genomic (chromosomal) stability. In contrast, Type II tumors harbours a high frequency of p53 mutation, dysfunctional BRCA1/2 DNA repair cascade, negligible RAS pathway activation with, high level of genomic instability with widespread DNA copy number changes. [159, 160]

Diagnosis of ovarian cancer:

Most patients with EOC displays the symptoms of very similar to other gynaecological and gastrointestinal problems and therefore often remains asymptamatic in nature. These symptoms include swelling of abdomen, alteration of bowel or bladder function, gas and bloating. Diagnosis is commonly performed through transvaginal ultrasound (US) and level of CA125 based on initial clinical suspicion of malignant growth. Other candidate secretory tumor marker includes glycoprotein human epididymis protein 4 (HE4), CEA, CA72-4, hCG, inhibin B and anti-Mullerian hormone (AMH).[161, 162] The combination of tumor marker CA125 and US imaging, are most preferred diagnostic tools for provisional clinical diagnosis of ovarian carcinima, using pre-operative algorithms such as the RMI (Risk of Malignancy Index). Other clinical imaging modalities such as computed tomography (CT) of the chest abdomen and pelvis, magnetic resonance imaging (MRI) and positron emission tomographic imaging (PET) are utilised for pre-operative tumor staging. [162, 163]

Treatment options:

The standard management of EOC comprises combination of debulking surgery along with either of neo-adjuvant or adjuvant combination chemotherapy.[156, 157, 164]

Surgery:

In EOC patients, debulking surgery is performed to achieve complete macroscopic cytoreduction of tumor tissue. Other than this goal, debulking surgery is also performed for patients with suspected ovarian cancer for tumor biopsy for histological diagnosis and staging of cancer tissue. [165, 166]

Chemotherapy

Over past few decades, platinum-based therapeutics persisted as the key first-line chemotherapy for management of ovarian cancer. The platinum-based compounds, cisplatin, or carboplatin, are the most effective single agents for treatment of ovarian cancer. A large clinical trial, GOG 111, compared efficacy of cisplatin in combination with cyclophosphamide or paclitaxel, which revealed survival advantage of the platinum-taxane arm. Ever since, combination of platinum-taxane has become standard first-line chemotherapy for ovarian cancer. [167] Another, less toxic platinum based compound-carboplatin, is introduced in 1980s which is as effective as and has been shown, in three randomised trials in combination with paclitaxel, to be as effective as combination of cisplatin-paclitaxel, but exert significantly less toxicity. Due to which, carboplatin has replaced cisplatin in most of the treatment centres. [168-170] First line chemotherapy with carboplatin (AUC 5-6) and paclitaxel (175 mg/m2) is usually administered every three weeks, for 6 successive cycles. Although the initial response to combination of platinum-taxane is excellent, with more than 80% responders with 40-60% complete responses, majority of these patients relapse within 18 months.[164, 171, 172] Tumors, which relapse with a PFI more than 12 months, are categorised as platinum sensitive tumors and have 40%

response rates to platinum-based therapy. Tumors which relapse between a span of 6 and 12 months are categorised as partial-sensitive tumors (platinum response rates upto 20-30%) and those which relapse within 6 months PFI are catogorised as platinum-resistant (response rate less than 10%).[164, 173] Chemorefractory tumors, are those tumors which do not respond to first-line therapy since the beginning of chemotherapy, as they are intrinsically resistant. In platinum-sensitive relapse, platinum-based combination therapy is used as therapeutic regiment. This is established based on combined outcome of several clinical trials, which have shown a survival benefit for combinatorial approach over single agent paclitaxel (single agent), carboplatin chemotherapy, gemcitabine, and liposomal doxorubicin.[174-178] With recurrent relapse, response rates to platinum-based combined therapy decreases dramatically and ultimately, all patients develop resistance agsinst platinum-based therapy.[164] In patients with platinum-resistant disease, liposomal doxorubicin and paclitaxel are most commonly used. Other agents used include topoisomerase inhibitors such as topotecan. However, only small numbers of platinum-resistant tumors respond to these agents, with relatively short response durations.[179-182]

Drug Resistance in Ovarian Cancer:

Even after diagnosis in advance stages, most of the EOC patients are primarily chemosensitive (platinum-sensitive), but they eventually acquire resistance to therapy. [156, 183] Therefore, understanding the molecular and cellular mechanism/s of drug resistance and development of novel therapeutic strategies for management of drug resistance are, therefore, crucial for improving EOC outcomes. Recent evidence pinpoints several molecular and cellular mechanism of chemo-resistance, which includes cancer cell-specific genomic alterations, and/or cellular heterogeneity, pharmacokinetic properties of drugs and tumor micro-environment-derived effects.[164] [184-186] Alterations in intracellular concentration of due to changes in expression level of cell membrane transport proteins which are involved

in drug influx and efflux has been shown to associate with chemoresistance *in vitro*.[187] Enhanced repair abilities for drug-induced DNA damage can also result in resistance.[188] Drug inactivation through cellular detoxification within a cell and alteration in interaction between drug and its target molecule are some of the potential mechanisms of drug resistance.[189-191] Recently, the role of the specific extracellular matrix (ECM) proteins and tumor microenvironment has been explored as potential targets for reversal of drug resistance. [192]

The efficacy of chemotherapeutics is highly dependent upon the their ability to propel apoptosis in cancer cell. It is now widely accepted that the decision to 'live or die' under treatment of a given drug is a reflection of the overall apoptotic-equilibrium in cellular ambiance. For example, cisplatin has been shown to upregulate and activate several pro-apoptotic factors such as p53, Fas, Bim, and Bax in a various cell types. [5–7] However, it also activates specific cell survival factors such as XIAP and AKT [8]. Hence, chemoresistance may represent an overall disparity between these two phenomena. In ovarian cancer, activation of PI3K/AKT has been demonstrated in cisplatin resistant ovarian cancer cell lines, compared to the respective cisplatin sensitive cell lines [149-152]. Peng et al., 2010, showed that cisplatin treatment can activate PI3K-AKT pathway along with induction of apoptosis [130]. Many *in vitro* evidences suggest that PI3K activation is associated with decreased sensitivity to several different chemotherapeutic agents, including paclitaxel, doxorubicin and 5-fluorouracil.

Oncogenic mutations in p53 confers chemoresistance through enhancing DNA repair, elevating expression of ABC transporters, attenuating cell death by activating anti-apoptotic pathways and inhibition of pro-apoptotic proteins; modulating expression of metabolic scavengers; and elevating expression of detoxifying enzymes [193]. The X-linked inhibitor of apoptosis (XIAP) levels are elevated in many cancer cell lines, and several reports have

shown that suppression of XIAP protein levels can sensitize cancer cells to chemotherapeutic drugs [194]. For both cisplatin and paclitaxel, BCl2 has shown to affect drug sensitivity *in vitro*. The role of BCl2, IAP, survivin in mediating drug resistance is also supported by clinical studies. However, in some studies, contrary to expectation, overexpression of BCl2 has been found to be a good prognostic marker in EOCs [195, 196]. It is also important to consider that cytotoxic agents are often more effective against proliferating cells. In 2010, Cooke et al provided confirmation through genomic analysis of high-grade serous carcinomas cell lines revealing pre-existing intra-tumour genetic heterogeneity, which attributes towards resistant relapse disease.[197] Currently, studies have revealed the existence of subset of rare, quiescent tumor population with intrinsic resistant to anti-cancer drugs called as cancer stem cells (CSCs), which can attribute to phenomena of chemoresistance.[198]

1.8 Cancer Stem cells:

Cancer stem cells (CSC) are the intrinsically resistant, small fraction of heterogeneous tumor population that is responsible for initiation of disease and relapses. Such subpopulations have been described for several cancer types, including ovarian, breast, lung and colon cancer. [184-186, 199-202] John Dick and colleagues, isolated a rare but highly tumorigenic cell-population from acute myeloid leukemia (AML) that could reinitiate the disease in immunocompromised mice, also termed as CSCs.[199, 203] In the majority of cancer types where CSCs have been recognised, the origin of this cell subpopulation is not necessarily lineage of a normal stem cell, ratherin most circumstances their origin is unknown.[204] Similar to normal stem cells, CSCs possess ability to either self-renew or differentiated to non-CSC tumor population.[205] These non-CSC, differentiated cells are highly proliferative in nature and rapidly forms the tumor burden. It is widely assumed that targeting CSC

component of tumor heterogenous population has great therapeutic potential, particularly in drug-resistant disease. It is generally agreed that CSCs possessfollowing characteristics:

• Increased tumorigenic potenitial when injected in xenograft models, where even with very few cells CSCs can establish tumors compared to whole/non-CSCs/ population of same origin

• Infinite self-renewal ability, i.e. CSCs can divide numerous times while still maintaining an undifferentiated state

• Pluripotency in terms of giving rise to new CSCs and to differentiated cancer cells

• Spontaneous formation of spheres in serum-free stem cell medium (SCM) when cultured *in vitro*

• Resistance to chemo- and radiotherapy

1.9 Cancer Stem cells in EOC:

Most common strategy to identify cancer stem cells is based on expression of cell surface marker. Though several CSC markers are proposed for ovarian cancer, no single marker clearly identifies ovarian CSCs and therefore combinations of markers are used to profiles CSC. Other than surface markers, CSC's has been identified based on their functional porperties , such as side population (SP) enrichment to sort out cells expressing high levels of drug transporters, and the ALDH (ALDEFLUOR) assay that detects activity of aldehyde dehydrogenase family (ALDH) enzyme. [201, 202] Commonly used markers and suggested CSC profiles are discussed below.

1.10 Cell surface markers for CSC:

In ovarian cancer, cancer stem cells are identified based on cell surface markers such as CD133, CD117, CD44, and CD24 as well as functional properties such as side population (SP) or aldehyde dehydrogenase (ALDH) activity. [199-202, 206]

CD133 (Prominin-1) is a transmembrane glycoprotein whose function is not well understood..[207] It is a commonly used surface marker for identification of ovarian cancer stem cells and increase in its expression is found to be associated with poor survival of EOC.[208-210] However, CD133 has been questioned as a CSC marker majorly due to the unidentified roles of its splice variants and various glycosylation forms, which cause inconsistent detection of CSC.[211-214]

CD44, is a hyaluronate receptor which is involved in cell adhesion, cell-cell interactions and cell migration. It is most frequently used surface marker for identification of both normal stem cells and cancer stem cells.[215] In EOC tumors, higher CD44 expression is shown to be associated with highly invasive and resistant CSC's and which correlates with shorter PFS. However, contradictory studies suggest that CD44+ cells are less aggressive and may be associated with good prognosis. [216-218]

CD117 (c-Kit) is a tyrosine kinase receptor that is activated upon its binding to stem cell factor (SCF) and initiates signal transduction through several pathways, including PI3K/AKT and Ras/ERK.[219, 220] Activation of c-KIT receptor mediates cell survival, proliferation, and migration and is frequently altered in various cancers. In ovarian cancer, CD117+ CSC shows higher self-renewal ability, high tumorigenic potential, and chemoresistance.[221-223]

Another cell adhesion molecule CD24 is another debatable cancer stem cell marker. In breast cancer CSCs, CD24 negative (CD44+/CD24) cells are defined as CSC while pancreatic CSCs are express CD44+/CD24+ surface markers, implying a tumor-tissue specific role for CD24.[224-226] Gao et al (2010) showed that in ovarian cancer, CD24+ cells are resistant

to chemotherapy and has ability to self-renewal. Morever, only CD24+ cells have displayed tumorogenic potential, but not CD24- cells, when injected into immuno-compromised mice.[227]

1.11 Intracellular markers and CSC profiles:

Aldehyde dehydrogenase (ALDH) enzymes are crucial player in oxidation of aldehydes to carboxylic acids and hence involved in detoxification of many drug intermediates. Classically, enzymatic activity of ALDH is measured though ALDEFLUOR assay which is most frequently assay for detection of ALDH+ normal and cancer stem cells.[228, 229] Higher ALDH activity in EOC tumors is associated with chemoresistance and tumorogenic potential. [230-232]

Several other CSC markers, individually or in combination, have been suggested to define CSCs in epithelial ovarian cancer cell lines and tissue, based on their tumorigenic potential, sphere forming ability, resistance towards chemotherapy and, in some cases, poor clinical outcome. These profiles include CD44+/CD24+/EpCAM+, CD44+/CD24-, CD44+/MyD88+, CD44+/CD117+ and ALDH1A1+/CD133+, which define potential CSC populations in EOC.[233-236]

Rationale & Hypothesis:

Constitutively active AKT has been found in chemoresistant lung, glioma and ovarian cancer cell lines, compared to their sensitive parental counterparts.[237-239] Peng et al., 2010, showed that cisplatin treatment can activate PI3K-AKT pathway along with induction of apoptosis [130]. Many *in vitro* evidences suggest that PI3K activation is associated with decreased sensitivity to several different chemotherapeutic agents, including paclitaxel, doxorubicin and 5-fluorouracil. Activation of PI3K/AKT has been demonstrated in cisplatin resistant ovarian cancer cell lines, compared to the respective cisplatin sensitive cell lines [149-152]. Amplification and/or overexpression of PIK3CA are one the factors that contributed towards activation of PI3K/AKT in chemoresistant ovarian cancer.[140, 147]. Lee et al, (2008) observed cisplatin escalated PIK3CA expression in OVCAR-3/CDDP cells, which inhibit BAX translocation via activated PI3K/AKT conforming platinum resistance.[149] However, the molecular mechanism of this effect of cisplatin remained unexplored. With the help of our isogenic A2780 chemoresistant model, we also observed that drug mediated repression of PIK3CA promoter activity gradually diminished with increased resistance towards cisplatin.[240] Interestingly, cisplatin induced PIK3CA expression in resistant A2780-CisR cells along with decreased p53 stabilization and increased phosphorylation of AKT. However, the molecular mechanism behind this contrasting effect of cisplatin between sensitive and acquired resistant cells and biological consequence was not examined. Also, whether and how cisplatin induced PI3CKA expression aid in maintenance of cancer stem cells has not been investigated.

In this study, we hypothesize that differential regulation of PIK3CA promoter mediated by differential binding of p53 occurs in chemoresistant cells leading to loss of PIK3CA attenuation and promoting survival mechanism. It is also possible that other unknown

positive regulators control the PIK3CA promoter activity in chemoresistant cells and thereby assist in maintenance of resistant scenario in ovarian cancer cells.

Based on the above facts we would like to address the following aim

Aim & Objectives:

To identify the potential regulators playing role in PIK3CA promoter modulation in chemoresistant ovarian cancer cells.

To achieve the above mentioned aim we designed our study by addressing the following key questions

Key questions:

- Out of four p53 binding sites, which is/are the most crucial site(s) in PIK3CA promoter modulation?

- How does p53 interact with PIK3CA promoter during acquired chemoresistance?

- Which are the other regulators of PIK3CA promoter in chemoresistant ovarian cancer cells?

Specific objectives for this study are -

Objective 1:

To study p53 mediated modulation of PIK3CA promoter in cisplatin chemoresistant ovarian cancer cells as follows:

    a. To study the dynamics of p53 binding to PIK3CA promoter in cisplatin resistant ovarian cancer cells

b. To identify p53 binding site/s that contribute/s major role in PIK3CA promoter regulation by reporter gene assay

c. To check p53 binding toPIK3CA promoter after cisplatin treatment by DNA binding assay

Objective 2:

To identify novel interacting partners for PIK3CA promoter in acquired chemoresistance

Chapter 2:

To study p53 mediated modulation of PIK3CA promoter in cisplatin chemoresistant ovarian cancer cells

Chapter 2: p53 mediated PIK3CA promoter modulation

To study p53 mediated modulation of PIK3CA promoter in cisplatin chemoresistant ovarian cancer cells

2.1 Introduction:

Cancer is a major killer and a perplexing malady for the healthcare worldwide. Traditional treatments for malignancies include surgery, radiation therapy, and chemotherapy.[22, 155] However, the effect of surgery and radiotherapy is only local and they cannot cure spread of advanced stage. Chemotherapy though is systemic, development of primary and secondary resistance limits its efficacy.[23, 24] Despite the promising potential of therapeutic intervention, some patients are intrinsically resistant to the therapy (primary or *de novo* resistance) while others respond initially to therapy, but ultimately acquire resistance (secondary resistance). [54-57] The mechanisms mediating chemoresistance and tactics to overcome them have been thoroughly studied, however, they are not yet fully understood. With increasing advancement in genome-wide association studies, it has become increasingly possible to relate acquirement of resistance to genetic alterations. Known alterations instigating therapy resistance include gene amplifications, activating mutations in kinase domain, gain-of function, and/or loss-of function mutations in regulatory proteins, which prime constant activation of downstream signalling cues, and cross-activation of parallel intracellular pathways.[58, 241-245] Understanding the molecular basis for therapeutic resistance should facilitate the identification of actionable targets and development of new paradigms for cancer treatment.

Chemotherapeutic agents majorly target actively proliferating cells. Typically, chemotherapy is used in combination with other treatment strategies such as surgery in local cancers. In

some cancers, like testicular cancer[246] and lymphoma[247], chemotherapy is the most successful regimen, while, in many recurrent and metastatic cancer settings, these chemotherapeutics are still ineffective.[156, 248, 249] Molecular changes in tumor cell, as they respond towards a chemotherapeutic drug determine their fate. The effect of chemotherapeutic agents is based on a variety of molecular mechanisms such as inhibition of enzymes involved in DNA and RNA synthesis, DNA/RNA damage, inhibition of mitosis through affecting the microtubule or cellular membranes damage.[183, 250-252] Platinum based compound, cisplatin (cis-diamminedichloro-platinum) has a major therapeutic effect on several solid neoplasm including testicular[253], ovarian[254], bladder[255], head and neck[256], breast[257], oesophageal[258], small cell lung cancer (SCLC)[259]. Other than the classical mode of action by DNA damage, oxidative and endoplamic stress followed by apoptosis induction, cisplatin modulate several signalling cascades driven by c-ABL, p53, MAPK/JNK/ERK, PI3K/AKT, NF-κB, focal adhesion kinases, and WNT.[58, 183, 260] Cisplatin-resistantance, a multifactorial phenomenon, is contributed by several mechanisms, including alterations that affect the intracellular uptake and detoxification of cisplatin and/or altered signaling pathways that ultimately influence the execution of the apoptotic program [10]. The induction and survival of cancer cells are highly dependent on specific aberrations in particular genes and/or proteins, which provide a favourable environment to maintain the diseased state. As a result, most cancer cells develop a dependency on particular oncogenic cue. Though platinum resistant cells are inert to therapy induced apoptosis, these cells respond to cisplatin by decreasing proliferation, protein synthesis and increased survival. Activation of signaling cascades either phosphorylates downstream targets or escalates their expression. Till now, a number of such molecular players like ABCG2, ATP7A, ATP7B (drug transport), glutathione, metalloproteases (detoxification of drug), HMGb1, RAG1, RAG2 (improved DNA repair), DNA polymerase η (DNA damage tolerance) and XIAP,

cFLIP, survivin, BCL2 family protein (anti-apoptotic) are known to be deregulated in platinum resistant ovarian cancer.[58] Although number of molecular interactions underlies the etiology of chemoresistance, these interactions are manipulated through signaling pathways. In many cancers, a key survival pathway –the phosphatidylinositol 3-kinase (PI3K) pathway can be regulated at one or several points and regulate above mentioned molecules.[115, 116, 261] The PI3K/AKT signalling pathway reportedly contributes to the progression of a variety of cancers.[115, 116, 148] This crucial cell survival pathway is also activated during course of resistance against various therapeutics such as gefitinib, letrozole, doxorubicin, paclitaxel, 5-flurouracil, etoposide and camptothecin and platinum based drugs, which often lead to failure in therapy outcome. [148] Activated AKT regulates cell growth and survival, which contributes to tumor growth, metastatic competence, and therapy resistance. Inhibition of PI3K/AKT cascade has a catastrophic effect on tumor growth, metastasis, and chemoresistance. In addition, activation of Akt can be induced by cisplatin in several cancer cell lines, including ovarian, breast, glioma, and pancreatic cancer cells. Constitutively active Akt has also been found in cisplatin-selected chemoresistant lung, glioma, and ovarian cancer cell lines, compared with their sensitive parental counterparts. [237-239]

Transmembrane receptor tyrosine kinases (RTKs) such as FGFR, EGFR and IGFR are stimulated through direct binding of mitogens present in the extracellular environment.[113, 114, 117, 262] RTKs, upon ligand binding, phosphorylate intracellular tyrosine and recruit Src homology (SH2) domain-containing molecules.[113, 114] Such molecules include the regulatory domains of class IA PI3Ks which recruit PI3Ks to the membrane and initiates PI3K/AKT/mTOR signaling. The PI3K/AKT signaling pathway is important for cell survival, and plays a critical role in a number of tumor-associated cellular processes, including cell

growth, and cell cycle progression[116]. Genomic alterations in class 1A Phosphoinositide 3-kinases (PIK3CA) such as amplification or mutation in kinase domain escalates its activity leading to activation of AKT. This activated AKT consecutively up-regulates cell survival, proliferation, and growth signalling and suppress apoptosis through phosphorylating multiple substrates like apoptosis-related proteins (BAD and FKHR), transcription factor activation (NF-κB, FOXO family, p53 and β-catenin) and the mTOR complex components (PRAS40 and mTOR). [113, 263] Many crucial factors such as BCL2, ribosomal protein S6, β-catenin and other transcriptional factors, which regulate apoptosis evasion, cell survival, proliferation, and cell cycle progression, are controlled under this central AKT node.[155] Phosphatidylinositol-4,5-bisphosphate 3-kinase catalytic subunit alpha (PIK3CA) gene codes for P110α protein which phosphorylates AKT and is frequently altered in breast, colon, lung and ovarian cancer.[115, 116, 148, 264] PI3K/AKT cascade is found to be upregulated in 50% of cancer cases due to gain-in function mutation (~ 23%) and amplification (~11%) in PIK3CA gene, loss of function mutations in PTEN (~11%) gene and amplification in AKT gene (~20%).[264] Gain-in-function mutation and amplification in PIK3CA gene alone escalate downstream PI3K-AKT-mTOR pathway within cancer cells.[116, 265] In ovarian cancer, mutations of the PIK3CA gene are rare, except for the endometrioid and clear cell types. High-grade serous OC is associated with 17-35% of PIK3CA copy number amplification.[265-267] The TCGA data for HGSOC provisional set (n=316) revealed a total of 9% cases associated with PIK3CA transcript upregulation without any changes in the gene copy numbers. (TCGA curated dataset from http://www.cbioportal.org/, march 2017) Such incidences indicate alteration in levels of specific regulators and subsequent promoter regulation in the cancer cells. Little is known about these mediators of upregulated PIK3CA transcription and their role during acquirement of chemoresistance in ovarian carcinoma.

PIK3CA is transcriptionally activated by FOXO3A [139], NF-κB [140] and YB-1 [268] proteins. Recent study using temperature sensitive SV40 mutant demonstrated that p53 represses *PIK3CA* transcription through direct binding to its promoter in ovarian surface epithelial cells [141]. Recently, our lab has shown that cisplatin and paclitaxel negatively modulate this PIK3CA promoter in ovarian cancer cells as well as in tumor xenografts using non-invasive optical imaging. The repressing activities of these drugs were probably mediated via p53 and mutation at three of the four p53 binding sites increased the promoter activity and decreased the effect of the drugs. However, mutations at all the four binding sites surprisingly decreased the promoter activity indicating a complex regulation of the PIK3CA promoter. A p53 deficient cell line (SKOV3), did not show the promoter attenuation by these drugs in *in vitro* as well as in *in vivo* tumor xenografts[269].

Tumor suppressor protein-p53 serves as a 'molecular hub' of complex cellular response towards stress signals.[270, 271] By nature p53 is a short-lived transcription factor, which coordinates between growth arrest, DNA-repair and/or apoptosis by differential transactivation and repression of genes under genotoxic stress.[272] Once 'activated', p53 plays a decisive role to drive cell arrest or apoptosis by either transactivating P21, GADD45A and repressing CYCLINB1, STMN1 and SHP-1 (growth arrest) or induces PUMA, BAX, AIP and represses BCL2, SGK1, PIK3CA, IGF1R (programmed cell death). [273, 274] As a mediator of these crucial functions, p53 is often referred as 'guardian of the genome'. The switching between growth arrest and apoptosis via p53 is controlled by the magnitude of protein stabilization, sequence specific DNA binding and posttranslational modifications (PTMs). [274-276] Various PTM's of p53 dictate its response towards diverse cellular signals and determine physiological function. P53 undergoes diverse posttranslational modifications such as ubiquitylation, phosphorylation, acetylation, sumoylation, methylation, and neddylation. [277] Acetylation and phosphorylation are the key PTM's which escalate p53-

binding to selective target promoters like P21 and MDM2 to initiate transcription. Phosphorylation of T18, S20 and/or S37 blocks Mdm2 association, with multisite phosphorylation more effective than isolated phosphorylation events.[278] Acetylation of C-terminal lysine residue (K370, K372, K373, K381, K382) by p300 and CBP (CREB-binding protein) promotes an open conformation of p53 and occlude the DNA binding domain, thereby enhancing p53 transcriptional activity.[279, 280] Lysine acetylation in the C-terminal regulatory domain affects interaction of p53 withits other interacting proteins.[281] In addition, phosphorylation at serine 46 is critical for induction of apoptosis related genes transcription, which is not required for growth arrest.[282, 283]

Stress condition like DNA damage induces p53 phosphorylation at various serine and threonine residue through kinases. ATM (ataxia telangiectasia mutated), ATR (ataxia telangiectasia and Rad3 related), and DNA-PK (DNA-dependent protein kinase) kinases phosphorylates S15 [284-287] followed by phosphorylation at S20 via both the Chk1 and Chk2 kinases.[288, 289] S37 is targeted by ATR, DNA-PK, and Chk2 (checkpoint kinase 2), whereas Chk1 and Chk2 target phosphorylation of p53 at T387 (Chk1), T18 and S366 (Chk2) and 4 other residues (S313, S314, T377, S378) in the C-terminus by both kinases.[281, 290, 291] Other kinases traditionally recognized for their roles in cell cycle progression or gene transcription, such as CAK (cyclin-dependent kinase activating kinase) or HIPK2 (homeodomain interacting protein kinase 2), can phosphorylate p53 at S33 or S46, respectively.[292, 293] These PTM's escalate binding of p53 to selective target promoters like P21 and MDM2, which is sufficient to induce their expression. HIPK2 and DYRK2, phosphorylates p53 in a context dependent manner at S46, which leads to transcriptional induction of apoptosis related genes.[294] Trichostatin A, cholera toxin B subunit and SIRT inhibitors induce p53 acetylation which governs sequence specific DNA binding.[280] However, acetylation status of p53 post cisplatin treatment is yet not investigated.

Deregulation in p53 PTM's are often associated with tumorigenesis and therapy resistance, which currently is an active area of research in cancer biology. [277] Ultra-Violet (UV) radiation induced phosphorylation at S392 residue of p53 is known to promote specific DNA binding activity through the stabilization of the p53 tetramer.[295] A Knock-in mouse model bearing a S389A (corresponds to the S392 residue of human p53) mutation displayed normal p53 stability but an increased predisposition to UV-induced skin cancer as well as altered expression of p53 target genes compared to wild-type mice. This supports a physiological role for S392 phosphorylation in the tumor suppressive responses of p53 to UV.[296-298] Mice bearing S15A and S20A phospho-deficient mutations exhibit spontaneous tumor formation.[297] Apoptosis associated p53-S46 phosphorylation has recently attracted much attention. S46 phosphorylation is not only escalates apoptotic related genes (AIP, NOXA, PUMA) but also represses survival associated genes (IGF1R, EGFR, AKT).[282, 283] Indeed, the resistance to induction of apoptosis in a human oral squamous cell carcinoma cell line HSC-3 upon p53 overexpression is attributed to deficiency in S46 phosphorylation, and the introduction of the exogenous phospho-mimic p53S46D (aspartic acid) mutant enhanced transcription of the pro-apoptotic target Noxa and restored apoptosis in HSC-3 cells.[299]

In HGSOC, p53 mutations in the form of missense mutation, non-sense, INDEL and frameshift mutations are the most common genetic change, causing complex effects on its transcriptional activity.[300-302] These p53 missense mutations are clustered to the DNA-binding domain, which leads not only to the loss of wild-type function (loss-of function, LOF mutations) but also gain of novel oncogenic functions (gain-of function, GOF mutations) based on its transcriptional activity.[303] LOF, can be either loss of p53 protein expression, due to insertions and deletions (causing frame shift) and splice mutations (cause major changes in the protein structure), or nonsense mutations that abruptly terminate translation or missense mutations which result in complete or partial loss of WT p53 function.[304, 305]

Partial LOF mutations such as substitution of arginine to proline at codon 175 (R175P) retain some WT p53 function, but lose other functions, hence, are more difficult to judge the overall consequence. Cells with R175P p53 mutation are capable of inducing cell cycle arrest but fail to activate apoptosis.[306] The 'hot-spot' p53 mutations (R248, R273, R175, G245, R249 and R282) are associated with low-to- moderate transcriptional activation of wild type-p53 target genes such as APAF1, P21, MDM2, GADD45A. At the same time, few of them possess gain-of function activity to increase the expression of the various oncogenes like ALDH2, BCL6, PIK3CA, Vimentin.[307-309] Though, majority of these hot-spot mutations exert gain-of-function properties, degree of their functionality vary within and between the amino acid residues to which they substitute. For instance, substitution of R248 to 248Q exhibits higher invasive properties compared to R248W in lung cancer cells.[310] Similarly, substitution of Arginine to Histidine (R273H) and Cysteine (R273C) impart more aggressive phenomenon compared to Glycine (R273G).[311] Chang et al, 2001, demonstrated that except R273H, other p53 mutants V143A, V173L, H179Q, and N247I confer enhanced sensitivity towards cisplatin and doxorubicin .[312] Though, posttranslational modifications of p53 can alter its sequence-specific transcriptional activity, very little has been studied on PTM's of mutated p53. Matsumoto et al, 2006 demonstrated that hyper-phosphorylation of Serine 392 and moderate levels of Serine 15 phosphorylation occur in unstressed cells.[295] Serine 15 phosphorylation confers the decoupling of mutant p53 from MDM2 due to which mutant p53 escapes degradation cycle. However, it is currently unknown how PTM's of missense p53 mutations influence its transcriptional activity.

Molecular imaging provides a platform to monitor treatment response accurately and noninvasively in live animals.[313] It exploits specific molecular probes as well as intrinsic tissue characteristics as a source of imaging contrast, which can be used to characterize and quantify biological processes. Molecular imaging modalities include optical imaging

(bioluminescence imaging (BLI) and fluorescence imaging), magnetic resonance imaging (MRI), ultrasound imaging, positron emission tomography (PET), single-photon emission computerized tomography (SPECT), and computed tomography (CT).[313, 314] It possesses several advantages over conventional biochemical assays, especially for research in animal models. Molecular imaging can be performed repetitively, non-invasively, and in a relatively short time in the same live animal.[314, 315] Therefore, it can reduce the number of animals required for research, which reduces cost while retaining the statistical power for longitudinal studies. Furthermore, molecular imaging can provide detailed spatial and temporal information of biological events in living animals, which sometimes is overlooked in studies with end-point assays. Bioluminescence is based on the luciferin-luciferase enzymatic reaction, where photons in visible light spectrum (bioluminescence) are generated as a by-product.[315] The luciferase-based system has long been utilized to reveal cell tracking, gene expression patterns and biological activities of protein in live cells or animals.[313, 314]

In this present study, we aim to understand the mechanism of p53 driven PIK3CA promoter regulation in response to cisplatin treatment for cisplatin sensitive cells and how this interaction is deregulated in resistant scenario using both *in vitro* as well as *in vivo* models. In addition, we aim to comprehend association of certain critical PTM's (phosphorylation and acetylation) with a few clinically associated p53 mutations and its impact on PIK3CA promoter modulation.

2.2 Materials and methods:

Plasmid constructs: Following are the plasmids used in this study-

The PIK3CA sensor: This consists of 934bp PIK3CA promoter driving *firefly-luciferase-2-tandem-dimer tomato* bifusion reporter (PIK3CA-*fl2-tdt*) in pcDNA 3.1 (+) backbone.[269] The bifusion reporter *fl2-tdt* comprises of a fusion reporter competent for both bioluminescence and fluorescence imaging studies. *Firefly luciferase-2* (*fl2*) is a codon-optimized version of bioluminescence reporter obtained from american firefly (*Photinus pyralis*) and *tandem dimer tomato* or (*tdt*) is a mutant red fluorescent proteins with 6 times higher photon efficiency compare to *egfp*.

CMV driven-*fl2-tdt*: This consists of CMV promoter driven *firefly-luciferase-2-tandem-dimer tomato* bifusion reporter in pcDNA 3.1 (+) backbone. This construct was used as a normalization vector while estimating promoter activity with *renilla luciferase* transient transfection experiments.

Modified pcDNA3.1(+)-CMV-β-galactosidase: Parent vector procured from clontech (cat# 631719) was cloned into pcDNA 3.1 (+) vector backbone and used as a normalisation vector.

SN3-p53 (pCMV-Neo-Bam p53 wt): This plasmid was procured from Addgene (plasmid # 16434) which expresses wild type p53 cDNA in mammalian system. This construct was used for overexpression wt p53 in cell lines.

Modified p53-nanoluc fusion reporter: The original vector p53NanoLuc® Fusion (Promega) was cloned in pcDNA 3.1 (+)-puromycin for generation of dual stable clone. A2780- stably expressing PIK3CA sensor (Selected with neomycin) (APFT) cells expressing p53-nanoluc construct were selected by puromycin selection.[269] This plasmid expresses fusion protein consisting of p53-cDNA fused with luciferase reporter -nanoluc.

Generation of PIK3CA single site mutant and deletion construct library:

A. Construction of PIK3CA-*hrl-egfp* construct:

Bifusion reporter from PIK3CA sensor (PIK3CA-*fl2-tdt*) was replaced with *hrl-egfp* (humanised renilla luciferase-enhanced green fluorescence protein) for studying PIK3CA promoter activity in APFT chemoresistant model. *fl2-tdt* bifusion cassette was replaced by *hrl-egfp* with NheI and BamHI restriction enzyme using standard cloning techniques. Figure 2.1 represents cloning steps. All these constructs were confirmed with restriction digestion and sequencing.

Figure 2. 1: Cloning strategy for the construction of the PIK3CA-hrl-egfp sensor.

A. Schematics of PIK3CA bifusion reporter construct. hrluc-egfp bifusion reporter was cloned into PIK3CA sensor with NheI and BamHI restriction enzyme. B. Agarose gel image of restriction digestion obtained from both the constructs, PIK3CA-fl2-tdt and CMV-hrl-egfp,

when digested with NheI and BamHI. C. Schematic map of expected clone (PIK3CA- hrl-egfp) representing unique restrictions sites of enzymes within reporter cassette and position of primers used for colony PCR. D&E. Positive clones were selected with colony PCR using two different primer sets (sequence described in Appendix B), first for hrluc-egfp (set 1, fig.1 D) then second for PIK3CA promoter (set 2, fig.1.E). F. Finally all clones confirmed with restriction digestion (either EcoRI or double digestion with NheI+BamHI) and sequencing.

PCR condition: colony PCR
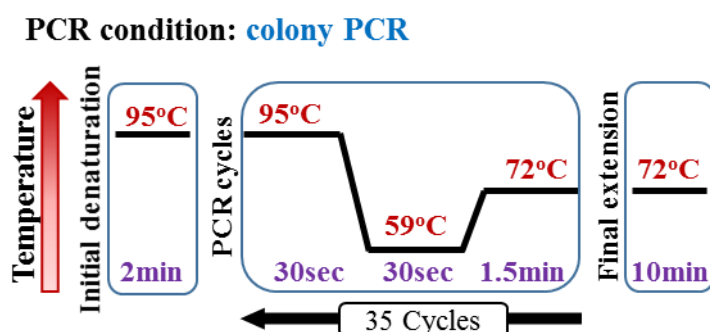
B. Construction of single site mutant constructs:

Standard SDM protocol was used to generate the mutations at the p53-response element in the PIK3CA promoter, modified from [269]. (Figure 2.2) A detailed protocol for the SDM is given in the Appendix A.3.5 and details of primers are given in Appendix C. All these constructs were confirmed with restriction digestion and sequencing. These construct were designated as S1-S4-PIK3CA.
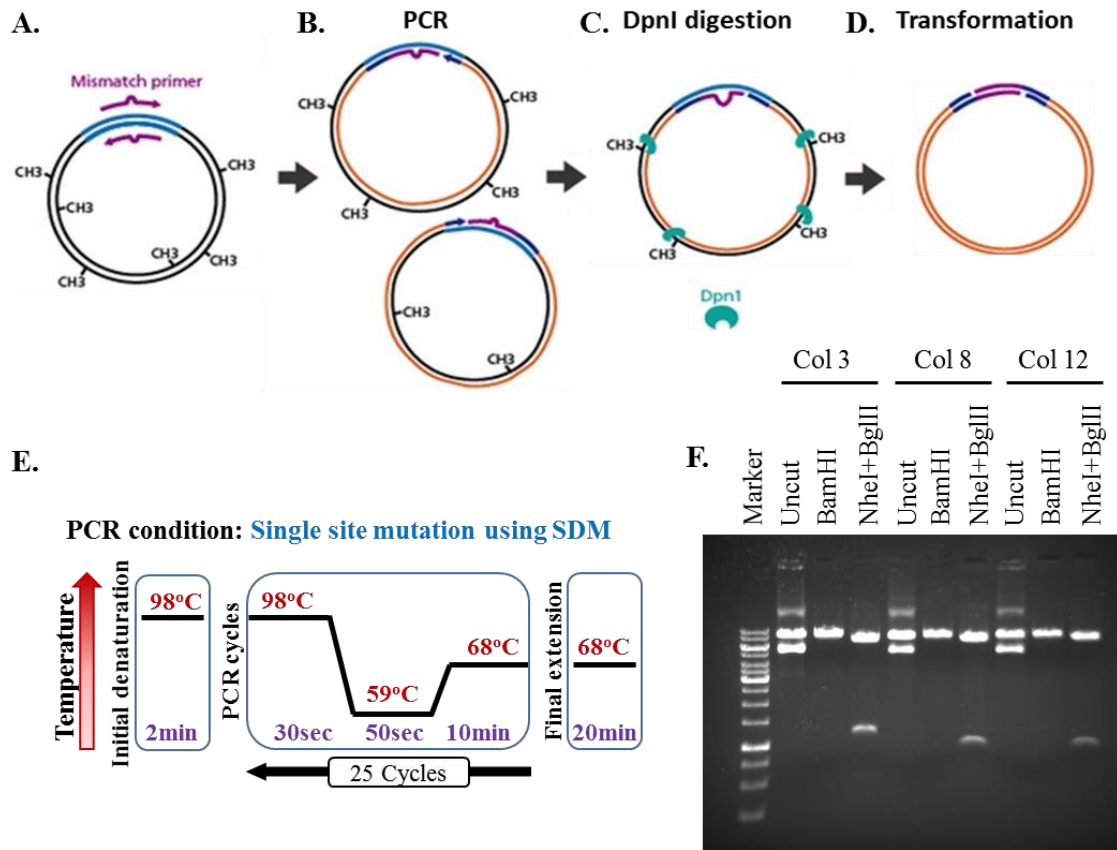
Figure 2. 2: Schematics of steps involved in site-directed mutagenesis.

A&B. PCR amplification of whole plasmid construct using mismatch primer (site-directed amplification). C&D. Template DNA was removed by digesting with methylation specific DpnI enzyme which cuts bacterial methylated plasmid. PCR-amplified plasmid was protected from such DpnI digestion as it did not harbour CpG-methylation. Digested product was then transformed to obtain colonies. E. PCR conditions used for site-directed mutagenesis PCR amplification. F. Plasmid DNA was isolated from colonies and positive clones were identified by restriction digestion (F) and sequencing.

C. Construction of single site containing deletion constructs:

Deletion constructs containing single p53 response element were created using PCR amplification of wild type PIK3CA promoter using primers given in Appendix D. (figure 3) Purified PCR product was further digested with NheI+BglII and cloned into

pcDNA3.1-hrl-egfp vector backbone. These deletion constructs were designated as OS1-4-PIK3CA promoter constructs. Similarly mutant version of these deletion construct were developed using amplification of single site mutant construct. All these constructs were confirmed with restriction digestion and sequencing.
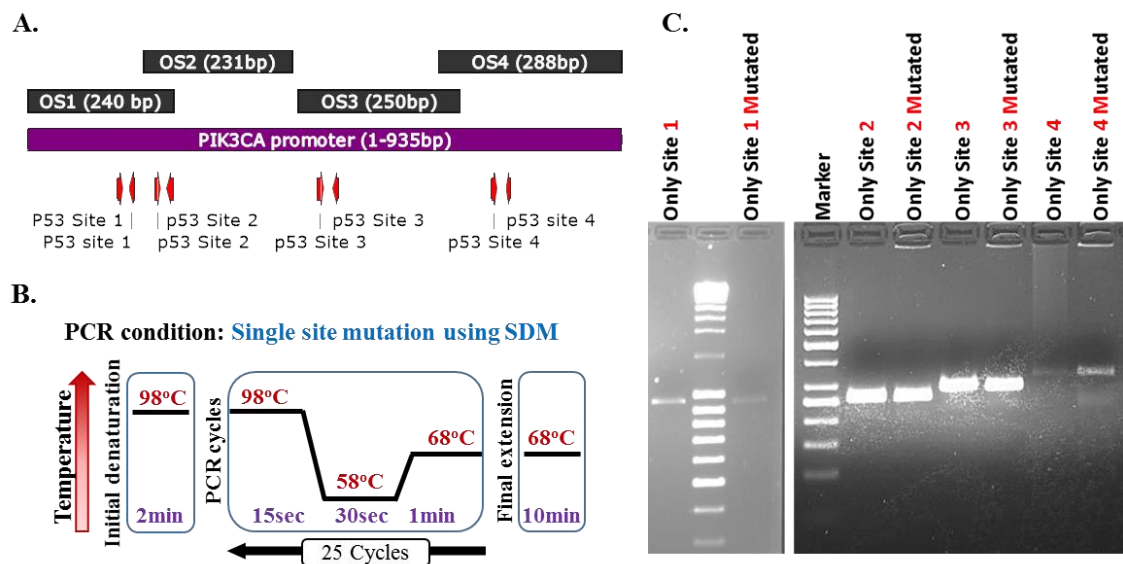
Figure 2. 3: Construction of single site containing deletion construct of PIK3CA promoter.

A. Schematics representation of single site containing deletion construct of PIK3CA promoter. OS1, OS2, OS3 and OS4 are the individual deletion constructs carrying single p53 response element site flanked by 50-100 base pairs of adjacent promoter region. B&C. PCR conditions used for amplification of deletion product and migration of PCR product in 1.2% agarose gel.

Site specific Chromatin immune precipitation (ChIP):

Site specific ChIP was performed as described earlier with few modifications [316]. Briefly, 3×10^6 cells were crosslinked with formaldehyde by adding directly to the culture medium to a final concentration of 0.75%. Glycine (125mM final concentration) was added to stop the crosslinking reaction and cells were washed with 1X chilled PBS for 3 times. Further, nuclei

was extracted using the lysis buffer (50mM HEPES-KOH pH7.5, 140mM NaCl, 1mM EDTA pH8, 1% TritonX 100, 0.1% SDS, 0.1% Sodium Deoxycholate, proteinase inhibitor) and subjected to sonication cycles to obtain an average of 200-400bp chromatin fragments. This step was crucial for achieving site specificity, as ensuring 200-400bp warrants independent pull down of individual sites. To check the specificity of p53 antibody for efficient pull-down, we precipitated chromatin fragments with ChIP-specific p53 antibody (raised in mouse) and immunoblotted with anti-p53 antibody (raised in rabbit). As only single band was detected corresponding to p53-molecular weight (53kDa), we used this antibody for our ChIP experiments.

Crosslinked, sonicated chromatin fragments were divided in three parts, as input, ChIP (precipitated with p53-antibody and protein A- sepharose beads) and bead only control. 25µg chromatin were precipitated with p53 specific antibody (SC-126X, ChIP grade, Santacruz) and DNA was eluted post reverse-crosslinking. Non-immunoprecipitated chromatin was used as total input control. DNA was isolated though column purification post RNAase A treatment. Further isolated DNA (ChIP-DNA) were analysed with real time PCR using site specific primers (Appendix E).

A. Schematic of ChIP protocol. **B.** Immunoblot for p53 showed p53-specific band after precipitation of chromatin using ChIP-specific p53 antibody. **C.** Chromatin fragments were
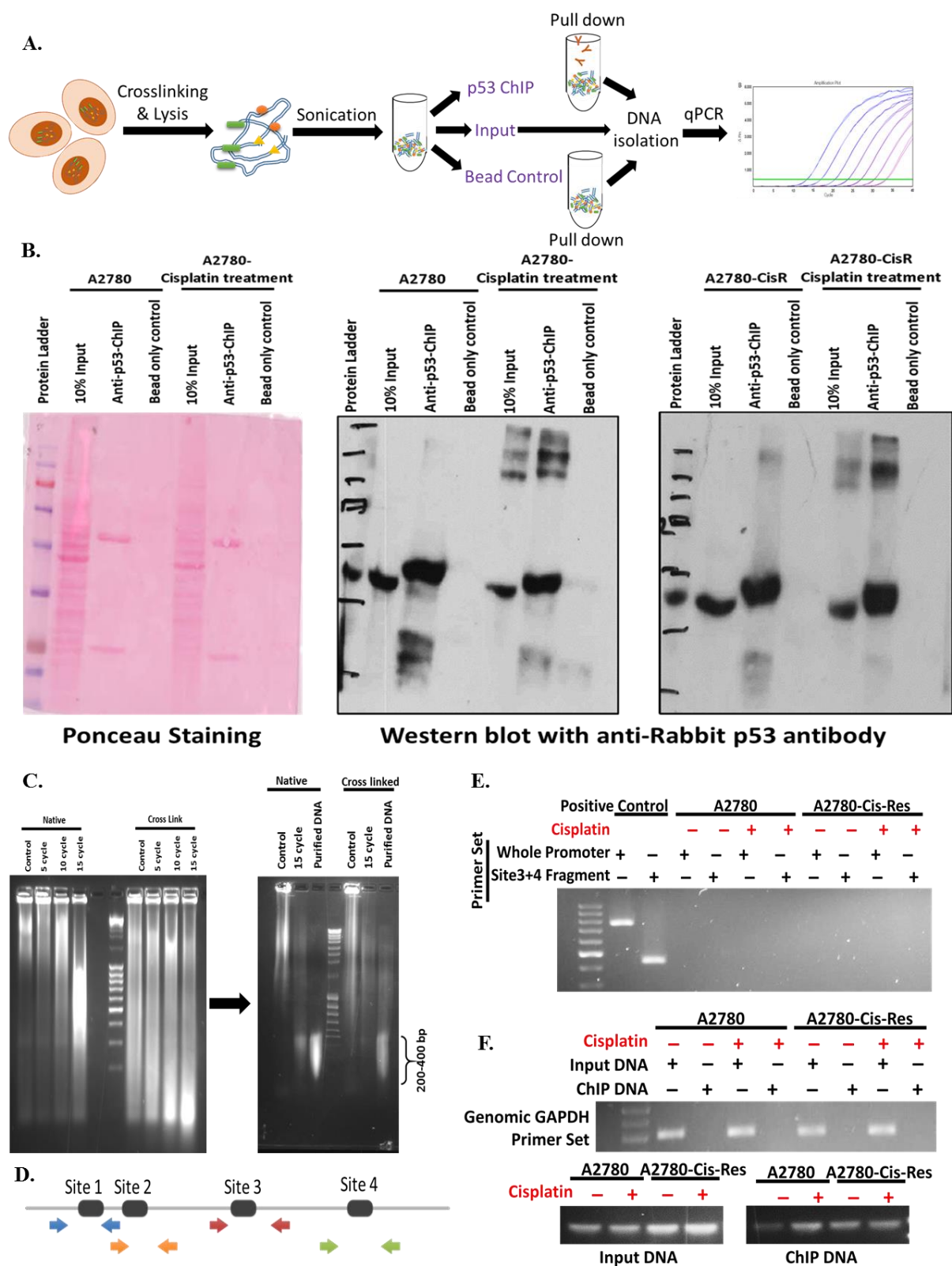
Figure 2. 4: Standardisation of site-specific chromatin immune-precipitation.

A. Schematic of ChIP protocol. B. Immunoblot for p53 showed p53-specific band after

precipitation of chromatin using ChIP-specific p53 antibody. C. Chromatin fragments were

sonicated and loaded on to 0.8% agarose gel for size estimation. As cross-linked DNA often migrates faster than native DNA, we ran native and cross-linked plasmid on same gel pre- and post- sonication cycles. Further, we affirmed size of sonicated fragment by purifing DNA from sonicated chromatin samples. D. Schematics of site-specific primers designed for ChIP. E. Semi-quantitative PCR showed the absence of amplification using primers flanking of site 3 (forward) and site 4 (reverse) validating site specificity for ChIP experiment. F. PCR using primer specific for GAPDH used as negative control to check the purity of antibody-specific pull-down. Presence of 120bp long specific amplicons post pull down confirmed specificity of site 4 primers for input and ChIP DNA.
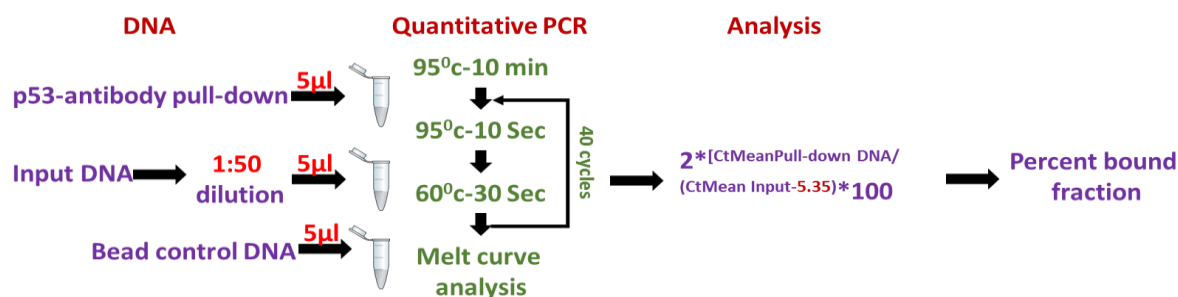
Figure 2. 5: Methodology for calculating DNA bound fraction of p53 using real-time PCR.

Results were plotted as percentage bound fraction compare to input DNA.

Live Cell Imaging

For live cell imaging, 5000 dually stable cells were seeded into 96 well black plates. These cells were treated with cisplatin for a specific time interval then incubated with fresh media. Bioluminescence of the seeded plate was first captured using furimazine (1:500 dilution) as a substrate for nanoluc activity, followed by washing with PBS and subsequent imaging with D-luciferine (1mg/ml) (fl2 activity measurement). All the images were analysed using Live Image (4.4) software. For quantification, Region of Interests (ROIs) were drawn over each

well and output luminescence was measured using the Live Image (4.4) software. Bioluminescence signals were recorded as photons/s/cm^2/sr.
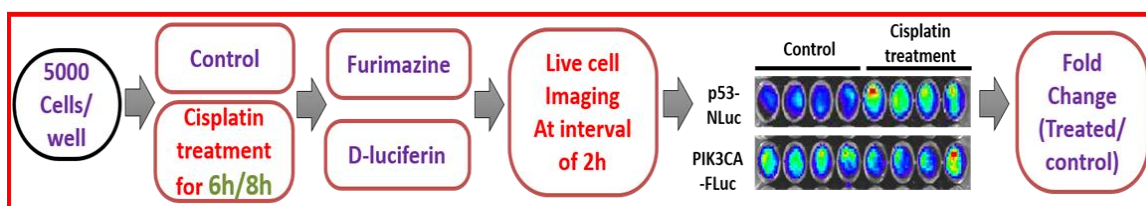
Figure 2. 6: Work plan for live cell imaging.

Bioluminescence imaging of tumor xenografts

Animal care and euthanasia were performed as per Institutional Animal Ethics Committee approval of ACTREC. SCID mice (n=10) were implanted with 4x 10^6 cells of either APN or APN-CisR dual stable cells and were allowed to grow palpable tumors (5-8 mm in size). Further, xenograft bearing mice were divided into two groups as control (injected with 0.9% saline, vehicle control) and treated group (injected with 8mg/kg cisplatin). Bioluminescence images of the mice were acquired after intraperitoneal injection of either Furimazine (1µl in 100µl/mouse) or 100µl D-luciferin (0.5mg/mouse). Image acquisition sequence involved p53-nanoluc imaging followed by *PIK3CA*-fl2 imaging after 8hr interval. ROIs were drawn over each of the tumors and quantified by using the Live Image (4.4) software. Bioluminescence signals were recorded as photons/s/cm^2/sr.
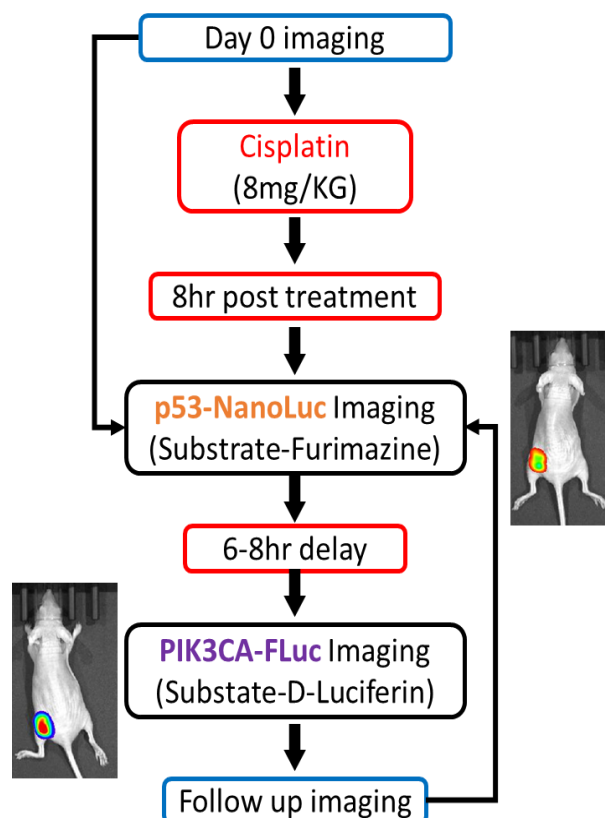
Figure 2. 7: Sequential acquisition of bioluminescence images for measurement of PIK3CA promoter and p53-protein activity in tumor xenografts.

Site directed mutagenesis for p53 serine 46 residue:

Standard SDM protocol was used to generate the mutations at the p53 serine 46 residue, modified from [269]. A detailed protocol for the SDM is given in the Appendix A.3.5. All these constructs were confirmed by sequencing. These clones were designated as S46A (serine to alanine conversion), S46D (serine to aspartate conversion), K5R (lysine to arginine mutation at 5 residue as K370, K372, K373, K381, K382) which act as phosphorylation-deficient mutant, phosphorylation-mimicking mutant, and acetylation-deficient mutation respectively.
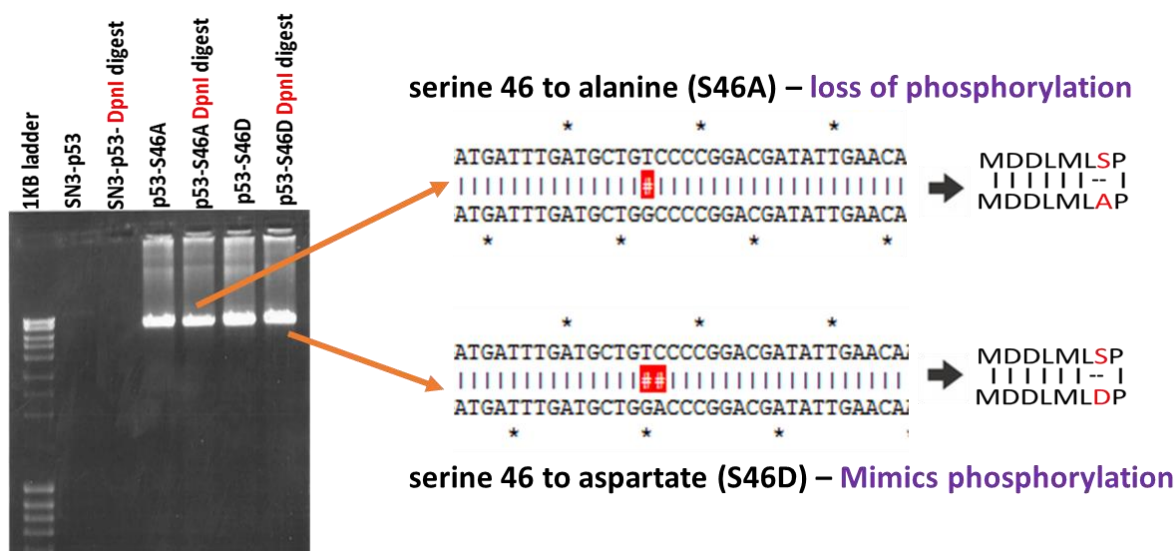
Figure 2. 8: Establishment of p53 mutation at serine 46 residue.

A. Wild type p53 plasmid was PCR amplified using mutagenic primers harbouring desired mutation and subjected to the DpnI digestion. Digested product was run on gel to confirm PCR amplification and DpnI digestion. Further, digested product was transformed and the colonies formed were screened by sequencing for desired mutation.

Co-relation analysis of mutant p53 and PIK3CA expression or phospho AKT levels in HGSOC patients (TCGA data)

To perform co-relation analysis from HGSOC-TCGA dataset, p53 mutation status, microarray data and RRPA level of PI3K/AKT associated genes were retrieved using cBioPortal (http://cbioportal.org) This data was combined using 'R-bind' R package with column binding function. To identify differential PIK3CA regulation, we categorized PIK3CA gene expression between low (PIK3CA regulator category) and high (PIK3CA non-regulator) expression based on mean of the expression level. Further, associated p53 mutations were grouped into five categories as 'wild type', 'non-functional mutation-splice varients, INDEL or non-sense mutation', 'Less frequent mutations-for >0.1% frequency in available dataset', and remaining mutations were divided into PIK3CA regulators and non-

regulators. From these two categories R273H, R248Q and C176Y and Y220C were studied further.

Statistical analysis: All the comparison between promoter activity measurements, cell culture and tumor xenografts were analysed using Student's *t* test in Microsoft EXCEL 2013. Values of *P*<0.05 were considered statistically significant. Error bars represents SD from at least three independent experiments.s

2.3 Results:

Cisplatin attenuated PIK3CA promoter activity only in sensitive but not in resistant cells:

Tumor suppressor protein 53 (p53) plays a crucial role in transcriptional regulation of PIK3CA oncogene in drug sensitive ovarian cancer cells, wherein it attenuated its promoter activity in response to various drugs including cisplatin.[269] Lee et al, (2008) also observed similar phenomenon where cisplatin repressed PIK3CA expression in OVCAR-3 cells. Surprisingly, treatment of cisplatin to resistant OVCAR-3/CDDP cells escalated PIK3CA expression.[149] Although cisplatin resistant cells can endure the cytotoxic action of chemotherapeutic drugs, treatment of cisplatin did induce p53 in these resistant cells similar to sensitive cells.[317-319] However, impact of p53 on PIK3CA promoter modulation in cisplatin resistant cells remained unexplored.

In order to understand cisplatin mediated PIK3CA promoter modulation in sensitive and resistant cells, various ovarian cancer cell lines were treated with cisplatin and levels PIK3CA, PARP, p53 and pAKT were assessed. Despite comparable levels of p53 stabilization by cisplatin treatment (except for SKOV3-p53 null cells), reduction in PIK3CA levels (both at transcript and protein) were observed in A2780 and OAW42 cell lines but not

in TOV21G and SKOV3 cell lines. (Figure 2.9 A-C) Subsequently, higher IC_{50} doses and absence of PARP cleavage after cisplatin treatment in TOV21G and SKOV3 cells affirmed their cisplatin resistant nature. While A2780 and OAW42 cells showed low IC_{50} doses and prominent PARP cleavage following cisplatin treatment indicating their sensitive character. (Figure 2. 9 B & C) These resistant cells are also accompanied with highly activated PI3K/AKT pathway as assessed by pAKT level. To understand the PIK3CA promoter modulation in sensitive and resistant cellular milieu, we assessed the promoter activity by transiently expressing a PIK3CA-hrl-egfp sensor after cisplatin treatment. While the sensitive cell lines (A2780 and OAW42) showed 0.4-0.5 fold decrease in promoter activity, the intrinsically resistant cell lines (TOV21G and SKOV3) showed 1.5-2 fold increase in PIK3CA promoter activity. (Figure 2. 9 D) In order to understand the global effect of cisplatin on PIK3CA promoter modulation, we had included two breast cancer cell lines, MCF7 (cisplatin sensitive) and ZR-75-1 (cisplatin resistant) in our study. Similar to ovarian cancer cells, we treated MCF7 and ZR-75-1 with cisplatin and assessed protein levels of PIK3CA, PARP, p53 and pAKT. Though cisplatin induced p53 stabilization in both, MCF7 and ZR-75-1 cells, only MCF7 cells showed reduction in PIK3CA promoter activity, PIK3CA transcript, and p110α level. (Figure 2. 9 C&D) In addition, PARP cleavage, a marker of apoptosis was observed only in MCF-7 but not in ZR-75-1 cell lines following treatment. (Figure 2. 9E) Higher levels of phosphorylated AKT were associated with cisplatin resistant cells (TOV21G, SKOV3 and ZR-75-1) compared to sensitive cells (A2780, OAW42 and ZR-75-1).

In order to nullify the effect of cellular heterogeneity, isogenic cisplatin resistant model developed with A2780 cells stably expressing a PIK3CA-fl2-tdt fusion reporter was used for further validation. These A2780-CisR cells exhibited higher IC_{50} (5μg/ml i.e., ~ 10 fold higher than IC_{50} of sensitive cells) [240], higher pAkt level and did not exhibit PARP

cleavage. (Figure 2. 9F) Interestingly, low level of p53 stabilisation was observed in A2780-CisR compare to A2780 upon cisplatin treatment. In addition, cisplatin treatment did not induce PIK3CA promoter attenuation as assessed at both promoter activity and expression level in these resistant cells even at high concentration. (Figure 9G&H)
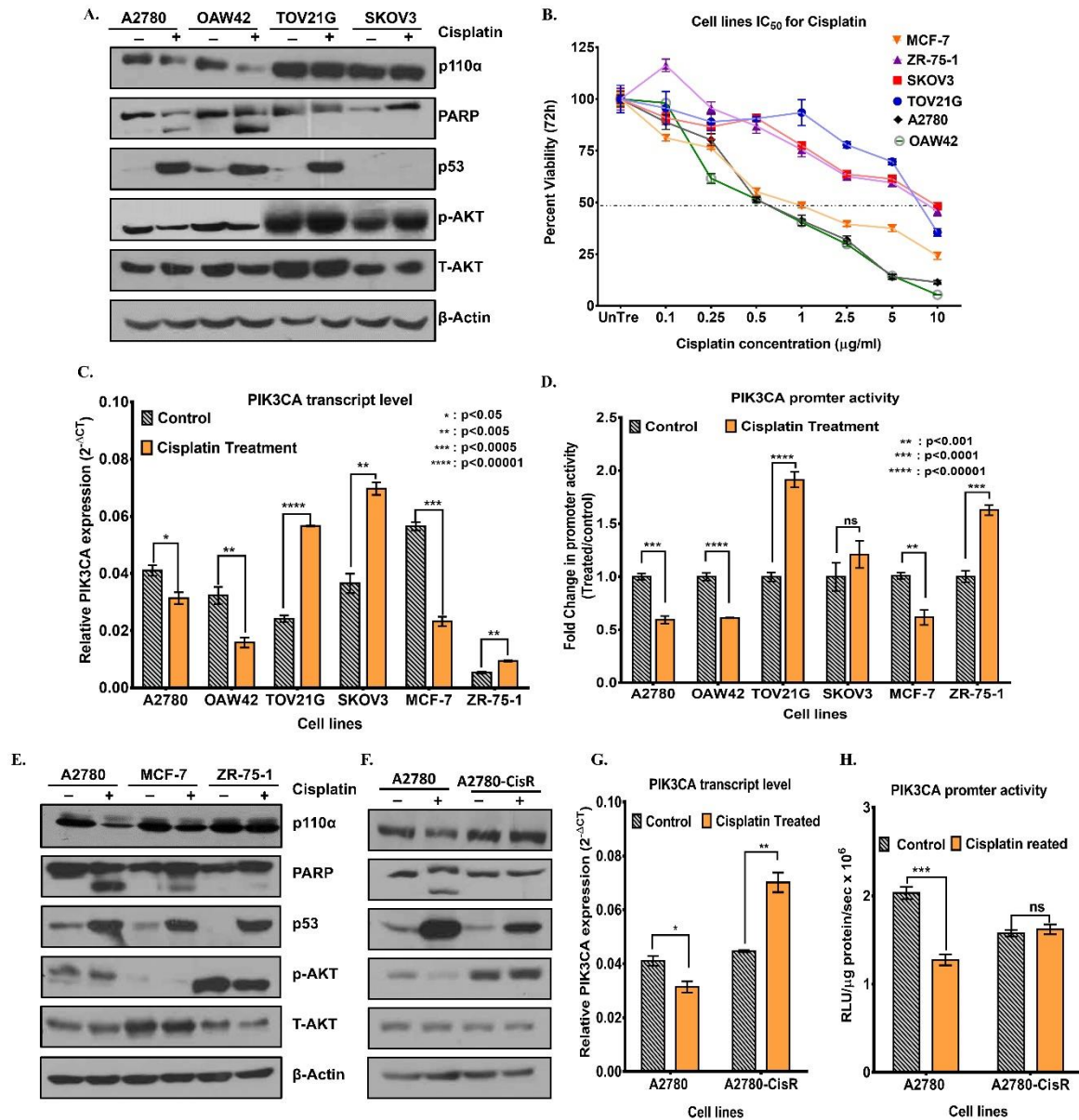
Figure 2. 9: Cisplatin negatively regulate PIK3CA expression in sensitive cells while it escalated PIK3CA expression in resistant cells.

A. Immunoblot analysis showed presence of cleaved PARP, and activated p53 along with decreased levels of p110α (PIK3CA) and pAKT in cisplatin treated sensitive A2780 and

OAW42cells which were not evident in resistant SKOV and TOV21G cells. SKOV3 being p53-deficient cell line did not show p53 expression. B. Status of cisplatin sensitivity for ovarian and breast cancer cell lines were evaluated by estimating their IC_{50} concentration for cisplatin by MTT assay. A2780, OAW42 and MCF7 cells demonstrated much lower IC_{50} for cisplatin (500ng/ml, 500ng/ml and 1000ng/ml respectively) affirming their sensitive nature towards cisplatin. Compared to sensitive cell lines, TOV21G, SKOV3 and ZR-75-1 cells showed much higher IC_{50} supporting their resistant nature. C. Upon cisplatin treatment, PIK3CA transcript level was decreased in cisplatin treated sensitive cells but not in resistant cells. Instead, resistant cells demonstrated increment in PIK3CA expression upon cisplatin treatment. D. Attenuated PIK3CA promoter activity was observed in cisplatin treated sensitive cells but not in resistant cells (n=4). E. MCF7 cells, upon cisplatin treatment showed decreased levels of p110α and pAKT, cleaved PARP, and activated p53, which were not evident in resistant ZR-75-1 cells. F-H. A2780 isogenic cisplatin resistant model also demonstrated abolished PIK3CA attenuation at transcript, protein, and reporter activity level in resistant cells after treatment.

Low level of p53 stabilization accounted for abolished PIK3CA promoter attenuation in resistant cells:

Since A2780-CisR cells showed low level of p53 stabilization, which might affect its transcriptional activity, we studied nuclear localization of p53 and assessed p21 and PUMA expression after cisplatin treatment. Nuclear localisation of p53 was not altered and induction in p21 and PUMA transcripts occurred in A2780-CisR cells upon cisplatin treatment. (Figure 2.10 A) However, fold induction in p21 and PUMA expression was much lower in A2780-CisR cells compared to sensitive A2780 cells. (Figure 2.10 B&C) This reduced p53 transcriptional activity in resistant cells could be due low level of p53 induction and reduced

nuclear localization in these cells. Intrinsically cisplatin resistant cells (TOV21G, SKOV3 and ZR-75-1) also showed low level of P21 induction post cisplatin treatment compared to sensitive (OAW42 and MCF7) cells. (Figure 2.10 D)

We assumed that diminished PIK3CA promoter modulation in resistant state could be due to low level of p53 induction. To understand the impact of p53 stabilization on its transcriptional regulation, we overexpressed p53 in A2780-CisR cells and assessed PIK3CA promoter luciferase activity. p53 overexpression mimicked the cisplatin mediated PIK3CA promoter attenuation in sensitive cells and combination of drug treatment with p53 expression aggravated this effect. (Figure 2.10 E) Interestingly, in A2780-CisR cells, significant promoter attenuation was observed only after p53 overexpression, which did not reduce further after concomitant drug exposure. Reduction in PIK3CA promoter activity was corroborated with endogenous p110a levels where combination of p53 overexpression along with cisplatin treatment decreased p110a levels, phosphorylated AKT and induced PARP cleavage in A2780-CisR cells. (Figure 2.10 F)
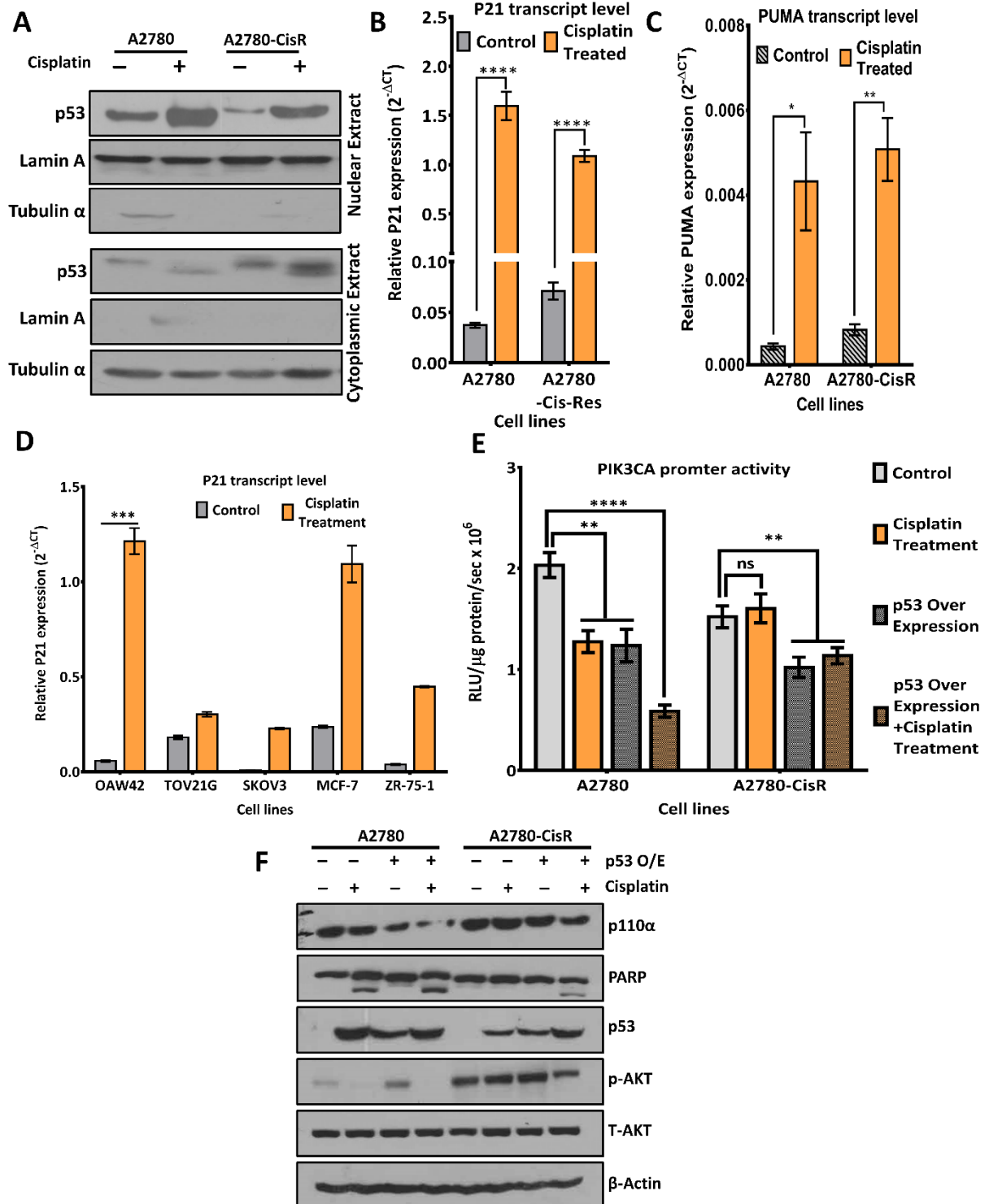
Figure 2. 10: Cisplatin-resistant cells demonstrate reduced p53 transcriptional ordinance.

A. In spite of lower level of p53 induction in resistant cells upon cisplatin treatment, p53 localized to nucleus as assessed cellular fractionation of cytoplasmic and nuclear extracts. In addition, we also observed higher level of cytoplasmic retention of p53 in resistant cells compared to sensitive cells. B&C. In accordance with reduced p53 levels, significantly lesser level induction in p53 immediate targets genes p21 (B) and PUMA (C) was observed in resistant cells (A2780-CisR) compare to sensitive (A2780) cells following cisplatin treatment. (n=3) D. Similar to isogenic A2780-cisplatin resistant model, intrinsically resistant cell lines (TOV21G, SKOV3 and ZR-75) also demonstrated lower level of induction in p21 expression compared to sensitive cells (OAW42 and MCF7) upon cisplatin treatment. (n=3) E. p53 overexpression simulated the effects of cisplatin treatment and aggravated the effect when used in combination in sensitive cells. In resistant cells, PIK3CA promoter attenuation was only observed after p53 overexpression (without or with drug combination). F. This modulation also corroborated with PIK3CA protein levels as examined by western blot analysis. Interestingly, PARP cleavage and reduced pAKT were found in resistant cells only during cisplatin treatment along with p53 overexpression.

Loss of p53 binding on site 3 and site 4 to PIK3CA promoter in resistant cells:

PIK3CA promoter harbours four complete p53 response elements and successive mutations at these sites abolish cisplatin mediated promoter attenuation.[269] To understand the strength of each site for p53 binding, we created single site mutant construct for PIK3CA promoter, S1 (mutation at site 1), S2 (mutation at site 2), S3 (mutation at site 3) and S4 (mutation at site 4). (Figure 2. 11 A&B) These single site mutant constructs were transiently transfected in cells with appropriate normalization vectors. (Figure 2. 11A) Cisplatin dependent promoter suppression was found to be alleviated from 0.5 fold to 0.75 fold after

mutating site 3 and site 4 in A2780 and OAW42 cells. (Figure 2. 11C) However, mutation at site 1 and site 2 did not result in any relief in promoter attenuation. TOV21G and SKOV3 being cisplatin resistant cells did not show any promoter modulation with these constructs. None of these mutations, however, altered PIK3CA promoter activity in A2780-CisR cells. (Figure 2. 11D)

To understand the influence of the adjacent bases of each p53 binding sites, we generated deletion constructs of PIK3CA promoter containing each p53 binding site flanked by 100-150 bases on either side. (Figure 2. 11B) Again, promoter modulation was observed only for site 3 and site 4 constructs but not with site 1 or site 2 constructs after transient expression of the mutants and cisplatin treatment in A2780 and OAW42 cell lines. (Figure 2. 11E) Both site 3 and site 4 independently showed PIK3CA promoter attenuation upon cisplatin treatment, suggesting that both sites individually contributes to PIK3CA promoter attenuation. To confirm specific involvement of site 3 and site 4, we mutated p53 response element in these deletion constructs and estimated promoter activity. Mutations at site 3 or site 4 p53 response element abolished cisplatin mediated PIK3CA promoter attenuation in both OS3- and OS4-PIK3CA constructs. (Figure 2. 11F) In cisplatin resistant cell lines (TOV21G, SKOV3 and A2780-CisR), similar to single site mutation constructs, the deletion constructs did not exhibit any promoter modulation upon cisplatin treatment. (Figure 2. 11G). Figure 2.12 represents the summary of promoter activity of PIK3CA constructs in various cisplatin sensitive and resistant cell lines.
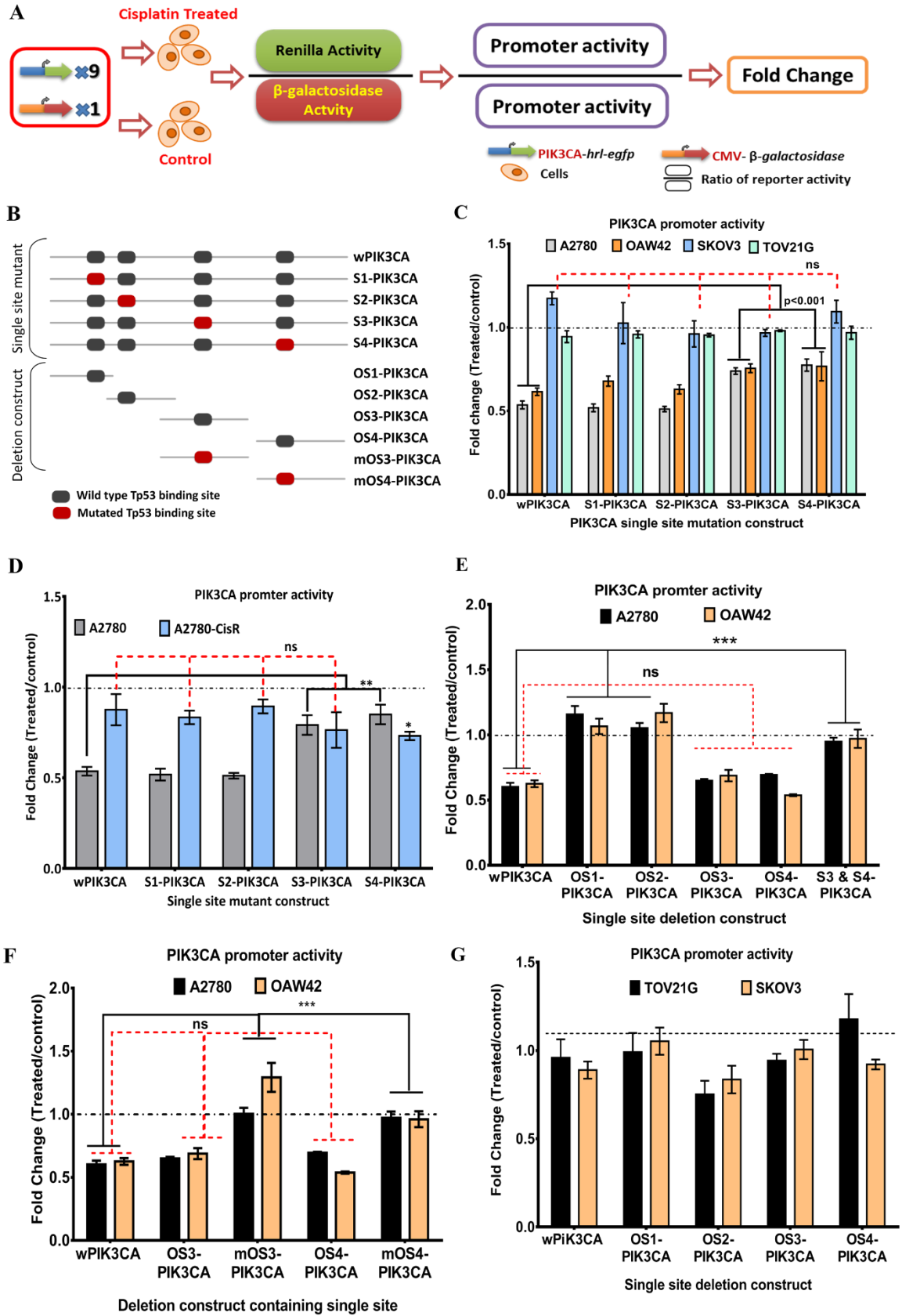
Figure 2. 11: Site 3 and site 4 p53 response element present on PIK3CA promoter are critical for cisplatin induced p53-PIK3CA attenuation in sensitive cell lines.

A. Work plan for estimation of promoter activity of different PIK3CA-promoter constructs. B. Schematic of PIK3CA promoter constructs which include single site mutant constructs and deletion constructs. Single site mutant constructs (S1-S4) harbours mutation in single p53 response elements disrupting binding of p53. Single site deletion constructs (OS1-OS4) are the deletion constructs carrying respective single p53 response element flanked by 50-100 adjacent base pairs. mOS3 and mOS4 are deletion constructs carry mutant form of p53 response element for site 3 or site 4 along with 50-100 base pairs of flanked region. C. In single site mutant PIK3CA promoter constructs, mutations in site 3 & 4 but not in site 1 & 2 abolished cisplatin mediated PIK3CA promoter attenuation in A2780 and OAW42 cells after transient transfection. Cisplatin resistant TOV21G and SKOV3 cells did not exhibit change in promoter activity upon cisplatin treatment for all four single site constructs (n=4). D. Similar to intrinsically resistant cell lines, A2780-CisR cells did not exhibit any change in promoter activity of single site mutant constructs (n=4). As a control, A2780 cells showed relieved promoter activity only in single site mutant construct harbouring mutations at site 3 and 4. E. Comparable to wild type PIK3CA promoter construct activity, cisplatin mediated promoter attenuation was observed for the deletion constructs comprised of only site 3 or 4 p53 response element (with flanking regions) but not for constructs bearing site 1 or 2 p53-RE after transient transfection in A2780 and OAW42 cells and cisplatin treatment. F. Further, mutating p53 binding sequences at site 3 or site 4 in these deletion constructs completely abolished cisplatin mediated PIK3CA promoter attenuation. G. Deletion constructs did not show any PIK3CA promoter attenuation in intrinsic cisplatin resistant cell lines (TOV21G and SKOV3).

A.

Schematics of PIK3CA promoter construct

B.

Promoter activity post cisplatin treatment				
Construct	A2780	OAW42	SKOV3	A2780-CisR
wPIK3CA	0.55	0.61	1.2	1.02
S1-PIK3CA	0.49	0.68	0.98	0.99
S2-PIK3CA	0.51	0.63	0.95	0.97
S3-PIK3CA	0.74	0.75	0.96	1.02
S4-PIK3CA	0.75	0.77	1.22	0.98
S3-S4-PIK3CA	1.16	1.01	1.09	1.2
OS1-PIK3CA	1.15	1.06	1.1	0.96
OS2-PIK3CA	1.05	1.17	1.05	0.94
OS3-PIK3CA	0.64	0.68	1.02	1.1
OS4-PIK3CA	0.69	0.54	1.2	0.98
mOS3-PIK3CA	1.12	1.01	1.1	1.03
mOS4-PIK3CA	1.09	0.99	1.07	1.1

No change | Moderate increase | Increase activity | Wild type activity

Figure 2. 12: Summary of modulation in PIK3CA promoter construct upon cisplatin treatment.

A. Schematics of single site mutant and single site containing deletion PIK3CA-promoter constructs. B. Quantification of fold change in promoter activity (treated/untreated) from each of the promoter constructs. Both, single site and deletion construct data indicates that p53 interacts with site 3 and site 4 p53-RE present on PIK3CA promoter and responsible for cisplatin mediated PIK3CA promoter modulation in sensitive cell line.

With stringent conditions as described in method section, we performed site-specific chromatin immune precipitation with p53 antibody to check site-specific p53 enrichment upon cisplatin treatment on four-p53 response element present on PIK3CA promoter. (Figure 2. 13A) Sensitive A2780 cells showed cisplatin responsive enrichment of p53 up to 1.5% and 2.5% of input on site 3 and 4 respectively. (Figure 2. 13B) Similarly, in OAW42 and MCF-7 cells, cisplatin induced p53 enrichment was observed only for site 3 and 4 wherein it enriched from 0.11% to 1.5% (site 3) and 0.11% to 2.9% (site 4) and 0.02% to 0.4% (site 3) and 0.02% to 1.14% (site 4) in respective cell lines. (Figure 2. 13 C&D) Interestingly, in untreated condition, p53 was found to occupy maximally site 1 but the binding was reduced (1.2% to

0.3% of input) post cisplatin treatment. In A2780-CisR cells, binding of p53 was minimal for site 1, 3 and 4, however it significantly enhances only at site 1 (0.13 to 1.4% of input) after cisplatin treatment. (Figure 2. 13B) Similarly, intrinsically cisplatin resistant TOV21G and ZR-75-1 cell lines did not show any drug dependent p53 enrichment for site 3 and 4 but enhanced binding at site 1 (from 0.05 to 0.75 and 0.1 to 0.45% of input respectively). (Figure 13C&D) No binding of p53 was found for Site 2 in any of these cells pre and post treatment.
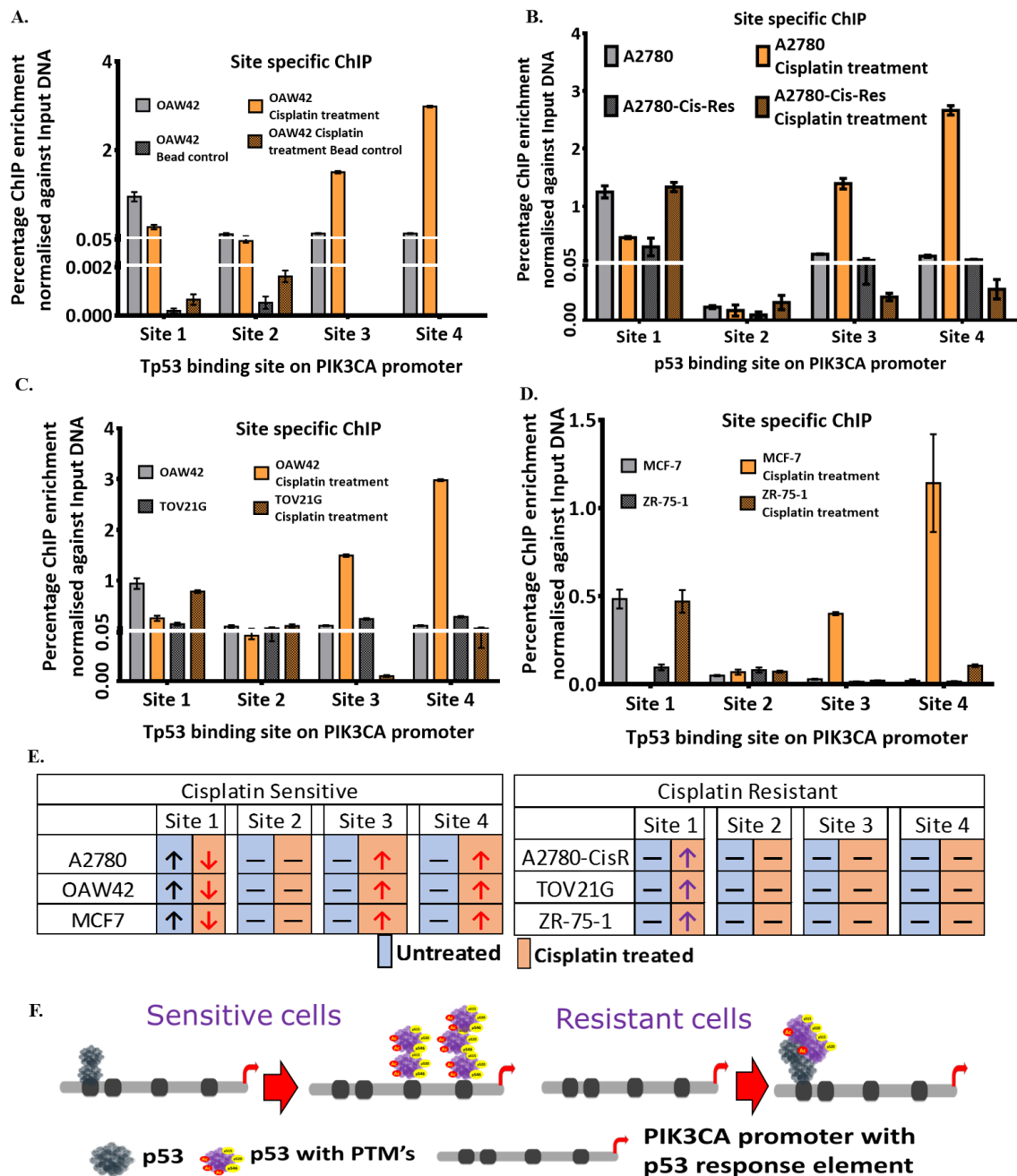
Figure 2. 13: p53 physically interacts with PIK3CA promoter at site 3 and site 4 following cisplatin treatment.

A. p53 occupancy on four-p53 response elements in DNA precipitated with p53 antibody or bead only control from pre- and post- cisplatin treated OAW42 cell lines. Bead only precipitated DNA was used as negative control. B-D. Quantification of site specific occupancy of p53 measured by ChIP in untreated and cisplatin treated A2780 (B), A2780-CisR (B), Oaw42 (C), TOV21G (C) MCF7 (D) and ZR-75-1 (D). Cisplatin incremented binding of p53 to site 3 and 4 from site 1 in A2780, OAW42 and MCF7 (sensitive cells) as determined by ChIP assay followed by real time PCR and compared with input DNA. In A2780 CisR, TOV21G and ZR-75-1 (resistant cells) such increased p53 occupancy was observed only at site 1 after cisplatin treatment. All the values were plotted as percent binding of p53 compared to input DNA. Site 2 showed negligible binding at all conditions (n=3). E. Summary of site-specific ChIP quantification, where arrow indicate increase or decrease in p53 occupancy while 'minus sign' represents no chance in p53 occupancy. F. Model depicting cisplatin mediated p53 binding on PIK3CA promoter in sensitive and resistant cells. In sensitive cell, cisplatin mediates alteration in p53 binding preference from site 1 to site 3 and 4 present on PIK3CA promoter, while in resistant cells, p53 occupancy was observed only after cisplatin treatment at site 1.

Monitoring dynamics of p53 activation and PIK3CA promoter modulation

To understand the dynamics of p53-PIK3CA promoter interaction in real time, we developed dual reporter stable cell lines as <u>A</u>2780-expressing <u>P</u>IK3CA-fl2-tdt and p53-<u>n</u>anoluc (**APN**) and its cisplatin resistant counterpart APN-CisR. APN and APN-CisR cells are dual reporter cell line genetically engineered to stable express <u>P</u>IK3CA-sensor (PIK3CA-promoter driving fl2-tdt) and p53-protein reporter (p53-protein fused with <u>n</u>anoluciferase reporter in sensitive

(A2780) and resistant (A2780-CisR) parent cells. This p53-protein reporter undergoes similar cellular fate as that of endogenous p53 where p53-nanoluc fusion protein was stabilized and translocated to nucleus following cisplatin treatment. Proteolytic cleavage of fusion protein is one the major concern for using a fusion reporter system. Hence, to evaluate whether p53-nanoluc endures any proteolytic cleavage, we transfected p53-reporter in SKOV3 cells (p53-deficient cell line) and carried out immunoblot with p53 antibody. Immunoblotting with p53 antibody only detected fusion reporter (~72kDa band) corresponding to p53-nanoluc fusion protein, while no band corresponding to 53kDa was observed in SKOV3 cell lysates. (Figure 2.14 A-B) Hence, the fusion protein does not experience any proteolytic cleavage. In addition, cisplatin treatment to only-nanoluc (CMV driven nanoluc) reporter construct did not change its activity. (Figure 2.14 C) Interestingly, expression of p53-nanoluc did not modulate PIK3CA promoter activity since it harbours P278A mutation in the DNA binding domain. (Figure 2.14 D) Substitution of proline to alanine at codon 278 is known to result in loss of p53 transcriptional activity.[320] Thus, p53-nanoluc reporter serves as a promising reporter for quantitative measurement of p53 activity as a function of Nanoluc activity. Further, we tested response of cisplatin towards dual stable cell lines, which demonstrated similar level of cytotoxic effect as that of parent sensitive and resistant cells. (Figure 2.14 E) Since over expression of fusion protein neither modulated PIK3CA promoter activity nor showed alteration in response towards cisplatin, we utilized these dual stable cell lines for studying p53 protein-PIK3CA promoter interaction dynamics in real time.
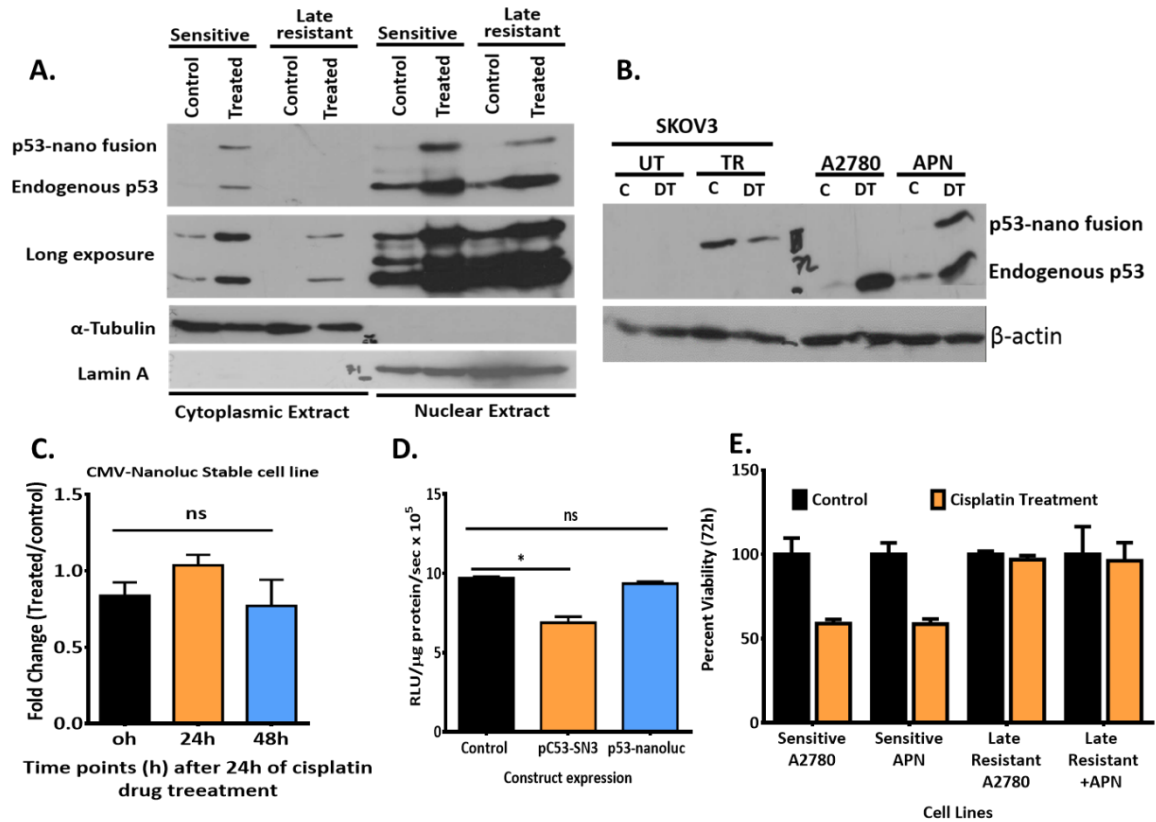
Figure 2. 14: p53 reporter (CMV driven p53 protein-nanoLuc fusion construct) as a potential p53-activation reporter.

A. p53-nanoluc in APN and APN-CisR dual reporter cells followed similar fate as that of endogenous p53 where both the proteins localized to nucleus following cisplatin treatment. Upper band (72kDa) corresponds to p53-nanoluc reporter while lower band (53kDa) represents endogenous p53, when immunoblotted with antibody against p53 B. Expression of p53-nanoluc fusion protein does not undergo any proteolytic cleavage in the cellular milieu pre- or post- cisplatin treatment as no p53 band corresponding to 53KDa was observed in SKOV3 (p53-deficient cell line) by immunoblot. C. Cisplatin treatment did not affect activity of CMV driven nanoluc (only nanoluc) reporter construct. D. Over-expression of p53 but not p53-Nanoluc fusion attenuated PIK3CA promoter activity. E. Cell lines stably expressing p53-nanoluc fusion construct behaves similar to parent cell lines and did not alter cell's response towards cisplatin.

To capture the dynamics of p53 activation and PIK3CA promoter modulation, we treated cells with cisplatin for 24h and monitored corresponding reporter activities for 72h by live cell imaging assay. (Figure 2.15 A-F) Maximum p53 induction was observed at 24hr and 48hr in sensitive and resistant cell lines respectively. Notably, resistant cells exhibited much lower level of p53 induction than sensitive cells, which was also confirmed by western blotting. (Figure 2.15 G&H) In contrary, PIK3CA promoter activity decreased over time only in sensitive cells but not in resistant cells.
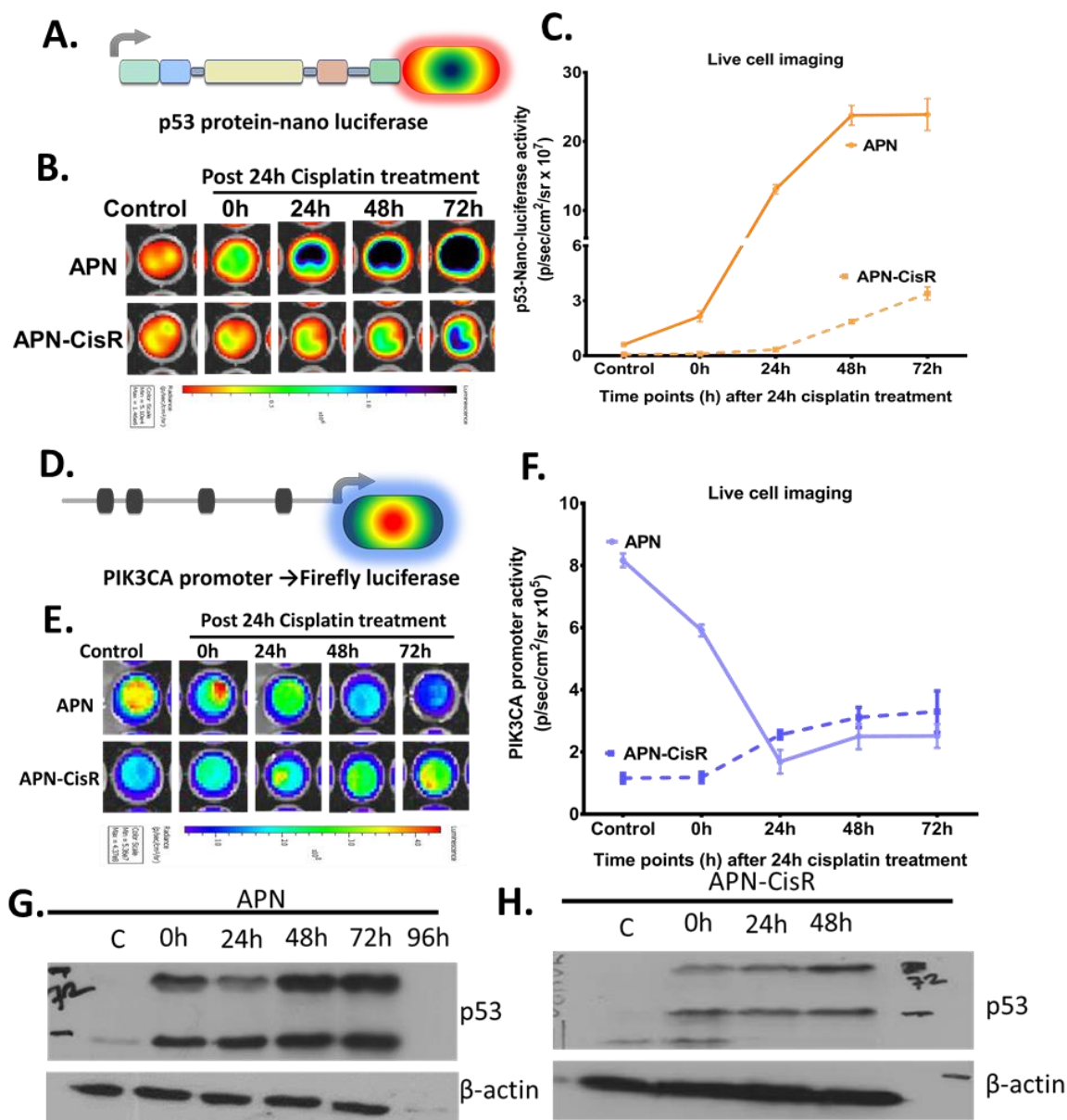
Figure 2. 15: Kinetic monitoring of p53-protein and PIK3CA promoter activity.

A Schematic representation of p53-nanoluc fusion reporter. B & C. Representative live cell images and quantification, displaying p53 stabilization as a function of nanoluc activity in APN and APN-CisR cells. APN (sensitive) cell displayed continues increase in p53 stabilisation over time, while APN-CisR exhibited delayed and reduced levels of p53 induction. Kinetics monitoring over time for p53 reporter demonstrated increased stabilization of p53 up to 26 and 10 fold in APN and APN-CisR cells following cisplatin treatment respectively. D. Schematic representation of PIK3CA promoter sensor. With the help of live cell imaging, PIK3CA promoter activity following cisplatin treatment were measured as a function of fl2 luciferase activity. E & F. Both sensitive and resistant cells demonstrated p53 stabilisation, yet PIK3CA promoter attenuation was observed only in sensitive but not in resistant cells. G & H. Immunoblot confirmed p53-nanoluc protein and endogenous-p53 stabilization post cisplatin treatment in APN (sensitive) as well as APN-CisR (resistant) cells over time.

Differential dynamics of p53 protein dependent PIK3CA promoter modulation in resistant tumor xenografts:

Assessing drug response only at cellular level often compromises with the outcomes and lead to failure in *in vivo* due to altered pharmacokinetics of the drug. To test whether p53-PIK3CA promoter interaction could be monitored in *in vivo* situation, APN-sensitive and resistant cells were grown as subcutaneous tumor in SCID mice and treated with cisplatin. Activation of p53 and modulation in PIK3CA promoter were visualized using nano-luciferase and firefly luciferase reporters respectively from the same tumor on day 4 and day 8 of post treatment. (Figure 2.16 A-H)

In sensitive tumor xenografts, cisplatin treatment increased p53 activity (measured as function of bioluminescence activity of p53-nanoluc) by 4.4±1.2 fold at day 4 and 7.4±0.7 fold at day 8 (Average radiance increased from $6.6x10^6±2.9x10^6$ p/sec/cm^2/sr to $2.7x10^7±8.5x10^6$ to $5.0x10^7±2.7x10^7$ p/sec/cm^2/sr from day 0 to day 4 to day 8). (Figure 15E) Resistant tumors also showed increased p53 activity by 1.6±0.35 fold on day 4 and 3.7±0.48 fold on day 8 (Average radiance increased from $1.1x10^6 ± 6.04x10^5$ to $1.7x10^6 ± 8.5x10^5$ to $4.1x10^6 ± 2.2x10^6$ p/sec/cm^2/sr from day 0 to day 4 to day 8) upon cisplatin treatment. (Figure 2.16 F) In untreated condition, due to increase in tumor size, nominal increase in p53 activity was observed for both sensitive and resistant tumors. Nanoluc activity of sensitive tumor xenograft increase by 1.3±0.11 fold at day 4 to 1.7±0.33 fold at day 8 ($4.6x10^7 ± 9.1x10^6$ to $5.7x10^7 ± 1.1x10^7$ to $7.5x10^7 ± 1.7x10^7$ p/sec/cm^2/sr). In resistant tumors, it increased to 1.3±0.7 and 1.2±0.13 fold by day 4 and day 8, respectively ($7.2x10^5 ± 1.3x10^5$ to $1.1x10^6 ± 4.6x10^5$ to $8.7x10^5 ± 8.7x10^4$ p/sec/cm^2/sr). (Figure 2.16 E&F)

In contrary, cisplatin treatment in sensitive tumors resulted in slight increase in PIK3CA promoter activity to 1.4 ± 0.5 fold at day 4 and then decreased to 0.4±0.1 fold ($1.3x10^9 ± 7.3x10^8$ to $1.9x10^9 ± 1.3x10^9$ to $5.7x10^8 ± 4.5x10^8$ p/sec/cm^2/sr). (Figure 2.16 G) Such decrease in PIK3CA promoter activity was not observed in resistant tumors, rather it sremained stabilised where PIK3CA promoter activity was increased by day 4 to 2.9 ± 0.45 fold then to 2.7±0.32 fold ($2.21x10^9 ± 4.8x10^8$ p/sec/cm^2/sr to $6.3x10^9 ± 1.5x10^9$ p/sec/cm^2/sr to $5.8x10^9 ± 1.12x10^9$ p/sec/cm^2/sr) post cisplatin treatment. (Figure 2.16 H) In sensitive untreated tumors, PIK3CA promoter activity increased from 2.6±1.5 fold at day 4 to 3.2±1 fold at day 8 ($1.3x10^9 ± 9.9x10^8$ p/sec/cm^2/sr to $2.6x10^9 ± 1.4x10^9$ p/sec/cm^2/sr to $3.7x10^9 ± 2.5x10^9$ p/sec/cm^2/sr) corroborating with tumor growth. Similarly PIK3CA promoter activity of untreated resistant tumor increased from 3.3±0.9 fold at day 4 to 5.4±0.7 fold at day 8 ($4.9x10^8 ± 2.4x10^8$ p/sec/cm^2/sr to $1.64x10^9 ± 1.1x10^9$ p/sec/cm^2/sr to $2.7x10^9 ± 1.4x10^9$

p/sec/cm^2/sr). (Figure 2.16 G&H) These observation also corroborates with tumor volume data where decrease in tumor volume was observed only in sensitive tumor xenograft whereas resistant tumor volume remain stabilised till day 8 (Figure 2.16 I&J). Body weights of cisplatin treated animals decreased significantly compared to untreated ones. (Figure 2.16 K&L)

When measured from tumor lysates, a 8.1±1.4 fold increase in p53 and an 0.38± 0.07 fold decrease in PIK3CA promoter activity were observed in cisplatin treated sensitive tumors compare to control ones. Whereas, *ex-vivo* luciferase activity of treated resistant tumors showed 4.25±2.3 fold increase in p53 activity but PIK3CA promoter activity remained unchanged (Fold Change by 1.05± 0.6) compared to untreated ones. (Figure 2.16 N&O) Western blot analysis of these tumor lysates confirmed p53 induction in cisplatin treated groups. (Figure 2.16 P)
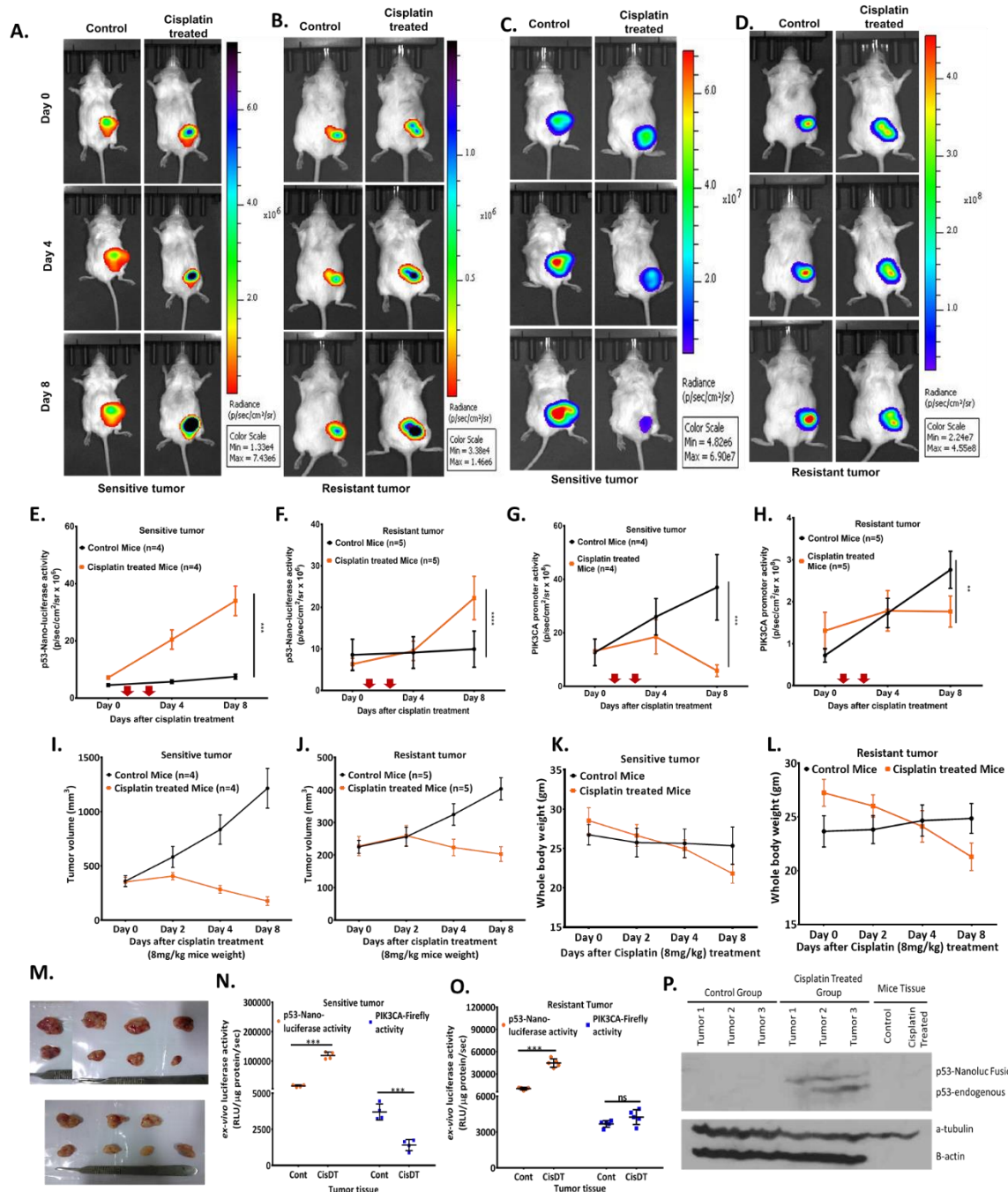
Figure 2. 16: Simultaneous in vivo monitoring of p53-protein stabilisation and PIK3CA promoter modulation.

A-D. Representative bioluminescence imaging of p53 protein and PIK3CA promoter activity modulation measured as a function of nanoluc and fl2 activity in SCID mice. Nanoluc activity representing p53- stabilisation profile in both control and cisplatin treated mice bearing sensitive and resistant tumors (A&B). fl2 activity denoting PIK3CA promoter activity

decreased with time in sensitive but remained stable in resistant tumors after cisplatin treatment (C&D). E & F. Graphical representation of quantified signal for nanoluc activity from cisplatin treated sensitive tumor xenograft (n=4) and resistant tumor xenografts (n=5). G & H. Graphical representation of quantified signal for fl2 from cisplatin treated sensitive (n=4) and resistant tumor xenografts (n=5). I & J. Kinetics of tumor growth for sensitive and resistant tumors pre and post cisplatin treatment. K & L. In treated group, cisplatin treatment reduced whole body weight of mice bearing sensitive or resistant tumor xenografts. M. Photographic image of tumors excised from control and treated groups (sensitive tumor xenografts-upper panel and resistant tumor xenografts-lower panel) N & O. Ex-vivo luciferase activities (nanoluc and fl2) from sensitive and resistant tumors lysates. P. Stabilization of p53-Nanoluc protein post cisplatin treatment in sensitive tumor xenograft was validated by presence of endogenous and p53-nanoluc fusion protein in protein extracted from excised tumor. α-tubulin and β-actin were used as controls. β-actin did not detect mouse actin while α-tubulin detects both human and mouse tubulin protein.

Reduced post-translational modification of p53 in resistant cells:

Our promoter activity with PIK3CA constructs demonstrated that in spite of p53 stabilisation, its ordinance was abolished on PIK3CA promoter in resistant cells. Hence, to comprehend this unexpected observation, we assessed posttranscriptional modification of p53 upon cisplatin treatment. p53 endures several post translational modifications (PTM) (phosphorylation, acetylation and sumoylation) and some of these modifications are critical for protein stabilization and transcriptional regulation.[290] To understand the role of PTMs in altered and reduced binding of p53 in PIK3CA promoter under influence of cisplatin, we looked at serine 15, 20 and 46 phosphorylation along with acetylation status of the p53 protein. While cisplatin treatment induced higher phosphorylation at S15, S20 and S46

residues in sensitive cells, the resistant cells showed minimal enhancement in pS15 and pS20 but not in pS46 level. In addition, higher level of un-acetylated p53 was found in resistant cells compared to the sensitive cells. (Figure 2.16 A) These results were also consistent in intrinsic resistant cell lines were p53 shows minimal level of S15 and S20 phosphorylation but not S46 phosphorylation. (Figure 2.16 B)
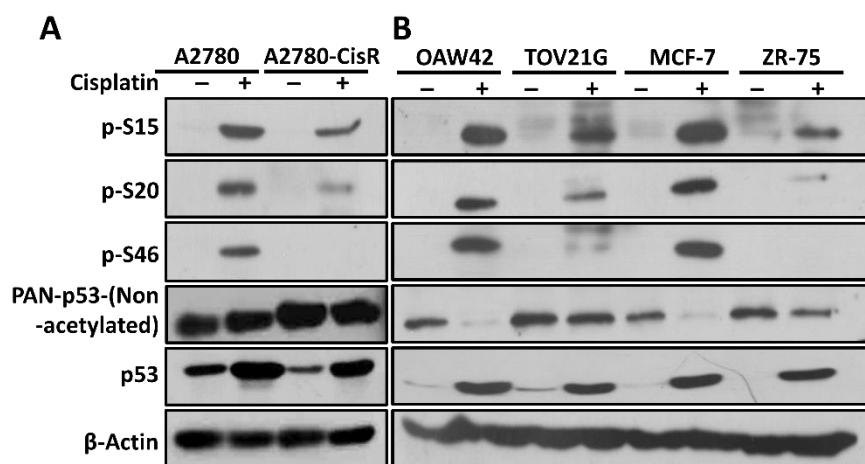
Figure 2. 17: Resistant cells exhibited discrete post translational modifications (PTM) of p53.

A & B. Immunoblotting showed differential phosphorylation at S15, S20 and S46 and differential acetylation in sensitive (A2780, OAW42 and MCF7) and resistant (A2780-CisR, TOV21G and ZR-75-1) cells post cisplatin treatment. In resistant cells, upon cisplatin treatment, p53 demonstrated hypo-acetylation, hypo-phosphorylation at serine 15 and 20 residue and loss of serine 46 phosphorylation compare to sensitive cells.

Delayed kinetics of p53 driven PIK3CA promoter modulation in response to drug:

p53 is known to bind its target genes with differential affinity and different kinetics.[274] To understand the kinetics of p53 activation-PIK3CA modulation by cisplatin in sensitive and resistant cells and the phosphorylation status of the above mentioned serine residues, we

followed p53/PIK3CA modulation every two hour interval by live cell imaging. (Figure 2.18 A&B) Significant p53 induction was observed after 6hr in sensitive cells which continued to increase and a ten-fold higher p53 activity was found at 48hr. In contrast, resistant cells took 8hr to induce noticeable p53 induction by cisplatin which increased with low level till 48hr (3.7 fold enhancement). (Figure 2.18 A) Reduction in the PIK3CA promoter activity started from 10-12hr post cisplatin treatment in sensitive cells and by 18hr PIK3CA promoter activity 50% decrease was evident. (Figure 2.18 B) Interestingly, resistant cells did not show any attenuation in PIK3CA promoter activity till 48hr. This trend was also corroborated with p110α level. Subsequently, PARP cleavage was not observed till 48hr in resistant cells compared to sensitive ones where cleavage was observed as early as at 12hr.

To understand the mechanism of this delayed kinetics, we looked at the kinetics of various PTMs in p53 post cisplatin treatment. In sensitive cells, phosphorylation of p53 at S15 and S20 residue reached to their peak at 12hr and 24hr respectively and then gradually decreased. Phosphorylation at S46 peaked at 24hr and remained stable till 48 hr. (Figure 2.18 C) Intriguingly, resistant cells exhibited these PTMs (S15 and S20) at much lower level and at later time points with no phosphorylation at serine 46 after treatment. Acetylation status of p53 remained higher in sensitive cells than resistant cells post cisplatin treatment. (Figure 2.18 C-H)

Figure 2. 18: Post translational modifications (PTM) in p53 are responsible for p53-PIK3CA promoter modulation dynamics.

A. Kinetics of p53 induction (A) and PIK3CA promoter modulation (B) in sensitive and resistant cells were monitored by live cell imaging post 6hr and 8hr of cisplatin treatment respectively. C-H. Differential induction in PTMs in p53 were measured from sensitive and resistant cells after 6hr and 8hr treatment, which indicated complete loss of pS46 and delayed and lower induction of phospho-S15, phospho-S20 and acetylation in p53. D-H. Represents the quantification of minimum three independent immunoblotting experiments for respective modifications I. Kinetics of cisplatin treatments were studied on protein levels of PARP, p110α and pAKT by immunoblotting.

Phospho-serine 46, a critical modulator p53-*PIK3CA* interaction in resistant cells

Complete loss of serine 46 phosphorylation and concomitant absence of p53 binding to PIK3CA promoter indicates a critical role of phospho- serine 46 in controlling p53 binding to PIK3CA promoter. To test this we created two p53 mutant constructs, S46A (serine to alanine-mimics non-phosphorylated serine) and S46D (serine to aspartate-mimics phosphorylated serine) by site directed mutagenesis. The phosphorylation-deficient S46A mutant expression in SKOV3 (p53-deficient cell line) did not show any repressive effect on PIK3CA promoter, however, expression of phosphorylation-mimicking mutant S46D showed attenuation of PIK3CA promoter activity. Similar observations were also observed in A2780 and A2780-CisR, wherein only S46D but not S46A mimicked similar scenario as that of wild type p53. (Figure 2.19 A-D) This data indicated that serine 46 phosphorylation in p53 indeed plays role in p53-PIK3CA regulatory mechanism. To evaluate the impact of p53 acetylation in governing p53-PIK3CA promoter interaction, we created K5R p53 mutant construct, which mimics as an acetylation deficient mutant. Here, lysine residues at 5 positions as K370, K372, K373, K381, K382 were mutated to arginine which act as acetylation deficient p53. Intriguingly, the acetylation-deficient K5R mutant expression in SKOV3 (p53-deficient cell line) did not show any repressive effect on PIK3CA promoter. (Figure 2.19 E) Further, to validate, whether overexpression of p53 leads to constitutive phosphorylation and acetylation, we checked the phospho serine 15, 20 and 46 levels along with its acetylation status in A2780 cells. Ectopic expression of SN3-p53 (wild type p53-expression construct), S46A, and S46D constructs in SKOV3 cells primes their phosphorylation and acetylation. Since serine was replaced with aspartic acid (S46D) and alanine (S46A), the phospho-serine antibody specific for 46 residue could not detect these mutant p53. (Figure 2.19 F) In order to comprehend the cause of loss of p53 serine 46 phosphorylation in resistant cells, we evaluated levels of two

kinases known to play role in this phosphorylation. Homeodomain-interacting protein kinase 2 (HIPK2) and Dual specificity tyrosine-phosphorylation-regulated kinase 2 (DYRK2) are serine/threonine-protein kinases involved in regulation of variety of transcription factors including p53-mediated cellular apoptosis and regulation of the cell cycle. Immunoblotting with whole cell lysate demonstrated that cisplatin induced low level of HIPK2 and DYRK2 in resistant cells compare to sensitive cells. (Figure 2.19 G) Both kinases are reported to undergo MDM2/4 mediated proteosomal degradation and similar to p53, their levels get stabilised in stress condition. We observed that both HIPK2 and DYRK2 were stabilised in resistant cells upon cisplatin treatment but the degree of stabilisation or total amount was lesser than that of present in sensitive cells. While, specific kinases phosphorylate p53 at serine 15 and 20 in the cytoplasm, serine 46 phosphorylation happens only in nucleus. Hence, to evaluate the causality of loss of serine 46 phosphorylation in resistant cells, we assessed nuclear localization of HIPK2 and DYRK2. In addition to reduced levels of HIPK2 and DYRK2, cisplatin resistant cells showed increased cytoplasmic retention of HIPK2 and DYRK2. (Figure 2.19 I) Hence, absence of p53-serine 46 phosphorylation might be due to improper localization of HIPK2 and DYRK2, which ultimately affects ability of p53 to attenuate PIK3CA promoter in resistant cells. (Figure 2.19 J)
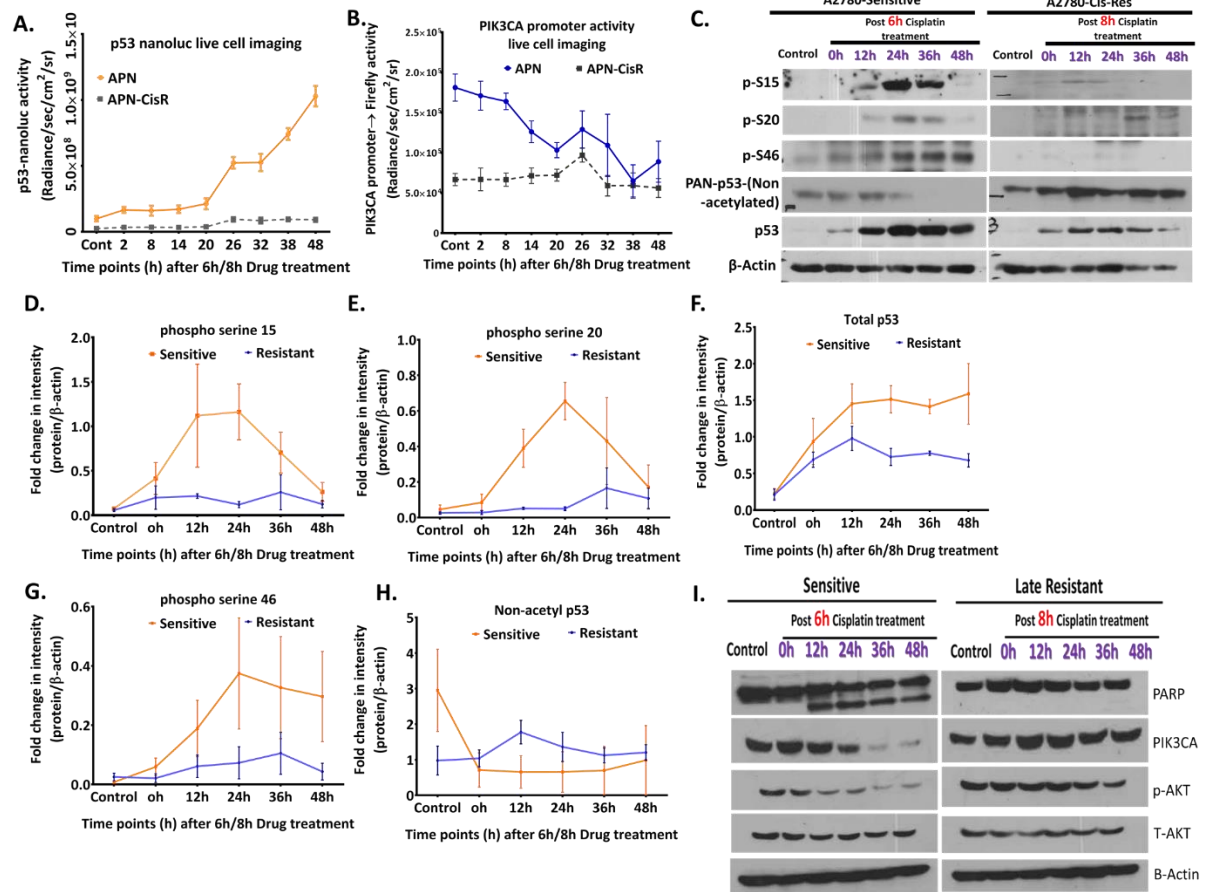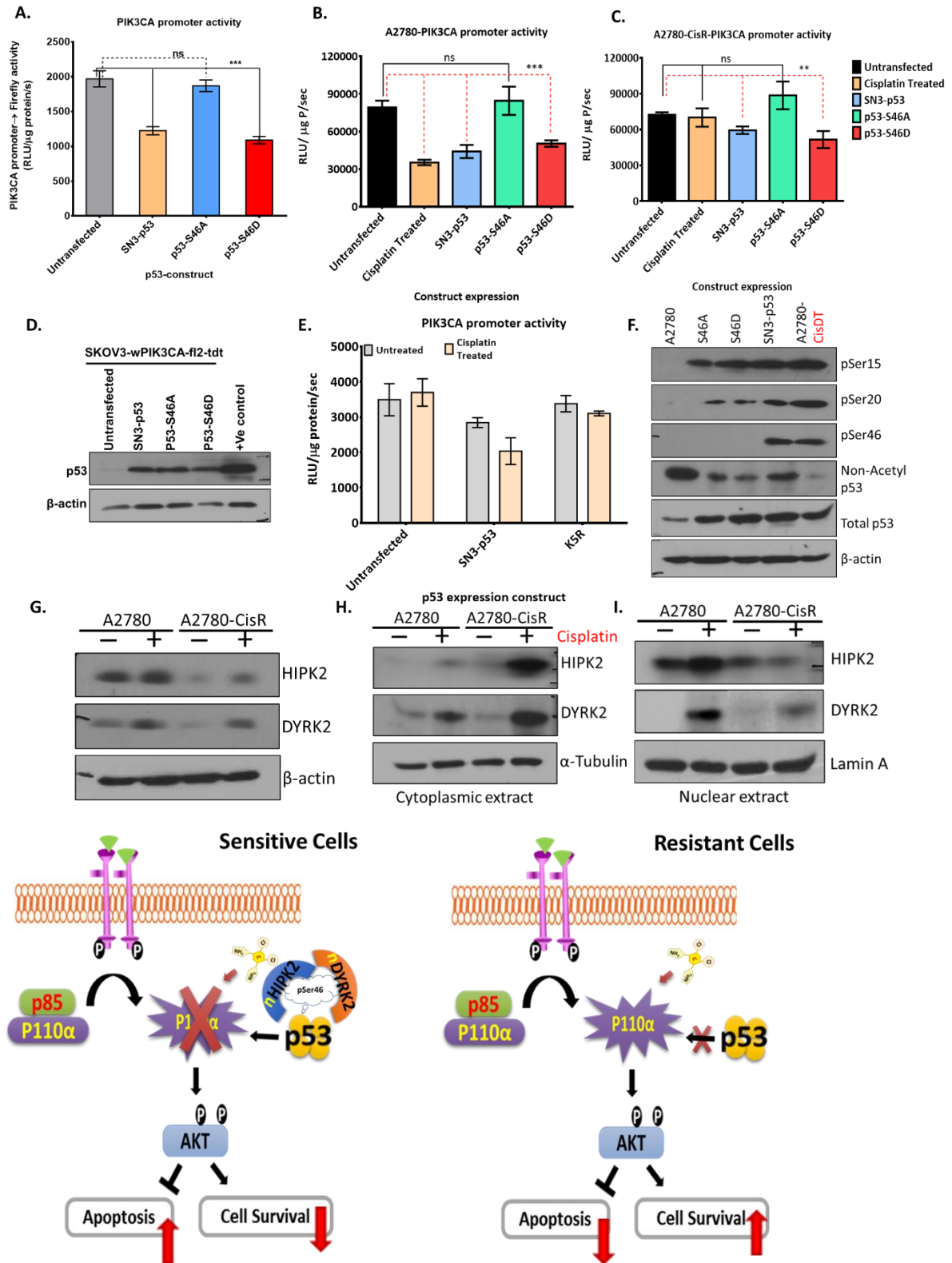
Figure 2. 19: Post translational modifications (PTM) in p53 are responsible for p53-PIK3CA promoter interaction dynamics.

A-C. Wild type p53 and p53 S46D over-expression but not p53 S46A reduces PIK3CA

promoter activity in SKOV3 (A), A2780 (B) and A2780-CisR (C) cell lines. D. Lower panel

depicts immunoblot showing expression of each of the p53 mutant construct in SKOV3 cell line. E. Expression of acetylation deficient p53 construct did not attenuated PIK3CA promoter activity. F. Immunoblotting showed differential phosphorylation at S15, S20 and S46 and differential acetylation in A2780 cell line upon overexpression of S46A, S46D and wild type (SN3-p53) construct. Cisplatin treated A2780 were used as positive control. G. Immunoblot analysis of HIPK2 and DYRK2 revealed reduced activation of both the kinases following cisplatin treatment in resistant cells compare to sensitive cells. H & I. Cellular fractionation revealed reduced level of nuclear localization and cytoplasmic retention of HIPK2 and DYRK2 was observed in resistant cells upon cisplatin treatment. J. Proposed mechanism of regulation of p53-PIK3CA promoter interaction in sensitive and resistant cells.

Effect of altered p53-PIK3CA interaction on downstream pathways in resistant cells:

To understand the consequence of altered p53-PIK3CA promoter interaction in resistant cells, we monitored various downstream targets of PI3K/AKT signalling cascade such as proliferation (P21, P27, CyclinD1, cMyc, β-catenin), protein synthesis (phosphorylation of S6 ribosomal protein), Pro-apoptotic (Bax) and Pro-survival (cFLIP, BCl2) after cisplatin treatment. Sensitive as well as resistant cell showed decreased phosphorylation of S6 ribosomal protein in response to cisplatin indicating a slower translation rate. (Figure 2.19 A) Resistant cells showed suppressed apoptotic machinery as evident by increased BCl2 and cFLIP, unaltered Bax, and loss of PARP cleavage level when compared to sensitive cells. (Figure 2.19 B&C) In response to cisplatin, only sensitive cells showed decreased level of Cyclin D1 and cMyc, but not resistant cells. (Figure 2.19 D&E) Hence, proliferation rate was severely affected only in sensitive cells but not in resistant cells. Interestingly p27- a regulator of G1 phase, showed 5-fold higher expression in untreated resistant cells and 9-fold

higher expression after cisplatin treatment. (Figure 2.19 F) Hence, resistant cells in response to cisplatin were able to evade apoptosis by inducing PI3K/AKT driven anti-apoptotic factor/s and decreased proliferation rate.
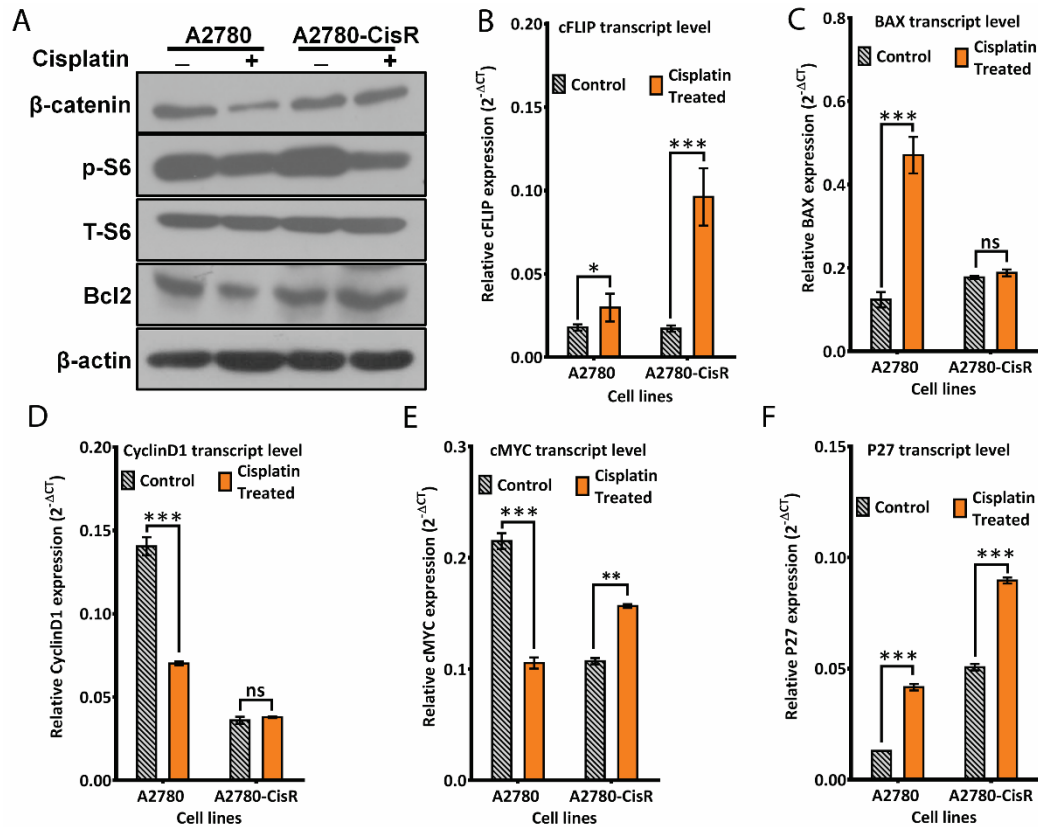
Figure 2. 20: Unaltered PI3K/AKT pathway aids resistant cell survival against cisplatin treatment.

A. Immunoblot analysis showed differential activation/repression of β-catenin, pS6, Bcl2 by cisplatin in sensitive and resistant cells. B-F. Real time PCR analysis showed differential activation/repression of cFLIP, BAX, CYCLIN-D1, cMYC and P27 expression after cisplatin treatment in sensitive and resistant cells. (n=3)

Clinically relevant mutation in p53 differentially regulates PIK3CA expression:

We elucidated the mechanism of how wild type p53 negatively regulates PIK3CA expression via its direct binding to the promoter in chemosensitive cells in presence of chemotherapeutic drugs. Such transcriptional ordinance was dictated by p53-PIK3CA promoter interaction as a result of p53 serine 46 phosphorylation, thereby suppressing PI3K/AKT cell survival pathway. Loss of p53 regulation on PIK3CA expression led to the activation of AKT, which assisted these cells to survive against chemotherapeutics. Our findings though made in cell lines showed a remarkable resemblance with clinical samples where increased activation of PI3K/AKT signalling is observed in p53 mutant HGSOC samples.[147] Mutation in p53 gene is a hallmark of 50% human malignancies including HGSOC. These samples revealed, mutations in p53 either in the form of substitution (missense) mutation, or non-sense, INDEL and frameshift mutations, which led to loss-of p53 wild type functioning.[300-302] However, there is no clear understanding whether a specific set of mutations are associated with PIK3CA/AKT signalling. We hypothesised that certain p53 mutations might possess differential regulatory effect on PIK3CA promoter that bestows upon tumor cells a proliferative advantage and help in tumor progression. Hence, to understand the relationship between mutant p53 and PIK3CA expression, we co-related publically available HGSOC patient dataset (n=316) for PIK3CA expression and associated p53 mutations. We divided the patient samples into two groups as 'high expressers' and 'low expressers' based on the median value of PIK3CA expression. Further, p53 mutational status and PIK3CA expression data was merged together using 'R-BIND' function with 'patient ID' as a reference point in R-program. In this study, we had excluded non-functional mutations (INDEL, splice variants and truncating mutations) as they did not express function p53. Remaining missense mutations were categorised into two major categories as 'PIK3CA regulators' and 'PIK3CA non-regulators' based on co-relation between mutant p53 and PIK3CA transcript along with

phosphorylated AKT status in ovarian cancer samples. (Figure 2.20 A-B) Summary of mutations belonging to these two categories is given in figure 2.20 C.

Next we generated two representative mutations from each group as R248Q, R273H (PIK3CA non-regulators category) and C176Y and Y220C (PIK3CA regulators). Stable expression of R248Q and R273C in p53-defecient SKOV3 cells did not reduce PIK3CA expression activity, while expression of C176Y and Y220C attenuated PIK3CA expression under cisplatin treatment. (Figure 2.20 D) Though R248Q and R273H belong to PIK3CA non regulator category, cisplatin treatment induced PIK3CA expression only in SKOV3 cells expressing R248Q p53 mutation while it remain unchanged in R273H expressing cells. Interestingly, only C176Y and Y220C mutants underwent p53 serine 46 phosphorylation after cisplatin treatment, which was absent in R248Q and R273C expressing SKOV3 cells. (Figure 2.20 E&F) However, cisplatin treatment induced phosphorylation of p53 at serine 15 and 20 for all four p53 mutants. Herein, with two exemplar p53 mutations, we demonstrated that different p53 missense mutations exert differential regulatory effect on the PI3K/AKT signaling based on their ability to acquire serine 46-phosphorylation status. Hence we believe that in clinical scenario, 'PIK3CA-non regulators' p53 mutations are addicted to PIK3CA signaling, which may mark their vulnerability towards PI3K inhibitor.

A. PIK3CA expression in Ovarian Cancer patients

B. AKT phosphorylation in Ovarian Cancer Patients

C.

p53 mutations													
PIK3CA regulators	<u>**Y220C**</u>	<u>**C176Y**</u>	V157F	H179R	G245S	H193R	G266R	G266V	K132N	V216M	V216M	C176F	R337C
Frequency	<u>**8**</u>	<u>**5**</u>	5	4	3	3	2	2	2	2	2	1	1
PIK3CA-Non regulators	<u>**R273H**</u>	R175H	<u>**R248Q**</u>	I195T	R248W	R282W	S241F	G245V	Y163C	Y234C	R273L	L194R	C238F
Frequency	10	8	8	7	5	5	4	3	2	2	2	2	1

D. PIK3CA transcript level

E. SKOV3 (p53-deficient cell line)

F.

GENE	R248Q		R273H		C176Y		Y220C	
	Control*	Cispaltin treated#	Control*	Cispaltin treated#	Control*	Cispaltin treated#	Control*	Cispaltin treated#
PIK3CA	↑↑	↑↑↑	↑↑	—	↑	↓↓	—	↓↓↓
P21	—	↑	↑↑	—	—	↑↑↑↑	—	↑↑↑↑
BAX	↑↑↑	↓↓	↑↑↑	—	↑↑↑	—	↑↑↑	—
PUMA	—	—	↑	—	↑	↑↑↑↑	↑	↑

*-Compare to wild type expression   #- Compare to control samples

Figure 2. 21: Mutant p53 exert distinct transcriptional regulation on PIK3CA promoter depending on its serine 46 phosphorylation.

A & B. Co-relation study with mutant p53 with PIK3CA transcript levels as well as phospho-AKT levels revealed two distinct classes of p53 as 'PIK3CA regulators' and 'PIK3CA non-regulators' in HGSOC patient data available with TCGA. C. Table representing frequency of each p53 mis-sense Smutation from both the catogories. From here we selected R248Q, R273H, C176Y and Y220C for further study based on their frequency. D. Modulation of PIK3CA transcript levels in SKOV3 cells (p53-deficient cell line) stably expressing individual p53 mutation. SKOV3 expressing p53 mutations C176Y and Y220C attenuates PIK3CA promoter activity similar to wild type p53, whereas SKOV3 cells expressing R248Q and R273H did not show such cisplatin responsive PIK3CA attenuation. E. Corroborating with PIK3CA transcript data, only C176Y and Y220C mutants underwent p53 serine 46 phosphorylation after cisplatin treatment, which was absent in R248Q and R273C expressing SKOV3 cells. F. Y220C and C176Y mutations escalated pro-apoptotic gene expression while R248Q and R273H lack such transcriptional activation of BAX and PUMA in response to cisplatin.S

2.4 Discussion:

Chemotherapy is one of the prevailing methods used to treat malignant tumors as they are effective against multiple tumor types.[23, 24] Though chemothrapeutic agents such as cisplatin, 5-fluorouracil, doxorubicin, camptothecin and paclitaxel differ in their mode of action, they target rapidly dividing tumor cells and kill them by inhibiting proliferation and/or inducing apoptosis. Platinum based therapeutics form the standard care of treatment for cervical, head and neck, non-small-cell lung, ovarian and testicular cancer; however, development of chemoresistance impedes success of therapy.[54-57] The essence of therapeutic success lies in the understanding how chemotherapeutics dictate cellular fate and translating this knowledge into development of innovative cancer therapeutics to overcome resistance. Molecular changes in tumor cell as a response towards a chemotherapeutic drug determines its fate. Cytotoxic damage induced by cisplatin forces platinum sensitive cells to proceed towards apoptosis as they lack activation of survival pathway. Deregulation of oncogenic signaling like MAPK/JNK/ERK, PI3K/AKT, NF-κB signalling, focal adhesion kinases and WNT signalling are the major cell-intrinsic molecular determinants that control and govern resistance.[183, 245] Among these, PI3K /AKT signalling cascade endows survival advantage against various therapeutics such as Adriamycin, paclitaxel, cisplatin, 5-fluorouracil, etoposide and camptothecin in multiple cancers including ovarian, breast and colon cancer.[148]

Ovarian cancer is the leading cause of mortality among patients suffering from gynaecological malignancies with high grade serous ovarian carcinoma (HGSOC) being the most frequent subtype. Due to its asymptomatic nature, only 15% of the patients are diagnosed in early stages, while most women remain undiagnosed until the cancer metastasizes resulting in poor prognosis and death.[156] Current clinical strategy for HGSOC management includes cytoreductive surgery followed by combination of platinum-taxol

based therapeutics for advanced stage disease. In spite of promising initial response of platinum based adjuvant therapy, most women succumb to the disease due to recurrence and chemoresistance. Apart from 18% PIK3CA amplification, 7% PTEN mutations and 3% AKT amplification, genetic alterations in components of PI3K/AKT signalling are rare in HGSOC.[133] Yet therapy resistant ovarian cancer displays 50% escalated AKT activity.[147] The TCGA data for HGSOC provisional set (n=316) revealed a total of 9% cases associated with PIK3CA transcript upregulation without any change in the gene copy number. Such incidences indicate alteration in levels of specific regulators and subsequent promoter regulation in the cancer cells. Little is known about these mediators of upregulated PIK3CA transcription and their role during acquirement of chemoresistance in ovarian carcinoma.

Chemotherapeutic agents like cisplatin and paclitaxel actives p53 which represses PIK3CA promoter in chemosensitive ovarian cancer cells.[269] Since little is understood about the overall mechanism of p53-PIK3CA interaction and influence of p53 upon transcriptional status of PIK3CA during cisplatin resistance, we attempted to explore the mechanism using different cell lines and acquired cisplatin resistant model developed indigenously in A2780 cells. With the help of various ovarian and breast cancer cell lines with varied p53 status (wild/ null) and platinum sensitivity status, we showed that binding of p53 at the four binding sites present in the PIK3CA promoter was drastically altered in resistant cells after cisplatin treatment. This alteration was associated with reduced PTM's (pS15, pS20, pS46 and acetylation) of the protein and altered expression of several vital genes involved in apoptosis, cell cycle and proliferation. Intriguingly, using an isogenic cisplatin resistant cell line, we found that the resistant cells not only exhibited altered binding of p53 but also a delayed kinetics of activation in a much lesser level and both these events were not sufficient enough to attenuate PIK3CA promoter activity. Using a dual reporter strategy, we for the first time

showed activation of p53 was associated with decreased PIK3CA expression after cispltain treatment from tumor xenografts bearing mice by real time optical imaging. The resistant tumor xenografts did show delayed p53 activation without any change in PIK3CA expression. Thus our data suggest that cisplatin resistant cells actively adapt a pro-survival fate by reduced PTM of p53 leading to altered binding to PIK3CA promoter.

As a response to chemotherapeutic drugs such as cisplatin, p53 gets stabilise and translocate to nucleus where it controls expression of various cellular determinants for cell cycle arrest and apoptosis[321-323]. A 900bp long PIK3CA promoter fragment containing four p53 binding sites was used to understand the influence of p53 activation upon PIK3CA in these cells. Corroborating with transcriptional induction, PIK3CA promoter activity was attenuated in cisplatin-sensitive but not in cisplatin-resistant cells. In fact, promoter activity increased at varied level in TOV21G and ZR-75-1 but not in SKOV3 cells. Since cells of different origin contain heterogeneous cellular milieu with various activated transcription factors that could influence the promoter activity differentially, we utilized an isogenic cisplatin-resistant cellular model developed in A2780 cells. Low level of p53 induction and unaltered PIK3CA promoter activity was found in A2780-cis-res cells after cisplatin treatment. Interestingly these resistant cells upon p53 overexpression exhibited PIK3CA promoter attenuation confirming abolished PIK3CA promoter modulation is due to loss of p53 ordinance. This was also consistent with intrinsic cisplatin resistant cell lines where TOV21G and ZR-75-1 shows low level of P21 activation compared to cisplatin sensitive OAW42, A2780 and MCF-7 cell lines post cisplatin treatment.

As a stress responsive molecule, p53 integrates signals from various stress induced signalling cascades, determines cellular fate towards growth arrest and apoptosis by differential transcriptional activity [324-326]. In order to understand the differential regulation of PIK3CA by p53 between sensitive and resistant stages, we critically analysed the influence of

each of the four p53 RE present on the promoter. Mutations at site 3 and 4 relieved cisplatin dependent promoter attenuation in sensitive (A2780 and OAW42) cells but not in A2780-cis-resistant cells. Deletion of site 3 and 4 (as in constructs OS1 and OS2) or promoter fragments carrying mutated site 3 and 4 (mOS3 and mOS4) abrogated the attenuation of the promoter in A2780 and OAW42 cells indicating an apparent preference of p53 towards site 3 and 4. Analysis by ChIP assay showed that p53 remained bound only to site 1 in sensitive unstressed cells but then moved to site 3 and 4 after cisplatin treatment. In contrary, low binding of p53 was observed to site 1, 3 and 4 in resistant cells without stress and binding was strengthened at site 1 after treated with cisplatin. Site 2, though was predicted as a p53 RE, didnot show any occupancy in any condition. Interestingly, similar trend of p53 occupancy to these REs were observed in OAW42 and MCF-7 (sensitive) and TOV21G and ZR-75-1 (resistant) cells pre and post cisplatin treatment.

Duration of stress is a critical factor for maximal induction of p53 which decides the fate of a cell. Using a dual reporter strategy and live cell imaging, we monitored the p53 activation and PIK3CA modulation in real time. Delayed initiation (6hr vs 8hr) and 4 fold of less induction of p53 in resistant cells by cisplatin were associated with lower levels of phosphorylation at S15/20 without any detectable pS46. PIK3CA expression simultaneously measured showed sharp decline by 14hr and continued to decline till 48hr. Interestingly, phosphorylation of p53S46 became evident from this time (14hr) which persisted till 48hr in cisplatin treated sensitive cells further proving that S46 phosphorylation is an important event for p53 mediated PIK3CA attenuation.

The altered dynamics of p53-PIK3CA promoter interaction in resistant cells showed a similar but delayed trend when measured from tumor xenografts of live mice in real time. This is the first report of imaging of p53 activation by cisplatin in live mice where significant induction in p53 was observed by day 1 after cisplatin treatment (Day 4 in the imaging sequence) which

continued till Day 5 (Day 8 in imaging sequence) with a 4-5 fold increase in p53-nanoluc activity in sensitive tumors. In contrary, only slight reduction in PIK3CA promoter activity observed by Day 1 but day 5, 4 fold reduction was evident. Reduction in tumor volume matched with PIK3CA expression indicating massive apoptosis occurring in these tumors. Though cisplatin showed an immediate effect on PIK3CA promoter attenuation in cell culture (14-16hrs), the effect was less prominent during the initial phase *in vivo* probably due to drug metabolism and different pharmacokinetics. In cisplatin treated resistant tumors, p53 induction was negligible by Day1 and achieved only 3 fold higher at Day 5. PIK3CA promoter activity and tumor volume remained stable over five days for this group. It seems that cisplatin though could not induce apoptosis in these resistant tumors but was still able to induce a growth arrest which was also supported by up regulated p27 and down regulated CyclinD1 expression.

Phosphorylation of S46 residue in p53 is an obligatory event in RITA induced apoptosis [327] which also requires simultaneous inhibition of PIK3CA and IGF1R oncogenes and activation of pro-apoptotic genes [328]. Phospho-S46 (under cytotoxic stress) induces a subtle change in p53 conformation and a stronger affinity for apoptosis-related genes (*BAX, PIG3*, and *p53AIP1*) [273, 274, 294]. Our results also demonstrated loss of serine 46 phosphorylation and abolished PIK3CA promoter attenuation in resistant cells. Hence, to comprehend the association between serine 46 phosphorylation and PIK3CA promoter attenuation, we developed two p53 mutations as phosphorylation-mimicking mutant S46D (serine to aspartate) and phosphorylation-deficient mutant S46A (serine to alanine). The phosphorylation-deficient S46A mutant did not show any repressive effect on PIK3CA promoter in SKOV3 (p53 deficient) cells while S46D attenuated PIK3CA promoter activity. To investigate causality of loss of serine 46 phosphorylation in resistant cells, we studied levels and nuclear localization of its kinases HIPK2 and DYRK2. As expected both kinases

HIPK2 and DYR2 showed reduced levels and cytoplasmic retention, which hinders p53 serine 46 phosphorylation in resistant cells after cisplatin treatment.

Cisplatin induces several pro-apoptotic pathways downstream p53 signalling cascade which are countered by survival pathways such as PI3K/AKT, MAPK pathways. Balance between these Pro and anti-apoptotic pathways determines cellular fate towards survival or cell death. Alteration in these signalling cascades leads to drug failure hence Chemoresistance. In sensitive scenario, DNA damage as a consequence of cisplatin treatment induces cell cycle arrest by induction of P21 and p27 levels. DNA damage, if not rectified leads to apoptosis through induction of pro-apoptotic genes such as Bim and Bax induction and suppression of anti-apoptotic genes such as BCl2and cFLIP. Whereas in case of resistant cells, cells underwent growth arrest similar to sensitive cells but evades apoptotic stimuli by inducing pro-survival molecules. Rather quiescence state achieved due to growth arrest help these cells to overcome drug induced damage.
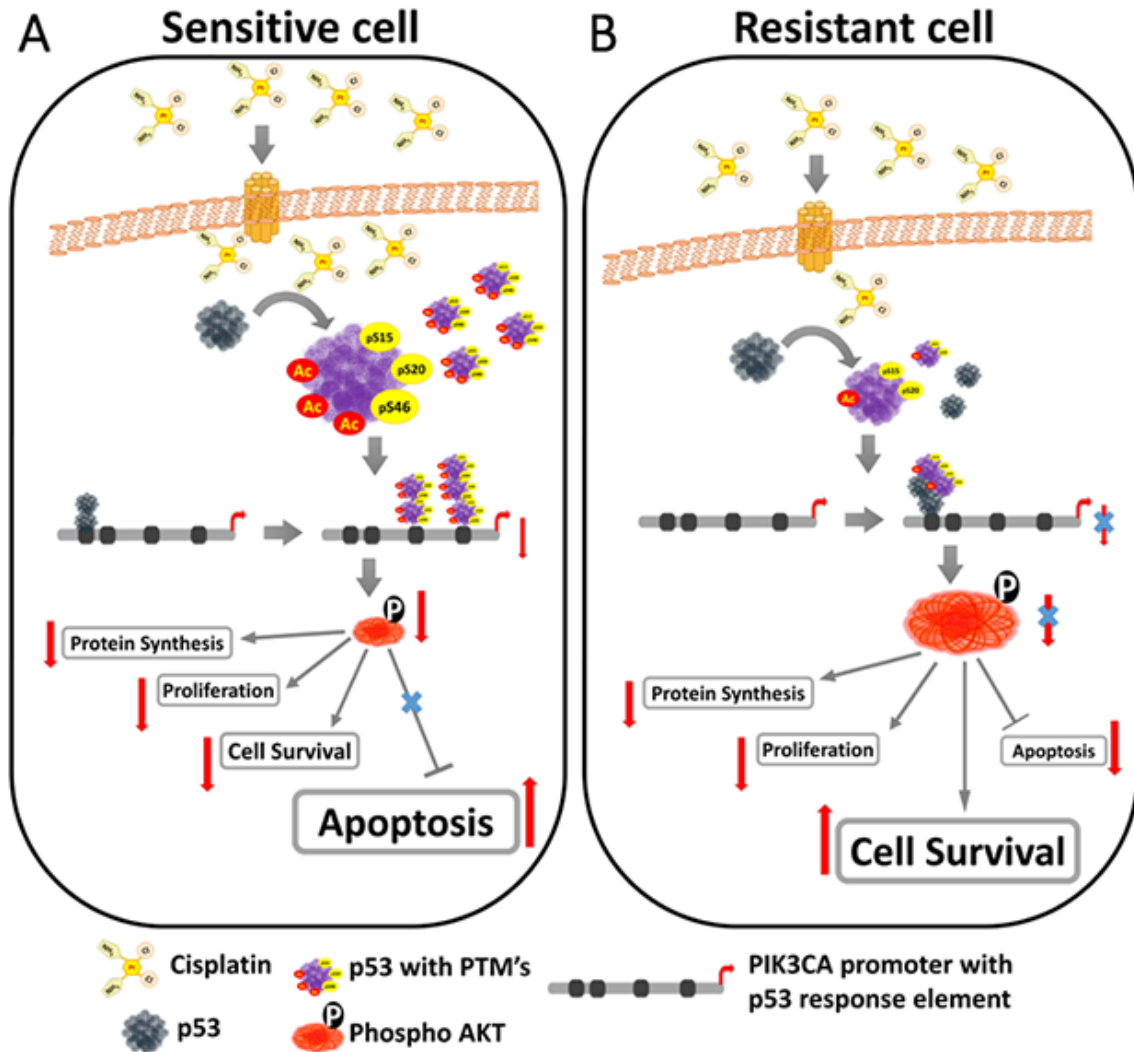
Figure 2. 22: Proposed model of p53 mediated PIK3CA regulation during stress.

A. In sensitive cell, cisplatin activates p53 via PTM's (acetylation, phospho-S15, phospho-S20 and phospho-S46) which alters p53 binding preference from binding site 1 to site 3 and 4 present on PIK3CA promoter. Altered p53-PIK3CA promoter interaction leads to PIK3CA attenuation and subsequently reduced AKT phosphorylation. Under these circumstances, cells experience reduced protein synthesis, survival and proliferation and up-regulation of apoptotic machinery. B. In contrary, resistant cells in response to cisplatin acquire a 'sensitive like' state in terms of p53-PIK3CA promoter interaction (occupancy only at site 1) and show reduced S15, S20 phosphorylation and acetylation with complete loss of pS46. Such p53-PIK3CA promoter interaction is insufficient to decrease PIK3CA transcript level

hence AKT phosphorylation remain unchanged. Under such condition, cells overcome the damage caused by cisplatin via active PI3K/AKT pathway and adapt an arrested state by down regulating apoptotic machinery.

Herein, we demonstrated that, wild type p53 negatively regulate PI3K/AKT signaling upon phosphorylation at serine 46 residue, which is absent in cisplatin resistant cell. However in clinical scenario, HGSOC demonstrated p53 gene mutations as a hallmark event. The quest of alternative treatment for ovarian cancers prompted a comprehensive genomic analysis through The Cancer Genome Atlas (TCGA) project, with the goal of identifying 'drugable' genetic abnormalities.[133] However, other than 96% of p53 mutations, mutation in HGSOC is a rare event. Many clinical studies have attempted to correlate the presence of a p53 mutation with patient survival or the development of chemoresistance.[147, 329-331] However, the conclusions of these studies are conflicting, majorly due to universal categorisation of mutant p53 into single group. Rather, the spectrum of mutations in p53 is extremely diverse, and a few particular mutations can actively promote oncogenesis. Moreover, studies on ovarian cancer cell lines [96, 149] and clinical studies [147, 332] demonstrated hyper-active PI3K/AKT pathway that contributed to therapy resistance. Hence, we hypothesize that certain p53 mutations are associated with loss of serine 46 phosphorylation and thereby favouring activation of PI3K/AKT survival signaling.

A well-established classification system categorised hot-spot p53 mutation as contact mutations (R273H, R248W, and R248Q), or conformational (structural) mutations (R175H, Y220C, G245S, R249S, R282W, etc), both of which theoretically interrupt wildtype p53 functionality. However, our analysis revealed unusual categorisation clinically relevant p53 mutations as 'PIK3CA regulators' and 'PIK3CA non-regulators'. As expected, patients with

'PIK3CA non-regulator' category are associated with higher activation of PI3K/AKT signaling compare to mutations from 'PIK3CA regulators' category. Though classical grouping put R248Q, R273H, C176Y, and Y220C mutation into non-wild type p53 category, we demonstrated that these mutations exert differential activity on PIK3CA promoter. Both C176Y and Y220C (PIK3CA regulators) exert wild type p53 activity and attenuate PIK3CA promoter upon chemotherapeutic agent. As expected other two mutations, R248Q, R273H (from PIK3CA non-regulators category) does not attenuates PIK3CA expression. In corroboration with our wild type p53-PIK3CA promoter dynamic, only C176Y and Y220C undergo phosphorylation at serine 46 residue but not R248Q and R273H. Importantly, we found that the p53 mutations on R248Q and R273H escalated PIK3CA expression compare to C176Y, Y220C and wild type p53, which corroborates with clinical scenario of association of activated AKT in PIK3CA-non regulator category. Interestingly, in response to cisplatin, R248Q exerts additional GOF activity, which increased PIK3CA expression even further. In summary, we provide a novel classification of p53-hotspot mutations in ovarian cancers, and their potential of R248Q/R273H in activation of PI3K/AKT survival pathway.

Altogether, our data suggest that genotoxic drug induced stress leads to downregulation of PI3KCA/AKT signalling through site specific recruitment of activated p53 in PIK3CA promoter. This recruitment is probably driven by S46 phosphorylation, which is lost in cisplatin resistant cells. Our study thus indicates S46 phosphorylation as a modulator of p53 binding for PIK3CA, an important cell survival gene. Detail mechanism of this modulation requires further investigation. Accumulation of cisplatin in drug resistant cells favours a quiescent, arrested growth, which is probably mediated by sub optimal binding of p53 to PIK3CA promoter. Increased expression of endogenous PIK3CA gene in resistant cells indicates another level of regulatory network involving sequences upstream to 900bp of transcription start point. In addition, we provided additional categorisation of clinically

relevant p53 hotspot mutation such as R248Q and R273H, which exert inadequate regulation on PIK3CA attenuation due to absence of serine 46 phosphorylation and activate PI3K/AKT signaling. We believe such PIK3CA-non regulatory p53 mutations associated with hyper-activated PI3K/AKT signaling can potentially be targeted through PIK3CA inhibitor. In addition, the unique in-vivo model of simultaneous monitoring of p53 activation and PIK3CA promoter modulation in real time developed in this study may be extended to other important p53 targets and in drug discovery research.

Chapter 3:
To identify novel interacting partners for PIK3CA promoter in

acquired chemoresistance.

Chapter 3: Novel regulators of PIK3CA promoter

To identify novel interacting partners for PIK3CA promoter in acquired chemoresistance.

3.1 Introduction

Therapy resistance is the major obstacle in clinical management of cancer. [21, 156, 183] Though, cytotoxic agents aimed to inflict DNA damage in proliferating cancer cells are the most commonly used cancer treatments, development of chemoresistance impedes its therapeutic efficiency. [59, 183] Well-established mechanisms that underpin the different routes to drug resistance in tumor cells, include drug export, augmented drug metabolism, and/or defects in signaling pathways that respond to the damage induced by cytotoxic chemotherapies.[58, 183, 260] Molecular changes in tumor cell as a response towards a chemotherapeutic drug determines its fate. The emerging concept states that, depending on cellular milieu the survival–death switch is turned on or off as a response by chemotherapeutic agent. The phosphatidylinositol 3-kinase (PI3K)/AKT signaling pathway is pivotal to several cellular processes including cell cycle progression and survival. [115, 116, 148, 261] Aberrant activation of this pathway has been widely implicated in many cancers, and increased activity of this pathway is often a hallmark of resistance to conventional treatment modalities. [131, 132] In addition, increased activation of the PI3K pathway is crucial to cancer cell survival under the stressful tumor environment of limited nutrients, oxygen, and reduced pH. [133, 134] For these reasons, PI3K pathway has emerged as a potential target in cancer treatment.

In many cancers, activation of PI3K/AKT, a key survival pathway contributes to tumor growth, metastatic competence, and therapy resistance.[115, 116, 261] Constitutive

activation of PI3K/AKT can result from the distinct and/or complementary biological events. These alterations include (i) constitutively active receptor tyrosine kinases (for example, activating mutations in EGFR or amplification of HER2) (ii) amplification of PI3K, (iii) presence of activating mutations in the PIK3CA gene encoding the p110a catalytic subunit, (iv) mutations in p85 regulatory subunit, (v) overexpression of the downstream kinase AKT; or (v) loss or inactivating mutations of the tumor suppressor gene PTEN. [93-95, 133, 134] These alterations trigger a cascade of biological events, from cell growth and proliferation to survival and migration, which drive tumor progression. In addition, activated AKT induces upregulation of anti-apoptotic proteins such as X-linked inhibitor of apoptosis (XIAP), BCL2, IAP, and survivin as a response towards cisplatin, paclitaxel, and etoposide conforming resistance against these drugs. [194-196, 333] Also, AKT phosphorylates BCl2 family members, FOXO3a, and MDM2. [334] Phosphorylation of BCl2 family such as Bad at Ser136[335, 336], Bax at Ser184[337], and Bim (EL) at Ser87[338] decrease their ability to hold mitochondria in an open configuration, and thereby reduce cytochrome C release. Phosphorylation of FOXO3a sequesters FOXO3a in the cytoplasm and supresses the expression of its target pro-apoptotic genes, such as Fas ligand, Bim and tumor necrosis factor-related apoptosis-inducing ligand (TRAIL).[139] MDM2 phosphorylation at Ser166 and Ser186 enhances p53 ubiquitination and degradation, reducing p53-mediated cell death.[339] Therefore, activation of PI3K/AKT pathway is one of the key regulator of survival of tumor cells to conventional cytotoxic and targeted anticancer therapies. PI3K/AKT cascade is associated with resistance against chemotherapeutics like cisplatin, doxorubicin, paclitaxel, 5-flurouracil, etoposide and camptothecin.[148]

Platinum-based therapeutics such as cisplatin or carboplatin forms the standard care of treatment for cervical, head and neck, non-small-cell lung, ovarian and testicular cancer, however, development of chemoresistance impedes success of therapy.[156, 183] Cisplatin

exerts its cytotoxic effect through DNA damage, oxidative and endoplasmic stress, which activates program cells death in sensitive cells. In addition, cisplatin modulates several signalling cascade including c-ABL, p53 signaling, MAPK/JNK/ERK, PI3K/AKT, NF-κB signalling, focal adhesion kinases and WNT signaling.[58, 183, 260]. Cisplatin resistance is a net effect of multiple mechanisms that either inhibit apoptosis, promote cell survival, or both. Activation of p53, c-JUN drives cells towards apoptosis, while PI3K/AKT, WNT signaling promote cell survival. Among these factors, nuclear Factor-kappa B (NF-κB) has been identified as one of the key players in resistance mechanisms regulating expression of genes involved in the various cellular processes.[340] A variety of stimuli coalesces on NF-κB activation, which can in turn mediate varied transcriptional programs. The IKK/NF-κB regulatory network controls a plethora of genes associated with inflammation (TNF, IL-6, and ICAM), cell survival (cIAP1/2, BCl2, and Bcl-xL), proliferation (CDK2), tumor progression (COX2), angiogenesis (VEGF), and apoptosis (Fas and FasL).[79, 341] NF-κB mediated upregulation of cFLIP, Bcl-XL, XIAP supress apoptosis, through which NF-κB favours survival of cisplatin resistant cells.[342-344] NF-κB-dependent transcription is not only tightly controlled by positive and negative regulatory mechanisms but also closely coordinated with other signaling pathways. In response to extracellular signals, a number of receptor tyrosine kinases can activate NF-κB via the PI3K/AKT or JNK/STAT pathway.[345] In previous chapter, we have demonstrated that phosphorylation of p53 at serine 46 accelerates p53-PIK3CA promoter interaction under cisplatin treatment. This interaction attenuated PIK3CA expression and PI3K/AKT mediated survival cascade thereby imposing sensitive cells towards apoptotic fate.[346] However, absence of p53 serine 46 phosphorylation in resistant cells hinders recruitment of p53 to site 3 and 4 on PIK3CA promoter. Rather, cisplatin mediates upregulation of PIK3CA expression in cisplatin resistant cells. Such transcriptional induction of PIK3CA primes activation of PI3K/AKT axis, which

up-regulates anti-apoptotic genes (cFLIP and Bcl2), cell-cycle arrest genes (p21, p27) and unaltered proliferation (CyclinD1). This cellular ambiance promotes a growth arrested and apoptotic resistant state in cisplatin resistant cells favouring survival against cytotoxic action of cisplatin.[346] Therefore, drug-induced transcriptional induction of PIK3CA might be one of the key mechanism that controls activation of PI3K/AKT in resistant cells. Though lack of attenuation in PIKCA promoter by cisplatin in platinum-resistant cells is indicative of loss of p53's repressive action, it does not explain the observed increase in PI3K expression and points toward a second level of regulation for this critical gene and associated signalling. However, regulators of such cisplatin-mediated PIK3CA upregulation expression in chemoresistant cells have not been investigated so far.

In addition to RTK mediated activation, PIK3CA gene is regulated by a few conspicuous transcription factors (p53, NF-κB, Foxo3A, YB-1) in chemosensitive tumor cells, however, whether such regulation exists or gets altered in chemoresistant cells particularly in response to chemotherapeutic drugs, is less explored. Cisplatin-induced stress differentially activates several transcription factors like p53/p73, Myc/Max, YB-1, CTF2, ATF4, ZNF143, mtTFA, Oct1, NF-κB and Sp1 which dictate cellular response towards damage. [23] YB-1 upregulates expression levels of MDR1, cyclin A/B1, TopoIIa, Fas, PTP1B, and GPX1 genes.[347-349] Both, GPX1 and MDR1 enhance cisplatin detoxification and extracellular export. Additionally, ATF4 induces expression of other transcription factors ZNF143 and CHOP, which participates in ER stress-induced gene expression and transactivation.[350, 351] Oct1 transcription factor is induced upon treatment with UV irradiation and anti-cancer agents, including cisplatin, which escalates expression of V-ATPase c subunit gene and HMG2 gene expression.[347, 352-354] V-ATPase regulates the modulation in intrinsic pH and supress necrosis, while HMG2 is involved in enhanced DNA repair.[347, 351] However, other than

NF-κB and YB-1 protein, whether these cisplatin-induced transcription factors escalate PIK3CA expression is not known.

Chemoresistance is a multifactorial phenomenon, governed by molecular changes within a cell and/or external stimuli. While molecular alteration in signaling cascade/s aid in acquirement and maintenance of resistance, a small fraction of inherently resistant cancer stem cells help in repopulating chemo resistant tumor. Due to intrinsically resistant nature, cancer stem cells are thought to be the prime culprit for therapy failure and tumor relapse. [184-186] Hence, in this part of the study, we majorly focused on how upregulation of PIK3CA influences survival of cancer stem cell. CSCs are a small fraction of heterogeneous tumor population identified by surface markers like CD34+/CD38- (AML) [199], ESA+CD44+CD24-/low (breast cancer) [200] as well as phenotypic markers such as side population (SP) or aldehyde dehydrogenase (ALDH) activity, which accounts for metastasis, relapse and therapy resistance. [201, 202] The clinical course of ovarian cancer, good initial response rates followed by high rates for relapse and the development of chemotherapy resistant disease, is consistent with the cancer stem cell model. The cellular hierarchy model describes cancer stem cells (CSC) on the top of the hierarchy and are the intrinsically resistant population which can self-renew or differentiate to non-CSC, hence responsible for initiation of disease and relapses.[164] Though relationship between CSCs and chemoresistance is well established, the key molecular events involved in the regulation of CSCs remain largely unknown. Till now differential activation of PI3K/AKT, WNT, NOTCH and NF-κB signaling are linked to maintenance of CSC phenotype and chemoresistance. [59, 355-357] Activation of WNT/β catenin pathway maintains resistance against Adriamycin and 5-FU in OV6+ HCC cancer stem cells. [358] Similarly, activated NF-κB signaling confers chemoresistance against paclitaxel and carboplatin in CD44+ ovarian CSCs and breast cancer cells. [359] Inhibition of NF-κB by Eriocalyxin B or disulfiram and copper sensitizes these

CSCs towards paclitaxel in Ovarian and Breast cancer cells. [360] Further Ma et al, (2008) demonstrated that chemotherapeutic drugs Adriamycin and 5-FU upregulate BCl2 family proteins in CD133+ colon cancer stem cells via activation of PI3K/AKT pathway. [141] However, regulators of PI3K/AKT signaling in chemoresistance and its impact on CSC's population have not been investigated so far.

In the present study, we aim to understand the mechanism of cisplatin mediated PIK3CA upregulation in cisplatin resistant cells and its impact on cancer stem cells.

3.2 Material and Methods

DNA-protein pulldown and nLC-MS analysis:

OS4-PIK3CA deletion construct (~340bp) was biotinylated by PCR amplification using 5'-biotin -labelled primers. DNA-protein pulldown was performed as described earlier (Drewett et al, 2001). (Figure 3.1) Briefly, biotinylated promoter fragment (200 pmol/mg of beads) was equilibrated with Dyanbead-streptavidin beads in buffer A (5 mM Tris pH 8.0, 0.5 mM EDTA, 1 M NaCl). Efficiency of biotin labelling was performed and quantified using dot-blot method. (Figure 3. 2 A&B) DNA-Dynabead complexes were blocked with 0.1% BSA and ssDNA in buffer C for 15 min. In parallel, nuclear protein extract from A2780-CisR cells pre- and post- cisplatin treatment was collected according to protocol described earlier. Further, DNA-Dynabead complexes were incubated with 300μg of nuclear protein extract in buffer C (20 mMTris pH 8.0, 1 mM EDTA, 10% glycerol, 1 mM DTT, 50 mMNaCl). These complexes were washed with buffer C, three times and DNA bound protein fraction was eluted with 0.1%SDS solution. Eluted protein mixture was digested with trypsin (in-solution digestion method) and subjected to Triple TOF 5500+ nano-LC-MS for acquiring peptide spectra. (Figure 3. 2 C)
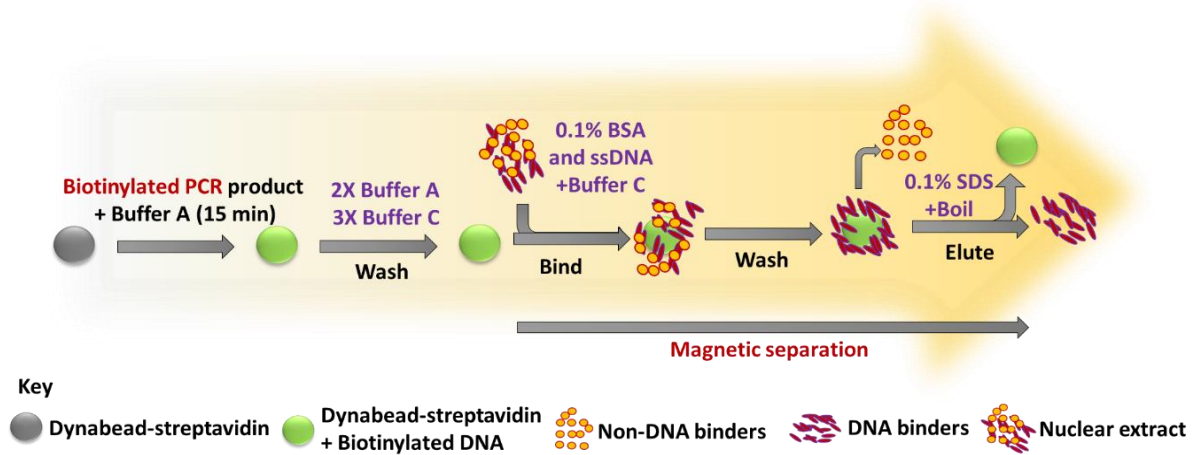
Figure 3. 1: Schematics of DNA-bound protein pull down using Dynabead-streptavidin magnetic beads.
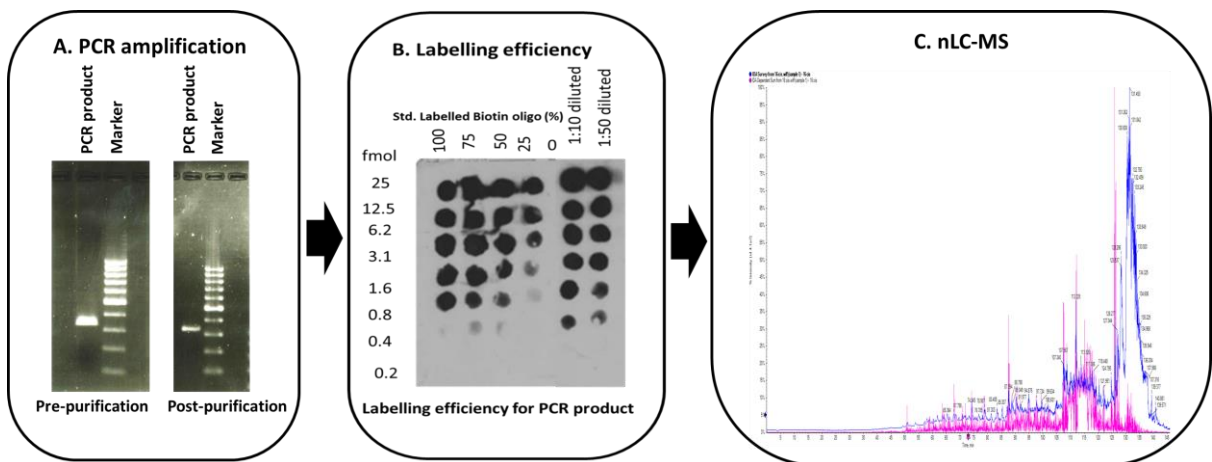
Figure 3. 2: Quantification of biotin labelled DNA and nano-LC-MS run.

A. Agarose gel image of PCR run using biotinylated oligo demonstrating amplification of OS4-PIK3CA promoter fragment (340bp) pre- and post- PCR clean up step. B. Representative Dot blot of biotin standard and labelled oligos showing labelling degree of biotinylation in PCR product. Both, biotin standard and biotinylated PCR product was dot blotted on nylon membrane and probed with HRP-labelled streptavidin. C. Representative chromatogram of nano-LC-MS run performed for 145 min.

Data analysis and candidate selection:

Significant protein candidates from the acquired mass spectra were identified using protein pilot software at 0.01% false discovery rate (FDR) and p=0.05 significance level. In each run, proteins associated with common 'biological' and 'molecular' processes were identified with GSEA server (http://software.broadinstitute.org/gsea/index.jsp). These common processes were identified for both independent biological replicates from pre and post cisplatin treated resistant cells (A2780-CisR). Only protein signatures associated with 'transcription factors and associated protein's were used for gene family overlap and pathway analysis via GSEA and Reactome server respectively. Functional overlap between control and cisplatin treated samples were computed with R-program. Transcription complexes identified exclusively in the cisplatin treated cells were used for further validation.

Promoter activity of PIK3CA promoter constructs:

Renilla (RL), Firefly luciferase (FL) and β galactosidase (β-gal) activities were measured using their respective substrates in a Berthold luminometer as described previously (Thakur et al, 2016). Detailed protocol for measurement of PIK3CA promoter activity was given in Appendix-Material and methods. All transfection experiments were performed in triplicates and repeated at least twice.

Chromatin immune precipitation (ChIP):

ChIP was performed as described earlier with few modifications (Garufi and D'Orazi, 2014). Briefly, 8x105 cells were cross linked with 0.75% formaldehyde and sonicated in lysis buffer (50mM HEPES-KOH pH7.5, 140mM NaCl, 1mM EDTA pH8, 1% TritonX 100, 0.1% SDS, 0.1% Sodium Deoxycholate, proteinase inhibitor) to obtain an average of 1000bp. 400ng chromatin was precipitated with NF-κBspecific antibody and DNA is eluted post reverse-

crosslinking. Non-immunoprecipitated chromatin was used as total input control. Further ChIP-DNA was analysed with semi-quantitative PCR using PIK3CA promoter primers.

Isolation of Side population:

Side and Non Side population cells are sorted as described earlier (Singh et al 2016) using Dye Cycle Violet (DCV) dye (Invitrogen) and BD FACS Aria with violet laser. Membrane drug transporter inhibitor Verapamil (50µM, Sigma) was used as negative control for gating. Data analysis was performed using DIVA software.

Immunofluorescence:

Immunofluorescence studies were performed as described earlier (Gaikwad et al., 2015) Briefly, cells plated on coverslips were fixed with 4% paraformaldehyde, permeabilized with 0.025% Triton-X and probed with NF-κB and OCT4 antibody for overnight at 4^0C. Next day, after two hours of incubation with secondary antibody, cells were counterstained with DAPI and images were observed under Carl Zeiss, LSM 710 microscope. At least 100-150 from five representative fields were quantified for NF-κB, Oct4, and DAPI staining.

Statistical analysis:

Data represents the mean $\pm$ SD of at least three independent experiments and were analysed as a biological replicates for significance using unpaired Student's t test. P value ≤ 0.05 was considered as significant.

3.3 Results:

Cisplatin treatment augments PIK3CA expression in platinum resistant cells:

In previous chapter, it was observed that treatment of cisplatin induced around 2 fold escalation of PIK3CA expression in three different platinum resistant cells (A2780-CisR, TOV21G and SKOV3) (Figure 3. 3A) due to loss of p53 binding at vital p53-RE in PIK3CA promoter. We therefore hypothesized that in absence of p53 regulation, cisplatin might induce other unidentified regulator/s, which escalate PIK3CA expression. Hence, to identify potent transcription regulators for PIK3CA promoter, initially we adopted transcription factor predictive approach through JASPER server. Transcription factor prediction with JASPER software revealed presence of 451 binding sites of known transcription factors on PIK3CA promoter. A few potential regulators for PIK3CA promoter like NF-κB, Hif-1α were already mentioned in literature (Astanehe et al 2009, Yang et al 2010). Hence, we used CoCl2 as an inducer for Hif-1α to study role of Hif-1α in PIK3CA promoter modulation. However, no significant PIK3CA promoter modulation was observed upon Hif-1α treatment. (Figure 3.3 B&C) Analysing the entire array of predicted transcription factor binding (~451) sites would not be feasible. Hence, to elucidate complex PIK3CA regulation as a response toward chemotherapeutic agent in resistant cells, we adopted promoter (DNA)-binder (protein) pull down strategy for identification of novel regulators.

Since pull down of whole length PIK3CA promoter (1kb) binders was not feasible due to obvious multi-target complexity, a smaller length PIK3CA fragment was used for DNA-protein pull down study. To select small fragment of PIK3CA promoter with optimal activity, promoter activity of PIK3CA deletion constructs containing single p53 response element were transiently transfected in cells with appropriate normalization vectors (Figure 3. 3D). The 3' PIK3CA deletion construct i.e. OS4-PIK3CA (340bp) augmented promoter activity in both sensitive A2780 and platinum resistant A2780-CisR cells (Figure 3. 3E). Interestingly

increase in promoter activity is more significant in A2780-CisR (2.6 fold) compared to

A2780 (1.4 fold). Other platinum resistant ovarian cancer cell lines TOV21G and SKOV3

also showed an increase in OS4-PIK3CA promoter activity (1.5-2.4 fold) compared to whole

length promoter (Figure 3. 3F). OAW42, a platinum sensitive cell line demonstrated only 1.5

fold increase in promoter activity, similar to A2780. Hence, OS4-PIK3CA deletion construct

of PIK3CA promoter was used for the pull down of promoter interacting factors.
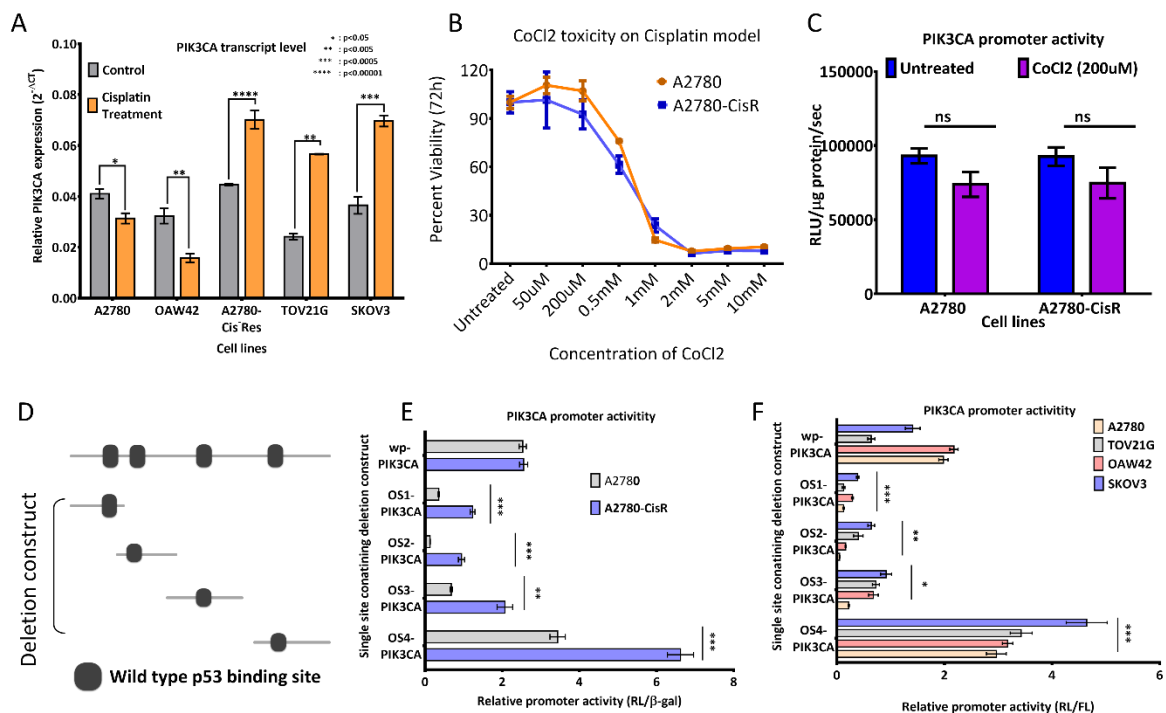
Figure 3. 3. 3: Identification of regulatory region on PIK3CA promoter.

A. *Cisplatin induced PIK3CA expression in cisplatin resistant cells (A2780-CisR, SKOV3*

and TOV21G), while PIK3CA expression was decreased in cisplatin sensitive cells (A2780

and OAW42) ***B.*** *MTT assay showing viability of A2780 and A2780-CisR cells against range*

of cobalt chloride (CoCl2) concentration. Non-toxic 200μM concentration was used for

studying PIK3CA promoter modulation. ***C.*** *Treatment of CoCl2 did not display PIK3CA*

promoter modulation in both sensitive (A2780) and resistant (A2780-CisR) cells. ***D.***

Schematic representation of PIK3CA promoter deletion constructs containing single p53

response element. ***E.*** *Deletion construct containing site 4 but not site 1, 2 & 3 showed*

augmented PIK3CA promoter activity compare to wild type PIK3CA promoter activity in A2780 and its cisplatin resistant counterpart A2780-CisR after transient transfection. **F.** *Only site 4 containing deletion construct showed augmented PIK3CA promoter activity compare to wild type PIK3CA promoter activity in A2780, OAW42, TOV21G and SKOV3 cells after transient transfection*

Identification of PIK3CA promoter interacting partners in platinum resistant cell line:

To identify novel interactors of PIK3CA promoter, biotin labelled OS4-PIK3CA (340bp) promoter fragment was used as bait for pull down of proteins (potential transcription factors). PIK3CA promoter binding proteins were isolated from A2780-CisR cells (control or cisplatin treated) by incubating nuclear extracts from respective cells with Biotin labelled OS4 PIK3CA promoter through streptavidin coupled Dynabeads and processed for nano-scale liquid chromatographic tandem mass spectrometry (nLC-MS/MS). Resultant MS/MS spectra were matched with human protein database (Homo sapiens) with protein pilot and Mascot server. Analysis of MS/MS spectra revealed 312 and 246 proteins in two biological replicates of cisplatin treated A2780-CisR cells, and 863 and 339 proteins in their untreated counterparts.

Further, obtained protein identities from two independent replicates of untreated or cisplatin treated A2780-CisR cells were clustered with GSEA-server based on their 'GO- biological and GO- molecular' functions.(Figure 3. 4A-C) A 0.01% false discovery rate (FDR) was pre-determined for clustering analysis. This functional classification of identified commonality within two independent samples and revealed 136 (untreated A2780-CisR) and 120 (treated A2780-CisR) protein signatures comprised of transcription factors, co-factors and general transcription assembly proteins. As our study focused on identifying transcriptional

regulator/s, only transcription associated factors were considered for further analysis. Protein overlap analysis using VENN 2.1 sever between control and cisplatin treated A2780-CisR cells revealed 67 common binders (36% of total binders) which comprised of general transcriptional assembly proteins including RNA-polymerase II subunit, PCNA and EP300. (Figure 3. 4D) A gist of these identified proteins/complexes is represented in Figure 3. 4E. Apart from the overlapping protein signatures we identified an exclusive set of 69 (36.4% of total identified binders) and 53 (27.7% of total identified binders) PIK3CA promoter binders in untreated and cisplatin treated A2780-CisR cells respectively. These proteins were further clustered based on a) their presence in biological replicates; b) presence of their known interacting partners in both replicates and c) presence of their binding sites (response element) on OS4 and on full-length PIK3CA promoter. We selected top scoring three promoter binders as NF-κB, β-catenin and CREB, which were known to regulate gene expression in cancer cells.
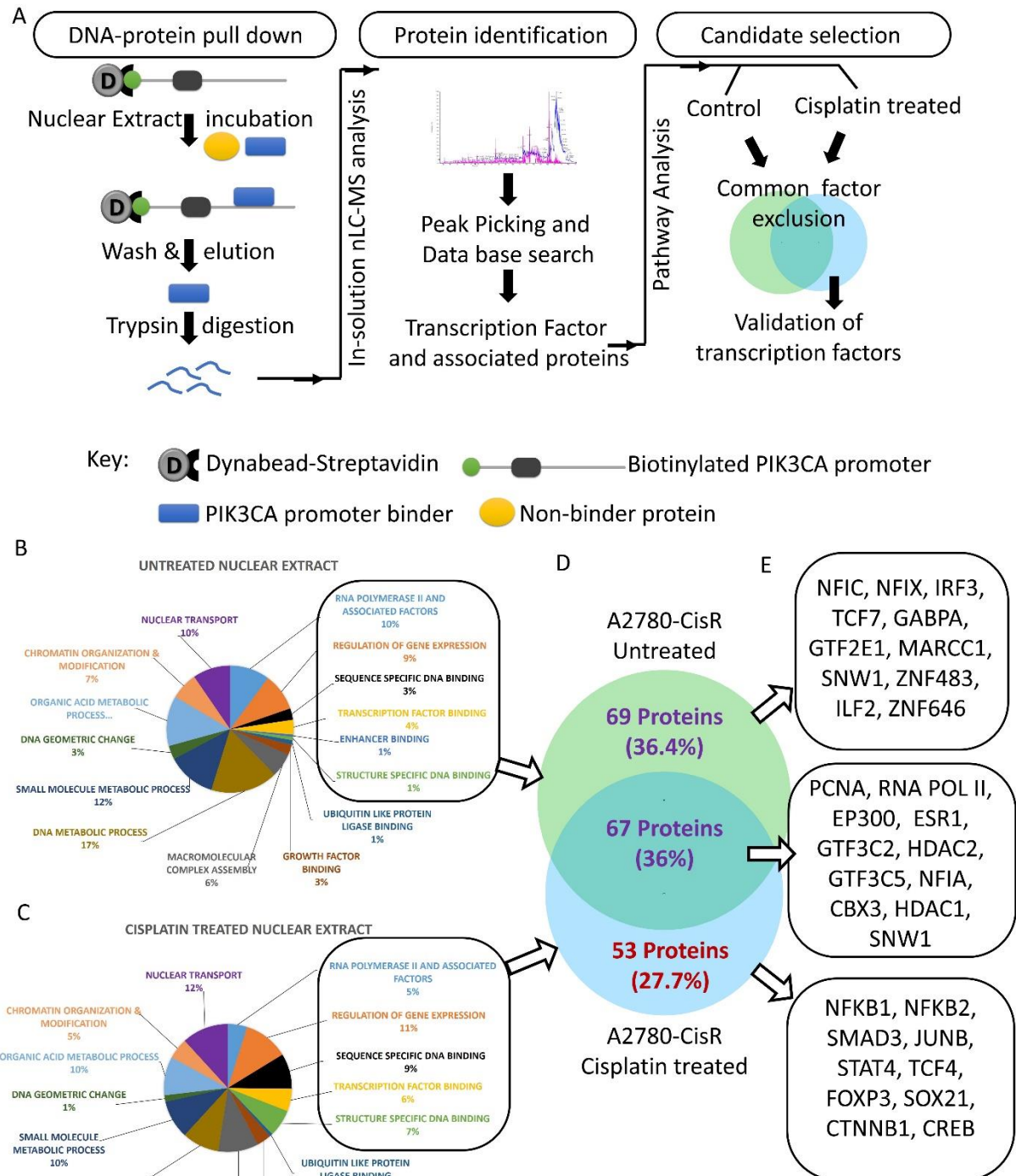
Figure 3. 4: Identification of cisplatin responsive PIK3CA regulator in resistant cells.

A. *Schematics of approach employed for identification of PIK3CA interacting protein in resistant (A2780-CisR) cells. DNA-bound proteins were pull-down using biotinylated PIK3CA promoter fragment in pre and post cisplatin treated A2780-CisR cells and subjected to nLC-MS analysis. Acquired MS/MS spectra of tryptic-digested bound fraction where used*

*for protein identification. Identified protein signatures from pre- and post- cisplatin treatment were categorised to obtain cisplatin responsive exclusive transcription factors. **B & C.** Categorisation of protein signatures based on 'GO-biological' and 'GO-molecular' functioning using GSEA server. Only transcription factors and their associated factors were employed for further analysis. **D & E.** Common factor identification between untreated and cisplatin treated A2780-CisR cells. From each category, top scoring factors were listed in the box.*

NF-κB escalated PIK3CA expression in resistant cells upon cisplatin treatment:

To confirm the extend of PIK3CA promoter regulation by NF-κB, β-catenin and CREB, we measured modulation in promoter activity of OS4-PIK3CA deletion construct in A2780 and A2780-CisR cells after TNFα, Lithium chloride and forskolin treatment. TNFα, Lithium chloride and forskolin are known to induce NF-κB, β-catenin and CREB transcriptional activity respectively. Number of identified sites for NF-κB, β-catenin and CREB and their position is represented in Figure 3. 5A. Induction of NF-κB and β-catenin transcriptional activity also increased OS4-PIK3CA promoter activity by 2.4 and 1.7 fold only in A2780-CisR cells respectively, but not in sensitive A2780 cells. (Figure 3. 5B and C) However, forskolin treatment induced OS4-PIK3CA promoter activity in both A2780 (1.6 fold) and A2780-CisR (1.5 fold) cells (Figure 3. 5D). In order to understand influence of NF-κB, β-catenin and CREB on whole promoter activity, we evaluated whole promoter activity in A2780 and A2780-CisR cells stably expressing PIK3CA promoter sensor. Similar to promoter activity of OS4-PIK3CA deletion construct, TNFα and Lithium chloride treatment escalated whole length promoter activity by 2.13 and 2.2 fold in A2780-CisR cells respectively, whereas it remained unchanged in A2780 cells. (Figure 3. 5E)

To evaluate role of NF-κB and β-catenin in cisplatin mediated transcriptional activation of PIK3CA, we assessed their nuclear localisation and PIK3CA transcript levels in A2780 and A2780-CisR cells. Nuclear translocation of transcription factor is a key event for their functioning as transcriptional regulators. Both, NF-κB and β-catenin are sequestered in the cytoplasm through binding with IκB and GSKβ:APC:AXIN respectively. Hence, we assessed level of nuclear localization of β-catenin and NF-κB in nuclear and cytoplasmic fraction of A2780 and A2780-cisR cells pre and post cisplatin treatment. Though cisplatin induced nuclear localization of β-catenin in both A2780 and A2780-CisR cells, level of nuclear translocation was higher in A2780-CisR cells. Interestingly, cisplatin treatment suppressed nuclear localization of NF-κB in sensitive A2780 while it induced nuclear localization of NF-κB in A2780-CisR. (Figure 3. 5H) Next, we tested impact of TNFα, Lithium chloride and forskolin treatment on endogenous PIK3CA expression. In accordance with PIK3CA promoter activity, TNFα and Lithium chloride treatment escalated PIK3CA expression by 2.2 and 1.7 fold in A2780-CisR cells but not in sensitive A2780 cells (0.8 and 0.5 fold compare to untreated respectively). Though forskolin increased PIK3CA promoter activity in both sensitive and resistant cells, increased PIK3CA expression was observed only in A2780-CisR cells (1.5 fold) but not in A2780 cells (0.7 fold). (Figure 3. 5I)

Herein, we identified NF-κB and β-catenin as potential regulators of PIK3CA promoter in response to cisplatin. However, among the large numbers of transcriptional partners of β-catenin complex, we could detect TCF4 and SMAD3 from our DNA-protein pull down complex, and whether they form an active transcriptional complex is yet to be determined. In contrast, both NF-κB 1 and NF-κB 2 were identified in DNA-protein pull down, which either homodimer or heterodimer sufficient to perform transcriptional function. Collectively these data of PIK3CA promoter activity and transcription levels under various treatments point towards a critical role of NF-κB in PIK3CA signalling in platinum resistant cells. Hence, we

pursued NF-κB mediated PIK3CA regulation and its effect on cell fate. Further, to evaluate physical interaction of NF-κB with PIK3CA promoter, we performed ChIP assay with antibody specific against NF-κB. ChIP revealed 1% bound fraction of NF-κB on PIK3CA promoter, which was enriched to 5% and 3.8% of input after TNFα or cisplatin treatment respectively in A2780-CisR cells. Similar to A2780-CisR, other two cell lines TOV21G and SKOV3 cells also showed increase in NF-κB occupancy from 0.3% to 6% and 0.1% to 3% post TNFα treatment respectively. Similar to TNFα induction, cisplatin treatment persuaded NF-κB occupancy on PIK3CA promoter upto 3.4% and 2.7% in TOV21G and SKOV3 respectively. (Figure 3. 5H) Together, our findings revealed imperative role of NF-κB in escalation of PIK3CA expression in platinum resistant cells.
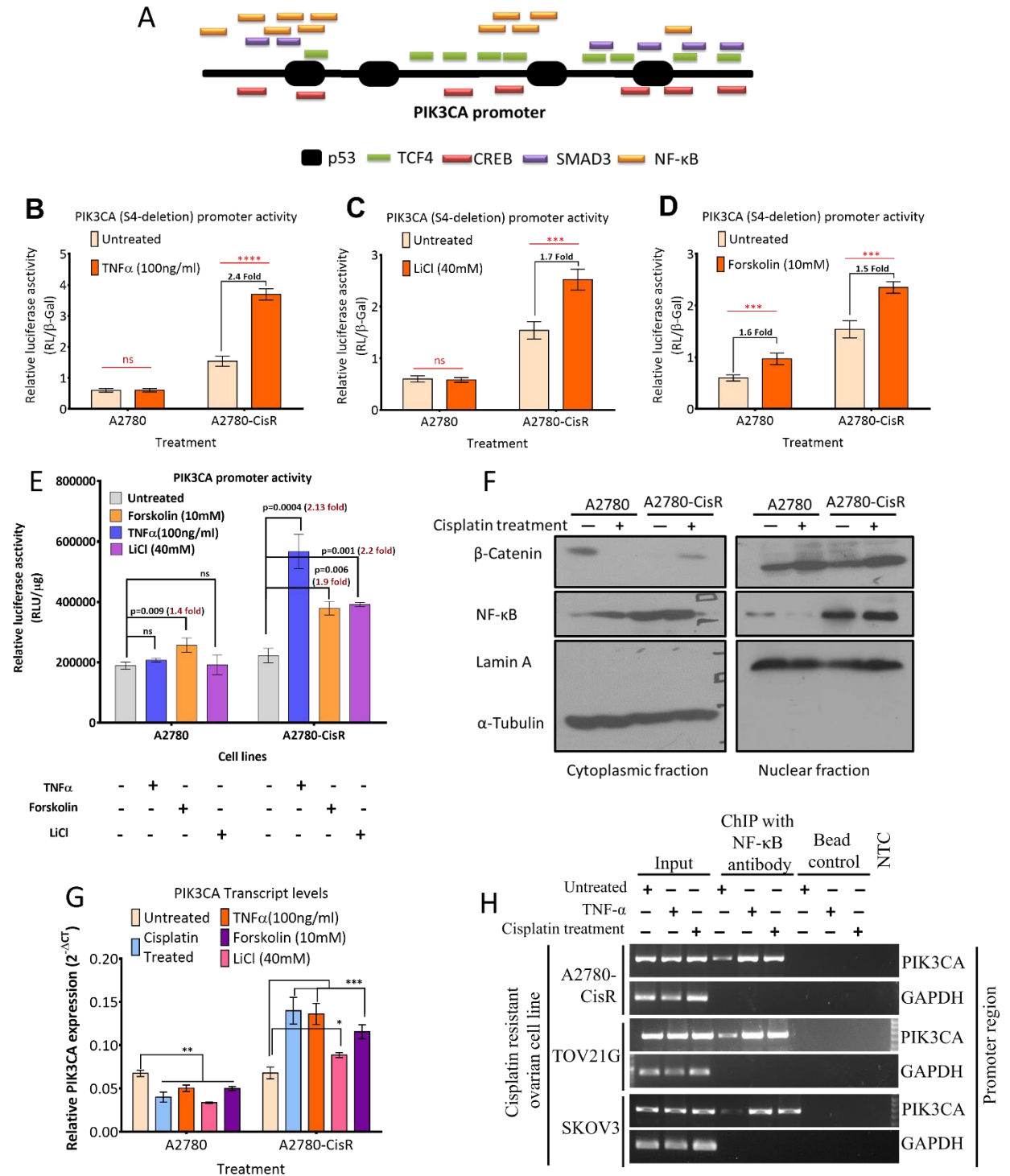
Figure 3. 5: Cisplatin responsive activation of NF-κB induces PIK3CA in resistant cells.

A. *Schematics of JASPER predicted response elements of putative transcription factors on PIK3CA promoter.* **B-D.** *PIK3CA promoter activity of transiently transfected OS4-PIK3CA deletion construct in A2780 and A2780-CisR cells after TNFα (B), lithium chloride (C) and forskolin (D) treatment.* **E.** *Whole length PIK3CA promoter activity of A2780-CisR stable*

clones increases post TNFα, lithium chloride while forsklin increased PIK3CA promoter activity in both A2780 and A2780-CisR cells. **F.** *Cellular fractionation showed increased β-catenin and NF-κB nuclear localization in response to cisplatin.* **G.** *TNFα, lithium chloride and forskolin treatment induced PIK3CA expression only in A2780-CisR but not in A2780 cells.* **H.** *Cisplatin and TNFα treatment augmented physical interaction of NF-κB on PIK3CA promoter as assessed by ChIP assay.*

Cisplatin mediates differential regulation of PIK3CA expression in cancer stem cells compare to non-cancer stem cells:

Chemoresistance is a multifactorial phenomenon, governed by molecular changes within a cell and/or external stimuli. While molecular alteration in signaling cascade aid in acquirement and maintenance of resistance, a small fraction of inherently resistant cancer stem cells help in repopulating chemo resistant tumor. CSCs are a small fraction of heterogeneous tumor population identified by surface markers like CD34+/CD38-(AML)[199], ESA+CD44+CD24-/low (breast cancer)[200] as well as phenotypic markers such as side population (SP) or aldehyde dehydrogenase (ALDH) activity, which accounts for metastasis, relapse and therapy resistance.[59] Though, chemotherapeutic intervention had shown rather unappreciated enrichment of CSC population, key molecules involved in such regulation of CSCs remain largely unknown. Intriguingly, concomitant activation of PI3K/AKT is one of such signaling cue linked with maintenance of CSC phenotype and chemoresistance. [141, 359] Hence, we hypothesised that transcriptional activation of PIK3CA may favours survival of cancer stem cells priming their enrichment upon therapeutic intervention. Hence, to understand the impact of PIK3CA promoter modulation on cancer

stem cell (CSC), we isolated CSC enriched SP fraction from platinum resistant cells and assessed the PIK3CA promoter activity in these cells.

Side population (SP) isolation is a functional assay to isolate the cancer stem cell enriched population (Singh et al, 2017). In accordance with our previous report (Singh et al. 2017), cisplatin resistant A2780-CisR, TOV21G and SKOV3 cells demonstrated 7.3$\pm$0.7% (0.65$\pm$0.45% verapamil inhibition), 5.9$\pm$0.65% (0.46$\pm$0.2% verapamil inhibition) and 4.8$\pm$0.66% (0.7$\pm$0.2% verapamil inhibition) of SP fraction respectively (Figure 3. 6A-C). To understand the regulation of PIK3CA expression in the SP and non-SP (NSP) cells, we assessed expression levels of PIK3CA in SP and NSP fraction pre and post cisplatin treatment. SP isolated from A2780-CisR, TOV21G and SKOV3 demonstrated 2.1, 2.2, and 1.7 fold increase in PIK3CA expression post cisplatin treatment (Figure 3. 6D-F). Though main population showed induction in PIK3CA expression in A2780-CisR, TOV21G and SKOV3 (1.4, 1.9 and 1.6 fold respectively), such increase was not observed in their respective NSP population. Hence, cancer stem cell enriched side population demonstrated a differential regulation of PIK3CA promoter in response to cisplatin treatment. Further, to study the regulators of PIK3CA promoter in the SP cells, TNFα, Lithium chloride and forskolin treatment was given to these cells. TNFα, Lithium chloride and forskolin to A2780-CisR cells induced PIK3CA promoter activity by 1.9, 1.1 and 0.9 fold. (Figure 3. 6G). NSP fraction did not drastic increase in PIK3CA promoter activity upon TNFα, forskolin and LiCl treatment. (Figure 3. 6H)
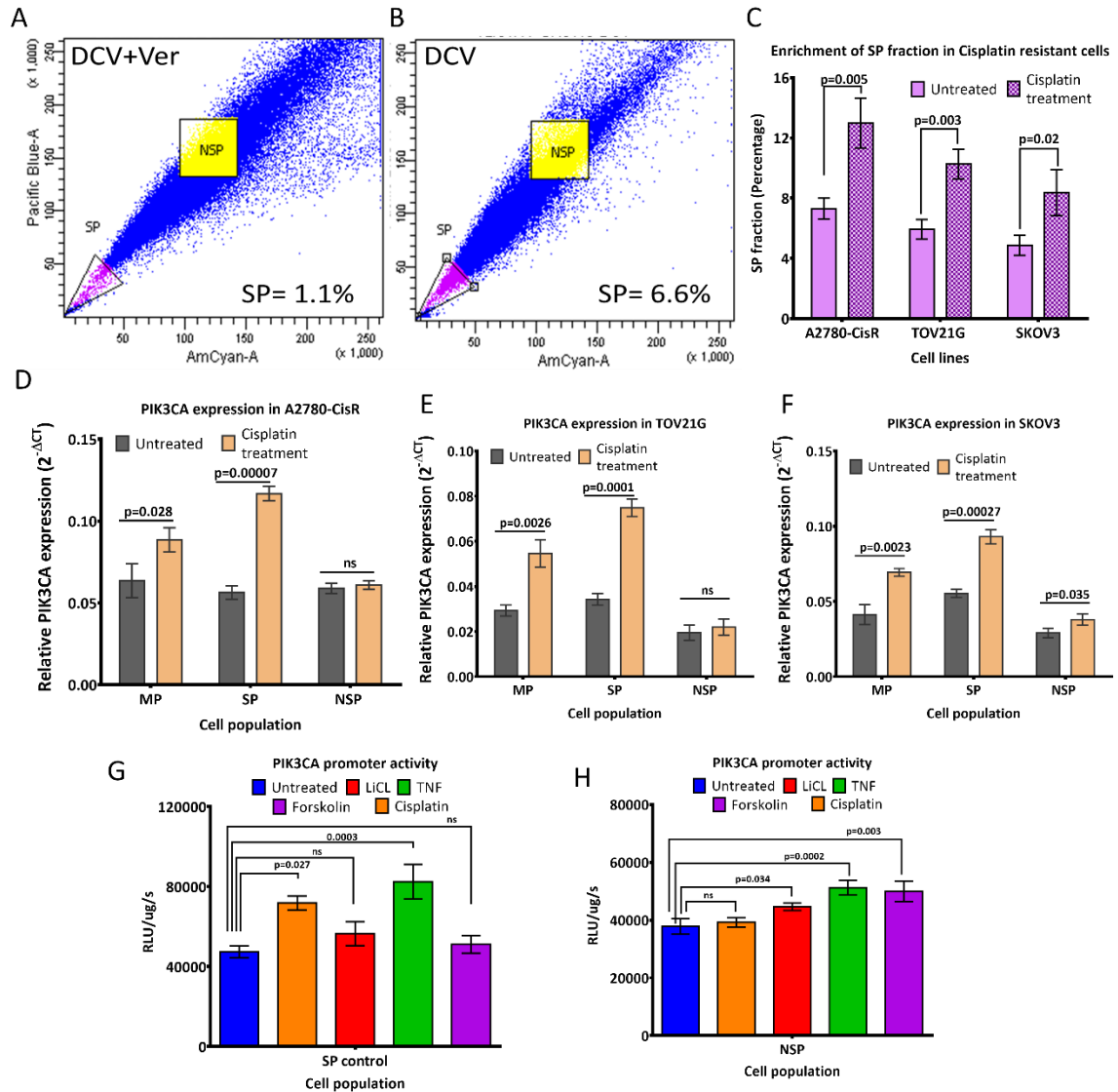
Figure 3. 6: Cisplatin augments side population fraction along with escalation of PIK3CA expression in resistant cells.

A & B. *Representative FACs dot plot showing SP fraction cells with (A) and without (B) verapamil.* ***C.*** *Quantification of SP fraction in A2780-CisR, TOV21G and SKOV3 cells pre and post cisplatin treatment from three independent experiments.* ***D-F.*** *Real time quantification of PIK3CA expression revealed treatment of cisplatin augmented PIK3CA expression in SP fraction but not in NSP fraction of A2780-CisR (D), TOV21G (E) and SKOV3 (F)* ***G.*** *Treatment of cisplatin and TNFα increased PIK3CA promoter activity, while such modulation was not observed after lithium chloride or forskolin treatment as assessed by PIK3CA promoter reporter assay.* ***H.*** *In, NSP fraction, only marginal increase in PIK3CA*

promoter upon TNFα, forskolin and LiCl treatment, while cisplatin did not induced PIK3CA promoter activity.

Differential transcriptional activity of NF-κB accounts for discrepant PIK3CA expression in CSC and non-CSC fraction:

To understand the role of NF-κB in cisplatin mediated PIK3CA upregulation, we first looked into activation of NF-κB upon cisplatin treatment. NF-κB is sequesters in the cytoplasm through its inhibitor IκB which leads to its proteosomal degradation. Activation of NF-κB signaling decouples interaction between IκB and NF-κB, which leads to its stabilisation and hence increases its protein level. Therefore, we looked into, level of NF-κB in MP, SP and NSP cells pre- and post- cisplatin treatment. Cisplatin treatment also induced total NF-κB level in MP, SP and NSP fraction compared to their untreated counterparts. However, we observed higher NF-κB protein level in untreated SP cells compare to untreated MP and NSP cells (Figure 3. 7A-C). Two other platinum resistant cells, TOV21G and SKOV3, also showed similar results where despite cisplatin mediated increment in NF-κB protein levels in MP, SP, NSP fraction, SP showed higher NF-κB compare to MP and NSP fraction.

To elucidate the correlation between NF-κB transcriptional activity and PIK3CA expression modulation in SP and NSP cells, we measured both NF-κB transcriptional activity and PIK3CA promoter activity in main population, SP and NSP cells isolated from A2780-CisR dual reporter cell line.[240]. This A2780-CisR dual reporter cell line expresses two reporters, one for measurement of NF-κB transcriptional activity (four adjacent NF-κB response elements driving a hRL-eGFP bifusion optical reporter) and the PIK3CA promoter sensor (PIK3CA promoter driving fl-tdt fusion reporter). We sorted SP and NSP fraction from these dual stable cells and treated with cisplatin or TNFα. We observed increased NF-κB

transcriptional activity by 3.5 and 4.8 fold after treatment of cisplatin or TNFα in SP fraction (Figure 3. 7D). Correspondingly, treatment with cisplatin or TNFα escalated PIK3CA promoter activity by 1.5 and 1.8 fold in SP cells (Figure 3. 7E). MP cells also showed a positive correlation in NF-κB transcriptional activity (3.5 fold) with 1.4 fold increase in PIK3CA promoter activity post TNFα treatment. Though cisplatin induced NF-κB transcriptional activity by 2.8 fold, no significant difference in PIK3CA promoter activity was observed in MP cells. In NSP cells, PIK3CA promoter activity remained unchanged (1 and 1.3 fold respectively) upon TNFα and cisplatin treatment while NF-κB transcriptional activity only showed increase with TNFα (1.7 fold) but not with cisplatin treatment (1.1 fold) (Figure 3. 7D & E). Further, a correlation analysis with all the replicates (untreated and cisplatin treated) showed a strong positive correlation between NF-κB reporter activity and PIK3CA promoter activity only in SP cells (Pearson correlation r=0.96). Such correlation was not observed in MP and NSP cells (r=0.12 and r=0.3 in MP and NSP respectively). (Figure 3. 7F-H)

NF-κB activation via cytotoxic stimuli like UV-C or doxorubicin is known to produce entirely different functional consequences than being activated by TNF☐ and a complete different set of target genes are induced.[344] Hence, to evaluate role of NF-κB in PIK3CA promoter modulation upon cisplatin treatment, we assessed its direct binding to PIK3CA promoter upon TNF☐ or cisplatin treatment. Our ChIP assay for quantifying physical interaction of NF-κB to PIK3CA promoter revealed that in SP fraction sorted from A2780-CisR cells, NF-κB was bound only to 0.9% (of input) PIK3CA promoter in untreated SP cells, which increased to 5.7 and 4.3% of input post TNFα or cisplatin treatment respectively (Figure 3. 7I). To our surprise, NSP fraction of A2780-CisR showed enhanced NF-κB binding only upon TNFα treatment (0% to 2.2% of input) but not by Cisplatin (0% to 0% of input) to PIK3CA promoter. (Figure 3. 7I) In SP fraction of TOV21G and SKOV3, NF-κB

binding increased on PIK3CA promoter upon TNFα (1.5% to 6.2 and 1.2% to 4.2% and of input, respectively) and cisplatin treatment (1.5% to 1.2% to 4.8% of input, respectively). NSP fraction, however, showed NF-κB and PIK3CA promoter interaction only after TNFα treatment (1.8 and 1.1% of input) in TOV21G and SKOV3 cells. (Figure 3. 7J & K)

Further to understand CSC specific NF-κB activation, we performed immunofluorescence studies with both NF-κB and OCT4 antibodies in MP, SP and NSP cells. As discussed earlier, active NF-κB translocate to nucleus. Hence, we quantified nuclear mean fluorescence intensity of NF-κB for assessing 'active' NF-κB in MP, SP and NSP cells. In accordance with our protein levels and reporter activity results, untreated SP cells showed highest nuclear localization of NF-κB compared to MP and NSP cells. (Figure 3. 8 A-C) Further, A2780-CisR MP and SP fraction showed increase in nuclear positive NF-κB cells from 5.2% to 10.8% (MP) and 17% to 33.4% (SP) upon cisplatin treatment (Figure 3. 5B-D). Similarly TOV21G and SKOV3 cells demonstrated ~2fold increase (from 7.8% to 14.5% and 18.3% to 27.3% in TOV21G MP and SP whereas 4.5% to 8.4% and 13.2% to 21.1% in SKOV3 MP and SP fractions respectively) in nuclear NF-κB (Figure 3. 8 F, G, J & K). NSP fraction from A2780-CisR, TOV21G and SKOV3 showed 3.6%, 5.8% and 3.4% cells with nuclear NF-κB localisation, which did not increase after cisplatin treatment. Further, we quantified Oct4 positive nuclei to detect CSC fraction from the MP, SP and NSP fraction. As expected, only SP fraction obtained from A2780-CisR, TOV21G and SKOV3 cells showed 44.3%, 36.7% and 32.4% Oct4 positive nuclei respectively. (Figure 3. 8 D, H & L) Number of Oct4 positive nuclei remains unchanged even after cisplatin treatment in all three cell line. Dual immunofluorescence with NF-κB and Oct4 antibody revealed 9.3%, 10% and 9% cells possess co-localization of both the transcription factors in untreated SP fraction of A2780-CisR, TOV21G and SKOV3 cells respectively. (Figure 3. 8 E, I & M) Contrarily, MP and NSP fractions did not show significant number of cells co-expressing OCT4 and NF-κB.

These dual nuclear positive cells (Oct4+ and NF-κB+) were further increased up to 23.4%, 14% and 15% post cisplatin treatment in SP fraction obtained from A2780-CisR, TOV21G and SKOV3. (Figure 3. 8 E, I & M)
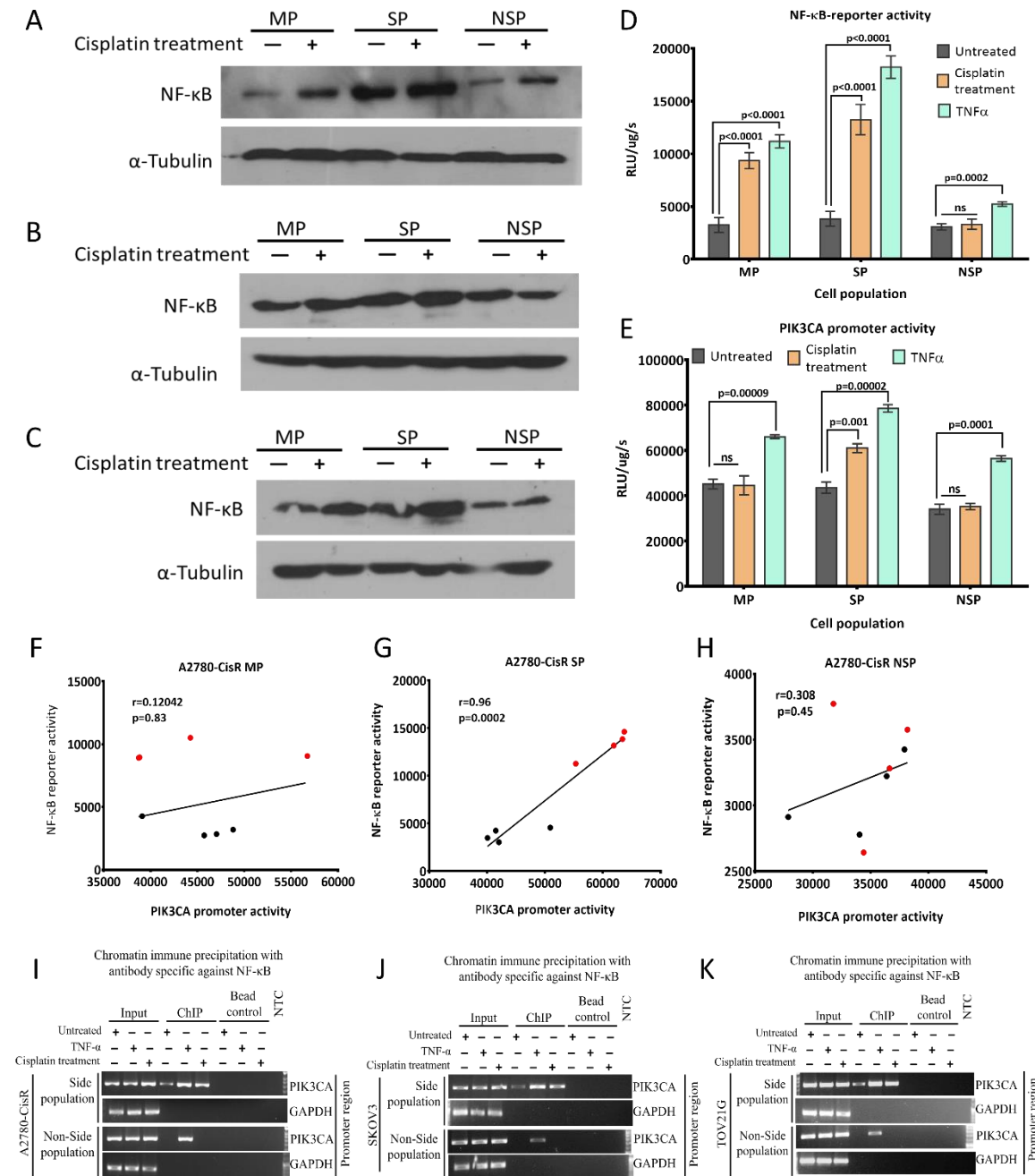
Figure 3. 7: Cisplatin mediates induction in NF-κB protein levels and its physical interaction with PIK3CA promoter in TOV21G and SKOV3 cells.

A-C. Though level of NF-κB increased in cell fraction of A2780-CisR (A), TOV21G (B) and SKOV3 (C) post cisplatin treatment, SP cells showed higher level of NF-κB compare to MP

*and NSP cells. All three sorted fraction from both the cell lines demonstrated cisplatin mediated increase in NF-κB protein levels. **D.** Treatment of TNFα or cisplatin dramatically increased renila activity driven by NF-κB response elements only in MP and SP fraction of A2780-CisR dual reporter cell line but not in NSP fraction. TNFα treatment to NSP fraction showed nominal increase in NF-κB transcriptional activity. **E.** Similar to NF-κB-reporter activity, TNFα treatment also induced PIK3CA promoter activity in MP, SP and NSP fractions. However, cisplatin mediated increased PIK3CA promoter activity was observed only in SP cells. SP cells showed much higher induction of PIK3CA promoter activity compare to MP cells after TNFα, cisplatin. **F-G.** Correlation analysis demonstrated a positive correlation (r=0.9) between NF-κB reporter activity and PIK3CA promoter activity only in SP cells in response to cisplatin. MP and NSP fraction did not show such significant correlation between NF-κB reporter activity and PIK3CA promoter activity. Black and red dots represent reporter activity from untreated and cisplatin treated replicated from each fraction respectively. (Note- Values of two replicate in cisplatin treated MP cells are overlapping with each other hence appear to be one) **I.** Both, TNFα or cisplatin treatment enriched NF-κB occupancy on PIK3CA promoter in SP cells while only TNFα showed NF-κB binding to PIK3CA promoter in NSP cells. Genomic GAPDH locus was used to show purity of chromatin immune-precipitation. **J & K.** Similar to A2780-CisR cells, TNFα or cisplatin treatment induced NF-κB occupancy on PIK3CA promoter only in SP fraction of TOV21G and SKOV3 cells. In NSP fraction, only TNFα treatment showed NF-κB binding to PIK3CA promoter in both the cell lines. Genomic GAPDH locus was used to show purity of chromatin immune-precipitation.*
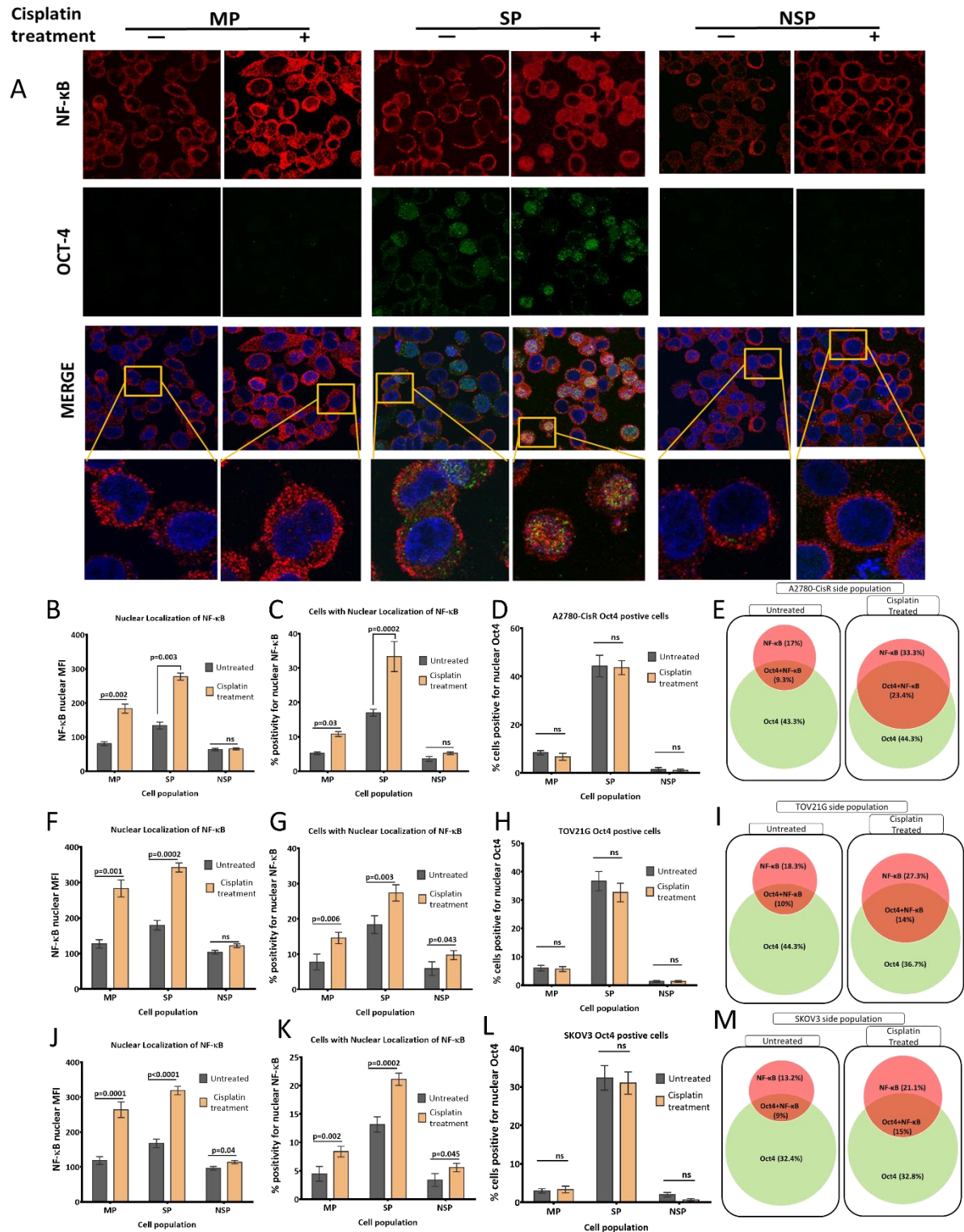
Figure 3. 8: Cisplatin induced NF-κB translocation to nucleus especially in OCT4 positive cells:

A. *Representative fluorescence images representing NF-κB (Red) and OCT4 (green) staining in A2780-Cis R MP, SP and NSP fractions pre- and post- cisplatin treatment.* **B & M.** *Quantification of nuclear mean fluorescence intensity for NF-κB, percent positive cells with*

NF-κB or Oct4 in A2780-CisR (B-E), TOV21G (F-I) and SKOV3 (J-M). Nuclear mean fluorescence intensity measurement for red channel demonstrated higher nuclear localization NF-κB in SP fraction of A2780-CisR (B), TOV21G (F) and SKOV3 (J). In MP and SP fractions of A2780-CisR, TOV21G and SKOV3, increased nuclear localization of NF-κB was observed upon cisplatin treatment. Percentage of cell with nuclear positive NF-κB, but not Oct4 cell increased after cisplatin treatment in MP and SP obtained from A2780-CisR (C & D), TOV21G (G & H) and SKOV3 (K & L) cell lines respectively. Further, overlap between cells with nuclear localized NF-κB and Oct4 in SP fraction through Venn diagram. Only fluorescence signal from nuclear region was quantified in at least 100 cells and represented as percentage positivity.

Cisplatin triggered enrichment of cancer stem cells in PIK3CA dependent manner: Clinical association between cancer stem cell (CSC) enrichment and chemoresistance is currently a well-established phenomenon in many cancers.[59, 361-364] Growing evidence indicate that, these drug tolerating CSC survive chemotherapy and repopulate further to develop into chemo-resistant tumor.[362-364] Our earlier study with A2780 and OAW42 isogenic chemoresistance models demonstrated that, CSC-enriched Side Population (SP) fraction was augmented during course of resistance acquirement. This SP fraction was associated with characteristic features of cancer stem cells such as increased spheroid formation ability, higher expression of pluripotent gene and tumorigenic ability at a fewer cell implantation in immune-compromised mice.[365] Intriguingly, recent evidence showed that this CSC fraction enriches upon therapeutic intervention. For example, ALDH+, CD44+, CD133+ CSC population from chemo-sensitive breast and colon cancer cells persist and enrich upon treatment with cisplatin, carboplatin and paclitaxel, 5-FU and Adriamycin.[59, 361] However, effect of chemotherapeutics on CSC's residing within chemo-resistant

tumors/cells is largely unknown. Recent evidences reveal involvement of activated PI3K/AKT/NF-κB cascade in maintenance and enrichment of colon, breast, ovarian and naopharyngeal cancer stem cells.[59, 366] Therefore, to understand the impact of PI3K/AKT signalling in drug resistant cancer stem cell (CSC) population, we assessed enrichment of SP fraction in cisplatin resistant cell lines post induction of PIK3CA expression using TNFα or cisplatin treatment. Treatment of cisplatin to A2780-CisR increased SP fractions from (7.3±0.7% (0.65±0.45% after verapamil inhibition)) increased to 13.7+2.6% (1.8±0.6% after verapamil inhibition). (Figure 3. 9 A-D) Similarly, other resistant cell lines also showed cisplatin mediated CSC enrichment wherein TOV21G and SKOV3 demonstrated increase in SP fraction from 5.9+0.65% to 10.2+0.4% and 4.9+0.7% to 8.4+1.5% respectively. (Figure 3. 9B) Similar to cisplatin treatment, TNFα also induced increase in SP fraction from 7.3+0.7% to 13.6+1.87% in A2780-CisR cells. (Figure 3. 9B) Other platinum resistant cells, TOV21G and SKOV3 also showed similar enrichment in SP fraction post TNFα wherein SP fraction increased from 5.9+0.65% to 9.1+1.6% in TOV21G cells and 4.9+0.7% to 7.7+0.8% in SKOV3 cells. (Figure 3. 9C & D) To assure whether cisplatin plays role in maintenance and differentiation of CSC fraction, we performed SP differentiation assay, where SP fraction were serially sorted till 3rd generation and SP fraction was assessed after TNFα or cisplatin treatment. [365] (Figure 3. 9A) We observed that, from 100% of A2780-CisR sorted SP fraction, only 38.7±3.5% of population persisted as SP fraction over 48hr while rest of the SP fraction differentiated into NSP fraction. (Figure 3. 9B) Interestingly, addition of TNFα or cisplatin in the media led to increase in SP fraction up to 67.1+7.23% and 59.9+12.2% respectively. Similar enrichment in SP fraction was also observed in TOV21G (31.5±1.3% to 45.8±7.9% by TNFα and 31.5±1.3% to 46.6±3.9% by cisplatin) cells and in SKOV3 (25.1±3% to 33.6±3.1% by TNFα and 25.1±3% to 33.6±3.1% by cisplatin) cells. (Figure 3. 9 C & D) NSP fraction from A2780-CisR, TOV21G, and SKOV3 cells did not show such

enrichment in SP fraction with either of the treatment. To affirm whether this enrichment of SP fraction also enriches CSC population, we accessed expression of pluripotency factors (Oct4, Nanog and Sox2) pre and post cisplatin treatment. Significantly higher levels of Oct4, Sox2 and Nanog in SP fraction compared to their MP and NSP counterparts were found in A2780-CisR, TOV21G and SKOV3 cells. (Figure 3. 9E-G) In response to cisplatin, Nanog and Sox2 level increased significantly only in the SP fraction of A2780-CisR, while Oct4 level remain constant. In TOV21G, only Oct4 transcript is increased significantly, while in SKOV3, both Oct4 and Nanog levels were induced post cisplatin treatment. (Figure 3. 9E-G)
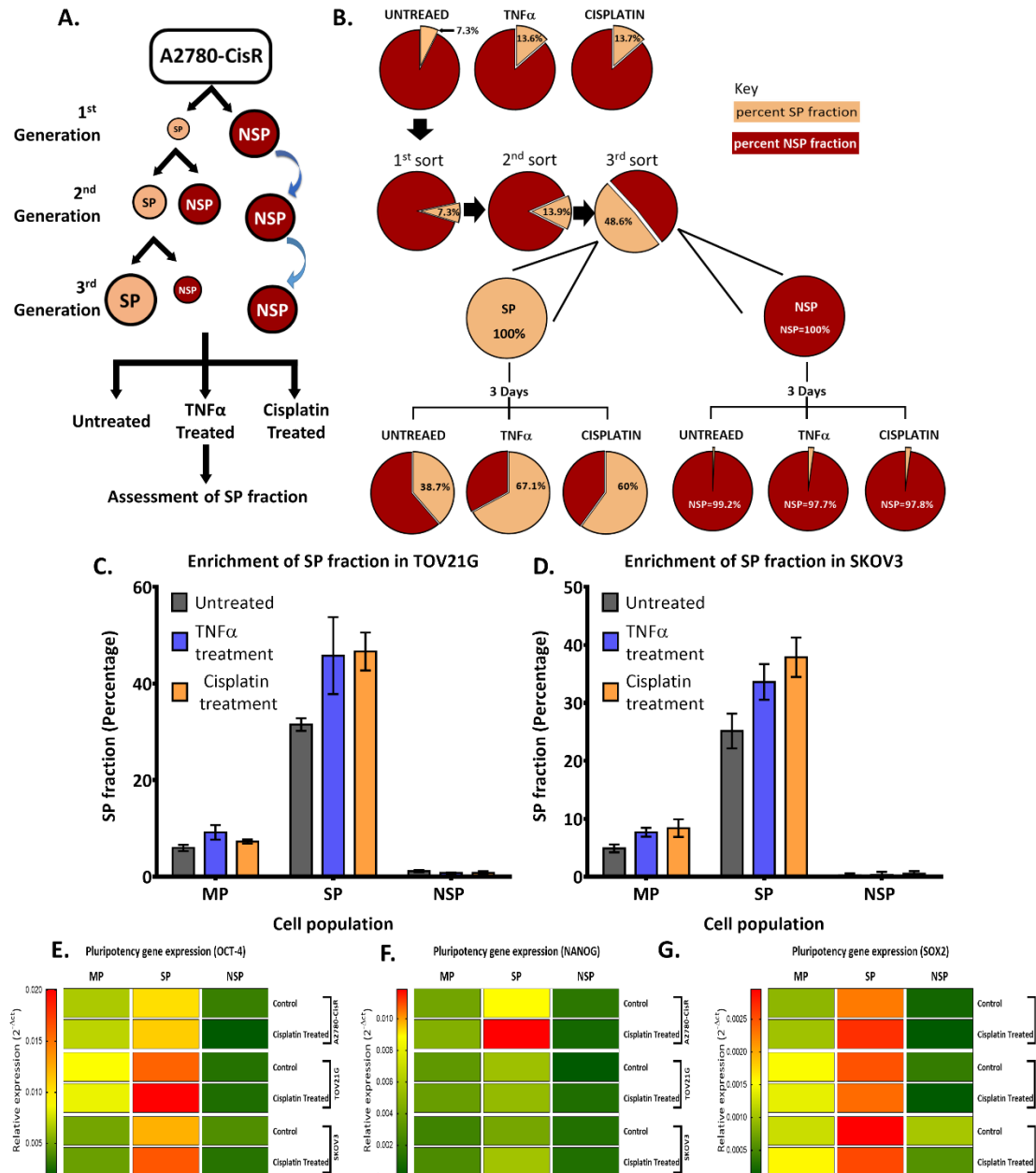
Figure 3. 9: Cisplatin treatment augmented cancer stem cell feature in resistant cells.

A. Schematic representation of SP-differentialtion assay. Serial sorting of SP fraction was performed for three successive generation and treated with either TNFα or cisplatin for 24hr. Further SP differentiation ability was evaluated by acquisition of SP fraction in 3ʳᵈ generation SP cells from untreated, TNFα or cisplatin treated A2780-CisR cells. B. Representative pie chart showing enrichment of SP fraction in MP and SP cells but not in NSP cells post TNFα or cisplatin treatment compared their untreated counterpart. C & D.

*Quantification of SP fraction in TOV21G (C) and SKOV3 (D) cells pre and post cisplatin treatment **E-G.** Heat map of pluripotency gene relative expression ($2^{-\Delta CT}$) showing increment in OCT4 (E), NANOG (F) and SOX2 (G) in response to cisplatin confirmed enrichment of CSC fraction in A2780-CisR, TOV21G and SKOV3 cells.*

Inhibition of PIK3CA activity suppresses cisplatin induced SP enrichment in platinum resistant cells: In spite of similar levels of PIK3CA expression in the main population, side population and non-side population, CSC enriched SP cells demonstrated relatively higher induction of PIK3CA expression in response to cisplatin. On other hand, cisplatin treatment persuades enrichment of SP fraction in A2780-CisR, TOV21G and SKOV3 cells. To ascertain that this enrichment depends on PIK3CA activity, we inhibited PIK3CA activity using a reversible PIK3CA inhibitor, wortmannin. Wortmannin treatment alone or in combination with cisplatin reduced SP fraction form $7.3\pm1.1\%$ (untreated) to $5.2\pm0.6\%$ (wortmanin alone) and $14.6\pm2.9\%$ (Cispatin treated) to $9.1\pm0.75\%$ (cisplatin and wortmannin combination treatment) respectively in A2780-CisR cells (Figure 3. 10A & B). Similar effect was observed in SKOV3 cells where SP fraction was reduced from $4.8\pm1.7\%$ (untreated) to $1.9\pm0.2\%$ (wortmanin) and $8.5\pm1.2\%$ (cisplatin) to $2.8\pm0.4\%$ (combination of cisplatin and wortmannin) (Figure 3. 7C). Effect of PIK3CA inhibition was more robust in serially cultured 3rd generation SP cells where ~50% decline in SP fraction was evident post 24hr of wortmannin treatment. NSP cells did not show any SP fraction after serial culturing with or without wortmannin treatment. (Figure 3. 10B-C)

To assess the consequence of activated PI3K/AKT cascade on CSC fraction, we monitored expression of specific downstream targets such as P21, P27, CYCLIN-D1 & Cyclin-E1 (cell cycle regulators), BAX, PUMA (pro-apoptotic) and cFLIP (anti-apoptotic) in MP, SP and

NSP cells after cisplatin treatment. Increased p21 and p27 levels and decreased cyclin D1 and E1 levels in SP cells compared to NSP cells marks growth arrested quiescent state of SP cells (Figure 3. 10 D-G). Interestingly, we observed sharp increase in cyclin D1 level indicating active proliferation of NSP cells after cisplatin treatment. Though cFLIP levels were increased in all three fractions, transcriptional increment in BAX and PUMA in NSP cells marked pro-apoptotic fate of these cells. However, increased cFLIP levels along with quiescent state of SP cells aid these cells to survive the action of chemotherapeutic drugs. In accordance with NF-κB-transcriptional reporter activity, its downstream targets IL6 and TNFα also showed higher expression levels in SP cells compare to MP and NSP fraction. Further, expression level of IL6 and TNFα increased significantly only in MP and SP fraction but not in NSP fraction. However, Cyclin D1, being transcriptional target of NF-κB did not show similar pattern of modulation in SP cells. Overall, CSC acquired anti-apoptotic, dormant state which provided survival advantage and hence CSC enrichment upon cisplatin treatment. (Figure 3. 11)
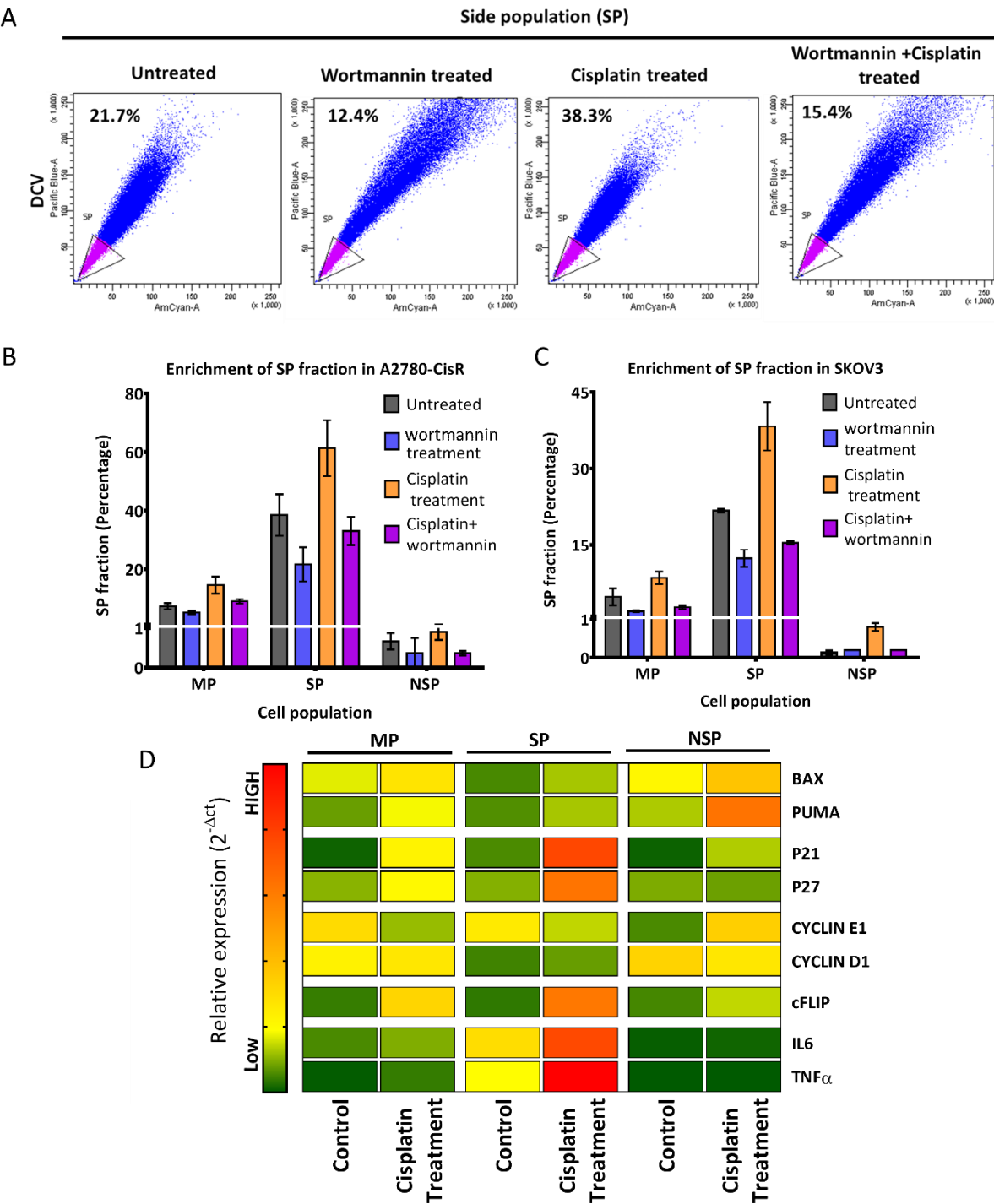
Figure 3. 10: Activation of PI3K/AKT cascade endorse anti-apoptotic, dormant state in SP fraction.

A-C. Inhibition of PIK3CA activity using wortmannin decreased SP fraction in MP and third generation SP cells. A. represents FACS dot plot demonstrating distribution of SP and NSP fraction in SKOV3 cells and B & C represents pie chart distribution of SP fraction from three independent biological replicates in A2780-CisR and SKOV3 cells. D. Heat map representing

gene expression normalised with GAPDH expression ($2^{-\Delta CT}$). Real time analysis showed a sharp increase in growth arrest proteins (p21 and p27 only in SP cells but not in NSP cells in response to cisplatin. Whereas cisplatin induced proliferation only in NSP cells as shown by Cyclin D1 levels. Though cFLIP levels were increased in all three MP, SP and NSP cells, sharp increase in BAX and PUMA forced NSP cells towards pro-apoptotic cellular fate. NF-κB target genes, IL6 and TNFα showed highest expression in SP cells, which was further increased upon cisplatin treatment.
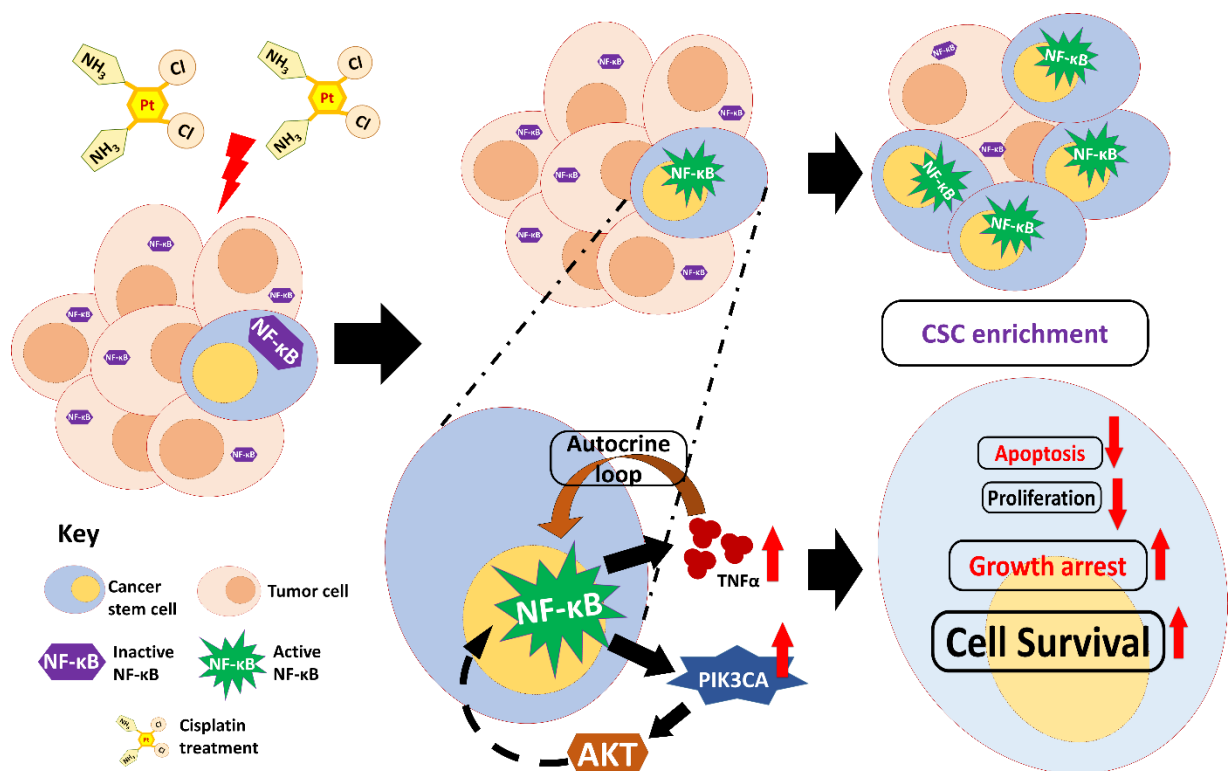
Figure 3. 11: Proposed model of cisplatin induced CSC enrichment during acquirement of cisplatin resistance.

Cisplatin activated NF-κB only in cancer stem cells, which in turn induces expression of TNFα and PIK3CA. Increase in TNFα expression of act as an autocrine loop activating NF-κB in CSC's while increased PIK3CA activated PI3K/AKT signaling. Activated PI3K/AKT confers resistance against cisplatin action through up regulation of anti-apoptotic genes such

as cFLIP. Overall, CSC acquired anti-apoptotic, quiescent state conferring survival advantage against action of chemotherapeutic drugs.

3.4 Discussion:

Cisplatin resistance is a net effect of multiple mechanisms that either inhibit apoptosis, promote cell survival, or both. While molecular alteration in signaling cascade aid in acquirement and maintenance of resistance, a small fraction of inherently resistant cancer stem cells help in repopulating chemo resistant tumor. The multifaceted nature of resistance continues to become more complex as more genes inducing cisplatin resistance are identified from gene expression profiles. Because many of these mechanisms coexist within a resistant tumor cell, the task of identifying therapeutic approaches that will be effective against cisplatin refractory disease become daunting. However, cell fate depends on net balance between pro-survival and prodeath signals induced by cisplatin. Activation of PI3K/AKT survival signaling is known to favour cellular endurance against drug treatment and maintenance of CSC population.[141, 361, 366] but regulators of this pathway in drug resistant cells are yet not well identified. Using transcription factor pull-down assay against PIK3CA promoter fragment, we identified NF-κB, β-catenin and CREB as cisplatin responsive transcriptional activators of PIK3CA promoter. Further, we found that NF-κB differentially activated PIK3CA only in cancer stem cell enriched side population but not in non-side population. Both cisplatin and TNF-a induced binding of NF-κB to PIK3CA promoter and led to enrichment of cancer stem cell enriched-SP fraction indicating an unique role of cisplatin in self-renewal of CSC. Such CSC enrichment was dramatically reduced upon inhibiting PIK3CA activity. Finally, gene expression analysis revealed that Cisplatin mediated activation of PI3K/AKT led to an anti-apoptotic, dormant stage, which aids CSC to evade therapeutic action while actively proliferating NSP cells succumb to cisplatin's action. Collectively, our data emphasize that therapeutic intervention to ovarian cancer cells, which

have already acquired chemoresistance favours a predominant quiescent stem cell like SP population state via NF-κB mediated upregulation of PIK3CA/AKT signalling.

Platinum based drugs, cisplatin and carboplatin are alkylating agents which play a central role in management of testicular, ovarian, cervical, head and neck and non-small cell lung cancer. They are alkylating agents which crosslink with adenine or guanine base resulting in DNA double strand breaks and DNA damage and repair.[183] Other than the classical mode of DNA damaging stress, cisplatin is known to induce oxidative and endoplasmic stress. Thus cisplatin induced stresses activate several signalling cascade including c-ABL, p53 signaling, MAPK/JNK/ERK and suppresses PI3K/AKT, NF-κB signalling, focal adhesion kinases and WNT signalling. Amongst several molecular determinants of cisplatin resistance, activated PI3K/AKTAKT pathway turns out to be a key signalling that also aids in cancer stem cell survival.[59, 268, 355, 361] Activated PIK3CA/AKT signalling bestows endurance against the action of chemotherapeutics and contributes to drug resistance in lung, ovarian, breast and gastric cancers.[237-239, 367] Especially in ovarian carcinoma, 50-75% of chemo-resistant tumors are associated with hyper-activation of PIK3CA/AKT cascade. Amplification of PIK3CA was associated with ovarian and uterine cervical carcinoma, which led to high pAKT level.[147, 368] Such activated pAKT levels confers resistance against platinum-based therapeutics. Lee et al, (2008) also showed such escalated PIK3CA expression in OVCAR-3/CDDP (resistant) cells, which led to inhibition of BAX translocation via activated PI3K/AKT conforming platinum resistance.[149] However, mechanism for augmented PIK3CA expression is less dissected at molecular level. As discussed in previous chapter, Our previous study demonstrates that in absence of a platinum induced serine phosphorylation, p53 fails to bind and represses PI3K promoter leading to activation of PI3K/AKT signalling that actively sustains survival not proliferation of platinum-resistant

cells.[346] Intriguingly, we observed cisplatin itself could induce upregulation of PIK3CA transcription in resistant cells but not in sensitive cells.

Several transcription factors (TF) such as p53, YB-1, ZNF143, mTFA, NF-κB, ATF-2, 3 and 4 transcription factors are known activated through cisplatin treatment. [240, 347] However, only p53, YB-1[268], NF-κB[140] and FOXO3a[139] are known to induce PIK3CA expression in un-stressed condition. However, no information is available on regulators of PIK3CA modulation in platinum-resistant cells in response to cisplatin. Thus to identify novel regulators of PIK3CA, we performed predictive transcription factor search on PIK3CA promoter with JASPER and Transfac. However, short listed transcription factors such as Hif-1α did not show significant PIK3CA promoter modulation. Since, analysis of the entire array of predicted transcription factor binding (~451) sites was not feasible, we adopted promoter (DNA)-binder (protein) pull down strategy for identification of PIK3CA regulators. Thus to identify cisplatin responsive regulators of PIK3CA promoter, we subjected PIK3CA promoter bound nuclear fraction (potential transcription factors) from untreated and cisplatin treated A2780-CisR cells to nLC-MS. We used a short (OS4-) PIK3CA promoter fragment (~340bp containing the fourth p53-RE) due to: A) site 4 is found to be the most critical regulatory site (highest promoter activity, binding sites for p53 as well as other transcription factor by JASPER analysis) & B) to avoid non-specific binding of protein complexes to the full length (1kb) promoter. Multiple putative candidate proteins bound to PIK3CA promoter in untreated (863 and 339) and cisplatin treated (312 and 246) A2780-CisR cells were identified which were further classified based upon their molecular and biological (transcription associated) functioning.

To pinpoint tangible transcription factors we performed pathway analysis, which revealed 36% of these interactors are shared between untreated and cisplatin treated PIK3CA binders, and majority of them are associated with general RNA polymerase transcriptional assembly.

Among the binders present exclusively in cisplatin treated samples (36%), we selected top three PIK3CA bound proteins (NF-κB, β-catenin and CREB) based on their identification scores as well as presence of their response elements on PIK3CA promoter for further validation. All the three transcription factors are known to influence cisplatin resistance in various cancer cells. Li et al (2016) demonstrated that cisplatin increases expression of β-catenin in oral squamous cell carcinoma, which aids these cells to develop resistance.[369] While CREB is shown to be activated by cisplatin treatment in ovarian cancer cells[370] and hyperactivation of NF-κB is associated with cisplatin resistant human epidermoid carcinoma KCP-4 cells[371]. Our earlier report also demonstrates that in absence of MyD88 adapter protein mediated TLR4 signalling, ovarian cancer chemoresistance is maintained by NF-κB transcriptional activation under cisplatin treatment.[240] Augmented PIK3CA expression in platinum resistant H460 cells also supported with increased NF-κB and β-catenin levels compared to their parental counterpart (GEO ID GSE21656).[367] However CREB does not show such correlation between parent and resistant H460 lung cancer cells. For this, we induced transcriptional activity of NF-κB, β-catenin or CREB by treating these cells with TNFα, Lithium chloride and forskolin respectively. Treatment with TNFα and Lithium chloride (inducers of NF-κB and β-catenin) augmented PIK3CA promoter activity only in platinum resistant cells but forksolin (CREB inducer) increased PIK3CA expression in both sensitive and resistant cells. Though forskolin increased PIK3CA expression in A2780-CisR cells, treatment to A2780 sensitive cells leads to reduction in PIK3CA transcript levels. Other than CREB, forskolin is known to induce binding of transcription factors Ets-2, phospho- p53 and AP1 to MMP-2 promoter.[372] Hence observed decrease in PIK3CA expression in A2780 sensitive cells may be influenced by its transcriptional repressor such as p53 which may be activated upon forskolin treatment. Till date NF-κB's role as a positive regulator for PIK3CA promoter in non-proliferating ovarian cancer cells by TNF-αis reported by Yang et

al.[140] Herein, we demonstrate a unique mechanism PIK3CA regulation by NF-κB induced by cisplatin, a cytotoxic drug in platinum resistant cells. Physical interaction of NF-κB to PIK3CA promoter by ChIP assay showed that NF-κB was nominally bound with PIK3CA promoter in untreated A2780-CisR, TOV21G, and SKOV3 cells whose occupancy increased several fold following TNFα or cisplatin treatment. Our data also suggest β-catenin complex to be another regulator of PIK3CA promoter, however, presence of only two interacting (SMAD3 & TCF4) partners of this complex among large numbers of identified binders and nominal fold increase in PIK3CA expression (1.5 fold in three cell lines) by lithium chloride does not signify a robust role of this complex. Further experimental studies are required to estimate the exact contribution of β-catenin complex.

Emerging evidence supports the concept that platinum-based therapies are able to eliminate the bulk of differentiated cancer cells, but are unable to eliminate tumor initiating cells. Other than perturbation of intrinsic survival pathway, chemoresistance is also maintained through extrinsic factors such as microenvironment and cancer stem cells. [184-186] Several correlative studies have shown that PI3K/AKT pathway activation is associated with poor outcomes in patients with high-grade serous ovarian cancer (HGSOC). However, the functional relevance of these findings in maintenance of chemoresistance remain to be delineated.

Till date, the relevant pathways that regulate ovarian cancer stem cells under the influence of chemotherapeutic drugs remain elusive. To explore the link between CSC and survival associated PIK3CA modulation, we assessed the expression levels of PIK3CA in the side population and their counterpart non-side population pre and post cisplatin treatment. To our surprise, we found augmented PIK3CA expression in response to cisplatin only in SP cells but not in NSP cells. Side population is a functional assay which distinguishes cancer stem cell enriched population. Next, for comprehensive understanding of what regulates PIK3CA

in SP cells, we treated these cells with inducers of NF-κB, β-catenin or CREB. Among these only TNFα treatment alone and in combination with cisplatin augmented PIK3CA promoter activity in SP cells but not in NSP cells indicating NF-κB could be one of the major contributor for differential activation of PIK3CA in SP cells. To affirm the differential regulation of PIK3CA via NF-κB is specific to CSC populations, immunofluorescence studies are performed over SP cells pre and post cisplatin treated. Surprisingly, most of cells with nuclear localisation of NF-κB is also demonstrated presence of nuclear Oct4. This confirms cisplatin induced NF-κB augments PIk3CA expression in CSC's. All these data lead us to hypothesize that NF-κB controlled PIK3CA expression coordinates the CSC survival. Several studies have shown a relationship between increased survival signals and the ability to increase growth of resistant phenotypes that show increase in cancer stem cell proportion. For instance, Tadoro et al (2007) demonstrated that activation of PI3K/AKT/BCl2 signalling enriches CD133+ colon cancer stem cells in response to Adriamycin and 5-FU. Similarly Kolev et al (2015) demonstrated that cisplatin treatment increases aldefluor+ve CSC population in breast cancer model in PI3K/AKT dependent manner.[361] So, we hypothesised that increasing PI3K/AKT survival can promote the plasticity in CSC population and enhanced its proportion under chemotherapeutic agent.

Nuclear factor-κB, (NF-κB), refers to a pivotal family of transcription factors, which controls expression of diverse genes related to immune responses, survival, proliferation, development, angiogenesis, and metastasis. In most cell types, inhibitor of κB (IκB) sequestered NF-κB/RelA heterodimer in the cytoplasm. [373] Phosphorylation of IκB relieves inhibition from NF-κB dimer, and activates NF-κB signalling. Both, PI3K/AKT and NF-κB signalling converges at IκB node, where activated AKT promotes IκB degradation via phosphorylating IKKα kinase. Along with phosphorylation of IKK at tyrosine 23 residue, AKT also phosphorylates NF-κB at serine 534 thereby stimulates NF-κB activity.[374] In

most tumors, NF-κB signaling is constitutively active, regulating gene induction associated with proliferation (cyclin D1, D2, CDK2 and c-Myc), growth signals (GM-CSF and IL6), anti-apoptosis (FLIP, BCL2, Bcl-xL and several IAPs) and angiogenesis (VEGF, TNF, IL1, and IL6).[79, 341] Further, Substantial evidence shows that NF-κB signaling pathway is constitutively active in cancer stem cells.[356] Especially in ovarian cancer stem cells, CD44+ cells, survives the treatment of paclitaxel and carboplatin through concomitant activation of NF-κB signalling confering resistance against paclitaxel and carboplatin.[359] Hence, to understand the CSC-specific activation of NF-κB in cisplatin resistant cells, we investigated co-localisation of Oct4 with NF-κB in MP, SP and NSP fraction. Dual immunofluorescence revealed 17.3% cells with nuclear NF-κB co-localises with Oct4 in SP fraction, which enhanced up to 43.4% once treated with cisplatin. Marginal increase in co-localisation of NF-κB & Oct4 in MP fraction and no change in NSP fraction clearly indicate contribution of NF-κb in CSC homeostasis and PIK3CA regulation in SP fraction alone. Enhanced expression in pluripotency gene (Oct4, Sox2 and Nanog) by cisplatin exclusively in SP cells but not in MP or NSP cells warranted escalation of CSC characteristics in SP fraction. Interestingly, same chemotherapeutic treatment induced distinct pluripotent gene expression in A2780-CisR, TOV21G and SKOV3 cells probably due to intercellular differences in genetic constituents. Further to inspect NF-κB mediated PIK3CA regulation, we assessed NF-κb-PIK3CA promoter physical interaction in SP and NSP cells pre and post TNFα or cisplatin treatment. Similar to MP, SP also demonstrated enhanced occupancy of NF-κB on PIK3CA promoter following TNFα or cisplatin treatment. NSP cells did not show such occupancy on PIK3CA promoter in untreated and cisplatin treated cells. TNFα, however, induced NF-κB binding on PIK3CA promoter in NSP fraction. This seemingly contradictory NF-κb-PIK3CA promoter interaction by two different stimuli is not surprising

as NF-κB activation by UV-C or doxorubicin is known to induce a complete different set of target genes than that by TNF☐ and produce entirely different functional consequences.[344] CSC is envisioned to be the key component leading to the relapse of tumor and chemoresistance. However, the knowledge on the etiology of ovarian CSC and mechanism of their enrichment is still limited. These therapy persister controls tumor development through their differentiation into non-CSC tumor cells. Chemotherapy has been shown to enrich cancer stem cells in tumors. If a cytotoxic drug can enrich CSC population in drug resistant cells, it would certainly affect either self renewal or their differentiation. We observed that, cisplatin or TNFα favours self-renewal of CSCs (SP fraction). All these data led us to hypothesize that NF-κB controlled PIK3CA expression coordinates the CSC survival and CSC plasticity under the influence of a chemotherapeutic agent. Indeed, treating SP cells with wortamanin, an irreversible PIK3CA inhibitor, with and without cisplatin diminished the percent positivity of SP cells. Further, to understand the fate of these CSC upon cisplatin treatment, we assessed their cellular fate through gene expression analysis. This revealed quiescent (increased p21, p27 decrease in cyclin D1 and cyclin E1), anti-apoptotic (increased FLIP) cell fate of SP fraction upon cisplatin treatment. In contrast, augmented cyclin D1 & E1 expression in cisplatin treated NSP cells indicated towards proliferative state making them vulnerable towards apoptosis. Our study demonstrated that cisplatin mediates cancer stem cell specific activation of NF-κB, which in turn induces expression of TNFα and PIK3CA. This incremented TNFα is known to act as an autocrine cue in concomitant NF-κB activation [341, 375], while activation of NF-κB escalates PIK3CA in CSC's. Activation of PI3K/AKT confers resistance against cisplatin action through up regulation of anti-apoptotic genes such as cFLIP. Overall, CSC's with active PI3K/AKT and NF-κB signaling acquire anti-apoptotic, quiescent state conferring survival advantage against action of chemotherapeutic drugs. (Figure 3. 11)

Resistance to anticancer drugs is widely observed *in vitro* and in cancer patients. Platinum compounds are in mainstay of cancer clinic for last few decades and will be continued for many more decades for their potent action against cell proliferation. However, resistance acquirement against platinum compounds is a major concern for several malignancies including epithelial ovarian cancer. The cellular and molecular mechanisms behind this resistance acquirement in a resistant cell treated with the same drug are therefore crucial to be identified and still remain poorly understood. The unanticipated finding of cisplatin inducing CSC enriched side population in platinum resistant cells opened a new dimension in our understanding on how action of a cytotoxic drug be modulated by cellular ambience. Activated NF-κB leading to upregulated PIK3CA expression is the key molecular feature behind this action of cisplatin. Though involvement of NF-κB mediated other signalling cascades are possible, our present data signifies PI3K/AKT pathway as the major determinant of cisplatin action in resistant cells.

Chapter 4: Summary and conclusion

Chapter 4: Summary and conclusion

Cancer refers to a collection of clinically diverse diseases aggravating worldwide burden of mortality.[155] Current strategies for cancer management include either targeting proliferative tumor cells through cytotoxic drugs or targeting molecular oncogenic drivers (targeted therapies) through antibodies or small molecules.[22, 36, 148] Chemotherapeutics hinder the homeostasis of these cancer cells hence enduring a key role in existing cancer treatment.[23, 24] Yet, cancer cells evolve new tactics to resist such setbacks, through manipulating survival signaling, which redirect towards same consequence: incessant growth. This primes tumor relapse, more often with chemoresistance, succumbing patient's survival. How chemotherapeutics dictate cellular fate and how to intervention this mechanism is one of the most confounding questions in cancer biology. In many cancers, a key survival pathway- the phosphatidylinositol 3-kinase (PI3K) pathway- can be activated at one or several points, encouraging endurance of a cell against stress such as drug treatment. Particularly, in lung, and ovarian cancer, hyper-activation of PI3K/AKT conforms platinum resistance.[149, 237-239] Though platinum resistance is a common problem for cervical, head and neck, and non-small-cell lung cancer management, it is particularly devastating for epithelial ovarian cancer (EOC) patients as 50% of the therapy responders ultimately show chemoresistant relapse.[156, 183] This thesis sought to dissect the mechanisms of differential activation of PIK3CA signaling in cisplatin-sensitive and resistant cells upon drug treatment.

Cells respond towards therapeutics though dynamically changing cascade of signaling events following therapeutic intervention. In the first part of the study, with the help of PIK3CA promoter sensor, we gain novel insight into PIK3CA promoter modulation in isogenic cisplatin resistant model upon cisplatin treatment. We find that cisplatin treatment represses PIK3CA promoter activity only in sensitive cells, but not in resistant cells. This is also

evident at protein levels, where P110α and pAKT levels are decreased in sensitive cells but not in resistant cells. Rather, cisplatin escalates PIK3CA expression and activates PI3K/AKT signaling, enduring cell survival. In sensitive cells, cisplatin activates p53, which negatively regulates PIK3CA promoter activity. Resistant cells show reduced p53 transcriptional ordinance on its target genes (P21, PUMA, and PIK3CA) and complete loss of PIK3CA regulation which is restored after overexpression of p53 in resistant cells. In order to clarify the molecular mechanism of such differential modulation of PIK3CA expression between sensitive and resistant cells, we have investigated the interaction dynamics of p53 protein with PIK3CA promoter. In order to enable the detection of molecular events longitudinally *in vivo*, we have utilized p53 protein fused with bioluminescence reporter (Nano luciferase-nanoluc) along with PIK3CA-sensor. The use of the bioluminescence reporter provides the ability to quantify the extent of p53-stabilisation and PIK3CA promoter modulation over time. We find that, both in *in vitro and in vivo* conditions, cisplatin activates p53 in both sensitive and resistant cells, however, PIK3CA promoter attenuation is observed only in sensitive cells. With dual-reporter cellular model, we have discovered reduced and delayed activation kinetics of p53 *in vitro* and *in vivo*, thus contributing to abolition of PIK3CA promoter attenuation. These finding may provide additional rationale for crosstalk between tumor suppressor (p53) and oncogenic (PI3K/AKT) signaling. Intriguingly, our dual reporter tumor xenograft model portrays clinical scenario, where stress signaling is activated in both sensitive and resistant cells, yet it is not sufficient to propel apoptosis in resistant cells.

p53 is often referred as 'guardian of the genome' whose transcriptional activity is dictated by the magnitude of protein stabilization, sequence specific DNA binding and posttranslational modifications (PTMs). [274-276] In order to understand the differential regulation of PIK3CA by p53 between sensitive and resistant stages, we have critically analysed binding of p53 on its four response elements present on PIK3CA promoter. With the help of single site

mutation and deletion constructs of PIK3CA promoter, we find that out of four p53 response element, site 3 and 4 p53-RE are crucial for PIK3CA promoter attenuation. This is also corroborated with p53-ChIP assay, which confirms physical interaction between p53 and PIK3CA promoter. In sensitive cells, p53 remain bound to site 1 in unstressed condition, while such occupancy is absent in resistant cells. In response to cisplatin, occupancy of p53 is decreased at site 1, and is increased at site 3 and 4 on PIK3CA promoter in sensitive cells. In contrary, resistant cells show increase in p53 occupancy only at site 1 after cisplatin treatment. This is the first report which demonstrate drug-induced 'relocation' of p53 between its RE on its target promoter dictating its transcriptional activity. Posttranslational modification (phosphorylation and acetylation) offers sequence-specific binding of p53 to its response elements. Hence, to investigate causality for decrease in p53 ordinance over PIK3CA promoter, we have assessed its PTMs as key regulator for its transcriptional activity in cisplatin resistant model. Sensitive cells show hyper-phosphorylation of p53 at serine 15, 20 and 46 along with hyper-acetylation, which is either low (phosphorylation at serine 15 and serine 20 and acetylation) or absent (phosphorylation at serine 46) in resistant cells. With the help of phosphorylation-mimicking (S46D) and phosphorylation-deficient (S46A) p53 mutant, we have confirmed that phosphorylation of serine 46 phosphorylation dictates PIK3CA promoter attenuation in sensitive cells. Further, we have showed reduced levels and cytoplasmic retention of HIPK2 and DYRK2- kinases, which phosphorylate p53 at serine 46- in resistant cells after cisplatin treatment.

The PI3K/AKT pathway plays an important role in the cell survival pathway. Our data indicate cisplatin facilitates activation of PI3K/AKT in resistant cells, which may, thereby prevent apoptosis in these cells. Indeed, in resistant cells, we have observed augmented expression of BCl2 and cFLIP and absence of PARP cleavage indicating an apoptosis resistant phase after cisplatin treatment. Though cisplatin decreases protein synthesis and

favors growth-arrest in sensitive as well as resistant cells, it activates apoptotic machinery only in the sensitive cells while favors a pro-survival fate in resistant cells.

Studies on ovarian cancer cell lines and clinical studies reveal an association between hyper-activation PI3K/AKT pathway and p53 mutations that contributes to therapy resistance. Mutation of p53 is a frequent event in HGSOC, however, whether individual mutations exert differential transcriptional regulation on PIK3CA promoter is still unexplored. To understand the link between mutant p53 and PIK3CA promoter modulation, we have classified clinically relevant p53 mutations into two groups as 'PIK3CA regulators' and 'PIK3CA non-regulators' on the basis of PIK3CA expression levels and status of PI3K/AKT signaling in patient data available with HGSOC-TCGA (n=316). In clinical scenario, as we have demonstrated through analysis of HGSOC-TCGA data, patients with 'PIK3CA non-regulator' category are associated with higher activation of PI3K/AKT signaling compare to mutations from 'PIK3CA regulators' category. We have also observed that, PIK3CA regulators (C176Y and Y220C) attenuate PIK3CA promoter upon chemotherapeutic agent and hence exert wild type p53-like activity on PIK3CA promoter. As per our expectation, PIK3CA promoter attenuation is not observed in cell lines expressing p53 mutations from PIK3CA non-regulator category (R248Q and R273H). Intriguingly, in corroboration with our wild type p53-PIK3CA promoter data, only C176Y and Y220C undergo phosphorylation at serine 46 residue but not R248Q and R273H. Rather, p53 mutations R248Q and R273H escalate PIK3CA expression compare to C176Y, Y220C, and wild type p53, which portraits clinical scenario of activation of AKT in PIK3CA-non regulator category. In summary, we provide a novel classification of p53-hotspot mutations in ovarian cancers, which conceptualise dependency on PI3K/AKT survival pathway. This study also underpins serine 46 phosphorylation as surrogate marker to categorise patients into PI3K/AKT inhibitor susceptible category.

The second part of this thesis focuses on understanding mechanisms of upregulation of PIK3CA expression in chemoresistant ovarian cancer. In resistant cells, when p53 losses its ability to bind at vital p53-RE on PIK3CA promoter, other unidentified regulator/s may play role in escalating PIK3CA expression as a response towards cisplatin. With promoter (DNA)-binder (protein) pull down strategy, we pinpoint 53 differential binders of PIK3CA promoter including NF-κB, β-catenin and CREB in cisplatin treated resistant cells. These are further validated using PIK3CA-promoter reporter assay, where only activation of NF-κB and β-catenin through TNFα, and Lithium chloride display increase in PIK3CA expression in resistant cells. Our study for first time pinpoints a novel mechanism of crosstalk between transcriptional regulations of PIK3CA through β-catenin. However, transcriptional regulation though β-catenin is a complex process which is mediated through its various interacting partners. As our analysis have identified only two interacting (SMAD3 & TCF4) partners, are among large numbers of identified binders, hence further experimental studies are required to estimate the exact contribution of β-catenin complex in PIK3CA promoter regulation.

Interestingly, we have observed differential regulation of NF-κB on PIK3CA expression in cancer stem cell which is absent in non-cancer stem cells. CSC is envisioned to be the key component leading to the relapse of tumor and chemoresistance, which often enriches upon drug treatment. In accordance with this, we have observed CSC-enrichment after cisplatin treatment. Both cisplatin and TNF-α induce binding of NF-κB to PIK3CA promoter and lead to enrichment of cancer stem cell enriched-SP fraction indicating an unique role of cisplatin in self-renewal of CSC. Such CSC enrichment is dramatically reduced upon inhibiting PIK3CA activity with wortmannin. Finally, gene expression analysis shows that cisplatin mediated PI3K/AKT activation lead to an anti-apoptotic, dormant stage, which aids CSC to evade therapeutic action while actively proliferating NSP cells succumb to cisplatin's action. Intriguingly, our study reveals cancer stem cell specific activation of NF-κB upon cisplatin

treatment, which in turn induces expression of TNFα and PIK3CA. This increment in TNFα levels may act as an autocrine cue leading to concomitant activation of NF-κB, while activation of NF-κB escalates PIK3CA in CSC's. Our study thus provides a mechanistic insight into CSC-enrichment by cisplatin treatment where NF-κB mediates activation of PI3K/AKT lead to anti-apoptotic quiescent state in cancer stem cells, enduring their survival against cisplatin.

Conclusion:

Several molecular players are known to play a role in acquirement of cisplatin resistance controlling their cellular fate. Many studies highlight mutations in components of PI3K/AKT pathway contributing to its dysregulation. In this study, we report a novel differential activity of cisplatin-a chemotherapeutic drug wherein it supresses PIK3CA expression through p53 in sensitive cells, while same drug up-regulates PIK3CA vis activation of NF-κB. In sensitive cells, phosphorylation of p53 at serine 46 accelerates its interaction with PIK3CA promoter at site 3 and 4 after cisplatin treatment. This interaction supresses activation of PI3K/AKT survival cascade thereby imposing sensitive cells towards apoptotic fate. Intriguingly, in absence of p53 ordinance, NF-κB escalates PIK3CA expression, priming activation of PI3K/AKT cascade. Overall, activation of PI3K/AKT and NF-κB signaling in resistant cells favours survival and enrichment of cancer stem cells by acquiring anti-apoptotic, quiescent state. Perhaps therapy-induce activation of PI3K/AKT pathway might be one of the radical alteration, which favours endurance of resistant cells and enrichment of cancer stem cells.

Appendices

Appendix A: Materials and methods

1. Reagents:

Table A. 1: Reagents used in this study and their source

Reagents	Catalogue No.	Company
Cisplatin	P4394	Sigma
G418 disulfate salt	G9516	Sigma
SuperFect Transfection Reagent	301307	Qiagen
D-Luciferin	L-8240	Biosynth
Coelenterazine, native	C-7001	Biosynth
Nano-Glo®(Furimazine)	N1110	Promega
RNease kit (RNA extraction kit)	74104	Qiagen
Superscript III (cDNA synthesis kit)	11752050	Thermo Fisher
SYBR® Green PCR Master Mix	4309155	Thermo Fisher

proteinase inhibitor cocktail	P8340	Sigma

2. Bacterial culture and cloning

All the bacterial culture work was performed with antibiotic sensitive E.coli strain DH5α and maintained in Luria-Bertani (LB) medium/LB-Agar plates. Powdered Luria Broth (HiMedia) (20g) was dissolved in 1L autoclaved MilliQ and sterilized by autoclaving. For making LB-agar plates, 35g Luria agar (HiMedia) powder was dissolved/ 1L of autoclaved MilliQ and sterilized by autoclaving. Further LB-agar was poured in 90 mm sterile Petri dish with (ampicillin) or without antibiotics as per the requirement.

2.1 Preparation of ultra-competent cells:

2.1.1 Reagents:

A. *Composition of Super Optimal Broth (SOB):*

Solution A: 2% Bactotryptone, 0.5% Yeast extract, 10mM NaCl, 2.5mM KCl, make the volume up to 100 ml with autoclaved MilliQ. Autoclave to sterilise SOB.

Solution B: Prepare the solution of 10mM MgCl2, 10mM MgSO4 and filter sterilize by passing through 0.2 μ membrane filter.

Add both, solution A and B at the time of inoculation to make SOB medium.

B. *Composition of Transformation Buffer (TB):*

10mM PIPES, 15mM CaCl2, 250mM KCl, adjusted pH to 6.7 with 5N KOH, 55mM MnCl2, make the volume till 100ml with autoclaved MQ. Filter sterilized by passing through 0.2 μ membrane filter.

2.1.2 *Procedure*:

1. E.coli strain DH5α strain glycerol stock was streaked on a fresh LB agar plates without antibiotics and incubated overnight at 37°C.

2. Single colony was inoculated in 200ml SOB broth and incubated at 18°C/150 rpm till it reaches to O.D.$_{(600nm)}$ ~0.4 (Approximately 2-3 days of incubation are required).

3. The cells were harvested by pelleting down by centrifugation at 3500rpm, 4°C and re-suspended in 80ml of TB. Further these cells were incubated on ice for 10min and centrifuged to pellet down.

4. The cell pellet was re-suspended in 18.6 ml TB. 1.4 ml (7%) DMSO was added to the cells and mixed completely.

5. 100μl aliquots of the cells were made in sterile microfuge tubes, snap frozen in liquid nitrogen and stored at -80°C.

2.2 Bacterial transformation:

1. Competent cells (100μl) were thawed on ice and mixed with 1-5 ng of plasmid DNA or 10μl of ligation mixture or 10μl of DpnI digested SDM product and incubated on ice for 30 min.

2. Heat shock was given to the mixture at 42°C for 60 sec and the sample was cooled down on ice.

3. LB medium was added to the cells and incubated at 37°C for 60 min at 170 rpm.

4. The cells were then plated on an LB agar plate with the appropriate antibiotic selection.

3. Molecular cloning and site-directed mutagenesis:

3.1 Protocol for agarose gel electrophoresis:

3.1.1 Reagents and their Source:

A. *Composition of the Tris Borate–EDTA buffer (TBE):*

Tris Borate EDTA (TBE) buffer: 0.9 M Tris base, 0.9 M Boric acid, 0.02 M EDTA (10X buffer stock is made and diluted to 1X for use)

Table A. 2: Reagents required for agarose electrophoresis and their source.

Reagents/Chemicals	*Source*
Tris Borate–EDTA buffer (TBE)	In house preparation
Agarose powder	HiMedia
6X gel loading dye	NEB
Ethidium bromide (EtBr)	SIGMA
DNA marker: 100bp ladder, 1kb ladder	NEB

3.1.2 Procedure

1. The agarose gel percentage varying from 0.7% – 2% (according to the size of the DNA to be resolved) was prepared along with EtBr as a DNA intercalating agent.

2. Solidified gel was transferred to the electrophoresis tank containing 1XTBE buffer.

3. The DNA samples such as PCR product, digestion reaction was mixed with the 6X DNA loading dye containing glycerol for viscosity and bromophenol blue as a tracking dye.

4. An appropriate reference DNA ladder was loaded in parallel. EtBr stained DNA bands were visualized and documented with Gel documentation system.

3.2 DNA extraction from Gel:

The PCR amplified product/restriction digested DNA was gel extracted and purified by using QIAGEN gel extraction kit. Briefly, the following procedure was followed:

3.2.1 Procedure

1. In the presence of UV-illuminator, desired DNA fragment from the agarose gel was excised with a clean, sharp scalpel.

2. The gel piece was weighed in a micro centrifuge tube. Buffer QG was added three time the volume of gel piece (100mg= ~100μl).

3. Reaction was incubated at 50°C for 10min (or until the no visible traces of agarose). The tube was vortexed every 2min.

4. 1 gel volume of isopropanol was added to the sample and mixed. Thereafter, a QIAquick spin column was placed on a 2ml collection tube and the above reaction mix was added to the column.

5. The tube was incubated for 1-2min and centrifuged for 1min at 13000rpm.

6. The flow-through was discarded and further washed with 0.5ml of buffer QG by centrifugation for 1min at 13000rpm.

7. Buffer PE (0.75ml) was added to QIAquick column and was incubated for 5min before centrifuging at 13000rpm for 1min. The flow-through was discarded and washed one more time with buffer PE.

8. An additional dry spin was given to the column and the column was placed in a clean 1.5ml micro centrifuge tube.

9. To elute DNA, 50μl Buffer EB (10mM TrisCl, pH 8.5) or water was added directly to the QIAquick membrane and centrifuged at 13000rpm for 1min.

3.3 Protocol for restriction digestion:

3.3.1 Reagents:

Restriction enzymes: NheI, BamHI, BglII, NotI, EcoRI and XhoI, NEB

Compatible buffers NEB

3.3.2 Procedure:

1. Vector plasmid or plasmid containing insert was digested with two restriction enzymes simultaneously or sequentially in a compatible buffer. NEB buffer which shows maximum activity of both the enzymes was chosen using the enzyme activity chart (provided by NEB).

2. Before beginning with digestion the recommended buffer was allowed to thaw completely on ice also the water bath is set at 37°C.

3. A typical restriction digestion mix consisted of following components:10X NEB buffer, DNA (insert/ vector), Enzyme/(s), Distilled water.

4. The reaction mixture was incubated at 37°C water bath, overnight.

3.4 **Protocol for Ligation**

Ligation was performed by using DNA ligase, which catalyses the formation of phosphodiester bond between juxtaposed 5'phosphate and 3'hydroxyl terminal in duplex DNA or RNA. This enzyme joins blunt and sticky ended termini as well as repair single stranded nicks in duplex DNA, RNA or DNA/RNA hybrids. The ligation reaction was set depending upon the concentration of the insert. Ideally, the vector to insert ratio is (1:3) which is essential for carrying out successful ligation reaction.

3.4.1 *Procedure*

1. Source of reagents: Quick ligase enzyme and its 10 X buffer was obtained from NEB, UK.

2. The ligation reaction was carried out at room temperature and incubated for 10-15 minutes before performing bacterial transformation.

3. After transformation the LB agar plates were placed in the incubator for overnight. After 16-18 hrs of incubation, the plates were checked for colonies.

4. Colonies are cultured in LB broth and plasmids were isolated. Screening for the positive clone was performed by restriction digestion.

5. Positive clone obtained by cloning was further verified by DNA sequencing.

6. Sequencing was performed using the ABI automated DNA sequencer available with Genomics facility of ACTREC.

3.5 **Site Directed Mutagenesis (SDM)**

SDM is a molecular technique that deliberately changes sequences in gene or DNA locus with specific intentions. It is used to create point mutation (single base pair change), deletion, insertion or substitution of more than one base pair. SDM is often used in application like

amino acid changes for protein structure and functional studies, promoter sequences changes to vary expression of the gene or to study binding affinity of transcription.

3.5.1 Guidelines for Primer Design

1. Both of the mutagenic primers must contain the desired mutation and anneal to the same sequence on opposite strands of the plasmid

2. Primers should be between 25 and 45 bases in length, with a melting temperature (Tm) of ≥78°C.

3. The desired mutation (deletion, insertion or substitution) should be in the middle of the primer with ~10–15 bases of correct sequence on both sides.

4. The primers optimally should have a minimum GC content of 40% and should terminate in one or more C or G bases.

5. 125 ng of each oligonucleotide primer is used in the amplification reaction. To convert nanograms to picomoles of oligo, use the following equation:

X picomoles of oligos = 125ng of oligo X 1000

330 X number of bases of oligo

Using SDM, site specific mutations can be generated in virtually any double-stranded plasmid using a four-step procedure. The steps are as follows:

3.5.2 Step I. Plasmid Preparation

Preparation of the plasmid (template DNA) for SDM by using miniprep plasmid isolation,bearing target DNA sequence for mutation. DNA is isolated from the E.coli strains that produce methylated DNA and are susceptible to DpnI digestion.

3.5.3 Step II. Temperature Cycling

a) Denaturation of the plasmid.

b) Annealing with the mutagenic primers (oligonucleotides primers containing desired mutation).

c) Pfu turbo DNA polymerase, that does not displace the newly synthesized strand and stops the extension, is used to extend and incorporate mutagenic primers resulting in the nicked circular DNA strands.

3.5.4 Step III. DpnI Digestion

The methylated and non-mutated template DNA is digested with DpnI restriction enzyme (overnight at 37°C).DpnI endonuclease (target sequence: 5´-Gm6ATC-3´) is specific for methylated and hemi-methylated DNA and is used to digest the parental DNA template and specifically select for mutation-containing synthesized DNA.

3.5.5 Step IV. Transformation

The circular nicked, ds DNA is transformed in DH5α-E.coli competent cells. After transformation the competent cells repairs the nicks in the mutated plasmids. Colonies obtained from this procedure are cultured and the plasmid obtained are confirmed for desired mutation by sequencing.

4. Cell culture:

All the cell culture maintenance and experimental procedures were performed following standard aseptic techniques. All the culture mediums were supplemented with 10% FBS, 1% 100U/ml penicillin and 100 µg/ml streptomycin(complete medium).

4.1 Cell lines and their p53 and PIK3CA genomic status:

Four human ovarian and two breast human cancer cell lines were utilised for this study respectively. (Table A. 3) Isogenic cisplatin chemoresistant model established in APFT (A2780 cells stably expressing PIK3CA sensor) were used for this study.[269] Both, A2780 (cisplatin sensitive) and A2780-CisR (cisplatin resistant) cells were maintained in complete

DMEM medium. All the media were supplemented with 10% FBS, 1% penicillin-streptomycin solutions. All the cells were cultures in their respective media and maintained under standard aseptic practice.

Table A. 3: Cisplatin sensitivity and PIK3CA, p53 genomic status of cell lines utilised in the study.

Cell line	*Cancer origin*	*p53 mutational status*	*PIK3CA mutational status*	*number*	*Cisplatin amplification sensitivity*	*Medium*
A2780	Ovarian	Wild type	Wild type	2	Sensitive	DMEM
OAW42	Ovarian	Wild type	Wild type	2	Sensitive	MEM
TOV21G	Ovarian	Wild type	Wild type	2	Resistant	RPMI
SKOV3	Ovarian	p53-deficient	Wild type	3	Resistant	RPMI
MCF7	Breast	Wild type	Wild type	2	Sensitive	RPMI
ZR-75-1	Breast	Wild type	Wild type	2	Resistant	RPMI

4.2 Maintenance of cell lines:

1. The entire medium from culture dish was removed and adherent cell monolayer was washed twice with 5ml of 1xPBS to remove any residual FBS.

2. 1ml of trypsin/EDTA solution was added to cover adhering cell layer in a 10cm dish and incubate for 1 to 2min at 37^0C.

3. Bottom of the plate was tapped on the countertop to dislodge cells. Culture was checked with an inverted microscope to ensure detached cells from the surface.

4. 3ml complete medium was added to stop trypsin action. Single cell suspension was made through gentle pipetting and cells are transferred into 15ml tube.

5. Cells were pelleted by centrifuged at 1000rpm, 4^0C for 5min. The supernatant was discarded and cells were re-suspended in the 1xPBS.

6. Viable cell count from cell suspension was estimated by trypan blue dye exclusion method using haemocytometer and cells number per ml was calculated using following formula: No of cells/ml =average number of cells per WBC chamber x 10^4 Generally, a 1:5 split ratio was used for subcultures.

7. All the cultures were maintained in a 37°C incubator with 5% CO2 and 95% humidity.

4.3 Cryopreservation:

1. Cells were trypsinised as described above, and cell suspension was centrifuged at 1000rpm for 5min at 4°C and the supernatant was discarded. Number of cells was calculated by trypan blue method using haemocytometer.

2. Freezing medium was prepared by adding 50-60% serum to complete medium along with 5%-8% of DMSO as per the requirement.

3. 1×10^6 - 2×10^6 cells were gently re-suspended in 1ml of chilled freezing medium with gentle pipetting and immediately transferred to a cryopreservation vial (cryo vials).

4. Cryo vials were then transferred to chiller to reduce temperature at the rate of $1\text{-}2^0/\text{hr}$ at -80^0C for overnight and then transferred to liquid nitrogen for cryopreservation.

4.4 **Revival of cryopreserved cells:**

1. Cryo vial from the liquid nitrogen was thawed at room temperature for approximately 3-5 minutes and immediately added to 15ml tube containing complete medium.

2. Components of freezing medium especially DMSO were removed from these cells by centrifugation at 700rpm for 5min at 4°C and the cell pellet was re-suspended in complete media with gentle pipetting.

3. The cell suspension was transferred to a new culture vessel or plate. Cells were allowed to adhere to the substratum by incubating at 37°C in 5% CO2 and 95% humidity.

5. **Transfection of adherent cell line:**

Transfection is the process of deliberately introducing nucleic acids (plasmid construct's) in eukaryotic cells by liposomal methods.

5.1 **Reagents:**

Superfect transfection reagent (Quigen),

Plasmid DNA (minimum 100ng/µl concentration), 1X PBS,

In-complete medium (without FBS and antibiotics, filter sterilised)

5.2 **Protocol:**

1. Viable cells were seeded at a particular density one day prior to transfection in culture vessel, primarily 24well plate.

2. DNA-Superfect reagent complex was prepared by adding required amount of plasmid/s (1µg) and transfection reagent (5µl) in appropriate amounts of incomplete

medium (100µl) with gentle tapping. This mixture was incubated for 10min at room temperature.

3. Meanwhile, the culture medium from the culture vessel was aspirated and washed twice with 1X PBS.

4. Definite amount of complete media (300µl) was added to the transfection mixture and administered to the cells. The plate was swirled gently to uniformly distribute the complex and incubated at 37°C, 5% CO2.

5. After 3hrs of incubation, the transfection media was aspirated washed with 1X PBS and complete media was added to these cells.

For stable transfection, after 24-48hrs of transfection in 60mm culture dish, the cells were trypsinized and sub-cultured in two 100mm culture dish with complete media containing either puromycin or G418 depending on the plasmid selection marker.

6. Cell viability assay (MTT assay):

6.1 Reagents

Table A. 4: Reagents required for MTT and their source

Reagents/Chemicals	Source
DMSO	HiMedia
MTT (3-(4,5-dimethylthiazol-2-yl)-2,5-diphenyltetrazolium bromide),	SIGMA
Reagents/Chemicals	Source
DMSO	HiMedia
MTT (3-(4,5-dimethylthiazol-2-yl)-2,5-diphenyltetrazolium bromide),	SIGMA

6.2 Procedure:

1. The cells were seeded in a 96 well plate (2000 cells/well). Each experiment was done in quadruplet and repeated at-least trice.

2. As per the requirement, a gradient or a specific concentration of inhibitor or drug was incubated with these cells for 72hrs at 37ºC, 5% CO_2.

3. At end points, cells were incubated with 20µl of 5mg/ml MTT and incubated for 3 hours.

4. The spent media from each well were removed completely without disturbing the formazan crystals. These crystals were solubilised by adding 100µl DMSO.

5. Optical density of solubilised formazan crystals was measured at wavelength 560nm and 670nm.Note- The absorbance at560nm was subtracted from the absorbance at 670nm to remove the background caused by the presence of DMSO.

6. Percent viability was counted using the formula [(Absorbance of Test ÷Absorbance of Control) ×100]. For drug treatment, freshly prepared cisplatin (30µg/µl) in 0.9% saline was used as stock solution. Different concentrations of cisplatin were prepared and incubated with sensitive and resistant cells. All experiments were performed at least three times.

7. Real time quantification of gene transcript (mRNA) levels

7.1 Total RNA Isolation and quality check:

7.1.1 Reagents and their Source:

Table A. 5: Chemicals required for RNA isolation and its quality check

Reagents/Chemicals	*Source*

RNeasy min total RNA isolation kit	QIAGEN
Diethyl Pyrocarbonate (DEPEC)	SIGMA
Ethanol	SIGMA
3-(N-morpholino) propanesulphonic acid (MOPS)	SIGMA
Formaldehyde	SIGMA
Formamide	SIGMA
EDTA 0.5M pH 8	SIGMA
Ethidium bromide	SIGMA
6X RNA loading	SIGMA
Agarose	INVITROGEN

A. *Composition of 10X MOPS buffer:*

0.2M MOPS, 50mM sodium acetate, 10mM EDTA.

B. *Composition of Running buffer:*

30 ml 10X MOPS buffer + 30 ml formaldehyde make up the volume to 300 ml.

C. *RNase Free water (DEPEC treated water):*

Add 1ml DEPEC in 999 ml of MilliQ and incubate overnight at 37°C.

Autoclave before use.

7.1.2 *Procedure:*

Total RNA from different cell lines was isolated using QUIGEN's total RNA isolation kit. Isolation of total cellular RNA:

1. 4×10^4 cells were harvested and washed with 1X PBS for 5min at 1200rpm 4°C.The supernatant was discarded.

2. The pellet was re-suspended in RLT (350µl) by pipetting and centrifuged for 3 min at 13000 rpm. Supernatant was collected in another tube.

3. Equal volume of 70% ethanol (350µl) was added in the supernatant, mixed well.700 µl of sample was transferred to RNeasy spin column placed in a fresh collection tube and centrifuged at 10000rpm for 15s. Flow-through was discarded.

4. 700µl of Buffer RW1 was added to the RNeasy spin column and centrifuged for 15s at 10000 rpm. Flow-through was discarded.

5. 500µl of Buffer RPE was added to the RNeasy spin column and centrifuged for 15s at 10000 rpm. Flow-through was discarded.

6. 500µl of Buffer RPE was added to the RNeasy spin column and centrifuged for 2min at 10000 rpm. Flow-through was discarded.

7. The RNeasy spin column was placed in a new 1.5ml collection tube and 30–50µl RNase-free water was added directly to the spin column membrane. Sample was then centrifuged at 10000 rpm for 1min to elute the RNA.

8. RNA was quantified with the help of Nano-drop. A good quality total RNA isolate has an O.D 260/280 ratio of 1.8-2 and O.D 260/230 ratio of 1.8 or more.

7.1.3 *Preparation of denaturing gel for visualisation of RNA (90ml):*

1.08g Agarose was added to RNase free water 76.5 ml and boiled to melt agarose completely. 10X MOPS buffer (9ml) and formaldehyde (4.5ml) and EtBr was added to melted agarose. The gel was poured in the gel-casting tray with a comb and allowed to solidify.

7.1.4 *Preparation of RNA sample for gel loading:*

Formaldehyde (1µl), Formamide (3µl), 10X MOPS buffer (1µl) and RNA quantity 1-2µg. The reaction mix was incubated for 5-10min a 65°C for denaturation. 6X RNA loading dye (1-2µl) was added and loaded on the gel. Once tracking dye reached to ¾ of gel, RNA bands were visualised on UV transilluminator.

7.2 cDNA Synthesis from Total RNA:

The cDNA was synthesized from total RNA using the superscript II first strand synthesis kit from INVITROGEN according to the manufacturer's protocol.

7.2.1 *Procedure:*

1. For each reaction, following components are combined in a 0.5-ml tube:

Component	Amount
RNA (1-2 µg)	X µl
10mM dNTP mix	1µl
Random hexamer (50ng/µl)	1µl
DEPC treated water to make volume	10µl

2. Starting material: 2µg total RNA

3. Control reactions: Use 1 µl of Control RNA (50 ng/µl)

4. The RNA/primer mixture was incubated at 65°C for 5min and placed immediately on ice for at least 1min.

5. In a separate tube, following 2X reaction mix was prepared by adding each component in the indicated order.

6. 9 µl of the 2X reaction mix was added to each RNA/primer mixture from step 3, mix gently, and collect by brief centrifugation.

7. The tube was then incubated at room temperature (~25°C) for 2 minutes.

8. 1 µl of SuperScript™ II RT was added to each tube.

9. Minus RT Control: 1 µl DEPC-treated water was added instead of the RT.

10. Incubate at room temperature for 10 minutes.

11. Incubate at 42°C for 50 minutes.

12. Terminate the reaction at 70°C for 15 minutes. Chill on ice.

13. Collect the reaction by brief centrifugation. Add 1 µl of RNase H to each tube and incubate for 20 minutes at 37°C. The reaction can be stored at -20°C.everse transcriptase PCR.

7.3 Quantification of gene expression (Real-time PCR):

7.3.1 Reagent:

Sybr Green, Primers

Table A. 6: Primer sequences used for real time PCR

Gene Name	Primer sequence
PIK3CA	TCAAAGGATTGGGCACTTTT GCCTCGACTTGCCTATTCAG
BAX	TGGAGCTGCAGAGGATGATTG GAAGTTGCCGTCAGAAAACATG
cFLIP	CCTAGGAATCTGCCTGATAATCGA TGGGATATACCATGCATACTGAGATG

P27	TGCAACCGACGATTCTTCTACTCAA CAAGCAGTGATGTATCTGATAAACAAGGA
P21	GGCAGACCAGCATGACAGATT GCGGATTAGGGCTTCCTCT
GAPDH	TGCACCACCAACTGCTTAGC GGCATGGACTGTGGTCATGAG
CYCLIN-D1	TATTGCGCTGCTACCGTTGA CCAATAGCAGCAAACAATGTGAAA
cMYC	AATGAAAAGGCCCCCAAGGTAGTTATCC GTCGTTTCCGCAACAAGTCCTCTTC

7.3.2 Procedure:

1. Normalize the primer concentrations and mix gene-specific forward and reverse primer pair. Each primer (forward or reverse) concentration in the mixture is 5 pmol/μl.

2. Set up the experiment and the following PCR program on ABI Prism SDS 7000. Do not click on the dissociation protocol if you want to check the PCR result by agarose gel. Save a copy of the setup file and delete all PCR cycles (used for later dissociation curve analysis). Following are the PCR cycle steps:

    a. 50°C 2 min, 1 cycle

    b. 95°C 10 min, 1 cycle

    c. 95°C 15 s → 60°C 30 s → 72°C 30 s, 40 cycles

    d. 72°C 10 min, 1 cycle

3. A real-time PCR reaction mixture can be either 20µl or 10µl. Prepare the following mixture in each optical tube.

   15 µl SYBR Green Mix (2x)

   3 µl prepared cDNA

   1.5 µl primer pair mix (5 pmol/µl each primer)

   9µl H2O

4. Reaction was divided into three replicates in individual well and ran with ABI Prism 7500 Quantstudio 12.0 software.

5. Analyze the real-time PCR result with the SDS 7000 software. Check to see if there is any bimodal dissociation curve or abnormal amplification plot.

8. Western blotting

Cell extracts were prepared by lysing the drug treated cells and control cells with Laemelli buffer.

8.1 Protein estimation by Bradford's method:

The extracts obtained from the lysis of drug treated sensitive and resistant cells were subjected to Bradford's test for estimation of the protein content.

8.1.1 Reagents:

1. SDS lysis buffer: (20mM Tris-HCl, 0.01% SDS, 0.02% β-mercaptoethanol with Sodium vanadate, Sodium fluoride and proteinase inhibitor cocktail)

2. Bradford's reagent

3. 1X PBS

4. Equipment: Microtitre plate reader and Magellen for F50 - software

8.1.2 *Procedure:*

1. Lysates were diluted 1:5 with PBS.

2. 5µl of the extract was added to 250µl of the Bradford reagent. The absorbance was recorded at 595 nm using plate reader. Using BSA standard curve, protein concentration was estimated.

8.2 SDS-Polyacrylamide Gel Electrophoresis:

Immunoblotting was done by first separation of proteins in cell lysate by SDS-PAGE. The proteins separated are transferred onto nitrocellulose membrane and then detection of the proteins is done by probing them against specific antibodies.

8.2.1 *Reagents:*

1. 29.2% Acrylamide (SIGMA, USA).

2. 0.8% Bis- acrylamaide (SIGMA, USA)

3. 10% SDS (SIGMA, USA).

4. Resolving gel buffer: 1.5mM Tris base, adjust the pH to 8.8 using 1N-HCl

5. Stacking gel buffer: 0.5mM Tris base, adjust the pH to 6.8 using 1N-HCl

6. 10% Ammonium persulfate (APS) (SRL Chemicals, India)

7. N, N, N', N'-tetramethylenediamine TEMED (SIGMA, USA)

8. Gel running buffer: 25mM Tris base, 190mM Glycine, 0.1% SDS.

9. 6X- gel loading dye: 50mM Tris HCl pH 6.8, 2% SDS, 20% Glycerol, 12.5mM EDTA, 0.02% Bromophenol blue.

10. Pre-stained protein marker (Prism11-245KDa).

11. SDS-PAGE composition

Table A. 7 Recipe for resolving gel composition: 10%

Reagent	Volume(For 10ml)
MilliQ	4.1ml
30% acrylamide	3.3ml
1.5M Tris (pH 8.8)	2.5ml
10% SDS	100 µl
10% APS	50 µl
TEMED	5µl

Table A. 8 Recipe for stacking gel composition: 4%

Reagent	Volume(For 10ml)
MilliQ	1.25ml
30% Acrylamide	260 µl

1.5M Tris (pH 6.8)	500 µl
10% SDS	20 µl
10% APS	10 µl
MilliQ	1.25ml

8.2.2 Procedure:

1. The protein sample (60 µg) was denatured using 5 µl 6x denaturing protein loading dye and heated on a heating block at 100°C for 5 min and then cooled.

2. Protein sample were loaded in each gel and run at 60V in stacking gel and at 80 V in resolving gel.

8.3 **Protein transfer to PVDF membrane (semi-dry blotting):**

8.3.1 Reagent:

1. Tween 20 (SIGMA)

2. 5% Bovine Serum Albumin (BSA) in TBS (blocking) (SIGMA)

3. Tris buffered saline (TBS): 50mM Tris base, 150mM NaCl, adjust the pH to 7.6 using 1N-HCL

4. TBST (TBS with 0.05% tween 20)

5. Enhanced Chemiluminescence ECL (TAKARA)

6. X-ray film

7. Stripping buffer

8. Transfer buffer: 25mM Tris base, 190mM Glycine, 0.04% SDS, 20% methanol.

9. Methanol

10. PVDF

11. Extra thick blot paper

8.3.2 *Equipment:*

1. Mini-PROTEAN Tetra system, Bio Rad

2. Transblot semi-dry transfer apparatus

3. Developing machine

8.3.3 *Procedure (Semi-dry transfer of proteins):*

1. Transfer buffer was prepared containing 20% methanol.

2. After completion of gel run gel and a nitrocellulose membrane also soaked in transfer buffer solution separately for 10 min.

3. Transfer assembly was set up by placing soaked fibre pads, then membrane and gel were placed over it such that both are in contact without any bubbles in between them and the gel is placed above the membrane. Two fibre pads are placed over it and pressed to remove any air spaces. Run transfer at 13V and 400mA for 60 minutes.

8.3.4 *Procedure (Wet transfer of proteins):*

Transfer buffer was prepared containing 20% methanol.

1. After completion of gel run, gel and a PVDF membrane were soaked in transfer buffer solution separately for 10 min. PVDF membrane is activated with methanol for 30 seconds prior to soaking in transfer buffer.

2. Transfer assembly was set up by placing soaked filter pads, then membrane and gel were placed over it such that both are in contact without any bubbles in between them and the gel is placed above the membrane. Two fibre pads are placed over it and

pressed to remove any air spaces. The assembly is placed in Transblot cell and transfer buffer is added upto the brim. Ice packs are kept to prevent heating.

3. Run transfer at 75V and 400mA overnight.

8.4 Immuno-detection:

Table A. 9: List of antibodies and their source

Target Name	Catalogue No.	Company Name
PIK3CA (p110α)	4255	Cell Signalling Technologies (Danvers, MA, USA)
PARP	9542	Cell Signalling Technologies (Danvers, MA, USA)
phospho-AKT (S473)	4058	Cell Signalling Technologies (Danvers, MA, USA)
Total-AKT	9272	Cell Signalling Technologies (Danvers, MA, USA)
phospho serine 15 p53	9286	Cell Signalling Technologies (Danvers, MA, USA)
phospho serine 20 p53	9287	Cell Signalling Technologies (Danvers, MA, USA)
phospho serine 46 p53	2521	Cell Signalling Technologies (Danvers, MA, USA)
Bcl-2	2876	Cell Signalling Technologies (Danvers, MA, USA)
phospho-S6 ribosomal protein	2211	Cell Signalling Technologies

		(Danvers, MA, USA)
Total-S6 ribosomal protein	2317	Cell Signalling Technologies (Danvers, MA, USA)
p53 (ChIP-grade)	SC-126-X	Millipore (MA, USA)
PAN-p53 (for non-acetylated p53)	OP-03	Millipore (MA, USA)
Total p53	SC-6243	Santacruz (Texas, USA)
β-actin	A5316	Sigma-Aldrich (USA)
α-tubulin	T5168	Sigma-Aldrich (USA)
HRP conjugated anti mouse secondary antibodies	A5316	Sigma-Aldrich (USA)
HRP conjugated anti rabbit secondary antibodies	A0545	Sigma-Aldrich (USA)
Lamin-A	AB26300	ABCAM (Cambridge, USA)
β-catenin	AB32572	ABCAM (Cambridge, USA)

8.4.1 Protocol:

1. After transfer, place the membrane in 5% BSA in 1×TBS containing 0.001% Tween 20 (Blocking buffer) or 5% Milk in 1X TBS as per requirement for 60 minutes, under constant agitation.

2. After incubation with blocking buffer, membrane was incubated in primary antibody overnight (12-16hrs) at 4°C under constant agitation.

3. After incubation with primary antibody the membrane was washed thrice with 0.05% TBST for 10 minutes each.

4. Membrane was further incubated with secondary antibody at room temparature for 2hrs under constant agitation.

5. For developing the blot, membrane was washed thrice with 0.05% TBST for 10 minutes each.

6. Develop blot in dark using ECL on an X-ray film.

8.5 Re-probing immunoblot:

1. The membrane was washed thrice with 0.05% TBST for 10 minutes each.

2. For stripping, membrane was placed in stripping buffer at room temperature for 15 minutes.

3. Blot was washed five times with 0.05% TBST for 10 minutes.

4. Re-probed stripped blot as above.

For validation of extracts, the blots were probed with cytoplasmic marker protein   beta actin (1:5000 dilution) in 5% milk was used.

Anti-mouse secondary antibody dilution 1:5000 in TBS and anti-rabbit secondary antibody dilution 1:3500 in TBS were used.

9. Luciferase Reporter Assay

The luciferase reporter assay is commonly used as a tool to study gene expression at the transcriptional level. Luciferases make up a class of oxidative enzymes found in several species that enable the organisms that express them to 'bioluminesce' or emit light. The light emitted is a by-product of the oxidative reaction catalyzed by the luciferase enzyme. In a luciferase reporter system, a gene promoter (of interest) is fused with the cDNA encoding a luciferase enzyme (either firefly luciferase or renilla luciferase). Modifications in the promoter activity can be monitored by the

measurement of luciferase enzyme activity which is directly proportional to the bioluminescence emitted.

9.1.1 Reagents:

Table A. 10 Source of Reagents for luciferase assay

Reagent/chemicals	Source
LAR II (Substrate for firefly luciferase *in vitro*)	Promega
Colenterazine (Substrate for renilla luciferase)	Biosynth
D-Luciferin (Substrate for firefly luciferase *in vivo*)	Biosynth
Dual Luciferase reporter assay system	Promega

9.1.2 Procedure for in vitro luciferase assay

1. 50µl of substrate was taken in the wells of 96-well plate

2. 10µl of lysate was added in each well

3. The combination was mixed properly with pipette tip.

4. Each of the luciferase reactions was measured in a Berthold luminometer for a period of 60 seconds.

5. The relative light unit per second (RLU/sec) obtained was normalised with protein estimated by Bradford method.

10. Immunofluorescence

Immunofluorescence is an antigen-antibody reaction where the antibodies are tagged (labelled) with a fluorescent dye and the antigen-antibody complex is visualized using ultra-violet (fluorescent) microscope. Immunofluorescence can be used to determine the localization, abundance and co-localization with another proteins.

10.1.1Reagents:

Table A. 11 List of reagents and their source required for immunofluorescence

Reagent/chemicals	Source
Paraformaldehyde	Sigma,USA
Bovine Serum Albumin	Sigma, USA
DAPI	Sigma, USA
Vectashield (Mounting media)	Vector Labs, USA
Triton X 100	Sigma, USA
Anti-Mouse FITC	Sigma, USA
Anti-Rabbit FITC	Sigma, USA
Anti- Rabbit FITC	Sigma, USA
Anti-Mouse Dy Light 633	Sigma, USA

Preparation of 4% paraformaldehyde

Paraformaldehyde was weighed equal to 4% volume of the final solution (for 100 ml final volume, weigh 4 g of paraformaldehyde) and added in 1X PBS (volume equal to

slightly less than 2/3 of the final desired volume). The mixture stirred at 60ºC using a magnetic stirrer and after complete dilution of PFA the final volume was made up. The solution was filtered by Watman filter paper and was chilled on ice before use. Freshly prepared paraformaldehyde solution was usually preferred for the experiment.

10.1.2 Procedure

Different staining and fixation procedures were followed to stain the cells with different antibodies. The general procedure for immuno-fluorescence was as follows:

6. 80% confluent plate was trypsinized and 30,000 - 40,000 cells were seeded per cover slip in a 6 well plate. Two cover slips per sample: One for secondary antibody control (without primary antibody) and the other as a test sample for staining were seeded.

7. Cells were then incubated in 5% $CO2$ at 37°C for 24h.

8. After 24h, the spent medium was aspirated and cells were washed twice with 1X PBS.

9. Cells were fixed on coverslip with 2ml of 4% PFA and incubated at room temperature for 10min. PFA was then removed and cells were washed thrice with PBS.

10. Permeabilization is often required for nuclear staining. Coverslips containing cells were then incubated in Triton X 100 (0.025 to 0.3%)in 4% PFA. The permeabilization solution was removed and cells were washed thrice with PBS.

11. The cells were now incubated with 5% BSA for 60 min at room temperature (blocking).

12. Each cover slip (containing cells) was then incubated with 50μl of primary antibody (1:100 dilution in 1X PBS) on a clean glass slide. Cover slip was placed with cell surface facing downward.

13. Cells were incubated with the primary antibody overnight in a moist chamber at 4°C.

14. On the next day, cover slips were washed thrice with PBS. Each cover slip (containing cells) was then incubated with 50μl of secondary antibody (1:200 dilution in 1X PBS) on a clean glass slide. Cover slip was placed with cell surface facing downward.

15. Incubation was carried out for 2 hours at room temperature in dark after which cells were washed thrice with PBS.

16. Cells were counter stained with 50μl of DAPI (0.05%) for 30 seconds and after washing for three times with PBS, coverslips were mounted on clean glassslide (cell surface facing downward) using Vectashield mounting medium.

17. Cells were observed under confocal laser scanning microscope within 1hour. Argon, Helium/Neon and diode lasers were used to capture images on a Carl Zeiss LSM 510 Meta confocal microscope and the images were analysed using LSM Image Browser.

11. *In vivo* Bioluminescence Imaging in Living Mice

In vivo bioluminescence imaging (BLI) is sensitive tool that is based on detection of light emission from cells or tissues. BLI allows a non-invasive, and real-time analysis of biological processes at the molecular level in living organisms. *In vivo* imaging allows longitudinal monitoring of disease like tumor formation in the same animal and offers desirable alternative to analyse number of animals at many time points during the progression of tumor formation. The *in vivo* BLI in mice uses the following procedure.

11.1 **Cell preparation**

Luciferase (firefly luciferase or renilla luciferase or nanoluc luciferase) expressing ovarian cancer cell lines (A2780, A2780-CisR, APN and APN-CisR) were established in the laboratory. These cells are highly tumorigenic and can be used in pre-clinical mouse models. The cells are cultured in standard growth conditions and amplified in amount required for implantation in specific number of mice. A 70-80% confluency flask is considered optimum for its use in implantation. An *in vitro* validation of the bioluminescence activity was performed earlier by luciferase assay.

11.2 **Animal Injection**

1. A 70-80% confluent flask cells were harvested by trypsinisation and counted using trypan blue.

2. Four-six million cells per mouse were used for implantation. Accordingly total number of cells required for all the mice were counted and collected in a microfuge tube. The final count of the cell number was dissolved in 100μl of 1X PBS and the cells were kept in ice. Care should be taken that the mice should be kept ready for implantation to avoid loss of viable cells and cells should be immediately implanted in mice.

3. Usually, in order to facilitate optimal formation of tumor athymic immunocompromised mice were preferred for implantation. Animal care and euthanasia were performed with the approval from Institutional Animal Ethics Committee of ACTREC. If SCID (Severe Combined Immuno-deficiency) mice were used, then the fur of the mice were removed by razor, to facilitate proper implantation and optical imaging. For nude mice no such pre-treatment is required.

4. Prior to implantation, animals were anesthetized by Xylazine (100 µl) -Ketamin (360 µl) combination.

5. Required amount of cells were loaded in a syringe with 26 guage needle.

6. The skin of the mice was lifted to make a tent and the cells were injected at the base to get a subcutaneous injection.

7. The newly injected mice can be imaged immediately.

11.3 **Animal imaging**

1. For each imaging session, D-luciferin (100 µl of 30mg/ml per mouse) or coelenterazine (50µg/mouse) was given through either intraperitoneal or tail-vein injection respectively.

2. After substrate injection the animals were imaged with IVIS-Spectrum optical imager.

3. In both the system, the bioluminescence signals from the animal were captured by a back-thinned charge coupled device camera cooled to -90°C.

4. For imaging through IVIS Spectrum optical imager, ROIs were drawn over the tumors and quantified by using the Live Image (4.4) software. Bioluminescence signals were recorded as maximum (photons/s/cm^2/sr). Photon flux (bioluminescence signal) from the tumor is proportional to the number of live cells expressing luciferase so bioluminescence correlates directly with tumor size.

5. Field of view is selected for the number of animals being imaged. Upto 5 animals can be maintained in the instrument under the influence of anaesthetic agent.

6. In Living Image software, exposure time, aperture size (f-stop) and pixel binning can be optimized based on the expression level of the cell line. These settings can be changed at any time during an experiment without impacting the quantitative result. However, for the WinlightOptimas Live image software, the above parameters cannot be tampered after capturing the image.

12. DCV Staining protocol

12.1.1 Solutions and Reagents:

DCV

Verapamil 50uM

12.1.2 Protocol:

1. Cells were used at 75% confluency

2. Cells were trypsinised and cell count taken using trypan blue

3. Three aliquots were made

    i. Tube 1 = 0.5 million cells unstained

    ii. Tube 2 = 1 million cells Verapamil+ DCV (Cover with foil)

    iii. Tube 3 = 1 million cells for DCV staining (Cover with foil)

4. These 3 tubes were centrifuged at 1200 rpm for 5 min to get rid of trypsin and 1 PBS wash.

5. Tube 1,2 & 3 were resuspended in 1 ml media and kept at 37^0C water bath

6. 1ul of 50uM stock verapamil was added to tube 2 for 15 min

7. 1ul of DCV dye was added to tube 2 and 3 after 15 min and kept at 37^0C for 90 min (every 15 minutes cells were mixed by tapping)

8. all the tubes were centrifuged at 1200 rpm at 4^0C

9. One PBS wash was given to each tube

10. Tube 1, 2 and 3 were resuspended in 500ul PBS in FACS tube and acquired within 3 hours.

Appendix B: Primers for colony PCR

Table B. 1 Primers used in colony PCR for plasmid clone screening: s

Primer	Sequences
hrl-egfp-forward primer (Set 1)	5'-ACGAGCTAGCATGGCTTCCAAGGTGTACGACCC-3'
hrl-egfp-reverse primer (Set 1)	5'-CCCGCGGTCTTGTACAGCTCGTCCATGCCGAGA-3'
PIK3CA-forward primer (Set 2)	5'-GTAAGATCTACTGCTCCTACGCTTC-3'
PIK3CA-reverse primer (Set 2)	5'-GCAGCTAGCTCGTGTAAACAAACAACG-3'

Appendix C: Primers for SDM- PIK3CA single site mutation

Table C. 1 Site directed mutagenesis primers used for generation of single site mutation at p53 response element on PIK3CA promoter.

Underlined sequence are mismatch bases for mutating p53-response element.

p53 binding sites	Mutagenic primers
Site 1	5'GGTACGCAG<u>CACTGTGACA</u>CTACCTTG 3' F 5' CAAGGTAG<u>TGTTACAGTG</u>CTGCGTACC 3' R

Site 2	5'CGCGAAAAAT<u>CCCCAGAATC</u>TTCTGAATAG 3'F
	5'CTATTCAGAA<u>GATTCTGGGG</u>ATTTTTCGC3' R
Site 3	5'TCCATAACCAC<u>GAGAATTAGC</u>CACTGAC3' F
	5' GTCAGTG<u>GCTAATTCTC</u>GTGGTTATGGA 3' R
Site 4	5'TCGGGCGGA<u>AAAGTGTGAC</u>GCAGGCG 3'F
	5'CGCCTGC<u>GTTACACTTT</u>TCCGCCCGA3' R

Appendix D: Primers for PIK3CA deletion constructs

Table D. 1: Primers used for generation of single site containing deletion constructs of PIK3CA promoter.

Primer	Deletion construct primers
OS1- PIK3CA	5'-GTAAGATCTACTGCTCCTACGCTTC-3' 5'-GCAGCTAGGCCAACAGAGACTTCAGAAAT-3'
OS2- PIK3CA	5'-GTAAGATCTCCTTGAATCAAATCTATAGCC-3' 5'-GCAGCTAGCGACATGGTTTAAGTTGTATAC-3'
OS3- PIK3CA	5'-GCAGCTAGCTAGGACAGCGTACGTGTA-3' 5'-GTAAGATCTGTATACAACTTAAACCATGTCG-3'
OS4- PIK3CA	5'-GTAAGATCTACACGTACGCTGTCCTA-3' 5'-GCAGCTAGCTCGTGTAAACAAACAACG-3'

Appendix E: Primers for Site specific ChIP

Table E. 1 Site specific ChIP-Primer

p53 Site specific primer	Primer sequence
Site 1	CGCACAGTACCGAACCCTTAT AATGCCAACAGAGACTTCAGAAATG
Site 2	CATTTCTGAAGTCTCTGTTGGCAT CGTGGAGACCTTTTGCTATGC
Site 3	ACCATGTCGGCAGAAGAACG AACGAGATTAGTTCGGGGGTG
Site 4	TACATAAACTTCGGGCGGAAA AAGAAGCGGAAGCGAAATTG

Reference:

Reference:

[1]Hackel PO, Zwick E, Prenzel N, Ullrich A. Epidermal growth factor receptors: critical mediators of multiple receptor pathways. Curr Opin Cell Biol. 1999;11(2):184-9.

[2]James A, Swann K, Recce M. Cell behaviour as a dynamic attractor in the intracellular signalling system. J Theor Biol. 1999;196(3):269-88.

[3]Hunter T. Signaling--2000 and beyond. Cell. 2000;100(1):113-27.

[4]Aplin AE, Howe A, Alahari SK, Juliano RL. Signal transduction and signal modulation by cell adhesion receptors: the role of integrins, cadherins, immunoglobulin-cell adhesion molecules, and selectins. Pharmacol Rev. 1998;50(2):197-263.

[5]Alroy I, Yarden Y. The ErbB signaling network in embryogenesis and oncogenesis: signal diversification through combinatorial ligand-receptor interactions. FEBS Lett. 1997;410(1):83-6.

[6]Yarden Y, Sliwkowski MX. Untangling the ErbB signalling network. Nat Rev Mol Cell Biol. 2001;2(2):127-37.

[7]Liebmann C, Bohmer FD. Signal transduction pathways of G protein-coupled receptors and their cross-talk with receptor tyrosine kinases: lessons from bradykinin signaling. Curr Med Chem. 2000;7(9):911-43.

[8]Schwartz MA, Baron V. Interactions between mitogenic stimuli, or, a thousand and one connections. Curr Opin Cell Biol. 1999;11(2):197-202.

[9]Breslin T, Krogh M, Peterson C, Troein C. Signal transduction pathway profiling of individual tumor samples. BMC Bioinformatics. 2005;6:163.

[10]Fisher MJ, Paton RC, Matsuno K. Intracellular signalling proteins as smart' agents in parallel distributed processes. Biosystems. 1999;50(3):159-71.

[11]Hurley JH, Meyer T. Subcellular targeting by membrane lipids. Curr Opin Cell Biol. 2001;13(2):146-52.

[12]Doughman RL, Firestone AJ, Anderson RA. Phosphatidylinositol phosphate kinases put PI4,5P(2) in its place. J Membr Biol. 2003;194(2):77-89.

[13]Anderson RA, Boronenkov IV, Doughman SD, Kunz J, Loijens JC. Phosphatidylinositol phosphate kinases, a multifaceted family of signaling enzymes. J Biol Chem. 1999;274(15):9907-10.

[14]Flynn DC. Adaptor proteins. Oncogene. 2001;20(44):6270-2.

[15]Hornberg JJ, Bruggeman FJ, Westerhoff HV, Lankelma J. Cancer: a Systems Biology disease. Biosystems. 2006;83(2-3):81-90.

[16]Kholodenko BN. Cell-signalling dynamics in time and space. Nat Rev Mol Cell Biol. 2006;7(3):165-76.

[17]Berg J, Tymoczko J, Stryer L. Defects in signaling pathways can lead to cancer and other diseases. Biochemistry 5th Edition New York: WH Freeman, Section. 2002;15.

[18]Berridge MJ. Module 7: Cellular Processes. Cell Signalling Biology. 2014;6.

[19]Sitaramayya A. Signal transduction: pathways, mechanisms and diseases: Springer Science & Business Media; 2009.

[20]Hanahan D, Weinberg RA. Hallmarks of cancer: the next generation. Cell. 2011;144(5):646-74.

[21]World Health Organization 2015 [cited 2017]. Mortality factsheets]. Available from: http://www.who.int/en/.

[22]Gatenby RA. A change of strategy in the war on cancer. Nature. 2009;459(7246):508-9.

[23]Piccolo MT, Menale C, Crispi S. Combined anticancer therapies: an overview of the latest applications. Anticancer Agents Med Chem. 2015;15(4):408-22.

[24]Chabner BA, Roberts TG, Jr. Timeline: Chemotherapy and the war on cancer. Nat Rev Cancer. 2005;5(1):65-72.

[25]Wilson WH. Treatment strategies for aggressive lymphomas: what works? Hematology Am Soc Hematol Educ Program. 2013;2013:584-90.

[26]Langlands FE, Horgan K, Dodwell DD, Smith L. Breast cancer subtypes: response to radiotherapy and potential radiosensitisation. Br J Radiol. 2013;86(1023):20120601.

[27]Kato H, Nakajima M. Treatments for esophageal cancer: a review. Gen Thorac Cardiovasc Surg. 2013;61(6):330-5.

[28]Vakaet LA, Boterberg T. Pain control by ionizing radiation of bone metastasis. Int J Dev Biol. 2004;48(5-6):599-606.

[29]Inaba H, Greaves M, Mullighan CG. Acute lymphoblastic leukaemia. Lancet. 2013;381(9881):1943-55.

[30]DeSantis CE, Lin CC, Mariotto AB, et al. Cancer treatment and survivorship statistics, 2014. CA Cancer J Clin. 2014;64(4):252-71.

[31]Stupp R, Hegi ME, Mason WP, et al. Effects of radiotherapy with concomitant and adjuvant temozolomide versus radiotherapy alone on survival in glioblastoma in a randomised phase III study: 5-year analysis of the EORTC-NCIC trial. Lancet Oncol. 2009;10(5):459-66.

[32]Aure JC, Hoeg K, Kolstad P. Clinical and histologic studies of ovarian carcinoma. Long-term follow-up of 990 cases. Obstet Gynecol. 1971;37(1):1-9.

[33]Sugiyama T, Kamura T, Kigawa J, et al. Clinical characteristics of clear cell carcinoma of the ovary: a distinct histologic type with poor prognosis and resistance to platinum-based chemotherapy. Cancer. 2000;88(11):2584-9.

[34]Winter WE, 3rd, Maxwell GL, Tian C, et al. Prognostic factors for stage III epithelial ovarian cancer: a Gynecologic Oncology Group Study. J Clin Oncol. 2007;25(24):3621-7.

[35]Cancer drug classification. Available from: http://www.cancer.ca/en/cancer-information/diagnosis-and-treatment/chemotherapy-and-other-drug-therapies/chemotherapy/types-of-chemotherapy/?region=on.

[36]Gerber DE. Targeted therapies: a new generation of cancer treatments. Am Fam Physician. 2008;77(3):311-9.

[37]Segovia-Mendoza M, Gonzalez-Gonzalez ME, Barrera D, Diaz L, Garcia-Becerra R. Efficacy and mechanism of action of the tyrosine kinase inhibitors gefitinib, lapatinib and neratinib in the treatment of HER2-positive breast cancer: preclinical and clinical evidence. Am J Cancer Res. 2015;5(9):2531-61.

[38]Yun S, Vincelette ND, Segar JM, et al. Comparative Effectiveness of Newer Tyrosine Kinase Inhibitors Versus Imatinib in the First-Line Treatment of Chronic-Phase Chronic Myeloid Leukemia Across Risk Groups: A Systematic Review and Meta-Analysis of Eight Randomized Trials. Clin Lymphoma Myeloma Leuk. 2016;16(6):e85-94.

[39]Burstein HJ. The distinctive nature of HER2-positive breast cancers. N Engl J Med. 2005;353(16):1652-4.

[40]Pozarowska D, Pozarowski P. The era of anti-vascular endothelial growth factor (VEGF) drugs in ophthalmology, VEGF and anti-VEGF therapy. Cent Eur J Immunol. 2016;41(3):311-6.

[41]Miller MJ, Foy KC, Kaumaya PT. Cancer immunotherapy: present status, future perspective, and a new paradigm of peptide immunotherapeutics. Discov Med. 2013;15(82):166-76.

[42]Nieder C, Milas L, Ang KK. Tissue tolerance to reirradiation. Semin Radiat Oncol. 2000;10(3):200-9.

[43]Yip D, Allen R, Ashton C, Jain S. Radiation-induced ulceration of the stomach secondary to hepatic embolization with radioactive yttrium microspheres in the treatment of metastatic colon cancer. J Gastroenterol Hepatol. 2004;19(3):347-9.

[44]Sartor O. Overview of samarium sm 153 lexidronam in the treatment of painful metastatic bone disease. Rev Urol. 2004;6 Suppl 10:S3-S12.

[45]Harrison LB, Chadha M, Hill RJ, Hu K, Shasha D. Impact of tumor hypoxia and anemia on radiation therapy outcomes. Oncologist. 2002;7(6):492-508.

[46]Maverakis E, Cornelius LA, Bowen GM, et al. Metastatic melanoma - a review of current and future treatment options. Acta Derm Venereol. 2015;95(5):516-24.

[47]Hanley J, Debois MM, Mah D, et al. Deep inspiration breath-hold technique for lung tumors: the potential value of target immobilization and reduced lung density in dose escalation. Int J Radiat Oncol Biol Phys. 1999;45(3):603-11.

[48]Lutz S, Berk L, Chang E, et al. Palliative radiotherapy for bone metastases: an ASTRO evidence-based guideline. Int J Radiat Oncol Biol Phys. 2011;79(4):965-76.

[49]Abdulkareem IH, Zurmi IB. Review of hormonal treatment of breast cancer. Niger J Clin Pract. 2012;15(1):9-14.

[50]Lobo RA. Hormone-replacement therapy: current thinking. Nat Rev Endocrinol. 2017;13(4):220-31.

[51]Alderton GK, Bordon Y. Tumour immunotherapy--leukocytes take up the fight. Nat Rev Immunol. 2012;12(4):237.

[52]Seton-Rogers S. Immunotherapy: Combinations that work. Nat Rev Cancer. 2012;12(4):231.

[53]Vanneman M, Dranoff G. Combining immunotherapy and targeted therapies in cancer treatment. Nat Rev Cancer. 2012;12(4):237-51.

[54]Longley DB, Johnston PG. Molecular mechanisms of drug resistance. J Pathol. 2005;205(2):275-92.

[55]Gottesman MM, Fojo T, Bates SE. Multidrug resistance in cancer: role of ATP-dependent transporters. Nat Rev Cancer. 2002;2(1):48-58.

[56]Borst P, Elferink RO. Mammalian ABC transporters in health and disease. Annu Rev Biochem. 2002;71:537-92.

[57]Fojo T, Bates S. Strategies for reversing drug resistance. Oncogene. 2003;22(47):7512-23.

[58]Pan ST, Li ZL, He ZX, Qiu JX, Zhou SF. Molecular mechanisms for tumour resistance to chemotherapy. Clin Exp Pharmacol Physiol. 2016;43(8):723-37.

[59]Abdullah LN, Chow EK. Mechanisms of chemoresistance in cancer stem cells. Clin Transl Med. 2013;2(1):3.

[60]Wilson TR, Longley DB, Johnston PG. Chemoresistance in solid tumours. Ann Oncol. 2006;17 Suppl 10:x315-24.

[61]Groenendijk FH, Bernards R. Drug resistance to targeted therapies: deja vu all over again. Mol Oncol. 2014;8(6):1067-83.

[62]Chen DH, Zhang XS. Targeted therapy: resistance and re-sensitization. Chin J Cancer. 2015;34(11):496-501.

[63]Johnstone RW, Ruefli AA, Smyth MJ. Multiple physiological functions for multidrug transporter P-glycoprotein? Trends Biochem Sci. 2000;25(1):1-6.

[64]Johnstone RW, Ruefli AA, Lowe SW. Apoptosis: a link between cancer genetics and chemotherapy. Cell. 2002;108(2):153-64.

[65]Volm M. Multidrug resistance and its reversal. Anticancer Res. 1998;18(4C):2905-17.

[66]Bush JA, Li G. Cancer chemoresistance: the relationship between p53 and multidrug transporters. Int J Cancer. 2002;98(3):323-30.

[67]Juliano RL, Ling V. A surface glycoprotein modulating drug permeability in Chinese hamster ovary cell mutants. Biochim Biophys Acta. 1976;455(1):152-62.

[68]Guminski AD, Harnett PR, deFazio A. Scientists and clinicians test their metal-back to the future with platinum compounds. Lancet Oncol. 2002;3(5):312-8.

[69]Wu H, Hait WN, Yang JM. Small interfering RNA-induced suppression of MDR1 (P-glycoprotein) restores sensitivity to multidrug-resistant cancer cells. Cancer Res. 2003;63(7):1515-9.

[70]Orr GA, Verdier-Pinard P, McDaid H, Horwitz SB. Mechanisms of Taxol resistance related to microtubules. Oncogene. 2003;22(47):7280-95.

[71]Katsumata K, Tomioka H, Sumi T, et al. Correlation between clinicopathologic factors and kinetics of metabolic enzymes for 5-fluorouracil given to patients with colon carcinoma by two different dosage regimens. Cancer Chemother Pharmacol. 2003;51(2):155-60.

[72]Banerjee D, Mayer-Kuckuk P, Capiaux G, et al. Novel aspects of resistance to drugs targeted to dihydrofolate reductase and thymidylate synthase. Biochim Biophys Acta. 2002;1587(2-3):164-73.

[73]Gatti L, Zunino F. Overview of tumor cell chemoresistance mechanisms. Methods Mol Med. 2005;111:127-48.

[74]Sokol AM, Cruet-Hennequart S, Pasero P, Carty MP. DNA polymerase eta modulates replication fork progression and DNA damage responses in platinum-treated human cells. Sci Rep. 2013;3:3277.

[75]Szakacs G, Paterson JK, Ludwig JA, Booth-Genthe C, Gottesman MM. Targeting multidrug resistance in cancer. Nat Rev Drug Discov. 2006;5(3):219-34.

[76]Anand S, Penrhyn-Lowe S, Venkitaraman AR. AURORA-A amplification overrides the mitotic spindle assembly checkpoint, inducing resistance to Taxol. Cancer Cell. 2003;3(1):51-62.

[77]Bast RC, Jr., Hennessy B, Mills GB. The biology of ovarian cancer: new opportunities for translation. Nat Rev Cancer. 2009;9(6):415-28.

[78]Brozovic A, Fritz G, Christmann M, et al. Long-term activation of SAPK/JNK, p38 kinase and fas-L expression by cisplatin is attenuated in human carcinoma cells that acquired drug resistance. Int J Cancer. 2004;112(6):974-85.

[79]Karin M. NF-kappaB as a critical link between inflammation and cancer. Cold Spring Harb Perspect Biol. 2009;1(5):a000141.

[80]Koti M, Gooding RJ, Nuin P, et al. Identification of the IGF1/PI3K/NF kappaB/ERK gene signalling networks associated with chemotherapy resistance and treatment response in high-grade serous epithelial ovarian cancer. BMC Cancer. 2013;13:549.

[81]Mabuchi S, Ohmichi M, Nishio Y, et al. Inhibition of inhibitor of nuclear factor-kappaB phosphorylation increases the efficacy of paclitaxel in *in vitro* and *in vivo* ovarian cancer models. Clin Cancer Res. 2004;10(22):7645-54.

[82]Nehra R, Riggins RB, Shajahan AN, et al. BCL2 and CASP8 regulation by NF-kappaB differentially affect mitochondrial function and cell fate in antiestrogen-sensitive and -resistant breast cancer cells. FASEB J. 2010;24(6):2040-55.

[83]Tang G, Minemoto Y, Dibling B, et al. Inhibition of JNK activation through NF-kappaB target genes. Nature. 2001;414(6861):313-7.

[84]Beale PJ, Rogers P, Boxall F, Sharp SY, Kelland LR. BCL-2 family protein expression and platinum drug resistance in ovarian carcinoma. Br J Cancer. 2000;82(2):436-40.

[85]Mabuchi S, Ohmichi M, Nishio Y, et al. Inhibition of NFkappaB increases the efficacy of cisplatin in *in vitro* and *in vivo* ovarian cancer models. J Biol Chem. 2004;279(22):23477-85.

[86]Deng J, Carlson N, Takeyama K, et al. BH3 profiling identifies three distinct classes of apoptotic blocks to predict response to ABT-737 and conventional chemotherapeutic agents. Cancer Cell. 2007;12(2):171-85.

[87]Zhivotovsky B, Orrenius S. The Warburg Effect returns to the cancer stage. Semin Cancer Biol. 2009;19(1):1-3.

[88]Duan Z, Feller AJ, Penson RT, Chabner BA, Seiden MV. Discovery of differentially expressed genes associated with paclitaxel resistance using cDNA array technology: analysis of interleukin (IL) 6, IL-8, and monocyte chemotactic protein 1 in the paclitaxel-resistant phenotype. Clin Cancer Res. 1999;5(11):3445-53.

[89]Sampath Ga. Resistance to Taxanes. In: B. Teicher © Humana Press Inc. T, NJ, editor. Cancer Drug Discovery and Development: Cancer Drug Resistance2006.

[90]Gadducci A, Cosio S, Muraca S, Genazzani AR. Molecular mechanisms of apoptosis and chemosensitivity to platinum and paclitaxel in ovarian cancer: biological data and clinical implications. Eur J Gynaecol Oncol. 2002;23(5):390-6.

[91]Giannakakou P, Poy G, Zhan Z, et al. Paclitaxel selects for mutant or pseudo-null p53 in drug resistance associated with tubulin mutations in human cancer. Oncogene. 2000;19(27):3078-85.

[92]Ferlini C, Raspaglio G, Mozzetti S, et al. Bcl-2 down-regulation is a novel mechanism of paclitaxel resistance. Mol Pharmacol. 2003;64(1):51-8.

[93]Slamon DJ, Clark GM, Wong SG, et al. Human breast cancer: correlation of relapse and survival with amplification of the HER-2/neu oncogene. Science. 1987;235(4785):177-82.

[94]Moscatello DK, Montgomery RB, Sundareshan P, et al. Transformational and altered signal transduction by a naturally occurring mutant EGF receptor. Oncogene. 1996;13(1):85-96.

[95]Hengstler JG, Lange J, Kett A, et al. Contribution of c-erbB-2 and topoisomerase IIalpha to chemoresistance in ovarian cancer. Cancer Res. 1999;59(13):3206-14.

[96]Hu L, Hofmann J, Lu Y, Mills GB, Jaffe RB. Inhibition of phosphatidylinositol 3'-kinase increases efficacy of paclitaxel in *in vitro* and *in vivo* ovarian cancer models. Cancer Res. 2002;62(4):1087-92.

[97]Hovinga KE, Shimizu F, Wang R, et al. Inhibition of notch signaling in glioblastoma targets cancer stem cells via an endothelial cell intermediate. Stem Cells. 2010;28(6):1019-29.

[98]Fan X, Matsui W, Khaki L, et al. Notch pathway inhibition depletes stem-like cells and blocks engraftment in embryonal brain tumors. Cancer Res. 2006;66(15):7445-52.

[99]Zou J, Li P, Lu F, et al. Notch1 is required for hypoxia-induced proliferation, invasion and chemoresistance of T-cell acute lymphoblastic leukemia cells. J Hematol Oncol. 2013;6:3.

[100]Wang J, Wakeman TP, Lathia JD, et al. Notch promotes radioresistance of glioma stem cells. Stem Cells. 2010;28(1):17-28.

[101]Yeung J, Esposito MT, Gandillet A, et al. beta-Catenin mediates the establishment and drug resistance of MLL leukemic stem cells. Cancer Cell. 2010;18(6):606-18.

[102]Anastas JN, Kulikauskas RM, Tamir T, et al. WNT5A enhances resistance of melanoma cells to targeted BRAF inhibitors. J Clin Invest. 2014;124(7):2877-90.

[103]O'Connell MP, Marchbank K, Webster MR, et al. Hypoxia induces phenotypic plasticity and therapy resistance in melanoma via the tyrosine kinase receptors ROR1 and ROR2. Cancer Discov. 2013;3(12):1378-93.

[104]Alvero AB. Recent insights into the role of NF-kappaB in ovarian carcinogenesis. Genome Med. 2010;2(8):56.

[105]Hu J, Friedman E. Depleting Mirk Kinase Increases Cisplatin Toxicity in Ovarian Cancer Cells. Genes Cancer. 2010;1(8):803-11.

[106]Vivanco I, Sawyers CL. The phosphatidylinositol 3-Kinase AKT pathway in human cancer. Nat Rev Cancer. 2002;2(7):489-501.

[107]Sharma SV, Gajowniczek P, Way IP, et al. A common signaling cascade may underlie "addiction" to the Src, BCR-ABL, and EGF receptor oncogenes. Cancer Cell. 2006;10(5):425-35.

[108]Choo AY, Blenis J. TORgeting oncogene addiction for cancer therapy. Cancer Cell. 2006;9(2):77-9.

[109]Vanhaesebroeck B, Waterfield MD. Signaling by distinct classes of phosphoinositide 3-kinases. Exp Cell Res. 1999;253(1):239-54.

[110]Stein RC, Waterfield MD. PI3-kinase inhibition: a target for drug development? Mol Med Today. 2000;6(9):347-57.

[111]Marte BM, Downward J. PKB/Akt: connecting phosphoinositide 3-kinase to cell survival and beyond. Trends Biochem Sci. 1997;22(9):355-8.

[112]Scheid MP, Woodgett JR. PKB/AKT: functional insights from genetic models. Nat Rev Mol Cell Biol. 2001;2(10):760-8.

[113]Manning BD, Cantley LC. AKT/PKB signaling: navigating downstream. Cell. 2007;129(7):1261-74.

[114]Manning BD, Toker A. AKT/PKB Signaling: Navigating the Network. Cell. 2017;169(3):381-405.

[115]Lien EC, Dibble CC, Toker A. PI3K signaling in cancer: beyond AKT. Curr Opin Cell Biol. 2017;45:62-71.

[116]Mayer IA, Arteaga CL. The PI3K/AKT Pathway as a Target for Cancer Treatment. Annu Rev Med. 2016;67:11-28.

[117]Yarden Y, Shilo BZ. SnapShot: EGFR signaling pathway. Cell. 2007;131(5):1018.

[118]Backer JM. The regulation and function of Class III PI3Ks: novel roles for Vps34. Biochem J. 2008;410(1):1-17.

[119]Cantley LC. The phosphoinositide 3-kinase pathway. Science. 2002;296(5573):1655-7.

[120]Osaki M, Oshimura M, Ito H. PI3K-Akt pathway: its functions and alterations in human cancer. Apoptosis. 2004;9(6):667-76.

[121]Koyasu S. The role of PI3K in immune cells. Nat Immunol. 2003;4(4):313-9.

[122]Thorpe LM, Yuzugullu H, Zhao JJ. PI3K in cancer: divergent roles of isoforms, modes of activation and therapeutic targeting. Nat Rev Cancer. 2015;15(1):7-24.

[123]Klippel A, Escobedo JA, Hirano M, Williams LT. The interaction of small domains between the subunits of phosphatidylinositol 3-kinase determines enzyme activity. Mol Cell Biol. 1994;14(4):2675-85.

[124]Ueki K, Fruman DA, Brachmann SM, et al. Molecular balance between the regulatory and catalytic subunits of phosphoinositide 3-kinase regulates cell signaling and survival. Mol Cell Biol. 2002;22(3):965-77.

[125]Geering B, Cutillas PR, Vanhaesebroeck B. Regulation of class IA PI3Ks: is there a role for monomeric PI3K subunits? Biochem Soc Trans. 2007;35(Pt 2):199-203.

[126]Yuan TL, Cantley LC. PI3K pathway alterations in cancer: variations on a theme. Oncogene. 2008;27(41):5497-510.

[127]Hennessy BT, Smith DL, Ram PT, Lu Y, Mills GB. Exploiting the PI3/AKT pathway for cancer drug discovery. Nat Rev Drug Discov. 2005;4(12):988-1004.

[128]Kim D, Dan HC, Park S, et al. AKT/PKB signaling mechanisms in cancer and chemoresistance. Front Biosci. 2005;10:975-87.

[129]Denley A, Kang S, Karst U, Vogt PK. Oncogenic signaling of class I PI3K isoforms. Oncogene. 2008;27(18):2561-74.

[130]Peng DJ, Wang J, Zhou JY, Wu GS. Role of the Akt/mTOR survival pathway in cisplatin resistance in ovarian cancer cells. Biochem Biophys Res Commun. 2010;394(3):600-5.

[131]Cully M, You H, Levine AJ, Mak TW. Beyond PTEN mutations: the PI3K pathway as an integrator of multiple inputs during tumorigenesis. Nat Rev Cancer. 2006;6(3):184-92.

[132]van der Heijden MS, Bernards R. Inhibition of the PI3K pathway: hope we can believe in? Clin Cancer Res. 2010;16(12):3094-9.

[133]Cancer Genome Atlas Research N. Integrated genomic analyses of ovarian carcinoma. Nature. 2011;474(7353):609-15.

[134]Bader AG, Kang S, Vogt PK. Cancer-specific mutations in PIK3CA are oncogenic *in vivo*. Proc Natl Acad Sci U S A. 2006;103(5):1475-9.

[135]Markman B, Atzori F, Perez-Garcia J, Tabernero J, Baselga J. Status of PI3K inhibition and biomarker development in cancer therapeutics. Ann Oncol. 2010;21(4):683-91.

[136]Bi L, Okabe I, Bernard DJ, Wynshaw-Boris A, Nussbaum RL. Proliferative defect and embryonic lethality in mice homozygous for a deletion in the p110alpha subunit of phosphoinositide 3-kinase. J Biol Chem. 1999;274(16):10963-8.

[137]Vanhaesebroeck B, Welham MJ, Kotani K, et al. P110delta, a novel phosphoinositide 3-kinase in leukocytes. Proc Natl Acad Sci U S A. 1997;94(9):4330-5.

[138]Geering B, Cutillas PR, Nock G, Gharbi SI, Vanhaesebroeck B. Class IA phosphoinositide 3-kinases are obligate p85-p110 heterodimers. Proc Natl Acad Sci U S A. 2007;104(19):7809-14.

[139]Hui RC, Gomes AR, Constantinidou D, et al. The forkhead transcription factor FOXO3a increases phosphoinositide-3 kinase/Akt activity in drug-resistant leukemic cells through induction of PIK3CA expression. Mol Cell Biol. 2008;28(19):5886-98.

[140]Yang N, Huang J, Greshock J, et al. Transcriptional regulation of PIK3CA oncogene by NF-kappaB in ovarian cancer microenvironment. PLoS One. 2008;3(3):e1758.

[141]Astanehe A, Arenillas D, Wasserman WW, et al. Mechanisms underlying p53 regulation of PIK3CA transcription in ovarian surface epithelium and in ovarian cancer. J Cell Sci. 2008;121(Pt 5):664-74.

[142]Singh B, Reddy PG, Goberdhan A, et al. p53 regulates cell survival by inhibiting PIK3CA in squamous cell carcinomas. Genes Dev. 2002;16(8):984-93.

[143]Samuels Y, Ericson K. Oncogenic PI3K and its role in cancer. Curr Opin Oncol. 2006;18(1):77-82.

[144]Samuels Y, Wang Z, Bardelli A, et al. High frequency of mutations of the PIK3CA gene in human cancers. Science. 2004;304(5670):554.

[145]Ma YY, Wei SJ, Lin YC, et al. PIK3CA as an oncogene in cervical cancer. Oncogene. 2000;19(23):2739-44.

[146]Byun DS, Cho K, Ryu BK, et al. Frequent monoallelic deletion of PTEN and its reciprocal associatioin with PIK3CA amplification in gastric carcinoma. Int J Cancer. 2003;104(3):318-27.

[147]Kolasa IK, Rembiszewska A, Felisiak A, et al. PIK3CA amplification associates with resistance to chemotherapy in ovarian cancer patients. Cancer Biol Ther. 2009;8(1):21-6.

[148]Cheaib B, Auguste A, Leary A. The PI3K/Akt/mTOR pathway in ovarian cancer: therapeutic opportunities and challenges. Chin J Cancer. 2015;34(1):4-16.

[149]Lee S, Choi EJ, Jin C, Kim DH. Activation of PI3K/Akt pathway by PTEN reduction and PIK3CA mRNA amplification contributes to cisplatin resistance in an ovarian cancer cell line. Gynecol Oncol. 2005;97(1):26-34.

[150]Servidei T, Riccardi A, Mozzetti S, Ferlini C, Riccardi R. Chemoresistant tumor cell lines display altered epidermal growth factor receptor and HER3 signaling and enhanced sensitivity to gefitinib. Int J Cancer. 2008;123(12):2939-49.

[151]Yang H, He L, Kruk P, Nicosia SV, Cheng JQ. Aurora-A induces cell survival and chemoresistance by activation of Akt through a p53-dependent manner in ovarian cancer cells. Int J Cancer. 2006;119(10):2304-12.

[152]Abedini MR, Muller EJ, Bergeron R, Gray DA, Tsang BK. Akt promotes chemoresistance in human ovarian cancer cells by modulating cisplatin-induced, p53-dependent ubiquitination of FLICE-like inhibitory protein. Oncogene2009. p. 11-25.

[153]Hafsi S, Pezzino FM, Candido S, et al. Gene alterations in the PI3K/PTEN/AKT pathway as a mechanism of drug-resistance (review). Int J Oncol. 2012;40(3):639-44.

[154]Page C, Lin HJ, Jin Y, et al. Overexpression of Akt/AKT can modulate chemotherapy-induced apoptosis. Anticancer Res. 2000;20(1A):407-16.

[155]Torre LA, Bray F, Siegel RL, et al. Global cancer statistics, 2012. CA Cancer J Clin. 2015;65(2):87-108.

[156]Matulonis UA, Sood AK, Fallowfield L, et al. Ovarian cancer. Nat Rev Dis Primers. 2016;2:16061.

[157]Raja FA, Chopra N, Ledermann JA. Optimal first-line treatment in ovarian cancer. Ann Oncol. 2012;23 Suppl 10:x118-27.

[158]Siegel R, Ma J, Zou Z, Jemal A. Cancer statistics, 2014. CA Cancer J Clin. 2014;64(1):9-29.

[159]Kaku T, Ogawa S, Kawano Y, et al. Histological classification of ovarian cancer. Med Electron Microsc. 2003;36(1):9-17.

[160]Kurman RJ, Shih Ie M. The origin and pathogenesis of epithelial ovarian cancer: a proposed unifying theory. Am J Surg Pathol. 2010;34(3):433-43.

[161]Drapkin R, von Horsten HH, Lin Y, et al. Human epididymis protein 4 (HE4) is a secreted glycoprotein that is overexpressed by serous and endometrioid ovarian carcinomas. Cancer Res. 2005;65(6):2162-9.

[162]Mohaghegh P, Rockall AG. Imaging strategy for early ovarian cancer: characterization of adnexal masses with conventional and advanced imaging techniques. Radiographics. 2012;32(6):1751-73.

[163]Rockall AG, Cross S, Flanagan S, Moore E, Avril N. The role of FDG-PET/CT in gynaecological cancers. Cancer Imaging. 2012;12:49-65.

[164]Agarwal R, Kaye SB. Ovarian cancer: strategies for overcoming resistance to chemotherapy. Nat Rev Cancer. 2003;3(7):502-16.

[165]Chaudhury S TB, Chatterjee S and Ray P. Molecular Imaging Aided Improvement in Drug Discovery and Development. Current Biotechnology. 2014;3(3):20.

[166]William R. Robinson GB, April S. Rogers. Neoadjuvant chemotherapy prior to intraperitoneal chemotherapy in women with advanced ovarian cancer. COMMUNITY ONCOLOGY. 2008;5:376–38.

[167]McGuire WP, Hoskins WJ, Brady MF, et al. Cyclophosphamide and cisplatin compared with paclitaxel and cisplatin in patients with stage III and stage IV ovarian cancer. N Engl J Med. 1996;334(1):1-6.

[168]du Bois A, Luck HJ, Meier W, et al. A randomized clinical trial of cisplatin/paclitaxel versus carboplatin/paclitaxel as first-line treatment of ovarian cancer. J Natl Cancer Inst. 2003;95(17):1320-9.

[169]Neijt JP, Engelholm SA, Tuxen MK, et al. Exploratory phase III study of paclitaxel and cisplatin versus paclitaxel and carboplatin in advanced ovarian cancer. J Clin Oncol. 2000;18(17):3084-92.

[170]Ozols RF, Bundy BN, Greer BE, et al. Phase III trial of carboplatin and paclitaxel compared with cisplatin and paclitaxel in patients with optimally resected stage III ovarian cancer: a Gynecologic Oncology Group study. J Clin Oncol. 2003;21(17):3194-200.

[171]Greenlee RT, Hill-Harmon MB, Murray T, Thun M. Cancer statistics, 2001. CA Cancer J Clin. 2001;51(1):15-36.

[172]Gore ME, Fryatt I, Wiltshaw E, Dawson T. Treatment of relapsed carcinoma of the ovary with cisplatin or carboplatin following initial treatment with these compounds. Gynecol Oncol. 1990;36(2):207-11.

[173]Harries M, Kaye SB. Recent advances in the treatment of epithelial ovarian cancer. Expert Opin Investig Drugs. 2001;10(9):1715-24.

[174]Oza AM, Cook AD, Pfisterer J, et al. Standard chemotherapy with or without bevacizumab for women with newly diagnosed ovarian cancer (ICON7): overall survival results of a phase 3 randomised trial. Lancet Oncol. 2015;16(8):928-36.

[175]Pfisterer J, Plante M, Vergote I, et al. Gemcitabine plus carboplatin compared with carboplatin in patients with platinum-sensitive recurrent ovarian cancer: an intergroup trial of the AGO-OVAR, the NCIC CTG, and the EORTC GCG. J Clin Oncol. 2006;24(29):4699-707.

[176]Sufliarsky J, Chovanec J, Svetlovska D, et al. Gemcitabine and carboplatin treatment in patients with relapsing ovarian cancer. Neoplasma. 2009;56(4):291-7.

[177]Luni C, Marth JD, Doyle FJ, 3rd. Computational modeling of glucose transport in pancreatic beta-cells identifies metabolic thresholds and therapeutic targets in diabetes. PLoS One. 2012;7(12):e53130.

[178]Lawrie TA, Bryant A, Cameron A, Gray E, Morrison J. Pegylated liposomal doxorubicin for relapsed epithelial ovarian cancer. Cochrane Database Syst Rev. 2013(7):CD006910.

[179]ten Bokkel Huinink W, Gore M, Carmichael J, et al. Topotecan versus paclitaxel for the treatment of recurrent epithelial ovarian cancer. J Clin Oncol. 1997;15(6):2183-93.

[180]Rose PG, Blessing JA, Buller RE, Mannel RS, Webster KD. Prolonged oral etoposide in recurrent or advanced non-squamous cell carcinoma of the cervix: a Gynecologic Oncology Group study. Gynecol Oncol. 2003;89(2):267-70.

[181]Gordon AN, Tonda M, Sun S, Rackoff W, Doxil Study I. Long-term survival advantage for women treated with pegylated liposomal doxorubicin compared with topotecan in a phase 3 randomized study of recurrent and refractory epithelial ovarian cancer. Gynecol Oncol. 2004;95(1):1-8.

[182]Naumann RW, Coleman RL. Management strategies for recurrent platinum-resistant ovarian cancer. Drugs. 2011;71(11):1397-412.

[183]Wang D, Lippard SJ. Cellular processing of platinum anticancer drugs. Nat Rev Drug Discov. 2005;4(4):307-20.

[184]Gasch C, Ffrench B, O'Leary JJ, Gallagher MF. Catching moving targets: cancer stem cell hierarchies, therapy-resistance & considerations for clinical intervention. Mol Cancer. 2017;16(1):43.

[185]Shibue T, Weinberg RA. EMT, CSCs, and drug resistance: the mechanistic link and clinical implications. Nat Rev Clin Oncol. 2017.

[186]Chien J, Kuang R, Landen C, Shridhar V. Platinum-sensitive recurrence in ovarian cancer: the role of tumor microenvironment. Front Oncol. 2013;3:251.

[187]Borst P, Evers R, Kool M, Wijnholds J. A family of drug transporters: the multidrug resistance-associated proteins. J Natl Cancer Inst. 2000;92(16):1295-302.

[188]Dijt FJ, Fichtinger-Schepman AM, Berends F, Reedijk J. Formation and repair of cisplatin-induced adducts to DNA in cultured normal and repair-deficient human fibroblasts. Cancer Res. 1988;48(21):6058-62.

[189]Giannakakou P, Sackett DL, Kang YK, et al. Paclitaxel-resistant human ovarian cancer cells have mutant beta-tubulins that exhibit impaired paclitaxel-driven polymerization. J Biol Chem. 1997;272(27):17118-25.

[190]Kavallaris M, Kuo DY, Burkhart CA, et al. Taxol-resistant epithelial ovarian tumors are associated with altered expression of specific beta-tubulin isotypes. J Clin Invest. 1997;100(5):1282-93.

[191]Sale S, Sung R, Shen P, et al. Conservation of the class I beta-tubulin gene in human populations and lack of mutations in lung cancers and paclitaxel-resistant ovarian cancers. Mol Cancer Ther. 2002;1(3):215-25.

[192]Tredan O, Galmarini CM, Patel K, Tannock IF. Drug resistance and the solid tumor microenvironment. J Natl Cancer Inst. 2007;99(19):1441-54.

[193]Shetzer Y, Solomon H, Koifman G, et al. The paradigm of mutant p53-expressing cancer stem cells and drug resistance. Carcinogenesis. 2014;35(6):1196-208.

[194]Obexer P, Ausserlechner MJ. X-linked inhibitor of apoptosis protein - a critical death resistance regulator and therapeutic target for personalized cancer therapy. Front Oncol. 2014;4:197.

[195]Sui L, Dong Y, Ohno M, et al. Survivin expression and its correlation with cell proliferation and prognosis in epithelial ovarian tumors. Int J Oncol. 2002;21(2):315-20.

[196]Mano Y, Kikuchi Y, Yamamoto K, et al. Bcl-2 as a predictor of chemosensitivity and prognosis in primary epithelial ovarian cancer. Eur J Cancer. 1999;35(8):1214-9.

[197]Zecri FJ, Albert R, Landrum G, et al. Pyrazole derived from (+)-3-carene; a novel potent, selective scaffold for sphingosine-1-phosphate (S1P(1)) receptor agonists. Bioorg Med Chem Lett. 2010;20(1):35-7.

[198]Shah MA, Schwartz GK. Cell cycle-mediated drug resistance: an emerging concept in cancer therapy. Clin Cancer Res. 2001;7(8):2168-81.

[199]Lapidot T, Sirard C, Vormoor J, et al. A cell initiating human acute myeloid leukaemia after transplantation into SCID mice. Nature. 1994;367(6464):645-8.

[200]Al-Hajj M, Wicha MS, Benito-Hernandez A, Morrison SJ, Clarke MF. Prospective identification of tumorigenic breast cancer cells. Proc Natl Acad Sci U S A. 2003;100(7):3983-8.

[201]Dalerba P, Dylla SJ, Park IK, et al. Phenotypic characterization of human colorectal cancer stem cells. Proc Natl Acad Sci U S A. 2007;104(24):10158-63.

[202]Cheung AM, Wan TS, Leung JC, et al. Aldehyde dehydrogenase activity in leukemic blasts defines a subgroup of acute myeloid leukemia with adverse prognosis and superior NOD/SCID engrafting potential. Leukemia. 2007;21(7):1423-30.

[203]Bonnet D, Dick JE. Human acute myeloid leukemia is organized as a hierarchy that originates from a primitive hematopoietic cell. Nat Med. 1997;3(7):730-7.

[204]Dean M. Cancer stem cells: Implications for cancer causation and therapy resistance. Discov Med. 2005;5(27):278-82.

[205]Alison MR, Lin WR, Lim SM, Nicholson LJ. Cancer stem cells: in the line of fire. Cancer Treat Rev. 2012;38(6):589-98.

[206]Shah MM, Dobbin ZC, Nowsheen S, et al. An ex vivo assay of XRT-induced Rad51 foci formation predicts response to PARP-inhibition in ovarian cancer. Gynecol Oncol. 2014;134(2):331-7.

[207]Mallard BW, Tiralongo J. Cancer stem cell marker glycosylation: Nature, function and significance. Glycoconj J. 2017.

[208]Liang J, Yang B, Cao Q, Wu X. Association of Vasculogenic Mimicry Formation and CD133 Expression with Poor Prognosis in Ovarian Cancer. Gynecol Obstet Invest. 2016;81(6):529-36.

[209]Zhang J, Guo X, Chang DY, et al. CD133 expression associated with poor prognosis in ovarian cancer. Mod Pathol. 2012;25(3):456-64.

[210]Silva IA, Bai S, McLean K, et al. Aldehyde dehydrogenase in combination with CD133 defines angiogenic ovarian cancer stem cells that portend poor patient survival. Cancer Res. 2011;71(11):3991-4001.

[211]Irollo E, Pirozzi G. CD133: to be or not to be, is this the real question? Am J Transl Res. 2013;5(6):563-81.

[212]Kusumbe AP, Mali AM, Bapat SA. CD133-expressing stem cells associated with ovarian metastases establish an endothelial hierarchy and contribute to tumor vasculature. Stem Cells. 2009;27(3):498-508.

[213]Hermansen SK, Christensen KG, Jensen SS, Kristensen BW. Inconsistent immunohistochemical expression patterns of four different CD133 antibody clones in glioblastoma. J Histochem Cytochem. 2011;59(4):391-407.

[214]Corbeil D, Joester A, Fargeas CA, et al. Expression of distinct splice variants of the stem cell marker prominin-1 (CD133) in glial cells. Glia. 2009;57(8):860-74.

[215]Senbanjo LT, Chellaiah MA. CD44: A Multifunctional Cell Surface Adhesion Receptor Is a Regulator of Progression and Metastasis of Cancer Cells. Front Cell Dev Biol. 2017;5:18.

[216]Lin J, Ding D. The prognostic role of the cancer stem cell marker CD44 in ovarian cancer: a meta-analysis. Cancer Cell Int. 2017;17:8.

[217]Shi YY, Jiang H. Prognostic role of the cancer stem cell marker CD44 in ovarian cancer: a meta-analysis. Genet Mol Res. 2016;15(3).

[218]Tjhay F, Motohara T, Tayama S, et al. CD44 variant 6 is correlated with peritoneal dissemination and poor prognosis in patients with advanced epithelial ovarian cancer. Cancer Sci. 2015;106(10):1421-8.

[219]Cardoso HJ, Figueira MI, Correia S, Vaz CV, Socorro S. The SCF/c-KIT system in the male: Survival strategies in fertility and cancer. Mol Reprod Dev. 2014;81(12):1064-79.

[220]Stankov K, Popovic S, Mikov M. C-KIT signaling in cancer treatment. Curr Pharm Des. 2014;20(17):2849-80.

[221]Ayub TH, Keyver-Paik MD, Debald M, et al. Accumulation of ALDH1-positive cells after neoadjuvant chemotherapy predicts treatment resistance and prognosticates poor outcome in ovarian cancer. Oncotarget. 2015;6(18):16437-48.

[222]Bonneau C, Rouzier R, Geyl C, et al. Predictive markers of chemoresistance in advanced stages epithelial ovarian carcinoma. Gynecol Oncol. 2015;136(1):112-20.

[223]Khalifeh I, Munkarah AR, Schimp V, et al. The impact of c-kit and ki-67 expression on patients prognosis in advanced ovarian serous carcinoma. Int J Gynecol Pathol. 2005;24(3):228-34.

[224]Kim YS, Kaidina AM, Chiang JH, Yarygin KN, Lupatov AY. [Molecular markers of cancer stem cells verified *in vivo*]. Biomed Khim. 2016;62(3):228-38.

[225]Carrasco E, Alvarez PJ, Prados J, et al. Cancer stem cells and their implication in breast cancer. Eur J Clin Invest. 2014;44(7):678-87.

[226]Jaggupilli A, Elkord E. Significance of CD44 and CD24 as cancer stem cell markers: an enduring ambiguity. Clin Dev Immunol. 2012;2012:708036.

[227]Gao MQ, Choi YP, Kang S, Youn JH, Cho NH. CD24+ cells from hierarchically organized ovarian cancer are enriched in cancer stem cells. Oncogene. 2010;29(18):2672-80.

[228]Rodriguez-Torres M, Allan AL. Aldehyde dehydrogenase as a marker and functional mediator of metastasis in solid tumors. Clin Exp Metastasis. 2016;33(1):97-113.

[229]Pors K, Moreb JS. Aldehyde dehydrogenases in cancer: an opportunity for biomarker and drug development? Drug Discov Today. 2014;19(12):1953-63.

[230]Mizuno T, Suzuki N, Makino H, et al. Cancer stem-like cells of ovarian clear cell carcinoma are enriched in the ALDH-high population associated with an accelerated scavenging system in reactive oxygen species. Gynecol Oncol. 2015;137(2):299-305.

[231]Liu S, Liu C, Min X, et al. Prognostic value of cancer stem cell marker aldehyde dehydrogenase in ovarian cancer: a meta-analysis. PLoS One. 2013;8(11):e81050.

[232]Ricci F, Bernasconi S, Porcu L, et al. ALDH enzymatic activity and CD133 positivity and response to chemotherapy in ovarian cancer patients. Am J Cancer Res. 2013;3(2):221-9.

[233]Ottevanger PB. Ovarian cancer stem cells more questions than answers. Semin Cancer Biol. 2017;44:67-71.

[234]Lupia M, Cavallaro U. Ovarian cancer stem cells: still an elusive entity? Mol Cancer. 2017;16(1):64.

[235]English DP, Menderes G, Black J, Schwab CL, Santin AD. Molecular diagnosis and molecular profiling to detect treatment-resistant ovarian cancer. Expert Rev Mol Diagn. 2016;16(7):769-82.

[236]Ozakpinar OB, Maurer AM, Ozsavci D. Ovarian stem cells: From basic to clinical applications. World J Stem Cells. 2015;7(4):757-68.

[237]Carpten JD, Faber AL, Horn C, et al. A transforming mutation in the pleckstrin homology domain of AKT1 in cancer. Nature. 2007;448(7152):439-44.

[238]Clark AS, West K, Streicher S, Dennis PA. Constitutive and inducible Akt activity promotes resistance to chemotherapy, trastuzumab, or tamoxifen in breast cancer cells. Mol Cancer Ther. 2002;1(9):707-17.

[239]Prasad G, Sottero T, Yang X, et al. Inhibition of PI3K/mTOR pathways in glioblastoma and implications for combination therapy with temozolomide. Neuro Oncol. 2011;13(4):384-92.

[240]Gaikwad SM, Thakur B, Sakpal A, Singh RK, Ray P. Differential activation of NF-kappaB signaling is associated with platinum and taxane resistance in MyD88 deficient epithelial ovarian cancer cells. Int J Biochem Cell Biol. 2015;61:90-102.

[241]Sartore-Bianchi A, Di Nicolantonio F, Nichelatti M, et al. Multi-determinants analysis of molecular alterations for predicting clinical benefit to EGFR-targeted monoclonal antibodies in colorectal cancer. PLoS One. 2009;4(10):e7287.

[242]Bonomi M, Blanco-Savorio A, Cerchietti L, et al. Continuous hyperfractionated accelerated radiation therapy week-end less in combination with neoadjuvant chemotherapy for the treatment of stage III non-small-cell lung cancer. Lung Cancer. 2008;60(1):75-82.

[243]Itamochi H, Kigawa J, Terakawa N. Mechanisms of chemoresistance and poor prognosis in ovarian clear cell carcinoma. Cancer Sci. 2008;99(4):653-8.

[244]Garraway LA, Janne PA. Circumventing cancer drug resistance in the era of personalized medicine. Cancer Discov. 2012;2(3):214-26.

[245]Chao SY, Chiang JH, Huang AM, Chang WS. An integrative approach to identifying cancer chemoresistance-associated pathways. BMC Med Genomics. 2011;4:23.

[246]Masters JR, Koberle B. Curing metastatic cancer: lessons from testicular germ-cell tumours. Nat Rev Cancer. 2003;3(7):517-25.

[247]Barrientos JC. Idelalisib for the treatment of indolent non-Hodgkin lymphoma: a review of its clinical potential. Onco Targets Ther. 2016;9:2945-53.

[248]Jacob LA, Chaudhuri T, Lakshmaiah KC, et al. Current status of systemic therapy for recurrent and/or metastatic squamous cell carcinoma of the head and neck. Indian J Cancer. 2016;53(4):471-7.

[249]Fakhrejahani F, Madan RA, Dahut WL. Management Options for Biochemically Recurrent Prostate Cancer. Curr Treat Options Oncol. 2017;18(5):26.

[250]Gaikwad SM, Ray P. Non-invasive imaging of PI3K/Akt/mTOR signalling in cancer. Am J Nucl Med Mol Imaging. 2012;2(4):418-31.

[251]Barbuti AM, Chen ZS. Paclitaxel Through the Ages of Anticancer Therapy: Exploring Its Role in Chemoresistance and Radiation Therapy. Cancers (Basel). 2015;7(4):2360-71.

[252]Murai J. Targeting DNA repair and replication stress in the treatment of ovarian cancer. Int J Clin Oncol. 2017.

[253]Hanna N, Einhorn LH. Testicular cancer: a reflection on 50 years of discovery. J Clin Oncol. 2014;32(28):3085-92.

[254]Lambert HE, Berry RJ. High dose cisplatin compared with high dose cyclophosphamide in the management of advanced epithelial ovarian cancer (FIGO stages III and IV): report from the North Thames Cooperative Group. Br Med J (Clin Res Ed). 1985;290(6472):889-93.

[255]Bellmunt J, Paz-Ares L, Cuello M, et al. Gene expression of ERCC1 as a novel prognostic marker in advanced bladder cancer patients receiving cisplatin-based chemotherapy. Ann Oncol. 2007;18(3):522-8.

[256]Amrein PC, Weitzman SA. Treatment of squamous-cell carcinoma of the head and neck with cisplatin and 5-fluorouracil. J Clin Oncol. 1985;3(12):1632-9.

[257]Erten C, Demir L, Somali I, et al. Cisplatin plus gemcitabine for treatment of breast cancer patients with brain metastases; a preferential option for triple negative patients? Asian Pac J Cancer Prev. 2013;14(6):3711-7.

[258]Polee MB, Hop WC, Kok TC, et al. Prognostic factors for survival in patients with advanced oesophageal cancer treated with cisplatin-based combination chemotherapy. Br J Cancer. 2003;89(11):2045-50.

[259]Karam I, Jiang SY, Khaira M, Lee CW, Schellenberg D. Outcomes of small cell lung cancer patients treated with cisplatin-etoposide versus carboplatin-etoposide. Am J Clin Oncol. 2015;38(1):51-4.

[260]Ali AY, Farrand L, Kim JY, et al. Molecular determinants of ovarian cancer chemoresistance: new insights into an old conundrum. Ann N Y Acad Sci. 2012;1271:58-67.

[261]Xia P, Xu XY. PI3K/Akt/mTOR signaling pathway in cancer stem cells: from basic research to clinical application. Am J Cancer Res. 2015;5(5):1602-9.

[262]Schwartz TW, Sakmar TP. Structural biology: snapshot of a signalling complex. Nature. 2011;477(7366):540-1.

[263]Steelman LS, Chappell WH, Abrams SL, et al. Roles of the Raf/MEK/ERK and PI3K/PTEN/Akt/mTOR pathways in controlling growth and sensitivity to therapy-implications for cancer and aging. Aging (Albany NY). 2011;3(3):192-222.

[264]Ciriello G, Miller ML, Aksoy BA, et al. Emerging landscape of oncogenic signatures across human cancers. Nat Genet. 2013;45(10):1127-33.

[265]Liang S, Yang N, Pan Y, et al. Expression of activated PIK3CA in ovarian surface epithelium results in hyperplasia but not tumor formation. PLoS One. 2009;4(1):e4295.

[266]Zhang W, Ding W, Chen Y, et al. Up-regulation of breast cancer resistance protein plays a role in HER2-mediated chemoresistance through PI3K/Akt and nuclear factor-kappa B signaling pathways in MCF7 breast cancer cells. Acta Biochim Biophys Sin (Shanghai). 2011;43(8):647-53.

[267]Abubaker J, Bavi P, Al-Haqawi W, et al. PIK3CA alterations in Middle Eastern ovarian cancers. Mol Cancer. 2009;8:51.

[268]Astanehe A, Finkbeiner MR, Hojabrpour P, et al. The transcriptional induction of PIK3CA in tumor cells is dependent on the oncoprotein Y-box binding protein-1. Oncogene. 2009;28(25):2406-18.

[269]Gaikwad SM, Gunjal L, Junutula AR, et al. Non-Invasive Imaging of Phosphoinositide-3-Kinase-Catalytic-Subunit-Alpha (PIK3CA) Promoter Modulation in Small Animal Models. PLoS One. 2013;8(2):e55971.

[270]Collavin L, Lunardi A, Del Sal G. p53-family proteins and their regulators: hubs and spokes in tumor suppression. Cell Death Differ. 2010;17(6):901-11.

[271]Joerger AC, Fersht AR. The tumor suppressor p53: from structures to drug discovery. Cold Spring Harb Perspect Biol. 2010;2(6):a000919.

[272]Aylon Y, Oren M. The Paradox of p53: What, How, and Why? Cold Spring Harb Perspect Med. 2016;6(10).

[273]Rinn JL, Huarte M. To repress or not to repress: this is the guardian's question. Trends Cell Biol. 2011;21(6):344-53.

[274]Szak ST, Mays D, Pietenpol JA. Kinetics of p53 binding to promoter sites *in vivo*. Mol Cell Biol. 2001;21(10):3375-86.

[275]Beckerman R, Prives C. Transcriptional regulation by p53. Cold Spring Harb Perspect Biol. 2010;2(8):a000935.

[276]Ray D, Murphy KR, Gal S. The DNA binding and accumulation of p53 from breast cancer cell lines and the link with serine 15 phosphorylation. Cancer Biol Ther. 2012;13(10):848-57.

[277]Dai C, Gu W. p53 post-translational modification: deregulated in tumorigenesis. Trends Mol Med. 2010;16(11):528-36.

[278]Wei J, Yang Y, Lu M, et al. Escape, or Vanish: Control the Fate of p53 through MDM2-Mediated Ubiquitination. Anticancer Agents Med Chem. 2015;16(2):174-89.

[279]Marouco D, Garabadgiu AV, Melino G, Barlev NA. Lysine-specific modifications of p53: a matter of life and death? Oncotarget. 2013;4(10):1556-71.

[280]Gu W, Roeder RG. Activation of p53 sequence-specific DNA binding by acetylation of the p53 C-terminal domain. Cell. 1997;90(4):595-606.

[281]Reed SM, Quelle DE. p53 Acetylation: Regulation and Consequences. Cancers (Basel). 2014;7(1):30-69.

[282]Taira N, Nihira K, Yamaguchi T, Miki Y, Yoshida K. DYRK2 is targeted to the nucleus and controls p53 via Ser46 phosphorylation in the apoptotic response to DNA damage. Mol Cell. 2007;25(5):725-38.

[283]Olsson A, Manzl C, Strasser A, Villunger A. How important are post-translational modifications in p53 for selectivity in target-gene transcription and tumour suppression? Cell Death Differ. 2007;14(9):1561-75.

[284]Banin S, Moyal L, Shieh S, et al. Enhanced phosphorylation of p53 by ATM in response to DNA damage. Science. 1998;281(5383):1674-7.

[285]Lees-Miller SP, Sakaguchi K, Ullrich SJ, Appella E, Anderson CW. Human DNA-activated protein kinase phosphorylates serines 15 and 37 in the amino-terminal transactivation domain of human p53. Mol Cell Biol. 1992;12(11):5041-9.

[286]Shieh SY, Ikeda M, Taya Y, Prives C. DNA damage-induced phosphorylation of p53 alleviates inhibition by MDM2. Cell. 1997;91(3):325-34.

[287]Siliciano JD, Canman CE, Taya Y, et al. DNA damage induces phosphorylation of the amino terminus of p53. Genes Dev. 1997;11(24):3471-81.

[288]Shieh SY, Ahn J, Tamai K, Taya Y, Prives C. The human homologs of checkpoint kinases Chk1 and Cds1 (Chk2) phosphorylate p53 at multiple DNA damage-inducible sites. Genes Dev. 2000;14(3):289-300.

[289]Dumaz N, Milne DM, Jardine LJ, Meek DW. Critical roles for the serine 20, but not the serine 15, phosphorylation site and for the polyproline domain in regulating p53 turnover. Biochem J. 2001;359(Pt 2):459-64.

[290]Lakin ND, Jackson SP. Regulation of p53 in response to DNA damage. Oncogene. 1999;18(53):7644-55.

[291]Nguyen TA, Menendez D, Resnick MA, Anderson CW. Mutant TP53 posttranslational modifications: challenges and opportunities. Hum Mutat. 2014;35(6):738-55.

[292]Hofmann TG, Moller A, Sirma H, et al. Regulation of p53 activity by its interaction with homeodomain-interacting protein kinase-2. Nat Cell Biol. 2002;4(1):1-10.

[293]D'Orazi G, Cecchinelli B, Bruno T, et al. Homeodomain-interacting protein kinase-2 phosphorylates p53 at Ser 46 and mediates apoptosis. Nat Cell Biol. 2002;4(1):11-9.

[294]Di Stefano V, Soddu S, Sacchi A, D'Orazi G. HIPK2 contributes to PCAF-mediated p53 acetylation and selective transactivation of p21Waf1 after nonapoptotic DNA damage. Oncogene. 2005;24(35):5431-42.

[295]Matsumoto M, Furihata M, Ohtsuki Y. Posttranslational phosphorylation of mutant p53 protein in tumor development. Med Mol Morphol. 2006;39(2):79-87.

[296]Bruins W, Bruning O, Jonker MJ, et al. The absence of Ser389 phosphorylation in p53 affects the basal gene expression level of many p53-dependent genes and alters the biphasic response to UV exposure in mouse embryonic fibroblasts. Mol Cell Biol. 2008;28(6):1974-87.

[297]Johnson TM, Attardi LD. Dissecting p53 tumor suppressor function *in vivo* through the analysis of genetically modified mice. Cell Death Differ. 2006;13(6):902-8.

[298]Bruins W, Jonker MJ, Bruning O, et al. Delayed expression of apoptotic and cell-cycle control genes in carcinogen-exposed bladders of mice lacking p53.S389 phosphorylation. Carcinogenesis. 2007;28(8):1814-23.

[299]Ichwan SJ, Yamada S, Sumrejkanchanakij P, et al. Defect in serine 46 phosphorylation of p53 contributes to acquisition of p53 resistance in oral squamous cell carcinoma cells. Oncogene. 2006;25(8):1216-24.

[300]Rojas V, Hirshfield KM, Ganesan S, Rodriguez-Rodriguez L. Molecular Characterization of Epithelial Ovarian Cancer: Implications for Diagnosis and Treatment. Int J Mol Sci. 2016;17(12).

[301]Chien J, Sicotte H, Fan JB, et al. TP53 mutations, tetraploidy and homologous recombination repair defects in early stage high-grade serous ovarian cancer. Nucleic Acids Res. 2015;43(14):6945-58.

[302]Cole AJ, Dwight T, Gill AJ, et al. Assessing mutant p53 in primary high-grade serous ovarian cancer using immunohistochemistry and massively parallel sequencing. Sci Rep. 2016;6:26191.

[303]Oren M, Rotter V. Mutant p53 gain-of-function in cancer. Cold Spring Harb Perspect Biol. 2010;2(2):a001107.

[304]Kern A, Taubert H, Scheele J, et al. Association of p53 mutations, microvessel density and neoangiogenesis in pairs of colorectal cancers and corresponding liver metastases. Int J Oncol. 2002;21(2):243-9.

[305]Brachova P, Thiel KW, Leslie KK. The consequence of oncomorphic TP53 mutations in ovarian cancer. Int J Mol Sci. 2013;14(9):19257-75.

[306]Rowan S, Ludwig RL, Haupt Y, et al. Specific loss of apoptotic but not cell-cycle arrest function in a human tumor derived p53 mutant. EMBO J. 1996;15(4):827-38.

[307]Hanel W, Marchenko N, Xu S, et al. Two hot spot mutant p53 mouse models display differential gain of function in tumorigenesis. Cell Death Differ. 2013;20(7):898-909.

[308]Weisz L, Oren M, Rotter V. Transcription regulation by mutant p53. Oncogene. 2007;26(15):2202-11.

[309]Strano S, Dell'Orso S, Di Agostino S, et al. Mutant p53: an oncogenic transcription factor. Oncogene. 2007;26(15):2212-9.

[310]Yoshikawa K, Hamada J, Tada M, et al. Mutant p53 R248Q but not R248W enhances *in vitro* invasiveness of human lung cancer NCI-H1299 cells. Biomed Res. 2010;31(6):401-11.

[311]Li J, Yang L, Gaur S, et al. Mutants TP53 p.R273H and p.R273C but not p.R273G enhance cancer cell malignancy. Hum Mutat. 2014;35(5):575-84.

[312]Chang FL, Lai MD. Various forms of mutant p53 confer sensitivity to cisplatin and doxorubicin in bladder cancer cells. J Urol. 2001;166(1):304-10.

[313]Thakur B, Chatterjee S, Chaudhury S, Ray P. Molecular Imaging of Therapeutic Potential of Reporter Probes. Curr Drug Targets. 2015;16(6):645-57.

[314]Massoud TF, Gambhir SS. Molecular imaging in living subjects: seeing fundamental biological processes in a new light. Genes Dev. 2003;17(5):545-80.

[315]Ray P. Multimodality molecular imaging of disease progression in living subjects. J Biosci. 2011;36(3):499-504.

[316]Garufi A, D'Orazi G. High glucose dephosphorylates serine 46 and inhibits p53 apoptotic activity. J Exp Clin Cancer Res. 2014;33:79.

[317]Shankar E, Basu C, Adkins B, Siede W, Basu A. NSC109268 potentiates cisplatin-induced cell death in a p53-independent manner. J Mol Signal. 2010;5:4.

[318]Xie X, He G, Siddik ZH. Functional Activation of Mutant p53 by Platinum Analogues in Cisplatin-Resistant Cells Is Dependent on Phosphorylation. Mol Cancer Res. 2017;15(3):328-39.

[319]Zhao Z, Wang J, Tang J, et al. JNK- and Akt-mediated Puma expression in the apoptosis of cisplatin-resistant ovarian cancer cells. Biochem J. 2012;444(2):291-301.

[320]Wang B, Niu D, Lam TH, Xiao Z, Ren EC. Mapping the p53 transcriptome universe using p53 natural polymorphs. Cell Death Differ. 2014;21(4):521-32.

[321]Kastan MB, Onyekwere O, Sidransky D, Vogelstein B, Craig RW. Participation of p53 protein in the cellular response to DNA damage. Cancer Res. 1991;51(23 Pt 1):6304-11.

[322]Benchimol S. p53-dependent pathways of apoptosis. Cell Death Differ. 2001;8(11):1049-51.

[323]Attardi LD, de Vries A, Jacks T. Activation of the p53-dependent G1 checkpoint response in mouse embryo fibroblasts depends on the specific DNA damage inducer. Oncogene. 2004;23(4):973-80.

[324]di Pietro A, Koster R, Boersma-van Eck W, et al. Pro- and anti-apoptotic effects of p53 in cisplatin-treated human testicular cancer are cell context-dependent. Cell Cycle. 2012;11(24):4552-62.

[325]Kracikova M, Akiri G, George A, Sachidanandam R, Aaronson SA. A threshold mechanism mediates p53 cell fate decision between growth arrest and apoptosis. Cell Death Differ. 2013;20(4):576-88.

[326]Kaeser MD, Iggo RD. Chromatin immunoprecipitation analysis fails to support the latency model for regulation of p53 DNA binding activity *in vivo*. Proc Natl Acad Sci U S A. 2002;99(1):95-100.

[327]Ma T, Yamada S, Ichwan SJ, et al. Inability of p53-reactivating compounds Nutlin-3 and RITA to overcome p53 resistance in tumor cells deficient in p53Ser46 phosphorylation. Biochem Biophys Res Commun. 2012;417(3):931-7.

[328]Grinkevich VV, Nikulenkov F, Shi Y, et al. Ablation of key oncogenic pathways by RITA-reactivated p53 is required for efficient apoptosis. Cancer Cell. 2009;15(5):441-53.

[329]Shahin MS, Hughes JH, Sood AK, Buller RE. The prognostic significance of p53 tumor suppressor gene alterations in ovarian carcinoma. Cancer. 2000;89(9):2006-17.

[330]Laframboise S, Chapman W, McLaughlin J, Andrulis IL. p53 mutations in epithelial ovarian cancers: possible role in predicting chemoresistance. Cancer J. 2000;6(5):302-8.

[331]Righetti SC, Della Torre G, Pilotti S, et al. A comparative study of p53 gene mutations, protein accumulation, and response to cisplatin-based chemotherapy in advanced ovarian carcinoma. Cancer Res. 1996;56(4):689-93.

[332]Woenckhaus J, Steger K, Sturm K, et al. Prognostic value of PIK3CA and phosphorylated AKT expression in ovarian cancer. Virchows Arch. 2007;450(4):387-95.

[333]Asselin E, Mills GB, Tsang BK. XIAP regulates Akt activity and caspase-3-dependent cleavage during cisplatin-induced apoptosis in human ovarian epithelial cancer cells. Cancer Res. 2001;61(5):1862-8.

[334]Huang WC, Hung MC. Induction of Akt activity by chemotherapy confers acquired resistance. J Formos Med Assoc. 2009;108(3):180-94.

[335]del Peso L, Gonzalez-Garcia M, Page C, Herrera R, Nunez G. Interleukin-3-induced phosphorylation of BAD through the protein kinase Akt. Science. 1997;278(5338):687-9.

[336]Datta SR, Dudek H, Tao X, et al. Akt phosphorylation of BAD couples survival signals to the cell-intrinsic death machinery. Cell. 1997;91(2):231-41.

[337]Gardai SJ, Hildeman DA, Frankel SK, et al. Phosphorylation of Bax Ser184 by Akt regulates its activity and apoptosis in neutrophils. J Biol Chem. 2004;279(20):21085-95.

[338]Qi XJ, Wildey GM, Howe PH. Evidence that Ser87 of BimEL is phosphorylated by Akt and regulates BimEL apoptotic function. J Biol Chem. 2006;281(2):813-23.

[339]Zhou BP, Liao Y, Xia W, et al. HER-2/neu induces p53 ubiquitination via Akt-mediated MDM2 phosphorylation. Nat Cell Biol. 2001;3(11):973-82.

[340]Li F, Sethi G. Targeting transcription factor NF-kappaB to overcome chemoresistance and radioresistance in cancer therapy. Biochim Biophys Acta. 2010;1805(2):167-80.

[341]Hoesel B, Schmid JA. The complexity of NF-kappaB signaling in inflammation and cancer. Mol Cancer. 2013;12:86.

[342]Takeuchi H, Kim J, Fujimoto A, et al. X-Linked inhibitor of apoptosis protein expression level in colorectal cancer is regulated by hepatocyte growth factor/C-met pathway via Akt signaling. Clin Cancer Res. 2005;11(21):7621-8.

[343]Abedini MR, Qiu Q, Yan X, Tsang BK. Possible role of FLICE-like inhibitory protein (FLIP) in chemoresistant ovarian cancer cells *in vitro*. Oncogene. 2004;23(42):6997-7004.

[344]Campbell KJ, Rocha S, Perkins ND. Active repression of antiapoptotic gene expression by RelA(p65) NF-kappa B. Mol Cell. 2004;13(6):853-65.

[345]Godwin P, Baird AM, Heavey S, et al. Targeting nuclear factor-kappa B to overcome resistance to chemotherapy. Front Oncol. 2013;3:120.

[346]Thakur B, Ray P. p53 Loses grip on PIK3CA expression leading to enhanced cell survival during platinum resistance. Mol Oncol. 2016.

[347]Torigoe T, Izumi H, Ishiguchi H, et al. Cisplatin resistance and transcription factors. Curr Med Chem Anticancer Agents. 2005;5(1):15-27.

[348]Ohga T, Uchiumi T, Makino Y, et al. Direct involvement of the Y-box binding protein YB-1 in genotoxic stress-induced activation of the human multidrug resistance 1 gene. J Biol Chem. 1998;273(11):5997-6000.

[349]Shen Q, Wu R, Leonard JL, Newburger PE. Identification and molecular cloning of a human selenocysteine insertion sequence-binding protein. A bifunctional role for DNA-binding protein B. J Biol Chem. 1998;273(10):5443-6.

[350]Averous J, Bruhat A, Jousse C, et al. Induction of CHOP expression by amino acid limitation requires both ATF4 expression and ATF2 phosphorylation. J Biol Chem. 2004;279(7):5288-97.

[351]Levenson VV, Davidovich IA, Roninson IB. Pleiotropic resistance to DNA-interactive drugs is associated with increased expression of genes involved in DNA replication, repair, and stress response. Cancer Res. 2000;60(18):5027-30.

[352]Zhao H, Jin S, Fan F, et al. Activation of the transcription factor Oct-1 in response to DNA damage. Cancer Res. 2000;60(22):6276-80.

[353]Torigoe T, Izumi H, Ise T, et al. Vacuolar H(+)-ATPase: functional mechanisms and potential as a target for cancer chemotherapy. Anticancer Drugs. 2002;13(3):237-43.

[354]Zwilling S, Konig H, Wirth T. High mobility group protein 2 functionally interacts with the POU domains of octamer transcription factors. EMBO J. 1995;14(6):1198-208.

[355]Holohan C, Van Schaeybroeck S, Longley DB, Johnston PG. Cancer drug resistance: an evolving paradigm. Nat Rev Cancer. 2013;13(10):714-26.

[356]Vazquez-Santillan K, Melendez-Zajgla J, Jimenez-Hernandez L, Martinez-Ruiz G, Maldonado V. NF-kappaB signaling in cancer stem cells: a promising therapeutic target? Cell Oncol (Dordr). 2015;38(5):327-39.

[357]Noda T, Nagano H, Takemasa I, et al. Activation of Wnt/beta-catenin signalling pathway induces chemoresistance to interferon-alpha/5-fluorouracil combination therapy for hepatocellular carcinoma. Br J Cancer. 2009;100(10):1647-58.

[358]Yang W, Yan HX, Chen L, et al. Wnt/beta-catenin signaling contributes to activation of normal and tumorigenic liver progenitor cells. Cancer Res. 2008;68(11):4287-95.

[359]Alvero AB, Chen R, Fu HH, et al. Molecular phenotyping of human ovarian cancer stem cells unravels the mechanisms for repair and chemoresistance. Cell Cycle. 2009;8(1):158-66.

[360]Leizer AL, Alvero AB, Fu HH, et al. Regulation of inflammation by the NF-kappaB pathway in ovarian cancer stem cells. Am J Reprod Immunol. 2011;65(4):438-47.

[361]Kolev VN, Wright QG, Vidal CM, et al. PI3K/mTOR dual inhibitor VS-5584 preferentially targets cancer stem cells. Cancer Res. 2015;75(2):446-55.

[362]Chen J, Li Y, Yu TS, et al. A restricted cell population propagates glioblastoma growth after chemotherapy. Nature. 2012;488(7412):522-6.

[363]Creighton CJ, Li X, Landis M, et al. Residual breast cancers after conventional therapy display mesenchymal as well as tumor-initiating features. Proc Natl Acad Sci U S A. 2009;106(33):13820-5.

[364]Gerber JM, Smith BD, Ngwang B, et al. A clinically relevant population of leukemic CD34(+)CD38(-) cells in acute myeloid leukemia. Blood. 2012;119(15):3571-7.

[365]Singh RK, Dhadve A, Sakpal A, De A, Ray P. An active IGF-1R-AKT signaling imparts functional heterogeneity in ovarian CSC population. Sci Rep. 2016;6:36612.

[366]Ma L, Zhang G, Miao XB, et al. Cancer stem-like cell properties are regulated by EGFR/AKT/beta-catenin signaling and preferentially inhibited by gefitinib in nasopharyngeal carcinoma. FEBS J. 2013;280(9):2027-41.

[367]Sun Y, Zheng S, Torossian A, et al. Role of insulin-like growth factor-1 signaling pathway in cisplatin-resistant lung cancer cells. Int J Radiat Oncol Biol Phys. 2012;82(3):e563-72.

[368]Bertelsen BI, Steine SJ, Sandvei R, Molven A, Laerum OD. Molecular analysis of the PI3K-AKT pathway in uterine cervical neoplasia: frequent PIK3CA amplification and AKT phosphorylation. Int J Cancer. 2006;118(8):1877-83.

[369]Li L, Liu HC, Wang C, et al. Overexpression of beta-Catenin Induces Cisplatin Resistance in Oral Squamous Cell Carcinoma. Biomed Res Int. 2016;2016:5378567.

[370]Bicaku E, Xiong Y, Marchion DC, et al. *In vitro* analysis of ovarian cancer response to cisplatin, carboplatin, and paclitaxel identifies common pathways that are also associated with overall patient survival. Br J Cancer. 2012;106(12):1967-75.

[371]Oiso S, Ikeda R, Nakamura K, et al. Involvement of NF-kappaB activation in the cisplatin resistance of human epidermoid carcinoma KCP-4 cells. Oncol Rep. 2012;28(1):27-32.

[372]Staun-Ram E, Goldman S, Shalev E. Ets-2 and p53 mediate cAMP-induced MMP-2 expression, activity and trophoblast invasion. Reprod Biol Endocrinol. 2009;7:135.

[373]Viatour P, Merville MP, Bours V, Chariot A. Phosphorylation of NF-kappaB and IkappaB proteins: implications in cancer and inflammation. Trends Biochem Sci. 2005;30(1):43-52.

[374]Bai D, Ueno L, Vogt PK. Akt-mediated regulation of NFkappaB and the essentialness of NFkappaB for the oncogenicity of PI3K and Akt. Int J Cancer. 2009;125(12):2863-70.

[375]Zhou A, Scoggin S, Gaynor RB, Williams NS. Identification of NF-kappa B-regulated genes induced by TNFalpha utilizing expression profiling and RNA interference. Oncogene. 2003;22(13):2054-64.

Reprints of Publications

RESEARCH

Open Access

CrossMark

Cisplatin triggers cancer stem cell enrichment in platinum-resistant cells through NF-κB-TNFα-*PIK3CA* loop

Bhushan Thakur[1,2] and Pritha Ray[1,2]*

Abstract

Background: Parallel to complex alteration in molecular and cellular events, enrichment of cancer stem cells (CSC) contributes significantly in deliberation and maintenance of cisplatin resistance. Cisplatin mediated CSC enrichment is well established in various cancers, yet the underlying mechanism is largely unknown. Cisplatin also promotes transcriptional upregulation of *PIK3CA*, hence activating PI3K/AKT signaling in resistant cells. However, such cisplatin-induced transcriptional regulators of *PIK3CA* and their impact on cancer stem cell population in resistant cells are largely unknown.

Methods: DNA-binding protein pulldown using *PIK3CA* promoter as bait followed by nLCMS was used to identify, cisplatin-induced potential transcriptional regulators of *PIK3CA* promoter. *PIK3CA* promoter activity was estimated by luciferase based reporter assay. ChIP was used to assess interaction of NF-κB with *PIK3CA* promoter. CSC-enriched side-population was sorted using DCV-dye exclusion methods. All the gene expression levels were assessed using qPCR.

Results: Using a transcription factor pull-down assay with *PIK3CA* promoter, we identified NF-κB as a prime regulator, which escalates both *TNFα* and *PIK3CA* expression only in CSC enriched side-population (SP) but not in non side-population (NSP) in platinum resistant ovarian cancer cells upon cisplatin treatment. This SP-specific NF-κB-TNFα-PIK3CA bi-modal loop, on one hand, maintains persistent activation of NF-κB through TNFα- NF-κB autocrine loop, while NF-κB-PIK3CA loop nurture CSC population under cisplatin treatment. Activation of PI3K/AKT signalling drives SP's into an undifferentiated, anti-apoptotic stage through upregulating *P21, P27,cFLIP* expression. Contrarily, lack of active NF-κB-TNFα-PIK3CA loop makes NSPs vulnerable towards cisplatin and undergoes apoptosis. Altogether, cisplatin enriches cancer stem cells properties in SP fraction, which is evident from increased levels of pluripotency gene *OCT4/SOX2/NANOG* expression. Disruption of *PIK3CA*-NF-κB loop by Wortamannin reduces SP fraction by 1.4–1.6 fold in control and treated cells.

Conclusion: Together, our study signifies an active role of NF-κB-TNFα-PIK3CA bi-modal loop in cisplatin-mediated promotion and maintenance of CSC-like population in platinum-resistant cells.

Keywords: CSC-enrichment, PIK3CA regulators, NF-κB-TNFα-*PIK3CA* loop

Background

Chemotherapy is one of the prevailing methods to manage neoplastic growth. Unfortunately, generation of resistance substantially handicaps the efficacy and results in significant mortality in cancer patients. While molecular alteration in signaling cascades aid in acquirement and maintenance of resistance, a small fraction of inherently resistant cancer stem cells (CSC) help in repopulating the chemoresistant tumor [1–3]. In particular, these drug resistant CSC's evolve to resist therapy setbacks resulting in incessant growth and relapse. Hence targeting the CSC component has a great therapeutic potential in therapy-resistant disease. However, theoretically achievable, such objective is extremely challenging and requires in depth understanding of how CSC's response towards chemotherapeutics.

CSC's are a small fraction of heterogeneous tumor population identified by surface markers like CD34+/CD38-(AML), ESA+/CD44+/CD24-(low) (breast cancer) and functional properties such as side-population (SP) or

---

* Correspondence: pray@actrec.gov.in
[1]Imaging Cell Signaling and Therapeutics Laboratory, Advanced Centre for Treatment, Research and Education in Cancer (ACTREC), Tata Memorial Centre, Navi Mumbai, India
[2]Homi Bhabha National Institute, Mumbai, Anushakti Nagar, India

aldehyde dehydrogenase activity [1]. Though association between CSCs and chemoresistance is well established, the key molecular events involved in the regulation of CSCs remain largely unknown. Till date, differential activation of PI3K/AKT, WNT, NOTCH and NF-κB signaling are linked to maintenance of CSC phenotype and chemoresistance [4–6]. However, the actions and the outcomes of cancer therapeutics on signaling cascades in CSCs still remain poorly understood.

Cisplatin, a DNA damaging agent, also modulates several signalling cues including c-ABL, p53 signaling, MAPK/JNK/ERK, PI3K/AKT, NF-κB-signalling, FAK and WNT-signaling [7]. Cisplatin resistance is a net effect of multiple mechanisms that either inhibit apoptosis, promote cell survival, or both. Amongst these, the nuclear Factor-kappa B (NF-κB) has been identified as a key player in platinum resistance [8, 9]. A variety of stimuli coalesces on NF-κB activation, which mediated upregulation of *cFLIP, BCl-XL, XIAP* and favours survival of cisplatin resistant cells [8, 9]. NF-κB also prevents cisplatin mediated histone acetylation and BRCA1 nuclear translocation in HNSCC and inhibit cisplatin cytotoxicity [10]. In response to extracellular signals, a number of RTKs can activate NF-κB via PI3K/AKT or JNK/STAT pathway [11]. In many cancers, hyperactivation of PI3K/AKT, a key survival pathway contributes to tumor growth, metastatic competence, and therapy-resistance [12]. Besides RTK mediated activation, PI3K gene is regulated by few central transcription factors (p53, NF-κB, FOXO3a, YB1) in chemosensitive cells [13], however, regulators of *PIK3CA* in chemoresistant cells particularly in response to drugs has never been identified. We have been investigating the underlying mechanism of upregulated PI3K expression in platinum-resistant cells, and demonstrated that in absence of a cisplatin-induced Ser46-phosphorylation, p53 failed to bind and represses *PIK3CA* promoter leading to activation of PI3K/AKT signalling that actively sustained survival but not proliferation of resistant cells [14]. Though lack of PI3K promoter attenuation by cisplatin in resistant cells is indicative of loss of p53's repressive action, it does not explain the observed increase in *PIK3CA* expression and points toward a second level of regulation for this critical gene and associated signalling.

In the present study, we identified cisplatin responsive potential transcriptional activators of *PIK3CA* in resistant cells and explored the consequence of this intricate regulation in preserving resistance and CSC-characteristics. Through DNA-protein pulldown, NF-κB was identified as a key cisplatin responsive transcription factor, which escalated *PIK3CA* specifically in CSC-enriched SP cells and governed an anti-apoptotic, dormant state. Lack of drug-induced quiescence in non-CSC fraction attributed to their susceptibility towards cisplatin. Cisplatin induced an intricate bi-modal feedback loop between TNFα-NF-κB & NF-κB-PI3K signalling leading to maintenance of CSC-phenotype. This is probably the first mechanistic report on how cisplatin drives enrichment of CSCs in platinum-resistant cells thereby favouring a tilt towards resistance maintenance.

Methods

Cell lines and treatment

A2780 (DMEM), A2780-CisR (DMEM), OAW42 (MEM), SKOV3 (RPMI) and TOV21G (RPMI) cells were cultured in the respective media supplemented with 10% fetal bovine serum (HiMedia) and 1% penicillin-streptomycin (GIBCO). Treatments of Cisplatin (10 μg/ml), TNFα (50 ng/ml), Forskolin (10 μM), LiCl (40 mM) and wortmanin (50 μM) were given for 24 h.

DNA-protein pulldown and nLC-MS analysis

OS4-*PIK3CA* deletion construct (340 bp) was biotinylated by PCR amplification and DNA-protein pulldown was performed using streptavidin-coupled Dynabeads as described earlier [15]. DNA bound protein fraction was eluted with 0.1% SDS solution and was digested with trypsin (in-solution method) and subjected to Triple TOF 5500+ nano-scale liquid chromatographic tandem mass spectrometry (nLC-MS/MS) for acquiring peptide spectra.

Data analysis and candidate selection

Significant protein candidates from each MS/MS spectra were identified using protein pilot software at 0.01% false discovery rate and $p = 0.05$ significance level. From each run, identified proteins were categorised based on GO-'biological' and 'molecular' functioning with GSEA server (http://software.broadinstitute.org/gsea/index.jsp). Only protein signatures associated with transcription factors and associated protein were used for gene family overlap and functional overlap between control and cisplatin treated samples were computed through Venn 2.1.0 server. List of identified proteins is given in Additional file 1: Table S1-S3.

Chromatin immune precipitation (ChIP)

ChIP was performed as described earlier with few modifications [14]. Briefly, 50 μg of crosslinked-chromatin were precipitated with 2 μg of NF-κB-specific antibody and DNA was eluted post reverse-crosslinking. ChIP-DNA was analysed with semi-quantitative PCR using whole length *PIK3CA* promoter primers (primer sequences adapted from [16]). Non-immuno-precipitated chromatin was used as total input control.

Isolation of side population

Side and non-side population cells are sorted as described earlier [17]. Membrane drug transporter inhibitor

Verapamil (50 μM, Sigma) was used as negative control for gating. Data analysis was performed using DIVA software.

Statistical analysis

All the quantitative data represents the mean ± SEM of at least three independent biological experiments and statistical significance were analysed using unpaired Student's t test. P value ≤ 0.05 was considered as significant. Additional supplementary method and materials (Additional file 8).

Results

Cisplatin enriched side-population fraction with augmented *PIK3CA* expression in resistant cells

We had earlier reported increase in CSC-enriched Side-population (SP) during acquirement of cisplatin resistance in A2780 and OAW42 cellular models. This SP fraction was associated with increased spheroid formation, upregulated pluripotent genes, and tumorigenic ability at fewer cell implantation in immune-compromised mice, the well-established characteristic features of CSCs [17]. Hence, to understand the impact of cisplatin on existing CSC-population of chemoresistant cells, we assessed the SP fraction in A2780-CisR cells pre and post cisplatin treatment. Cisplatin enhanced SP fraction from 7.3 ± 0.7% (0.65 ± 0.45% with verapamil) to 13.7 ± 2.6% (1.8 ± 0.6% with verapamil) (Fig. 1a-c). Similar cisplatin dependent increase in SP fraction was also found in other resistant cell lines like TOV21G (from 5.9 ± 0.7% to 10.2 ± 0.4%) and SKOV3 (from 4.9 ± 0.7% to 8.4 ± 1.5%) cells (Fig. 1c). These cells showed low level of cell death (15–20%) upon 24 h of sub-lethal cisplatin treatment (10 μg/ml) (Additional file 2: Figure S1A). However, drug mediated enrichment of a specific cell fraction (SP) was quite unexpected and therefore we attempted to decipher the molecular mechanism. Recent evidences revealed active involvement of PI3K/AKT/NF-κB cue in maintenance and enrichment of colon, breast, and ovarian CSCs [1]. Hence, to understand the impact of PI3K/AKT signalling in CSC, we assessed *PIK3CA* expression in main population (MP), SP, and non-SP (NSP) fraction of resistant cells pre and post cisplatin treatment. Cisplatin augmented *PIK3CA* expression in MP (1.4, 1.9 and 1.6 fold) and SP fraction (2.1, 2.2, and 1.7 fold) in A2780-CisR, TOV21G and SKOV3 cells respectively (Fig. 1d, Additional file 2: Figure S1B&C). However, such increase in *PIK3CA* expression was not observed in their respective NSP fractions.

DNA-protein pull down identified critical *PIK3CA* promoter binders in platinum resistant cells
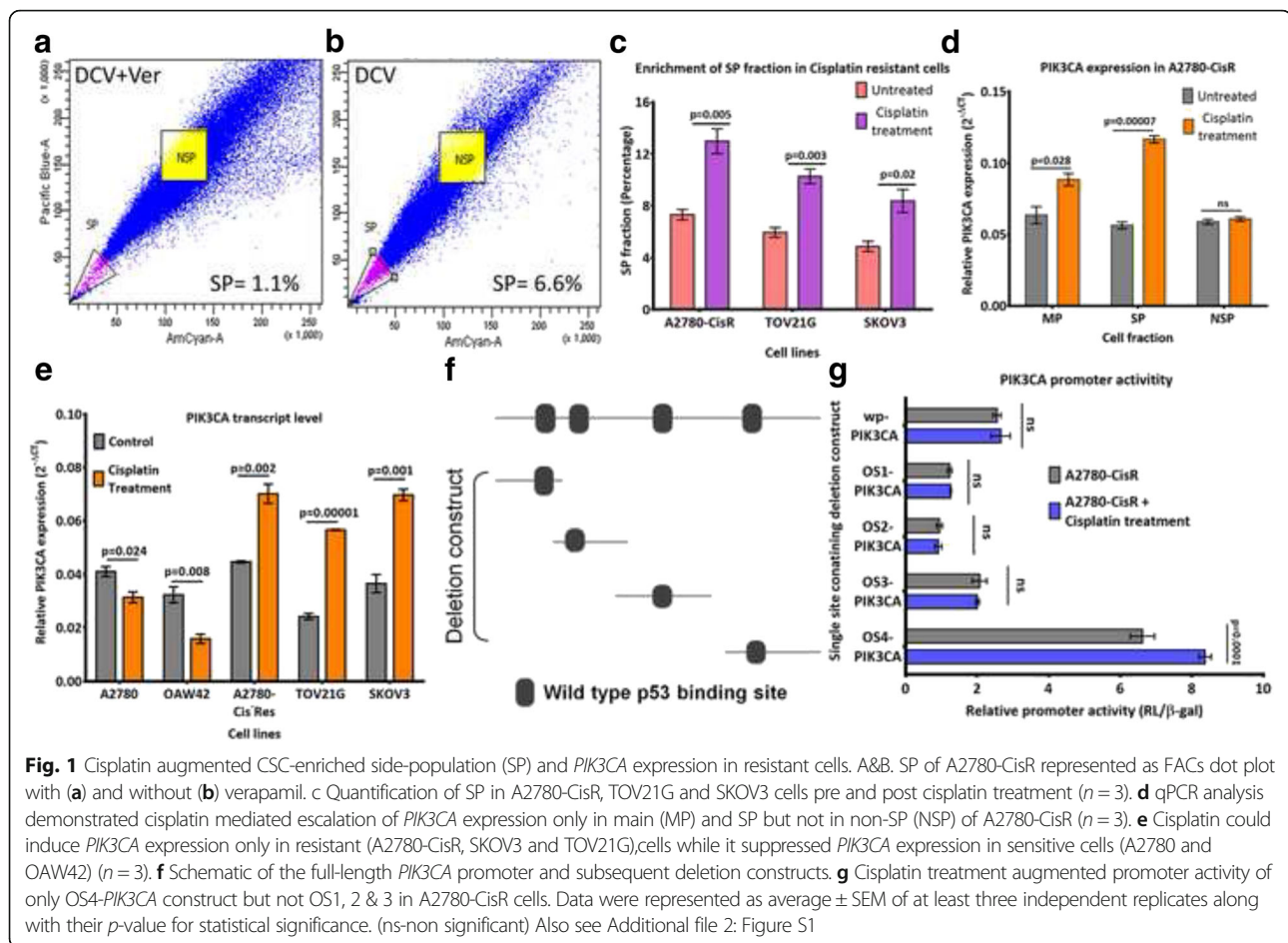
To identify the potential regulators, we adopted a magnetic bead-separation methodology where DNA-binder proteins were pulled down using biotinylated *PIK3CA* promoter as a bait. Since pulldown with the full-length *PIK3CA* promoter (1 kb) was not feasible due to obvious multi-target complexity, a smaller promoter fragment was used. To select the appropriate fragment of *PIK3CA* promoter, promoter activity of all four deletion constructs each with p53 binding site were assessed (Fig. 1f). The 5′-*PIK3CA* deletion construct (OS4-*PIK3CA*) exhibited maximal promoter activity (1.5–2.4 fold) in resistant (A2780-CisR, TOV21G, and SKOV3) cells compared to the full-length promoter, which was further increased (~1.3 fold) upon cisplatin treatment (Fig. 1g, Additional file 2: Figure S1D&E). Bioinformatic analysis with JASPER revealed presence of 116 putative transcription factor-binding sites in OS4, majority of which are also present on the full-length promoter sequence.

Using DNA-protein pull down assay, putative binders were isolated from nuclear extracts of A2780-CisR cells (control or cisplatin treated) and processed for nLC-MS analysis. These MS/MS spectra were analysed by protein pilot/Mascot server and identified 312 and 246 (cisplatin treated) and 863 and 339 (untreated) proteins in two biological replicates of A2780-CisR cells. We clustered protein signatures from each independent replicates of untreated and cisplatin treated A2780-CisR cells based on their 'GO- biological and GO- molecular' functions using GSEA (Fig. 2a-c). Pathway analysis of the identified hits revealed 136 (untreated) and 120 (treated) protein signatures comprised of transcription factors and their associated factors. Protein overlap analysis using VENN 2.1.0 sever revealed 67 common binders (36% of total hits) in both untreated and cisplatin-treated A2780-CisR cells (Fig. 2d) which comprised of general transcriptional assembly including RNA pol-II, PCNA and EP300 (Fig. 2e). List of these identified proteins is given in Additional file 1: Table S1–3. Apart from these overlapping *PIK3CA* promoter binders, we found an exclusive set of 69 (36.4%) and 53 (27.7%) hits in untreated and cisplatin treated A2780-CisR cells respectively. These proteins were further clustered based on a) presence in both replicates; b) presence of their interacting partners in replicates and c) predicted binding sites on *PIK3CA* promoter (Fig. 3a). The top three promoter binders found to be NF-κB, β-catenin and CREB which are known to maintain self-renewal and differentiation of CSCs in ovarian (NF-κB) [4], nasopharyngeal (β-catenin) [18] and oral cancer (CREB) [19] cells.

Cisplatin mediated induction of NF-κB transcriptionally activated *PIK3CA* expression in resistant cells

To compare the specificity of *PIK3CA* regulation by NF-κB, β-catenin and CREB, we assessed promoter activity of OS4-*PIK3CA* in A2780 and A2780-CisR cells after TNFα, Lithium chloride (LiCl) and forskolin treatment which are known inducers of these factors. Treatment of

Fig. 1 Cisplatin augmented CSC-enriched side-population (SP) and *PIK3CA* expression in resistant cells. A&B. SP of A2780-CisR represented as FACs dot plot with (**a**) and without (**b**) verapamil. c Quantification of SP in A2780-CisR, TOV21G and SKOV3 cells pre and post cisplatin treatment (*n* = 3). **d** qPCR analysis demonstrated cisplatin mediated escalation of *PIK3CA* expression only in main (MP) and SP but not in non-SP (NSP) of A2780-CisR (*n* = 3). **e** Cisplatin could induce *PIK3CA* expression only in resistant (A2780-CisR, SKOV3 and TOV21G),cells while it suppressed *PIK3CA* expression in sensitive cells (A2780 and OAW42) (*n* = 3). **f** Schematic of the full-length *PIK3CA* promoter and subsequent deletion constructs. **g** Cisplatin treatment augmented promoter activity of only OS4-*PIK3CA* construct but not OS1, 2 & 3 in A2780-CisR cells. Data were represented as average ± SEM of at least three independent replicates along with their *p*-value for statistical significance. (ns-non significant) Also see Additional file 2: Figure S1

TNFα and LiCl increased OS4-*PIK3CA* promoter activity by 2.4 and 1.7 fold in A2780-CisR cells but not in sensitive A2780 cells (Fig. 3b). However, forskolin induced OS4-*PIK3CA* promoter activity by 1.5 fold in both A2780 and A2780-CisR cells (Fig. 3b) indicating a more general transcriptional regulation. Similar trend was also observed for full-length *PIK3CA* promoter activity (data not shown). In accordance with promoter activity, TNFα and LiCl escalated endogenous *PIK3CA* expression by 2.2 and 1.7 fold in A2780-CisR but not in A2780 cells (Fig. 3c). However, forskolin enhanced *PIK3CA* expression only in A2780-CisR (1.5 fold) but not in A2780 cells (0.7 fold) (Fig. 3c).

Collectively our data point towards a critical role of NF-κB in PI3K/AKT signalling in platinum-resistant cells. Next, to study the SP-specific *PIK3CA* regulators, we assessed *PIK3CA* promoter activity in SP fraction after treatment of cisplatin, TNFα, LiCl or forskolin. Promoter activity was induced by cisplatin (1.5 fold) and TNFα (1.9 fold) but not by LiCl (1.1 fold) and forskolin (0.9 fold) (Additional file 3: Figure S2). This was also corroborated with NF-κB binding on *PIK3CA* promoter, where cisplatin and TNFα enhanced NF-κB occupancy

from 1% to 5% and 3.8% of input in A2780-CisR SP fraction. Similarly, TOV21G and SKOV3 cells showed increased NF-κB binding from 0.3% to 6% and 0.1% to 3% post TNFα and from 0.3% to 3.4% and 0.1% to 2.7% post cisplatin respectively (Fig. 3d).

Differential activity of NF-κB was responsible for discrepant *PIK3CA* expression in SP and NSP fraction

To understand NF-κB driven *PIK3CA* promoter regulation, we measured NF-κB transcriptional activity and *PIK3CA* promoter activity in MP, SP and NSP fraction of A2780-CisR dual reporter cells [20]. This dual reporter cells expresses a NF-κB transcriptional reporter (4xNF-κB binding sites driving a hRL-eGFP) along with the *PIK3CA* promoter sensor (*PIK3CA* promoter driving fl2-tdt). SP showed increase in NF-κB reporter activity after cisplatin (3.5 fold) or TNFα (4.8 fold) treatment (Additional file 4: Figure S3A). Correspondingly, cisplatin or TNFα escalated *PIK3CA* promoter activity by 1.5 and 1.8 fold in SP cells, respectively (Additional file 4: Figure S3B). Only MP but not NSP showed augmented NF-κB reporter and *PIK3CA* promoter activity after TNFα treatment. Though cisplatin induced NF-κB transcriptional
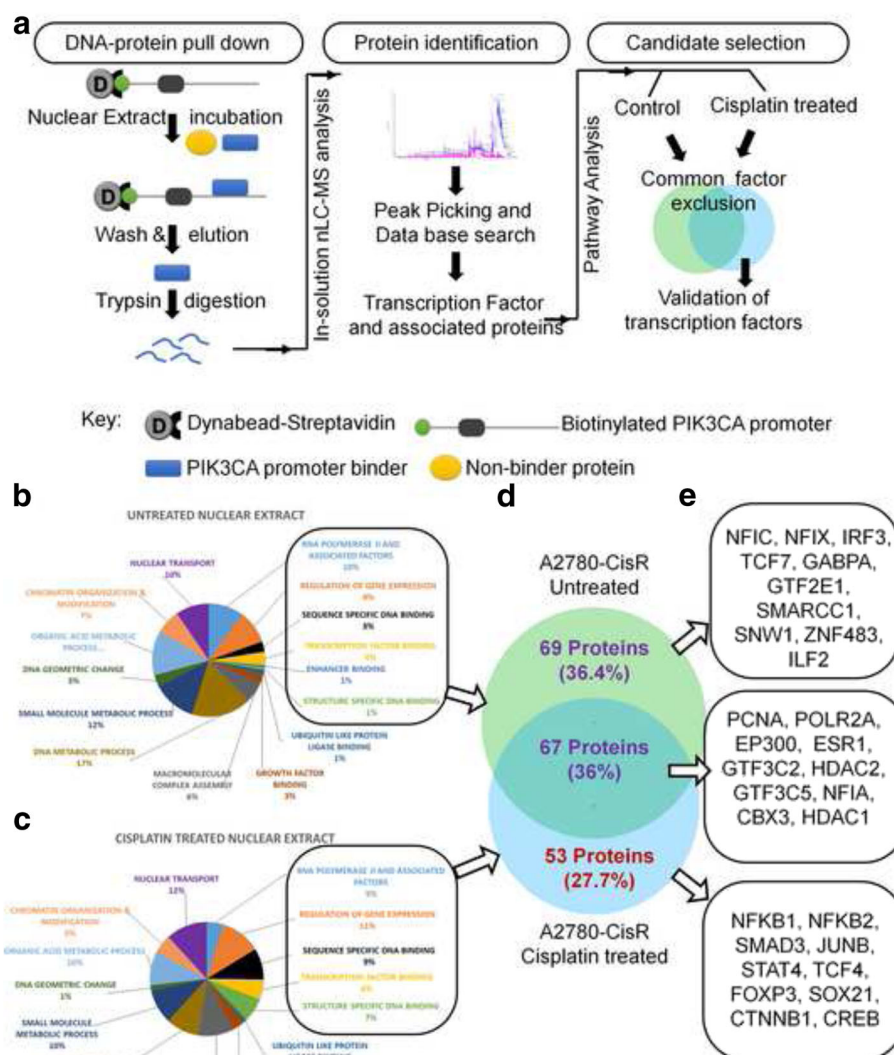
Fig. 2 Identification of cisplatin responsive *PIK3CA* regulator in resistant cells: **a** Flow-chart of DNA-protein pulldown assay performed with nuclear extracts of pre and post cisplatin treated A2780-CisR cells. **b**&**c.** Identified protein signatures were functionaly categorised using GSEA server. Only transcription factors and their associated partner proteins were used for further analysis. **d**&**e.** potential binders were grouped from mutually inclusive or exclusive hits from untreated and treated A2780-CisR cells using Venn 2.1.0 server. Ten top scoring factors from each category were listed in the representative boxes. The complete list is given in the Additional file 1: Table S1-S3

activity (2.8 fold), no significant difference was observed in *PIK3CA* promoter activity in MP cells (Additional file 4: Figure S3). Further, statistical analysis showed a strong positive correlation between NF-κB reporter activity and *PIK3CA* promoter activity in SP cells (Pearson correlation, $r = 0.96$). Such correlation was not observed in MP and NSP cells ($r = 0.12$ and $r = 0.3$ respectively) (Fig. 3e-g).

Cisplatin treatment induced total NF-κB level in MP, SP and NSP fraction compared to their untreated counterparts. Notably, control SP showed highest NF-κB level compared to MP and NSP cells (Fig. 3h). Further, NF-κB binding to *PIK3CA* promoter in untreated SP cells (0.9%), was increased up to 5.7 and 4.3% post TNFα or cisplatin

treatment (Fig. 3i). In accordance with this and to our surprise, enhanced binding of NF-κB upon *PIK3CA* promoter by TNFα (0% to 2.2%) but not by cisplatin (0% to 0%) was observed in NSP fraction of A2780-CisR cells (Fig. 4g). TOV21G and SKOV3 also showed similar results with physical-interaction of NF-κB with *PIK3CA* promoter (Additional file 5: Figure S4A-C).

To understand CSC specific NF-κB activation, we performed co-localization studies for NF-κB and OCT4 in MP, SP and NSP fraction. Cisplatin treatment to A2780-CisR increased nuclear NF-κB+ cells from 5.2% to 10.8% (MP) and 17% to 33.4% (SP) (Fig. 4a-d). Similarly, TOV21G and SKOV3 cells showed ~2 fold increase (from
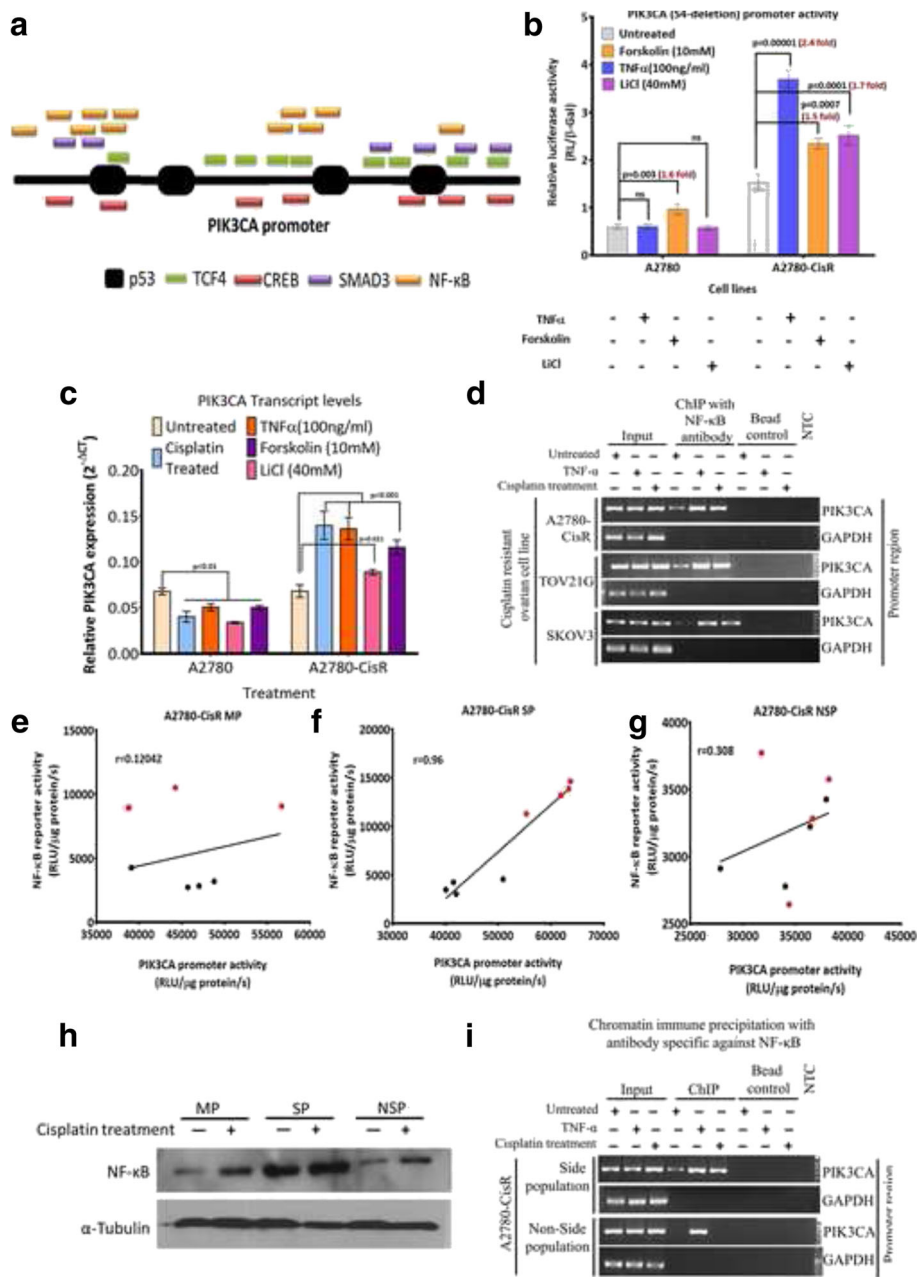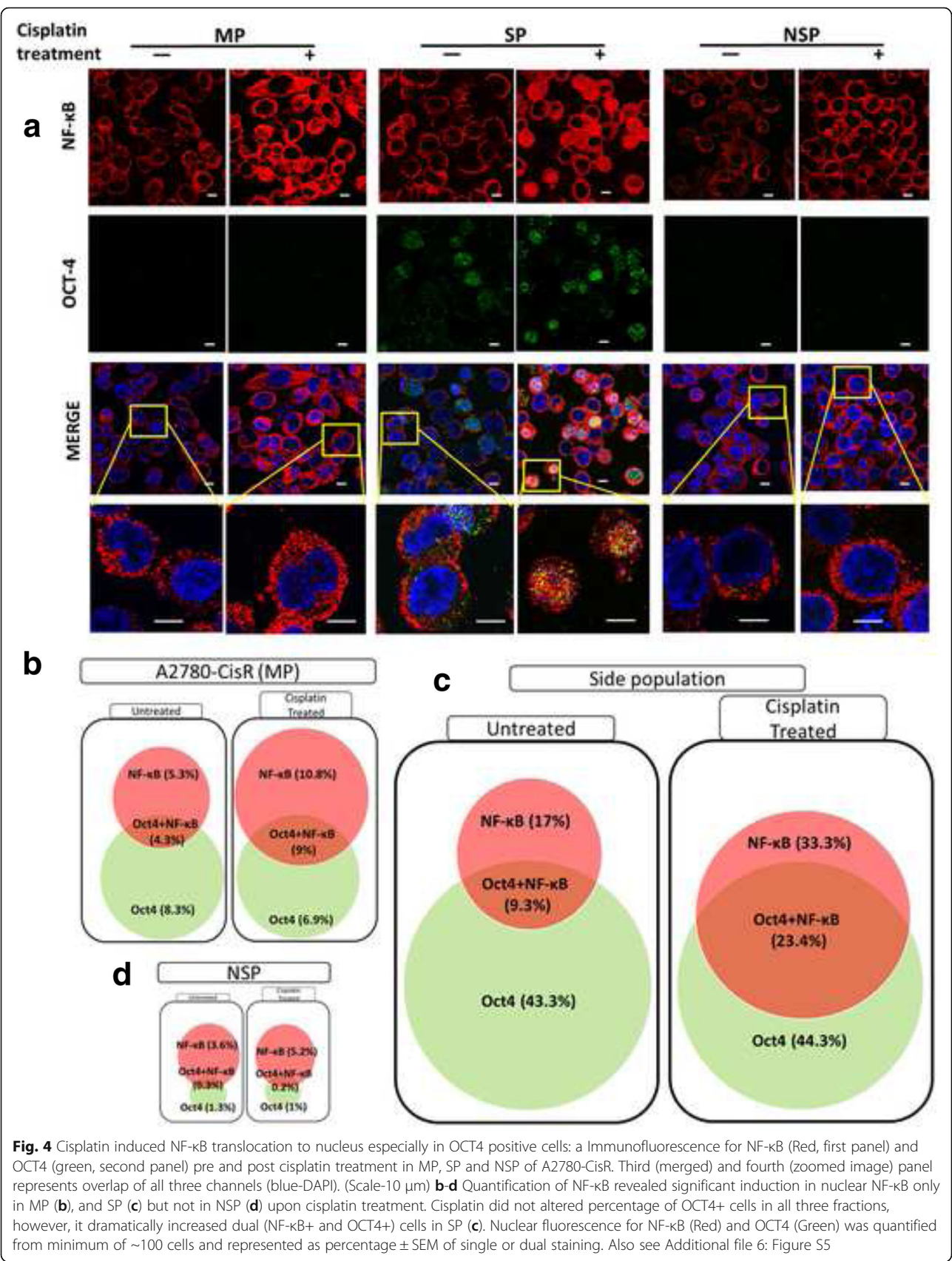
Fig. 3 Cisplatin responsive activation of NF-κB induced *PIK3CA* in SP fraction of resistant cells. **a** Schematic of predicted response elements of five transcription factors on full-length *PIK3CA* promoter identified using JASPER server. **b** TNFα and LiCl treatment increased OS4-*PIK3CA* promoter activity only in A2780-CisR but not in A2780. Forskolin induced marginal change in both cells. Fold change (treated/control) were represented in red font (*n* = 4). **c** qPCR showed induction in *PIK3CA* expression only in A2780-CisR but not in A2780 cells after TNFα, LiCl and forskolin treatment. **d** Both cisplatin and TNFα augmented interaction of NF-κB on *PIK3CA* promoter as assessed by ChIP assay in A2780-CisR, TOV21G, and SKOV3 cells. **e-g** Pearson correlation analysis showed a strong positive correlation between NF-κB reporter and *PIK3CA* promoter activity only in SP but not in MP or NSP cells in response to cisplatin. Black -untreated and red -treated. (Note- overlapping values in cisplatin treated MP are appeared as a single dot) (*n* = 4). **h** Protein levels of NF-κB pre and post cisplatin treatment. **i** ChIP assay for NF-κB occupancy on *PIK3CA* promoter in SP and NSP after TNFα and cisplatin treatment. GAPDH was used as control for ChIP experiments. Data represented as average ± SEM of four independent replicates with their actual p-value for statistical significance (ns-non significant). Also see Additional file 3: Figure S2, Additional file 4: Figure S3 and Additional file 5: Figure S4

7.8% to 14.5% (MP) and 18.3% to 27.3% (SP) in TOV21G, 4.5% to 8.4% (MP) and 13.2% to 21.1% (SP) in SKOV3 in nuclear NF-κB+ cells (Additional file 6: Figure S5A-D).

Nuclear NF-κB+ cells in NSP fraction remained unchanged after cisplatin treatment in A2780-CisR (3.8%), TOV21G (5.8%) and SKOV3 (3.4%) cells (Fig. 4d,

Fig. 4 Cisplatin induced NF-κB translocation to nucleus especially in OCT4 positive cells: a Immunofluorescence for NF-κB (Red, first panel) and OCT4 (green, second panel) pre and post cisplatin treatment in MP, SP and NSP of A2780-CisR. Third (merged) and fourth (zoomed image) panel represents overlap of all three channels (blue-DAPI). (Scale-10 μm) **b-d** Quantification of NF-κB revealed significant induction in nuclear NF-κB only in MP (**b**), and SP (**c**) but not in NSP (**d**) upon cisplatin treatment. Cisplatin did not altered percentage of OCT4+ cells in all three fractions, however, it dramatically increased dual (NF-κB+ and OCT4+) cells in SP (**c**). Nuclear fluorescence for NF-κB (Red) and OCT4 (Green) was quantified from minimum of ~100 cells and represented as percentage ± SEM of single or dual staining. Also see Additional file 6: Figure S5

Additional file 6: Figure S5A-D). Further, we quantified nuclear OCT4+ cells to detect CSC fraction from the MP, SP and NSP fraction. As expected, only SP obtained from A2780-CisR (44.3%), TOV21G (36.7%) and SKOV3 (32.4%) cells showed OCT4+ nuclei and cisplatin treatment did not alter their percent OCT4 positive cells (Fig. 4b-d, Additional file 6: Figure S5E&F). Notably, SP fraction of A2780-CisR, TOV21G and SKOV3 cells possessed 9.3%, 10% and 9% cells with NF-κB+ and OCT4+ nuclei respectively (Fig. 4, Additional file 6: Figure S5G&H). Contrarily, MP showed only 4.3%, 2.3%, and 1.3% cells with OCT4+ and NF-κB+ nuclei, while NSP fractions did not show any OCT4+ and NF-κB+ nuclei in A2780-CisR, TOV21G and SKOV3 respectively (Fig. 4b, d, Additional file 6: Figure S5G&H). These dual positive (OCT4+ and NF-κB+) nuclei were further increased up to 23.4%, 14% and 15% post cisplatin treatment in SP obtained from A2780-CisR, TOV21G and SKOV3 cells (Fig. 4c, Additional file 6: Figure S5G&H). Only MP fraction from A2780-CisR cells demonstrated increase in OCT4+ and NF-κB+ cells up to 9% (Fig. 4b), however, such increase was not observed in TOV21G (2.6%) and SKOV3 (2%) cells after cisplatin treatment (Additional file 6: Figure S5G&H). OCT4+ and NF-κB+ cells remained unchanged in NSP of in all three cells (Fig. 4d, Additional file 6: Figure S5G&H).

Cisplatin triggered enrichment of cancer stem cells in *PIK3CA* dependent manner

To understand the impact of *PIK3CA* expression modulation on the CSC-phenotype, we assessed enrichment of SP fraction in resistant cells post induction of *PIK3CA* using TNFα or cisplatin. Similar to cisplatin treatment (Fig. 1c), TNFα also augmented SP fraction from 7.3 ± 0.7% to 13.6 ± 1.9% in A2780-CisR cells (Fig. 6a, b). In other resistant cells, SP fraction increased from 5.9 ± 0.7% to 9.1 ± 1.6% (TOV21G) and 4.9 ± 0.7% to 7.7 ± 0.8% (SKOV3) post TNFα (Additional file 7: Figure S6A&B). To determine whether cisplatin plays a role in maintenance and/or differentiation of CSC fraction, we repeatedly sorted SP from resistant cells and cultured for three generation as reported earlier [17] (Fig. 5a). We observed that, from 100% of A2780-CisR sorted SP fraction, only 38.7 ± 3.5% of population persisted as SP fraction over 48 h while rest of the cells differentiated into NSP fraction (Fig. 5b). Interestingly, addition of TNFα or cisplatin in the media led to increase in SP fraction up to 67.1 ± 7.2% and 59.9 ± 12.2% respectively (Fig. 5b). Similar enrichment in SP fraction was also observed in TOV21G (31.5 ± 1.3% to 45.8 ± 7.9% by TNFα and 31.5 ± 1.3% to 46.6 ± 3.9% by cisplatin) and SKOV3 (25.1 ± 3% to 33.6 ± 3.1% by TNFα and 25.1 ± 3% to 33.6 ± 3.1% by cisplatin) cells (Additional file 7: Figure S6). NSP fraction from all three cells did not show any enrichment in SP fraction with either of the treatments

(Fig. 5b, Additional file 7: Figure S6). To confirm whether this enrichment of SP fraction also enriches CSC-characteristics, we assessed expression of pluripotency factors (OCT4, NANOG and SOX2) pre and post cisplatin treatment. Cisplatin had also increased one or more pluripotency gene signatures in SP fraction of A2780-CisR (NANOG, SOX2), TOV21G (OCT4), and SKOV3 (OCT4, NANOG) (Fig. 5c-e). MP and NSP fraction did not show such alteration.

Inhibition of *PIK3CA* activity suppresses cisplatin induced SP enrichment in platinum resistant cells

We observed relatively higher induction of *PIK3CA* expression in SP compared to MP and NSP upon cisplatin treatment, which also persuaded enrichment of SP fraction in A2780-CisR, TOV21G and SKOV3 cells. To ascertain that this enrichment depends on *PIK3CA* activity, we inhibited PI3K-activity using a reversible PI3K inhibitor, wortmannin. PI3K inhibition reduced SP fraction from 7.3 ± 1.1% (untreated) to 5.2 ± 0.6% (wortmanin) and 14.6 ± 2.9% (cisplatin) to 9.1 ± 0.8% (cisplatin and wortmannin) in A2780-CisR MP fraction (Fig. 5f). Similar effect was also observed in SKOV3 cells where SP fraction was reduced from 4.8 ± 1.7% (untreated) to 1.9 ± 0.2% (wortmannin) and 8.5 ± 1.2% (cisplatin) to 2.8 ± 0.4% (cisplatin and wortmannin) (Fig. 5g). Effect of PI3K inhibition was more robust in serially sorted 3rd generation SP where ~50% decline in SP-enrichment was evident post wortmannin treatment (24 h). In 3rd generation A2780-CisR cells, *PIK3CA* inhibition reduced SP from 38.5 ± 7.1% (untreated) to 21.6 ± 5.8% (wortmanin) and 61.3 ± 9.5% (cisplatin) to 33 ± 4.8% (cisplatin and wortmannin) (Fig. 5f). Similarly SP percentage of 3rd generation SP fraction obtained from SKOV3 cells was reduced from 21.7 ± 0.4% (untreated) to 12.3 ± 1.7% (wortmannin) and 38.3 ± 4.7% (cisplatin) to 15.4 ± 0.4% (cisplatin and wortmannin) (Fig. 5g). NSP cells did not show significant percentage of SP fraction after serial culturing with or without wortmannin treatment (Fig. 5f, g).

To assess the consequence of activated PI3K/AKT cascade on CSCs, we monitored expression of specific downstream targets such as *P21, P27, CYCLIN-D1 & CYCLIN-E1* (cell cycle regulators), *BAX, PUMA* (pro-apoptotic) and *cFLIP* (anti-apoptotic) in MP, SP and NSP fractions pre and post cisplatin treatment. Increased *P21* and *P27* levels and decreased *CYCLIN-D1&*E1 levels in SP fractions compared to NSP cells marks growth-arrested, quiescent state of SP (Fig. 5h). Interestingly, we observed sharp increase in *CYCLIN-D1* level indicating active proliferation of NSP cells after cisplatin treatment. Though *cFLIP* levels were increased in all three fractions, transcriptional increment in *BAX* and *PUMA* in NSP fractions marked their pro-apoptotic fate (Fig. 5h). However, increased *cFLIP* levels along with quiescent-state of SP aid these cells to survive the action of chemotherapeutics. In accordance with NF-
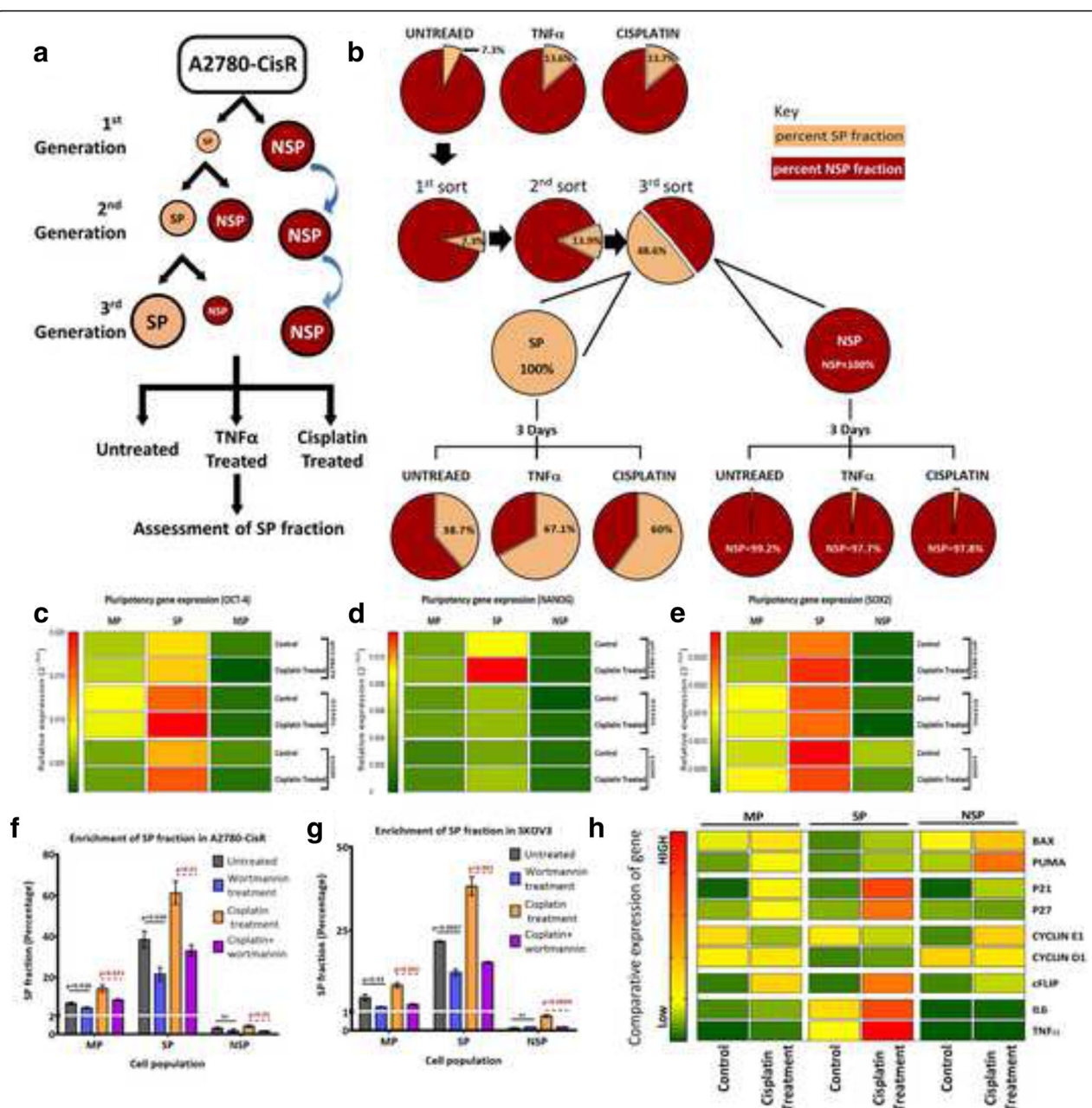
Fig. 5 Cisplatin mediated activation of PI3K/AKT endorsed an anti-apoptotic, dormant state, augmenting CSC in resistant cells. **a** Flow-chart of SP-differentiation assay, where SP was serially sorted for three successive generation and %SP was determined pre and post TNFα or cisplatin treatment (24 h). **b** Pie chart showing SP enrichment after TNFα or cisplatin in A2780-CisR cells (MP, top panel). The middle panel depicted the percent increase in SP over generations as described in A and the lower panel depicted %SP after respective condition. The NSP cells did not showed any SP fraction. Data represented as average %SP obtained from three independent biological replicates. **c-e.** Heat map of relative expression ($2^{-\Delta CT}$) of pluripotent genes *OCT4* (**c**), *NANOG* (**d**) and *SOX2* (**e**) in response to cisplatin in MP, SP and NSP of A2780-CisR, TOV21G and SKOV3 cells (*n* = 3). **f&g.** Inhibition of *PIK3CA* activity using wortmannin decreased %SP in MP and 3rd gen SP of control and cisplatin treated A2780-CisR and SKOV3 cells (*n* = 3). **h** Comparative expression of the indicated genes in MP, SP and NSP fraction of A2780-CisR cells with and without cisplatin treatment where the least relative expression ($2^{-\Delta CT}$) value was considered be the lowermost color (dark green) of the scale. Data represented as mean of at least three independent replicates, and heat maps were generated with GraphPad prism 7. Also see Additional file 7: Figure S6

κB-transcriptional reporter activity, its downstream targets (*IL6* and *TNFα*) also showed higher expression in SP fractions compared to MP and NSP, which further increased significantly upon cisplatin treatment in MP and SP but not in NSP. However, *CYCLIN-D1*, another target of NF-κB did not show similar modulation in SP fractions. Overall, anti-apoptotic, dormant state provided survival advantage to CSC against
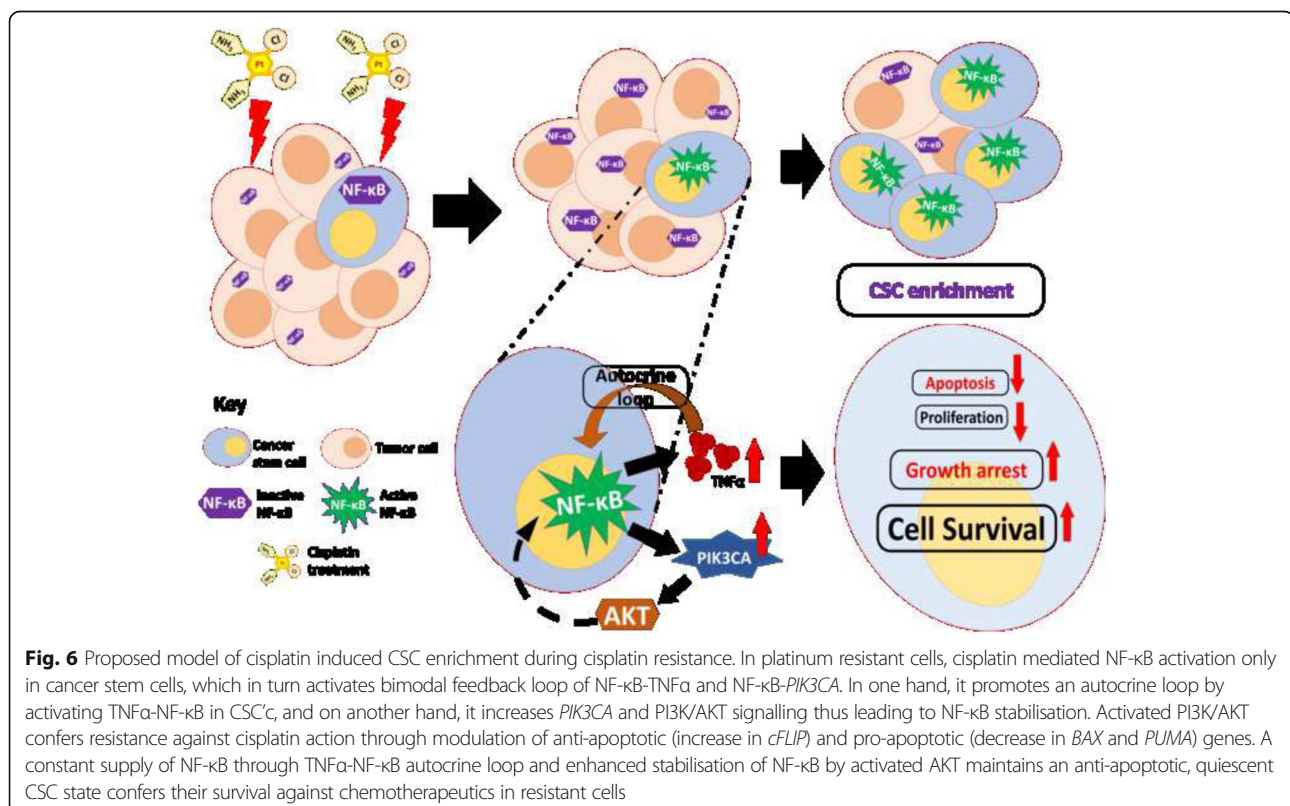
cisplatin cytotoxicity and led to their enrichment upon cisplatin treatment (Fig. 6).

Discussion

Chemoresistance, either intrinsic or acquired, substantially handicaps the efficacy of chemotherapy, escalating mortality rates in cancer patients. Acquirement of resistance towards chemotherapeutics is a dynamic and multifactorial process and influenced by cancer stem cell (CSC) enrichment [3, 21, 22]. Though platinum resistance is a common problem for cervical, head and neck, and non-small-cell lung cancer management, it is particularly devastating for epithelial ovarian cancer (EOC) patients as 50% of the therapy-responders ultimately show chemoresistant-relapse [7, 23]. Utilizing A2780-cisplatin resistant cellular model and two naturally occurring cisplatin resistant cells (TOV21G and SKOV3) [14], we attempted to address a unique question of how cisplatin impact existing CSCs in resistant cells. In all these cells, cisplatin enhanced the inherently drug resistant side-population with increased *PIK3CA* expression. Activation of PI3K/AKT pathway is known to favour cellular endurance against chemotherapeutics and maintenance of CSC-population [2, 18] but regulators of this pathway in drug-resistant cells are yet to be identified. Using transcription-factor pulldown assay, we identified NF-κB, β-catenin and CREB as cisplatin-responsive

transcriptional activators of *PIK3CA* promoter. Amongst them, NF-κB differentially activated *PIK3CA* only in CSC-enriched side-population but not in non-SP. Both cisplatin and TNFα induced interaction between NF-κB and *PIK3CA* promoter. Further, inhibition of PI3K-activity dramatically reduced this CSC-enriched SP fraction. Enhanced nuclear co-localization of NF-κB with OCT4 and augmented expression of *OCT4*, *SOX2* and *NANOG* in SP signified enrichment of CSC properties by cisplatin. Finally, gene expression analysis revealed that cisplatin mediated activation of PI3K/AKT led to an anti-apoptotic, dormant stage, which aided CSC to evade therapeutic action while actively proliferating non-CSC cells succumbed to cisplatin's action. Intriguingly, TNFα, a well-known activator of NF-κB and an NF-κB–regulated gene showed enhanced expression following cisplatin treatment only in SP cells. Collectively, our data emphasize that therapeutic intervention to platinum-resistant ovarian cancer cells favours a predominant quiescent state in SP via an interdependent positive feedback loop between TNFα-NF-κB and PI3K/AKT signalling.

Cisplatin forms the first line therapy against malignancies including ovarian, breast and colorectal cancer, however, acquirement of resistance impaired therapeutic efficacy [6, 7]. Amongst several molecular determinants of cisplatin resistance, activated PI3K/AKT pathway turns out to be a key signalling that also aids in survival

Fig. 6 Proposed model of cisplatin induced CSC enrichment during cisplatin resistance. In platinum resistant cells, cisplatin mediated NF-κB activation only in cancer stem cells, which in turn activates bimodal feedback loop of NF-κB-TNFα and NF-κB-*PIK3CA*. In one hand, it promotes an autocrine loop by activating TNFα-NF-κB in CSC'c, and on another hand, it increases *PIK3CA* and PI3K/AKT signalling thus leading to NF-κB stabilisation. Activated PI3K/AKT confers resistance against cisplatin action through modulation of anti-apoptotic (increase in *cFLIP*) and pro-apoptotic (decrease in *BAX* and *PUMA*) genes. A constant supply of NF-κB through TNFα-NF-κB autocrine loop and enhanced stabilisation of NF-κB by activated AKT maintains an anti-apoptotic, quiescent CSC state confers their survival against chemotherapeutics in resistant cells

of CSCs [1, 2]. Lee et al., (2005) showed that escalated *PIK3CA* expression in OVCAR-3/CDDP (resistant) cells leads to inhibition of *BAX* translocation via activated PI3K/AKT conforming platinum-resistance [24]. Amplification of *PIK3CA* was associated with ovarian and uterine cervical carcinoma, which led to active PI3K/AKT signaling and resistance acquirement [25, 26]. However, mechanism for augmented *PIK3CA* expression is less dissected at molecular level. Intriguingly, we observed cisplatin itself could upregulate *PIK3CA* expression in resistant but not in sensitive cells [14]. Several transcription-factors (TF) such as p53/p73, cMyc, YB-1, CTF-2, ATF-4, ZNF143, mTFA, AP1, NF-κB, OCT1, SP1, β-catenin and CREB are known to be associated with cisplatin resistance, regulating expression of resistance associated genes [27, 28]. Among all these TFs, cisplatin directly influences transcriptional activities of p53, YB-1, ZNF143, mTFA, NF-κB, ATF-2, 3 and 4 [27]. We earlier reported that cisplatin-mediated phosphorylation of p53 at Ser46 promotes its binding, and repress *PIK3CA* promoter in sensitive cells. Absence of such phosphorylation in cisplatin-treated resistant cells resulted in loss *PIK3CA* attenuation [14] which, however, does not explain the apparent increase in *PIK3CA* expression level. Till now, only YB-1, NF-κB and FOXO3a are known to induce *PIK3CA* expression in unstressed condition [13]. No information is available on regulators of *PIK3CA* modulation in platinum-resistant cells in response to cisplatin. Thus to identify cisplatin-responsive regulators of *PIK3CA* promoter, we subjected *PIK3CA* promoter bound nuclear fraction (potential transcription-factors) from untreated and cisplatin treated A2780-CisR cells to nLC-MS. We used a short OS4-*PIK3CA* promoter fragment due to: A) it shows augmented promoter activity upon cisplatin treatment, B) Contains binding sites for p53, and other transcription-factors & C) to avoid multi-target binding complexity possible for full-length (1 kb) promoter. Multiple putative candidate proteins bound to *PIK3CA* promoter in untreated (863 and 339) and cisplatin treated (312 and 246) A2780-CisR cells were identified which were further classified based upon their transcription associated functioning. Among the binders present exclusively in cisplatin treated samples (36%), we selected the top three *PIK3CA* binders (NF-κB, β-catenin and CREB) for further validation. All these three transcription-factors are known to influence cisplatin resistance in various cancer cells. Li et al., (2016) demonstrated that cisplatin-mediated increase in β-catenin expression aids in resistance-development in oral squamous cell carcinoma [25, 29]. While CREB is shown to be activated by cisplatin in ovarian cancer cells [28] and hyperactivation of NF-κB is associated with cisplatin resistant human epidermoid carcinoma, KCP-4 cells [30]. Our earlier report also demonstrates that in absence of TLR4/MyD88

signalling, ovarian cancer chemoresistance is maintained by NF-κB transcriptional activation under cisplatin treatment [20]. Augmented *PIK3CA* expression in platinum resistant H460 cells was also supported with increased NF-κB and β-catenin but not in CREB levels compared to their parental counterpart [31]. In accordance with this, we observed augmented *PIK3CA* promoter activity only in platinum resistant cells upon treatment with TNFα (NF-κB inducer) or LiCl (β-catenin inducer), while, forskolin (CREB inducer) increased *PIK3CA* promoter activity in both sensitive and resistant cells. Though forskolin increased *PIK3CA* expression in A2780-CisR cells, its treatment to A2780 sensitive cells led to reduction in *PIK3CA* transcript levels. Other than CREB, forskolin is known to induce binding of Ets-2, phospho-p53 and AP1 TFs to MMP-2 promoter [32]. Hence, observed decrease in *PIK3CA* expression in A2780 cells may be influenced by other forskolin-induced TFs such as p53. Till date NF-κB's role as a positive regulator for *PIK3CA* promoter in ovarian cancer cells by TNFα is known [33]. Herein, we demonstrate a unique mechanism of *PIK3CA* transcriptional upregulation by NF-κB upon cisplatin, a cytotoxic drug treatment in platinum-resistant cells. ChIP assay showed that NF-κB-*PIK3CA* promoter interaction increased several fold following TNFα or cisplatin treatment in A2780-CisR, TOV21G, and SKOV3 cells. Our data also suggest β-catenin complex to be another regulator of *PIK3CA* promoter, however, presence of only two interacting (SMAD3 & TCF4) partners of this complex among large numbers of identified binders and minimal (~1.5) fold increase in *PIK3CA* expression by LiCl did not suggest a robust role of this complex. Further experimental studies are required to elucidate the exact contribution of β-catenin complex.

Two distinct observations that cisplatin mediates SP-enrichment and increased NF-κB-*PIK3CA* promoter interaction, prompted us to assess the expression level of *PIK3CA* in MP, SP, and NSP fractions. Surprisingly, augmented *PIK3CA* expression in response to cisplatin found only in SP but not in NSP cells. Next, for comprehensive understanding of what regulates *PIK3CA* in SP, we treated SP cells with inducers of NF-κB, β-catenin or CREB. Among them, only TNFα augmented *PIK3CA* promoter activity in SP but not in NSP cells, indicating NF-κB as distinct activator of *PIK3CA* in SP cells. Further, to verify whether SP does contain transcriptionally active NF-κB, we used a dual-stable cellular system of A2780-CisR expressing NF-κB-transcriptional reporter and *PIK3CA* sensor [20]. Cisplatin treatment resulted in strong positive correlation between NF-κB activity and *PIK3CA* promoter activity only in SP but not in MP or NSP.

Nuclear factor-κB, (NF-κB) belongs to a pivotal transcription-factor family, which controls expression of diverse genes related to immune-response, survival, proliferation, angiogenesis, and metastasis. In most cells,

inhibitor of κB, (IκB) regulates NF-κB transcriptional activity [34] and dissociation of NF-κB/IκB heterodimer leads to nuclear-translocation of NF-κB where it functions as transcription-factor. The NF-κB signalling cascade converges with several cellular pathways including PI3K/AKT, where activated AKT promotes IκB degradation via phosphorylating IKKα kinase. In most tumors, NF-κB signaling is constitutively active, regulating gene induction associated with proliferation (*CYCLIN-D1&D2, CDK2* and c-*MYC*), growth signals (*GM-CSF* and *IL6*), anti-apoptosis (*cFLIP, BCL2, Bcl-xL* and *IAPs*) and angiogenesis (*VEGF, TNFα,* and *IL1*) [35]. Further, ovarian CD44 + CSCs, survive the treatment of paclitaxel and carboplatin through concomitant activation of NF-κB signalling and conferring resistance against these drugs [4]. Hence, to understand the CSC-specific activation of NF-κB in cisplatin resistant cells, we investigated co-localisation of OCT4 with NF-κB in MP, SP and NSP. ~2–3 fold increase in nuclear NF-κB+ and OCT4 + cells in only SP but not in MP or NSP upon cisplatin treatment, clearly indicating contribution of NF-κB in both CSC-homeostasis and *PIK3CA*-regulation. Enhanced expression in pluripotency gene (*OCT4, SOX2* and *NANOG*) by cisplatin exclusively in SP but not in MP or NSP warranted escalation of CSC-characteristics in SP fraction. Interestingly, same drug treatment induced distinct pluripotent gene expression in A2780-CisR, TOV21G, and SKOV3 cells probably due to intercellular differences in genetic constituents. Further to inspect NF-κB mediated *PIK3CA* regulation, we assessed NF-κB-*PIK3CA* promoter interaction in SP and NSP cells pre and post TNFα or cisplatin treatment. Similar to MP, SP but not NSP showed enhanced occupancy of NF-κB on *PIK3CA* promoter following cisplatin treatment. TNFα, however, induced NF-κB binding on *PIK3CA* promoter in both SP and NSP. This seemingly contradictory NF-κB-*PIK3CA* promoter interaction by two different stimuli is not surprising as NF-κB activation by UV-C or doxorubicin is known to induce a complete different set of target genes than that by TNFα and produce entirely different functional consequences [9].

Self-renewal and differentiation are the two major characteristics of stem cells that influence and regulate organogenesis and normal development. Likewise, cancer stem cells control tumor development through self-renewal and differentiation into proliferating tumor cells. If a cytotoxic drug can enrich CSC-population in resistant cells, it would certainly affect one of these two crucial properties. Both cisplatin and TNFα were found to favour a self-renewing undifferentiated state of CSCs as evident from 1.7–2 fold enrichment of SP. In addition, our study revealed that cisplatin mediates CSC-specific activation of NF-κB, which in turn induces expression of *TNFα* and *PIK3CA*. This incremented TNFα is known to act as an autocrine cue in concomitant NF-κB activation [35, 36], while activation of NF-κB

escalates *PIK3CA* in CSC's. All these data led us to hypothesize that NF-κB controlled *PIK3CA* expression coordinates the CSC-survival and CSC-plasticity under the influence of a chemotherapeutics. Indeed, treating SP with wortamannin, an irreversible PI3K-inhibitor, with and without cisplatin diminished the SP fraction. Gene expression analysis showed increased *P21, P27* and *cFLIP* and decrease in *CYCLIN-D1* and *CYCLIN-E1* in cisplatin treated SP cells pointing towards an anti-apoptotic, quiescent phase. In contrast, augmented *CYCLIN-D1&E1* expression in cisplatin treated NSP cells marking their proliferative state make them vulnerable towards drug. Activation of PI3K/AKT confers resistance against cisplatin action through up regulation of anti-apoptotic genes such as *cFLIP*. Overall, CSC's with active PI3K/AKT and NF-κB signaling acquire anti-apoptotic, quiescent state conferring survival advantage against action of chemotherapeutic drugs (Fig. 6).

Conclusion

Platinum-salts are in mainstay of cancer clinic for last few decades and will be continued for decades due to their potent action against proliferating cells. Resistance acquirement against platinum-compounds is a major concern for several malignancies including epithelial ovarian cancer. The unanticipated finding of cisplatin inducing CSC-enriched side-population in platinum-resistant cells opened a new dimension in our understanding on how action of a cytotoxic drug be modulated by cellular ambience. Activated NF-κB leading to upregulated *PIK3CA* expression is the key molecular feature behind this action of cisplatin. Though involvement of NF-κB mediated other signalling cascades are possible, our present data signifies PI3K/AKT pathway as the major determinant of cisplatin action in resistant cells. Perturbation in CSC homeostasis through blocking PI3K/AKT signalling might become a rational approach to intervene Platinum-resistant relapse.

Additional file

Additional file 3: Figure S2. NF-κB escalated PIK3CA promoter activity in SP cells. Cisplatin and TNFα but not lithium chloride or forskolin increased PIK3CA promoter activity in SP collected from A2780-CisR cells (n = 4, p-value denoted significant statistical different, ns- non significant). (TIFF 400 kb)

Additional file 4: Figure S3. NF-κB drove PIK3CA expression in SP cells upon cisplatin treatment. A. Treatment of TNFα or cisplatin dramatically increased renila activity driven by NF-κB response elements only in MP and SP fractions of A2780-CisR dual reporter cell line but not in NSP fraction. TNFα treatment to NSP fraction showed minimal increase in NF-κB transcriptional activity (n = 4). B. Similar to NF-κB-reporter activity, TNFα treatment also induced PIK3CA promoter activity in MP, SP and NSP fractions of A2780-CisR dual reporter cell line. However, cisplatin mediated increase in PIK3CA promoter activity was observed only in SP fraction. SP fraction showed much higher induction of PIK3CA promoter activity compared to MP cells after TNFα, or cisplatin (n = 4). (TIFF 403 kb)

Additional file 5: Figure S4. Cisplatin induced NF-κB and its physical interaction with PIK3CA promoter in TOV21G and SKOV3 cells. A & B. Similar to A2780-CisR cells, both TOV21G (A) and SKOV3 (B) cells showed higher NF-κB protein levels in SP fraction compared to MP and NSP cells as assessed through immunoblotting. All three fraction from both the cell lines demonstrated cisplatin mediated increase in NF-κB protein levels. C. Similar to A2780-CisR cells, TNFα or cisplatin treatment induced NF-κB occupancy on PIK3CA promoter only in SP fraction of TOV21G and SKOV3 cells. In NSP fraction, only TNFα treatment showed NF-κB binding to PIK3CA promoter in both the cell lines. PCR using primers for GAPDH was used to show purity of chromatin immune-precipitation. (TIFF 357 kb)

Additional file 6: Figure S5. Cisplatin triggers nuclear localization of NF-κB in OCT4 positive SP cells. A-H. Confocal microscopy for NF-κB and OCT4 staining was performed pre and post cisplatin treatment in TOV21G (upper panel) and SKOV3 (lower panel) cells and quantification were graphically represented. A & B. Mean nuclear fluorescence intensity measurement demonstrated higher nuclear localization NF-κB in SP fractions of TOV21G (A) and SKOV3 (B) compared to their MP and NSP fractions. Intriguingly, nuclear localization of NF-κB was further increased upon cisplatin treatment in MP and SP fractions of both, TOV21G and SKOV3 cells. C-F. Cisplatin treatment increases only NF-κB nuclear positive cells but not OCT4 positive cells in MP, SP and NSP fractions obtained from TOV21G (C & E) and SKOV3 (D & F) cells. G & H. Similar to A2780-CisR, cisplatin increased NF-κB nuclear translocation in SP fractions, especially in OCT4 positive cells of TOV21G and SKOV3 cells. Only MP but not NSP fractions showed nominal increase in co-nuclear localised NF-κB and OCT4 positive cells upon cisplatin treatment. All the quantifications were performed from minimal of ~100 cells and data was represented as either mean + SEM or percent + SEM. p-value represents statistical significance (student t-test) and ns- no significant difference. (TIFF 513 kb)

Additional file 7: Figure S6. SP differentiation assay for evaluation of CSC enrichment in TOV21G and SKOV3. A & B. Quantification of percent SP fraction in demonstrated enrichment of SP fraction in MP (top panel) and SP (middle panel) fractions but not in NSP (lower panel) fractions after TNFα or cisplatin treatment compared their untreated counterpart. Represented percentage SP fraction was obtained from three independent biological replicates. (TIFF 240 kb)

Additional file 8: Supplementary Methods. (DOCX 23 kb)

Abbreviations
CSC: Cancer stem cells; MP: Main population (whole population); NF-κB: Nuclear factor kappa-light-chain-enhancer of activated B cells; NSP: Non side population (Non-CSC population); PIK3CA: Phosphoinositide-3-kinase catalytic unit alpha; SP: Side population (CSC-enriched population); TNFα: Tumor necrosis factor alpha

Acknowledgements
Not applicable

Funding
BT acknowledges CSIR for fellowship. PR acknowledges DST for funding.

Availability of data and materials
All data generated or analysed during this study are included in this published article [and its Additional files].

Authors' contributions
BT performed research; BT and PR designed, analyzed research and wrote the paper. All authors read and approved the final manuscript.

Ethics approval and consent to participate
Not applicable

Consent for publication
Not applicable

Competing interests
The authors declare that they have no competing interests.

Publisher's Note
Springer Nature remains neutral with regard to jurisdictional claims in published maps and institutional affiliations.

References
1. Abdullah LN, Chow EK. Mechanisms of chemoresistance in cancer stem cells. Clin Transl Med. 2013;2(1):3.
2. Kolev VN, Wright QG, Vidal CM, Ring JE, Shapiro IM, Ricono J, Weaver DT, Padval MV, Pachter JA, Xu Q. PI3K/mTOR dual inhibitor VS-5584 preferentially targets cancer stem cells. Cancer Res. 2015;75(2):446–55.
3. Chien J, Kuang R, Landen C, Shridhar V. Platinum-sensitive recurrence in ovarian cancer: the role of tumor microenvironment. Front Oncol. 2013;3:251.
4. Alvero AB, Chen R, Fu HH, Montagna M, Schwartz PE, Rutherford T, Silasi DA, Steffensen KD, Waldstrom M, Visintin I, et al. Molecular phenotyping of human ovarian cancer stem cells unravels the mechanisms for repair and chemoresistance. Cell Cycle. 2009;8(1):158–66.
5. Alison MR, Lin WR, Lim SM, Nicholson LJ. Cancer stem cells: in the line of fire. Cancer Treat Rev. 2012;38(6):589–98.
6. Holohan C, Van Schaeybroeck S, Longley DB, Johnston PG. Cancer drug resistance: an evolving paradigm. Nat Rev Cancer. 2013;13(10):714–26.
7. Wang D, Lippard SJ. Cellular processing of platinum anticancer drugs. Nat Rev Drug Discov. 2005;4(4):307–20.
8. Abedini MR, Qiu Q, Yan X, Tsang BK. Possible role of FLICE-like inhibitory protein (FLIP) in chemoresistant ovarian cancer cells in vitro. Oncogene. 2004;23(42):6997–7004.
9. Campbell KJ, Rocha S, Perkins ND. Active repression of antiapoptotic gene expression by RelA(p65) NF-kappa B. Mol Cell. 2004;13(6):853–65.
10. Almeida LO, Abrahao AC, Rosselli-Murai LK, Giudice FS, Zagni C, Leopoldino AM, Squarize CH, Castilho RM. NFkappaB mediates cisplatin resistance through histone modifications in head and neck squamous cell carcinoma (HNSCC). FEBS Open Bio. 2014;4:96–104.
11. Godwin P, Baird AM, Heavey S, Barr MP, O'Byrne KJ, Gately K. Targeting nuclear factor-kappa B to overcome resistance to chemotherapy. Front Oncol. 2013;3:120.
12. Mayer IA, Arteaga CL. The PI3K/AKT pathway as a target for cancer treatment. Annu Rev Med. 2016;67:11–28.
13. Kok K, Geering B, Vanhaesebroeck B. Regulation of phosphoinositide 3-kinase expression in health and disease. Trends Biochem Sci. 2009;34(3):115–27.
14. Thakur B, Ray P. p53 loses grip on PIK3CA expression leading to enhanced cell survival during platinum resistance. Mol Oncol. 2016;10(8):1283–95.
15. Drewett V, Molina H, Millar A, Muller S, von Hesler F, Shaw PE. DNA-bound transcription factor complexes analysed by mass-spectrometry: binding of novel proteins to the human c-fos SRE and related sequences. Nucleic Acids Res. 2001;29(2):479–87.
16. Gaikwad SM, Gunjal L, Junutula AR, Astanehe A, Gambhir SS, Ray P. Non-invasive imaging of Phosphoinositide-3-Kinase-catalytic-subunit-alpha (PIK3CA) promoter modulation in small animal models. PLoS One. 2013;8(2):e55971.
17. Singh RK, Dhadve A, Sakpal A, De A, Ray P. An active IGF-1R-AKT signaling imparts functional heterogeneity in ovarian CSC population. Sci Rep. 2016;6:36612.
18. Ma L, Zhang G, Miao XB, Deng XB, Wu Y, Liu Y, Jin ZR, Li XQ, Liu QZ, Sun DX, et al. Cancer stem-like cell properties are regulated by EGFR/AKT/beta-catenin signaling and preferentially inhibited by gefitinib in nasopharyngeal carcinoma. FEBS J. 2013;280(9):2027–41.
19. Misuno K, Liu X, Feng S, Hu S. Quantitative proteomic analysis of sphere-forming stem-like oral cancer cells. Stem Cell Res Ther. 2013;4(6):156.

20. Gaikwad SM, Thakur B, Sakpal A, Singh RK, Ray P. Differential activation of NF-kappaB signaling is associated with platinum and taxane resistance in MyD88 deficient epithelial ovarian cancer cells. Int J Biochem Cell Biol. 2015; 61:90–102.

21. Gasch C, Ffrench B, O'Leary JJ, Gallagher MF. Catching moving targets: cancer stem cell hierarchies, therapy-resistance & considerations for clinical intervention. Mol Cancer. 2017;16(1):43.

22. Shibue T, Weinberg RA. EMT, CSCs, and drug resistance: the mechanistic link and clinical implications. Nat Rev Clin Oncol. 2017;14(10):611–29.

23. Matulonis UA, Sood AK, Fallowfield L, Howitt BE, Sehouli J, Karlan BY. Ovarian cancer. Nat Rev Dis Primers. 2016;2:16061.

24. Lee S, Choi EJ, Jin C, Kim DH. Activation of PI3K/Akt pathway by PTEN reduction and PIK3CA mRNA amplification contributes to cisplatin resistance in an ovarian cancer cell line. Gynecol Oncol. 2005;97(1):26–34.

25. Kolasa IK, Rembiszewska A, Felisiak A, Ziolkowska-Seta I, Murawska M, Moes J, Timorek A, Dansonka-Mieszkowska A, Kupryjanczyk J. PIK3CA amplification associates with resistance to chemotherapy in ovarian cancer patients. Cancer Biol Ther. 2009;8(1):21–6.

26. Bertelsen BI, Steine SJ, Sandvei R, Molven A, Laerum OD. Molecular analysis of the PI3K-AKT pathway in uterine cervical neoplasia: frequent PIK3CA amplification and AKT phosphorylation. Int J Cancer. 2006;118(8):1877–83.

27. Torigoe T, Izumi H, Ishiguchi H, Yoshida Y, Tanabe M, Yoshida T, Igarashi T, Niina I, Wakasugi T, Imaizumi T, et al. Cisplatin resistance and transcription factors. Curr Med Chem Anticancer Agents. 2005;5(1):15–27.

28. Bicaku E, Xiong Y, Marchion DC, Chon HS, Stickles XB, Chen N, Judson PL, Hakam A, Gonzalez-Bosquet J, Wenham RM, et al. In vitro analysis of ovarian cancer response to cisplatin, carboplatin, and paclitaxel identifies common pathways that are also associated with overall patient survival. Br J Cancer. 2012;106(12):1967–75.

29. Li L, Liu HC, Wang C, Liu X, Hu FC, Xie N, Lu L, Chen X, Huang HZ. Overexpression of beta-catenin induces Cisplatin resistance in oral Squamous cell carcinoma. Biomed Res Int. 2016;2016:5378567.

30. Oiso S, Ikeda R, Nakamura K, Takeda Y, Akiyama S, Kariyazono H. Involvement of NF-kappaB activation in the cisplatin resistance of human epidermoid carcinoma KCP-4 cells. Oncol Rep. 2012;28(1):27–32.

31. Sun Y, Zheng S, Torossian A, Speirs CK, Schleicher S, Giacalone NJ, Carbone DP, Zhao Z, Lu B. Role of insulin-like growth factor-1 signaling pathway in cisplatin-resistant lung cancer cells. Int J Radiat Oncol Biol Phys. 2012;82(3):e563–72.

32. Staun-Ram E, Goldman S, Shalev E. Ets-2 and p53 mediate cAMP-induced MMP-2 expression, activity and trophoblast invasion. Reprod Biol Endocrinol. 2009;7:135.

33. Yang N, Huang J, Greshock J, Liang S, Barchetti A, Hasegawa K, Kim S, Giannakakis A, Li C, O'Brien-Jenkins A, et al. Transcriptional regulation of PIK3CA oncogene by NF-kappaB in ovarian cancer microenvironment. PLoS One. 2008;3(3):e1758.

34. Viatour P, Merville MP, Bours V, Chariot A. Phosphorylation of NF-kappaB and IkappaB proteins: implications in cancer and inflammation. Trends Biochem Sci. 2005;30(1):43–52.

35. Hoesel B, Schmid JA. The complexity of NF-kappaB signaling in inflammation and cancer. Mol Cancer. 2013;12:86.

36. Zhou A, Scoggin S, Gaynor RB, Williams NS. Identification of NF-kappa B-regulated genes induced by TNFalpha utilizing expression profiling and RNA interference. Oncogene. 2003;22(13):2054–64.

p53 Loses grip on *PIK3CA* expression leading to enhanced cell survival during platinum resistance

CrossMark

Bhushan Thakur, Pritha Ray*

Advanced Centre for Treatment, Research and Education in Cancer (ACTREC), Tata Memorial Centre, Navi Mumbai, Maharashtra, India

ABSTRACT

Tumour suppressor p53, a master transcriptional regulator determines cell fate through preferential activation/repression of a myriad of genes during stress. Till date, activation and preferential binding of p53 on different promoters was reported to be influenced by the nature, strength and duration of stress which mediates its post translational modifications. Cisplatin, a widely used cytotoxic drug represses *PIK3CA* promoter activity and attenuates PI3K/AKT cell survival pathway through p53 activation in sensitive cells. However, very little is understood about the overall mechanism of p53-*PIK3CA* interaction and influence of p53 on the transcriptional status of *PIK3CA* during cisplatin resistance. Here we showed that cisplatin could dynamically alter p53 occupancy between the p53 binding sequences present in *PIK3CA* promoter in ovarian and breast cancer cells. This altered occupancy is dictated by higher acetylation and hyper-phosphorylation at serine 15, serine 20 and serine 46 residues. Interestingly, cisplatin resistant cells when challenged with cisplatin demonstrated abolished *PIK3CA* promoter attenuation, low level of p53 binding, and loss of p53 serine 46 phosphorylation. A phosphorylation deficient S46A mutant failed to repress *PIK3CA* in p53 deficient cells. Elevated expression of Bcl2, *P27* and *cFLIP* indicated a pro-survival state in these resistant cells. Non-invasive real time imaging using two different luciferase reporters showed that cisplatin could simultaneously induce *PIK3CA* attenuation and p53 activation with growth regression in sensitive tumours but not in the resistant tumours where only low level of p53 activation and sustained growth was observed. This is the first report on phosphorylation of p53 serine 46 as a modulator of p53-*PIK3CA* promoter interaction which influences altered binding of p53 at different consensus sequences in the same promoter in response to chemotherapeutic stress. Absence of such modulation in resistant cellular milieu influences cellular homoeostasis in platinum-resistant cells probably due to altered post translational modification of p53.

© 2016 Federation of European Biochemical Societies. Published by Elsevier B.V. All rights reserved.

1.   Introduction

Despite of promising initial response exhibited by cisplatin treatment, recurrence due to acquired resistance is the major obstacle for successful platinum-based therapy in many cancers (Loizzi et al., 2003). Other than the classical mode of action by DNA intercalation, replication stalling followed by apoptosis induction, cisplatin is known to inhibit AKT activation and thereby cell proliferation. Presence of activated Phosphatidylinositol 3-kinase/AKT (PI3K/AKT) signalling is a common characteristics of many cancer cells resistant to drugs like doxorubicin, paclitaxel, 5-flurouracil, etoposide and camptothecin and might be responsible for treatment failure (Knuefermann et al., 2003).

Amplification or activating mutation in *PIK3CA* gene results in AKT activation which in turn promotes cell survival, proliferation and growth signalling and suppresses apoptosis through phosphorylation of multiple targets like Bcl2, Bad and FKHR (apoptosis-related proteins), CREB, TWIST1 and YB1 (transcription factors), ribosomal protein-S6, β-catenin and the mTOR complex components (PRAS40 and mTOR) (Steelman et al., 2011). *PIK3CA* is transcriptionally activated by Foxo3a (Hui et al., 2008), NF-κB (Yang et al., 2008) and YB1 (Astanehe et al., 2009) proteins. Recent study using temperature sensitive SV40 mutant demonstrated that p53 represses *PIK3CA* transcription through direct binding to its promoter in ovarian surface epithelial cells (Astanehe et al., 2008). Subsequently our lab demonstrated that cisplatin and paclitaxel attenuate *PIK3CA* expression through p53 activation and sequential deletion of p53 response elements (RE) in *PIK3CA* promoter abolish this attenuation in ovarian cancer cells and in tumour xenografts as monitored by optical imaging (Gaikwad et al., 2013). Yet, how this p53-*PIK3CA* association is controlled at molecular level remains elusive.

During stress, p53 plays a decisive role in determining cell fate and drives cellular programming either towards growth arrest followed by survival or towards apoptosis. This choice between life and death is dictated by the ability of p53 to preferentially activate or repress particular subsets of genes. Cell cycle arrest governed by p53 is synchronised with transactivation of *P21, GADD45A* and transrepression of *CYCLINB1, STMN1* and *SHP-1* (Rinn and Huarte, 2011). In response to severe stress, apoptosis is favoured through simultaneous activation of *PUMA, BAX, AIP* and repression of *BCL2, SGK1, IGF1R* genes by p53 (Rinn and Huarte, 2011). Such dualistic action of p53 is regulated by extent of protein stabilization, differential affinity towards specific DNA sequences and various post translational modifications (PTMs) (Beckerman and Prives, 2010). Szak et al. (2001) showed delayed transcriptional induction of *PIG3* gene than *P21* and *MDM2* genes is caused by lower affinity of p53 to binding sequences present on *PIG3* promoter compared to sequences present on *P21* and *MDM2* promoters (Szak et al., 2001). Similarly, p53 exhibits higher binding affinity towards *P21, FAS* and *SURVIVIN*, moderate affinity to *CDC25C, CYCLIN G, MDM-2, NOXA* and *PCNA* and weak binding to *MDR1, PUMA* and *Kai 1* genes in H_2O_2 treated MCF7 cells (Ray et al., 2012). Selective transcriptional regulation of p53-target genes are also facilitated by various post translational modifications (phosphorylation and

acetylation) of different residues of p53 (Dai and Gu, 2010). Cisplatin induced DNA damage initiates phosphorylation of p53 at S15 by ATM, ATR and/or DNA-PK kinases followed by phosphorylation at other serine and threonine residues (S20, S33, S37 and T18, T81) (Appella and Anderson, 2001). These modifications escalate binding of p53 to selective target promoters like *P21* and *MDM2* to initiate transcription (Appella and Anderson, 2001). In addition, HIPK2 kinase phosphorylates p53 at S46 which specifically drives transcriptional induction of apoptosis related genes (Di Stefano et al., 2005). Acetylation of p53 is responsible for destabilization of p53-MDM2 interaction and could also lead to abolishment of transactivation of *P21* (Tang et al., 2008). However, acetylation status of p53 following cisplatin treatment is unknown.

Altered p53 PTMs are often associated with tumorigenesis (Dai and Gu, 2010). However, little is understood about reworking of these PTMs and subsequent transcriptional regulation of p53 in drug resistant scenario. Here we showed that cisplatin dynamically altered occupancy of p53 to its response elements (RE) present in *PIK3CA* promoter in ovarian and breast cancer cells. Such alteration was governed by acetylation and hyper phosphorylation of p53 at S15, S20 and S46 residues. Intriguingly, in cisplatin treated resistant cells, p53 exhibited basal level of promoter binding and complete loss of S46 phosphorylation in conjunction with up-regulated Bcl2, *P27* and *cFLIP* expression. A phosphorylation-mimicking mutant S46D (serine to aspartate) but not a phosphorylation-deficient mutant S46A (serine to alanine) was able to attenuate *PIK3CA* expression in p53 null cell line. Real time imaging using two different luciferase reporters showed cisplatin simultaneously induced *PIK3CA* attenuation and p53 activation in sensitive tumours but not in the resistant tumours where only low level of p53 activation was observed. This is the first report on how cisplatin-resistant cells can actively adapt a pro-survival fate by altering influence of p53 upon *PIK3CA* transcription.

2.   Material and methods

2.1.   Reagents and plasmids

Chemicals and antibodies used in this study are enlisted in Supplementary Tables 1 and 2. The *PIK3CA* sensor (*PIK3CA* promoter driving firefly-luciferase-2-tandem-dimer tomato, PIK3CA-fl2-tdt (Gaikwad et al., 2013)), p53-nanoluc fusion reporter (Promega), CMV-fl2-tdt (Gaikwad et al., 2013), modified pcDNA3.1-CMV-β-galactosidase (Clontech) and SN3-p53 were previously reported. To transiently assess the *PIK3CA* promoter activity, the fl2-tdt bifusion reporter was replaced with hrl-egfp (humanised renilla luciferase-enhanced green fluorescence protein). Single site mutant constructs were generated using site directed mutagenesis (SDM) as described earlier (Gaikwad et al., 2013). Deletion constructs containing single site were created using PCR amplification of required sequence and cloning into pcDNA3.1-hrl-egfp vector backbone. All these constructs were confirmed with sequencing.

2.2. Cell line, culture conditions and transfection

A2780, OAW42, SKOV3 and TOV21G cells were cultured in DMEM, MEM and RPMI (GIBCO), respectively, supplemented with 10% foetal bovine serum (HiMedia) and 1% penicillin-streptomycin (GIBCO). MCF7 and ZR-75-1 were gifted by Dr. Abhijit De. A2780-Cisplatin resistant model is previously reported (Gaikwad et al., 2015). Stable clones of *PIK3CA* sensors and p53-nanoluc fusion for A2780 (APN/APN-CisR) were created using G418 and puromycin selection. Similarly, SKOV3 stably expressing *PIK3CA* sensor was generated using G418 selection. The p53 mutant constructs, S46A (serine to alanine) and S46D (serine to aspartate) were generated using the SDM with the oligonucleotides 5′-GCTGGCCCCGGACGA-TATTGAACA-3′ and 5′-CGGGGCCAGCATCAAATCATCCATT-3′ and 5′-GCTGGACCCGGACGATATTGAACA-3′ and 5′-CGGGTCCAGCATCAAATCATCCATT-3′, respectively. The constructs were confirmed by DNA sequencing.

2.3. Promoter activity of PIK3CA promoter constructs

To measure *PIK3CA* promoter activity, cells were transiently transfected with *PIK3CA*-hrl-egfp and CMV-fl2-tdt (9:1 ratio) and fold change (treated/untreated) was calculated as a ratio of renilla luciferase/firefly luciferase (RL/FL) activity. FL and RL activities were measured using luciferase assay system (Promega) and coelenterazine in a Berthold luminometer as described previously (Gaikwad et al., 2013). For promoter activity with transient transfection, cells were treated for 2 h with cisplatin (10 μg/ml) and incubated in fresh media for 22 h. For stable reporter cell lines, cells were incubated for 24 h with cisplatin (10 μg/ml). All transfection experiments were performed in triplicates and repeated at least twice.

2.4. Preparation of proteins extract and immunoblotting

Whole cell extract from cells were collected in SDS buffer (20 mM Tris–HCl, 0.01% SDS, 0.02% β-mercaptoethanol with Sodium vanadate, Sodium fluoride and proteinase inhibitor cocktail). Cytosolic and nuclear extracts preparation and immunoblot were done as described earlier (Gaikwad et al., 2013).

2.5. Quantitative RT-PCR

cDNA was synthesised using 2 μg of total RNA extracted from cells and qRT-PCR was performed using SYBR-Green method. The relative expression levels of mRNAs were calculated by the $2^{-\Delta Ct}$ method with GAPDH as an internal control (Gaikwad et al., 2013). Primer sequences used are listed in Supplementary table 3.

2.6. Site specific chromatin immune precipitation (ChIP)

ChIP was performed as described earlier with few modifications (Garufi and D'Orazi, 2014). Briefly, 3×10^6 cells were cross linked with 0.75% formaldehyde. Nuclei collected in lysis buffer (50 mM HEPES-KOH pH7.5, 140 mM NaCl, 1 mM EDTA pH8, 1% TritonX 100, 0.1% SDS, 0.1% Sodium Deoxycholate, proteinase inhibitor) were sonicated to obtain an average of 200–400 bp chromatin fragments. 25 μg chromatin were

precipitated with p53 specific antibody (SC-126X, Santacruz) and DNA was eluted post reverse-crosslinking. Non-immuno-precipitated chromatin was used as total input control. Further ChIP-DNA were analysed with real time PCR using site specific primers (Supplementary table 3).

2.7. Live cell imaging

For live cell imaging, 5000 dually stable cells were seeded into 96 well black plates. These cells were treated with cisplatin for specified time frame then incubated with fresh media. Bioluminescence of whole plate was first captured using furimazine (1:500 dilution), washed with PBS and followed by imaging with D-luciferine (1 mg/ml). Region of Interests (ROIs) were drawn over each well and quantified by using the Live Image (4.4) software. Bioluminescence signals were recorded as photons/s/cm²/sr.

2.8. Bioluminescence imaging of tumour xenografts

Animal care and euthanasia were performed as per Institutional Animal Ethics Committee approval of ACTREC. SCID mice (n = 5) implanted with 4×10^6 cells stably expressing dual luciferases were allowed to grow tumours till 5–8 mm and divided into control and treated group (injected with 8 mg/kg cisplatin). Bioluminescence imaging of the mice were obtained after intraperitoneal injection of either 100 μl D-luciferin (0.5 mg/mouse) or Furimazine (1 μl in 100 μl/mouse). Image acquisition sequence involved p53-nanoluc imaging followed by *PIK3CA*-fl2 imaging after 1 h interval. ROIs were drawn over the tumours and quantified by using the Live Image (4.4) software. Bioluminescence signals were recorded as photons/s/cm²/sr.

2.9. Statistical analysis

All cell culture and mouse group comparisons were analysed with a Student's *t* test by using Microsoft EXCEL 2013. Values of $P < 0.05$ were considered statistically significant. Error bars represents SD from at least three independent experiments.

3. Result

3.1. Abrogation of PIK3CA promoter response to cisplatin in resistant cells

Reduced transcriptional and translational levels of *PIK3CA* gene were observed in A2780, OAW42 and MCF7 cells (platinum-sensitive) but not in TOV21G, SKOV3 and ZR-75-1 cells (platinum-resistant) (Figure 1A–C) after 24 h of cisplatin treatment. Absence of PARP cleavage and higher IC_{50} doses after cisplatin treatment in TOV21G, SKOV3 and ZR-75-1 cells affirmed their cisplatin-resistant nature when compared to A2780, OAW42 and MCF-7 cells (Figure 1B and Figure S1). Though cisplatin induces p53 stabilization in all cells, only the resistant cells showed high levels of activated AKT. When *PIK3CA* promoter modulation was assessed using a *PIK3CA* promoter sensor (*PIK3CA*-hrl-egfp), the sensitive cells showed 0.4–0.5 fold reduction and the resistant cells showed
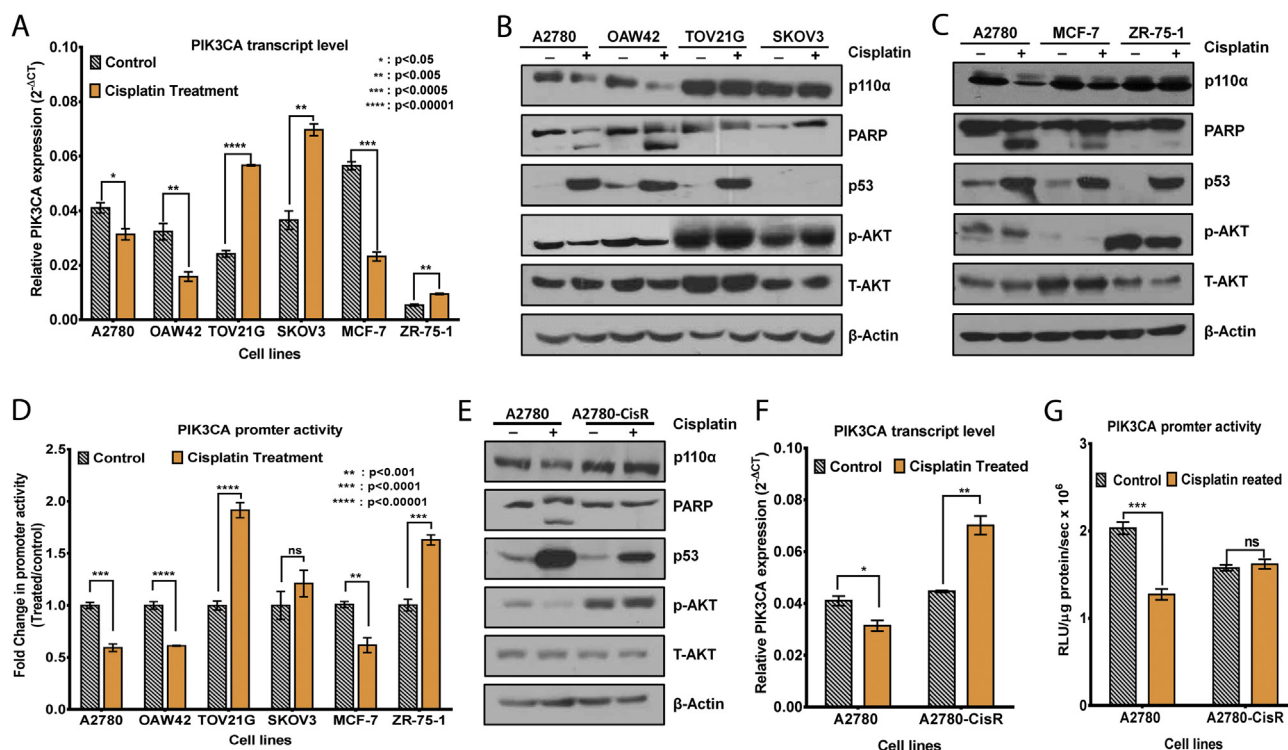
Figure 1 − Cisplatin modulates *PIK3CA* level in ovarian and breast cancer cell lines. A. Reduced expression of *PIK3CA* transcript level was observed in cisplatin treated sensitive cells but not in resistant cells. B−C. Immunoblot analysis showed decreased p110α and pAKT, cleaved PARP, and activated p53 (except SKOV3) in cisplatin treated sensitive (A2780, OAW42 and MCF7) cells which were not evident in resistant (SKOV3, TOV21G and ZR-75-1) cells. D. Attenuated *PIK3CA* promoter activity was observed in cisplatin treated sensitive cells but not in resistant cells (n = 4). E−G A2780 isogenic cisplatin resistant model also demonstrated abolished PIK3CA attenuation at transcript, protein and reporter activity level in resistant cells after treatment.

1.5−2 fold induction in promoter activity (Figure 1D). To nullify the effect of cellular heterogeneity, isogenic cisplatin-resistant model developed in A2780 cells expressing the *PIK3CA*-fl2-tdt fusion reporter was used for further validation (Gaikwad et al., 2013). These A2780-CisR cells exhibited 10-fold higher IC$_{50}$ (5 μg/ml) (Gaikwad et al., 2013), low level of p53 stabilization, higher pAKT level and absence of PARP cleavage (Figure 1E) and loss of *PIK3CA* promoter attenuation in comparison to their sensitive counterpart even at high cisplatin concentration (Figure 1F and G).

Despite of low induction, p53 did localise to nucleus (Figure S2A) and induced *P21* (Figure 2A) and *PUMA* (Figure S2B) in resistant cells. However, fold induction of *P21* expression was lesser in A2780-CisR and other resistant cells than in sensitive cells. p53 Overexpression mimicked the cisplatin induced reduction in *PIK3CA* expression in sensitive cells which was aggravated after cisplatin treatment. In resistant cells, reduced *PIK3CA* expression was mediated by exogenous p53 which did not enhance after treatment. These cells however showed PARP cleavage (Figure 2C and D).

3.2. Sequence specific occupancy of p53 to PIK3CA promoter is altered in resistant cells

We have earlier shown that sequential mutations in the four p53-RE situated in the *PIK3CA* promoter abolish cisplatin

mediated *PIK3CA* promoter attenuation (Gaikwad et al., 2013). To understand the strength of each individual element for p53 binding, single site mutants and deletion mutant constructs containing single p53 response element were transiently transfected in cells with appropriate normalization vectors (Figure 3A). Mutations at site 3 and 4 alleviated (0.5 fold−0.75 fold) cisplatin dependent promoter suppression in A2780 and OAW42 cells while mutations at site 1 and 2 did not show any effect. TOV21G and SKOV3 being cisplatin-resistant cell lines did not exhibit any alteration in promoter activity after being transfected with all four mutant constructs (Figure 3B). These mutations did not alter *PIK3CA* promoter activity in A2780-CisR cells (Figure S3A).

To understand the influence of the adjacent bases for each of the p53 binding sites, we generated deletion mutants of *PIK3CA* promoter containing each p53 binding site flanked by 100−150 bases on either side (Figure 3A). Again, promoter modulation in A2780 and OAW42 was observed only for site 3 and site 4 constructs but not with site 1 or site 2 constructs after transient expression and cisplatin treatment (Figure 3C). When mutations were introduced at site 3 and 4 in these deletion constructs, promoter attenuation was not observed after cisplatin treatment (Figure S3B). The resistant cells (TOV21G and SKOV3) did not exhibit any alteration in promoter activity under similar conditions (Figure S3C). Site specific chromatin immune precipitation (ChIP) with p53
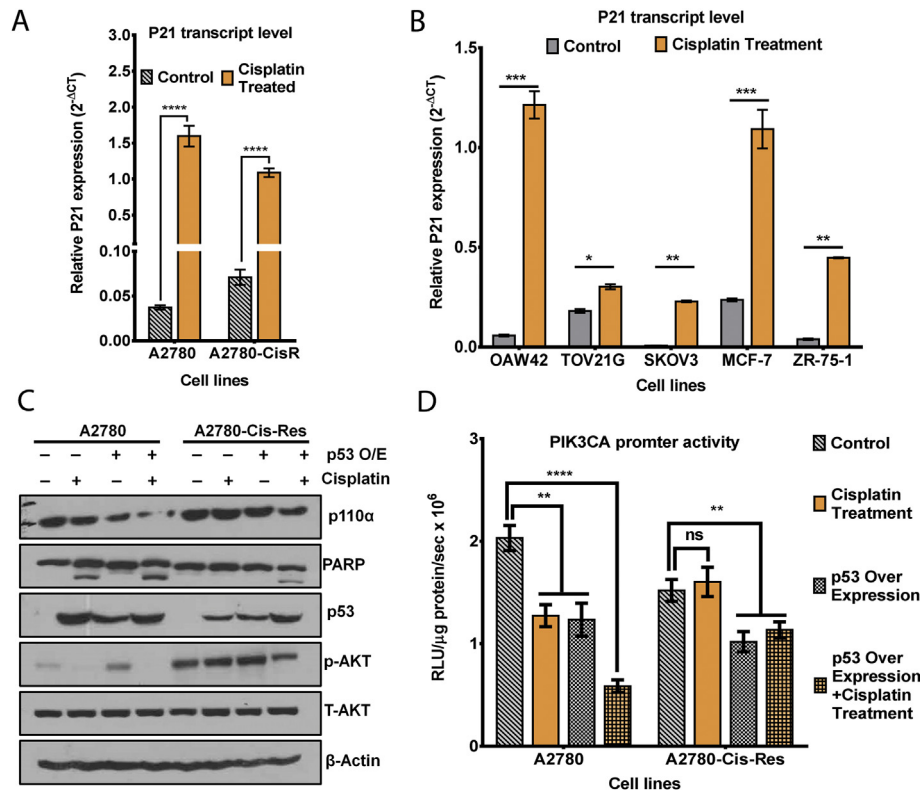
Figure 2 − Cisplatin-resistant cells demonstrate reduced p53 transcriptional activity compare to sensitive cells. A−B. Cisplatin resistant cell lines (A2780-CisR, TOV21G, SKOV3 and ZR-75) showed lower induction in *P21* expression compared to sensitive cells (A2780, OAW42 and MCF7) post cisplatin treatment (n = 3). C. p53 Over-expression alone could reduce p110α, which was aggravated along with cisplatin treatment in both sensitive and resistant cells. However, PARP cleavage and reduced pAKT were found in resistant cells only during cisplatin treatment along with p53 overexpression. D. *PIK3CA* promoter modulation after p53 overexpression without/with cisplatin treatment in sensitive and resistant cells.

antibody in cisplatin treated A2780 cells showed 1.5 and 2.5% of input enrichment of p53 on site 3 and 4, respectively (Figure 3D and E). Interestingly, in untreated condition, p53 was bound maximally to site 1 but the occupancy was reduced (1.2−0.3% of input) by cisplatin. Similarly, in OAW42 and MCF7 cells, cisplatin induced p53 enrichment was observed only for site 3 and 4 (Figure 3F). In A2780-CisR cells, binding of p53 was minimal at site 1, 3 and 4, but significantly enhanced at site 1 (0.13−1.4% of input) after treatment. TOV21G and ZR-75-1 cells showed drug induced enhanced binding only at site 1 (Figure 3G). No binding of p53 was found for Site 2 in any of these cells during pre and post treatment. No promoter fragments were precipitated in bead control samples for all the cells (Figure S3D).

3.3.   Differential dynamics of p53 dependent PIK3CA promoter modulation in resistant tumour xenografts

To understand the dynamics of p53-*PIK3CA* promoter interaction in real time, we created cells expressing sensors for both *PIK3CA* promoter and p53 (termed as APN and APN-CisR, respectively). This p53-nanoluc reporter serves as a promising reporter for quantitative measurement of p53 activity as a function of nanoluc activity. Since overexpression of p53-nanoluc neither modulated *PIK3CA* promoter activity nor showed altered response towards cisplatin (Figure S4), we

utilized these dual stable cell lines for studying p53-*PIK3CA* promoter interaction in real time. Live cell imaging of APN-CisR cells exhibited delayed and reduced level of p53 induction after cisplatin treatment (Figure 4A−C, Figure S5A & B). Time dependent reduction in *PIK3CA* promoter activity after 24 h of cisplatin treatment was observed in sensitive cells but not in resistant cells (Figure 4D−F).

Non-invasive optical imaging of mice bearing tumours of APN origin and treated with cisplatin showed continuous increase in p53-nanoluc activity from day 0 to day 8. However, the resistant tumours (APN-CisR origin) exhibited the increment only after day 4 (Figures 4G and 4H, 4K & 4L) and with much lower level of induction. In contrary, cisplatin treatment of sensitive tumours resulted in slight (not significant) increase in *PIK3CA* promoter activity by day 4 which then decreased significantly by day 8. Such decrease in *PIK3CA* promoter activity was not observed in control resistant tumours and it remained rather stabilised (Figure 4I, J, M & N). These observations also corroborated with tumour volume data where tumour regression was observed only in sensitive tumour xenografts while resistant tumour volume remained stabilised till day 8 (Figure 4O & P, Figure S6A & B).

When measured from tumour lysates, a 8.1 ± 1.4 fold increase in p53 and an 0.38 ± 0.07 fold decrease in *PIK3CA* promoter activity were observed in cisplatin treated sensitive tumours compared to control ones (Figure 4Q). Similarly,
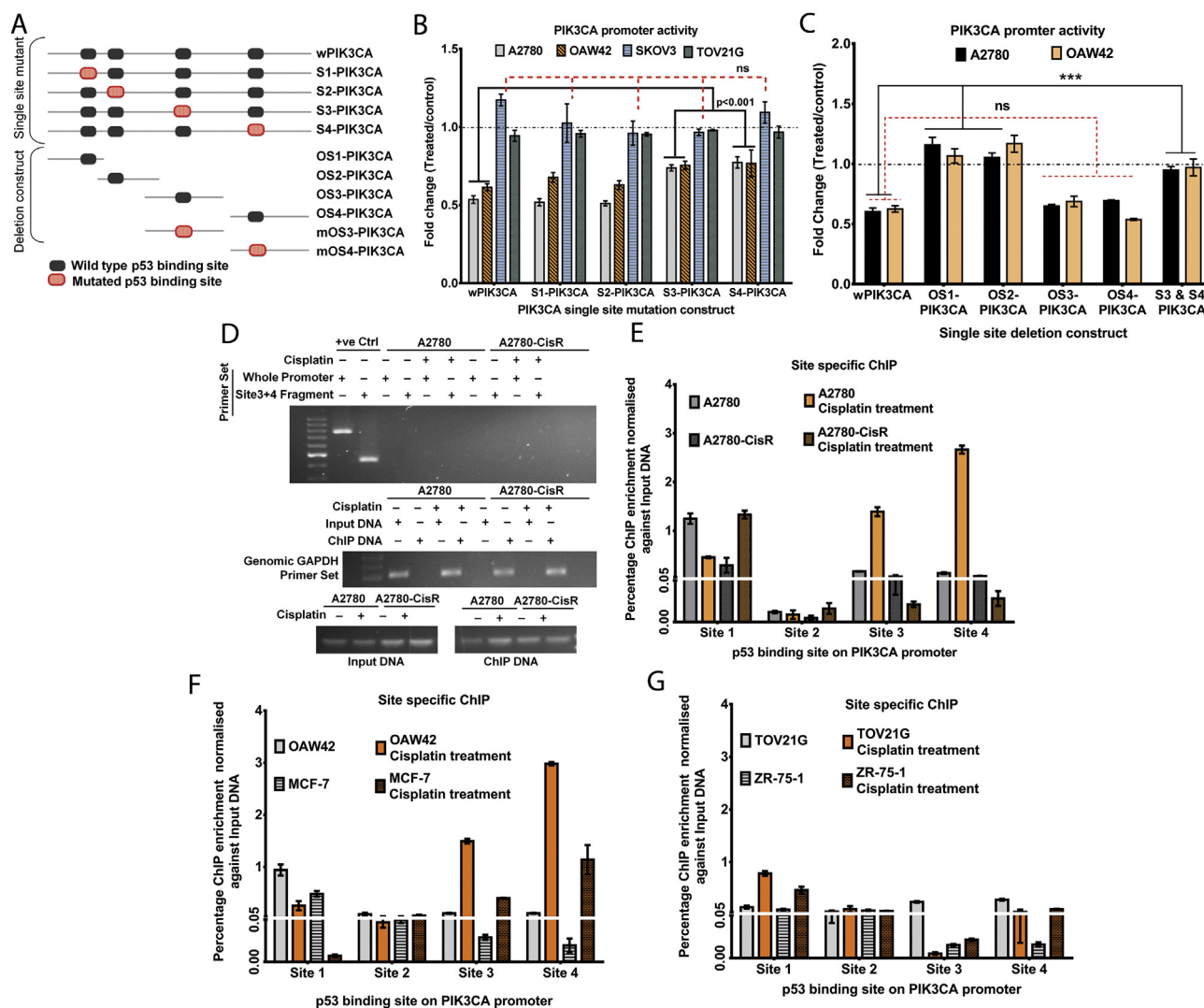
Figure 3 — Site 3 and site 4 p53 response element present on *PIK3CA* promoter are critical for cisplatin induced p53-*PIK3CA* promoter interaction in sensitive cell line. A. Schematics of single site mutant constructs and deletion constructs of *PIK3CA* promoter. S1—S4 are the constructs carrying single site mutation in p53 response elements. OS1—OS4 are the deletion constructs carrying respective binding sites flanked by 50—100 base pairs. mOS3 and mOS4 are deletion constructs carrying mutated site 3 and site 4 sequences and flanked by 50—100 base pairs. B. Mutations in site 3 & 4 but not in site 1 & 2 abolished cisplatin induced *PIK3CA* promoter attenuation in A2780 and OAW42 cells after transient transfection. SKOV3, TOV21G cells being resistant cell lines did not exhibit any change in promoter activity for all four mutations (n = 4). C. Promoter attenuation was observed for the deletion constructs comprised of only site 3 or 4 (with neighbouring sequences) but not for constructs bearing site 1 or 2 after transient transfection in A2780 and OAW42 cells and cisplatin treatment. D. qRT-PCR showed absence of amplification using primers flanking of site 3 (forward) and site 4 (reverse) validating site specificity for ChIP experiment (upper panel). PCR using primer specific for GAPDH used as negative control (middle panel). Presence of 120 bp long specific amplicons post pull down confirmed specificity of site 4 primers for input and ChIP DNA. E—G. Site specific chromatin immune-precipitation experiment for untreated and cisplatin treated A2780, A2780-CisR (E), Oaw42, MCF7 (F), TOV21G and ZR-75-1 (G). Incremented binding of p53 to site 3 and 4 from site 1 was observed in cisplatin treated A2780, OAW42 and MCF7 sensitive cells as determined by ChIP assay followed by real time PCR. In A2780 CisR, TOV21G and ZR-75-1 resistant cells increased binding at site 1 was observed after treatment (values were plotted as % binding of p53 compared to input DNA). Site 2 showed negligible binding at all conditions (n = 3).

treated resistant tumours showed 4.3 ± 2.3 fold higher p53-nanoluc activity but no change in *PIK3CA* promoter activity as compared to untreated ones (Figure 4R). Significant decrease in body weight in treated animals was observed (Figure S6C & D). Immunoblot analysis of these tumour lysates confirmed p53 induction in cisplatin treated groups (Figure S6E).

3.4.   Phospho-serine 46, a critical modulator p53-PIK3CA interaction in resistant cells

Phosphorylation at S15, S20 and S46 residues critically regulate stabilization, DNA-binding and pathway specific gene induction ability of p53. While cisplatin induced higher phospho-S15, phospho-S20, phospho-S46 levels in
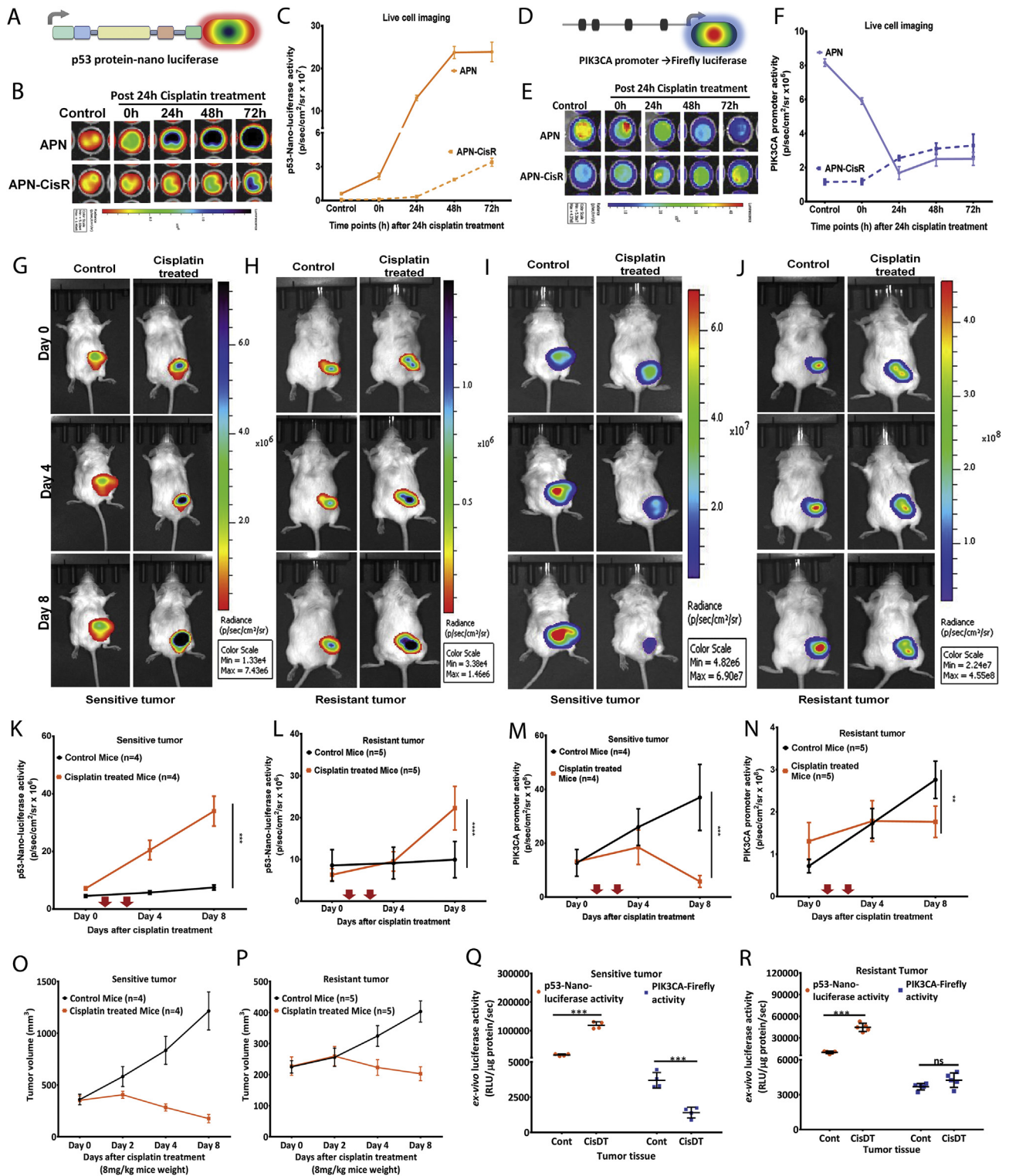
Figure 4 — Resistant tumour xenograft demonstrate abolished *PIK3CA* promoter modulation and delayed p53 activation compared to sensitive tumour xenografts. A. Schematic representation of p53-nanoluc fusion reporter. B & C. Representative live cell images and their quantification for p53-nanoluc fusion reporter and PIK3CA promoter sensor activity in APN and APN-CisR cells. Kinetics monitoring of p53 reporter shows increased stabilization of p53 up to 26 and 10 fold in APN and APN-CisR cells, respectively. D. Schematic representation of *PIK3CA* promoter sensor. E—F. Representative live cell images and their quantification of *PIK3CA* promoter demonstrated *PIK3CA* attenuation only in case of sensitive but not in resistant cells. G—J. Representative Bioluminescence images of p53 protein and *PIK3CA* promoter signature. Nanoluc activity representing p53 profile increased with time in both control and cisplatin treated mice bearing sensitive and resistant tumours (G & H). fl2 Activity denoting *PIK3CA* promoter activity decreased with time in sensitive but remained stable in resistant tumours after cisplatin treatment (I & J). K & L. Graphical representation of quantified signal for *nanoluc* from cisplatin treated sensitive (n = 4) and resistant tumours (n = 5). M—N. Graphical representation of quantified signal for fl2 from cisplatin treated sensitive (n = 4) and resistant tumours (n = 5). O & P. Kinetics of tumour growth for sensitive and resistant tumours pre and post cisplatin treatment. Q & R. *Ex vivo* luciferase activities (nanoluc and fl2) from sensitive and resistant tumours lysates.

A2780 cells, the resistant counterpart showed minimal enhancement in phospho-S15 and phospho-S20 and complete loss of phospho-S46 (Figure 5A). These results were in accordance with other resistant cells where p53 showed minimal level of phospho-S15 and phospho-S20 without any phospho-S46. Higher level of un-acetylated p53, an indication of less DNA binding activity was found in resistant cells compared to the sensitive cells (Figure 5A). Overexpression of phosphorylation-deficient mutant S46A did not suppress PIK3CA promoter activity, whereas expression of wild-type

p53 and phosphorylation-mimicking mutant S46D attenuated PIK3CA promoter activity in p53 null SKOV3 cells stably expressing PIK3CA-fl2-tdt (Figure 5B).

3.5. Delayed kinetics of p53 driven PIK3CA promoter modulation in response to cisplatin

Kinetics of p53 mediated PIK3CA modulation was measured at two hour intervals by live cell imaging (Figure S5C & D). Significant p53 induction was initiated at 6 h by cisplatin which
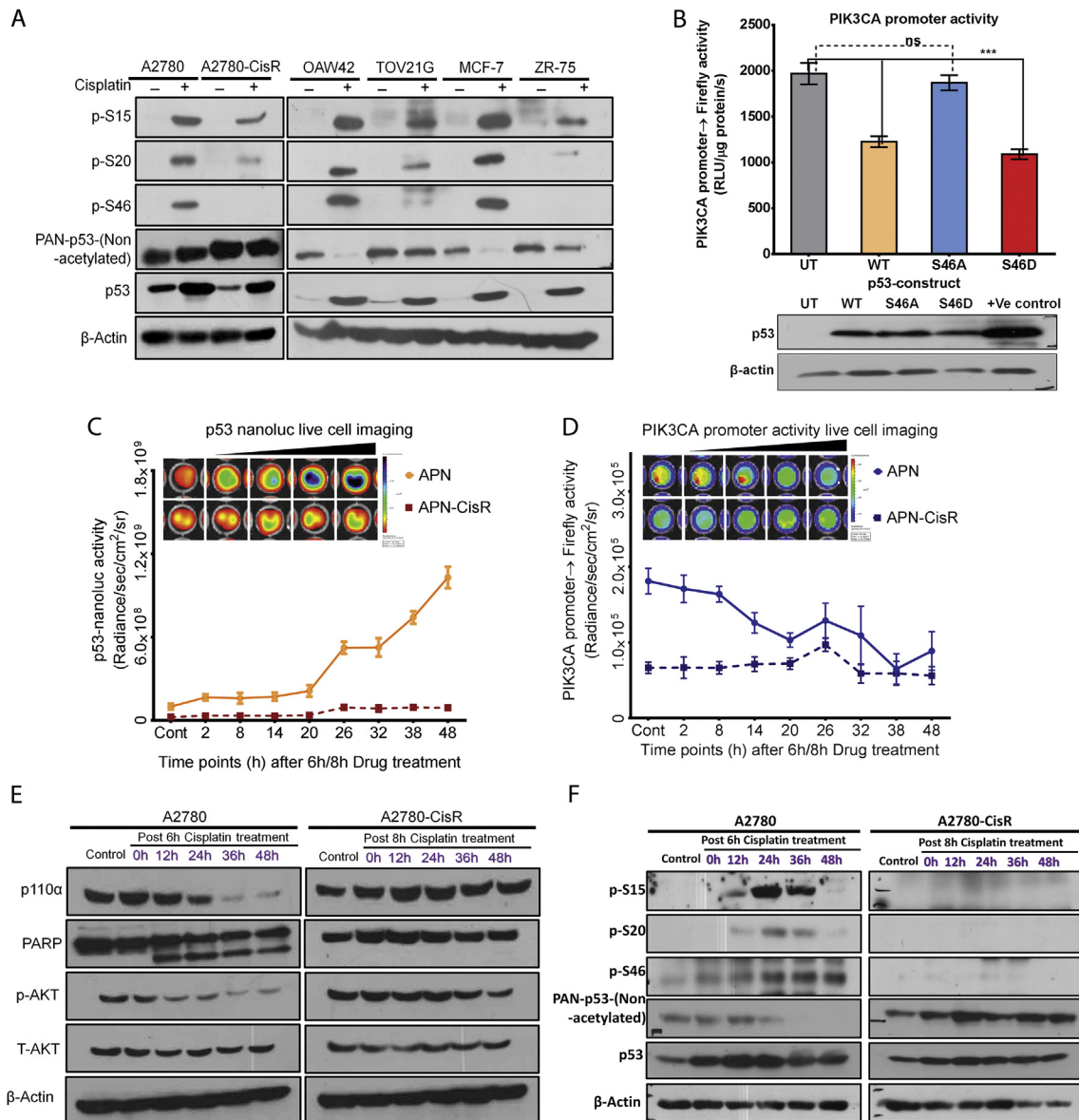
Figure 5 – Post translational modifications (PTM) in p53 are responsible for p53-PIK3CA promoter interaction dynamics. A. Immunoblotting showed differential phosphorylation at S15, S20 and S46 and differential acetylation in sensitive and resistant cells post cisplatin treatment. B. Wild type p53 and p53 S46D over-expression but not p53 S46A reduces PIK3CA promoter activity in SKOV3 cell line (UT-untreated, WT-wild type p53). Cisplatin treated A2780 were used as positive control. Lower panel depicts immunoblot showing expression of each of the p53 mutant construct in SKOV3 cell line. C–D. Kinetics of p53 induction (B) and PIK3CA promoter modulation (C) from sensitive and resistant cells were monitored by live cell imaging post 6 h and 8 h of cisplatin treatment, respectively. E. Kinetics of cisplatin treatments were studied on protein levels of PARP, p110α and pAKT by immunoblotting. F. Differential induction in PTMs as stated in A were measured from sensitive and resistant cells after 6 h and 8 h treatment indicated complete loss of pS46 and delayed and lower induction of phospho-S15, phospho-S20 and acetylation in p53.

reached to ten-fold high in sensitive cells at 48 h. In contrast, resistant cells took 8 h to induce noticeable p53 activation which then increased at low level (3.7-fold) till 48 h (Figure 5C). Attenuation in *PIK3CA* promoter activity started from 10 to 12 h post cisplatin treatment in sensitive cells and 50% decrease was evident by 18 h. Resistant cells did not show *PIK3CA* promoter attenuation till 48 h (Figure 5D). p110α Level followed this trend. PARP cleavage was evident around 12 and 48 h, respectively in sensitive and resistant cells (Figure 5E).

When cisplatin induced PTM kinetics of p53 were assessed, sensitive cells exhibited peak phosphorylation at S15 and S20 residues at 12 and 24 h, respectively which then gradually declined. S46 phosphorylation peaked at 24 h and remained stable till 48 h. Intriguingly, resistant cells exhibited phosphorylation at S15 and pS20 at much lower level and at later time points without any detectable phospho-S46 after treatment. Similarly acetylation status of p53 remained higher in sensitive cells than resistant cells (Figure 5F).

3.6. Effect of altered p53-PIK3CA interaction on downstream pathways in resistant cells

To assess the consequence of this altered p53-*PIK3CA* interaction, we monitored expression of specific downstream targets such as phospho-S6-ribosomal protein (protein synthesis), *P21*, *P27*, *CYCLIN-D1*, *cMYC*, β-catenin (proliferation), *BAX* (pro-apoptotic) and *cFLIP*, Bcl2 (anti-apoptotic) after cisplatin treatment. Both treated sensitive and resistant cells showed decreased S6-ribosomal protein phosphorylation indicating slower translation rate. Increased Bcl2 and *cFLIP*, unaltered *BAX* (Figure 6A−C), and loss of PARP cleavage (Figure 1E) in cisplatin treated resistant cells indicated suppression of apoptosis. Proliferation was severely affected in sensitive cells as cisplatin treatment decreased both *CYCLIN-D1* and *cMYC* transcription but not in resistant cells which could be due to unaltered β-catenin level (Figure 6D and E). Interestingly *P27*, a regulator of G1 phase, showed 5-fold higher expression in untreated resistant cells and 9-fold higher expression after cisplatin treatment than sensitive cells (Figure 6F).

4. Discussion

Perturbation in the PI3K/AKT signal transduction pathway, a critical regulator of cell proliferation, differentiation and apoptosis underlies many pathological diseases including cardiac, neurological, inflammation and cancer (Franke, 2008). Activated PI3K/AKT signalling endows with survival advantage and contributes to drug resistance in ovarian, breast
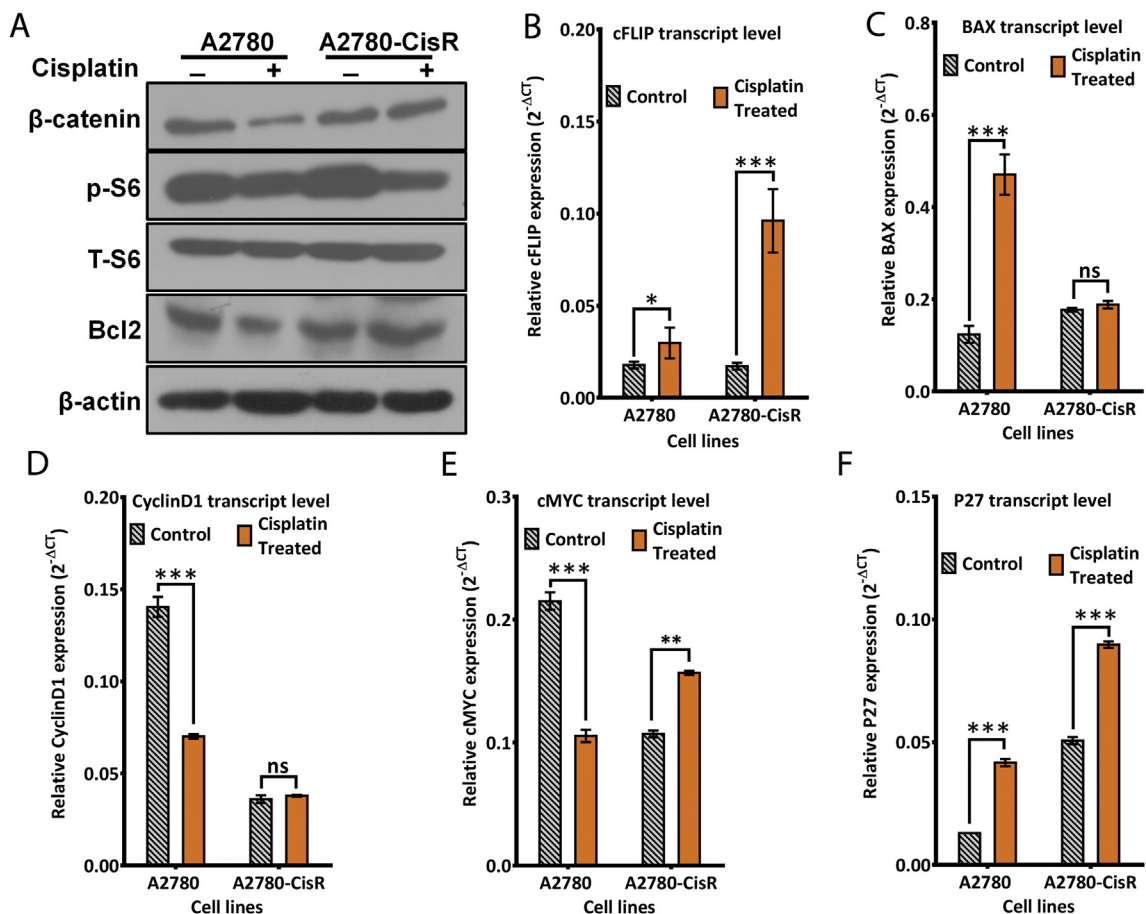
Figure 6 − Unaltered PI3K/AKT pathway aids resistant cell survival against cisplatin treatment. **A.** Immunoblot analysis showed differential activation/repression of β-catenin, pS6, Bcl2 by cisplatin in sensitive and resistant cells. **B−F.** Real time PCR analysis showed differential activation/repression of *cFLIP*, *BAX*, *CYCLIN-D1*, *cMYC* and *P27* expression after cisplatin treatment in sensitive and resistant cells (n = 3).

and gastric cancers (Cheaib et al., 2015). While NF-κβ and FOXO3a induce *PIK3CA* expression, p53 acts as a major repressor thereby enforcing an initial check on cell proliferation during stress (Gaikwad et al., 2013). p53 Attenuates *PIK3CA* expression in normal epithelial ovarian cells (Astanehe et al., 2008), ovarian cancer cells (Gaikwad et al., 2013) and upper aero-digestive tract carcinoma cells (Singh et al., 2002). However, no information is available on modulation of *PIK3CA* expression in cisplatin-resistant cells. Using various ovarian and breast cancer cells of varied p53 (wild/null) and platinum-sensitivity statuses, we showed that p53 binding in *PIK3CA* promoter was drastically altered after cisplatin treatment. This alteration was associated with increased phospho-S15, phospho-S20, phospho-S46 and hyper-acetylation of p53 in sensitive cells and complete loss of phospho-S46, reduced phospho-S15 and phospho-S20 and hypo-acetylation in resistant cells. Altered expression of several essential genes involved in apoptosis, cell cycle and proliferation were evident. Intriguingly, using an isogenic cisplatin-resistant cell line, we found that the resistant cells not only exhibited altered binding of p53 but also a delayed kinetics of activation (at a much lower level) and both these events were not sufficient enough to attenuate *PIK3CA* promoter activity. Serine 46 phosphorylation acts as a prime modulator for this altered/reduced binding of p53 to *PIK3CA* promoter as observed by the inability of a phosphorylation-deficient mutant S46A to attenuate *PIK3CA* expression in p53 null background. Using a dual reporter strategy, we for the first time showed that activation of p53 is associated with decreased *PIK3CA* expression after cisplatin treatment from tumour xenografts bearing mice by real time optical imaging. The resistant tumour xenografts showed delayed p53 activation without any change in *PIK3CA* expression. Thus our data suggest that cisplatin-resistant cells actively adapt a pro-survival fate through reduced post-translational modification and altered binding of p53 to *PIK3CA* promoter.

Inhibition of PI3K/AKT pathway often sensitizes the cancer cells to cisplatin (Cheaib et al., 2015). However, cisplatin could up-regulate *PIK3CA* transcription in cisplatin-resistant OVCAR3 cells but not in control cells (Lee et al., 2005) indicating a differential regulation of *PIK3CA* promoter in chemoresistantance. We found that while platinum-sensitive ovarian and breast cancer cells (A2780, OAW42, MCF7) exhibited decreased p110α level, the naturally resistant TOV21G, SKOV3 and ZR-75-1 cells showed increased expression of *PIK3CA* under cisplatin treatment. Interestingly, SKOV3 cells do not possess functional p53. All these resistant cells exhibited higher phospho-AKT and absence of PARP cleavage.

To elucidate the mechanism behind differential expression of *PIK3CA* gene between the sensitive and resistant cells, we used a 900 bp long promoter fragment (containing four p53 response elements) driving firefly luciferase to mimic *PIK3CA* expression (Astanehe et al., 2008). In agreement with the observed transcriptional modulation, *PIK3CA* promoter activity was attenuated in cisplatin-sensitive but not in cisplatin-resistant cells. Lower *P21* activation was found in cisplatin treated intrinsically resistant cells. Since cells of different origin contain heterogeneous cellular milieu with various activated transcription factors and could differentially influence promoter activity, we utilized an isogenic cisplatin-resistant

model developed in A2780 cells (Gaikwad et al., 2015). Since the panel of cell lines utilized in this study showed varied sensitivity to cisplatin, an uniform concentration of maximum tolerable dose (10 μg/ml for 24 h) as determined by viable cell counting (data not shown) was used. Reduced p53 induction and unaltered *PIK3CA* promoter activity were characteristics of A2780-CisR cells after cisplatin treatment. Upon p53 overexpression, these resistant cells exhibited *PIK3CA* promoter attenuation confirming that the abolished *PIK3CA* promoter modulation is due to loss of p53 ordinance.

Under stress, p53 drives cellular fate towards growth arrest or apoptosis through differential regulation of various target genes (di Pietro et al., 2012; Kracikova et al., 2013). To understand why *PIK3CA* experiences differential regulation by p53 between sensitive and resistant stages, influence of individual p53-RE was critically analysed. Mutations at site 3 and 4 relieved cisplatin dependent promoter attenuation in sensitive (A2780 and OAW42) cells but not in A2780-CisR cells. ChIP assay showed that p53 remained bound to site 1 in unstressed sensitive cells but shifted to site 3 and 4 following cisplatin treatment. Till date only Hepatitis virus-B infection has been found to induce similar altered binding of p53 at different p53-RE in *p53AIP* promoter. This altered site selection was shown to be influenced by acetylation at lysine320 in p53 protein (Chan et al., 2013). In contrary to cisplatin induced altered occupancy of p53 in sensitive cells, resistant cells exhibited low binding of p53 at site 1, 3 and 4 which enhanced only at site 1 after treatment indicating the importance of site 3 and 4 for p53-*PIK3CA* interaction. Site 2, though was predicted as a p53-RE did not show any occupancy at any condition (Astanehe et al., 2008). Similar shift in p53 occupancy to selective binding sites were observed in OAW42 and MCF7 (sensitive) and TOV21G and ZR-75-1 (resistant) cells at pre and post cisplatin treatment. p53 Displays preferential binding to specific gene promoters under different stresses (UV vs IR), at different concentrations (1.75 μg/ml vs 5 μg/ml of cisplatin) and at different time points (24 h vs 48 h) (Di Stefano et al., 2005). Szak et al. (2001) reported for low affinity and delayed binding of p53 on *PIG3* promoter compared to *P21* and *MDM2* promoters. However, our report is possibly the first to demonstrate altered and preferential binding of p53 to different sequences present in the same promoter during stress in both sensitive and resistant cells. This differential binding could be due to differential affinity of p53 to its RE and might be dictated by PTMs of p53. As expected, high phospho-S15, phospho-S20 and phospho-S46 were observed in cisplatin treated sensitive cells which were either low or absent in resistant cells. Phospho-S15 is considered to be an initiating and nucleating event for p53 activation. Phospho-S20 in combination with phospho-S15 and phospho-T18 uncouples p53/MDM2 interaction and stabilise p53 (Appella and Anderson, 2001). Thus reduced phospho-S15 and phospho-S20 after treatment indicated lower levels of activation and stabilization of p53 in resistant cells. Phospho-S46 (under cytotoxic stress) induces a subtle change in p53 conformation and a stronger affinity for apoptosis-related genes (*BAX*, *PIG3*, and *p53AIP1*) (Di Stefano et al., 2005; Rinn and Huarte, 2011; Szak et al., 2001). We hypothesize that phospho-S46 drives preferential recruitment of p53 to site 3 and 4 on *PIK3CA* promoter after cisplatin treatment, attenuates PI3K/AKT

signalling and cellular proliferation and thereby compels the cells towards apoptosis. Absence of phospho-S46 in resistant cells hinders recruitment of p53 to site 3 and 4 favouring increased *PIK3CA* transcription. The critical role of phospho-S46 in controlling p53 binding was further confirmed using two p53 mutant constructs, S46A and S46D as described earlier (Mayo et al., 2005). In accordance with our data, the phosphorylation-deficient S46A mutant did not show any repressive effect on *PIK3CA* promoter in p53 null cells. In contrast a phosphorylation-mimicking mutant S46D showed similar level of *PIK3CA* attenuation. Simultaneous augmented expression of Bcl2 and *cFLIP*, absence of PARP cleavage and decreased expression of *BAX* also pointed towards an apoptosis resistant phase in these cells. Accumulation of un-acetylated p53 indicated lower level of transcriptionally active p53 in resistant cells and explained relatively lower *P21* expression (Di Stefano et al., 2005).

Duration of stress is a critical determinant for maximal p53 induction. Using a dual reporter strategy and live cell imaging, delayed initiation (6 h vs 8 h) and 4-fold less induced p53 were found in resistant cells. Simultaneously *PIK3CA* expression that remained stable in resistant cells, showed sharp decline by 14 h which continued till 48 h in sensitive cells. To avoid loss of signal due to cell death for incubating cells for 48 h at 10 μg/ml of Cisplatin, a lower dose (5 μg/ml) was used for time kinetics analyses. Interestingly, phospho-S46 became evident from this time (14 h) which persisted till 48 h in cisplatin treated sensitive cells further proving that phospho-S46 is a critical event in p53 mediated *PIK3CA* attenuation.

The altered dynamics of p53, *PIK3CA* modulation in resistant cells were also evident in tumour xenografts of live mice in real time. This is the first report of non-invasive imaging p53 activation by cisplatin where significant induction in p53-nanoluc activity was observed on 1st day after treatment which increased upto 7-fold on 5th day in sensitive tumours. In contrary, slight reduction in *PIK3CA* promoter activity observed on 1st day and 4-fold attenuation was found on 5th day. Reduction in tumour volume matched with *PIK3CA* expression indicating massive apoptosis in these tumours. Though cisplatin showed an immediate effect on *PIK3CA* promoter in cell culture (by 14−16 h), the effect was less prominent *in vivo* due to altered metabolism and pharmacokinetics. In cisplatin treated resistant tumours, p53 induction was negligible by Day 1 and attained 3-fold
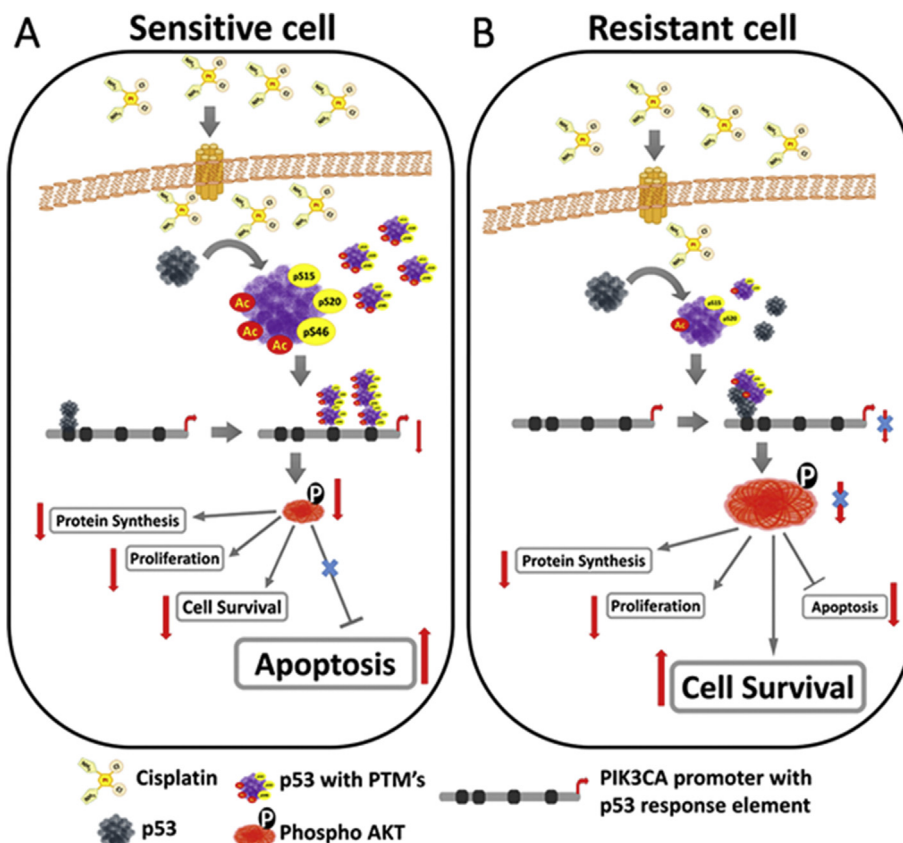

Figure 7 — Proposed model of p53 mediated *PIK3CA* regulation during stress. A. In sensitive cell, cisplatin activates p53 via PTM's (acetylation, phospho-S15, phospho-S20 and phospho-S46) which alters p53 binding preference from binding site 1 to site 3 and 4 present on *PIK3CA* promoter. Altered p53-*PIK3CA* promoter interaction leads to *PIK3CA* attenuation and subsequently reduced *AKT* phosphorylation. Under these circumstances, cells experience reduced protein synthesis, survival and proliferation and up-regulation of apoptotic machinery. B. In contrary, resistant cells in response to cisplatin acquire a 'sensitive like' state in terms of p53-*PIK3CA* promoter interaction (occupancy only at site 1) and show reduced S15, S20 phosphorylation and acetylation with complete loss of pS46. Such p53-*PIK3CA* promoter interaction is insufficient to decrease *PIK3CA* transcript level hence AKT phosphorylation remain unchanged. Under such condition, cells overcome the damage caused by cisplatin via active PI3K/AKT pathway and adapt an arrested state by down regulating apoptotic machinery.

higher induction on 5th day. *PIK3CA* promoter activity and tumour volume remained stable over five days for this group. It seemed that though cisplatin was unable to promote apoptosis in resistant tumours, it could induce a growth arrest which was supported by enhanced *P27* and decreased *CYCLIN-D1* expression.

Phosphorylation of S46 residue in p53 is an obligatory event in RITA induced apoptosis (Ma et al., 2012) which also requires simultaneous inhibition of *PIK3CA* and *IGF1R* oncogenes and activation of pro-apoptotic genes (Grinkevich et al., 2009). We therefore hypothesize that genotoxic drug induced stress leads to repression of PI3K/AKT signalling through site specific recruitment of activated p53 in *PIK3CA* promoter (Figure 7). This recruitment is driven by S46 phosphorylation which is lost in cisplatin-resistant cells. Our study thus indicates phospho-S46 as a modulator of p53 binding to *PIK3CA*, an important cell survival regulator. Detail mechanism of this modulation and how it influences site specificity requires further investigation. Lower accumulation of cisplatin in drug resistant cells favours a quiescent, growth arrested state which is mediated by sub optimal binding of p53 to *PIK3CA* promoter. Increased expression of endogenous *PIK3CA* gene in resistant cells indicates another level of regulatory network involving sequences upstream to 900 bp of transcription start point. The unique *in vivo* model of simultaneous monitoring of p53 activation and *PIK3CA* promoter modulation in real time developed in this study can be extended to other important p53 targets and in drug discovery research.

5.   Conclusion

In conclusion, we report a novel mechanism of cisplatin induced site specific alteration of p53 occupancy on *PIK3CA* promoter resulting in attenuated *PIK3CA* expression in chemo-sensitive cells. This differential binding of p53 on site 3 and site 4 on *PIK3CA* promoter is dictated by serine 46 phosphorylation of p53. In chemo-resistant cells, cisplatin fails to attenuate *PIK3CA* expression as p53 losses ability to interact with *PIK3CA* promoter at site 3 and site 4. Hypo-phosphorylation at Serine 15 and 20 and complete loss of Serine 46 phosphorylation are responsible for this discrepant p53-*PIK3CA* promoter interaction in resistant cells. Real time imaging reveals that these chemo resistant tumours bear lower level of p53 activation without any changes in *PIK3CA* expression and a low proliferative and stable growth after cisplatin treatment. Our data thus provides a new mechanistic insight of p53 mediated transcriptional regulation of *PIK3CA* gene in platinum-resistant cells.

Author contributions

B.T. performed research; B.T. and P.R. designed, analysed research and wrote the paper.

Conflict of interest

The authors declare no conflict of interest.

Appendix A.
Supplementary data

Supplementary data related to this article can be found at http://dx.doi.org/10.1016/j.molonc.2016.06.006.

R E F E R E N C E S

Appella, E., Anderson, C.W., 2001. Post-translational modifications and activation of p53 by genotoxic stresses. Eur. J. Biochem./FEBS 268, 2764–2772.

Astanehe, A., Arenillas, D., Wasserman, W.W., Leung, P.C., Dunn, S.E., Davies, B.R., Mills, G.B., Auersperg, N., 2008. Mechanisms underlying p53 regulation of PIK3CA transcription in ovarian surface epithelium and in ovarian cancer. J. Cell Sci. 121, 664–674.

Astanehe, A., Finkbeiner, M.R., Hojabrpour, P., To, K., Fotovati, A., Shadeo, A., Stratford, A.L., Lam, W.L., Berquin, I.M., Duronio, V., Dunn, S.E., 2009. The transcriptional induction of PIK3CA in tumor cells is dependent on the oncoprotein Y-box binding protein-1. Oncogene 28, 2406–2418.

Beckerman, R., Prives, C., 2010. Transcriptional regulation by p53. Cold Spring Harbor Perspect. Biol. 2, a000935.

Chan, C., Wang, Y., Chow, P.K., Chung, A.Y., Ooi, L.L., Lee, C.G., 2013. Altered binding site selection of p53 transcription cassettes by hepatitis B virus X protein. Mol. Cell. Biol. 33, 485–497.

Cheaib, B., Auguste, A., Leary, A., 2015. The PI3K/Akt/mTOR pathway in ovarian cancer: therapeutic opportunities and challenges. Chin. J. Cancer 34, 4–16.

Dai, C., Gu, W., 2010. p53 post-translational modification: deregulated in tumorigenesis. Trends Mol. Med. 16, 528–536.

di Pietro, A., Koster, R., Boersma-van Eck, W., Dam, W.A., Mulder, N.H., Gietema, J.A., de Vries, E.G., de Jong, S., 2012. Pro- and anti-apoptotic effects of p53 in cisplatin-treated human testicular cancer are cell context-dependent. Cell Cycle 11, 4552–4562.

Di Stefano, V., Soddu, S., Sacchi, A., D'Orazi, G., 2005. HIPK2 contributes to PCAF-mediated p53 acetylation and selective transactivation of p21Waf1 after nonapoptotic DNA damage. Oncogene 24, 5431–5442.

Franke, T.F., 2008. PI3K/Akt: getting it right matters. Oncogene 27, 6473–6488.

Gaikwad, S.M., Gunjal, L., Junutula, A.R., Astanehe, A., Gambhir, S.S., Ray, P., 2013. Non-invasive imaging of phosphoinositide-3-kinase-catalytic-subunit-alpha (PIK3CA) promoter modulation in small animal models. PLoS One 8, e55971.

Gaikwad, S.M., Thakur, B., Sakpal, A., Singh, R.K., Ray, P., 2015. Differential activation of NF-kappaB signaling is associated with platinum and taxane resistance in MyD88 deficient epithelial ovarian cancer cells. Int. J. Biochem. Cell Biol. 61, 90–102.

Garufi, A., D'Orazi, G., 2014. High glucose dephosphorylates serine 46 and inhibits p53 apoptotic activity. J. Exp. Clin Cancer Res. 33, 79.

Grinkevich, V.V., Nikulenkov, F., Shi, Y., Enge, M., Bao, W., Maljukova, A., Gluch, A., Kel, A., Sangfelt, O., Selivanova, G., 2009. Ablation of key oncogenic pathways by RITA-reactivated p53 is required for efficient apoptosis. Cancer Cell 15, 441–453.

Hui, R.C., Gomes, A.R., Constantinidou, D., Costa, J.R., Karadedou, C.T., Fernandez de Mattos, S., Wymann, M.P., Brosens, J.J., Schulze, A., Lam, E.W., 2008. The forkhead transcription factor FOXO3a increases phosphoinositide-3 kinase/Akt activity in drug-resistant leukemic cells through induction of PIK3CA expression. Mol. Cell. Biol. 28, 5886–5898.

Knuefermann, C., Lu, Y., Liu, B., Jin, W., Liang, K., Wu, L., Schmidt, M., Mills, G.B., Mendelsohn, J., Fan, Z., 2003. HER2/PI-3K/Akt activation leads to a multidrug resistance in human breast adenocarcinoma cells. Oncogene 22, 3205–3212.

Kracikova, M., Akiri, G., George, A., Sachidanandam, R., Aaronson, S.A., 2013. A threshold mechanism mediates p53 cell fate decision between growth arrest and apoptosis. Cell Death Differ. 20, 576–588.

Lee, S., Choi, E.J., Jin, C., Kim, D.H., 2005. Activation of PI3K/Akt pathway by PTEN reduction and PIK3CA mRNA amplification contributes to cisplatin resistance in an ovarian cancer cell line. Gynecol. Oncol. 97, 26–34.

Loizzi, V., Chan, J.K., Osann, K., Cappuccini, F., DiSaia, P.J., Berman, M.L., 2003. Survival outcomes in patients with recurrent ovarian cancer who were treated with chemoresistance assay-guided chemotherapy. Am. J. Obstet Gynecol. 189, 1301–1307.

Ma, T., Yamada, S., Ichwan, S.J., Iseki, S., Ohtani, K., Otsu, M., Ikeda, M.A., 2012. Inability of p53-reactivating compounds Nutlin-3 and RITA to overcome p53 resistance in tumor cells deficient in p53Ser46 phosphorylation. Biochem. Biophys. Res. Commun. 417, 931–937.

Mayo, L.D., Seo, Y.R., Jackson, M.W., Smith, M.L., Rivera Guzman, J., Korgaonkar, C.K., Donner, D.B., 2005. Phosphorylation of human p53 at serine 46 determines promoter selection and whether apoptosis is attenuated or amplified. J. Biol. Chem. 280, 25953–25959.

Ray, D., Murphy, K.R., Gal, S., 2012. The DNA binding and accumulation of p53 from breast cancer cell lines and the link with serine 15 phosphorylation. Cancer Biol. Ther. 13, 848–857.

Rinn, J.L., Huarte, M., 2011. To repress or not to repress: this is the guardian's question. Trends Cell Biol. 21, 344–353.

Singh, B., Reddy, P.G., Goberdhan, A., Walsh, C., Dao, S., Ngai, I., Chou, T.C., O-Charoenrat, P., Levine, A.J., Rao, P.H., Stoffel, A., 2002. p53 regulates cell survival by inhibiting PIK3CA in squamous cell carcinomas. Genes Dev. 16, 984–993.

Steelman, L.S., Chappell, W.H., Abrams, S.L., Kempf, R.C., Long, J., Laidler, P., Mijatovic, S., Maksimovic-Ivanic, D., Stivala, F., Mazzarino, M.C., Donia, M., Fagone, P., Malaponte, G., Nicoletti, F., Libra, M., Milella, M., Tafuri, A., Bonati, A., Basecke, J., Cocco, L., Evangelisti, C., Martelli, A.M., Montalto, G., Cervello, M., McCubrey, J.A., 2011. Roles of the Raf/MEK/ERK and PI3K/PTEN/Akt/mTOR pathways in controlling growth and sensitivity to therapy-implications for cancer and aging. Aging 3, 192–222.

Szak, S.T., Mays, D., Pietenpol, J.A., 2001. Kinetics of p53 binding to promoter sites in vivo. Mol. Cell. Biol. 21, 3375–3386.

Tang, Y., Zhao, W., Chen, Y., Zhao, Y., Gu, W., 2008. Acetylation is indispensable for p53 activation. Cell 133, 612–626.

Yang, N., Huang, J., Greshock, J., Liang, S., Barchetti, A., Hasegawa, K., Kim, S., Giannakakis, A., Li, C., O'Brien-Jenkins, A., Katsaros, D., Butzow, R., Coukos, G., Zhang, L., 2008. Transcriptional regulation of PIK3CA oncogene by NF-kappaB in ovarian cancer microenvironment. PLoS One 3, e1758.

CrossMark

Tumor suppressor protein p53 exerts negative transcriptional regulation on human sodium iodide symporter gene expression in breast cancer

Madhura G. Kelkar[1,3] · **Bhushan Thakur**[2,3] · **Abhishek Derle**[1] · **Sushmita Chatterjee**[1] ·
Pritha Ray[2,3] · **Abhijit De**[1,3]

Abstract

Purpose Aberrant expression of human sodium iodide symporter (NIS) in breast cancer (BC) is well documented but the transcription factors (TF) regulating its aberrant expression is poorly known. We identify the presence of three p53 binding sites on the human NIS promoter sequence by conducting genome-wide TF analysis, and further investigate their regulatory role.

Methods The differences in transcription and translation were measured by real-time PCR, luciferase reporter assay, site-directed mutagenesis, in vivo optical imaging, and chromatin immunoprecipitation. The relation of NIS and

✉ Abhijit De
ade@actrec.gov.in

Madhura G. Kelkar
madhuragk@yahoo.com

Bhushan Thakur
bhushan0331@gmail.com

Abhishek Derle
derle.abhishek90@gmail.com

Sushmita Chatterjee
sushmita.microbio@gmail.com

Pritha Ray
pray@actrec.gov.in

1 Molecular Functional Imaging Lab, Tata Memorial Centre, ACTREC, Sector 22, Kharghar, Navi Mumbai 410210, India

2 Imaging Cell Signaling and Therapeutics Lab, Tata Memorial Centre, ACTREC, Navi Mumbai, India

3 Homi Bhabha National Institute, Anushakti Nagar, Mumbai, India

p53 in clinical samples was judged by TCGA data analysis and immunohistochemistry.

Results Overexpression of wild-type p53 as a transgene or pharmacological activation by doxorubicin drug treatment shows significant suppression of NIS transcription in multiple BC cell types which also results in lowered NIS protein content and cellular iodide intake. NIS repression by activated p53 is further confirmed by non-invasive bioluminescence imaging in live cell and orthotropic tumor model. Abrogation of p53-binding sites by directional mutagenesis confirms reversal of transcriptional activity in wild-type p53-positive BC cells. We also observe direct binding of p53 to these sites on the human NIS promoter. Importantly, TCGA data analysis of NIS and p53 co-expression registers an inverse relationship between the two candidates.

Conclusion Our data for the first time highlight the role of p53 as a negative regulator of functional NIS expression in BC, where the latter is a potential targeted radioiodine therapy candidate. Thus, the study provides an important insight into prospective clinical application of this approach that may significantly impact the patient with mutant versus wild-type p53 profile.

Abbreviations

atRA	All-trans retinoic acid
BC	Breast cancer
ChIP	Chromatin immunoprecipitation
Dox	Doxorubicin
IHC	Immunohistochemistry
NIS	Sodium iodide symporter

🙋 Springer

NUE	NIS upstream enhancer
RAR	Retinoic acid receptor
RXR	Retinoid X receptor
TNBC	Triple-negative breast cancer
TF	Transcription factor
TSH	Thyroid-stimulating hormone

Introduction

The human sodium iodide symporter (NIS) is a distinguished target for radioiodine therapy in thyroid carcinoma [1–3]. Other than thyroid, NIS is naturally expressed in breast tissue only during lactation phase to support iodide concentration for neonatal nutrition [4]. In a breakthrough study, Tazebay et al. [5] showed overexpression of NIS protein in breast malignancies over normal breast tissue. Subsequently, several groups including ours have reported aberrant NIS protein expression in different subsets of breast cancer (BC), signifying its therapeutic potential in disease management [6–9]. However, realization of NIS-based targeted radioiodine therapy in BC is yet to happen as NIS gene regulation in BC is poorly understood.

Transcriptional regulation of human NIS expression is a comprehensive research area primarily studied in thyroid. In thyroid tissue, NIS upstream enhancer (NUE) is strongly responsive to thyroid-stimulating hormone (TSH) stimulation, mediating transcriptional regulation via Pax8, Nkx2.1, and CREB [10–12]. Recently, FoxE1/TTF-2 and miRNA146b-3p are identified as NIS modulators in thyroid cells [13, 14]. However, NIS gene is differentially regulated in breast tissue which is largely unknown [15, 16]. In BC context, the cardiac homeobox transcription factor Nkx2.5 is reported as a NIS regulator [17]. All-trans retinoic acid (atRA) and retinoic acid receptor (RAR) synthetic ligands induce functional NIS expression in estrogen receptor-positive cells by binding of an intronic enhancer to RARα and retinoid X receptor (RXR) [18–22]. Additionally, epigenetic modulators like histone deacetylase inhibitors induce NIS expression in BC [23, 24]. Although these studies are informative, it is of great interest to investigate the potential transcriptional regulators of NIS in BC.

The p53 protein is a critical tumor suppressor protein in cancer biology. Mutation or changes in p53 expression are found almost universally in many cancer types. Beyond indisputable important role as a tumor suppressor, p53 acts as a transcription factor regulating diverse array of genes involved in various cellular processes [25]. Mutations of p53 are frequently present (25%) in BC [26] and specially the triple-negative BC (TNBC) cases with

mutant p53 have poor prognosis [27]. In the current study, the regulatory role of the tumor suppressor gene p53 is investigated revealing its negative impact on NIS gene expression in BC. To the best of our understanding, this is the first report presenting evidences on regulation of NIS expression and function by p53 in BC, suggesting important clinical implication for translation of this potential therapeutic approach.

Materials and methods

Chemicals and cell lines

1.34 kb human NIS promoter from Dr. Kenneth Ain, University of Kentucky, USA, wild-type p53 expression plasmid from Dr. Sorab Dalal, ACTREC, India and p53.Nanoluc fusion plasmid from Promega, USA were kind gifts. Doxorubicin hydrochloride was purchased from Sigma. Following antibodies were used: anti-p53 (DO-1, Santa Cruz Biotechnology), phospho-serine15 p53 (#9286, Cell Signaling Technology), anti-human NIS (FP5A, Abcam), β-actin (A5316, Sigma), anti-α-tubulin (T9026, Sigma). MCF-7, Zr-75-1, and MDA-MB-453 cells (ATCC) were used for experiments. Refer to Supplementary material for details.

Plasmid construction and site-directed mutagenesis

Human NIS promoter driven Fluc2.TurboFP bi-fusion reporter vector (pNIS-Fluc2.TurboFP) was developed as described previously [24]. pNIS-Fluc2.TurboFP vector comprising three p53 binding sites was sequentially mutated using the oligonucleotides (listed in Supplementary Table 1) by site-directed mutagenesis.

Reporter assay

Renilla and Firefly luciferase and β-galactosidase activity were measured as previously described [28].

Live cell bioluminescence and fluorescence imaging

For live cell imaging, MCF-7 cells stably overexpressing p53.Nanoluc fusion reporter were used. Refer to Supplementary material for experimental details.

Quantitative real-time PCR

The TaqMan probes for human NIS and GAPDH (assay IDs Hs00166567_m1 and Hs02758991_g1 respectively)(Applied

Biosystems) were used. Refer to Supplementary material for details.

Immunoblotting, immunofluorescence, and immunohistochemistry (IHC)

Immunoblotting and immunofluorescence were performed as described previously [24]. Immunohistochemistry was performed as previously described [9].

Iodide uptake assay

Iodide uptake study was performed as described previously with minor modifications [24, 29, 30].

In vivo optical imaging

Animal imaging experiments were performed following approval by Institutional Animal Ethics Committee (IAEC) at ACTREC and according to the guidelines for the care and use of the laboratory animals. Refer to Supplementary material for experimental details.

Chromatin immunoprecipitation (ChIP)

ChIPed DNA was analyzed by PCR using primer set as shown in Supplementary Table 2. Refer to Supplementary material for experimental details.

Ethics statement

The clinical study protocol was approved by the TMC-ACTREC Institutional Ethical Committee III and informed consents were obtained as per regulatory provision. Demographic details of patient cohort are provided in Supplementary Table 3.

TCGA data analysis of NIS and p53 expression

BC TCGA data were curated from cBioPortal (http://www.cbioportal.org/index.do). Refer to Supplementary material for details.

Statistical analysis

Assays were performed in duplicates, and data were expressed as mean $\pm$ SE (standard error of mean). Statistical significance was analyzed by student t test. For IHC analysis, Fischer's exact test was performed. P values of ≤ 0.05 were considered as statistically significant.

Results

Human NIS is a transcriptional target of tumor suppressor gene p53

To get a rational insight on candidate transcriptional regulators of NIS, we performed a genome-wide in silico analysis of the human NIS promoter sequence (-1298 to $+32$ basepairs) [31]. Bioinformatics analysis using the Transfac and Genomatix softwares (with 80% cut off score) predicts the presence of ~ 64 putative TF binding sites including AP1, CREB, Pax8, etc. Interestingly, two complete and a half-binding consensus sequence (RRRCNNGYYY) for p53 are found on this promoter between -595 and -80 basepairs (Fig. 1a). Since both p53 and NIS are pertinent in BC context, the above findings instigated us to discern the role of p53 in NIS regulation. We used two wild-type p53 expressing cell lines (MCF-7 and Zr-75-1) (Supplementary Fig. 1) and another cell line lacking functional p53 protein (MDA-MB-453). These cells were treated with a common chemotherapeutic drug, Doxorubicin (Dox), which is known to activate wild-type p53 [32, 33]. Treatment of the cells with Dox showed upregulation of endogenous p53 protein in MCF-7 and Zr-75-1 cells but not in MDA-MB-453 cells (Fig. 1b). p53 protein content after wild-type plasmid overexpression and activation by Dox treatment in MCF-7 cells was verified by semi-quantitative western blotting (Supplementary Fig. 2). To verify modulation of NIS transcription by p53 overexpression or activation, cell lines transiently overexpressing pNIS-Fluc2.TurboFP reporter plasmid were used. Dox treatment shows significant reduction of normalized luciferase reporter activity in MCF-7 (0.7fold; $p \leq 0.001$) and Zr-75-1 (0.6fold; $p \leq 0.001$), but not in MDA-MB-453 cells (1.34fold increase; $p = 0.064$). Further, in response to wild-type p53 overexpression or when combined with Dox treatment, significant loss of promoter activity is observed in all the three cell lines (0.2–0.7fold; $p \leq 0.05$) (Fig. 1c). Mammalian TK promoter driving luciferase (pTK-RL) reporter was used for transfection normalization after verifying its unaltered activity upon p53 activation (data not shown). Additionally, similar trend of NIS promoter attenuation is also observed in engineered MCF-7 and Zr-75-1 cells stably overexpressing the same reporter construct (Fig. 1d). Moreover, p53 activation in response to Dox treatment leads to a significant reduction in endogenous NIS mRNA content in MCF-7 (0.4fold; $p = 0.001$) and Zr-75-1 cells (0.5fold; $p = 0.046$), but a non-significant increase is observed in MDA-MB-453 cells (1.46fold; $p = 0.121$) (Fig. 1e). Together, these results confirm that NIS transcriptional activity is modulated by wild-type p53 in BC cell lines.
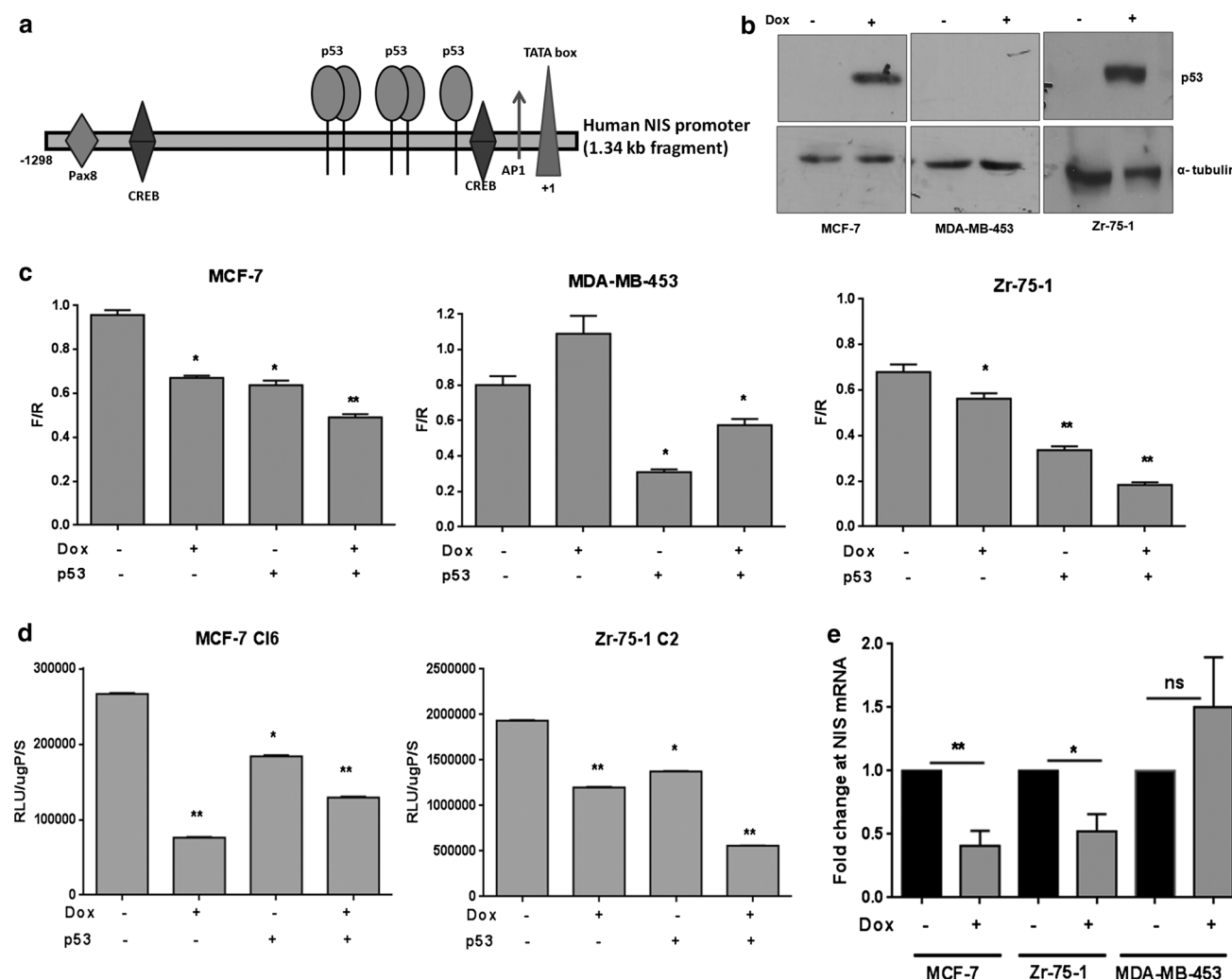
Fig. 1 NIS is a transcriptional target of cellular p53 in breast cancer. a Schematic representation of 1.34 kb length human NIS promoter DNA showing respective positions of important transcription factor binding sites including the three binding sites for p53. b Western blots verifying the p53 status in MCF-7, MDA-MB-453, and Zr-75-1 cells in response to p53 activation by doxorubicin (Dox) treatment. α-tubulin was used as loading control. c Charts showing normalized luciferase activity in response to wild-type p53 overexpression or endogenous p53 activation by Dox treatment in two wild-type p53 (MCF-7 and Zr-75-1) cells and MDA-MB-453 cells lacking functional p53 protein. These breast cancer cells were transiently transfected with pNIS-Fluc2.TurboFP reporter construct and pTK-

hRL was used for transfection normalization. Dox treatment (1 μg/ml, for 24 h) was given to activate cellular p53. d Chart showing the luciferase activity in response to exogenous wild-type p53 overexpression or endogenous p53 activation in engineered MCF-7 clone6 and Zr-75-1 cloneC2 cells stably expressing pNIS-Fluc2.TurboFP reporter. **indicates high significance $p < 0.001$, *indicates $p < 0.05$, ns indicates non-significant. e Graphs showing the effect of activated p53 on endogenous NIS transcript measured by quantitative real-time PCR in the three breast cancer cell lines. Results were normalized for housekeeping gene GAPDH. **indicates high significance $p < 0.001$, *indicates $p < 0.05$

Disruption of the DNA sequence for p53 binding sites by mutagenesis restores NIS promoter activity

To verify the role of p53 in NIS transcription regulation, p53 binding sites on the human NIS promoter sequence were disrupted either individually or in combination by site-directed mutagenesis. The core CNNG sequence motif of p53 response element was either substituted with AATT sequence or the entire response element was deleted (Del) as represented in Fig. 2a. Compared to the wild-type promoter,

introduction of point mutations at sites1 or 2 results in a moderate increase of reporter signal, while mutations at site3 or at all sites show significant increase of reporter activity (1.2–1.8fold; $p \leq 0.05$) in the cell lines with endogenous wild-type p53 (Fig. 2b). Further, in response to Dox treatment, baseline promoter exhibits 0.4-0.5fold reduction ($p \leq 0.05$), whereas site3 mutation alone shows 1.5fold gain in MCF-7 ($p \leq 0.005$) and 1.7fold gain in Zr-75-1 ($p \leq 0.001$) cells. Mutation at all three sites shows 1.5fold increase of reporter activity in both cell lines ($p \leq 0.001$).

Fig. 2 Mutations in NIS promoter sequence for p53 binding sites result in augmentation of transcriptional activity in breast cancer cells expressing endogenous wild-type p53. **a** Schematic design of mutagenic promoter sequence by either base pair substitution or by site-specific deletion to disrupt the core CNNG nucleotide sequence. **b** Charts showing effect of AATT substitution at individual or all sites, on normalized luciferase reporter activity measured from MCF-7 and Zr-75-1 cells. Cells were transfected with either wild-type or mutant human NIS promoter plasmids or reporter activity was measured in the presence or absence of doxorubicin treatment. **c** Similarly, effect of deletion mutations was tested for either individual or all binding sites using the same breast cancer cell lines. ***indicates high significance $p < 0.0001$, **indicates $p < 0.005$, *indicates $p < 0.05$, ns indicates non-significant
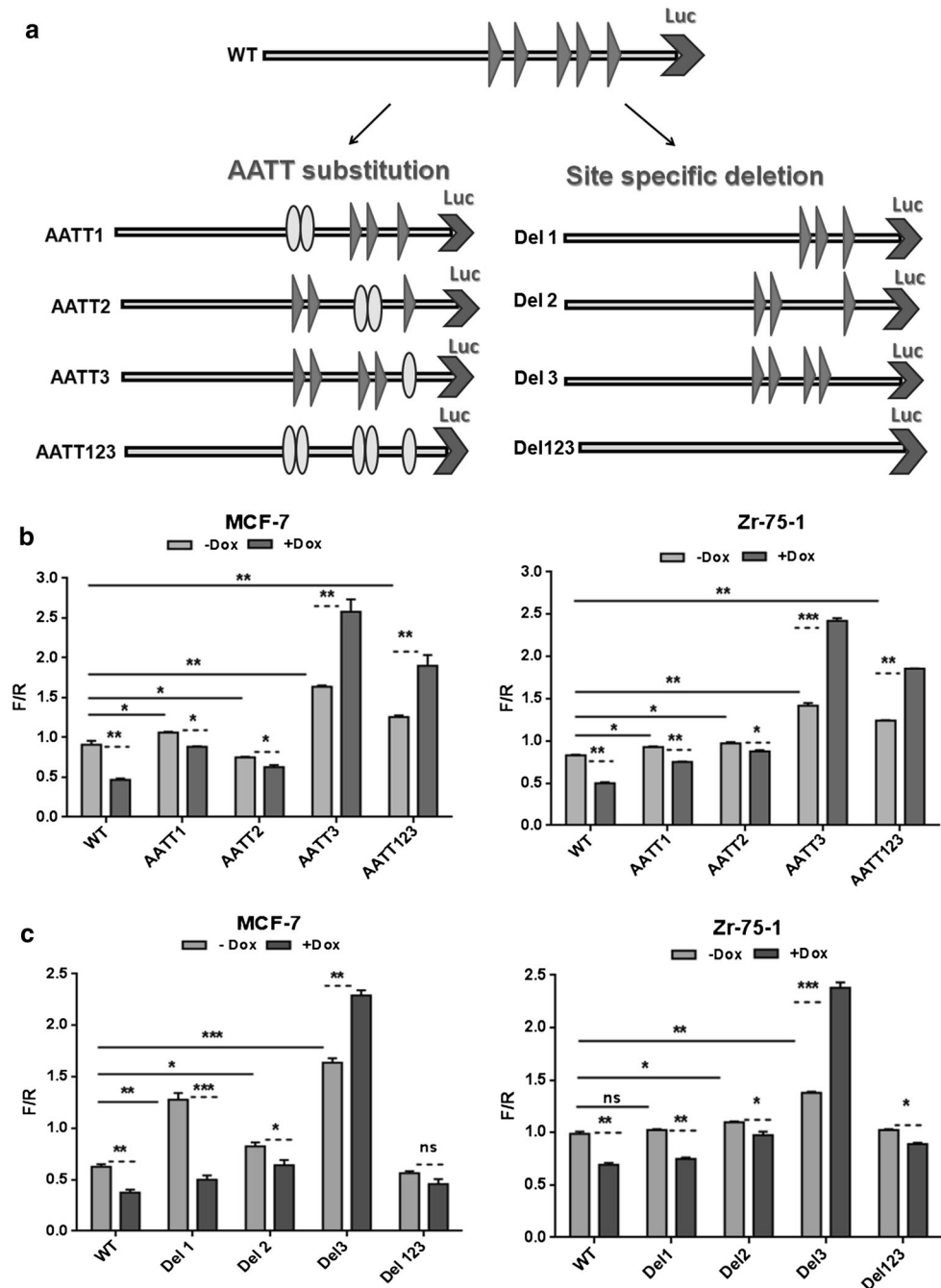
Complete deletion of p53 binding sequence at site3 shows an increase in gene expression (1.4fold for MCF-7 and 2.6fold for Zr-75-1; $p \leq 0.0001$) compared to the wild-type promoter (Fig. 2c). Deletion at site2 shows moderate effect (~ 1.2–1.3fold) while site1 deletion shows heterogeneous response in the cell lines studied. Deletion of site1 results in significant increase in transcriptional activity in MCF-7 cells (2fold) but non-significant change in luciferase signal is observed in Zr-75-1 cells (1.03fold). Upon Dox treatment, site3 deletion exhibits higher reporter activity (1.4–1.7fold; $p \leq 0.0001$) confirming temporary release from p53-mediated repression at this region (Fig. 2c). Combined deletion of all sites shows no major release of transcriptional activity under untreated or Dox-treated condition in both the cell lines. Overall, these findings suggest probable binding of p53 to the identified sites of human NIS promoter, thereby exerting gene regulation.

Multiplexed live cell imaging confirms NIS promoter modulation is a p53-dependent event

Next, we designed a live cell in vivo imaging experiment involving simultaneous measurement of three molecular events in real-time using multiplexed reporters. MCF-7 cell stably overexpressing p53.Nanoluc fusion construct was transfected with either wild-type or site3 deleted (Del3) pNIS-Fluc2.TurboFP construct and transcription was monitored in response to Dox treatment. Inherent fluorescence of doxorubicin (Fig. 3a), bioluminescence signal from Nanoluc-furimazine reaction (Fig. 3b), and Fluc2-D-Luciferin reaction (Fig. 3c) were captured in sequence from live cells. For transfection normalization, β-galactosidase expression was measured from cell lysates (Fig. 3d). Natural fluorescence of doxorubicin was imaged to demonstrate how Dox-mediated p53 activation affects NIS promoter expression. The Dox fluorescence data also indicate equal dose of drug added in wild-type and Del3 NIS promoter-transfected cells. As evident from bioluminescence imaging data, 6-7fold induction in p53 activity is noted in both wild-type and Del3 promoter construct-transfected cells after Dox treatment indicating comparable activation of p53.Nanoluc fusion transgene in both the promoter constructs (Fig. 3b). Interestingly, Fluc2 scan clearly demonstrates that deletion of p53 response element (Del3) enhances normalized reporter signal by at least 2-fold when compared to wild-type promoter, corroborating our in vitro findings (Fig. 3e). As shown in Supplementary Fig. 3, p53.Nanoluc fusion protein overexpression causes considerable drop in NIS mRNA content, suggesting that p53.Nanoluc fusion retains transcriptional regulation ability. To validate similar modification of endogenous p53 and p53.Nanoluc protein in response to DNA damage, we have further checked serine15 phosphorylation levels after Dox treatment. The immunoblot clearly indicates increased phospho-serine15 and corresponding total p53 levels after Dox treatment as represented in Fig. 3f.

Extending these results, we measured the effect of p53 activation on NIS gene regulation in vivo. We implanted engineered Zr-75-1-pNIS-Fluc2.TurboFP reporter cells (clone C2) orthotropically in a set of immunocompromised
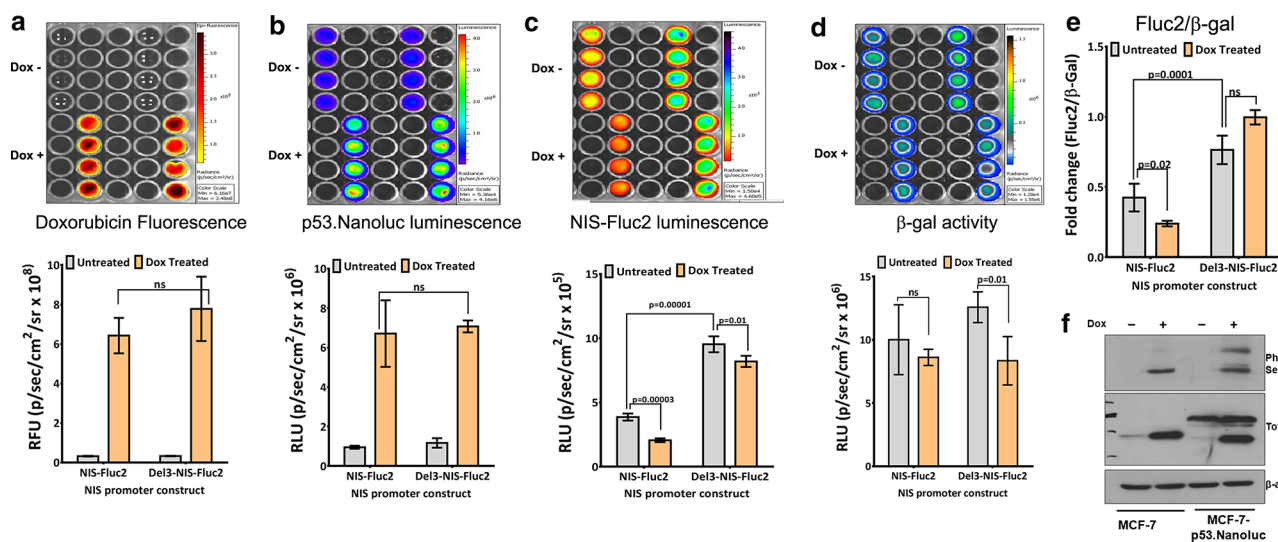

Fig. 3 Non-invasive optical imaging analysis showing NIS gene expression is directly related to the wild-type p53 status in breast cancer cells. Simultaneous measurements of four imaging signatures captured from live cells in culture are shown in (a–e). Natural fluorescence of doxorubicin was imaged to demonstrate how Dox-mediated p53 activation affects NIS promoter expression. The Dox fluorescence data indicates equal dose of drug added in wild-type and Del3 NIS promoter-transfected cells; bioluminescence signal from Nanoluc-furimazine reaction represents activation of p53 while bioluminescence imaging of Fluc2-D-Luciferin reaction indicates NIS promoter modulation in the presence or absence of doxorubicin. β-galactosidase activity was measured from cell lysates for transfection normalization. **a** Representative image (*upper panel*) and chart (*lower panel*) showing doxorubicin fluorescence in wild-type and Del3-NIS promoter-transfected MCF-7 cells. **b** Image (*upper panel*) and chart (*lower panel*) of bioluminescence signal captured from the same plate by adding furimazine substrate to measure p53.Nanoluc expression in the presence and absence of doxorubicin treatment (ns indicates non-significant). **c** Image (*upper panel*) and chart (*lower panel*) indicating Firefly luciferase signal respectively without normalization in wild-type and Del3-NIS promoter constructs. **d** Image (*upper panel*) and chart (*lower panel*) indicating β-galactosidase activity signal used for normalization. **e** Normalized Fluc activity of wild-type and Del3-NIS promoter constructs showing p53-specific promoter modulation in breast cancer cells. **f** Western blot indicating p53 activation in response to doxorubicin treatment in both parental MCF-7 and engineered MCF-7-p53.Nanoluc cells using phospho-serine p53- and p53-specific monoclonal antibody, respectively. β-actin was used as an endogenous control. The upper band ($\sim$71 kDa) in the immunoblot represents p53 protein fused to Nanoluc reporter while the lower band ($\sim$53 kDa) represents endogenous p53 protein in MCF-7-p53.Nanoluc reporter cells

mice. Once the tumors were formed, mice in the Dox treatment group were injected with low Dox dose (1.5 mg/kg) as reported before [34] to keep tumor cytotoxicity minimal while measuring reporter activity as a measure of gene regulation. The treatment group exhibits 50% reduction in luciferase activity after 48-h drug treatment ($1.61 \times 10^8 \pm 5.87 \times 10^7$ to $8.07 \times 10^7 \pm 2.01 \times 10^7$ Photon/s/cm^2/sr), whereas the untreated control group shows non-significant increment in bioluminescence signal due to tumor growth ($1.18 \times 10^8 \pm 4.83 \times 10^7$ to $1.48 \times 10^8 \pm 7.79 \times 10^7$ Photon/s/cm^2/sr) (Supplementary Fig. 4). Altogether, the results from in vivo live cell and animal imaging confirm possible involvement of p53 in downregulating NIS gene transcription in BC.

Transcription factor p53 exerts negative regulation on NIS function in breast cancer cells

Following the experimental evidences obtained so far, effect of p53 activation on NIS protein expression and function was further investigated. Since endogenous level of NIS protein is lower than the assay detection threshold and activated p53 further lowers its expression, a NIS overexpressing MCF-7 cell line (Clone31) established in our laboratory before [35] was used to verify NIS functional response (Supplementary Fig. 5a–b). In these cells, NIS-mediated iodide uptake is well above the detection threshold as shown in Supplementary Fig. 5c. Dox-mediated endogenous p53 activation or exogenous wild-type p53 overexpression and their combination result in marked reduction of NIS protein content as shown in Fig. 4a. Reduced NIS protein content did result in 30–50% reduction ($p \leq 0.05$) of cellular iodide uptake (Fig. 4b). These findings together demonstrate that p53 negatively affects NIS expression and thus lowers iodine intake ability.
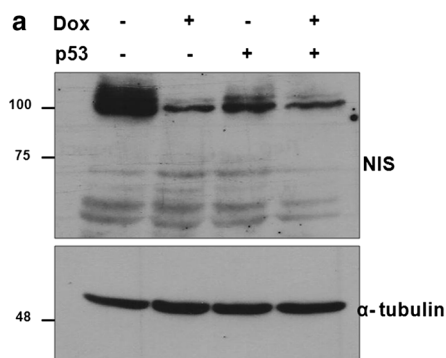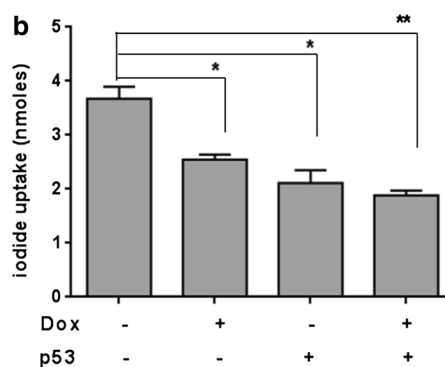
Wild-type p53 directly binds to the specific DNA-binding sites identified on human NIS promoter

Since the endogenous NIS expression is significantly altered by cellular p53, direct binding of p53 to the human NIS promoter was tested by ChIP assay. Cross-linked chromatin from BC cell lines was pulled with p53 antibody and PCR amplified for NIS promoter using primer set I (Supplementary Table 2). Our results indicate that activated p53 is bound to 450 basepairs region of NIS promoter DNA covering all three binding sites, both in MCF-7 and Zr-75-1 cell lines, but not in MDA-MB-453 cells (Fig. 5a–b). The sequencing of ChIPed DNA shows complete match with the NIS promoter sequence (Fig. 5c). To validate p53-specific binding on NIS promoter, we knocked down p53 in MCF-7 cells [36] (Fig. 5d) and observed 50% reduction in amplification of pulled NIS promoter, confirming the recruitment of wild-type p53 (Fig. 5e–f). We also used primers to PCR amplify the promoter area outside the putative p53 binding sites. However, PCR with this primer set did not amplify ChIPed product (Supplementary Fig. 6a) confirming sequence-specific p53 binding on NIS promoter. Since p21 is a known target of p53, binding of p53 to p21 promoter sequence was also verified. As expected, p53 binding on p21 promoter was observed in Zr-75-1 cells but not in MDA-MB-453 cells (Supplementary Fig. 6b). In summary, these observations confirm sequence-specific binding of p53 to human NIS promoter in vivo in regulation of gene expression.

Relationship of human NIS and p53 expression in breast cancer clinical cases

Taking a step forward, breast cancer TCGA data including p53 genomic sequencing and NIS (SLC5A5) gene

Fig. 4 NIS expression and function in MCF-7 cells are p53 dependent. **a** Semi-quantitative western blot showing downregulation of the major band of fully matured NIS protein (~ 100 kDa) in MCF-7 Cl31 cells in response to wild-type p53 overexpression and/or Dox activation state. **b** Effect of p53 activation on NIS function in MCF-7 Cl31 cells. Since NIS protein functions to pump iodine inside the cells, iodide uptake under p53 activating conditions was measured. The Y axis *scale bar* represents nanomoles (nmoles) of iodide uptake in cells. **indicates $p < 0.005$, *indicates $p < 0.05$
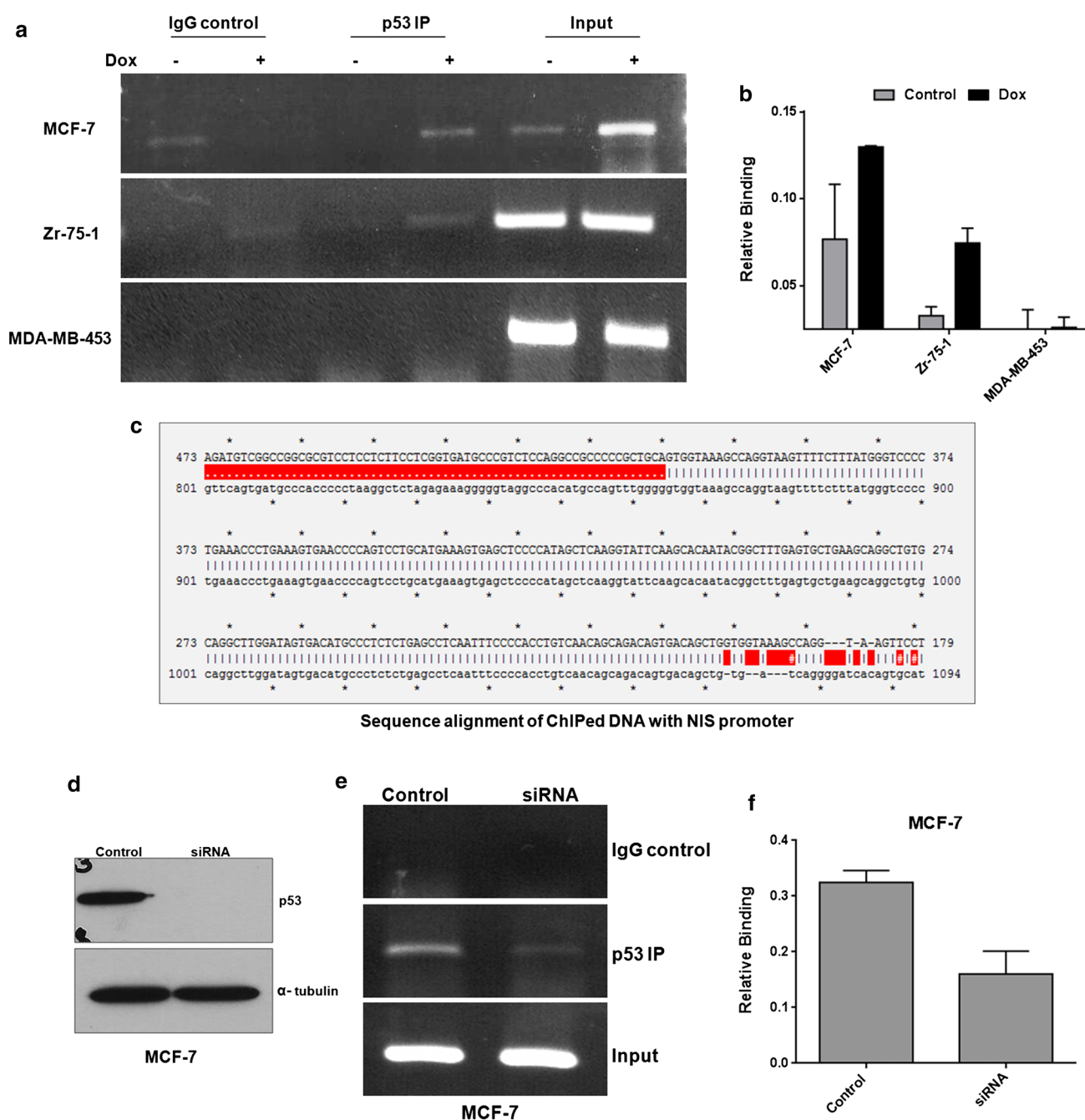
Fig. 5 Evidence of direct binding of p53 to the human NIS promoter DNA. **a** Recruitment of p53 onto the human NIS promoter checked by using primer set I. Sonicated chromatin fragments were pulled with α-p53 antibody with and without doxorubicin treatment and PCR amplified for the 450 basepairs region product verified from cells. Input represents total sonicated genomic DNA, IP eluate represents the pulled chromatin fraction by p53 antibody and IgG control is the isotype control. **b** Charts representing relative binding of p53 to the NIS promoter DNA in the presence or absence of doxorubicin treatment in MCF-7, Zr-75-1, and MDA-MB-453 cells. Relative band intensity normalized by input DNA was calculated and plotted. **c** Alignment of ChIPed DNA to the human NIS promoter establishes the identity of immunoprecipitated PCR product. **d** Immunoblot indicating p53 knockdown in MCF-7 cells. **e–f** Agarose gel image and chart representing quantitative estimation of band intensity of the gel picture indicating loss of p53 binding to NIS promoter in p53 knockdown condition in MCF-7 cells

expression profile [37] were curated from cBioPortal (http://www.cbioportal.org/index.do) [38, 39]. The p53 mutations were categorized into non-functional (14%) and missense mutations (22%) as shown in Fig. 6a. Based on the analysis of 513 samples, significant variation in NIS mRNA expression level is not observed in wild-type or

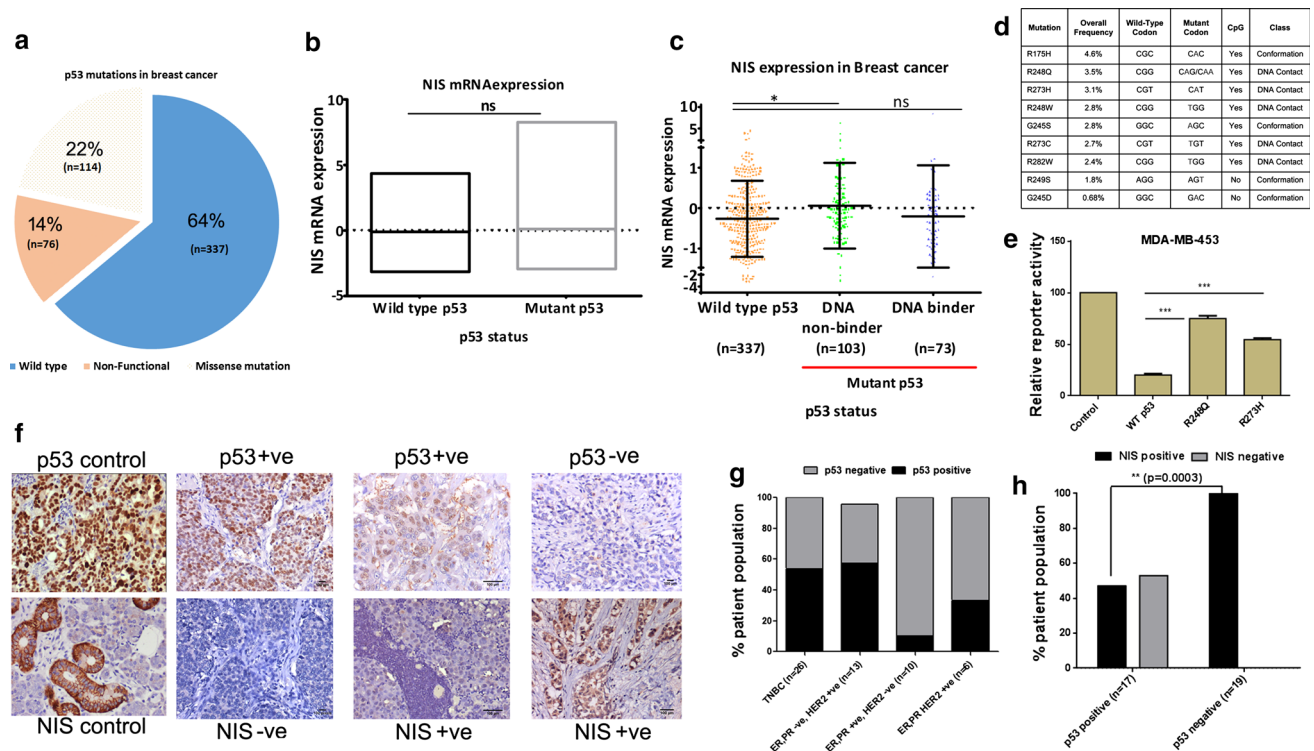**Fig. 6** Breast cancer patient sample analysis to confirm inverse association between NIS and p53. **a** Chart showing classified p53 status in breast cancer patients, data curated from cBioPortal. **b** Graph represents NIS mRNA expression variation (Y axis) against wild-type and mutant cases of p53; ns indicates data non-significant. **c** Correlative analysis of TCGA breast cancer dataset to understand the relationship between NIS (SLC5A5) and p53 expression profile. The p53 genomic sequencing and NIS gene expression profile data were obtained from cBioPortal. Missense mutations which lack DNA binding ability along with truncated mutations and splice variants of p53 are classified as 'DNA non-binder,' while the rest of the p53 mutations belong to 'DNA binder' category. *indicates $p < 0.05$. **d** List of 9 missense 'non-binder' mutations with compromised DNA binding ability of p53 is shown. **e** Chart showing the effect of wild-type and p53 mutants R248Q and R273H expression on human NIS promoter transcription measured by luciferase reporter activity in

MDA-MB-453 cells lacking functional p53. Data represented as relative reporter activity in cells co-transfected with wild-type and mutant p53 vector. The activity of reporter vector alone transfected cells is set as 100%. A thymidine kinase promoter driven humanized *Renilla* luciferase (pTK-hRL) was used for transfection normalization. ***indicates high significance $p < 0.0001$. **f** Representative IHC images of human breast tumor tissue samples with correlated expression of three basic types, i.e., p53 +/NIS-, p53 +/NIS +, and p53-/NIS + cases. All images were captured at ×20 magnification. A high-grade ovarian serous carcinoma section and a normal salivary gland were shown as positive staining control for p53 and NIS, respectively. **g** Chart representing breast cancer subtype-specific analysis of p53 positive and negative cases. A total of 55 cases were evaluated. **h** Chart representing comparison of NIS staining between the p53-positive and -negative patient samples

mutant p53 cases. But when NIS mRNA expression is compared between wild-type p53 (337 cases) versus the p53 mutations abrogating its DNA binding ability (103 cases), significantly higher NIS expression is noticed in p53 mutant cases ($p < 0.05$) (Fig. 6b–c). As p21 is a direct transcriptional target of p53 and p53 is known to transactivate p21 gene, we have also verified p53 and p21 correlative expression in the same dataset which shows that p21 expression is significantly reduced in the p53 mutant cases (both binder and non-binder cases) (Supplementary Fig. 7). Figure 6d represents various p53 mutants along with their mode of action and frequency of occurrence in BC. Encouraged by these findings, two mutations commonly occurring in BC patients, i.e., R248Q and R273H, affecting DNA binding ability of the p53 protein were

chosen and tested in MDA-MB-453 cell overexpressing NIS promoter driven luciferase reporter sensor to verify if their co-expression cause any difference. As expected, in comparison to the wild-type protein, R248Q and R273H p53 mutants release the repressive activity on NIS transcription and thus reporter expression increases (Fig. 6e).

To verify the inverse relationship of NIS and p53 proteins in a clinical setting, we performed immunostaining using p53 antibody in a subset of 55 tumor tissue samples collected at our hospital with reported NIS expression [9]. Of the total number of tissues stained for p53, 44% cases turned out to be positive with clear nuclear staining in majority of them as represented in Fig. 6f. BC subtype-specific analysis shows that p53 positive cases are predominant in TNBC (54% i.e., 14 out of 26 cases) and

HER2 subtypes (57% i.e., 8 out of 13 cases) than the hormone receptor +ve subtypes (Fig. 6g).

Finally, a correlative expression of NIS and p53 protein was judged from a total of 36 cases. 47% (8 of 17) p53-positive cases display NIS positive stain, which is significantly different ($p = 0.003$) as all 19 samples stained negative for p53 turn out to be positive for NIS (Fig. 6h), indicating an inverse association between NIS and p53 protein immunostaining in breast tumor specimens. Various literatures have reported that the judgement of wild-type or mutant status in formaldehyde fixed tissue samples may be ambiguous [40, 41]. Considering these technical limitations, determining p53 mutational status will help understand the association of the two proteins in future. Altogether, accumulated observations from these experiments point out an inverse relationship of NIS and p53 in human BC dataset.

Discussion

In quest of identifying important NIS transcriptional regulators, here we report the presence of multiple p53 response elements on the human NIS promoter sequence. The p53 protein is a critical tumor suppressor and nearly one-third of all breast cancers have p53 gene mutations, which are associated with high histological grade and clinical aggressiveness [26]. In this context, we hypothesized that p53 status in BC cells may have profound impact on observed NIS expression and subsequently its function in terms of iodide transport activity. Our findings suggest that p53 acts as a transcriptional repressor of NIS expression in BC. So far, the only report by Guerrieri et al. has shown that in liver cancer cells, NIS is a transcriptional target of p53 family of proteins and its expression is shown to be upregulated upon binding of p53 family members [42]. Such opposing role of p53 on NIS gene regulation in breast or liver cancer cells is possible, which may be due to the complexity of how p53 family proteins function in nature. It has been reported that available isoforms (p63, p73 etc.) may exert opposite transcriptional effects in cell types of different tissue origin or even their states [43, 44]. Further, the functional outcome of p53 depends on its quantity, association with specific co-regulatory proteins (which could be tissue-specific), as well as specific post-translational modifications induced by a variety of stress-induced response [25, 45–47]. As discussed before, NIS gene regulation differs significantly in different cell types based on their tissue origin [15, 16]. By now, aberrant NIS expression in BC is a well-reported fact, and therefore understanding how NIS function is regulated in cancer condition representing wild-type or mutant p53 is of great relevance as

this may have immense impact on proposed role of NIS in radioiodine therapy for BC.

Therefore, during this study, we have performed a range of molecular characterization in vitro, in vivo or even clinical sample analysis to establish how cellular p53 status may alter NIS expression and/or function. Transcriptional repression by p53 can occur through steric interference with the functions of transcriptional activators by the binding of p53 protein to the transcription factor itself or by the direct binding of p53 protein to the target gene promoter DNA. Alternatively, repression can be brought about by p53-mediated recruitment of transcriptional repressors like histone deacetylases (HDACs) [48]. Our experimental findings suggest that p53 directly binds to the NIS promoter in a sequence-specific manner. Abrogating p53 binding sequence from the NIS promoter, particularly at site3, results in remarkable induction of NIS transcription. Interestingly, it is observed that Sp1 site is retained in AATT123 substitution while this site is lost in Del123 mutation. Now, Sp1 is an established as a transcriptional inducer of NIS in breast cancer [49]. It is noteworthy here that the analysis of human NIS promoter sequence has revealed the presence of overlapping binding sites for RXR, Zn finger containing transcription factor and octamer binding protein at site1 region and Pax4, Smad and GATA binding sites at site2 region and Sp1, Zn finger containing transcription factor for the site3 region of NIS promoter. During mutagenesis, disrupting p53 binding sequence might have resulted in interruption of predicted binding of some of these factors. Therefore, co-operative binding of p53 interacting proteins or even additional binding sites formed due to mutational rearrangements require full consideration in future to understand how NIS gene regulation operates through overlapping binding sites in BC cells.

Multiplexed optical imaging using multimodality fusion reporter genes has been shown to be an effective measure to monitor gene expression in live cell in vivo [28]. Combining the power of dual luciferases i.e., Fluc2 and Nanoluc, simultaneous measure of NIS expression and activated p53 expression respectively was adopted, which has also provided concrete evidence on lowered NIS gene function when wild-type p53 is present in the cell. Further, the p53 activator drug doxorubicin-mediated loss of luciferase reporter signal also confirms the same in physiological context. This finding is in concordance with our in vitro results. Such engineered cells overexpressing pNIS-Fluc2.TurboFP fusion reporter may be a very useful tool to conduct screening of various other transcriptional regulators of NIS in future.

Based on experimental evidences gathered, inhibition of wild-type p53 may allow induction of NIS expression for therapeutic intervention in BC patients. However, since

p53 acts as a guardian of the genome protecting normal cells and tissues, use of wild-type p53 inhibitors is not a practical approach [50, 51]. Instead, determining patient's p53 status may aide in achieving good therapeutic benefit. As observed from TCGA data, not all but specific mutations hampering the DNA binding capacity of p53 may result in higher NIS expression and function. Out of the two p53 mutants tested, R248Q is found to reverse p53-mediated transcriptional repression more effectively although complete loss of transcriptional repression is not observed. Mutant p53 can also interact with other p53 family members like p63 and p73, or other cellular transcription factors like Sp1, Ets-1 and can exert transcriptional regulation [52, 53]. Further studies on such interactions may delineate the differences observed in mutation studies here. Earlier, we have analyzed NIS expression in near 200 patient samples [9]. Now, we have reanalyzed a subset of these patient samples ($n = 55$) using p53 antibody. Our IHC results provide an impression of inverse association between NIS- and p53-positive cases. However, these results are technically challenged as wild-type p53 is unstable in fixed tissue samples. As p53 gene mutations often cause stabilization of the protein, it permits immunohistochemical detection [54, 55]. Still, immunohistochemical detection of p53 protein does not reflect accurately p53 gene mutations. At times, non-sense or null mutations of p53 remain undetected while cellular stress sometimes results in delayed degradation of wild-type p53 making it detectable by IHC [40, 41]. Therefore, it is imperative to determine correct status of p53 using appropriate antibody in BC cases in future.

In conclusion, for the first time, this study brings out molecular evidence showing that NIS is a direct target of wild-type p53 and its activation upon Doxorubicin drug exposure results in suppression of NIS expression and function in breast cancer cells. Our study remains limited in completing the assessment of correlative expression of the two targets in patient tissue samples, which is primarily because: i) wild-type p53 is unstable in tissue samples and therefore IHC-based detection in formalin fixed tissue is complicated; and ii) NIS gene regulation in breast cancer is not solely dependent on p53. However, the leads generated from experiments conducted here including the TCGA data analysis clearly indicate that a judgement of p53 status and/ or prior Doxorubicin chemo exposure should be included in patient selection criteria to succeed in targeted radioiodine therapy trials in future.

References

1. Spitzweg C, Harrington KJ, Pinke LA, Vile RG, Morris JC (2001) Clinical review 132: the sodium iodide symporter and its potential role in cancer therapy. J Clin Endocrinol Metab 86(7):3327–3335. doi:10.1210/jcem.86.7.7641

2. Micali S, Bulotta S, Puppin C, Territo A, Navarra M, Bianchi G, Damante G, Filetti S, Russo D (2014) Sodium iodide symporter (NIS) in extrathyroidal malignancies: focus on breast and urological cancer. BMC Cancer 14:303. doi:10.1186/1471-2407-14-303

3. Ahn BC (2012) Sodium iodide symporter for nuclear molecular imaging and gene therapy: from bedside to bench and back. Theranostics 2(4):392–402. doi:10.7150/thno.3722

4. Cho JY, Leveille R, Kao R, Rousset B, Parlow AF, Burak WE Jr, Mazzaferri EL, Jhiang SM (2000) Hormonal regulation of radioiodide uptake activity and Na$^+$/I- symporter expression in mammary glands. J Clin Endocrinol Metab 85(8):2936–2943

5. Tazebay UH, Wapnir IL, Levy O, Dohan O, Zuckier LS, Zhao QH, Deng HF, Amenta PS, Fineberg S, Pestell RG, Carrasco N (2000) The mammary gland iodide transporter is expressed during lactation and in breast cancer. Nat Med 6(8):871–878

6. Wapnir IL, Goris M, Yudd A, Dohan O, Adelman D, Nowels K, Carrasco N (2004) The Na$^+$/I- symporter mediates iodide uptake in breast cancer metastases and can be selectively down-regulated in the thyroid. Clin Cancer Res 10(13):4294–4302

7. Renier C, Yao C, Goris M, Ghosh M, Katznelson L, Nowles K, Gambhir SS, Wapnir I (2009) Endogenous NIS expression in triple-negative breast cancers. Ann Surg Oncol 16(4):962–968

8. Moon DH, Lee SJ, Park KY, Park KK, Ahn SH, Pai MS, Chang H, Lee HK, Ahn IM (2001) Correlation between 99mTc-pertechnetate uptakes and expressions of human sodium iodide symporter gene in breast tumor tissues. Nucl Med Biol 28(7):829–834

9. Chatterjee S, Malhotra R, Varghese F, Bukhari AB, Patil A, Budrukkar A, Parmar V, Gupta S, De A (2013) Quantitative immunohistochemical analysis reveals association between sodium iodide symporter and estrogen receptor expression in breast cancer. PLoS ONE 8(1):e54055. doi:10.1371/journal.pone.0054055

10. Puppin C, Arturi F, Ferretti E, Russo D, Sacco R, Tell G, Damante G, Filetti S (2004) Transcriptional regulation of human sodium/iodide symporter gene: a role for redox factor-1. Endocrinology 145(3):1290–1293. doi:10.1210/en.2003-1250

11. Ohno M, Zannini M, Levy O, Carrasco N, di Lauro R (1999) The paired-domain transcription factor Pax8 binds to the upstream enhancer of the rat sodium/iodide symporter gene and participates in both thyroid-specific and cyclic-AMP-dependent transcription. Mol Cell Biol 19(3):2051–2060

12. Kogai T, Brent GA (2012) The sodium iodide symporter (NIS): regulation and approaches to targeting for cancer therapeutics. Pharmacol Ther 135(3):355–370. doi:10.1016/j.pharmthera.2012.06.007

13. Riesco-Eizaguirre G, Wert-Lamas L, Perales-Paton J, Sastre-Perona A, Fernandez LP, Santisteban P (2015) The miR-146b-3p/

PAX8/NIS regulatory circuit modulates the differentiation phenotype and function of thyroid cells during carcinogenesis. Cancer Res 75(19):4119–4130. doi:10.1158/0008-5472.CAN-14-3547

14. Fernandez LP, Lopez-Marquez A, Martinez AM, Gomez-Lopez G, Santisteban P (2013) New insights into FoxE1 functions: identification of direct FoxE1 targets in thyroid cells. PLoS ONE 8(5):e62849. doi:10.1371/journal.pone.0062849

15. Spitzweg C (2003) [The sodium-iodide symporter. Pathophysiologic, diagnostic and therapeutic significance]. Der Internist 44(4):396–402

16. Kogai T, Kanamoto Y, Li AI, Che LH, Ohashi E, Taki K, Chandraratna RA, Saito T, Brent GA (2005) Differential regulation of sodium/iodide symporter gene expression by nuclear receptor ligands in MCF-7 breast cancer cells. Endocrinology 146(7):3059–3069. doi:10.1210/en.2004-1334

17. Dentice M, Luongo C, Elefante A, Romino R, Ambrosio R, Vitale M, Rossi G, Fenzi G, Salvatore D (2004) Transcription factor Nkx-2.5 induces sodium/iodide symporter gene expression and participates in retinoic acid- and lactation-induced transcription in mammary cells. Mol Cell Biol 24(18):7863–7877

18. Kogai T, Schultz JJ, Johnson LS, Huang M, Brent GA (2000) Retinoic acid induces sodium/iodide symporter gene expression and radioiodide uptake in the MCF-7 breast cancer cell line. Proc Natl Acad Sci U S A 97(15):8519–8524. doi:10.1073/pnas.140217197

19. Kogai T, Kanamoto Y, Che LH, Taki K, Moatamed F, Schultz JJ, Brent GA (2004) Systemic retinoic acid treatment induces sodium/iodide symporter expression and radioiodide uptake in mouse breast cancer models. Cancer Res 64(1):415–422

20. Ohashi E, Kogai T, Kagechika H, Brent GA (2009) Activation of the PI3 kinase pathway by retinoic acid mediates sodium/iodide symporter induction and iodide transport in MCF-7 breast cancer cells. Cancer Res 69(8):3443–3450

21. Alotaibi H, Yaman E, Salvatore D, Di Dato V, Telkoparan P, Di Lauro R, Tazebay UH (2006) Intronic elements in the Na +/I-symporter gene (NIS) interact with retinoic acid receptors and mediate initiation of transcription. Nucleic Acids Res 38(10):3172–3185

22. Tanosaki S, Ikezoe T, Heaney A, Said JW, Dan K, Akashi M, Koeffler HP (2003) Effect of ligands of nuclear hormone receptors on sodium/iodide symporter expression and activity in breast cancer cells. Breast Cancer Res Treat 79(3):335–345

23. Baldan F, Lavarone E, Di Loreto C, Filetti S, Russo D, Damante G, Puppin C (2014) Histone post-translational modifications induced by histone deacetylase inhibition in transcriptional control units of NIS gene. Mol Biol Rep 41(8):5257–5265. doi:10.1007/s11033-014-3397-x

24. Kelkar MG, Senthilkumar K, Jadhav S, Gupta S, Ahn B-C, De A (2016) Enhancement of human sodium iodide symporter gene therapy for breast cancer by HDAC inhibitor mediated transcriptional modulation. Sci Rep 6:19341. doi:10.1038/srep19341

25. Menendez D, Inga A, Resnick MA (2009) The expanding universe of p53 targets. Nat Rev Cancer 9(10):724–737. doi:10.1038/nrc2730

26. Alsner J, Yilmaz M, Guldberg P, Hansen LL, Overgaard J (2000) Heterogeneity in the clinical phenotype of TP53 mutations in breast cancer patients. Clin Cancer Res 6(10):3923–3931

27. Shapira I, Lee A, Vora R, Budman DR (2013) P53 mutations in triple negative breast cancer upregulate endosomal recycling of epidermal growth factor receptor (EGFR) increasing its oncogenic potency. Crit Rev Oncol/Hematol 88(2):284–292. doi:10.1016/j.critrevonc.2013.05.003

28. Ray P, De A, Min JJ, Tsien RY, Gambhir SS (2004) Imaging tri-fusion multimodality reporter gene expression in living subjects. Can Res 64(4):1323–1330

29. Mandell RB, Mandell LZ, Link CJ Jr (1999) Radioisotope concentrator gene therapy using the sodium/iodide symporter gene. Cancer Res 59(3):661–668

30. Waltz F, Pillette L, Ambroise Y (2010) A nonradioactive iodide uptake assay for sodium iodide symporter function. Anal Biochem 396(1):91–95. doi:10.1016/j.ab.2009.08.038

31. Venkataraman GM, Yatin M, Ain KB (1998) Cloning of the human sodium-iodide symporter promoter and characterization in a differentiated human thyroid cell line, KAT-50. Thyroid 8(1):63–69. doi:10.1089/thy.1998.8.63

32. Bode AM, Dong Z (2004) Post-translational modification of p53 in tumorigenesis. Nat Rev Cancer 4(10):793–805. doi:10.1038/nrc1455

33. Meek DW (2004) The p53 response to DNA damage. DNA Repair 3(8–9):1049–1056. doi:10.1016/j.dnarep.2004.03.027

34. Briat A, Vassaux G (2008) A new transgenic mouse line to image chemically induced p53 activation in vivo. Cancer Sci 99(4):683–688. doi:10.1111/j.1349-7006.2008.00742.x

35. Chatterjee S, Thaker N, De A (2015) Combined 2-deoxy glucose and metformin improves therapeutic efficacy of sodium-iodide symporter-mediated targeted radioiodine therapy in breast cancer cells. Breast Cancer 7:251–265. doi:10.2147/BCTT.S84648

36. Nair AR, Schliekelman M, Thomas MB, Wakefield J, Jurgensen S, Ramabhadran R (2005) Inhibition of p53 by lentiviral mediated shRNA abrogates G1 arrest and apoptosis in retinal pigmented epithelial cell line. Cell Cycle 4(5):697–703. doi:10.4161/cc.4.5.1672

37. Ellis MJ, Ding L, Shen D, Luo J, Suman VJ, Wallis JW, Van Tine BA, Hoog J, Goiffon RJ, Goldstein TC, Ng S, Lin L, Crowder R, Snider J, Ballman K, Weber J, Chen K, Koboldt DC, Kandoth C, Schierding WS, McMichael JF, Miller CA, Lu C, Harris CC, McLellan MD, Wendl MC, DeSchryver K, Allred DC, Esserman L, Unzeitig G, Margenthaler J, Babiera GV, Marcom PK, Guenther JM, Leitch M, Hunt K, Olson J, Tao Y, Maher CA, Fulton LL, Fulton RS, Harrison M, Oberkfell B, Du F, Demeter R, Vickery TL, Elhammali A, Piwnica-Worms H, McDonald S, Watson M, Dooling DJ, Ota D, Chang LW, Bose R, Ley TJ, Piwnica-Worms D, Stuart JM, Wilson RK, Mardis ER (2012) Whole-genome analysis informs breast cancer response to aromatase inhibition. Nature 486(7403):353–360. doi:10.1038/nature11143

38. Cerami E, Gao J, Dogrusoz U, Gross BE, Sumer SO, Aksoy BA, Jacobsen A, Byrne CJ, Heuer ML, Larsson E, Antipin Y, Reva B, Goldberg AP, Sander C, Schultz N (2012) The cBio cancer genomics portal: an open platform for exploring multidimensional cancer genomics data. Cancer Discov 2(5):401–404. doi:10.1158/2159-8290.CD-12-0095

39. Gao J, Aksoy BA, Dogrusoz U, Dresdner G, Gross B, Sumer SO, Sun Y, Jacobsen A, Sinha R, Larsson E, Cerami E, Sander C, Schultz N (2013) Integrative analysis of complex cancer genomics and clinical profiles using the cBioPortal. Sci Signal 6(269):pl1. doi:10.1126/scisignal.2004088

40. Yemelyanova A, Vang R, Kshirsagar M, Lu D, Marks MA, Shih Ie M, Kurman RJ (2011) Immunohistochemical staining patterns of p53 can serve as a surrogate marker for TP53 mutations in ovarian carcinoma: an immunohistochemical and nucleotide sequencing analysis. Modern Pathol 24 (9):1248-1253. doi:10.1038/modpathol.2011.85

41. Zaika A, Marchenko N, Moll UM (1999) Cytoplasmically "sequestered" wild type p53 protein is resistant to Mdm2-mediated degradation. J Biol Chem 274(39):27474–27480

42. Guerrieri F, Piconese S, Lacoste C, Schinzari V, Testoni B, Valogne Y, Gerbal-Chaloin S, Samuel D, Brechot C, Faivre J, Levrero M (2013) The sodium/iodide symporter NIS is a transcriptional target of the p53-family members in liver cancer cells. Cell Death Dis 4:e807. doi:10.1038/cddis.2013.302

43. Marcel V, Olivier M, Mollereau B, Hainaut P, Bourdon JC (2011) First International p53 Isoforms Meeting: 'p53 isoforms through evolution: from identification to biological function'. Cell Death Differ 18(3):563–564. doi:10.1038/cdd.2010.156

44. Marcel V, Fernandes K, Terrier O, Lane DP, Bourdon JC (2014) Modulation of p53beta and p53gamma expression by regulating the alternative splicing of TP53 gene modifies cellular response. Cell Death Differ 21(9):1377–1387. doi:10.1038/cdd.2014.73

45. Braithwaite AW, Prives CL (2006) p53: more research and more questions. Cell Death Differ 13(6):877–880. doi:10.1038/sj.cdd.4401938

46. Brandt T, Townsley FM, Teufel DP, Freund SM, Veprintsev DB (2012) Molecular basis for modulation of the p53 target selectivity by KLF4. PLoS ONE 7(10):e48252. doi:10.1371/journal.pone.0048252

47. Meek DW, Anderson CW (2009) Posttranslational modification of p53: cooperative integrators of function. Cold Spring Harbor Perspect Biol 1(6):a000950. doi:10.1101/cshperspect.a000950

48. Ho J, Benchimol S (2003) Transcriptional repression mediated by the p53 tumour suppressor. Cell Death Differ 10(4):404–408. doi:10.1038/sj.cdd.4401191

49. Xu J, Kogai T, Brent GA, Hershman JM (2002) A GC box in the human sodium iodide symporter gene promoter is essential for full activity. Thyroid 12(2):107–114

50. Bouchet BP, Caron de Fromentel C, Puisieux A, Galmarini CM (2006) p53 as a target for anti-cancer drug development. Crit Rev Oncol/Hematol 58(3):190–207. doi:10.1016/j.critrevonc.2005.10.005

51. Fuster JJ, Sanz-Gonzalez SM, Moll UM, Andres V (2007) Classic and novel roles of p53: prospects for anticancer therapy. Trends Mol Med 13(5):192–199. doi:10.1016/j.molmed.2007.03.002

52. Freed-Pastor WA, Prives C (2012) Mutant p53: one name, many proteins. Genes Dev 26(12):1268–1286. doi:10.1101/gad.190678.112

53. Sun Y, Cheung JM, Martel-Pelletier J, Pelletier JP, Wenger L, Altman RD, Howell DS, Cheung HS (2000) Wild type and mutant p53 differentially regulate the gene expression of human collagenase-3 (hMMP-13). J Biol Chem 275(15):11327–11332

54. Menezes MV, Cestari AL, Almeida O, Alvarenga M, Pinto GA, Gurgel MS, Souza GA, Zeferino LC (2006) Protein expression of c-erbB-2 and p53 in normal ducts, ductal carcinoma in situ and invasive carcinoma of the same breast. Sao Paulo Med J 124(3):121–124

55. Mirza AN, Mirza NQ, Vlastos G, Singletary SE (2002) Prognostic factors in node-negative breast cancer: a review of studies with sample size more than 200 and follow-up more than 5 years. Ann Surg 235(1):10–26

Research Paper

Assessing Therapeutic Potential of Magnetic Mesoporous Nanoassemblies for Chemo-Resistant Tumors

Lina Pradhan[1, 4*], Bhushan Thakur[2*], Rohit Srivastava[3], Pritha Ray[2✉], Dhirendra Bahadur[4✉]

1. Centre for Research in Nanotechnology and Sciences, IIT Bombay, Mumbai, 400076,India.
2. Advance Centre for Treatment, Research and Education in Cancer, Tata Memorial Centre, Kharghar, Navi Mumbai, 410210, India.
3. Department of Biosciences and Bioengineering, IIT Bombay, Mumbai, 400076, India.
4. Department of Metallurgical Engineering and Materials Science, IIT Bombay, Mumbai, 400076 India.

*These authors contributed equally.

✉ Corresponding authors: Tel.: +91 22 2740 5119 (P. Ray). Tel.: +91 22 25767632 (D. Bahadur). E-mail addresses: pray@actrec.gov.in (P. Ray), dhirenb@iitb.ac.in (D. Bahadur).

Abstract

Smart drug delivery system with strategic drug distribution is the future state-of-the-art treatment for any malignancy. To investigate therapeutic potential of such nanoparticle mediated delivery system, we examined the efficacy of dual drug-loaded, pH and thermo liable lipid coated mesoporous iron oxide-based magnetic nanoassemblies (DOX:TXL-LMMNA) in mice bearing both drug sensitive (A2780^S) and drug resistant (A2780-CisR) ovarian cancer tumor xenografts. In presence of an external AC magnetic field (ACMF), DOX:TXL-LMMNA particles disintegrate to release encapsulated drug due to hyperthermic temperatures (41-45 °C). *In vivo* bio distribution study utilizing the optical and magnetic properties of DOX:TXL-LMMNA particles demonstrated minimum organ specific toxicity. Noninvasive bioluminescence imaging of mice bearing A2780^S tumors and administered with DOX-TXL-LMMNA followed by the application of ACMF revealed 65% less luminescence signal and 80% mice showed complete tumor regression within eight days. A six months follow-up study revealed absence of relapse in 70% of the mice. Interestingly, the A2780-CisR tumors which did not respond to drug alone (DOX:TXL) showed 80% reduction in luminescence and tumor volume with DOX:TXL-LMMNA after thermo-chemotherapy within eight days. Cytotoxic effect of DOX:TXL-LMMNA particles was more pronounced in A2780-CisR cells than in their sensitive counterpart. Thus these novel stimuli sensitive nanoassemblies hold great promise for therapy resistant malignancies and future clinical applications.

Key words: Mesoporous magnetic nanoassembly, Dual drug carrier, Fluorescence and Bioluminescence imaging, Cisplatin resistance, Ovarian cancer xenografts, Combined thermo-chemotherapy effect.

1. Introduction

Cancer is one of the most fatal anomalies of human body whose cure is still a challenging task to the clinicians and scientists worldwide. Majority of the novel therapeutic strategies that were discovered and found to be effective against various malignancies in recent times fall short in treating radiation or chemo resistant diseases. Drug resistance is a multifactorial phenomenon comprising of abridged intracellular drug concentration, altered drug-target interaction, enhanced cell survival and defects in apoptotic pathways [1-3]. All these mechanisms may or may not be interdependent and hence pose a major road block to drug efficacy. This necessitates development of smarter treatment strategies, which will also be effective against therapy resistant malignancies. Nanoparticles based

multi-drug delivery systems promise to improve the efficacy, delivery and dose optimization over the existing chemotherapeutics in biomedical applications [1, 3-6]. Recent studies demonstrated that physico-chemical factors such as AC magnetic field, electric field, ultrasound, temperature and pH in combination with nano-carrier can act as triggers for chemotherapeutics release and exhibit synergistic effect on chemo-sensitive cancer [7-10]. Such strategy of combination therapy exhibits superior anti-tumor effects even against drug resistant tumor cells compared to photo/hyperthermia or chemo treatment alone [7]. However, efficacy of such stimuli sensitive nanoparticle mediated combination therapy on a chemoresistant cancer model is yet to be evaluated.

One of the major challenges in combined thermo-chemotherapy is to develop an efficient drug delivery system that amalgamates multiple drugs with controlled release, thereby increasing tumor regression capabilities [7, 11, 12]. It is challenging to integrate various requirements such as biocompatibility, good colloid stability, efficient multiple drug loading capacity and multi stimuli sensitivity for an ideal carrier molecule. An adjuvant externally applied AC magnetic field (ACMF) with superparamagnetic nanoassembly generates local hyperthermic temperature (41-45 °C) which enhances cellular permeability and retention effects (EPR). This improves the efficacy of drug accumulation at targeted lesions, decreases systemic toxicity, inducing apoptosis at the target tumor site synergistically [7, 8, 12-14]. Effect of such thermo-chemo therapy might become equally efficient against both sensitive and resistant tumors through targeting their biophysical characteristics.

Epithelial ovarian cancer is infamous for acquirement of resistance against the first line treatment regimen-cisplatin [15]. The current challenge lies in the management of platinum resistant ovarian tumor which is a leading cause of relapse and morbidity (5 year survival rate being 45%) [16]. Second line therapy involving paclitaxel, doxorubicin and etoposide drugs which produce significant toxicity and side effects, are the ultimate choice for these patients [17]. However, these drugs only increase overall survival without any significant increase in progression-free survival [17]. The lack of effective treatment modality against platinum resistant ovarian carcinoma thus till date remains an area of active research.

So far, there has been no study on the usage of magnetic nano-assemblies (which is an aggregation of single nanoparticles) for dual drug delivery as well as hyperthermia. These nano-assemblies have added advantages such as: higher magnetization, higher drug loading capacity for both hydrophilic and hydrophobic drugs and good colloidal stability in different solution over single nanoparticles.

Here, we report a smart pH- and thermo liable drug-delivery system that consists of a thin lipid layer with mesoporous magnetite nanoassemblies (LMMNA) as an effective therapeutic regimen against platinum resistant ovarian carcinoma. These nanoassemblies are capable of carrying and simultaneously delivering two anticancer drugs after suitable temperature or pH stimulation. As reported by us earlier, these LMMNA are characterized with high loading efficiency of hydrophilic doxorubicin hydrochloride (DOX) and hydrophobic paclitaxel (TXL) [18]. In the present study, cytotoxic effects of these particles were first tested in combination with hyperthermia against sensitive (A2780^S) and cisplatin-resistant (A2780-CisR) ovarian cancer cells. Interestingly, the particles produced higher lethality as compared to drug alone in A2780-CisR cells but not in A2780^S cells. Next these LMMNA have been explored as a dual drug delivery system (DOX:TXL-LMMNA) for *in vivo* bio distribution and thermo-chemotherapeutic effects in tumor bearing mice through fluorescence and bioluminescence imaging (Scheme 1). Bio distribution and long term effect of these non-targeted nanoparticles were studied in mice by optical fluorescence imaging, transmission electron microscopy (TEM) of tissues and by measuring the "Fe" concentrations of vital organs through ICP-AES and magnetic measurement. Real time monitoring of the combined thermo-chemotherapy with DOX:TXL-LMMNA particles by optical imaging showed significant decrease in bioluminescence signal and tumour volume in comparison to control group for both A2780^S and A2780-CisR tumor models. The efficacy was more pronounced in platinum resistant tumors as compared to drug alone treatment and in the sensitive tumors. Notably we did not observe any tumor relapse in 70% of the mice even after six months of completion of therapy. This is probably the first report and validation of a smart and stimuli sensitive magneto-nanoassembly system that shows enhanced toxicity against cisplatin resistant ovarian tumor xenografts using noninvasive optical imaging.

2. Experimental procedure

Preparation and characterization of DOX:TXL-LMMNA

MMNA and LMMNA preparation and characterization were described by us previously [18]. To load doxorubicin (Sigma Aldrich) into MMNA

particles, aquous solution of doxorubicin (500 µg/ml) was added to a suspension of 10 mg/ml of MMNA. Post overnight incubation, the DOX-MMNA were collected by centrifugation at 6720g for 10 min and stored at 4 °C for further experiments [18]. The concentration of unloaded drug in the supernatant was measured from the fluorescence spectra as described earlier. The percentage entrapment efficiency was calculated using the following calculation.

$$\% \text{ entrapment efficiency} = \frac{Ic - Sc}{Ic} \times 100; \qquad \ldots(1)$$

where *Ic* and *Sc* are the respective initial concentrations of the DOX added and the DOX content of the supernatant.

Further dual drug–loaded (DOX and TXL) LMMNA (DOX:TXL-LMMNA) were prepared by the thin film hydration method described earlier [18]. Briefly, 2 mg of preloaded DOX-MMNA (containing equivalent of 80 µg DOX) was added into the lipid mixture of DPPC, Chol. and DSPE-PEG$_{2000}$ in a 5:2:2 *w/w* ratio. For dual drug-encapsulated LMMNA, TXL (100 µg) was added concurrently to the synthesis of DOX-LMMNA. The encapsulation efficiency of DOX and TXL in LMMNA (labelled as DOX:TXL-LMMNA) was determined using UV-visible spectrophotometer (Super Aurius CE3021, Cecil Instruments, UK). The encapsulation efficiency and loading capacity of the drugs were calculated on the 5:2:2:2 *w/w* ratio of DOX:TXL-LMMNA with the initially added amount of the drug during the loading process using the following relations: (Eqn. 1) and,

$$\text{loading capacity} = \frac{\text{amount of drug incorporated in LMMNA (mg)}}{\text{LMMNA mass (mg)}};$$
$$\ldots(2)$$

Cell culture

A2780^S (human ovarian cancer cells) cell line was obtained from ATCC, USA. Cisplatin resistant counterpart for A2780 (A2780-CisR) was described earlier (Gaikwad et al. [19]). The cells were grown in Dulbecco's Modified Eagle's Medium (DMEM; HiMedia) supplemented with 10% fetal bovine serum (HiMedia) and 1% antibiotic antimycotic solution (HiMedia) in a humidified incubator at 37 °C, 5% CO_2. The resistant cells were maintained in 500 ng/ml of cisplatin.
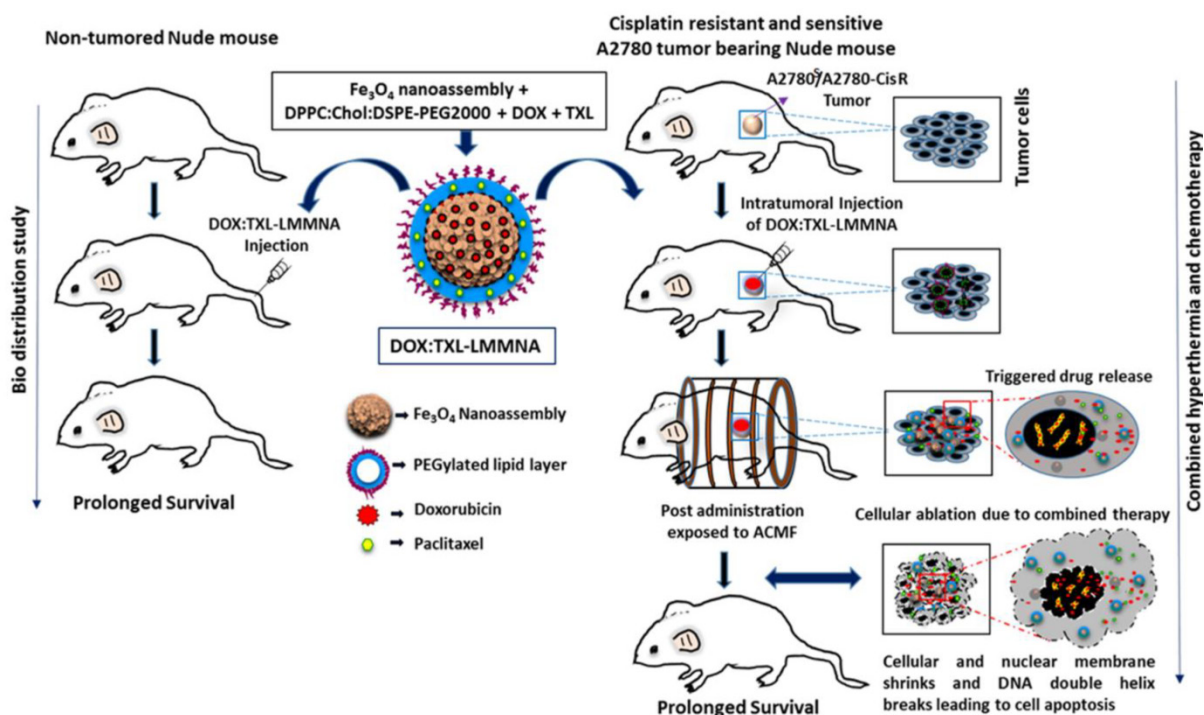
Scheme 1. Illustration of *in vivo* bio distribution in non-tumored mice and combined hyperthermia and chemotherapy with DOX:TXL-LMMNA as a dual drug delivery system on sensitive A2780^S and A2780-CisR tumor xenografts mice. The combination treatment of intratumoral injection of DOX:TXL-LMMNA along with ACMF leads to DNA damage as well as complete ablation of sensitive A2780^S and A2780-CisR cancerous tumor. This treatment ensures recovery and prolonged survival of tumor xenograft bearing mice as inferred by our investigation.

In vitro cytotoxicity measurement

The cytotoxicity of LMMNA, cisplatin (Sigma Aldrich), doxorubicin:paclitaxel (DOX:TXL) and DOX:TXL-LMMNA were assessed by Sulforhodamine-B assay for A2780^S and A2780-CisR cells. The cells were seeded into 96-well plates at 1 × 10^4 density per well overnight and incubated with defferent concentrations of LMMNA, cisplatin, DOX:TXL and DOX:TXL-LMMNA diluted in media for 24 h or 48 h. Cytotoxicity was assessed using Sulforhodamine-B (SRB, Sigma-Aldrich) assay as per manufacture's instruction and viability (%) was calculated using the following formula,

$$\% \text{ cell viability} = \frac{\text{absorbance of treated sample}}{\text{absorbance of control}} \times 100; \quad \ldots(3)$$

In vitro thermo-chemotherapy

For *in vitro* thermo-chemotherapy, 1 × 10^6 cells were seeded into 35 mm dish and treated with either DOX:TXL (40+30 µg/ml) or Cisplatin (5 µg/ml), LMMNA (1 mg/ml), or DOX:TXL-LMMNA (0.5 and 1 mg/ml) for 1 h. Simultaneously, another set of cells treated with LMMNA and DOX:TXL-LMMNA were kept under ACMF for 20 min at 376 Oe (250 kHz). Following this treatment cycle, all cells were incubated at 37 °C for 24 h, washed thrice with PBS and harvested by trypsinization. The percentage viability after different treatments was determined using trypan blue dye exclusion assay [20]. For quantification of apoptotic population, trypsinized cells were stained with Propidium Iodide (PI) as described earlier [18] and a minimum 10,000 events were recorded using flow cytometry (BD FACSCalibur) and analyzed by Motif software to determine the percentage of apoptotic population.

Fluorescent imaging of in vivo bio distribution of DOX:TXL-LMMNA particles

All animal experimentations were performed as per approval of the Institutional Animal Ethics Committee of Advanced Centre for Treatment, Research and Education in Cancer (ACTREC). Female BALB/c NUDE (6–8 weeks old) mice were used for bio distribution study of DOX:TXL-LMMNA. Utilizing the fluorescent properties of Doxorubicin entrapped into DOX:TXL-LMMNA biodistribution study was performed in real time for six time points (Day 0, Day 1, Day 2, Day 7, Day 30 and Day 60) (n=5 for each group) by *in vivo* fluorescent imaging with IVIS imaging system (see ESI Table S1). All these mice except the control ones were injected with 50 mg/kg of DOX:TXL-LMMNA (in 70 µl of sterile PBS) either by intra-peritoneal or intra-venous injections. The mice were anesthetized using isoflurane and whole body fluorescence spectra was acquired pre and post particle administration [21, 22]. Fluorescence spectra from each mice image was spectrally unmixed and analyzed using Live Imaging Software, 4.0. At the end of each imaging experiment, mice were sacrificed for organ specific iron content measurement.

ICP-AES, and magnetization properties of residual particles in organ

Iron quantity of LMMNA accumulated in different organs from bio distribution and thermo-chemotherapy studies was determined by ICP-AES and magnetization measurement. All the tissues were collected, fixed with 10% formaldehyde solution for overnight and were vacuum-dried for 2 days at 50 °C and then crushed to obtain powder. The mixed powder was used for magnetization measurements at room temperature using a superconducting quantum interference device (SQUID) magnetometer (MPMS). For ICP-AES analysis, powder samples were dissolved thoroughly in concentrated hydrochloric acid and filtered through filter paper to determine the iron concentration in different organs [23, 24].

TEM analysis of different organs

The vital organs harvested from control or treated mice were collected at different time points and fixed with 1 ml of 2.5% glutaraldehyde for 1 h at room temperature. The small portion of tissues were rinsed thrice with PBS and treated with 100 µl of 1% osmium tetroxide solution for 1 h and dehydrated with different ratios of alcohol. The tissues were then fixed in a 50:50 mixture of propylene oxide and resin overnight. Ultrathin sections were prepared from tissue embedded resin mold and placed on a copper grid for TEM analysis [22].

Table 1: Represent the level of "Fe" content in different organs pre and post administration of DOX:TXL-LMMNA at different time poionts.

Organs	Day 0	Day 1	Day 7	Day 60
Spleen	~ 0.1%	~ 16%	~ 17%	~ 0.4%
Lung	~ 1%	~ 12%	~ 13%	~ 0.9%

Bioluminescence imaging of A2780^S and A2780-CisR tumor xenografts

Animal care and euthanasia were performed with the approval from Institutional Animal Ethics Committee of ACTREC. Mice were implanted with 7 × 10^6 cells of either A2780^S or A2780-CisR stably expressing bi-fusion reporter (firefly luciferase-tandom tomato red (*fl2-tdt*)) and tumors were allowed to grow till 5-8 mm. For estimating anti-tumor activity of DOX:TXL-LMMNA nanoassembly, mice (n=15) were divided into three groups: I) untreated II) injected with DOX:TXL-LMMNA (50 mg/kg of DOX:TXL-LMMNA) (once intratumorally) without ACMF and III) injected with DOX:TXL-LMMNA and treated with ACMF (see ESI Table S2). For ACMF treatment, mice were anaesthetized with avertin (150 mg/kg mice weight) and subjected to ACMF at 376 Oe, 250 kHz (hyperthermia double dose: 1st dose at 0 h and 2nd dose at 24 h) by placing them into the 6 cm coil. The temperature of tumor surface was measured with an alcohol thermometer (Paico deluxe) at different time points. Whole body bioluminescence imaging of mice using IVIS-Spectrum optical imager was obtained after intra-peritoneal injection of 100 µl D-luciferin (0.4 mg/mouse) diluted in phosphate-buffered saline. Region of Interests (ROIs) were drawn over the tumors and quantified by using the Live Image (4.4) software. Bioluminescence signals were recorded as maximum (photons/s/cm^2/sr). The volume of the tumors and body weights were recorded and compared across the groups. The tumor volume was calculated using the following formula [24, 25]:

$$Tumor\ volume = \frac{1}{2}(length \times width^2) \qquad ...(4)$$

After completion of imaging experiments, mice from all groups (group I, II and III) were sacrificed at Day 7 and organs, namely, the large intestine, small intestine, lung, liver, spleen, heart, kidney, stomach, brain, tumor, and normal skin were collected and preserved in 10% formalin to determine the amount of "Fe". Toxicity was evaluated by measuring the total body weight and weights of all the organs before proceeding for preservation [23]. For the follow up study, mice with completely regressed tumors were kept for six months and monitored for physical appearance of tumor mass.

For the resistant tumor xenograft study, A2780-CisR cells were implanted at two sites per mouse and tumors were allowed to grow till 5-8 mm. A2780-CisR-tumor-bearing mice were divided into four major groups (n=5) according to treatment modality, that is, I) cisplatin (3.5 mg/kg), II) DOX:TXL (3.5 mg/kg), III) LMMNA and IV)

DOX:TXL-LMMNA (see ESI Table S3). Each of these groups was treated with intra-tumoral injection of respective therapy regiment and tumor growth kinetics was measured by bioluminescence imaging and tumor volume.

Immunofluorescence studies and H&E staining

Immunofluorescence studies were performed as described earlier (Gaikwad et al. [19]). Briefly, cells seeded on coverslips were fixed with 4% paraformaldehyde, permeabilized with 0.025% Triton-X and probed with γH2.X antibody for overnight at 4 °C. Next day, after two hours of incubation with secondary antibody, cells were counterstained with DAPI and images were observed under Carl Zeiss, LSM 710 microscope. At least 50 cells were analysed from each group. Hematoxylin & eosin (H & E) staining was performed according to standard procedure on tissue sections.

Statistical analysis

Each experiment was carried out in triplicate at least three different times. The data are expressed as mean ± standard deviation (SD). The statistical analysis was determined by an unpaired two-tailed T-test using GraphPad Prism 6 software. The significant differences between the values are denoted as follows: $p < 0.05$ (denoted *****), $p < 0.01$ (denoted ******) and $p < 0.001$ (denoted *******).

3. Results and discussion

Characterization of DOX:TXL-LMMNA particles

Detailed characterisation and size distribution of MMNA and LMMNA particles were already reported in our earlier study [18]. Briefly, TEM images demostrated spherical structure of MMNA with a diameter of 73 nm which after coating (LMMNA) increased to 92 nm (as demonstrated in our pevious study), (see ESI Figure S1) [18]. The hydrodynamic diameter of LMMNA did not alter significantly (157 nm vs. 159 nm) when measured in PBS or serum-supplemented growth medium (DMEM) using dynamic light scattering (DLS) (see ESI Figure S2). This result indicated that LMMNA provide good suspension stability in PBS as well as in DMEM. A stable and consistant magnetic properties of these particles were also confirmed by VSM (evaluated in our previous report and data not shown) [18]. We also reported that DOX:TXL-LMMNA particles are able to release higher amount of DOX (~88%) and TXL (~53%) in the acidic media (pH 4.3) compared to ~28% of DOX and 26% of TXL at neutral condition (pH 7.4) over a period of 172 h. These DOX:TXL-LMMNA also show temperature dependent increased drug

discharge where ~23% of DOX and ~32% of TXL were released at 43 °C as compared to ~18% of DOX and ~21% of TXL at 37 °C [18]. For the current *in vivo* study, the loading efficiency of DOX and TXL was determined to be 81±2 and 60±3% and the loading capacity were 0.04±0.0004 and 0.03±0.0018 mg/mg at 5:2:2:2 ratio of LMNNA, respectively (ESI Figure S3).

Effect of combined thermo-chemotherapy *in vitro* on A2780^S cells

The cytotoxic effect of the combined thermo-chemotherapy was evaluated on A2780^S cells using dye exclusion assay as indicated in Figure 1. Administration of ACMF field decreased viability of A2780^S cells (86±2.57% to 48±0.41%) after LMMNA treatment (Figure 1A). Interestingly, dual drug loaded with DOX:TXL-LMMNA (0.5 mg/ml) nanoassembly

demonstrated a significant decrease in viability (21.6±1%) compared to LMMNA+ACMF treatment (48±0.41%) (p < 0.001). Similarly, administration of higher dosage of DOX:TXL-LMMNA (1 mg/ml) showed further decrease in cell viability (6±0.3%) in these cells. These high doses of drug loaded particles were particularly chosen to mimic the *in vivo* dose condition where maximal magnetization was observed earlier [18]. DOX alone treatment (40 µg/ml) showed cellular viability of 34.5±4.5% compared to the control. Treatment of free DOX:TXL showed an increased cytotoxicity in dose dependent manner where cell viability decreased form 17±2.9% to 7.2±0.26% at a concentration of 35 and 70 µg/ml respectively. However, toxicity exerted by the free drugs were 5-7% more severe than the DOX:TXL-LMMNA particles. Both 35 and 70 µg/ml
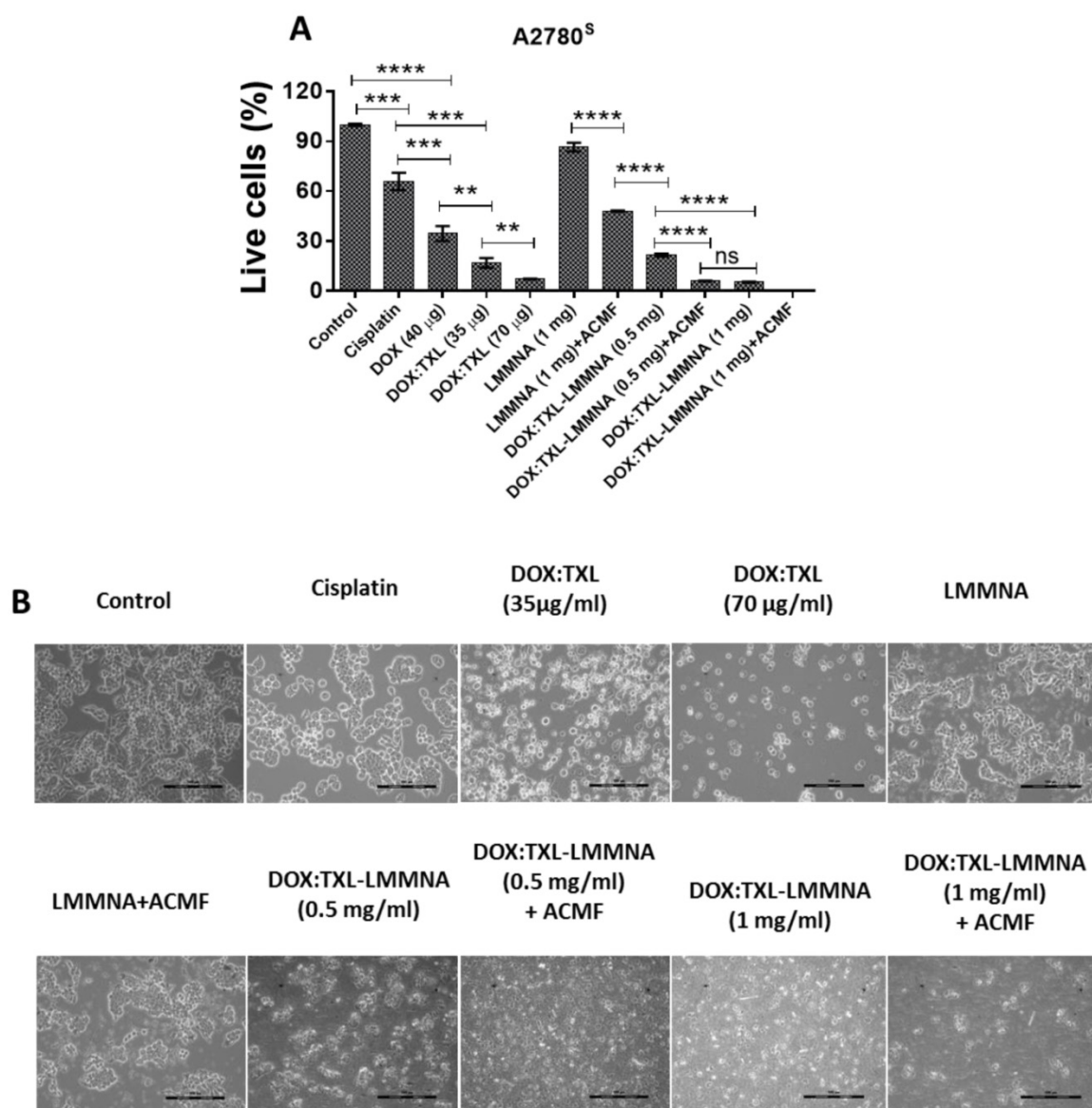

Figure 1. *In vitro* thermo-chemotherapy study on A2780^S cell line post 24 h of treatment. (A) Percent live cell count and (B) cellular morphology changes by optical microscopy after indicated treatment to A2780^S cells. Data expressed as mean ± SD (n=3). Significance is denoted as ** p < 0.01, *** p < 0.001 and **** p < 0.0001 and *ns* as no significance. Scale bar 100 µm.

concentration of free DOX:TXL correspond to drug loaded into 0.5 and 1 mg/ml of DOX:TXL-LMMNA respectively. ACMF administration to DOX:TXL-LMMNA (both at 0.5 and 1 mg/ml) further decreased viability from 21±1% to 6±0.3% and 5.4±0.3 to 0%, respectively. These observations indicate that hyperthermia induced by ACMF field improves efficacy of heat sensitive DOX:TXL-LMMNA in A2780^S cells. This improved drug efficacy can be due to enhanced uptake and accumulation of intracellular DOX:TXL from temperature induced hyper-permeability of the cell membrane and DNA damage [8, 13, 14, 26, 27]. Additionally, microscopic examination revealed drastic changes in cellular morphology when A2780^S cells were treated with DOX:TXL-LMMNA+ACMF compared to either treatment alone (Figure 1B). The rounded appearance of the cells subjected to all treatments including DOX:TXL, LMMNA+ACMF, DOX:TXL-LMMNA with/without ACMF (at 0.5-1 mg/ml) were indicative of cell apoptosis. Further, apoptosis induction in these cells were quantified using PI staining. Cells treated with LMMNA and DOX:TXL-LMMNA in presence of ACMF showed higher percentage of apoptotic cells (13% and 38%) compared to absence of ACMF for both LMMNA (~0.45%) and DOX:TXL-LMMNA (~21%) treatment (ESI page 7).

In vivo bio distribution of DOX:TXL-LMMNA

In order to evaluate the toxicity of DOX:TXL-LMMNA *in vivo*, overall growth and tissue bio distribution were investigated in NUDE mice. DOX:TXL-conjugated LMMNA offers an added advantage of fluorescence property of doxorubicin which can be imaged in *in vivo* [14, 28] and therefore both non-invasive fluorescence imaging and ICP-AES analysis of tissue homogenates were utilized to monitor the kinetics of distribution and retention properties of these particles. As shown in Figure 2A, higher fluorescence signal demonstrated the presence of non-targeted DOX:TXL-LMMNA mainly in the abdominal area immediately after intra-peritoneal or intra-venous injection. On second day, fluorescence signal was observed from all over the body in the mice which were subjected to intravenous injection. In contrast, intraperitoneal injection of the particles showed a localized (abdominal) signal indicating a lower/slower distribution rate. The signals remained stabilized for 7 days and decreased with time and completely disappeared by Day 60. This indicates that DOX:TXL-LMMNA are cleared from NUDE mice over a period of 60 days.

The organ-specific retention of DOX:TXL-LMMNA was estimated by measuring 'Fe' content in different organs through ICP-AES analysis.

Corroborating to our non-invasive fluorescence bio distribution studies, increased 'Fe' level was observed in all organs except skin and brain tissue post 24 h DOX:TXL-LMMNA administration (Figure 2(B & C)). Interestingly, intra-venous administration showed relatively higher 'Fe' content in spleen, stomach and heart compared to intra-peritoneal administration of DOX:TXL-LMMNA (Figure 2C). No significant difference was observed in iron retention for other organs based on route of administration. Iron content in all tissues remained stable till Day 7 and then decreased over time for both intra-venous and intra-peritoneal mode of administration. This data was also corroborated with magnetization properties of these particles measured from each organ. The highest magnetization value of all organs based on the amount of "Fe" concentration was obtained with M-H loop (see ESI Figure S4). As shown in Figure 2D, the highest magnetization values were obtained from the large intestine (0.03±0.004 emu/g), lung (0.03±0.004 emu/g), spleen (0.06±0.011 emu/g), liver (0.012±0.001 emu/g) and kidney (0.03±0.002 emu/g) till Day 7, which decreased gradually over a period of 60 days indicating both hepatobiliary and renal excretion mode of clearance. The accumulation of "Fe" in the small intestine, kidney, stomach, and the heart were found to be minimal at Day 60. As shown in Figure 2E, no significant differences were observed in the organ weight profile between control and DOX:TXL-LMMNA treated mice except for large intestine and the mice did not show any discomfort or any overt clinical signs of toxicity.

In vivo disassembly of DOX:TXL-LMMNA in different organs

Spontaneous disassembly of DOX:TXL-LMMNA is required to avoid toxicity and clearance from body. Since our bio-distribution data indicated maximal accumulation of DOX:TXL-LMMNA in spleen and lung, TEM analysis was performed to confirm particle integrity. As shown in Figure 3B & C, intact DOX:TXL-LMMNA were found at Day 1. By Day 7 (Figure 3D & E), most of these assemblies were disintegrated and very few of them retained their original morphology. In addition, localization of nanoassemblies inside the tissue by Day 7 can also be confirmed in the ESI Figure S5. Further these particles were cleared out from the spleen and the lung as TEM analysis did not detect presence of these particles by Day 60 (Figure 3F). As shown in Table 1, percent weight accumulation of 'Fe' gradually decreased over a period of 60 days in the spleen and lung tissues. Thus we believe that these nanoassemblies undergo spontaneous degradation which facilitates their clearance from the organs over time.
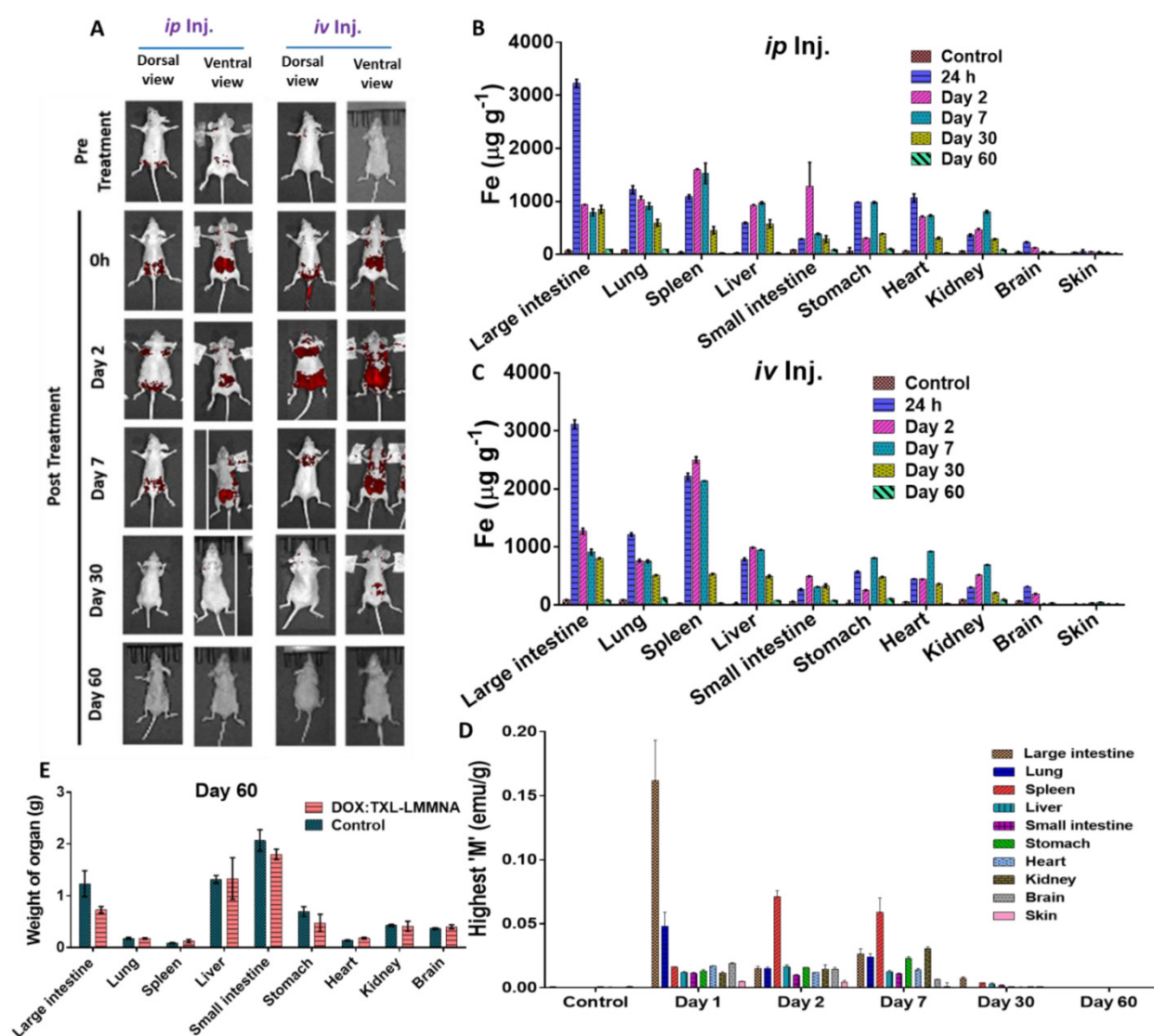
Figure 2. *In vivo* bio distribution and clearance of DOX:TXL-LMMNA post intra-venous (iv) and intra-peritoneal (ip) administration in female NUDE mice (n=5). (A) Representative whole body fluorescence imaging of DOX:TXL-LMMNA bio distribution over a period of 2 months. (Red color represents the spectrally unmixed fluorescence signal of the DOX at 580 nm). A gradual reduction in the fluorescence intensity indicates disintegration and excretion of the nanoparticles by the hepatobiliary route. (B & C) Iron content 'Fe' (µg/g) of each organ tissue post DOX:TXL-LMMNA administration as determined by ICP-AES analysis at various time points. (D) Highest magnetization values of vital organ tissues at various time points and (E) Comparison between organ tissue weights of the treated and untreated mice at Day 60.
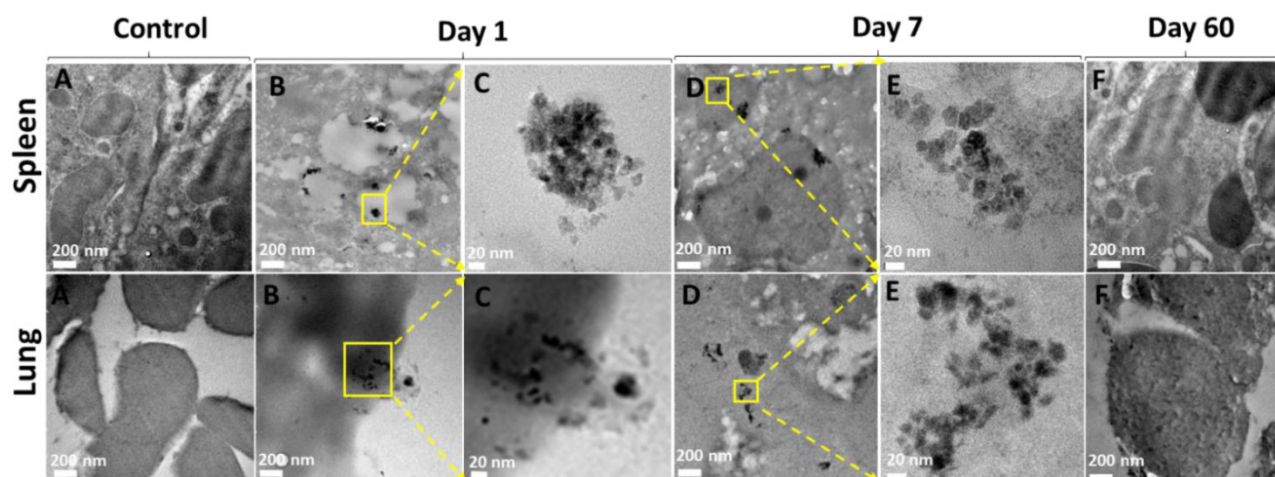
Figure 3. TEM images of uptake and accumulation of nanoparticles in spleen and lung tissues after Day 1, Day 7 and Day 60 treatment. Column (A) untreated spleen and lung tissue, column (B) both tissues show morphology with accumulation of LMMNA after Day 1, column (C) magnified image of the area indicated by the yellow box in column (B), column (D) shows morphology with accumulation of LMMNA after Day 1, column (E) magnified image of column (D) marked as yellow box, showing the nanoassemblies into tissue at Day 7, column (F) shows tissues morphology at Day 60 which is similar to the untreated control column.
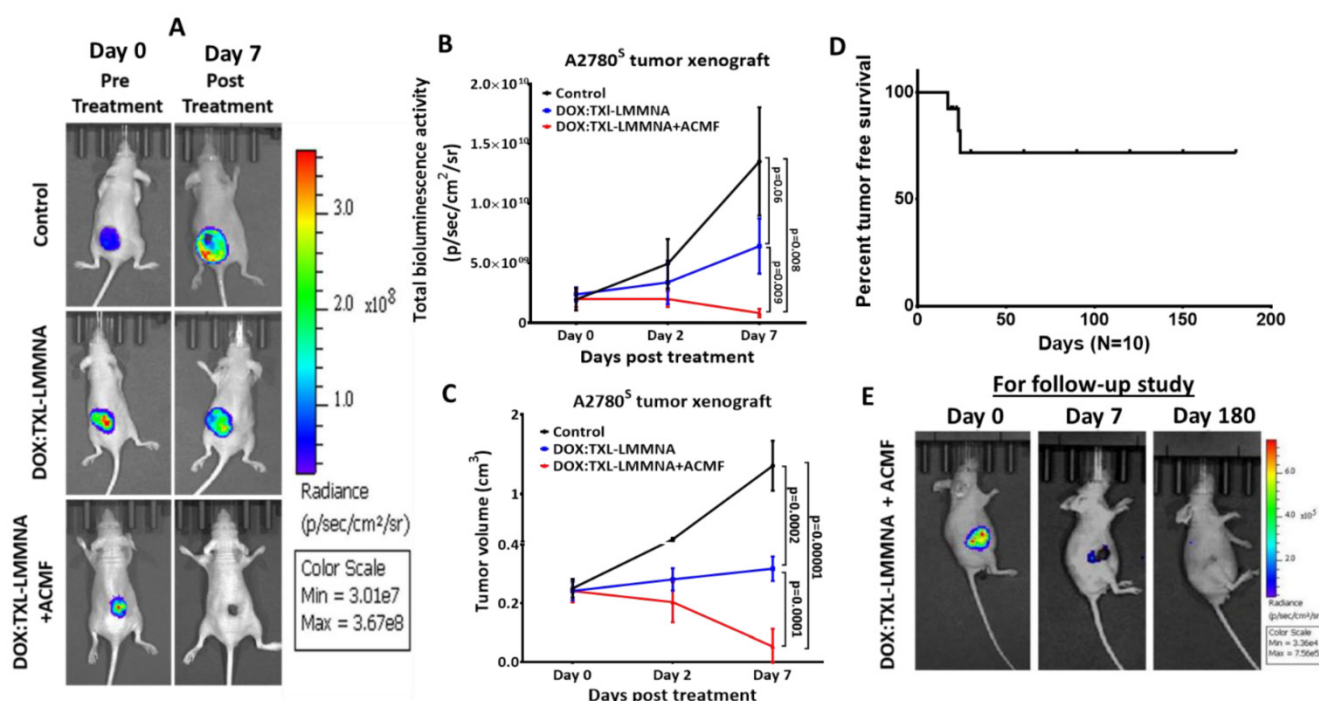
Figure 4. *In vivo* combined therapy using 1 mg of DOX:TXL-LMMNA in mice bearing A2780^S tumor xenografts (n=5). Tumor regression was monitored by bioluminescence imaging in the absence/presence of ACMF at 376 Oe, 250 kHz frequency on the A2780^S tumor xenografts after intratumoral injections. (A) Representative bioluminescence images of *in vivo* combined therapy evaluation against A2780^S tumor xenografts. (B) Graphical quantification of bioluminescence signal showed significant decrease in bioluminescence of tumor post DOX:TXL-LMMNA compare to control by Day 7 on A2780^S tumor xenografts (significance difference indicates as p= 0.06, p= 0.009 and p= 0.008). (C) Tumor volume measurement of A2780^S tumor xenografts showed decrease in tumor volume post DOX:TXL-LMMNA with and without treatment of ACMF at different time points (significance difference indicates as p= 0.0002, p= 0.0001 and p= 0.00001). (D) Kaplan-Meier survival curve for the tumor free survival of mice treated with DOX:TXL-LMMNA+ACMF combined therapy (A2780^S tumor). (E) Representative bioluminescence imaging for 6 month follow-up study of DOX:TXL-LMMNA+ACMF treatment on mice bearing A2780^S tumor xenografts.

In vivo therapeutic efficacy of DOX:TXL-LMMNA on A2780 ^{S} tumor xenografts

To study the anticancer activity of DOX:TXL-LMMNA in combination with ACMF, mice carrying A2780^S tumor xenografts were injected with the particles and subjected to ACMF treatment. Administration of DOX:TXL-LMMNA increased the temperature of the tumor surface up to 41±0.25 °C within 15 min and remained constant over time (ESI Figure S6). For group III animals (as mentioned in method section), ACMF was given twice for 20 min within 48 h after single dose of DOX:TXL-LMMNA injection. Our study revealed a significant reduction in tumor bioluminescence signal for group III by 0.34 ± 0.18 fold change (from $2.26\times10^9 \pm 2.39\times10^9$ to $7.7\times10^8 \pm 1.3\times10^9$ p/sec/cm^2/sr) as compared to group I (from $3.46\times10^9 \pm 3.37\times10^9$ to $3.13\times10^{10} \pm 3.37\times10^{10}$ p/sec/cm^2/sr, 8.7 ± 1.25 fold change) (p= 0.002) or group II (from $4.65\times10^9 \pm 5.17\times10^9$ to $2.46\times10^{10} \pm 4.1 \times 10^{10}$ p/sec/cm^2/sr, 4.15±2.61 fold change) (p= 0.0068) animals (Figure 4A & B). This was also corroborated with tumor volume where in group III, all animals except one showed complete tumor regression (0.2±0.21 fold change) compared to the control (group I) and only DOX:TXL-LMMNA treated animals

(group II) showed a fold change of 5.4±0.7 and 1.32±0.03 in tumor volume respectively (Figure 4C).

To monitor long term potential of these particles, mice (n=10) showing complete tumor regression were followed upto 6 months. As shown in Figure 4D, only 3 out of 10 mice showed relapse while the rest did not show any palpable tumors. Bio luminescence imaging of these mice (with no relapse) after 6 months also did not show any signal indicating complete absence of viable tumor cells (Figure 4E). All these data indicate a remarkable potential of these magnetic nanoparticles containing very low doses of drugs to effectively kill tumor cells. The possible mechanism involves hyperthermia induced enhanced permeability of the cell membrane through ACMF, and higher accumulation of drugs in the tumor site [8, 13, 14].

DOX:TXL-LMMNA particle retention in the different organs post thermo-chemotherapy

In order to understand the effect of ACMF on the organ specific retention of DOX:TXL-LMMNA nanoassembly, iron content of each organ was estimated using ICP-AES analysis at Day 7. As shown in Figure 5A, no significant alteration in organ specific accumulation was observed post application of ACMF except for tumor tissue. Low level 'Fe' accumulation in tumor tissues explains disassembly

of these nanoparticles after ACMF exposure, suggesting site specific drug release at the tumor site for the DOX:TXL-LMMNA+ACMF treatment group, in comparison to the DOX:TXL-LMMNA treatment group (Figure 5A). As an additional validation for disassembly of DOX:TXL-LMMNA in tumors, assessment of magnetization properties and fluorescence imaging were performed in absence/presence of ACMF at the end of Day 7. Higher magnetization values were observed in tumors treated with DOX:TXL-LMMNA (0.4±0.04 emu/g) as compared to DOX:TXL-LMMNA+ACMF (0.02±0.003 emu/g) treatment (ESI Figure S7A).

Fluorescence signal in DOX:TXL-LMMNA+ACMF treated mice completely disappeared in comparison to DOX:TXL-LMMNA treated mice at Day 7 (ESI Figure S7B). These results confirm occurrence of rapid disintegration of nanoassemblies under the action of ACMF. For both DOX:TXL-LMMNA and DOX:TXL-LMMNA+ACMF conditions, higher accumulation of "Fe" was observed in lung, spleen and liver compared to other organs at Day 7. In order to understand the toxic effects of these particles, all organs collected from the three groups of animals were weighed.
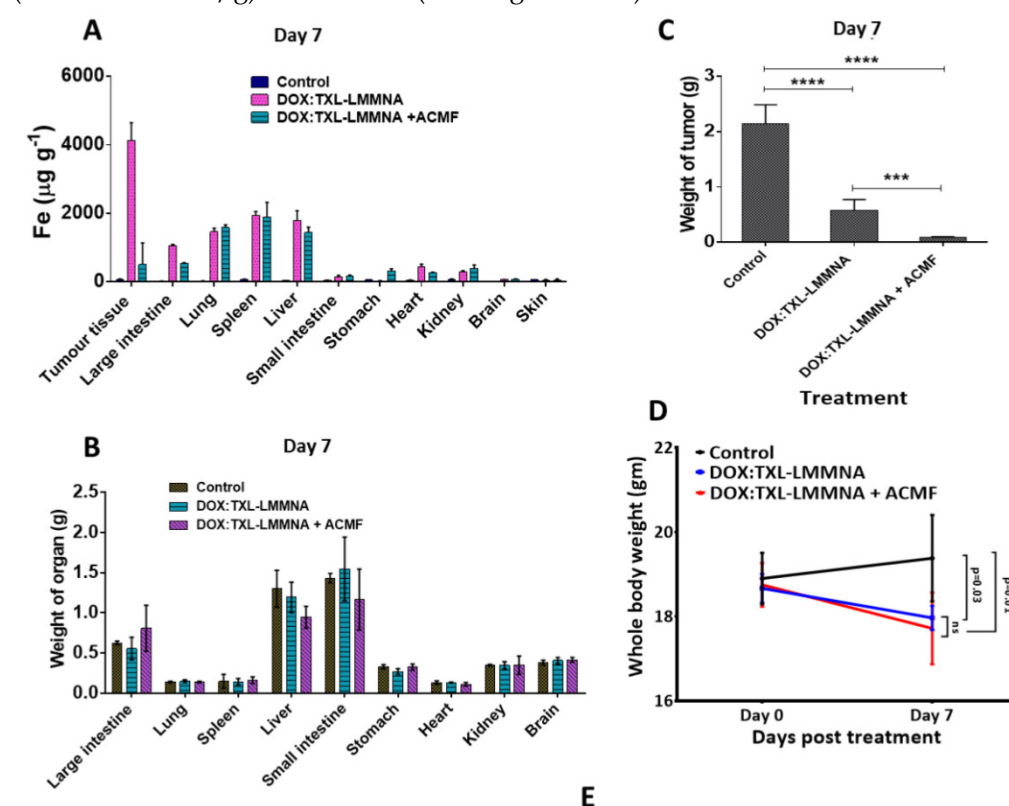
Figure 5. *In vivo* cytotoxicity studies using 1 mg of DOX:TXL-LMMNA in the absence/presence of ACMF at Day 7 in the A2780^S sensitive tumor xenograft bearing NUDE mice. (A) Quantitative estimation of the 'Fe' from different organs of the mice at Day 7. (B) Measurement of weight of all organs after treatment at Day 7. (C) Graphical representation of the tumor weight showed decreases tumor weight after combined therapy at Day 7. (D) Whole body weight of mice treated with DOX:TXL-LMMNA decreases due regression of tumor post therapy. (Significance difference indicates as p= 0.03, p= 0.01 and *ns* as no significance). (E) Histological analysis of tumor tissue using DOX:TXL-LMMNA in the absence/presence of ACMF. All sections stained with Hematoxylin & Eosin (H & E). DOX:TXL-LMMNA treated tumor section shows necrotic lesion which increases in the tumor tissue treated with DOX:TXL-LMMNA+ACMF. Yellow star indicate necrotic cells whereas red arrow indicate immune-associated cells in the tumor sections. Significance is denoted as *** p < 0.001 and **** p < 0.0001 and *ns* as no significance.
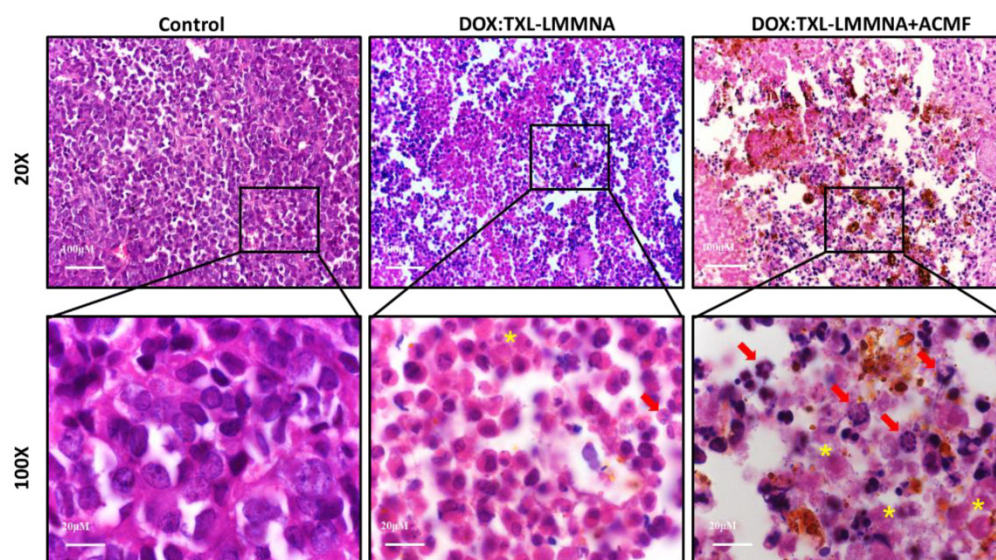
As shown in Figure 5B, no significant difference was observed in the organ weights among each group. A significant decrease in the total tumor weight from Day 0 to Day 7 was observed for group II-DOX:TXL-LMMNA (0.6±0.2 fold) animals compared to the control group (increased by 2±0.4 fold) (Figure 5C). The slight increase in total body weight in control group from Day 0 (19±1)g to Day 7 (20±1)g was possibly resulted from increased tumor volume. In contrast, in mice treated with DOX:TXL-LMMNA and DOX:TXL-LMMNA+ACMF, slight decline in body weights were observed (18±0.5)g and (17±1)g at Day 7 in comparison (~(19±0.6)g and (18±1)g) at Day 0 (Figure 5D). This data was also corroborated with histopathological analysis of H & E stained tumor tissue sections from control mice and mice treated with DOX:TXL-LMMNA and DOX:TXL-LMMNA+ACMF. As shown in Figure 5E, the control tumor tissue section did not show any noticeable inflammatory or necrotic lesion. However, the DOX:TXL-LMMNA treated tumor tissue sections showed various necrosis lesions (shown with yellow star), degree of which increased post ACMF treatment. Interestingly, tumor treated with DOX:TXL-LMMNA showed increased immune-associated cells indicating inflammatory response (shown with red arrow in Figure 5E). This inflammatory response escalated after ACMF application in combination with DOX:TXL-LMMNA treatment. Thus altogether our data suggest that this thermo-chemo combined therapy with drug loaded smart nanoparticle is able to exert complete regression of tumors without any toxic effect on the vital organs of mice.

In vitro cytotoxicity assay of DOX:TXL-LMMNA on cisplatin resistant cell line A2780-CisR

Development of resistance towards the first line chemotherapy (platinum and taxol based drugs) is a serious problem for epithelial ovarian cancer patients and no alternate therapy has shown success in the relapse setting. *In vitro* cytotoxicity of DOX:TXL-LMMNA was previously reported with various sensitive cell lines across different cancer types (HeLa, MCF-7 and HepG2 cells) respectively. The viability of HeLa, MCF-7 and HepG2 cells were observed to be ~41±1%, ~40±1% and ~44±2% respectively [18]. In order to evaluate the effect of these magnetic nanoparticles on cisplatin resistant (A2780-CisR) ovarian cancer cell line, both A2780^S and A2780-CisR cells were treated with LMMNA, cisplatin, doxorubicin+paclitaxel (DOX:TXL) and DOX:TXL-LMMNA and cytotoxicity were estimated post 24 and 48 h of treatment. While the A2780^S cells

exhibited ~69±1% and ~38±4% viability at 24 and 48 h respectively (Figure 6A & C), A2780-CisR cells demonstrated more than 90% viability post 24 and 48 h of treatment, (Figure 6B & D) when treated with 5 µg/ml of cisplatin. However, both these cells showed 90% viability when incubated with 1 mg/ml of LMMNA upto 48 h indicating good biocompatibility. This again suggested the non-toxic nature of LMMNA particles. Further, to determine the anticancer effect of DOX:TXL-LMMNA, 1 mg/ml (correspond to 40 and 30 µg/ml concentration of DOX and TXL respectively) particles and similar amount of free drugs were added to A2780^S and A2780-CisR cells for 24 and 48 h. In presence of particles, both A2780^S and A2780-CisR cells exhibited cell viability upto 9±0.5% at 24 h and 4±0.4% at 48 h and 12±2% at 24 h and 8±1% at 48 h respectively. Though A2780-CisR cells are resistant towards cisplatin, they showed sensitivity to free DOX:TXL drugs with 37±1% and 30±2% viability (24 h and 48 h respectively) compared to 12.2±1.7% and 8.6±1.2% viability in sensitive cells. Interestingly, in presence of DOX:TXL-LMMNA particles, the A2780-CisR cells exhibited significantly higher cell death (36%) compared to the free DOX:TXL treatment. Altered pH gradient and increased lysosomal compartmentalization of chemotherapeutic agents are known to induce drug resistance in cancer cells [31-34]. The drug loaded nanoassemblies have shown to accumulate in the lysosomal compartment of cells after endocytosis [18]. Thus this hypersenstivity of drug resistant cells towards the nanoparticles might be due to highly acidic lysosomal milieu which is a known feature of drug resistant cells.

Effect of combined thermo-chemotherapy on cisplatin resistant A2780-CisR cells

Next the cytotoxic effect of combined thermo-chemotherapy with 0.5 and 1 mg/ml concentrations of DOX:TXL-LMMNA was evaluated in A2780-CisR cells for 24 h. The viability of resistant cells significantly reduced from 87±3.2 (treated with 1 mg/ml of LMMNA in absence of ACMF) to 50±3.4% (p < 0.001) after LMMNA+ACMF treatment (Figure 7A). Further, we observed that the viability was significantly decreased in a concentration-dependent manner of DOX:TXL-LMMNA (0.5 and 1 mg/ml) from 21 to 4.3% (p < 0.01) in the absence of ACMF. Administration of free DOX:TXL (at a concentration of 35 and 70 µg/ml) treatment showed that the cell viability decreased to 56.6±3.3% and 33±4% (p < 0.01) respectively, while DOX alone treatment at concentration of 40 µg/ml showed 69.1±4.3% cell viability. However, this sensitizing effect was observed in case of free DOX alone and DOX:TXL treatment and not with cisplatin (at 70 µg/ml)

treatment (87±2.3%) in A2780-CisR cells. Interestingly, when ACMF (for 20 min at 376 Oe, 250 kHz) was applied to cells treated with DOX:TXL-LMMNA+ ACMF (0.5 mg/ml) a significant reduction in viability (4.7±1.5%) was observed compared to only DOX:TXL-LMMNA treatment (21±4.2%) (p < 0.01). Similarly, ACMF application to cells incubated with 1 mg/ml of DOX:TXL-LMMNA decreased viability from 4.3±3.8% to 0% respectively. These results suggested that hyperthermia treatment with heat sensitive DOX:TXL-LMMNA enhanced the cytotoxic effect in A2780-CisR cells. More interestingly, the combined hyperthermia and chemotherapy can enhance the DNA damage and destroy the cell membrane in A2780-CisR and A2780^S cells [18]. Significant morphological changes of cells occur when

A2780-CisR was treated with DOX:TXL-LMMNA+ ACMF compared to either treatment alone as shown in Figure 7B. Administration of DOX:TXL, LMMNA+ACMF, DOX:TXL-LMMNA with/without ACMF (at 0.5-1 mg/ml) showed the typical round morphology of apoptotic cells. Further, cells undergoing apoptosis were quantified using PI staining post respective treatments (see ESI Figure S8). Similar to A2780^S cells, A2780-CisR cells also showed higher apoptotic population in presence of ACMF after treatment with LMMNA or DOX:TXL-LMMNA (11% and 33%, respectively) compared to LMMNA or DOX:TXL-LMMNA treatment in absence of ACMF (0.2% and 20% respectively).
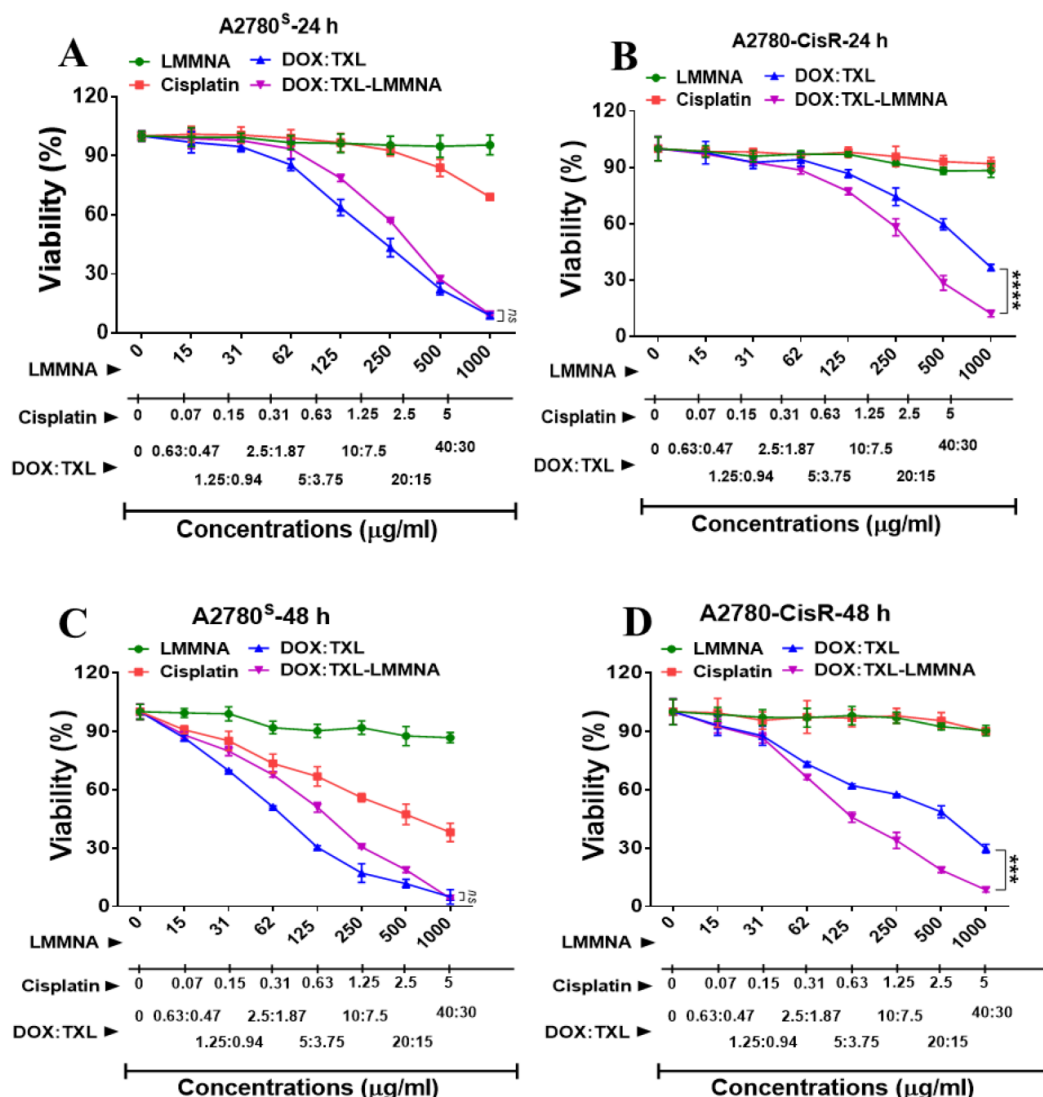
Figure 6. Time dependent *in vitro* cytotoxicity effect of LMMNA, free cisplatin, free DOX:TXL and DOX:TXL-LMMNA upto 1 mg/ml with different drug contents (A & B) at 24 h and (C & D) at 48 h on A2780^S and A2780-CisR cells. Data expressed as mean ± SD (n=3). Significance is denoted as *** p < 0.001 and **** p < 0.0001 and *ns* as no significance.
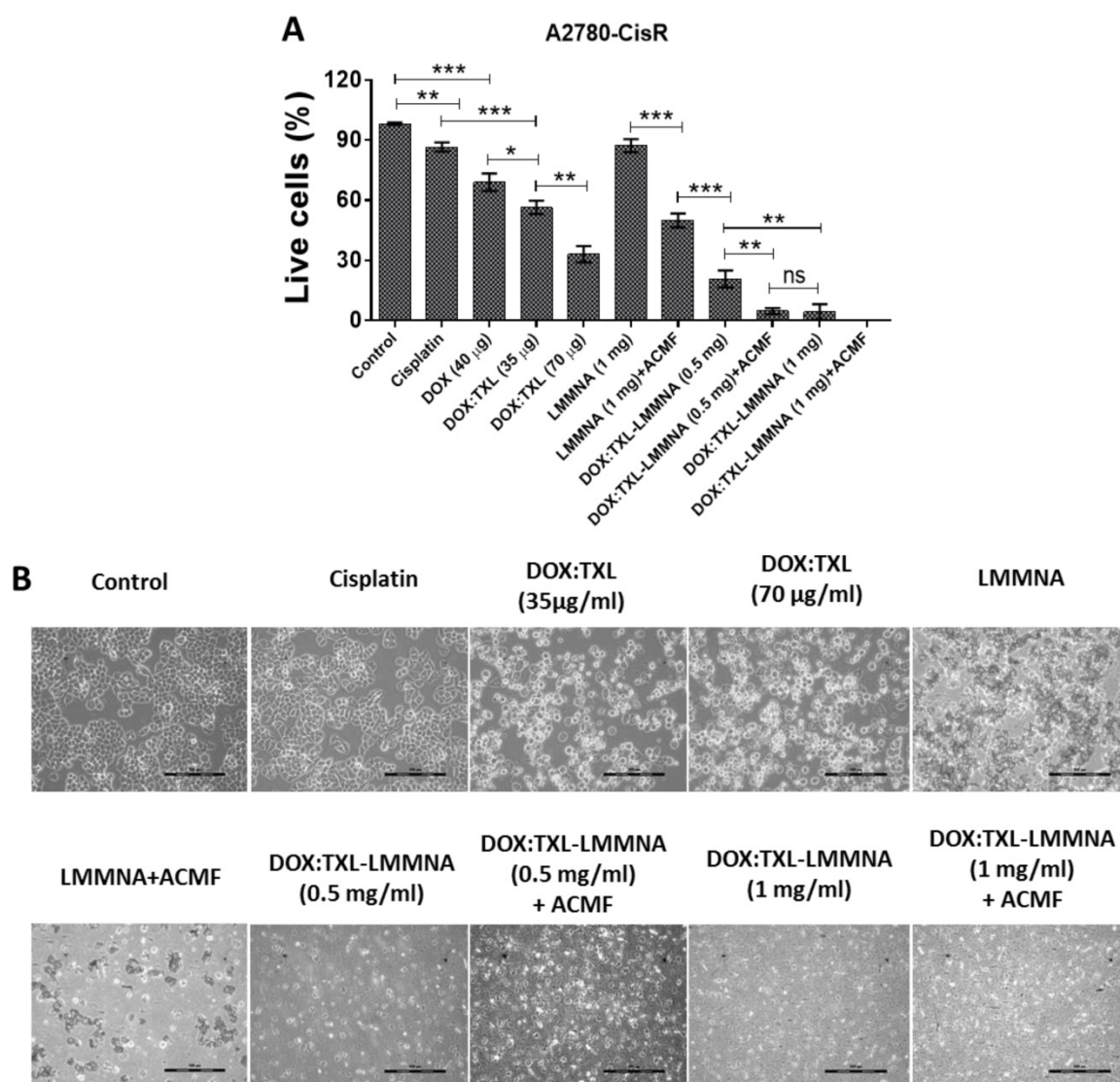
Figure 7. *In vitro* thermo-chemotherapy study on A2780-CisR cell line at 24 h. (A & B) efficiency of live cells after treatment and (C) optical microscopy images for morphological study. Data expressed as mean ± SD (n=3). Significance is denoted as ** p < 0.01 and *** p < 0.001 and *ns* as no significance. Scale bar 100 µm.

Efficacy of DOX:TXL-LMMNA with hyperthermia against cisplatin resistant A2780-CisR tumor xenografts

To understand the efficacy of thermo-chemotherapy *in vivo* on drug resistant tumors, 5×10^6 of A2780-CisR-cells were implanted either on two shoulders or shoulder and flank region of NUDE mice. All mice from each group were exposed to ACMF under the same conditions which have been previously described and imaged by injecting D-luciferin. Representative images of tumor regression evaluated using bioluminescence imaging are shown in Figure 8A. As shown in Figure 8B, in group IV mice (DOX:TXL-LMMNA+ACMF treated), tumor bioluminescence signal was decreased by 0.22±0.18 fold (from $2.2 \times 10^7 \pm 1.9 \times 10^7$ to $4.9 \times 10^6 \pm 5.2 \times 10^6$ p/sec/cm^2/sr) post hyperthermia treatment.

Resistant tumor treated with cisplatin or DOX:TXL alone showed increased bioluminescence activity from $2.1 \times 10^7 \pm 1.2 \times 10^7$ to $5.5 \times 10^7 \pm 3.03 \times 10^7$ p/sec/cm^2/sr (3.7±1.96 fold change) and from $2.1 \times 10^7 \pm 1.7 \times 10^7$ to $6.7 \times 10^7 \pm 1.6 \times 10^7$ p/sec/cm^2/sr (fold change by 4.79±3.27) respectively (Figure 8B). The increase in tumor signal by DOX:TXL is contrary to our *in vitro* data and occurred due to lower doses than the optimal one to show any effect in *in vivo* condition [34-37]. Resistant tumor on treatment with only LMMNA particles followed by hyperthermia showed minor change in bioluminescence activity (from $1.8 \times 10^7 \pm 9.8 \times 10^6$ to $1.5 \times 10^7 \pm 1.1 \times 10^7$ p/sec/cm^2/sr (0.8±0.3 fold change) indicating cytostatic effect of these particles in combination with hyperthermia. Interestingly, the bioluminescence signal significantly (p = 0.016) decreased in A2780-CisR tumor as compared to A2780^s tumor xenograft undergoing

similar treatment of DOX:TXL-LMMNA+ACMF (ESI Figure S9A).

The imaging results were also corroborated with tumor volume data where cisplatin and DOX:TXL treated tumor showed increased tumor mass by 2.18±0.49 and 3.52±1.3 fold respectively. Interestingly, LMMNA treated tumors demonstrated slight decrease in volume (0.65±0.2 fold change) whereas DOX:TXL-LMMNA+ACMF showed around 80% regression of tumor (0.22±0.18 fold change) volume (Figure 8C). DOX:TXL-LMMNA+ACMF treated resistant tumor showed significant (p = 0.04) decrease in tumor volume as compared to sensitive tumor as shown in ESI Figure S9B. To understand the effect of hyperthermia alone, we treated A2780-CisR cells with DOX:TXL in absence and presence of hyperthermia (incubated at 42 °C to mimic hyperthermia effect) and processed for γH2.X foci formation analysis as a marker of DNA damage at various time intervals (Figure 8D). As shown in Figure 8E, cells incubated at 37 °C showed highest mean fluorescence intensity of

foci formation at 12 h which decreased by 24 h. This indicates that the DOX:TXL treatment is most effective till 12 h at 37 °C. Interestingly, cells incubated at 42 °C showed slightly lesser foci formation at 12 h which increased by 24 h. This indicated that hyperthermia (42 °C) enhances the efficacy and duration of DOX:TXL treatment.

Again minimal change in body weights of mice were observed for to cisplatin (17±1)g, DOX:TXL+ACMF (18±2)g, LMMNA+ACMF (18±1)g and for DOX:TXL-LMMNA+ACMF (18±1)g treatment groups at Day 7 in comparison to Day 0 (19±1), (19±1), (19±1), and (20±1)g, respectively (Figure 8F). All together our data indicate that these novel nanoassemblies developed in this study have the potential to exert maximum cytotoxicity with low drug concentration without affecting the mouse physiology when induced by hyperthermia. Intriguingly, we have found that this cytotoxic effect is more pronounced in drug resistant cells/tumors.
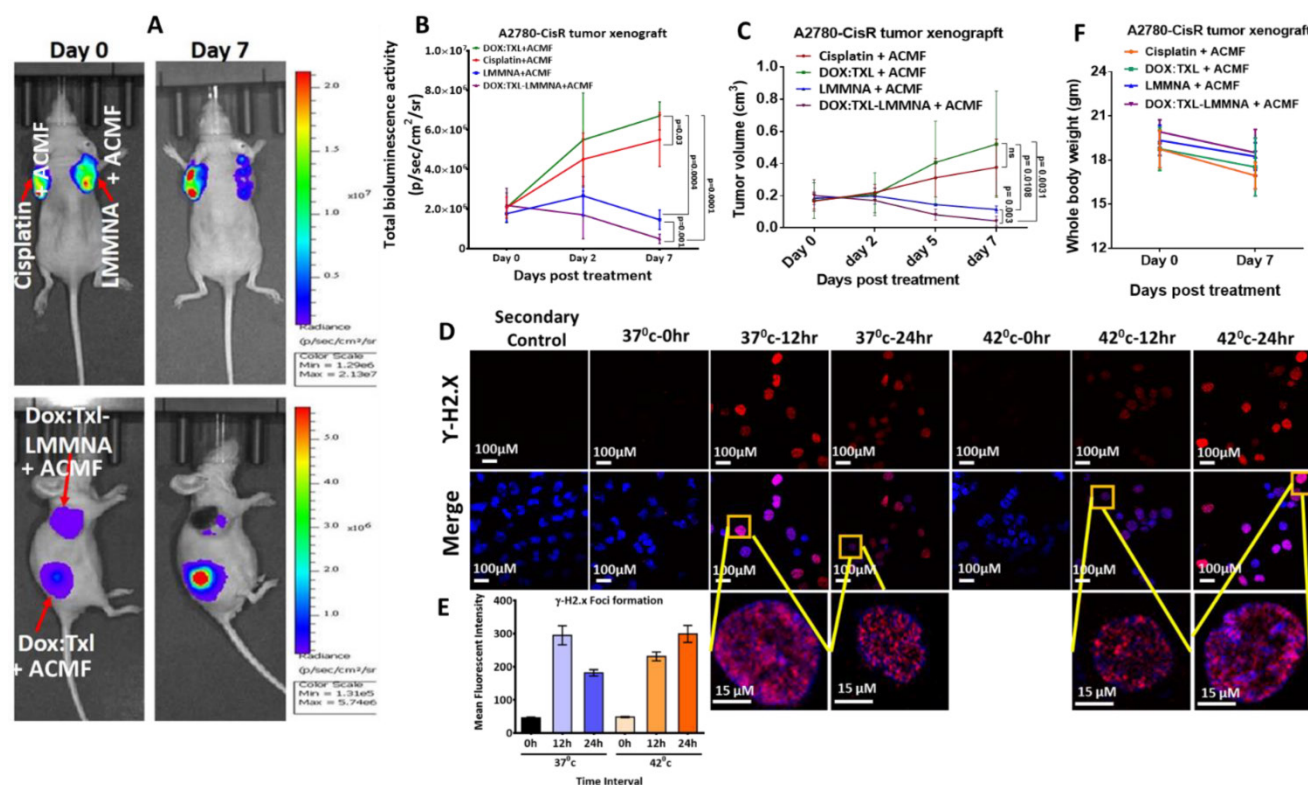
Figure 8. *In vivo* combined therapy using 1 mg of DOX:TXL-LMMNA in A2780-CisR tumor xenografts NUDE mice (n=5). Tumor regression study monitored by bioluminescence imaging in the absence/presence of ACMF at 376 Oe, 250 kHz frequency on the A2780-CisR tumor xenografts after intratumoral injections. (A) Representative bioluminescence images of A2780-CisR tumor xenografts after intratumoral injections of free cisplatin (3.5 mg/kg), DOX:TXL+ACMF (2:1.5 mg/kg), LMMNA+ACMF (50 mg/kg) and DOX:TXL-LMMNA+ACMF (2:1.5:50 mg/kg). (B) Quantitative assessment of bioluminescence signal showed significant decrease in bioluminescence signal of A2780-CisR tumor xenografts post combined therapy (p= 0.03, p= 0.001, p= 0.0004 and p= 0.0001). (C) Graphical representation of the tumor volume for A2780-CisR tumor xenografts showed decreases tumor volume post combined therapy (p= 0.003, p= 0.0108, p= 0.0031 and *ns* as no significance). (D & E) Effect of hyperthermia on drug efficacy assessed by γH2.X foci formation assay in A2780-CisR cancer cells. Hyperthermia increases the efficacy drug leads to increased γH2.X foci formation at 42 °C compare to 37 °C. (E) Graphical quantitation of γH2.X foci after each treatment. (F) Whole body weight measurement of mice bearing A2780-CisR tumor xenograft after each treatments at Day 0 and Day 7.

Conclusion

In summary, we have successfully developed a novel pH and thermo liable lipid-coated mesoporous magnetic nanoassembly for dual drug delivery and hyperthermia applications. This fomulation was optimized for combined hyperthermia and chemotherapy. The therapeutic efficacy was evaluated both *in vtro* and *in vivo* in cisplatin resistant and cisplatin sensitive ovarian cancer model (A2780^S and A2780-CisR tumor xenograft animals) using molecular imaging techniques. The enhanced cytotoxic effect of DOX:TXL-LMMNA under ACMF resulted in higher cell death than treatment with only DOX:TXL-LMMNA on A2780^S and A2780-CisR cells and tumors without any adverse effect on body physiology. The dual drug-delivery system is found to be effective and exhibits optimal therapeutic efficacy and complete tumor ablation at low concentrations, *in vivo*. Most importantly we found that the effect of these particles is more pronounced in drug resistant cells and tumors probably due to its inherent lysosomal acidic environment. Thus these novel stimuli sensitive nanoassemblies hold great promise for therapy of resistant malignancies and may be translated to clinics in near future. However, the non-targeted nature of these particles still pose limitation for ultimate application hence further improvement towards targeted delivery are under investigation.

Supplementary Material

Supplementary tables and figures.
http://www.thno.org/v06p1557s1.pdf

Abbreviations

ACMF, AC magnetic field; Chol., cholesterol; CisR, cisplatin resistant; DOX, doxorubicin hydrochloride; DMEM, Dulbecco's Modified Eagle's Medium; DPPC, 1,2-dipalmitoyl-sn-glycero-3-phosphocholine; DSPE-PEG$_{2000}$, 1,2-distearoyl-sn-glycero-3-phosphoethanolamine-N-[amino (polyethylene glycol)-2000]; EPR, enhances cellular permeability and retention effects; *fl2-tdt*, firefly luciferase-tandom tomato red; (H & E), Hematoxylin & eosin; ICP-AES, Inductively coupled plasma atomic emission spectroscopy; LMMNA, thin lipid layer with mesoporous magnetite nanoassemblies; MMNA, mesoporous magnetite nanoassemblies; ROIs, Region of Interests; SRB, Sulforhodamine-B; TEM, transmission electron microscopy; TXL, paclitaxel.

Competing Interests

The authors have declared that no competing interest exists.

References

1. Zafar S, Negi LM, Verma AK, Kumar V, Tyagi A, Singh P, et al. Sterically stabilized polymeric nanoparticles with a combinatorial approach for multi drug resistant cancer: *in vitro* and *in vivo* investigations. Int J Pharm. 2014; 477: 454-68.
2. He Q, Gao Y, Zhang L, Zhang Z, Gao F, Ji X, et al. A pH-responsive mesoporous silica nanoparticles-based multi-drug delivery system for overcoming multi-drug resistance. Biomaterials. 2011; 32: 7711-20.
3. Wu JL, Wang CQ, Zhuo RX, Cheng SX. Multi-drug delivery system based on alginate/calcium carbonate hybrid nanoparticles for combination chemotherapy. Colloids Surf., B. 2014; 123: 498-505.
4. Ahmed F, Pakunlu RI, Brannan A, Bates F, Minko T, Discher DE. Biodegradable polymersomes loaded with both paclitaxel and doxorubicin permeate and shrink tumors, inducing apoptosis in proportion to accumulated drug. J Controlled Release. 2006; 116: 150-8.
5. Miao J, Du YZ, Yuan H, Zhang XG, Hu FQ. Drug resistance reversal activity of anticancer drug loaded solid lipid nanoparticles in multi-drug resistant cancer cells. Colloids Surf., B. 2013; 110: 74-80.
6. Zhang L, Radovic-Moreno AF, Alexis F, Gu FX, Basto PA, Bagalkot V, et al. Co-delivery of hydrophobic and hydrophilic drugs from nanoparticle-aptamer bioconjugates. Chem Med Chem. 2007; 2: 1268-71.
7. Elumalai R, Patil S, Maliyakkal N, Rangarajan A, Kondaiah P, Raichur AM. Protamine-carboxymethyl cellulose magnetic nanocapsules for enhanced delivery of anticancer drugs against drug resistant cancers. Nanomed Nanotechnol Biol Med. 2015; 11: 969-81.
8. Chen Y, Jiang L, Wang R, Lu M, Zhang Q, Zhou Y, et al. Injectable smart phase-transformation implants for highly efficient *in vivo* magnetic-hyperthermia regression of tumors. Adv Mater. 2014; 26: 7468-73.
9. Kheirolomoom A, Lai CY, Tam SM, Mahakian LM, Ingham ES, Watson KD, et al. Complete regression of local cancer using temperature-sensitive liposomes combined with ultrasound-mediated hyperthermia. J Controlled Release. 2013; 172: 266-73.
10. Di Corato R, Bealle G, Kolosnjaj-Tabi J, Espinosa A, Clement O, Silva AK, et al. Combining magnetic hyperthermia and photodynamic therapy for tumor ablation with photoresponsive magnetic liposomes. ACS Nano. 2015; 9: 2904-16.
11. Ren Y, Zhang H, Chen B, Cheng J, Cai X, Liu R, et al. Multifunctional magnetic Fe$_3$O$_4$ nanoparticles combined with chemotherapy and hyperthermia to overcome multidrug resistance. Int J Nanomed. 2012; 7: 2261-9.
12. W-CH CCH, Lin YW, Yu TW, Chen HH, Lin SC, Chiang WH, Chiu HC. Active Tumor permeation and uptake of surface charge-switchable theranostic nanoparticles for imaging-guided photothermal/chemo combinatorial therapy. Theranostics. 2016; 6: 302-17.
13. Ryu JS, Raucher D. Elastin-like polypeptides: the influence of its molecular weight on local hyperthermia-induced tumor accumulation. Eur J Pharm Biopharm. 2014; 88: 382-9.
14. Al-Ahmady ZS, Chaloin O, Kostarelos K. Monoclonal antibody-targeted, temperature-sensitive liposomes: *in vivo* tumor chemotherapeutics in combination with mild hyperthermia. J Controlled Release. 2014; 196: 332-43.
15. Jayson GC, Kohn EC, Kitchener HC, Ledermann JA. Ovarian cancer. Lancet. 2014; 384: 1376–88.
16. Nossov V, Amneus M, Su F, Lang J, Janco JMT, RT Srinivasa, et al. The early detection of ovarian cancer: from traditional methods to proteomics. Can we really do better than serum CA-125?. Am J Obstet Gynecol. 2008; 199: 215-23.
17. Baumann KH, Wagner U, du Bois A. The changing landscape of therapeutic strategies for reccurrent ovarian cancer. Future Oncol. 2012; 8: 1135-47.
18. Pradhan L, Srivastava R, Bahadur D. pH- and thermosensitive thin lipid layer coated mesoporous magnetic nanoassemblies as a dual drug delivery system towards thermochemotherapy of cancer. Acta biomater. 2014; 10: 2976-87.
19. Gaikwad SM, Thakur B, Sakpal A, Singh RK, Ray P. Differential activation of NF-kappaB signaling is associated with platinum and taxane resistance in

MyD88 deficient epithelial ovarian cancer cells. Int J Biochem Cell Biol. 2015; 61: 90-102.

20. Swain AK, Pradhan L, Bahadur D. Polymer stabilized Fe_3O_4-graphene as an amphiphilic drug carrier for thermo-chemotherapy of cancer. ACS Appl Mater Interfaces. 2015; 7: 8013-22.

21. Chytil P, Hoffmann S, Schindler L, Kostka L, Ulbrich K, Caysa H, et al. Dual fluorescent HPMA copolymers for passive tumor targeting with pH-sensitive drug release II: impact of release rate on biodistribution. J Controlled Release. 2013; 172: 504-12.

22. Rengan AK, Bukhari AB, Pradhan A, Malhotra R, Banerjee R, Srivastava R, et al. *In vivo* analysis of biodegradable liposome gold nanoparticles as efficient agents for photothermal therapy of cancer. Nano Lett. 2015; 15: 842-8.

23. Jaiswal MK, Gogoi M, Sarma HD, Banerjee R, Bahadur D. Biocompatibility, biodistribution and efficacy of magnetic nanohydrogels in inhibiting growth of tumors in experimental mice models. Biomater Sci-Uk. 2014; 2: 370-80.

24. Jose S, Anju SS, Cinu TA, Aleykutty NA, Thomas S, Souto EB. *In vivo* pharmacokinetics and biodistribution of resveratrol-loaded solid lipid nanoparticles for brain delivery. Int J Pharm. 2014; 474: 6-13.

25. Jensen MM, Jorgensen JT, Binderup T, Kjaer A. Tumor volume in subcutaneous mouse xenografts measured by microCT is more accurate and reproducible than determined by 18F-FDG-microPET or external caliper. BMC Med Imaging. 2008; 8: 16.

26. Kruse AM, Meenach SA, Anderson KW, Hilt JZ. Synthesis and characterization of CREKA-conjugated iron oxide nanoparticles for hyperthermia applications. Acta biomater. 2014; 10: 2622-9.

27. Rao W, Zhang W, Poventud-Fuentes I, Wang Y, Lei Y, Agarwal P, et al. Thermally responsive nanoparticle-encapsulated curcumin and its combination with mild hyperthermia for enhanced cancer cell destruction. Acta biomater. 2014; 10: 831–842.

28. Ding H, Wu F. Image guided biodistribution and pharmacokinetic studies of theranostics. Theranostics. 2012; 2: 1040-53.

29. Nazir S, Hussain T, Ayub A, Rashid U, MacRobert AJ. Nanomaterials in combating cancer: therapeutic applications and developments. Nanomed Nanotechnol Biol Med. 2014; 10: 19-34.

30. LW QZ, Cheng R, Mao L, Arnold RD, Howerth EW, ZG C, Platt S. Magnetic nanoparticle-based hyperthermia for head & neck cancer in mouse models. Theranostics. 2012; 2: 113-21.

31. Mani J, Vallo S, Rakel S, Antonietti P, Gessler F, Blaheta R, et al. Chemoresistance is associated with increased cytoprotective autophagy and diminished apoptosis in bladder cancer cells treated with the BH3 mimetic (−)-Gossypol (AT-101). BMC Cancer. 2015; 15: 224.

32. Gong Y, Duvvuri M, Krise JP. Separate roles for the golgi apparatus and lysosomes in the sequestration of drugs in the multidrug-resistant human leukemic cell line HL-60. J Biol Chem. 2003; 278: 50234-39.

33. Larsen AK, Escargueil AE, Skladanowski A. Resistance mechanisms associated with altered intracellular distribution of anticancer agents. Pharmacol Ther. 2000; 85: 217–229.

34. Nicoletti MI, Lucchini V, Massazza G, Abbott BJ, D'Incalci M, Giavazzi R. Antitumor activity of taxol (NSC-125973) in human ovarian carcinomas growing in the peritoneal cavity of nude mice. Ann Oncol. 1993; 4: 151-5.

35. Nicoletti MI, Lucchini V, D'Incalci M, Giavazzi R. Comparison of Paclitaxel and Docetaxel Activity on Human Ovarian Carcinoma Xenografts. Euro J Cancer. 1994; 30: 691-96.

36. Iliopoulos D, Hirsch HA, Struhl K. Metformin decreases the dose of chemotherapy for prolonging tumor remission in mouse xenografts involving multiple cancer cell types. Cancer Res. 2011; 71: 3196-201.

37. Jin C, Li H, He Y, He M, Bai L, Cao Y, et al. Combination chemotherapy of doxorubicin and paclitaxel for hepatocellular carcinoma in vitro and in vivo. J Cancer Res Clin Oncol. 2010; 136: 267–274.

Differential activation of NF-κB signaling is associated with platinum and taxane resistance in MyD88 deficient epithelial ovarian cancer cells

Snehal M. Gaikwad [1], Bhushan Thakur [1], Asmita Sakpal, Ram K. Singh, Pritha Ray *

Advanced Centre for Treatment, Research and Education in Cancer (ACTREC), Tata Memorial Centre, Navi Mumbai, Maharashtra, 410210, India

ABSTRACT

Development of chemoresistance is a major impediment to successful treatment of patients suffering from epithelial ovarian carcinoma (EOC). Among various molecular factors, presence of MyD88, a component of TLR-4/MyD88 mediated NF-κB signaling in EOC tumors is reported to cause intrinsic paclitaxel resistance and poor survival. However, 50–60% of EOC patients do not express MyD88 and one-third of these patients finally relapses and dies due to disease burden. The status and role of NF-κB signaling in this chemoresistant MyD88[negative] population has not been investigated so far. Using isogenic cellular matrices of cisplatin, paclitaxel and platinum-taxol resistant MyD88[negative] A2780 ovarian cancer cells expressing a NF-κB reporter sensor, we showed that enhanced NF-κB activity was required for cisplatin but not for paclitaxel resistance. Immunofluorescence and gel mobility shift assay demonstrated enhanced nuclear localization of NF-κB and subsequent binding to NF-κB response element in cisplatin resistant cells. The enhanced NF-κB activity was measurable from *in vivo* tumor xenografts by dual bioluminescence imaging. In contrast, paclitaxel and the platinum-taxol resistant cells showed down regulation in NF-κB activity. Intriguingly, silencing of MyD88 in cisplatin resistant and MyD88[positive] TOV21G and SKOV3 cells showed enhanced NF-κB activity after cisplatin but not after paclitaxel or platinum-taxol treatments. Our data thus suggest that NF-κB signaling is important for maintenance of cisplatin resistance but not for taxol or platinum-taxol resistance in absence of an active TLR-4/MyD88 receptor mediated cell survival pathway in epithelial ovarian carcinoma.

© 2015 Elsevier Ltd. All rights reserved.

1. Introduction

Ovarian cancer primarily the epithelial ovarian cancer (EOC) has the highest mortality rate of all gynaecologic malignancies in women. In spite of improved treatment modalities in recent years, about 60% patients succumb to the disease within 5 years due to recurrence and acquired drug resistance (Armstrong et al., 2006; Rocconi et al., 2006). Patients with relapsed disease either show intrinsic resistance or develop resistance through repetitive exposures to drugs. Among various factors contributing to chemoresistance, genes involved in cell death and cell survival pathways play major role in acquirement and sustainment of resistance phenotype (Chaudhury et al., 2014; Gaikwad and Ray, 2012; Gottesman, 2002; Kartalou and Essigmann, 2001; Kim et al.,

2005; Siddik, 2002; Singh et al., 2014). Altered expression of anti-apoptotic proteins such as members of Bcl-2 family proteins and components of mitogen-activated proteins kinase (MAPK) pathway, PI3K/AKT/mTOR pathway and NF-κB signaling are shown to be involved in resistance and recurrence (Beale et al., 2000; Brozovic et al., 2004; Karin, 2009; Koti et al., 2013; Mabuchi et al., 2004a; Nehra et al., 2010; Tang et al., 2001). The NF-κB family of transcription factors are induced by a broad range of stimulators and can initiate dynamic modulations in gene expressions of immune surveillances, differentiation, proliferation, apoptosis, angiogenesis, cell cycle progression and drug resistance (Hayden and Ghosh, 2012).

The Toll-like receptor (TLR) family plays a central role in commencement of innate immunity through activation of NF-κB (Blasius and Beutler, 2010). The activation of TLR signaling pathways originates from the cytoplasmic TIR domains and TIR domain containing adapter protein, myeloid differentiation factor88 or MyD88. Among all the TLRs, TLR-4 and TLR-3 induce NF-κB activation either through MyD88 (MyD88 dependent) or

via another adapter protein called TICAM-1 (MyD88 independent) (Akira, 2003; Kawai and Akira, 2006, 2007). Both MyD88 and TICAM-1 activate IκB kinases (IKKα/IKKβ or IKKε/IKKι) via activation of either IRAK/TRAF-6 or IRF-3/TBK1 which are responsible for phosphorylation and degradation of inhibitory κB (IκB) proteins, nuclear localization of NF-κB and initiation of the cascade of gene expression.

Interestingly, active TLR-4/MyD88 signaling is also found on epithelial ovarian cancer cells and presence of MyD88 but not TLR-4 significantly influences the drug response (Kelly et al., 2006; Muccioli et al., 2012; Silasi et al., 2006; Szajnik et al., 2009). Following paclitaxel treatment, MyD88 positive EOC cells show increased proliferation and tumor growth, activated NF-κB and AKT signaling and overexpression of antiapoptotic proteins. However, MyD88 negative EOC cells do not show proliferation rather induce caspase dependent apoptosis after paclitaxel treatment (Szajnik et al., 2009). Patients devoid of MyD88 expression show a significantly higher disease free progression interval compared to the patients whose tumors express MyD88 (Kim et al., 2012). Thus MyD88 has been proposed as a potential biomarker for determining chemo-response to paclitaxel in ovarian cancer (Kelly et al., 2006). Recently, the relationships between the expression of TLR-4, MyD88 and NF-κB were examined in a large cohort of 123 cases of epithelial ovarian cancer patients using immunohistochemistry (Kim et al., 2012). While this study indicated that MyD88 expression was associated with poor survival in patients, it also revealed that a significant percentage of EOC patients (~60%) were MyD88[negative] and around 40% (32/78) of them exhibited disease recurrence. The status and role of NF-κB signaling in these chemoresistant MyD88[negative] populations is unclear and certainly requires further investigation for devising new therapeutic strategies.

In this study, using isogenic cellular matrices of cisplatin, paclitaxel and platinum-taxol resistant MyD88[negative] ovarian cancer cells (A2780) expressing a NF-κB reporter sensor, we showed that enhanced NF-κB activity was only required for cisplatin resistance but not for paclitaxel or platinum-taxol resistance. This enhanced NF-κB activity was evident from higher nuclear expression and could be imaged from cisplatin resistant tumor xenografts in real time. Increased expression associated with cisplatin resistance indicated Bcl-2 as a possible molecular player for sustained resistance. In contrast, paclitaxel and platinum-taxol resistant cells were not associated with NF-κB activation. Cisplatin, paclitaxel and platinum taxol treatment did not exhibit any change in NF-κB activity in MyD88[positive] and naturally occurring cisplatin resistant TOV21G cells. However, when MyD88 expression was suppressed using sh-RNA mediated silencing; only cisplatin treatment exhibited enhanced NF-κB activity. Similar result was observed in SKOV3, another MyD88[positive] and naturally occurring cisplatin resistant cell line. Taken together, these data show the complexity of the NF-κB signaling pathway involved in acquired drug resistance and dispensability of MyD88 during development of cisplatin resistance in epithelial ovarian cancer.

2. Material and methods

2.1. Reagents and antibodies

Cisplatin (cis-Diammineplatinum (II) dichloride), Paclitaxel, G418 disulfate salt, puromycin, Lipopolysaccharide (LPS), polybrene, primary antibodies (β-actin and α-tubulin), and HRP conjugated secondary antibodies (anti-mouse and anti-rabbit) were purchased from Sigma–Aldrich (USA). Luciferase assay system was procured from Promega. D-luciferin and coelenterazine were procured from Biosynth International (Switzerland). NF-κB (p65), Lamin-A, MyD88, TLR-4 and Bcl-2 antibodies were procured from ABCAM (Cambridge, USA) and Cell Signaling Technologies (Danvers, MA, USA) respectively.

2.2. Construction of NF-κB sensor

The 160 bp sequence consisting of NF-κB response element (composed of four tandem copies of the NF-κB consensus binding sequence) followed by a minimal TA promoter was PCR amplified from pNF-κB-Met-Luc-2 plasmid (Clontech, USA). The amplified product was cloned in place of CMV promoter of pcDNA-3.1(+)-puro vector carrying the hRL-eGFP or hRL-mRFP bi-fusion reporter (Ray et al., 2003). Positive clones of pNF-κB-hRL-eGFP/mRFP-pcDNA3.1 (+)-puro were confirmed by PCR amplification, restriction digestion and sequencing.

2.3. Cell line, culture conditions and transfection

A2780 cells (undifferentiated EOC cell), SKOV3 (high grade serous), OAW42 (high grade serous) and TOV21G (clear cell) cells obtained from ATCC (Manassas, VA, USA) were cultured in DMEM, RPMI, and MEM medium (GIBCO, Carlsbad, CA) respectively supplemented with 10% fetal bovine serum (HiMedia) and 1% penicillin-streptomycin (GIBCO). For NF-κB activity, cells were transiently transfected with pNF-κB-hRL-eGFP/mRFP and CMV-fl2-tdt (9:1 ratio) and ratiometrically measured by Renilla luciferase/ Firefly luciferase (RL/FL) activity. A2780 cells stably expressing PIK3CA promoter driving firefly luciferase were engineered for stably expressing the NF-κB sensor (Gaikwad et al., 2013). All the transient and stable transfections with NF-κB sensor were carried out using Superfect transfection reagent (Qiagen, Valencia, CA) and stable cells were selected using puromycin. For all the drug treatments, cells were incubated for 24 h with cisplatin (10 μg/ml) or carboplatin (0.5–1.25 μg/ml) or paclitaxel (5 μg/ml) diluted in DMSO or water. Combinatorial treatments were given with both cisplatin (1 μg/ml) and paclitaxel (500 ng/ml) for 24 h. All transfection and drug treatment experiments were performed in triplicates and repeated at least twice.

2.4. MyD88 silencing by lentiviral mediated sh-RNA constructs

Lentivirus mediated RNA interference was used to silence the expression of MyD88 gene. First the pLL3.7 lentiviral vector was used to clone the target (5′ GACCCAATGTACCAGTATT, adapted from Yang et al., 2013) and scramble sequence (5′ ATAATCGC-CGTGAATTCC) between Hpa1 and Xho1 sites. Positive clones were verified by restriction digestion and sequencing. Later 2×10^6 293FT cells were seeded in 100 mm culture dish followed by cotransfection of vector plasmid carrying the desired shRNA construct along with the packaging plasmids (pδ 8·9, VSVG) using lipofectamine 2000 (Invitrogen). After 16 h of transfection, supernatant was removed and supplemented with 10 ml fresh medium. Viruses were harvested post 48 h and filtered through 0.45 μm filter and stored at −80 °C.

2.5. FACs sorting of MyD88 stable knockdowns cells

TOV21G and SKOV3 cells transiently or stably expressing pNF-κB hRL-mRFP reporter were seeded at 60% confluency in 100 mm culture dish. Transduction with lentivirus particles was performed by adding 2 ml of viral particles and 4 ml of complete media in presence of polybrene (4 μg/ml). Stable clones were isolated by FACS sorting using the eGFP reporter present in the lentiviral vector.

2.6. Establishment of cisplatin, paclitaxel and combinatorial resistance in A2780 cells

To develop cisplatin, paclitaxel and platinum-taxol resistant models, 1×10^6 A2780 cells were treated with incremental doses for a period of 6 months with each dose repeated for three cycles. Based upon percent viability, cells were categorized as A2780-Cis^{LR} (cells resistant to cisplatin), A2780-Pac^{LR} (resistant to paclitaxel) and A2780-Cis-Pac^{LR} (resistant to both cisplatin and paclitaxel). Both TOV21G and SKOV3 cells are known to show resistance towards different concentration of cisplatin (Dier et al., 2014; Koh et al., 2012; Yuan et al., 2011).

2.7. Luciferase reporter assay

Renilla and Firefly luciferase activities were measured using luciferase assay system (Promega) and coelenterazine in a Berthold luminometer as described previously (Gaikwad et al., 2013).

2.8. MTT assays

Cell viability was assessed using the standard thiazolyl blue tetrazolium bromide (MTT) method and percent viability was counted using the formula {[Absorbance$^{(Test)}$ ÷ Absorbance$^{(Control)}$] × 100}. Drugs were added at different concentrations and the inhibitory concentrations were calculated for the sensitive and resistant cells. All experiments were performed at least three times. Resistance index (RI) for each model was calculated using the formula (IC$_{50}$ of resistant cells/IC$_{50}$ of sensitive cells). For calculating doubling time, 5×10^2 cells/well were plated in 96 well plates and cell viability was assessed by MTT in quadruplicate every 24 h interval for 6 days. The data were subjected to linear regression analysis and doubling time (Td) was calculated using online calculator of doubling time (Roth, 2006).

2.9. Clonogenic assay

Single-cell suspensions were plated in six well dishes at a density of 500 cells/well. Once adhered, cells were treated with increasing concentrations of drugs for 24 h. The plates were further incubated for 7 days and colonies were stained with 0.05% crystal violet and counted under inverted microscope. Colonies consisting more than 50 cells were counted. Plating efficiencies (PE) and survival fractions (SF) were calculated using the formula: PE = Number of colonies/Number of cells seeded; SF = Number of colonies/Number of cells seeded × PE and plotted graphically to obtain survival curves.

2.10. Immunofluorescence

Immunofluorescence studies were performed as described earlier (Gaikwad et al., 2013) Briefly, cells plated on coverslips were fixed with 4% paraformaldehyde, permeabilized with 0.025% Triton-X and probed with NF-κB or TLR-4 antibody for overnight at 4 °C. Next day, after 2 h of incubation with secondary antibody, cells were counterstained with DAPI and images were observed under Carl Zeiss, LSM 710 microscope. At least five representative fields were studied.

2.11. Preparation of nuclear and cytosolic proteins and Western blotting

1×10^7 cells were lysed with 400 μl (five times the cells pellet volume) of Cytoplasmic Extract (CE) buffer [(10 mM KCl, 0.1 mM EDTA, 10 mM HEPES and 0.3% NP-40 with proteinase inhibitor cocktail (Sigma))] at 4 °C for 10 min. The lysate was centrifuged for 15 min at 6000 rpm at 4 °C and supernatants were collected as cytosolic extract. The resulting pellet was re-suspended in CE buffer and washed for 2–3 times for 15 min at same conditions. Further, the pellet was resuspended in 50 μl of ice-cold 20 mM HEPES (pH 7.9), 420 mM NaCl, 20% (v/v) glycerol, 1 mM EDTA and proteinase inhibitor cocktail. After 5 min incubation at 4 °C, the lysate was centrifuged for 10 min at 14,000 rpm at 4 °C, and the supernatant was collected as nuclear extract. The concentrations of cytosolic and nuclear extracts were determined using Bradford Reagent (Sigma). Western blot analysis was done as described earlier (Gaikwad et al., 2013).

2.12. Quantitative and semi-quantitative RT-PCR

2 μg of total RNA extracted from cells using RNeasy kit (Qiagen, Netherland) was reverse transcribed using cDNA synthesis kit (Invitrogen, Carlsbad, CA). Quantitative-PCR (q-PCR) was performed using SYBR Green method (Invitrogen). GAPDH was used as an internal control. Primer sequences used were as follows: GAPDH (forward TGCACCACCAACTGCTTAGC, reverse GGCATG-GACTGTGGTCATGAG); MyD88 (forward CGCCGGATGGTGGTG-GTTGT, reverse TGTAGTCGCAGACAGTGATGAACC); Cyclin D1 (forward TATTGCGCTGCTACCGTTGA, reverse CCAATAGCAGCAAA-CAATGTGAAA); XIAP (forward GATGATGTGAGTTCTGATAGG and reverse CTTAATGTCCTTGAAACTGAAC). The relative expression levels of mRNAs were calculated by the $2^{-\Delta Ct}$ and fold change measurement by $2^{-\Delta\Delta Ct}$ method. Semi-quantitative RT-PCR was done as mentioned earlier (Gaikwad et al., 2013).

2.13. Electrophoretic mobility shift assay (EMSA)

NF-κB DNA binding activity was assessed by EMSA using biotin labeled oligo probes. Briefly, oligomers containing NF-κB consensus sequences were labeled using Biotin 3′ End DNA labeling kit (Thermo Scientific). 10 μg of respective nuclear lysates were equilibrated in binding buffer containing 10 mM Tris, 50 mM KCl, 1 mM DTT, 5 mM MgCl$_2$, 2.5% glycerol, 0.05% NP40, 20 ng/μl sheared salmon sperm DNA and 0.1% BSA for 5 min at room temperature. For binding reaction, 250 fmol of labeled oligo were added in each reaction and incubated for 30 min at room temperature. Competition assay was performed using 100 fold excess unlabeled oligo added during equilibration step prior to addition of labeled oligo. DNA-protein complexes were separated using 5% polyacrylamide gel and transferred to nylon membrane. DNA-protein complexes and free oligo were detected using chemiluminescent nucleic acid detection kit (Thermo scientific, USA).

2.14. Bioluminescence imaging of tumor xenografts

Animal care and euthanasia were performed with the approval from Institutional Animal Ethics Committee of ACTREC. Mice were implanted with 6×10^6 cells stably expressing either single or dual luciferases and tumors were allowed to grow till 5–8 mm. Mice were divided into two groups and one (treated) group was injected with cisplatin (8 mg/kg). Whole body images of anaesthetized mice using IVIS Spectrum optical imaging system were obtained after 100 μl intra-peritoneal injection of ᴅ-luciferin (3 mg/mouse) or tail-vein injection of coelenterazine (50 μg/mouse) diluted in phosphate-buffered saline. Region of Interests (ROIs) were drawn over the tumors and quantified by using the Live Image (4.4) software. Bioluminescence signals were recorded as maximum (photons/s/cm^2/sr). Bioluminescence imaging of the same mouse was acquired in sequence (first NF-κB-renilla luciferase followed by firefly luciferase).
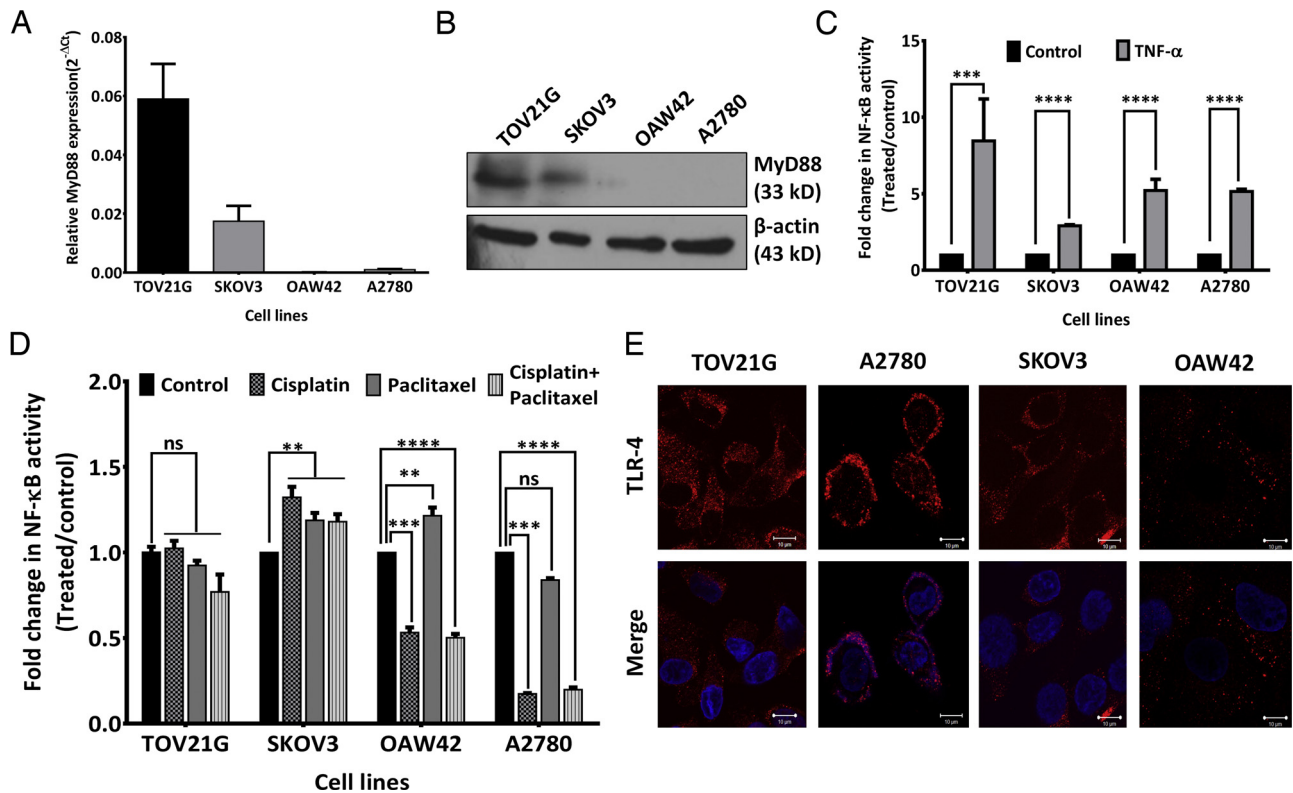
Fig. 1. Characterization of cell lines for TLR-4/MyD88/NF-κB pathway: A–B. MyD88 expression analysis. Quantitative-PCR (qPCR) and Western blot analysis showed positive expression for MyD88 in TOV21G and SKOV3 cells while A2780 and OAW42 were found to be negative for MyD88 expression, GAPDH and β-actin were used as internal control respectively. C–D. Transient transfection study for NF-κB activity TOV21G, SKOV3, OAW42 and A2780 cells were transiently transfected with pNF-κB-RE-driven-renilla luciferase and CMV driven-firefly luciferase constructs followed by TNF-α (200 ng/ml), cisplatin (10 μg/ml), paclitaxel (5 μg/ml) and cisplatin-paclitaxel (1 μg/ml; 500 ng/ml) treatment for 24 h. Relative NF-κB activity were calculated ratiometrically as RL/FL activity which showed significant increase by TNF-α treatment (C) (***$p < 0.001$), however reduced luciferase activity was observed with cisplatin and cisplatin-paclitaxel treatment (****$p < 0.0001$) and no change after paclitaxel treatment (D). E. Immunofluorescence study. Membrane localization of TLR-4 was observed in all the cells where upper panel represents the staining pattern of the TLR-4 and lower panel showing merged images with nuclear stain (DAPI).

3. Results

3.1. Differential activation of NF-κB was associated with differential drug treatments in MyD88^{negative} but not in MyD88^{positive} cells

Though absence of MyD88 expression is thought to associate with effective paclitaxel treatment and longer survival in epithelial ovarian cancer patients, a significant number of them exhibit disease recurrence (Kim et al., 2012). In order to understand the status of NF-κB activation in MyD88^{positive} and MyD88^{negative} cells by various chemotherapeutics, a panel of cell lines (TOV21G, SKOV3, OAW42 and A2780) were analyzed for the level of MyD88 expression by real time PCR and Western blot. As shown in Fig. 1A and B, while OAW42 and A2780 cells were devoid of MyD88 expression, TOV21G exhibited 3-fold higher expression than SKOV3. All these cells were then transiently transfected with NF-κB sensor and normalization plasmid and treated with various drugs and inducers. While 2 h of TNF-α treatment induced 5 fold increase, cisplatin and cisplatin + paclitaxel treatments resulted in 50–80% decrease in NF-κB-renilla luciferase activity in MyD88^{negative} OAW42 and A2780 cells. No significant change in luciferase activity was observed after paclitaxel treatment (Fig. 1C and D). In contrary both the MyD88^{positive} cells (TOV21G and SKOV3) did not exhibit any significant change in NF-κB activity after cisplatin, paclitaxel and cisplatin + paclitaxel treatments though a trend in enhanced activation was observed in SKOV3 cells (Fig. 1D). Two hours of TNF-α treatment induced ∼8 fold and 3 fold increase in NF-κB activity in these cells (Fig. 1C). All these cells showed prominent

TLR-4 expression and membrane localization except for OAW42 cells where only low cytoplasmic expression was observed (Fig. 1E).

Since the transient expression of any reporter gene is often influenced by the heterogeneity of the experimental procedure, two A2780 cell clones stably expressing the NF-κB sensor were generated. TNF-α showed increased (6–7 fold) NF-κB activity while LPS, a paclitaxel analogue did not induce NF-κB activation (Fig. 2A). These stable clones also displayed no change in NF-κB reporter activity after paclitaxel treatment but significant attenuation after cisplatin and combinatorial treatments (Fig. 2B).

In accordance with luciferase activity, changes in NF-κB expression in nuclear extracts were found after paclitaxel, cisplatin and dual treatments by Western blotting (Fig. 2C). Nuclear localization of NF-κB, a key event for NF-κB transcriptional action was differentially altered by various drug treatments. Minimal nuclear localization of NF-κB was found after cisplatin and dual treatments while enhanced localization was observed after paclitaxel treatment. An overall increase in NF-κB expression was evident in paclitaxel treated cells (Fig. 2D) by immunoflorescence.

3.2. Cisplatin and paclitaxel resistant cells with enhanced AKT phosphorylation exhibited slower proliferation and lower clonogenicity than the dual resistant cells

To understand the drug resistant characteristics of MyD88^{negative} cells, three isogenic cellular models of resistance (cisplatin, paclitaxel and cisplatin-paclitaxel) were developed
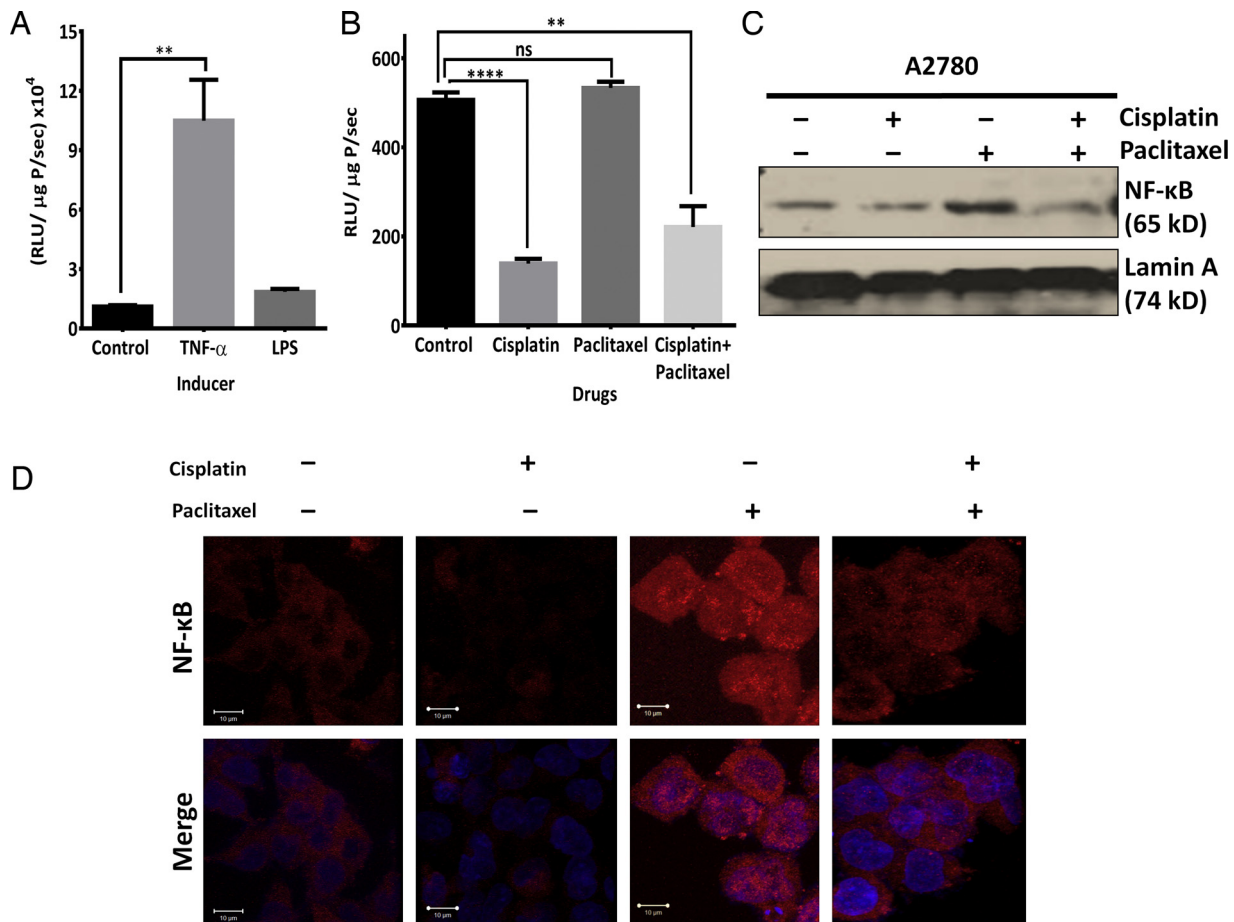
Fig. 2. Different chemotherapeutics showed differential expression of NF-κB upon treatments in MyD88 negative EOC cells: A–B. Stable expression study. An increased NF-κB luciferase activity was observed with TNF-α (**$p < 0.01$) but not with Lipopolysaccharide (LPS) treatment (A). A2780 cells stably expressing NF-κB sensor showed significant decrease in luciferase activity after cisplatin (****$p < 0.0001$) and combinational treatment of cisplatin and paclitaxel (**$p < 0.01$) while no changes were observed after paclitaxel treatment (B). C. Immunoblotting study. Increased NF-κB levels were observed after paclitaxel treatment but not after cisplatin and dual drug treatment in nuclear lysates of the drug treated A2780 cells. Lamin A was used as loading control. D. Immunofluorescence study. Increased nuclear localization of NF-κB was observed in A2780 cells after paclitaxel treatment, however, such localization were absent in cisplatin and platinum-taxol treated cells. Upper panel showed the staining pattern of the NF-κB and lower panel showed merged images with DAPI.

using A2780 cells with sequential treatment of increasing doses of drugs. The MyD88 deficient status of A2780 cells and their resistant counterparts was confirmed again (Fig. 3B). The late resistant cells demonstrated 92% viability for A2780-Cis^{LR}, 68% viability for A2780-Pac^{LR} and 96% viability for A2780-Cis-Pac^{LR} cells at IC$_{50}$ concentration of respective drugs. The resistance indices (RI) for A2780-Cis^{LR}, A2780-Pac^{LR} and A2780-Cis-Pac^{LR} cells were found to be 7.5, 5 and 10 fold higher than the sensitive counterparts respectively (Fig. 3A). The A2780-Cis^{LR} cells also demonstrated resistance to carboplatin, another platinum drug often used in clinics (Suppl. Fig. 1). Interestingly, proliferation rate for the dual resistant model was found to be comparable to sensitive cells (Doubling time: 27.70 ± 1.15 h vs. 25.30 ± 1.22 h) while both the single drug resistant cells showed much slower proliferation (Cis^{LR}: 33.44 ± 1.35 h and Pac^{LR}: 37.55 ± 1.86 h) (Fig. 3D). Similarly, the A2780-Cis-Pac^{LR} cells demonstrated a much higher rate of colony formation (1,000 fold) at an elevated drug concentration than A2780-Cis^{LR} and A2780-Pac^{LR} cells (~10 fold) when compared to the sensitive cells (Fig. 3E–G and supplementary Fig. 1). All the three cellular models showed gradual activation of AKT with acquirement of resistance without any significant change in total AKT level. The activation of AKT seemed to occur at much earlier stages for cisplatin and dual resistance than paclitaxel resistance (Fig. 3C).

3.3. The A2780 cisplatin resistant cells retained the resistant characteristics in vivo

One of the caveats of establishment of in vitro drug resistant cells is frequent reversal of the resistant phenotype and they often require to be maintained under drug selection. To test whether our cellular models could retain their resistant properties without any selection and in in vivo situation, A2780-Cis^{LR} cells were grown as tumors in nude mice and treated with cisplatin (8 mg/kg) and change in cellular viability was measured by bioluminescence imaging (all these cellular models stably express a PIK3CA promoter driven firefly luciferase reporter) (Gaikwad et al., 2013). In corroboration with the proliferation data, the tumors of resistant cells had slower growth than their sensitive counter parts (data not shown). The bioluminescence activity of these cisplatin resistant tumors ($n = 3$) did not decrease after treatment rather slightly increased ($3.72 \times 10^8 \pm 1.99 \times 10^8$ p/s/cm^2/sr to $1.19 \times 10^9 \pm 4.31 \times 10^8$ p/s/cm^2/sr) due to tumor growth. This increase was consistent even after another dose of cisplatin treatment ($3.36 \times 10^9 \pm 1.26 \times 10^9$ p/s/cm^2/sr). The untreated resistant tumors ($n = 3$) exhibited increased bioluminescence ($2.46 \times 10^8 \pm 4.81 \times 10^7$ p/s/cm^2/sr to $9.89 \times 10^8 \pm 2.78 \times 10^8$ p/s/cm^2/sr to $5.59 \times 10^9 \pm 1.03 \times 10^9$ p/s/cm^2/sr) over time (Fig. 4A and C). Tumor volume of the treated A2780-Cis^{LR} tumors
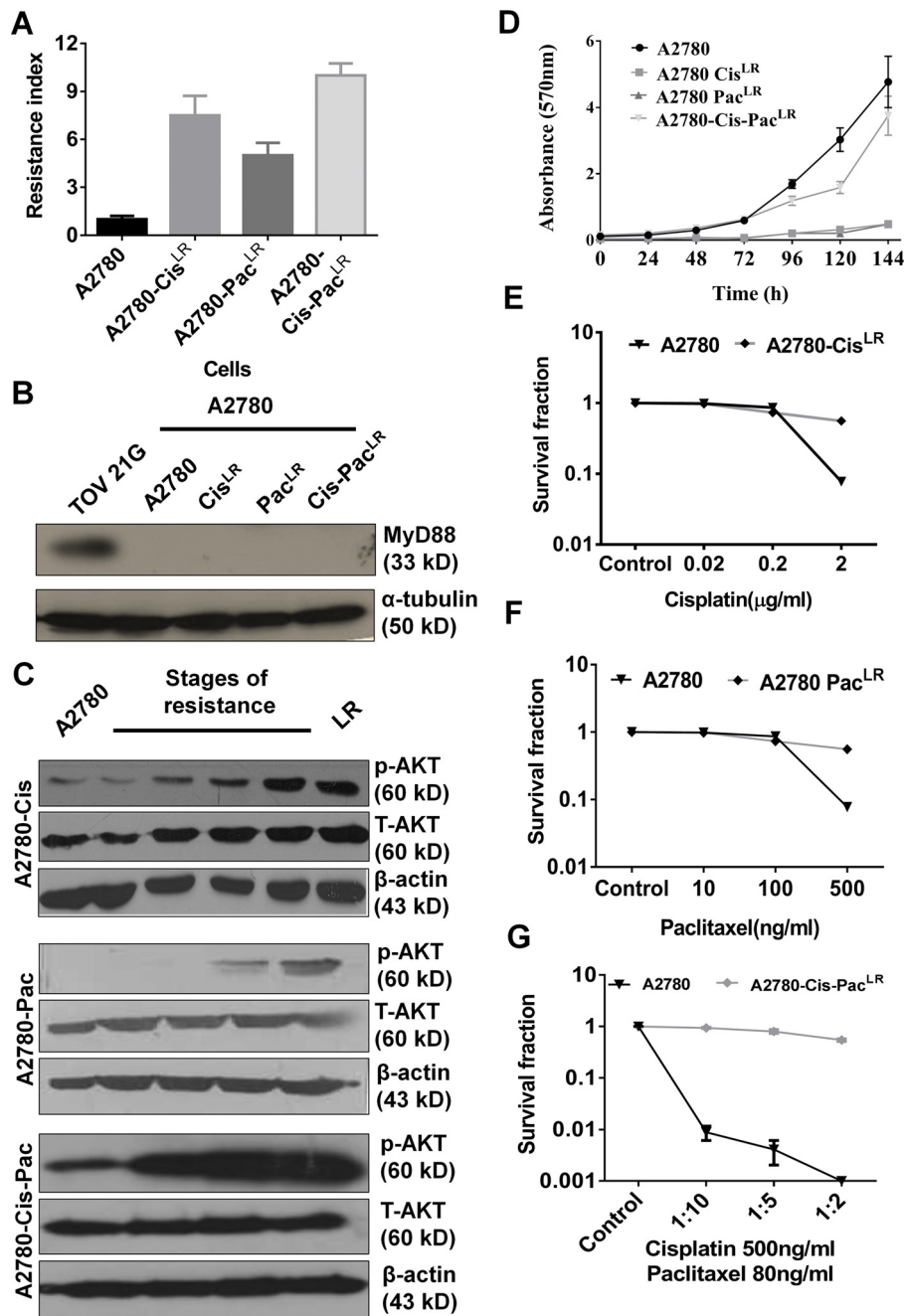
Fig. 3. Characterization of the isogenic resistant variants of A2780 cells: A. Resistance index. Resistance index of A2780 cells, A2780-Cis[LR], A2780-Pac[LR] and A2780-Cis-Pac[LR] were calculated using IC$_{50}$ doses of cisplatin, paclitaxel and platinum-taxol for A2780 and the resistant variants as described in methods. The three resistant variants of A2780 cells, A2780-Cis[LR], A2780-Pac[LR] and A2780-Cis-Pac[LR] demonstrated 8, 5 and 10 fold higher resistance than control respectively. B. MyD88 status. Western blot analysis showed absence of MyD88 protein in A2780 and its resistant variants. TOV21G cells were used as positive control and α-tubulin as a loading control. C. Immunoblotting study. High expression of phosphorylated AKT was observed in late stages of all resistant cells, however, no change was observed with total AKT. β-actin was used as loading control. D. Proliferative rate of the resistant cells. MTT assay of A2780 and its isogenic resistant variants to estimate growth rate showed a much slower proliferative capacity for A2780-Cis[LR], A2780-Pac[LR] than A2780 cells. Interestingly, A2780-Cis-Pac[LR] cells demonstrated a proliferation rate comparable to A2780 cells. E–G. Clonogenic assay. A2780 cells and all the isogenic resistant variants showed higher clonogenic potential (***$p < 0.001$) with increasing concentration of drugs.

remained stable whereas the control tumors exhibited gradual increase (Fig. 4B).

3.4. Acquirement of cisplatin resistance augmented NF-κB activity

Activated AKT is a critical regulator of NF-κB signaling which phosphorylates and activates inhibitory κB kinase (IKK) leading to phosphorylation and degradation of IKBα. Since all our resistant

models exhibited gradual increase in AKT phosphorylation, we sought to monitor the changes in NF-κB signaling by stably expressing the NF-κB sensor in these resistant (A2780-Cis[LR], A2780-Pac[LR] and A2780-Cis-Pac[LR]) cells. Interestingly, A2780-Cis[LR] cells stably expressing the NF-κB sensor exhibited a significant increase in luciferase activity (∼10 fold) after cisplatin treatment (Fig. 5A). This increase was not clone specific and observed independently in two other clones (data not shown). NF-κB also showed distinct nuclear localization in A2780-Cis[LR] cells with or without cisplatin
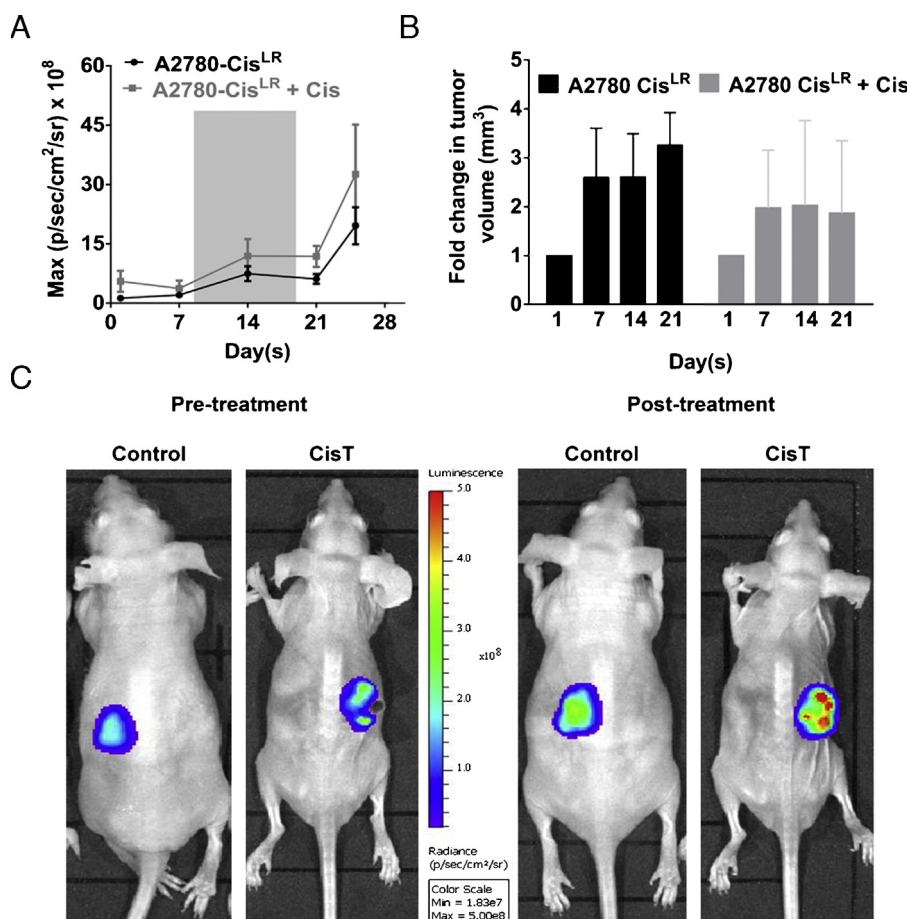
Fig. 4. Non-invasive imaging of A2780-Cis[LR] tumor xenografts demonstrated resistant characteristics after cisplatin treatment: A. Bioluminescence signal analysis. Graphical representation of the bioluminescent signals of pre and post-treated A2780-Cis[LR] tumor xenografts showed increased luminescence with time after two rounds of cisplatin treatment in both control ($n = 3$) and treated mice ($n = 3$). Shaded area displays the day/s of cisplatin treatment. B. Tumor volume assessment. Measurement of fold change in tumor volume (mm^3) of cisplatin treated mice showed similar trend of tumor growth in both control and treated mice. C. Bioluminescence imaging. Representative bioluminescent images of A2780-Cis[LR] tumor xenografts bearing mice before and after treatment did not exhibit attenuated luciferase activity after two treatments of cisplatin (post-treatment). The control group was injected with normal saline and exhibited increased luciferase activity.

treatment (Fig. 5D). Immunoblotting of nuclear lysates did not show any change in NF-κB level after cisplatin treatment to the A2780-Cis[LR] cells (Fig. 5G).

On contrary, A2780-Pac[LR] cells demonstrated a significant decrease in NF-κB activity after paclitaxel treatment (Fig. 5B). In contrast to the sensitive cells, where paclitaxel could induce nuclear localization, the A2780 Pac[LR] cells did not exhibit nuclear localization of NF-κB in pre and post treatment (Fig. 5G). Western blot analysis showed decreased nuclear NF-κB after treatment (Fig. 5D). Interestingly, about 1.5 fold induction in NF-κB activity was observed when A2780-Pac[LR] cells were challenged with cisplatin (Fig. 5E). However, similar cross treatment of paclitaxel to A2780-Cis[LR] cells resulted in reduction (∼1.5 fold) in NF-κB activity (Fig. 5F).

Surprisingly, A2780-Cis-Pac[LR] cells stably expressing the NF-κB sensor showed decreased NF-κB activity after combinatorial drug treatment (Fig. 5C). This decrease was found to be associated with reduced expression and localization of NF-κB in nucleus (Fig. 5D and G).

3.5. Cisplatin resistant cells showed enhanced NF-κB DNA binding activity

To evaluate the DNA binding capacity of NF-κB in sensitive and resistant cells, a biotinylated NF-κB response sequence was used for gel shift assay. Paclitaxel and combinatorial drug treatments

in sensitive cells slightly reduced the intensity of the DNA-protein complex; however, cisplatin treatment resulted in complete abolishment of the complex. A 100 fold excess cold probe could compete and abolish the complex while a scrambled oligonucleotide did not exhibit such competition indicating the specificity of the observed high molecular weight DNA-protein complex (Fig. 6A). In cisplatin resistant cells, cisplatin treatment did not abolish and rather slightly increased the intensity of the DNA-protein complex. In paclitaxel treated A2780 and cisplatin-paclitaxel treated A2780-Cis-Pac[LR] cells slight decrease in the DNA-protein complex formation was observed after treatments (Fig. 6B). A graphical representation of semi-quantitative comparison between the untreated and treated DNA-protein complex is shown in Fig. 6C.

3.6. Differential expression of Bcl-2 was associated with differential resistance

Activated NF-κB controls cell proliferation and apoptosis by directly regulating various molecular players like Cyclin-D1, Bcl-2, and XIAP. While Cyclin-D1 expression did not show significant alteration in A2780-Cis[LR] and A2780-Pac[LR] cells, A2780-Cis-Pac[LR] cells exhibited two-fold increase in Cyclin-D1 expression (Fig. 7A).

Among the two important antiapoptotic proteins controlled by NF-κB, Bcl-2 expression was enhanced in cisplatin resistant cells but was down-regulated in paclitaxel and platinum-taxol cells (Fig. 7C). In contrary, anti-apoptotic protein XIAP transcripts
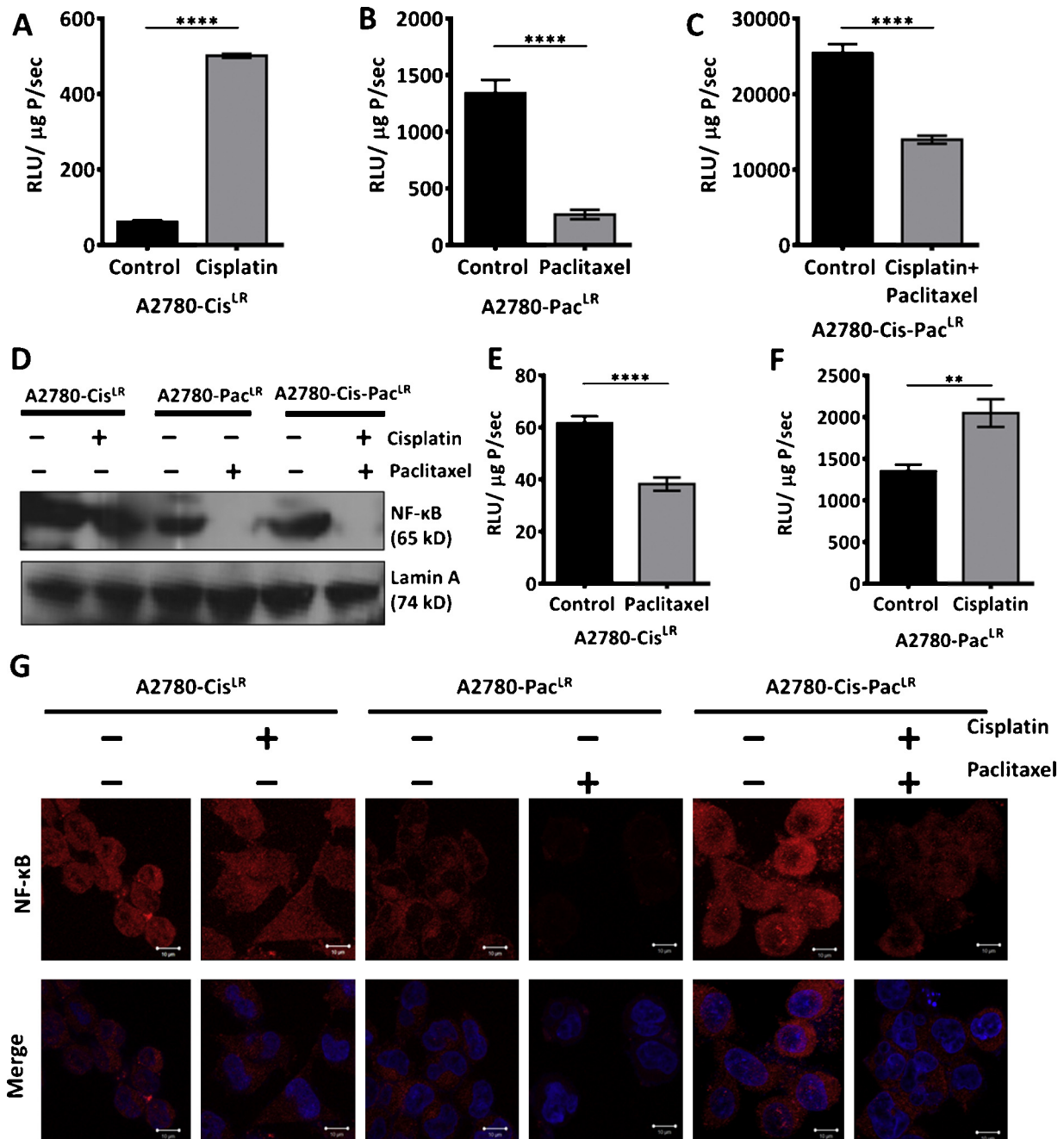
Fig. 5. Upregulated NF-κB activity was associated with cisplatin resistant cells but not with paclitaxel and dual resistant cells: A–C. Luciferase assay study A2780-Cis^LR cells stably expressing NF-κB sensor showed significant increase (****$p < 0.0001$) in luciferase activity after cisplatin treatment (A). A2780-Pac^LR and A2780-Cis-Pac^LR with stably expressing NF-κB sensor showed significant decrease (****$p < 0.0001$) in luciferase activity after paclitaxel and platinum-taxol treatment respectively (B and C). D. Immunoblotting study. Decreased NF-κB levels were evident in nuclear cell lysates of drug treated of A2780-Pac^LR and A2780-Cis-Pac^LR cells. However, no obvious change was observed after cisplatin treatment in A2780-Cis^LR. Lamin A was used as loading control. E–F. NF activity after cross treatment A2780-Cis^LR cells showed significant decrease (****$p < 0.0001$) in luciferase activity after paclitaxel treatment (E) whereas A2780-Pac^LR showed significant increase (**$p < 0.01$) in luciferase activity after cisplatin treatment (F). G. Immunofluorescence study. No apparent change was observed in the nuclear staining of NF-κB in A2780-Cis^LR after cisplatin treatment. However, decreased in NF-κB staining was evident in A2780-Pac^LR and A2780-Cis-Pac^LR (upper panel) cells after treatment. Lower panels showed the merged images with DAPI.

though decreased after cisplatin treatment showed slight change after drug treatments to A2780-Cis^LR, A2780-Pac^LR, and A2780-Cis-Pac^LR cells (Fig. 7B).

3.7. Cisplatin treatment to the A2780-Cis^LR cells augmented NF-κB activity in vivo

To non-invasively monitor NF-κB activation, subcutaneous tumor xenografts of A2780-Cis^LR cells stably expressing the NF-κB sensor were developed in nude mice ($n = 7$) and sequential

bioluminescence imaging for firefly and renilla luciferase were performed. As expected firefly luciferase activity of A2780-Cis^LR tumor xenografts ($n = 4$) showed no change after cisplatin treatment ($6.2 \times 10^6 \pm 1.6 \times 10^5$ p/s/cm^2/sr to $7.1 \times 10^6 \pm 2.1 \times 10^5$ p/s/cm^2/sr) in comparison to control tumor xenografts ($8.7 \times 10^6 \pm 1.3 \times 10^5$ to $6.8 \times 10^6 \pm 1.7 \times 10^5$ p/s/sr) ($n = 3$). However, a 14 fold increase in NF-κB-RL activity was found after cisplatin treatment ($n = 4$) ($5.43 \times 10^5 \pm 8.4 \times 10^3$ p/s/cm^2/sr to $4.31 \times 10^6 \pm 1.4 \times 10^4$ p/s/cm^2/sr) as compared to the control tumor xenografts ($n = 3$) ($3.8 \times 10^5 \pm 1.3 \times 10^4$ to $3.8 \times 10^5 \pm 1.2 \times 10^4$)
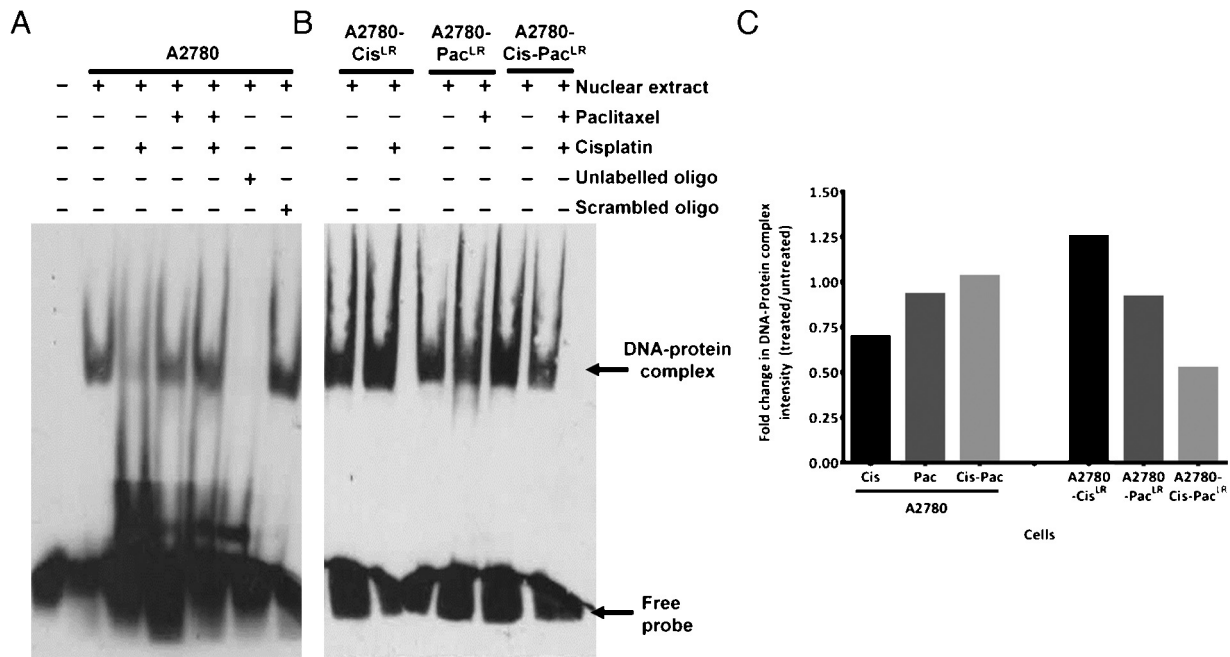
Fig. 6. Cisplatin resistant cells showed enhanced NF-κB DNA binding activity: A. NF-κB DNA binding activity in control cells. Electrophoretic mobility shift assay was performed to analyze the binding of NF-κB to respective response elements using nuclear extracts of A2780 cells treated with cisplatin, paclitaxel and both the drugs and a biotin labeled 22 bp long NF-κB response element. In comparison to paclitaxel and dual drug treatments, cisplatin treatment resulted in significant decrease in the DNA-protein complex. Disappearance of the DNA-protein complex after challenging with an unlabeled oligo confirmed the specificity of NF-κB binding. A scrambled oligo could not compete and abolish the complex. B. NF-κB DNA binding activity in drug resistant cells. The A2780-Cis^{LR} cells showed high NF-κB binding after cisplatin treatment while both A2780-Pac^{LR} and A2780-Cis-Pac^{LR} cells showed decrease in the DNA-protein complex. C. Densitometric analysis. A graphical representation of the ratiometric analysis of the intensity of the DNA-protein complexes represented the fold changes in NF-κB binding of pre and post treatments.
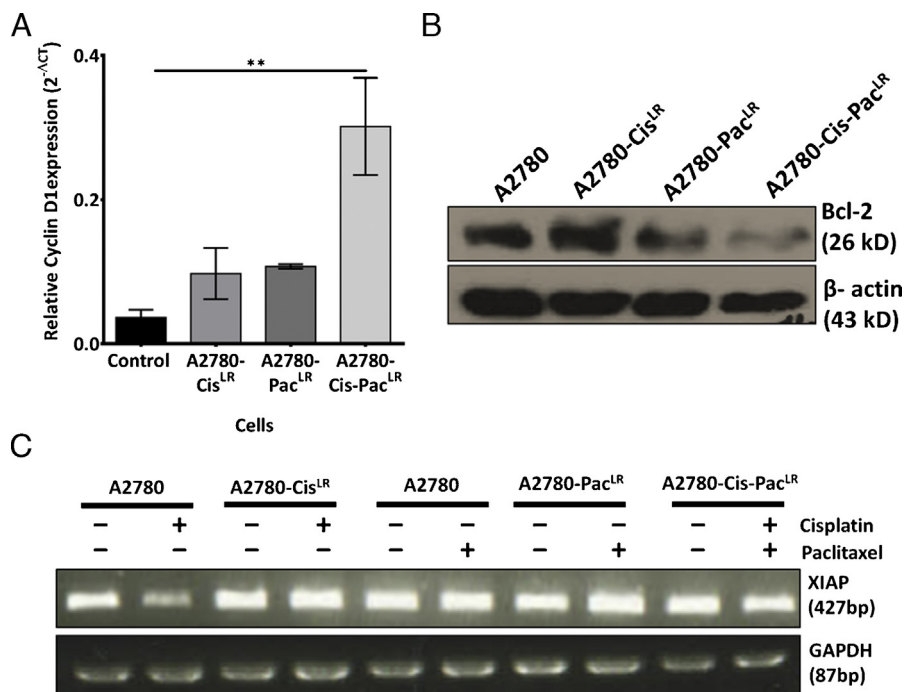
Fig. 7. Differential expression of downstream target genes of NF-κB: A–B. Expression analysis. qPCR of Cyclin D1 expression in A2780 and its isogenic resistant variants showed maximum expression in Cis-Pac^{LR} dual resistant cells ($**p < 0.01$) (A). Semi-quantitative analysis of XIAP expression in the same cells showed no change in expression level (B) C. Immunoblotting study. Endogenous Bcl-2 expression was highest in A2780-Cis^{LR} in comparison to A2780 and paclitaxel and dual resistant cells.
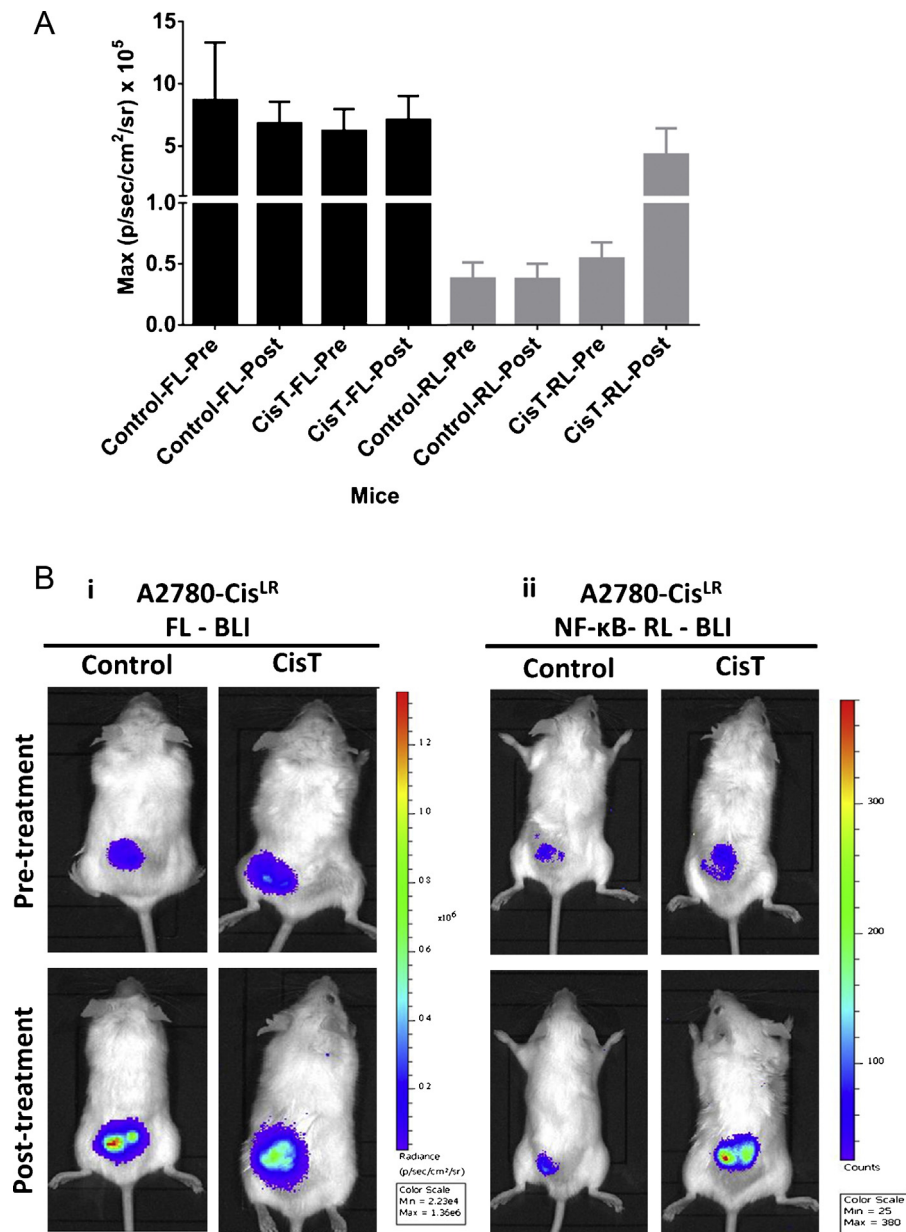
Fig. 8. Non-invasive imaging of NF-κB activity in A2780-Cis[LR] tumor xenografts after cisplatin treatment: A. Graphical representation of bioluminescence signals. Bioluminescence signals for both firefly luciferase and NF-κB-renilla luciferase were calculated for the respective ROIs drawn over tumors of control and cisplatin treated mice. No change was observed for firefly luminescence (before and after treatment), however, a 14 fold increased luminescence was observed for NF-κB-renilla luciferase after cisplatin treatment. B. Bioluminescence imaging. Representative bioluminescent images of the same mouse bearing A2780-Cis[LR] tumors are shown for pre- and post- cisplatin treatment. The left panel (7Bi) showed the mouse imaged for firefly luciferase signal and the right panel showed the same mouse imaged sequentially for the renilla luciferase signal (7Bii). The upper panel depicts images before treatment and lower panel depicts images after treatment.

(Fig. 8A). Representative images of same mouse scanned for firefly and renilla luciferase pre and post cisplatin treatment phases were shown in Fig. 8B.

3.8. Silencing of MyD88 did not affect cisplatin mediated NF-κB activation in cisplatin resistant TOV21G and SKOV3 cells

To ascertain that acquirement and maintenance of cisplatin resistance depends on TLR-4/MyD88 independent NF-κB activation in EOC cells, we suppressed MyD88 expression using lentiviral mediated MyD88 specific sh-RNA construct in naturally occurring cisplatin resistant TOV21G and SKOV3 cells and then evaluated the effect of the therapeutics. In MyD88 knock down TOV21G cells, transient transfection of NF-κB sensor showed 50% reduction in luciferase activity compared to cells transduced with a scrambled

sh-RNA construct. After paclitaxel and cisplatin + paclitaxel treatments, NF-κB activity reduced to 40% and 50% respectively, however cisplatin treatment retained 80% of NF-κB activity (compared to similar treatments to cells transduced with the scrambled sh-RNA). A comparison between MyD88 knockdown control and MyD88 knockdown cisplatin treated cells showed 1.5 fold induction in NF-κB activity (Fig. 9A). Western blot analysis confirmed the reduction in MyD88 expression level after transduction of MyD88 specific sh-RNA construct (Fig. 9C).

To monitor the effect cisplatin on stable expression of NF-κB sensor in another cisplatin resistant EOC cell line, we first generated clones of SKOV3 cells stably expressing NF-κB promoter driving a renilla luciferase-monomeric red fluorescent fusion reporter (hRL-mRFP) by puromycin selection. Since our strategy to isolate cells stably expressing the sh-RNA constructs depended on the eGFP
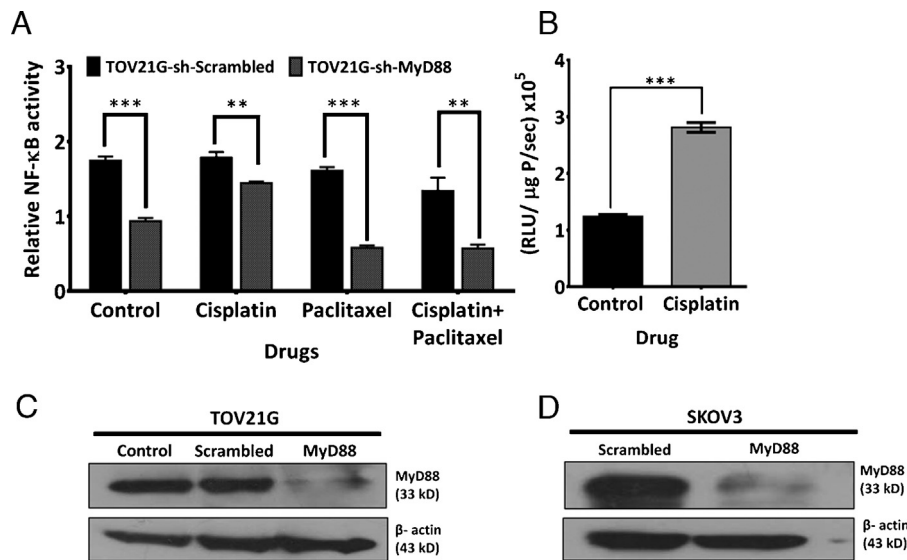
Fig. 9. Effect of MyD88 knockdown on NF-κB activity: A–B. NF-κB activity. Transient transfection of NF-κB driven-renilla luciferase-mRFP reporter in TOV21G stably expressing either sh-MyD88 or sh-scrambled constructs after cisplatin (10 μg/ml), paclitaxel (5 μg/ml) and cisplatin-paclitaxel (1 μg/ml; 500 ng/ml) treatment for 24 h resulted in significant decrease in NF-κB activity (A). Increased luciferase activity was observed after cisplatin treatment in SKOV3 cells stably expressing the NF-κB-renilla luciferase-mRFP reporter and sh-MyD88 construct (B). C–D. Validation of MyD88 knockdown cells. Western blot analysis for MyD88 protein showed significant level of knockdown in TOV21G (C) and SKOV3 (D) cells.

based FACS sorting (after lentiviral transduction), we had to use the pNF-κB–hRL-mRFP fusion reporter instead of pNF-κB–hRL-eGFP reporter which was used for other experiments. This stable clone was then transduced with MyD88 sh-RNA and then further treated with cisplatin. As expected a 2.8 fold higher NF-κB activity was observed with cisplatin treatment (Fig. 9B). The level of MyD88 suppression in these cells was analyzed as well (Fig. 9D).

4. Discussion

Despite significant improvements in clinical outcome, platinum resistance is still a major obstacle for effective treatment of epithelial ovarian carcinoma. Recent reports identified various candidate genes responsible for underlying molecular mechanisms of resistance (Chaudhury et al., 2014). MyD88, an essential adapter protein in TLR-4 mediated NF-κB signaling pathway has shown to influence the response of EOC cells to paclitaxel treatment. Though MyD88[negative] population (~40% of total EOC patients) show better prognosis and longer survival, a significant proportion of them (~40%) acquire resistance over time (Kim et al., 2012). Moreover, NF-κB signaling shows a delayed kinetics in MyD88-independent pathway and induces IFN-β and IFN-responsible genes (Kawai and Akira, 2006). In this study we investigated the state of NF-κB signaling in MyD88 deficient EOC cell lines after making them resistant towards paclitaxel, cisplatin and combinatorial treatments. Our results indicated that cisplatin down-regulated NF-κB activity in sensitive cells as shown by luciferase assay, Western blot and EMSA. Such down-regulation was also found with cisplatin-paclitaxel treatment but not with paclitaxel. Interestingly we found that while NF-κB was down-regulated in paclitaxel and platinum-taxol resistance, acquirement of cisplatin resistance showed increased activation of NF-κB. In contrary, no difference in NF-κB activity was found in MyD88 positive and cisplatin resistant TOV21G and SKOV3 cells after all the drug treatments. Silencing of MyD88 resulted in induction in NF-κB activity only after cisplatin treatment but not after paclitaxel or combinatorial treatment in these cells. This activation can be imaged noninvasively from *in vivo* tumor xenografts of cisplatin resistant and MyD88 deficient A2780 cells. Bcl-2, but not XIAP, a downstream target of NF-κB showed differential expression

in cisplatin and paclitaxel/platinum-taxol resistant cells. Thus our data indicates that an active NF-κB signaling and over expression of Bcl-2 is an essential phenomenon for acquirement of cisplatin resistance but not for paclitaxel or platinum-taxol resistance in MyD88[negative] epithelial ovarian cancer cells.

The standard therapeutic regimen for management of EOCs is a combinatorial treatment of platinum (cisplatin or carboplatin) and taxane (paclitaxel) drugs. However, their clinical utility is often limited by development of drug resistance, partly owing to our poor understanding of the underlying mechanism of resistance (Chaudhury et al., 2014; Gaikwad and Ray, 2012). Several mechanisms like alterations in drug transport and drug targets, detoxification of drug, changes in DNA repair mechanisms, activation/down regulation of genes involved in survival and cell death pathways are shown as contributory factors to poor chemoresponse of ovarian cancer (Chaudhury et al., 2014; El-Deiry, 1997). Among various survival pathways, activated PI3K/AKT/mTOR and NF-κB signaling play important roles in development and maintenance of platinum and paclitaxel resistance (Agarwal and Kaye, 2003; Alvero, 2010; Annunziata et al., 2010; Peng et al., 2010). These two pathways are often found to be mutually dependent on each other for maximal activation. Via phosphorylation of IκB kinase (IKK) that phosphorylates and directs degradation of IκB, AKT activates NF-κB, which depending upon cellular context induces cell survival or cell death (Mabuchi et al., 2004a). Thus presence of high level of phosphorylated AKT in our cisplatin, paclitaxel and platinum-taxol resistant cells indicated a possible involvement of NF-κB signaling for maintenance of resistant characteristics. However, the differential activation of NF-κB by the three different treatments in these resistant cells indicates an additional layer of regulation.

The IKK family of proteins is also known be induced by various compounds through the Toll-like Receptors (TLRs) present on myeloid and non-myeloid cells (Akira et al., 2001). After stimulated by LPS, TLR-4, a member of TLR family activates IL-1R-associated kinase (IRAK)/TRAF-6 via recruitment of an adaptor protein (myeloid differentiation factor 88). Activated IRAK/TRAF-6 further phosphorylates IKKα/IKKβ and mediates NF-κB activation through degradation of IκB proteins. In absence of MyD88, TLR-4 induces late activation and delayed response of NF-κB possibly

through association of TIRAP (Toll-IL-Receptor Adaptor Protein) via activation of IKKε/IKKι kinases and degradation of IκB proteins (Kawai and Akira, 2006).

TLR-4 driven signaling cascade which primarily triggers inflammatory and immune response is found in ovarian cancer cells and is shown to influence the drug response towards paclitaxel, a TLR-4 ligand and analogue of lipopolysaccharide. Earlier reports showed that in MyD88positive EOC cells, treatment with LPS and paclitaxel showed enhanced cell proliferation, activation of NF-κB, constitutive secretion of pro-inflammatory cytokines promoting tumor growth and thus rendering paclitaxel resistance. In contrast, MyD88negative cells undergo apoptosis and do not secrete cytokines/chemokines in response to paclitaxel treatment. Induction of MyD88 expression in MyD88negative EOC cells contributed to paclitaxel resistance (Kelly et al., 2006; Szajnik et al., 2009). MyD88 deficient A2780 cells exhibited decreased NF-κB activity after 6 h of cisplatin treatment (Mabuchi et al., 2004b). In this study, we found NF-κB activity did not alter significantly after cisplatin, paclitaxel or cisplatin + paclitaxel treatment in MyD88positive EOC cells though there was a trend in increased NF-κB activation in SKOV3 cells. However, in MyD88negative A2780 cells, reduced nuclear localization (by Western blotting and immunofluorescence assay) and decreased NF-κB activity (by reporter assay) were observed after 24 h of cisplatin treatment. Interestingly, treatment with cisplatin and paclitaxel together exhibited the similar pattern. Both these treatments resulted in complete or partial abolishment of NF-κB binding to the respective response elements. In contrast, no significant decrease in NF-κB activity and increased nuclear localization of NF-κB protein were found in paclitaxel treated cells with a slight reduction in the DNA-protein complex formation. The discrepancy found in NF-κB nuclear localization pattern after paclitaxel treatment between Szajnik et al. (2009) and us could be due to differential exposure time of the drug. Altogether our results like others indicate that MyD88 deficiency could influence the effect of different drugs upon NF-κB activation.

Previously, two subsequent studies had suggested MyD88 as a potential biomarker for measuring clinical response to paclitaxel in epithelial ovarian cancer (Kelly et al., 2006; Silasi et al., 2006). However the patient cohort in these studies was relatively small (12 in Kelly et al.'s study and 20 in Silasi et al.) and even in such small cohorts, around 50% epithelial ovarian tumors were found to be MyD88 negative. In a recent study by Kim et al. (2012), association of TLR-4/MyD88/NF-κB with survival and disease recurrence was investigated in 123 patients. Though higher disease recurrence was found in MyD88 positive tumors (∼36%), around 40% of the MyD88 negative patients (60% of total population) showed relapse and 65% of these patients were turned to be NF-κB positive. Therefore expression of MyD88 seems to create a delicate balance between *Intrinsic* and *Acquired* drug resistance in EOC where both the situations involve NF-κB activation. To understand the status of NF-κB in acquirement of cisplatin, paclitaxel and combinatorial treatment resistance in absence of MyD88 adapter protein, we generated isogenic cellular matrices of acquired drug resistant cells using a well-known MyD88negative cell line. To understand the effect of different drugs in single or in combination upon various pathways in resistant milieu, we challenged these cells with high dose of drugs for longer time period. Intriguingly, we found cisplatin treatment augmented NF-κB in cisplatin resistant cells while paclitaxel and combinatorial treatments down regulated NF-κB activity in paclitaxel and platinum-taxol resistant cells. This contrary effect was evident from luciferase, Western and immunofluorescence data. The DNA binding activity of NF-κB was increased in cisplatin treated A2780-CisLR cells while the same was reduced after paclitaxel or dual drug treatments in A2780-PacLR or A2780-Cis-PacLR cells. Cross treatments of cisplatin and paclitaxel

to A2780-PacLR or A2780-CisLR cells also showed the same induction phenotype indicating role of NF-κB signaling evading cisplatin mediated cellular toxicity in drug resistant cells. Intriguingly, when MyD88 expression was silenced in MyD88positive and cisplatin resistant cells, only cisplatin but not paclitaxel or combinatorial treatments could enhance NF-κB activity. Enhanced expressions of anti-apoptotic genes have been found to sustain the resistance properties of cancer cells (Cepeda et al., 2007). Enhanced Bcl-2 expression observed in A2780-CisLR cells is probably involved in maintenance of cisplatin resistance in our model. In contrast, decreased expression of Bcl-2 in paclitaxel and platinum-taxol resistant cells might have resulted from down-regulated NF-κB activity. Thus our data indicate that MyD88 expression is dispensable for acquirement of resistance towards cisplatin in epithelial ovarian cancer. The underlying molecular mechanism is not known and is currently under investigation.

Non-invasive imaging of molecular events in small animals has become an ideal practice to understand molecular mechanism at organ level and to evaluate therapeutic molecules (Chan et al., 2009; Chen et al., 2012). Reporter genes single or in combination, fused with gene of interest or driven by promoter of interest are frequently used with multiple imaging devices with appropriate probe/substrate. Using bioluminescence imaging modality, we first demonstrated that the cisplatin resistant tumors could effectively retained their resistant phenotype and did not exhibit attenuation in luciferase signal or tumor regression after cisplatin treatment. When these resistant cells were further engineered to stably express the NF-κB sensor, a 14 fold increase in NF-κB activity was observed after cisplatin treatment. Real time monitoring of NF-κB activity in animal models using various luciferases (renilla luciferase or gaussia luciferase) have already been demonstrated using TNF alpha as an inducer (Badr et al., 2009; Roth et al., 2006). However, to the best of our knowledge this is the first report in which NF-κB reporter activity was studied non-invasively in effect of cisplatin treatment. This unique model would be useful in screening therapeutic molecules against NF-κB or Bcl-2 for platinum resistant ovarian cancer cells particularly in a MyD88 compromised background.

5. Conclusion

MyD88, an adapter protein in TLR-4/MyD88 driven NF-κB signaling, imparts crucial influence on intrinsic taxol resistance in epithelial ovarian carcinoma. Since, about 50–60% EOC are MyD88 deficient, it is critical to understand how drug resistance is acquired in absence of MyD88. Our results demonstrated that paclitaxel, a TLR-4 ligand did not induce NF-κB in sensitive or in taxol/platinum resistant cells without MyD88 indicating an absolute dependency. In contrary, NF-κB upregulation by cisplatin and high Bcl-2 expression in MyD88 deficient cisplatin resistant cells indicated dispensability of MyD88 in acquired cisplatin resistance. In fact that silencing of MyD88 in MyD88positive cisplatin resistant cells led to NF-κB activation by cisplatin strengthens our hypothesis. Thus our data has provided a new insight into the molecular complexity associated with chemoresistance which may be exploited for developing better therapeutic strategy for ovarian cancer in future.

Appendix A. Supplementary data

Supplementary data associated with this article can be found, in the online version, at http://dx.doi.org/10.1016/j.biocel.2015.02.001.

References

Agarwal R, Kaye SB. Ovarian cancer: strategies for overcoming resistance to chemotherapy. Nat Rev Cancer 2003;3:502–16.

Akira S. Toll-like receptor signaling. J Biol Chem 2003;278:38105–8.

Akira S, Takeda K, Kaisho T. Toll-like receptors: critical proteins linking innate and acquired immunity. Nat Immunol 2001;2:675–80.

Alvero AB. Recent insights into the role of NF-kappaB in ovarian carcinogenesis. Genome Med 2010;2:56.

Annunziata CM, Stavnes HT, Kleinberg L, Berner A, Hernandez LF, Birrer MJ, et al. Nuclear factor kappaB transcription factors are coexpressed and convey a poor outcome in ovarian cancer. Cancer 2010;116:3276–84.

Armstrong DK, Bundy B, Wenzel L, Huang HQ, Baergen R, Lele S, et al. Intraperitoneal cisplatin and paclitaxel in ovarian cancer. N Engl J Med 2006;354:34–43.

Badr CE, Niers JM, Tjon-Kon-Fat LA, Noske DP, Wurdinger T, Tannous BA. Real-time monitoring of nuclear factor kappaB activity in cultured cells and in animal models. Mol Imaging 2009;8:278–90.

Beale PJ, Rogers P, Boxall F, Sharp SY, Kelland LR. BCL-2 family protein expression and platinum drug resistance in ovarian carcinoma. Br J Cancer 2000;82:436–40.

Blasius AL, Beutler B. Intracellular toll-like receptors. Immunity 2010;32:305–15.

Brozovic A, Fritz G, Christmann M, Zisowsky J, Jaehde U, Osmak M, et al. Long-term activation of SAPK/JNK, p38 kinase and fas-L expression by cisplatin is attenuated in human carcinoma cells that acquired drug resistance. Int J Cancer 2004;112:974–85.

Cepeda V, Fuertes MA, Castilla J, Alonso C, Quevedo C, Perez JM. Biochemical mechanisms of cisplatin cytotoxicity. Anticancer Agents Med Chem 2007;7:3–18.

Chan CT, Paulmurugan R, Reeves RE, Solow-Cordero D, Gambhir SS. Molecular imaging of phosphorylation events for drug development. Mol Imaging Biol 2009;11:144–58.

Chaudhury S, Maheshwari A, Ray P. Ovarian cancer an ever challenging malady. Biomed Res J 2014;1:34–55.

Chen HH, Yuan H, Josephson L, Sosnovik DE. Theranostic imaging of the kinases and proteases that modulate cell death and survival. Theranostics 2012;2:148–55.

Dier U, Shin DH, Hemachandra LP, Uusitalo LM, Hempel N. Bioenergetic analysis of ovarian cancer cell lines: profiling of histological subtypes and identification of a mitochondria-defective cell line. PloS One 2014;9:e98479.

El-Deiry WS. Role of oncogenes in resistance and killing by cancer therapeutic agents. Curr Opin Oncol 1997;9:79–87.

Gaikwad SM, Gunjal L, Junutula AR, Astanehe A, Gambhir SS, Ray P. Non-invasive imaging of phosphoinositide-3-kinase-catalytic-subunit-alpha (PIK3CA) promoter modulation in small animal models. PloS One 2013;8:e55971.

Gaikwad SM, Ray P. Non-invasive imaging of PI3K/Akt/mTOR signalling in cancer. Am J Nucl Med Mol Imaging 2012;2:418–31.

Gottesman MM. Mechanisms of cancer drug resistance. Annu Rev Med 2002;53:615–27.

Hayden MS, Ghosh S. NF-kappaB, the first quarter-century: remarkable progress and outstanding questions. Genes Dev 2012;26:203–34.

Karin M. NF-kappaB as a critical link between inflammation and cancer. Cold Spring Harb Perspect Biol 2009;1:a000141.

Kartalou M, Essigmann JM. Mechanisms of resistance to cisplatin. Mutat Res 2001;478:23–43.

Kawai T, Akira S. TLR signaling. Cell Death Differ 2006;13:816–25.

Kawai T, Akira S. Signaling to NF-kappaB by Toll-like receptors. Trends Mol Med 2007;13:460–9.

Kelly MG, Alvero AB, Chen R, Silasi DA, Abrahams VM, Chan S, et al. TLR-4 signaling promotes tumor growth and paclitaxel chemoresistance in ovarian cancer. Cancer Res 2006;66:3859–68.

Kim D, Dan HC, Park S, Yang L, Liu Q, Kaneko S, et al. AKT/PKB signaling mechanisms in cancer and chemoresistance. Front Biosci 2005;10:975–87.

Kim KH, Jo MS, Suh DS, Yoon MS, Shin DH, Lee JH, et al. Expression and significance of the TLR4/MyD88 signaling pathway in ovarian epithelial cancers. World J Surg Oncol 2012;10:193.

Koh J, Lee SB, Park H, Lee HJ, Cho NH, Kim J. Susceptibility of CD24(+) ovarian cancer cells to anti-cancer drugs and natural killer cells. Biochem Biophys Res Commun 2012;427:373–8.

Koti M, Gooding RJ, Nuin P, Haslehurst A, Crane C, Weberpals J, et al. Identification of the IGF1/PI3K/NF kappaB/ERK gene signalling networks associated with chemotherapy resistance and treatment response in high-grade serous epithelial ovarian cancer. BMC Cancer 2013;13:549.

Mabuchi S, Ohmichi M, Nishio Y, Hayasaka T, Kimura A, Ohta T, et al. Inhibition of inhibitor of nuclear factor-kappaB phosphorylation increases the efficacy of paclitaxel in in vitro and in vivo ovarian cancer models. Clin Cancer Res 2004a;10:7645–54.

Mabuchi S, Ohmichi M, Nishio Y, Hayasaka T, Kimura A, Ohta T, et al. Inhibition of NFkappaB increases the efficacy of cisplatin in in vitro and in vivo ovarian cancer models. J Biol Chem 2004b;279:23477–85.

Muccioli M, Sprague L, Nandigam H, Pate M, Benencia F. Toll-like receptors as novel therapeutic targets for ovarian cancer. ISRN Oncol 2012;2012:642141.

Nehra R, Riggins RB, Shajahan AN, Zwart A, Crawford AC, Clarke R. BCL2 and CASP8 regulation by NF-kappaB differentially affect mitochondrial function and cell fate in antiestrogen-sensitive and -resistant breast cancer cells. FASEB J 2010;24:2040–55.

Peng DJ, Wang J, Zhou JY, Wu GS. Role of the Akt/mTOR survival pathway in cisplatin resistance in ovarian cancer cells. Biochem Biophys Res Commun 2010;394:600–5.

Ray P, Wu AM, Gambhir SS. Optical bioluminescence and positron emission tomography imaging of a novel fusion reporter gene in tumor xenografts of living mice. Cancer Res 2003;63:1160–5.

Rocconi RP, Case AS, Straughn JM Jr, Estes JM, Partridge EE. Role of chemotherapy for patients with recurrent platinum-resistant advanced epithelial ovarian cancer: a cost-effectiveness analysis. Cancer 2006;107:536–43.

Roth DJ, Jansen ED, Powers AC, Wang TG. A novel method of monitoring response to islet transplantation: bioluminescent imaging of an NF-kB transgenic mouse model. Transplantation 2006;81:1185–90.

Roth V. Doubling time calculator; 2006.

Siddik ZH. Biochemical and molecular mechanisms of cisplatin resistance. Cancer Treat Res 2002;112:263–84.

Silasi DA, Alvero AB, Illuzzi J, Kelly M, Chen R, Fu HH, et al. MyD88 predicts chemoresistance to paclitaxel in epithelial ovarian cancer. Yale J Biol Med 2006;79:153–63.

Singh RK, Gaikwad SM, Jinager A, Chaudhury S, Maheshwari A, Ray P. IGF-1R inhibition potentiates cytotoxic effects of chemotherapeutic agents in early stages of chemoresistant ovarian cancer cells. Cancer Lett 2014;354:254–62.

Szajnik M, Szczepanski MJ, Czystowska M, Elishaev E, Mandapathil M, Nowak-Markwitz E, et al. TLR4 signaling induced by lipopolysaccharide or paclitaxel regulates tumor survival and chemoresistance in ovarian cancer. Oncogene 2009;28:4353–63.

Tang G, Minemoto Y, Dibling B, Purcell NH, Li Z, Karin M, et al. Inhibition of JNK activation through NF-kappaB target genes. Nature 2001;414:313–7.

Yang G, Zhou Y, Liu X, Xu L, Cao Y, Manning RJ, et al. A mutation in MYD88 (L265P) supports the survival of lymphoplasmacytic cells by activation of Bruton tyrosine kinase in Waldenstrom macroglobulinemia. Blood 2013;122:1222–32.

Yuan Z, Cao K, Lin C, Li L, Liu HY, Zhao XY, et al. The p53 upregulated modulator of apoptosis (PUMA) chemosensitizes intrinsically resistant ovarian cancer cells to cisplatin by lowering the threshold set by Bcl-x(L) and Mcl-1. Mol Med 2011;17:1262–74.

　　　　1

Design and Synthesis of Novel Schiff Base-Benzothiazole Hybrids as Potential Epidermal Growth Factor Receptor (EGFR) Inhibitors

Meenakshi Singh[a], Sudhir Kumar Singh[b], Bhushan Thakur[c], Pritha Ray[c] and Sushil K. Singh[a,*]

[a]*Department of Pharmaceutics, Indian Institute of Technology (BHU), Varanasi-221005, U.P., India;* [b]*Molecular and Structural Biology Division, CSIR-Central Drug Research Institute, Lucknow- 226031, U.P., India;* [c]*Advanced Centre for Treatment, Research and Education in Cancer (ACTREC), Tata Memorial Centre, Navi Mumbai-410210, Maharashtra, India*

Sushil K. Singh

Abstract: A series of novel Schiff bases -benzothiazole hybrids was designed, synthesized and evaluated for their anticancer activity by MTT assay and western blot method. Antiproliferative screening indicated that compound containing dihydroxy substituents had potent inhibitory activity with IC_{50} value 34μg/ml against SKOV3, A2780-S and A2780-CR cell lines. It showed more potent cytotoxicity in combination with cisplatin and paclitaxel than alone in the selected cell lines (SKOV3, A2780 and A2780-CR models). The *in vitro* cytotoxicity of the compounds on IOSE 364 cell line was evaluated to establish the selectivity. Molecular docking study exhibited good binding against epidermal growth factor receptor, which was further ascertained by immunoblot assay using specific antibody against phosphorylated EGFR, and thus unravelling the targeted anticancer mechanism.

1. INTRODUCTION

Research and development of new anticancer therapeutic agents are of paramount importance because of the innate ability of tumor cells to develop resistance to existing therapies. The progression of multiple drug resistance to anticancer agents in human tumor cells has been recognized as major impediment to unbeaten cancer chemotherapy. Thus, studies for the identification of novel drugs and targets for the management of these diseases are at the cutting edge. The clinical significance of benzothiazole moiety as antitumor [1-4], antimicrobial [5, 6], antitubercular [7], antimalarial [8], anticonvulsant [9, 10], antihelmintic [11], analgesic [12], anti-inflammatory [13] antidiabetic [14] etc., has attracted continuing interest and therefore are useful scaffold for the upgradation of pharmacologically active compounds.

The illustrious presence of biologically active benzothiazole nucleus serves a prominent role in various marine and terrestrial natural compounds. Some of the biologically active natural benzothiazoles include compounds from the dercitin (1) and kuanoniamine (2a,b) families, derived from bottom-dwelled marine sponge (*Dercitus sp.*) and from *Micronesian purple tunicate*, respectively. Benzothiazole nucleus is also found in complex molecules Rifamycin P and Q (3), Sponge-derived bronchodilator S1319 (4), the aroma fractionate of tea leaves and in the tail-gland of the red deer *Cervus elaphus* (5) as well as in antibiotic C304Aor M4582 (6) known as 6-Hydroxybenzothiazole-5-acetic acid [15] (Fig. **1**). Riluzole (PK-26124, RP-25279), Diamthazoledihydrochloride, Ethoxzolamide and pramipexole are also examples of benzothiazole bearing drugs [16].

Schiff bases, characterized by the presence of azomethine group (-C=N-) have also achieved significance due to the array of pharmacological activities viz. anti- bacterial, antifungal, anti-inflammatory, anti-cancer and anti-viral [17, 18]. These are generally synthesized by the condensation of primary amines with active carbonyl groups.

Literature survey shows that substituted 2-arylbenzothiazoles have emerged as an important pharmacophore for the development of antitumor agents [19, 20]. Synthesis of benzothiazole derivatives by different approaches with their pharmacological activities has been described by many researchers [21-26]. Modification of scaffold with different substituents is a general method for drug design and development with the possibility to be modified for obtaining more successful next generation derivatives. In Fig. (**2**), Compounds 1, 2, 3, 4 and 5 are the benzothiazole derivatives with anticancer activity [27]. Compound 6 is reported to have antitumor, antiviral, antitubercular and antimicrobial effects [28]. In the present study, we designed novel benzothiazoles possessing an azomethine linkage - a promising approach in designing drug-like molecules (Fig. **2**).

Over expression of Epidermal growth factor receptor (EGFR) is allied with several types of cancers viz. lung, ovarian and other malignancies. Over expression of 33 to 75% EGFR is reported in ovarian cancers and is associated with poor survival [29, 30]. Due to the implication of this receptor in growth and progression of ovarian cancer, it represents a promising target for anticancer drug development. A variety of strategies have been developed to obstruct the activation of EGFR including the anti- EGFR blocking monoclonal antibodies and EGFR-targeted tyrosine kinase inhibitors. Designing of EGFR- TK inhibitors is a salient approach for the improvement of new therapeutic agents [31, 32]. Gefitinib (ZD-1839, Iressa) [33] and erlotinib (OSI-774, Tarceva) [34] were approved as EGFR-TK inhibitors for the treatment of ovarian and non-small cell lung cancers, respectively.

Continuing our study on the Benzothiazole scaffold [35-38], and in view of above findings, we designed and synthesized novel Schiff base-benzothiazole hybrids and further evaluated the *in vitro* anti-tumor activity in normal, sensitive and resistant EGFR over expressed in ovarian cell lines. In addition, we have explored the potential of newly synthesized derivatives as EGFR targeted tyrosine kinase inhibitor. Finally, the synthesised compounds were docked with the crystal structure of EGFR to establish their mechanism of action [39, 40].

*Address correspondence to this author at the Pharmaceutical Chemistry Research Laboratory, Department of Pharmaceutics, Indian Institute of Technology (BHU), Varanasi-221005, U.P., India; Tel: 0542-26702749; Fax: +915422368428; E-mail: sksingh.phe@iitbhu.ac.in

(1)

(2a)   R= COCH$_2$CHMe$_2$,
          COCH$_2$Me,
          COMe

(2b)

P : R= H
Q : R=CH$_2$OH

(3)

(4)

(5)

(6)
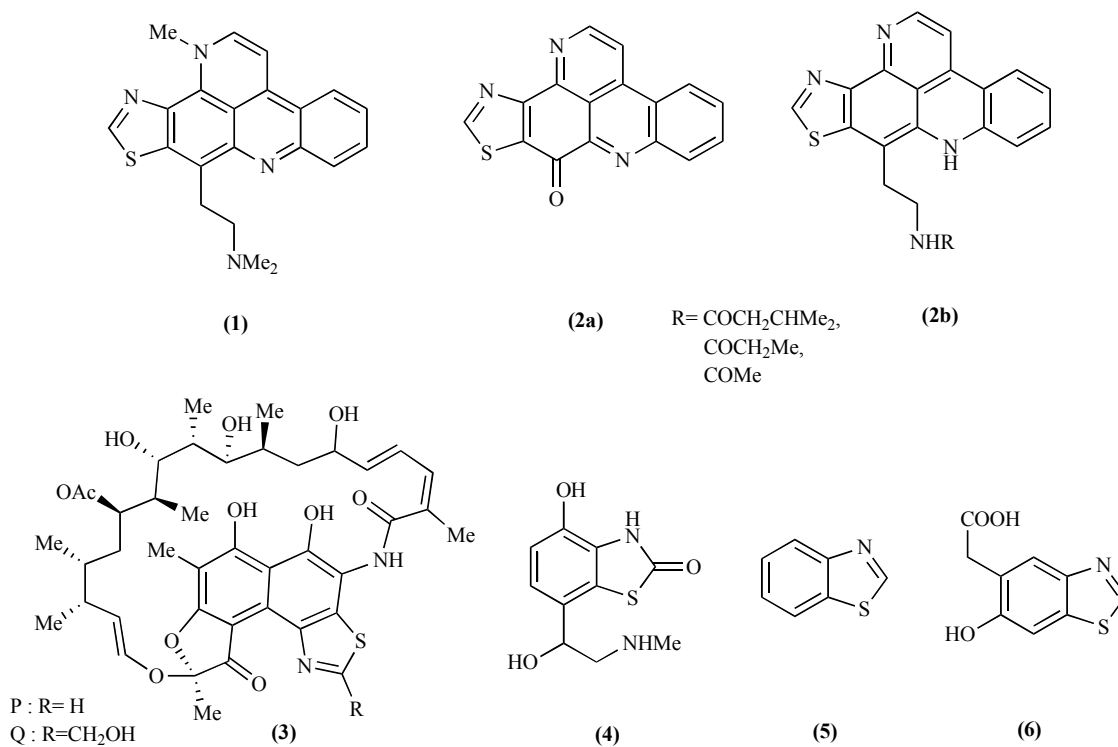
Fig. (1). Chemical structures of biologically important benzothiazole compounds.

(Frentizole)

[2]

(Phortress)

[1]

(CJM 126)

[3]

Common structural motiff

R = H, halogen, alkoxy
R' = substituted phenyl

[6]

(DF203, R=H)
(5F203, R=F)

[4]

(PMX610)

[5]
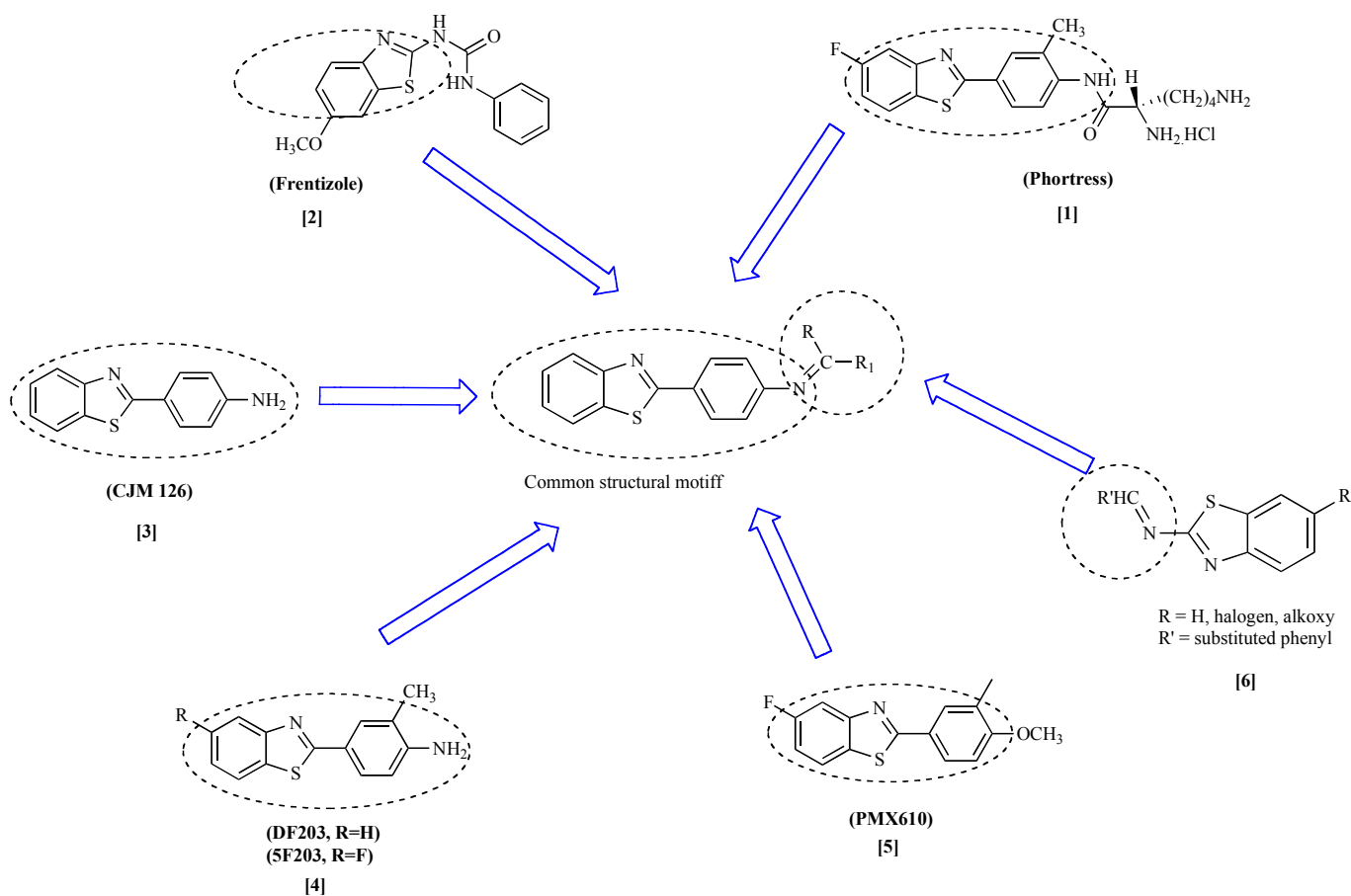
Fig. (2). Rationale of design of target compounds (**S01-20**).
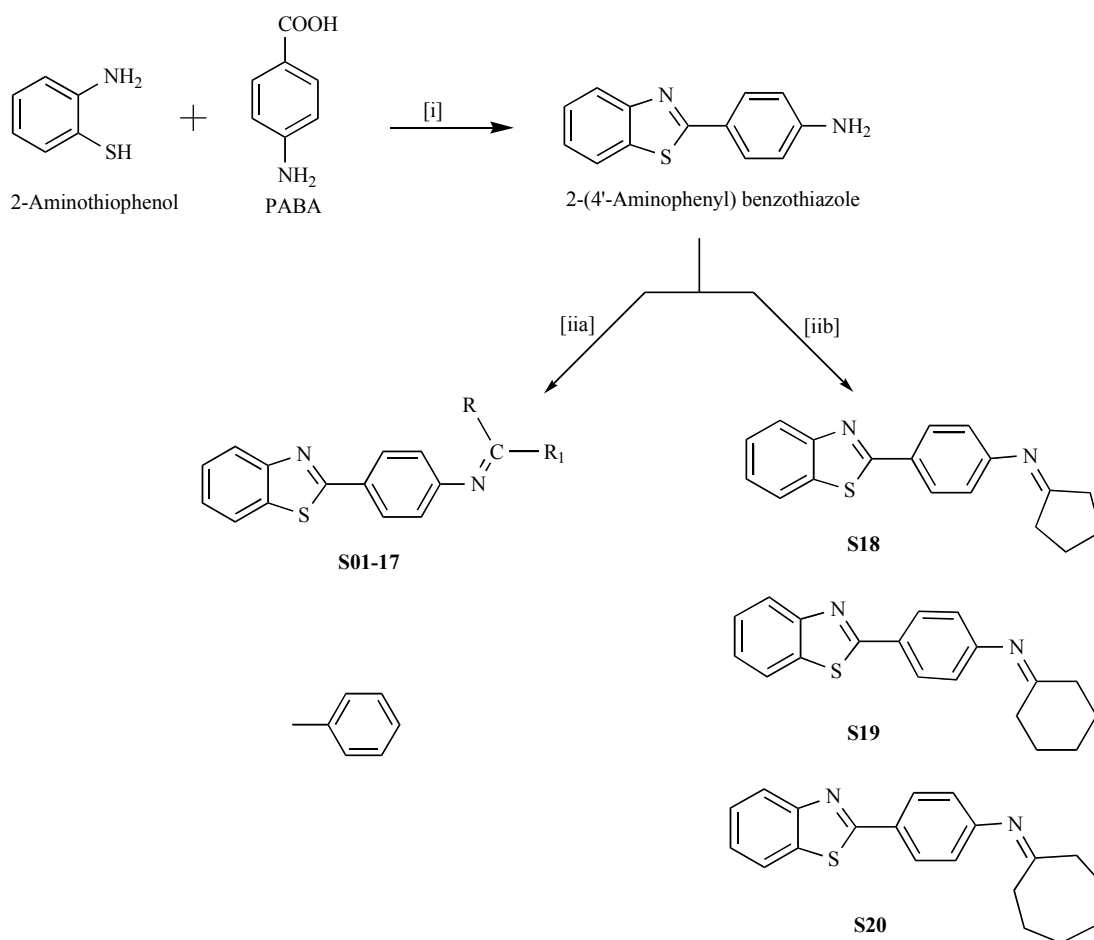
Scheme 1. Reagents and conditions: (i) Polyphosphoric acid (PPA), 220°C, 1-2 h reflux with stirring (iia) Aromatic aldehydes, CH$_3$OH/C$_2$H$_5$OH, AcOH, 4–6 h reflux (iib) Cyclic ketones, CH$_3$OH/C$_2$H$_5$OH, conc. H$_2$SO$_4$, 6–10 h reflux.

2. MATERIALS AND METHODS

2.1. Chemistry

All the chemicals and solvents were of analytical grade or purified by standard methods prior to use [41]. These were purchased from Merck (Germany), M.P. bio medicals, S.D.Fine (Mumbai) and Sigma Aldrich (USA). The progress of the reactions was monitored with the help of thin-layer chromatography (TLC) on precoated aluminium plate (silica gel GF-254, 0.25 mm). Phosphorylated EGFR (PY20) and anti-Actin antibodies (I-19) were purchased from Santa Cruz Biotechnology (Mumbai). Melting points were recorded on Stuart-SMP10 melting point apparatus and were uncorrected. FTIR spectra were measured on Shimadzu FTIR-8400s spectrophotometer. ^{1}H NMR and ^{13}C NMR spectrum was recorded on JEOL AL300 FTNMR spectrophotometer, operating at 300 MHz. Chemical shifts were reported in parts per million (ppm) downfield from TMS. Mass spectra were obtained on Micromass Quattro II spectrometer. Elemental analysis (C, H, N) were performed on Exeter Analytical Inc., USA, CE-440 elemental analyzer within 0.03% of the theoretical values.

2.2. Pharmacology

The evaluation of anticancer activity of novel hybrids (**S01-20**) was performed on two human ovarian cancer cell lines A2780 (undifferentiated EOC cell) and SKOV3 (endometroid adeno-carcinoma). Cellular chemoresistant models were developed in A2780 cells by incubating them to increasing dosages of cisplatin and paclitaxel in a cyclic manner. The resistant models (cisplatin resistant model, A2780-CR and paclitaxel resistant model, A2780-PR) represent ~90% survival at IC$_{50}$ of sensitive cells (A2780-S). Assessment of *in vitro* cytotoxicity of the synthesized compounds on sensitive and resistant models was performed by standard 3-(4, 5-dimethylthiazol-2-yl)-2, 5-diphenyltetrazolium bromide (MTT) bioassay at 48 h of drug exposure.

2.3. General Procedure for the Synthesis of Schiff base Benzothiazole Hybrids

2.3.1. General Procedure for the Synthesis of Schiff bases from Aromatic Aldehydes [N-(arylidene)-4-(benzo[d] thiazol-2-yl)benzenamines (S01-17)]

A reaction mixture coupled with 2-aminothiophenol (0.053 M) and para amino benzoic acid (PABA) (0.05 M) in polyphosphoric acid (PPA; 85 g) was refluxed with stirring at 220°C for 4 h, yielded 2-(4'-aminophenyl) benzothiazole. The solution was cooled and poured into ice-cold 10% aqueous sodium carbonate. The solid product was collected, washed with water and purified with aq. methanol in satisfactory yield, as described previously [42]. Equimolar quantities of 2-(4'-aminophenyl) benzothiazole (0.01mol) in ethanol (20ml) and the appropriate substituted aldehyde/ketone (0.01mol) in ethanol/methanol (20ml) were set to reflux for 4-6 h in the presence of few drops of glacial acetic acid. After completion of the reaction, as monitored by TLC, the reaction mixture was cooled, poured into ice cold water (five times its volume), the resultant solid was filtered and dried. Finally, the desired products obtained were recrystallized with ethanol-ethylacetate (1:1) or ethanol-dichloromethane (1:2) mixture.

2.3.2. General Procedure for the Synthesis of Schiff bases from cyclic Ketones [4-(benzo[d]thiazol-2-yl)-N-cyclopentylidene/cyclo-hexylidene/cycloheptylidene benzenamines (S18-20)]

To the equimolar ethanolic solutions of 2-(4'-aminophenyl) benzothiazole (0.01 mol) and of respective cyclic ketones (0.01 mol), few drops of conc. H_2SO_4 was added as catalyst. The reaction mixture was refluxed for 6-10 h and after cooling, the solution was poured on to crushed ice and neutralized with K_2CO_3. The separated solid was filtered and dried. Finally, the product thus obtained was recrystallized from ethyl acetate and ethanol in graded proportions depending on the nature of the compound.

2.4. Characterization of Compounds

2.4.1. N-(4-methoxybenzylidene)-4-(benzo[d]thiazol-2-yl)benzen-amine (S01)

IR (KBr, υmax cm^{-1}): 3081 (Aromatic C-H str.), 2924, 2853 (C-H str., N=CH group), 2850 (C-H str., O-CH$_3$ group), 1591 (C=N str., azomethine); ^{1}H NMR (DMSO-d$_6$, 300 MHz) δ (ppm): 3.82 (s, 3H, OCH$_3$), 6.60-6.67 (m, 4H, benzylidene-C2'', C3'', C5'', C6''), 6.83 (q, 2H, benzenamine-C3', C5'), 7.41 (q, 3H, benzenamine-C2', C6' & benzothiazole-C7), 7.63 (d, 1H, benzothiazole-C6), 7.71-7.74 (m, 1H, benzothiazole-C8), 7.82 (d, 1H, benzothiazole-C5), 8.47 (s, 1H, -N=CH); ^{13}C NMR (DMSO-d$_6$) δ (ppm): 55.69 (OCH$_3$), 141.33 (C=N-), 165.51 (benzothiazole-C-2), 164.24 (Ar-C-OCH$_3$), 129.67, 129.80, 130.47, 130.67, 130.76, 130.96, 131.13, 131.19, 131.32, 133.83, 135.11, 135.16, 140.05 (Aromatic-C, C$_4$-C$_9$ C$_1$-C$_6$, C$_1$-C$_6$); MS (m/z, %): 345 (M + 1, 100).

2.4.2. N-(4-chlorobenzylidene)-4-(benzo[d]thiazol-2-yl)benzena-mine (S02)

IR (KBr, υmax cm^{-1}): 3127, 3087 (Aromatic C-H str.), 2926, 2846 (C-H str., N=CH group), 1621 (C=N str., azomethine), 1065 (C-Cl str.); ^{1}H NMR (DMSO-d6, 300 MHz) δ (ppm): 7.26 (q, 3H, benzylidene-C3'', C5''& benzenamine-C5'), 7.42 (t, 2H, benzylidene-C2'', C6''), 7.54 (d, 3H, benzenamine-C2', C3', C6'), 7.69 (t, 1H, benzothiazole-C7), 8.01 (d, 1H, benzothiazole-C6), 8.14 (t, 2H, benzothiazole-C5, C8), 8.52 (s, 1H, -N=CH); ^{13}C NMR (DMSO-d$_6$) δ (ppm): 149.62 (C=N-), 166.35 (benzothiazole-C-2), 121.34, 121.45, 123.17, 124.33, 124.83, 126.63, 127.18, 127.82, 129.50, 131.96, 133.66, 141.66, 146.04, 146.73 (Aromatic-C, C4-C9 C1'-C6' C1''-C6''); MS (m/z, %): 349, 351 [M + 1, M + 2 (3:1)].

2.4.3. N-(2,4-dichlorobenzylidene)-4-(benzo[d]thiazol-2-yl)ben-zenamine (S03)

IR (KBr, υmax cm^{-1}): 3118, 3083 (Aromatic C-H str.), 2919, 2841 (C-H str., N=CH group), 1627 (C=N str., azomethine), 1108, 1065 (C-Cl str.); ^{1}H NMR (DMSO-d$_6$, 300 MHz) δ (ppm): 7.34 (s, 1H, benzenamine-C5'), 7.62 (t, 3H, benzenamine-C2', C3', C6'), 7.92 (d, 3H, benzylidene-C3'', C5'', C6''), 8.06 (d, 2H, benzothiazole-C7, C6), 8.22 (d, 2H, benzothiazole-C5, C8), 8.83 (s, 1H, -N=CH); ^{13}C NMR (DMSO-d$_6$) δ (ppm): 151.22 (C=N-), 165.15 (benzothiazole-C-2), 123.39, 123.397, 123.40, 123.41, 123.419, 123.78, 124.28, 126.08, 126.87, 127.27, 128.95, 131.40, 133.10, 141.10, 145.73 (Aromatic-C, C$_4$-C$_9$ C$_1$-C$_6$, C$_1$-C$_6$); MS (m/z, %): 384, 386, 388 [M + 1, M + 2, M + 4 (9:6:1)].

2.4.4. 4-(benzo[d]thiazol-2-yl)-N-(pyridin-4-ylmethylene)benzena-mine (S04)

IR (KBr, υmax cm^{-1}): 3112, 3089 (Aromatic C-H str.), 2929, 2854 (C-H str., N=CH group), 1632 (C=N str., azomethine); ^{1}H NMR (DMSO-d$_6$, 300 MHz) δ (ppm): 7.23 (d, 1H, benzenamine-C5'), 7.42 (q, 3H, benzenamine-C2', C6'), 7.75 (d, 3H, benzothiazole-C6, C7, C8), 7.87 (d, 3H, benzothiazole-C5 & pyridine-C3'', C5''), 8.26 (s, 1H, -N=CH), 8.52 (q, 2H, pyridine-C2'', C6''); ^{13}C NMR (DMSO-d$_6$) δ (ppm): 151.22 (C=N-), 166.51

(benzothiazole-C-2), 124.19, 128.21, 128.41, 128.58, 129.30, 129.53, 129.78, 131.49, 134.15, 135.46, 141.22, 143.27, 155.39 (Aromatic-C, C$_4$-C$_9$ C$_1$-C$_6$, C$_1$-C$_6$); MS (m/z, %): 316 (M + 1, 100).

2.4.5. N-(2, 4-dihydroxybenzylidene)-4-(benzo[d]thiazol-2-yl)ben-zenamine (S05)

IR (KBr, υmax cm^{-1}): 3126 (O-H str., br.), 3102 (Aromatic C-H str.), 2924, 2852 (C-H str., N=CH group), 1631 (C=N str., azomethine); ^{1}H NMR (DMSO-d$_6$, 300 MHz) δ (ppm): 6.31 (d, 1H, benzylidene-C3''), 6.80 (m, 1H, benzylidene-C5''), 7.19 (m, 3H, benzylidene-C6'' & benzenamine-C3', C5'), 7.35 (t, 4H, benzenamine-C2', C6' & benzothiazole-C6, C7), 7.52 (d, 2H, benzothiazole-C5, C8), 8.35 (s, 1H, -N=CH), 9.92 (s, 1H, *p*-OH group), 10.69 (br, s, 1H, *o*-OH group); ^{13}C NMR (DMSO-d$_6$) δ (ppm): 163.27 (Ar-C-OH), 143.20 (C=N-), 165.23 (benzothiazole-C-2), 110.29, 110.84, 111.27, 113.65, 114.14, 114.21, 118.50, 118.68, 122.13, 122.60, 124.46, 132.43, 132.75, 132.99 (Aromatic-C, C$_4$-C$_9$ C$_1$-C$_6$, C$_1$-C$_6$); MS (m/z, %): 347 (M + 1, 100).

2.4.6. N-(3-bromobenzylidene)-4-(benzo[d]thiazol-2-yl)benzen-amine (S06)

IR (KBr, υmax cm^{-1}): 3107 (Aromatic C-H str.), 2931, 2835 (C-H str., N=CH group), 1636 (C=N str., azomethine), 765 (C-Br str.); ^{1}H NMR (DMSO-d$_6$, 300 MHz) δ (ppm): 7.21-7.32 (m, 2H, benzylidene-C5'', C6''), 7.43-7.50 (m, 7H, benzylidene-C2'', C4'', benzenamine-C2', C3', C5', C6' & benzothiazole-C7), 7.73 (d, 2H, benzothiazole-C6, C8), 8.17 (d, 1H, benzothiazole-C5), 8.82 (s, 1H, -N=CH); ^{13}C NMR (DMSO-d$_6$) δ (ppm): 148.42 (C=N-), 165.32 (benzothiazole-C-2), 123.48, 124.89, 127.73, 127.86, 128.28, 128.39, 129.14, 129.25, 129.46, 129.77, 129.89, 132.96, 133.93, 133.98, 139.42, 145.73 (Aromatic-C, C$_4$-C$_9$ C$_1$-C$_6$, C$_1$-C$_6$); MS (m/z, %): 394, 396 [M + 1, M + 2 (1:1)].

2.4.7. N-(4-hydroxybenzylidene)-4-(benzo[d]thiazol-2-yl)benzena-mine (S07)

IR (KBr, υmax cm^{-1}): 3426 (O-H str.), 3132 (Aromatic C-H str.), 2924, 2813 (C-H str., N=CH group), 1634 (C=N str., azomethine); ^{1}H NMR (DMSO-d$_6$, 300 MHz) δ (ppm): 7.11-7.25 (m, 4H, benzylidene-C2'', C3'', C5'', C6''), 7.34 (t, 2H, benzenamine-C3', C5'), 7.53 (d, 2H, benzenamine-C2', C6'), 7.87-7.94 (m, 4H, benzothiazole-C5-C8), 8.32 (s, 1H, -N=CH), 9.72 (s, 1H, -OH); ^{13}C NMR (DMSO-d$_6$) δ (ppm): 160.17 (Ar-C-OH), 141.20 (C=N-), 166.83 (benzothiazole-C-2), 112.79, 120.91, 122.25, 122.51, 124.10, 125.35, 126.69, 130.18, 130.47, 132.39, 133.96, 135.58, 138.91 (Aromatic-C, C$_4$-C$_9$ C$_1$-C$_6$, C$_1$-C$_6$); MS (m/z, %): 331 (M + 1, 100).

2.4.8. 4-((4-(benzo[d]thiazol-2-yl)phenylimino)methyl)-N,N-dime-thylbenzenamine (S08)

IR (KBr, υmax cm^{-1}): 3067 (Aromatic C-H str.), 2921, 2827 (C-H str., N=CH group), 2878 (C-H str., -CH$_3$ group), 1621 (C=N str., azomethine), 1336 (-C-N str.); ^{1}H NMR (DMSO-d$_6$, 300 MHz) δ (ppm): 3.23(s, 6H, -CH$_3$), 7.06-7.09 (d, 2H, benzylidene-C3'', C5''), 7.23 (t, 2H, benzylidene-C2'', C6''), 7.38 (d, 3H, benzenamine-C2', C3', C5'), 7.49 (t, 2H, benzenamine-C6' & benzothiazole-C6), 8.23 (d, 3H, benzothiazole-C5, C7, C8), 8.61 (s, 1H, -N=CH); ^{13}C NMR (DMSO-d$_6$) δ (ppm): 44.21 (2CH$_3$-), 144.52 (C=N-), 166.10 (benzothiazole-C-2), 112.37, 121.17, 122.59, 123.21, 123.46, 123.72, 125.20, 126.62, 126.87, 127.53, 128.32, 133.47, 136.73, 140.73 (Aromatic-C, C$_4$-C$_9$ C$_1$-C$_6$, C$_1$-C$_6$); MS (m/z, %): 358 (M + 1, 100).

2.4.9. 4-(benzo[d]thiazol-2-yl)-N-benzylidenebenzenamine (S09)

IR (KBr, υmax cm^{-1}): 3147 (Aromatic C-H str.), 2938, 2815 (C-H str., N=CH group), 1630 (C=N str., azomethine); ^{1}H NMR (DMSO-d$_6$, 300 MHz) δ (ppm): 7.22 (s, 1H, benzylidene-C2''),

7.51-7.56 (m, 6H, benzylidene-C3''-C6'' & benzenamine-C3', C5'), 7.79-7.83 (m, 2H, benzenamine-C2', C6'), 7.89 (d, 2H, benzothiazole-C6, C7), 7.95 (s, 1H, benzothiazole-C8), 7.98 (s, 1H, benzothiazole-C5), 8.48 (s, 1H, -N=CH); ^{13}C NMR (DMSO-d$_6$) δ (ppm): 142.34 (C=N-), 165.09 (benzothiazole-C-2), 124.98, 126.97, 127.28, 127.76, 129.86, 130.02, 130.11, 130.31, 131.13, 131.34, 131.77, 134.20, 139.02, 139.17 (Aromatic-C, C$_4$-C$_9$ C$_1$'-C$_6$', C$_1$''-C$_6$''); MS (m/z, %): 315 (M + 1, 100).

2.4.10.   N-(4-methylbenzylidene)-4-(benzo[d]thiazol-2-yl)benzenamine (S10)

IR (KBr, υmax cm^{-1}): 3068 (Aromatic C-H str.), 2936, 2829 (C-H str., N=CH group), 2892 (C-H str., -CH$_3$ group), 1691 (C=N str., azomethine); ^{1}H NMR (DMSO-d$_6$, 300 MHz) δ (ppm): 2.82 (s, 3H, -CH$_3$), 7.06-7.24 (m, 8H, benzylidene-C2'', C3'', C5'', C6'' & benzenamine- C2', C3', C5', C6'), 7.48 (d, 1H, benzothiazole-C6), 7.55-7.58 (m, 2H, benzothiazole-C7, C8), 7.80 (d, 1H, benzothiazole-C5), 8.28 (s, 1H, -N=CH); ^{13}C NMR (DMSO-d$_6$) δ (ppm): 22.36 (-CH$_3$), 140.12 (C=N-), 166.15 (benzothiazole-C-2), 112.46, 118.87, 119.12, 127.66, 127.90, 128.11, 128.54, 128.78, 130.27, 130.52, 132.64, 132.88, 134.71, 139.03 (Aromatic-C, C$_4$-C$_9$ C$_1$'-C$_6$' C$_1$''-C$_6$''); MS (m/z, %): 329 (M + 1, 100).

2.4.11.   N-(3-nitrobenzylidene)-4-(benzo[d]thiazol-2-yl)benzenamine (S11)

IR (KBr, υmax cm^{-1}): 3127 (Aromatic C-H str.), 2939, 2831(C-H str., N=CH group), 1632 (C=N str., azomethine), 1351 (N=O str.); ^{1}H NMR (DMSO-d$_6$, 300 MHz) δ (ppm): 7.12 (s, 1H, benzylidene-C6''), 7.51-7.65 (m, 7H, benzylidene-C2'', C4'', C5'' & benzenamine-C2', C3', C5', C6'), 7.90 (d, 3H, benzothiazole-C6, C7, C8), 8.10 (s, 1H, benzothiazole-C5), 8.74 (s, 1H, -N=CH); ^{13}C NMR (DMSO-d$_6$) δ (ppm): 149.40 (C=N-), 165.02 (benzothiazole-C-2), 121.98, 122.94, 123.64, 124.10, 126.24, 129.95, 132.02, 132.94, 135.44, 141.42, 142.32, 146.74, 147.15, 147.30, 147.49, 147.73 (Aromatic-C, C$_4$-C$_9$ C$_1$'-C$_6$' C$_1$''-C$_6$''); MS (m/z, %): 360 (M + 1, 100).

2.4.12.   N-(2-chlorobenzylidene)-4-(benzo[d]thiazol-2-yl)benzenamine (S12)

IR (KBr, υmax cm^{-1}): 3116 (Aromatic C-H str.), 2942, 2844 (C-H str., N=CH group), 1646 (C=N str., azomethine), 1061 (C-Cl str.); ^{1}H NMR (DMSO-d$_6$, 300 MHz) δ (ppm): 7.06 (s, 1H, benzylidene-C6''), 7.51-7.68 (m, 7H, benzylidene-C3''-C5'' & benzenamine- C2', C3', C5', C6'), 7.90-7.95 (m, 3H, benzothiazole-C6, C7, C8), 8.26 (s, 1H, benzothiazole-C5), 8.69 (s, 1H, -N=CH); ^{13}C NMR (DMSO-d$_6$) δ (ppm): 148.02 (C=N-), 166.05 (benzothiazole-C-2), 122.84, 123.17, 123.28, 124.71, 126.22, 126.59, 128.18, 129.05, 129.09, 129.54, 130.58, 130.59, 132.44, 133.32, 145.57, 148.33 (Aromatic-C, C$_4$-C$_9$ C$_1$'-C$_6$' C$_1$''-C$_6$''); MS (m/z, %): 349, 351 [M + 1, M + 2 (3:1)].

2.4.13.   5-((4-(benzo[d]thiazol-2-yl)phenylimino)methyl)-2-methoxyphenol (S13)

IR (KBr, υmax cm^{-1}): 3458 (O-H str.), 3088, 3054 (Aromatic C-H str.), 2930, 2843 (C-H str., N=CH group), 2885 (C-H str., O-CH$_3$ group), 1641 (C=N str., azomethine); ^{1}H NMR (DMSO-d$_6$, 300 MHz) δ (ppm): 3.80 (s, 3H, -OCH$_3$), 6.96 (d, 2H, benzylidene-C2'', C6''), 7.37-7.49 (m, 3H, benzylidene-C5'' & benzenamine-C3', C5'), 7.59-7.70 (m, 6H, benzenamine- C2', C6' & benzothiazole-C5-C8), 8.34 (s, 1H, -N=CH), 10.36 (br, s, 1H, -OH group); ^{13}C NMR (DMSO-d$_6$) δ (ppm): 56.06 (OCH$_3$), 145.33 (C=N-), 165.01 (benzothiazole-C-2), 124.67, 126.18, 127.01, 128.34, 128.54, 129.38, 129.72, 130.43, 130.75, 130.94, 137.53, 138.98, 142.71, 143.53, 144.15 (Aromatic-C, C$_4$-C$_9$ C$_1$'-C$_6$' C$_1$''-C$_6$''); MS (m/z, %): 361 (M + 1, 100).

2.4.14.   N-(2-nitrobenzylidene)-4-(benzo[d]thiazol-2-yl)benzenamine (S14)

IR (KBr, υmax cm^{-1}): 3169 (Aromatic C-H str.), 2973, 2845 (C-H str., N=CH group), 1643 (C=N str., azomethine), 1365 (N=O str.); ^{1}H NMR (DMSO-d$_6$, 300 MHz) δ (ppm): 7.11 (d, 1H, benzylidene-C6''), 7.25 (s, 1H, benzylidene-C5''), 7.30-7.38 (m, 4H, benzylidene-C3'', C4'' & benzenamine- C3', C5'), 7.47-7.60 (m, 2H, benzenamine- C2', C6'), 7.70-7.78 (m, 1H, benzothiazole-C6), 7.97-8.07 (m, 2H, benzothiazole-C7, C8), 8.43 (d, 1H, benzothiazole-C5), 8.84 (s, 1H, -N=CH); ^{13}C NMR (DMSO-d$_6$) δ (ppm): 150.94 (C=N-), 164.70 (benzothiazole-C-2), 126.08, 126.15, 126.30, 126.49, 127.84, 128.18, 129.50, 131.51, 133.91, 135.59, 136.26, 141.47, 143.01,143.10, 143.27 (Aromatic-C, C$_4$-C$_9$ C$_1$'-C$_6$' C$_1$''-C$_6$''); MS (m/z, %): 360 (M + 1, 100).

2.4.15.   N-(3,4,5-trimethoxybenzylidene)-4-(benzo[d]thiazol-2-yl)benzenamine (S15)

IR (KBr, υmax cm^{-1}): 3146, 3120, 3068 (Aromatic C-H str.), 2924, 2854 (C-H str., N=CH group), 2915, 2835, 2812 (C-H str., O-CH$_3$ group), 1634 (C=N str., azomethine); ^{1}H NMR (DMSO-d$_6$, 300 MHz) δ (ppm): 3.72 (s, 3H, OCH$_3$), 3.87 (s, 6H, OCH$_3$), 6.96-6.98 (m, 3H, benzylidene-C2'', C6'' & benzenamine-C5'), 7.28 (d, 2H, benzenamine-C3', C6), 7.42 (d, 2H, benzenamine-C2' & benzothiazole-C6), 7.60 (s, 1H, benzothiazole-C7), 7.87 (d, 2H, benzothiazole-C5, C8), 8.23 (s, 1H, -N=CH); ^{13}C NMR (DMSO-d$_6$) δ (ppm): 56.20, 56.50 (OCH$_3$), 142.03 (C=N-), 165.66 (benzothiazole-C-2), 114.67, 123.0, 126.18, 127.01, 128.34, 128.54, 129.38, 129.72, 130.43, 130.75, 130.94, 132.53, 134.85 (Aromatic-C, C$_4$-C$_9$ C$_1$'-C$_6$' C$_1$''-C$_6$''); MS (m/z, %): 405 (M + 1, 100).

2.4.16.   N-(3-fluorobenzylidene)-4-(benzo[d]thiazol-2-yl)benzenamine (S16)

IR (KBr, υmax cm^{-1}): 3183 (Aromatic C-H str.), 2933, 2821(C-H str., N=CH group), 1653 (C=N str., azomethine); ^{1}H NMR (DMSO-d$_6$, 300 MHz) δ (ppm): 7.14 (d, 2H, benzylidene-C2'', C6''), 7.50 (s, 1H, benzylidene-C5''), 7.83 (d, 2H, benzylidene-C4'' & benzenamine- C5'), 8.06 (s, 1H, benzenamine- C3'), 8.22-8.28 (m, 5H, benzenamine- C2', C6' & benzothiazole- C6, C7, C8), 8.55 (s, 1H, benzothiazole-C5), 8.75 (s, 1H, -N=CH); ^{13}C NMR (DMSO-d$_6$) δ (ppm): 149.02 (C=N-), 165.09 (benzothiazole-C-2), 118.34, 118.63, 120.13, 122.22, 123.28, 124.27, 125.43, 126.35, 126.66, 128.27, 129.53, 133.71, 136.18, 138.06, 138.18, 139.13 (Aromatic-C, C$_4$-C$_9$ C$_1$'-C$_6$' C$_1$''-C$_6$''); MS (m/z, %): 333 (M + 1, 100).

2.4.17.   N-((1H-indol-3-yl)methylene)-4-(benzo[d]thiazol-2-yl)benzenamine (S17)

IR (KBr, υmax cm^{-1}): 3276 (-N-H str.), 3095 (Aromatic C-H str.), 2941, 2856 (C-H str., N=CH group), 1614 (C=N str., azomethine); ^{1}H NMR (DMSO-d$_6$, 300 MHz) δ (ppm): 7.01 (d, 2H, Indole), 7.22 (d, 2H, Indole), 7.49-7.53 (m, 3H, Indole & benzenamine-C2', C6'), 7.64 (d, 1H, benzenamine-C3'), 7.78 (d, 4H, benzenamine-C5' & benzothiazole-C6-C8), 7.89 (s, 1H, benzothiazole-C5), 8.37 (s, 1H, -N=CH), 11.35 (s, 1H, Indole NH); ^{13}C NMR (DMSO-d$_6$) δ (ppm): 142.82 (C=N-), 165.41 (benzothiazole-C-2), 121.74, 121.77, 122.74, 125.98, 126.05, 127.53, 127.71, 128.08, 129.38, 130.18, 131.04, 131.21, 132.71, 134.59, 134.62, 140.30, 140.33 (Aromatic-C, C$_4$-C$_9$ C$_1$'-C$_6$' C$_1$''-C$_6$''); MS (m/z, %): 354 (M + 1, 100).

2.4.18.   4-(benzo[d]thiazol-2-yl)-N-cyclopentylidenebenzenamine (S18)

IR (KBr, υmax cm^{-1}): 3071, 3039 (Aromatic C-H str.), 2920, 2825 (C-H str. of cylopentyl group), 1647 (C=N str., azomethine); ^{1}H NMR (DMSO-d$_6$, 300 MHz) δ (ppm): 1.41-1.52 (m, 6H, cyclopentylidene-H), 1.85 (s, 2H, cyclopentylidene-H), 7.31-7.47 (m, 2H, benzenamine-C3', C5'), 7.54 (t, 1H, benzenamine-C6'),

7.78 (q, 3H, benzenamine-C2' & benzothiazole-C6, C7), 8.13 (d, 1H, benzothiazole-C8), 8.44 (t, 1H, benzothiazole-C5); ^{13}C NMR (DMSO-d$_6$) δ (ppm): 22.03, 34.38 (cyclopentyl-C), 141.53 (C=N-), 165.41 (benzothiazole-C-2), 121.34, 121.68, 126.75, 126.82, 127.0, 127.82, 128.84, 129.25, 130.69, 134.38 (Aromatic-C, C$_4$-C$_9$ C$_1$'-C$_6$', C$_1$''-C$_6$''); MS (m/z, %): 293 (M + 1, 100).

2.4.19. 4-(benzo[d]thiazol-2-yl)-N-cyclohexylidenebenzenamine (S19)

IR (KBr, υmax cm^{-1}): 3118, 3049 (Aromatic C-H str.), 2923, 2834 (C-H str. of cylohexyl group), 1618 (C=N str., azomethine); ^{1}H NMR (DMSO-d$_6$, 300 MHz) δ (ppm): 1.78-1.97 (m, 8H, cyclohexylidene-H), 2.35 (s, 2H, cyclohexylidene-H), 7.34 (s, 1H, benzenamine-C6'), 7.40 (t, 2H, benzenamine-C3', C5'), 7.53 (t, 2H, benzenamine-C2' & benzothiazole-C6), 7.65 (t, 1H, benzothiazole-C7), 8.01 (d, 1H, benzothiazole-C8), 8.18 (s, 1H, benzothiazole-C5); ^{13}C NMR (DMSO-d$_6$) δ (ppm): 24.37, 25.22, 36.58 (cyclohexyl-C), 146.42 (C=N-), 166.01 (benzothiazole-C-2), 123.94, 127.35, 127.77, 127.82, 127.95, 129.29, 129.47, 131.67, 131.76, 140.28 (Aromatic-C, C$_4$-C$_9$ C$_1$'-C$_6$', C$_1$''-C$_6$''); MS (m/z, %): 307 (M + 1, 100).

2.4.20. 4-(benzo[d]thiazol-2-yl)-N-cycloheptylidenebenzenamine (S20)

IR (KBr, υmax cm^{-1}): 3131, 3058 (Aromatic C-H str.), 2933, 2854 (C-H str. of cyloheptyl group), 1637 (C=N str., azomethine); ^{1}H NMR (DMSO-d$_6$, 300 MHz) δ (ppm): 1.86-2.08 (m, 10H, cycloheptylidene-H), 2.63 (s, 2H, cycloheptylidene-H), 7.31 (t, 1H, benzenamine-C6'), 7.52 (d, 2H, benzenamine-C3', C5'), 7.81 (t, 2H, benzenamine-C2' & benzothiazole-C6), 8.02 (d, 1H, benzothiazole-C7), 8.19 (t, 2H, benzothiazole-C8, C5); ^{13}C NMR (DMSO-d$_6$) δ (ppm): 27.17, 29.10, 38.68 (cyloheptyl-C), 148.22 (C=N-), 165.72 (benzothiazole-C-2), 124.94, 127.11, 127.29, 128.03, 129.0, 130.52, 134.64, 140.01, 143.17, 143.18 (Aromatic-C, C$_4$-C$_9$ C$_1$'-C$_6$', C$_1$''-C$_6$''); MS (m/z, %): 321 (M + 1, 100).

2.5. In-Silico Studies

2.5.1. Docking Study

Molecular docking was performed using the X-ray crystal structure of tyrosine kinase as a template retrieved from protein data bank (PDB ID: 2J5F) and further modified for docking calculations. Protein preparation was carried out by deleting the water molecules and adding the hydrogen atoms, where they were missing. Further, grids of default box size were defined using the ligand binding site of the crystal structure. The 3D structure of the ligands was built with the help of Arguslab server, energetically minimized upto 0.01 rms gradient using Merck Molecular Universal Force Field (MMUFF) [43] and Gasteigere-Marsili partial charges were assigned to the ligands for docking calculations. Furtherance, the Lamarckian genetic algorithm and the Pseudo-Solis as well as Wets methods were applied using default parameters for minimization. The receptor tyrosine kinase was docked with ligand having lowest energy conformation using the generated grid. The number of docking runs, genetic algorithm population, energy evaluations and the maximum number of iterations were 50, 250, 10000 and 100000, respectively. The results were interpreted on the basis of docking score and best binding pose was considered as the final output. The docking results also showed optimized binding energy, inhibition constant, intermolecular energy and subsequently analysed for other interactions like hydrogen bonding, hydrophobic and vander Waal's interaction.

2.5.2. Pharmacokinetic Predictions

The *in silico* pharmacokinetic prediction study was performed on preADMET server for ligands that acquired good docking

scores, in order to remove compounds with poor pharmokinetic properties and hence minimises expensive and time consuming steps. This program simultaneously calculates physically important descriptors and pharmaceutically related properties to predict experimentally various human ADMET processes as well as other significant pharmacokinetic parameters such as oral absorption, bioavailability, skin penetration, clearance (C$_L$), volume of distribution (V$_d$), and metabolism [44, 45].

2.6. Evaluation of Anti-Cancer Activity

2.6.1. Maintenance of Cancer Cell Lines

Human ovarian cancer cell lines, A2780 parent cells and their respective resistant counterparts were cultured in DMEM supplemented with 10% FBS. IOSE 364 (normal ovarian surface epithelial cell line) was cultured in MCDB-M199 medium supplemented with 15% FBS. SKOV3 cells were cultured in McCoy's medium supplemented with 10% FBS along with 1% glutamine and 50 mM/ml antibiotic solution in a CO$_2$ incubator with humidified atmosphere of 5% CO$_2$ and 95% air.

2.6.2. Cytotoxicity Assessment

The 3-(4, 5-dimethylthiazol-2-yl)-2, 5-diphenyltetrazolium bromide (MTT) dye reduction assay was used to determine cytotoxic effect of S-series compounds in ovarian cancer cell lines. The test compounds were dissolved in 0.1% Dimethyl sulfoxide (DMSO) for the assay. To estimate the half maximal inhibitory concentration (IC$_{50}$), cells were incubated with each drug at different concentrations (1mM, 0.1mM and 0.01mM) for 48 hours. This was followed by MTT (5mg/ml) incubation for 3 hr at 37°C. Formazan crystal was solubilised with DMSO and absorbance was measured spectrophotometrically on ELISA plate reader at 540 nm [2]. The experiments were performed in triplicate.

2.7. Immunoblot Analysis

Western blot analysis was used to assess the phosphorylation pattern of EGFR. The assay was performed as described previously [46]. Briefly, the ovarian cancer cells were grown overnight in 60 cm^2 tissue culture dish until sub confluence, then were exposed with different chemical treatments at single concentration 100 μM and also without any chemical treatment. A single dose of 10 μM gefitinib was used as positive control. After 48 hours, cells were pellet down and washed thrice in cold PBS and further lysed using buffer [50 mM Tris-HCl (pH 7.5), 250 mM NaCl, 5 mM EDTA, 50 mM NaF, 1 mM DTT, 50 mM Na$_3$VO$_4$ and 0.5% NP-40] containing protease inhibitor cocktails (Roche Diagnostics, IN). Protein estimation of the cell lysates was determined using BCA assay kit (Thermo Scientific). 50 μg of proteins were resolved by 10% SDS-PAGE and transferred onto PVDF membrane (Millipore, Bedford, MA). After 1 hour, blot was blocked with 5% non fat dry milk and 5% BSA in TBST at room temperature and further probed overnight at 4°C with desired phosphorylated EGFR antibody. To ensure equal loading, another blot containing actin was blocked in 5% non fat dry milk and probed overnight with anti-actin antibody at 4°C. Membranes were then washed thrice with TBST, incubated with peroxidase conjugated secondary antibody for 1 hour at room temperature, and specific protein bands were detected by X-ray film (Kodak, Rochester, NY) using the enhanced chemiluminescence (ECL) detection system (GE Healthcare). The densitometry of the western blots was calculated by Image J (IJ1.46r).

3. RESULTS AND DISCUSSION

3.1. Chemistry

The synthesis of target compounds viz. N-(arylidene)-4-(benzo[d]thiazol-2-yl)benzenamines (**S01-17**) and 4-(benzo[d]thiazol-2-yl)-N-cyclopentylidene/cyclohexylidene/cycloheptylidene

benzenamines (**S18-20**) were achieved by adopting the steps outlined in Scheme **1**. The final product was obtained in the following steps. In the first step, the key intermediate *i.e.*, 2-(4'-aminophenyl) benzothiazole was prepared by coupling 2-amino thiophenol with para amino benzoic acid (PABA) in polyphosphoric acid. In the second step, a mixture of equimolar quantities of substituted aryl aldehydes/cyclic ketones and key intermediate obtained in the first step was refluxed in appropriate solvent (methanol/ethanol) in the presence of few drops of glacial acetic acid/conc.H_2SO_4 used as catalyst, yielding Schiff bases (**S01-17**) and (**S18-20**), respectively. All the characterization data of synthesized compounds (**S01-20**) were in accordance with the proposed molecular structures. The purity assessment of the synthesized compounds was analysed by TLC and established by elemental analysis.

The structure of Schiff bases of 2-(4'-aminophenyl) benzothiazole was confirmed by the comprehensive spectral data. The FT-IR spectra showed absorption bands at 3039 and 3183 cm^{-1} for aromatic C-H and at 1591 and 1691 cm^{-1} for azomethine group (-CH=N-). Formation of Schiff bases was confirmed by the absence of characteristic IR absorption peak (3140-3400 cm^{-1}) of N-H stretching, due to conversion of -NH$_2$ group to -CH=N- group. The ^{1}H NMR showed sharp singlet peak in the range of δ 8.23-8.84 ppm indicating the presence of azomethine proton (-CH=N-). The multiplet at δ 6.31-8.65 ppm was due to aromatic protons. The ^{13}C NMR spectra revealed all the corresponding peaks in the range of δ 140.12-151.22 ppm and δ 110.29-155.39 ppm which were due to azomethine (-CH=N-) carbon and aryl carbon respectively. The peak appearing in the range of δ 165.01-166.83 ppm corresponded to C2 of the benzothiazole ring. Phenolic-OH proton and methoxy protons of compound **S13** exhibited singlet at δ 10.36 and δ 3.80 ppm respectively. Methoxy protons of compounds **S01** and **S15** exhibited singlet at δ 3.82 and δ 3.88 ppm respectively. The phenolic-OH groups of compound **S05** showed broad singlet for *o*-OH proton at about δ 10.69 and singlet for *p*-OH proton at δ 9.92. The phenolic-OH proton for compound **S07** showed singlet at δ 9.72 ppm. Further, ESI-MS spectra gave all the (M+1) peaks related to molecular weight of the compounds. Compound **S05** showed peak at m/z 347(M+1,100%), which is in compliance with the molecular formula $C_{20}H_{14}N_2O_2S$. Physicochemical data and CHN results (microanalysis data) of the compounds are listed in Table **1**. The characteristic spectral data of the compounds are given in Section 2.

3.2. Docking Study

The molecular docking software, Autodock 4.0 was used to study the binding behaviour of the ligands onto receptor binding pockets. The association of EGFR family of tyrosine kinases in cancer proliferation suggest ligands which block the kinase activity of the entire EGFR family and may have profound therapeutic potential [47]. With the exposition of the 3D-structures of kinase domains, ATP-binding pocket has been the spotlight of small molecular inhibitor design [48, 49]. Benzothiazoles act *via* challenging with ATP intended for binding at the catalytic domain of tyrosine kinase [50]. The ATP binding site has the following features: Adenine region - plays an important role in hydrogen bonding; Sugar region - a hydrophilic region; Hydrophobic pocket - though not used by ATP but plays an imperative role in inhibitor selectivity; Hydrophobic channels - even if not used by ATP but may be exploited for inhibitor specificity; and Phosphate binding region - precisely used for improving inhibitor selectivity [51]. Thus, we selected EGFR target to carry out the docking study of synthesized compounds and delineate their best possible mechanism of action. The proposed hypothetical model of the highly active N-(2,4-dihydroxybenzylidene)-4-(benzo[d]thiazol-2-yl)benzenamine (**S05**) bound to ATP binding site of EGFR tyrosine kinase is shown in Fig. (**3**).

Molecular docking studies of the target compounds were performed to explore the possible interaction between target (ATPase domain of tyrosine kinase) and synthesised compounds. A number of general residues involved in this type of interaction are LYS745, VAL726, MET766, ASP800 and MET793. Almost all the compounds were found to reveal hydrogen bonding with wide range of residues. Lys745 was found to be common residue involved in the docking of maximum number of ligands. Although, MET793 contributes to the hinge binding with the ligands but it is not necessary that all the ligands exhibit such an interaction. Due to different conformational changes and orientation behaviour of the ligands in the amino acid pool of receptor, only 'O' atom of methoxy group contributed hinge binding with the residues MET793, as found in compounds **S01** and **S13**. Despite tri-methoxy substitution in compound **S15**, hinge interaction was absent in it due to its bulkiness nature, resulting in altered conformational position. Binding pose of compound **S01** in the ATP binding site of EGFR-TK showing hinge binding, is shown in Fig. (**4**).
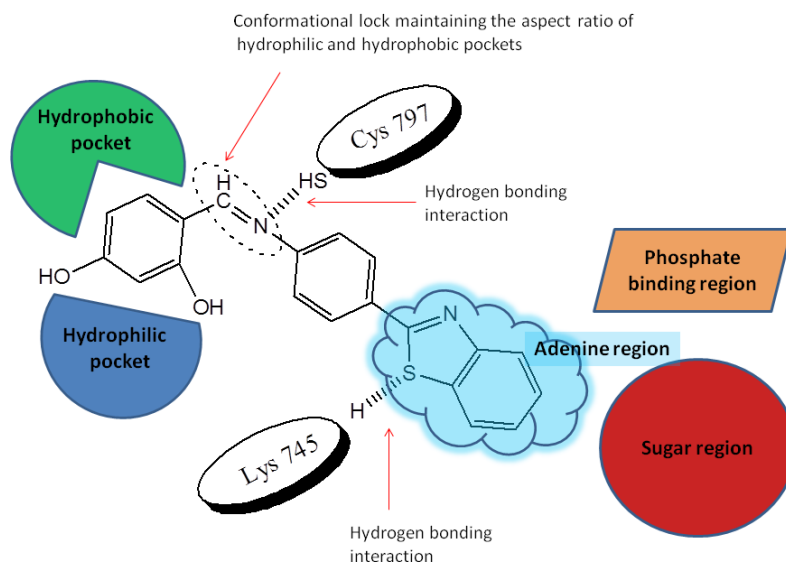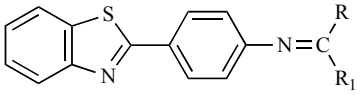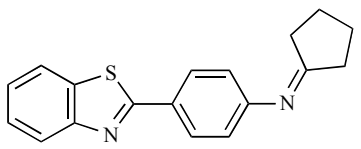
Fig. (3). Proposed hypothetical model of the highly active N-(2, 4-dihydroxybenzylidene)-4-(benzo[d]thiazol-2-yl)benzenamine (**S05**) bound to ATP binding site of EGFR Protein tyrosine kinase.
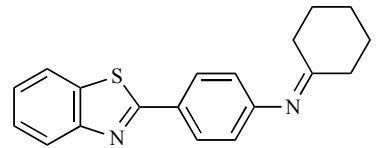
Table 1. **Analytical and physicochemical data of the synthesized compounds.**
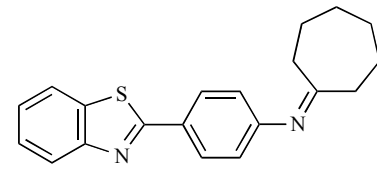
S01-17

S18

S19

S20
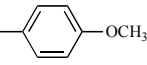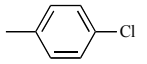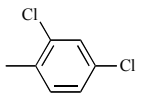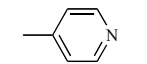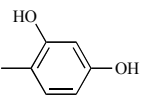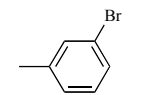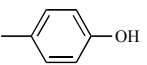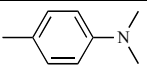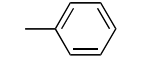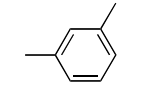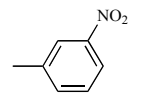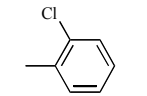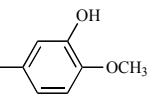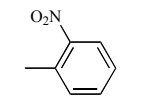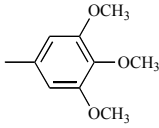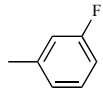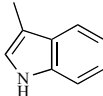
Compound Code	R	R₁	Molecular Formula	M.W.ᵃ	M.p.(°C)ᵇ	Yield (%)	% Analysis of C, H,N Found (calc.)ᶜ		
							C	H	N
S01	H	―〈 〉―OCH₃	$C_{21}H_{16}N_2OS$	344.43	181-183	84	73.21(73.23)	4.62(4.68)	8.09(8.13)
S02	H	―〈 〉―Cl	$C_{20}H_{13}ClN_2S$	348.85	171-173	68	68.85(68.86)	3.74(3.76)	8.04(8.03)
S03	H	Cl / ―〈 〉―Cl	$C_{20}H_{12}Cl_2N_2S$	383.29	157-159	56	62.35(62.37)	3.18(3.16)	7.29(7.31)
S04	H	―〈 〉―N	$C_{19}H_{13}N_3S$	315.39	146-147	65	72.35(72.36)	4.12(4.15)	13.30(13.32)
S05	H	HO / ―〈 〉―OH	$C_{20}H_{14}N_2O_2S$	346.40	125-127	73	69.35(69.35)	4.08(4.07)	8.07(8.09)
S06	H	Br / ―〈 〉	$C_{20}H_{13}BrN_2S$	393.30	199-201	51	61.05(61.08)	3.31(3.33)	7.10(7.12)
S07	H	―〈 〉―OH	$C_{20}H_{14}N_2OS$	330.40	138-140	75	72.71(72.70)	4.25(4.27)	8.46(8.48)
S08	H	―〈 〉―N<	$C_{22}H_{19}N_3S$	357.47	176-178	81	73.90(73.92)	5.35(5.36)	11.74(11.75)
S09	H	―〈 〉	$C_{20}H_{14}N_2S$	314.40	188-190	70	76.38(76.40)	4.49(4.49)	8.90(8.91)
S10	H	―〈 〉―	$C_{21}H_{16}N_2S$	328.43	194-196	66	76.78(76.80)	4.90(4.91)	8.50(8.53)
S11	H	NO₂ / ―〈 〉	$C_{20}H_{13}N_3O_2S$	359.40	168-170	43	66.85(66.84)	3.63(3.65)	11.68(11.69)
S12	H	Cl / ―〈 〉	$C_{20}H_{13}ClN_2S$	348.85	175-177	61	68.85(68.86)	3.74(3.76)	8.02(8.03)
S13	H	OH / ―〈 〉―OCH₃	$C_{21}H_{16}N_2O_2S$	360.43	196-198	78	69.95(69.98)	4.95(4.97)	7.75(7.77)
S14	H	O₂N / ―〈 〉	$C_{20}H_{13}N_3O_2S$	359.40	134-136	49	66.84(66.84)	3.63(3.65)	11.66(11.69)

Table 1. Contd……

Compound Code	R	R$_1$	Molecular Formula	M.W.[a]	M.p.(°C)[b]	Yield (%)	% Analysis of C, H,N Found (calc.)[c]		
							C	H	N
S15	H	OCH$_3$ / OCH$_3$ / OCH$_3$	C$_{23}$H$_{20}$N$_2$O$_3$S	404.48	222-224	82	68.29(68.30)	4.96(4.98)	6.91(6.93)
S16	H	F	C$_{20}$H$_{13}$FN$_2$S	332.39	155-157	59	72.25(72.27)	3.93(3.94)	8.40(8.43)
S17	H	(indole)	C$_{22}$H$_{15}$N$_3$S	353.44	208-210	64	74.75(74.76)	4.27(4.28)	11.90(11.89)
S18	-	-	C$_{18}$H$_{16}$N$_2$S	292.40	165-166	60	73.92(73.94)	5.50(5.52)	9.56(9.58)
S19	-	-	C$_{19}$H$_{18}$N$_2$S	306.42	178-180	56	74.45(74.47)	5.91(5.92)	9.13(9.14)
S20	-	-	C$_{20}$H$_{20}$N$_2$S	320.45	191-192	52	74.95(74.96)	6.29(6.29)	8.72(8.74)

[a]Molecular weight of the compound.
[b]Melting point of the compound at their decomposition.
[c]Elemental analyses for C, H and N were within ±0.03% of the theoretical value.
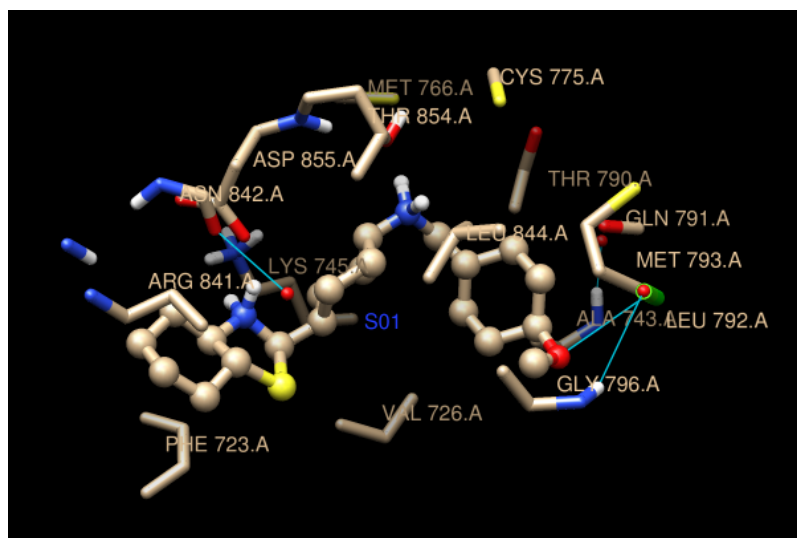
Fig. (4). Predicted binding pose of compound **S01** at the ATP-binding site of EGFR-TK.

The compounds **S01**, **S02**, **S05**, **S11** and **S13** were found to have high negative docking energy or score ranging from −8.94 to −9.85 kcal/mol (Table **2**) indicating that these compounds formed most stable drug-receptor complexes. The minimum docking energy was found in compound **S05** (-9.85 kcal/mol) with an estimated inhibition constant of 36.75µM and RMSD 0.89. Fig. (**5a**) demonstrates binding mode of compound **S05** in the ATP binding site of EGFR-TK**.** The sulphur atom of benzothiazole ring system in compound **S05** is involved in hydrogen bond formation with LYS-745 and nitrogen atom of azomethine linkage of Schiff base shows hydrogen bond interaction with CYS-797. The azomethine linkage at 4th position of 2-phenyl substituted benzothiazoles behaves as a conformational lock and extends substituted -CH=N- portion into the lipophilic pockets of EGFR tyrosine kinase, making it predominantly hydrophobic/lipophilic. Residues within 5 Å area of compound **S05** is shown in Fig. (**5b**) and Fig. (**5c**) depicts the color-coded visualization of electrostatic potential surface owing to the charge density of the compound. The color scale of the electrostatic potential shows red for the highest magnitude, blue for the lowest magnitude and white for neutral.

The aforesaid-findings confirm that the experimental results of wet lab are in good agreement with the predicted ones as observed from the dock scores. However, compounds **S01**, **S11** and **S13** exhibited good docking scores but did not show significant activities. It is possible that these compounds might have some permeability problems, and further studies are required to elucidate this.

3.3. Pharmacokinetic Predictions of the Best Fit Molecules

The best-fit ligands **S01**, **S02**, **S05**, **S11** and **S13** were subjected to preADMET server to predict the *in silico* pharmacokinetic properties. The numerous molecular descriptors have been employed to predict human ADMET processes and other significant pharmacokinetic parameters such as log P analysis, drug-likeliness, human intestinal absorption, *in vitro* plasma protein binding and water solubility in buffer system of all the synthesized Schiff base analogues of benzothiazole. The predicted drug likeliness of the synthesized compounds follows the Lipinski''Rule of Five''. All the four parameters for a compound, *i.e.* Log P <5, H-bond donors <5, H-bond acceptors <10 and molecular weight <500

Table 2. Docking results based on hydrophobic interaction, hydrogen bonding interaction, docking energy/ score, inhibition constant, bond length and RMSD.

Compound No.	Hydrophobic Interaction (Within 5 Å)	H-bond Interaction	Docking Energy/Score [kcal/mol]	Inhibition Constant [µM]	Bond Length [A⁰]	RMSD
S01	LYS745, ALA743, VAL726, PHE723, THR790, GLN791, MET793, ASP855, THR855, ARG841, LEU844.	O- of OCH3 group and H atom of amino acid backbone of MET-793	-9.17	1.44	1.75	0.83
S02	LYS745, VAL726, THR790, THR855, ARG841, LEU844, ASP 800, CYS797, MET766, LEU788, ILE789.	S- of benzothiazole and H atom of amino acid backbone of LYS-745 =N- of azomethine linkage and S atom of amino acid backbone of CYS-797	-9.45	22.44	2.61 2.28	0.39
S03	LYS745, ALA743, VAL726, PHE723, MET793, ASP855, THR855, ARG841, LEU788, CYS79, LYS797.	S- of benzothiazole and H atom of amino acid backbone of LYS-745	-6.98	12.29	2.75	0.68
S04	ALA743, VAL726, PHE723, MET793, ASP855, CYS797, ILE789, MET766, GLU762, LYS797, LEU792, ILE 744.	No H-bonds	-6.47	16.85	----	1.08
S05	LYS745, ALA743, VAL726, THR790, MET766, ASP855, ARG841, LEU788, ASP 800, CYS797, ILE789, ILE 744.	S- of benzothiazole and H atom of amino acid backbone of LYS-745 =N- of azomethine linkage and S atom of amino acid backbone of CYS-797	-9.85	36.75	2.79 2.24	0.89
S06	LYS745, ALA743, VAL726, PHE723, THR790, ASP855, ASP 800, CYS797, ILE789, MET766, GLU762, LYS797.	No H-bonds	-6.90	13.96	----	0.83
S07	LYS745, ALA743, VAL726, PHE723, GLN791, MET793, ASP855, LEU844, ASP 800, MET766, GLU762, LYS797.	S- of benzothiazole and H atom of amino acid backbone of LYS-745	-7.28	23.11	2.63	1.26
S08	LYS745, ALA743, THR790, GLN791, MET793, LEU844, ASP 800, CYS797, MET766, GLU762, LYS797, ILE 744.	S- of benzothiazole and H atom of amino acid backbone of LYS-745	-7.17	5.34	2.55	1.11
S09	LYS745, VAL726, PHE723, THR790, GLN791, ASP855, LEU844, LEU788, ASP 800, CYS797, LYS797, ILE744.	S- of benzothiazole and H atom of amino acid backbone of LYS-745	-6.13	19.89	2.67	0.76
S10	LYS745, ALA743, VAL726, PHE723, THR790, MET793, ASP855, LEU844, LEU788, ASP 800, CYS797, ILE789, MET766.	S- of benzothiazole and H atom of amino acid backbone of LYS-745	-6.65	28.74	2.60	0.66
S11	LYS745, ALA743, VAL726, PHE723, THR790, MET793, ASP855 LEU788, ASP 800, CYS797, LYS797, LEU792, ILE 744.	O- of nitro group and H atom of amino acid backbone of ASP-855 =N- of azomethine linkage and O- atom of amino acid backbone of ASP-855	-9.32	58.74	1.09 1.72	0.58
S12	LYS745, VAL726, THR790, THR855, ARG841, LEU844, ASP 800, CYS797, MET766, LEU788, ILE789, MET793.	S- of benzothiazole and H atom of amino acid backbone of LYS-745	-6.74	26.43	2.70	0.55

Table 2. Contd…..

Compound No.	Hydrophobic Interaction (Within 5 Å)	H-bond Interaction	Docking Energy/Score [kcal/mol]	Inhibition Constant [μM]	Bond Length [A⁰]	RMSD
S13	LYS745, ALA743, VAL726, PHE723, THR790, MET793, ASP855, LEU844, LEU788, ASP 800, CYS797, ILE789, MET766, LEU792.	S- of benzothiazole and H atom of amino acid backbone of LYS-745 O- of OCH₃ group and H atom of amino acid backbone of MET-793	-8.94	67.14	2.42 1.09	0.94
S14	LYS745, ALA743, VAL726, PHE723, THR790, MET793, ASP855 LEU788, ASP 800, CYS797, LYS797, LEU792, ILE 744, LEU844.	=N- of azomethine linkage and O- atom of amino acid backbone of ASP-855	-6.82	41.69	1.89	1.05
S15	LYS745, ALA743, VAL726, THR790, MET793, ASP855, ARG841, LEU844, ASP 800, CYS797, GLU762, LEU792, ILE 744.	S- of benzothiazole and H atom of amino acid backbone of LYS-745	-7.08	96.74	2.44	0.99
S16	LYS745, ALA743, VAL726, PHE723, THR790, MET793, ARG841, CYS797, GLU762, LYS797, LEU792.	S- of benzothiazole and H atom of amino acid backbone of LYS-745	-6.78	24.96	2.63	0.78
S17	LYS745, ALA743, VAL726, PHE723, THR790, GLN791, MET793, ASP855, THR855, ARG841, LEU844, ILE 744.	No H-bonds	-6.41	13.96	----	0.71
S18	LYS745, ALA743, VAL726, MET793, ASP855, THR855, ARG841, LEU844, ASP 800, MET766, GLU762, LYS797.	S- of benzothiazole and H atom of amino acid backbone of LYS-745	-6.32	84.32	2.34	0.96
S19	LYS745, ALA743, VAL726, MET793, ASP855, THR855, LEU844, LEU788, ASP 800, CYS797, GLU762, LYS797.	S- of benzothiazole and H atom of amino acid backbone of LYS-745	-6.73	76.63	2.45	0.87
S20	LYS745, ALA743, VAL726, MET793, ASP855, THR855, ARG841, ASP 800, CYS797, GLU762, LYS797, ILE 744.	S- of benzothiazole and H atom of amino acid backbone of LYS-745	-6.96	79.12	2.77	0.99

Table 3. **Theoretical prediction of different properties of novel Schiff base benzothiazole hybrids using PreADMET Server.**

Compound No.	Log p	LogS$_b$ (mg/L)	HIA (%)	*In-vitro* PPB (%)	HB-donors	HB-acceptors
S01	5.5	117.01	100	91.08	0	4
S02	4.7	0.262	92.72	96.65	0	3
S05	3.6	56.84	98.46	89.51	2	3
S11	4.9	5.08	96.76	90.12	0	4
S13	5.3	20.33	99.42	83.27	1	4

suggested that the compounds might have good absorption or permeability properties [52]. The results are summarized in Table **3** and description of descriptors is given in Table **4**.

3.4. Antiproliferative Activity of N-(arylidene/cycloalkylidene)-4-(benzo[d]thiazol-2-yl)benzenamine Derivatives (S01-20) Against Ovarian Cancer Cell Lines

The compounds **S01-20** were subjected to MTT assay against human ovarian sensitive (A2780 and SKOV3) and resistant (A2780-CR and A2780-PR) cell lines in order to determine growth inhibitory/cytotoxic capability. The IC$_{50}$ values derived from *in vitro* screening revealed that compounds **S02** and **S05** possess significant cytotoxicity against A2780 and SKOV3 and compound

S05 also showed significant cytotoxcity against A2780-CR cell line. However, no cytotoxicity was observed against A2780-PR cell line for all the compounds (Table **5** and Table **S1**). The detailed % cell viability results of compounds **S02** and **S05** in A2780, SKOV3 and A2780-CR cell lines are represented graphically in Figs. (**S1**, **S2** and **S3**) in supplementary file. Statistical analysis was performed by using non linear regression analysis on Graph Pad prism 5.0. IC$_{50}$ values were calculated from each set of triplicate wells. The synthesized compounds **S01**, **S11** and **S13** showed cytotoxic activity with IC$_{50}$ values over 100 µg/ml on A2780 and SKOV3 and compound **S13** also displayed same cytotoxicity on A2780-CR. Rest of the compounds did not display any cytotoxicity on all the cell lines used in the study (Table **5**). Five benzothiazole derivatives

(a)

(b)

(c)
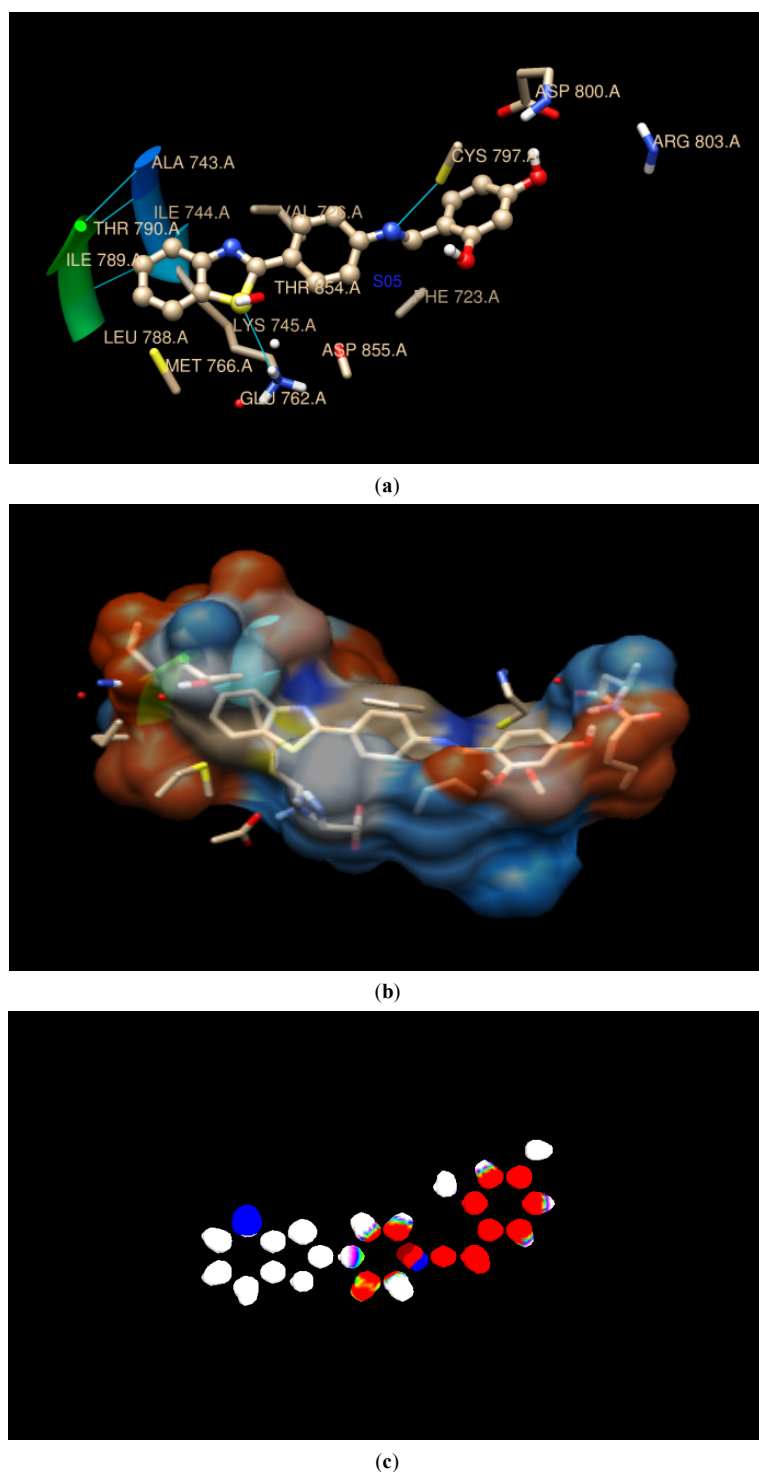
Fig. (5). (a) Predicted binding pose of compound **S05** at the ATP-binding site of EGFR **(b)** Hydrophobic surface regions of EGFR kinase domain. **(c)** Electrostatic potential regions over molecule **S05**, The coloring for regions is described as follows: red, negative electricity region; blue, positive electricity region; white, neutral region.

viz., **S01**, **S02**, **S05**, **S11** and **S13** with good docking scores were subjected to pharmacokinetic prediction analysis using Lipinski's Rule of Five. Further, these five derivatives were evaluated in detail for anticancer activity in order to support dry lab findings.

3.4.1. Screening of Novel Compounds Against Ovarian Cancer Cells

To understand the cytotoxic potential of these molecules, both A2780 and SKOV3 cell lines were treated with the five S-series

compounds for 48 hrs and analyzed by MTT assay. As represented in Fig. (**6**), compounds **S02** and **S05** exhibited low cell killing effect at lower concentration (91% cell survival at 4.9 and 3.4µg/ml, respectively) compared to significantly high cell killing effect at highest concentration (21% cell survival at 490 and 340 µg/ml, respectively) in A2780 cells. Similar effects were also observed in SKOV3 cell line except for compound **S02** that showed reactivity with McCoy's medium at higher concentration. For both cell lines, IC$_{50}$ values of compounds **S02** and **S05** were found to be 49 µg/ml

Table 4.   PreADMET Server properties and descriptors.

Sr. No.	Descriptor	Description	Recommended Range
1	Log P	physicochemcal descriptor	-2 to 8
2	Log S_b	physicochemcal descriptor	broad range
3	HIA (%)	It predicts human intestinal absorption on 0–100 % scale.	Poorly absorbed: 0 to 20%, moderately absorbed: 20- 70% and well absorbed compounds: 70-100%.
4	In-vitro PPB (%)	In-vitro plasma protein binding prediction tool predicts percent drug bound in plasma protein as *in vitro* data on human.	Strongly bound chemicals >90% Weakly bound chemicals <90%
5	HB-donors	Estimated number of hydrogen bonds that would be donated by the solute to water molecules in an aqueous solution.	0.0–6.0
6	HB-acceptors	Estimated number of hydrogen bonds that would be accepted by the solute from water molecules in an aqueous solution.	2–20
7	Rule of five (Lipinski's rule)	Tool for predicting drug-likeness, discriminating between drug-like compounds and non-drug compounds. Number of violations of Lipinski's rule of five. The rules are: mol_MW<500, log P<5, HB donor<= 5, HB acceptor<= 10. Compounds that satisfy these rules are considered drug-like.	Maximum is 4

Table 5.   IC$_{50}$ of synthesized Schiff bases S01-S20, Cisplatin and Paclitaxel in SKOV3, A2780-S, A2780-CR, A2780-PR cell lines.

Compound Code	SKOV3	A2780-S	A2780-CR	A2780-PR
S01	>100	>100	-	-
S02	49	49	-	-
S03	-	-	-	-
S04	-	-	-	-
S05	34	34	34	-
S06	-	-	-	-
S07	-	-	-	-
S08	-	-	-	-
S09	-	-	-	-
S10	-	-	-	-
S11	>100	>100	-	-
S12	-	-	-	-
S13	>100	>100	>100	-
S14	-	-	-	-
S15	-	-	-	-
S16	-	-	-	-
S17	-	-	-	-
S18	-	-	-	-
S19	-	-	-	-
S20	-	-	-	-
Cisplatin	-	500ng/ml	5μg/ml	NA
Paclitaxel	-	4.3ng/ml	NA	21.3ng/ml
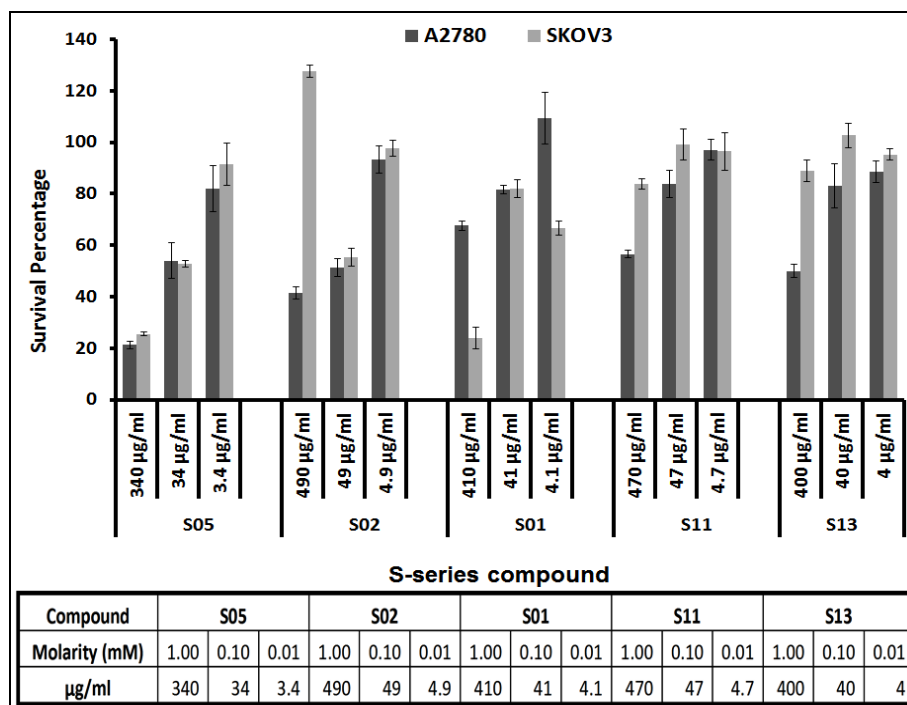
Fig. (6). Effect of different concentrations (1mM, 0.1mM and 0.01mM) of compounds **S05, S02, S01, S11** and **S13** on viability of ovarian cancer cell lines (A2780 and SKOV3).

and 34μg/ml. The rest three compounds did not show any growth inhibitory effect and therefore, compound **S05** was used for further evaluation (Fig. **6**). The IC$_{50}$ values of compounds **S02, S05**, Cisplatin and Paclitaxel in sensitive (SKOV3, A2780-S) and resistant (A2780-CR and A2780-PR) cells are mentioned in Table **5**. However, to establish the specificity of compound **S05** towards cancer cells, normal ovarian surface cell line IOSE 364 was incubated with different concentrations of compound **S05**. As represented in Fig. (**7**), only ~20% reduction in cell viability was seen at 34 μg/ml of compound **S05**, which was found to induce 50% lethality in other two cancer cell lines (A2780 & SKOV3) indicating the specificity of the compound.
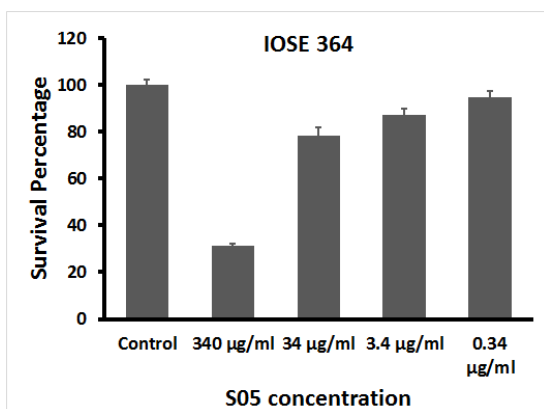
Fig. (7). Growth inhibitory effect of compound **S05** on viability of normal ovarian cancer surface epithelial cell line (IOSE 364).

3.4.2. Effect of Compound S05 Against A2780-CR and A2780-PR Cells

In vitro growth inhibitory effect of compound **S05** was assessed using MTT reduction assay as shown in Fig. (**8**). Interestingly, A2780-CR showed similar response as its sensitive counterpart A2780-S (IC$_{50}$ at 34μg/ml, Fig. **8A**) on treatment with compound **S05**. However, in paclitaxel resistant cells (A2780-PR) compound

S05 showed inhibitory effect only at higher dosage (~20% at 340μg/ml) compared to intermediate and lower dosage (~80% for both 34 μg/ml and 3.4 μg/ml) (Fig. **8B**).

3.4.3. Influence of Compound S05 as a Combinatorial Treatment

To evaluate the influence of compound **S05** as a combinatorial therapeutic agent with cisplatin or paclitaxel, A2780-S cells were treated with IC$_{50}$ dosage of each drug alone and/or in combination. Compound **S05** along with cisplatin and paclitaxel showed significant growth inhibition (50% to 20%) (p= 0.006 and p= 0.003, respectively) compared to individual drug treatments indicating a synergistic effects.

Further, this synergistic effect of compound **S05** was studied in the cisplatin and paclitaxel resistant models. When cisplatin resistant cells were treated with compound **S05** alone and **S05** with cisplatin (at IC$_{50}$ dose for A2780-CR cells), a significant growth inhibition (40%, p=0.02) was observed in combinatorial treatment. The synergistic effect of compound **S05** was also observed with lower concentration of cisplatin (IC$_{50}$ dose for A2780-S) in A2780-CR cells. When A2780-CR was treated with cisplatin (500ng/ml) and compound **S05** together, significant growth inhibition (39%) compared to individual drugs (50% for **S05** and 90% cisplatin, p=0.0245 & p=0.0009) treatments was found (Fig. **9A**).

The paclitaxel resistance cells (A2780-PR) were also used to study the similar synergistic effect of compound **S05** with paclitaxel. However, no significant growth inhibition was observed with combination treatment of compound **S05** and paclitaxel compared to individual treatments (Fig. **9B**).

Platinum/taxane based chemotherapy serves as excellent first line treatment for ovarian cancer, but majority of these tumors recur due to acquirement of resistance to chemotherapy. Herein, we investigated novel EGFR ligand inhibitor as a therapeutic agent for ovarian cancer. When all newly synthesized derivatives were tested for their cytotoxic activities in two different ovarian cancer cells, compound **S05** showed the maximal effect in both. In combination with cisplatin and paclitaxel, compound **S05** significantly decreased the viability by 33% & 24% in A2780 sensitive cells. We have also
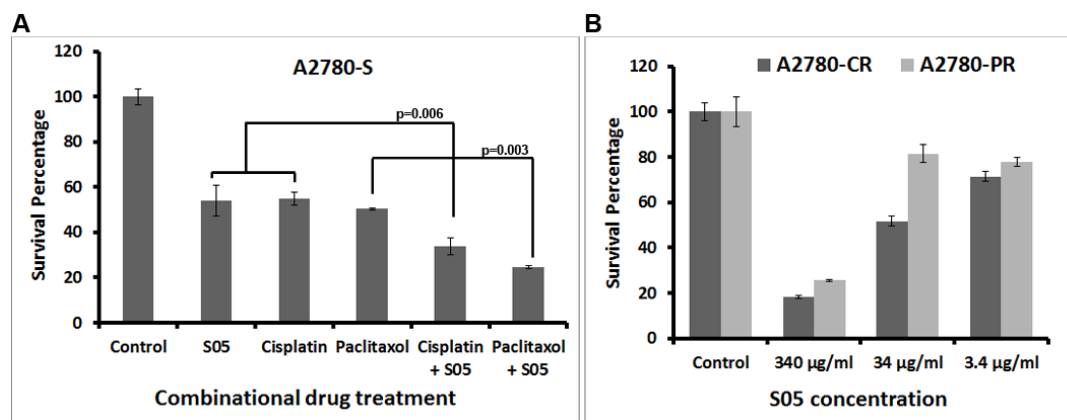
Fig. (8). Growth inhibitory effect of compound **S05** on (A) A2780-S (B) A2780-CR and A2780-PR cell lines.
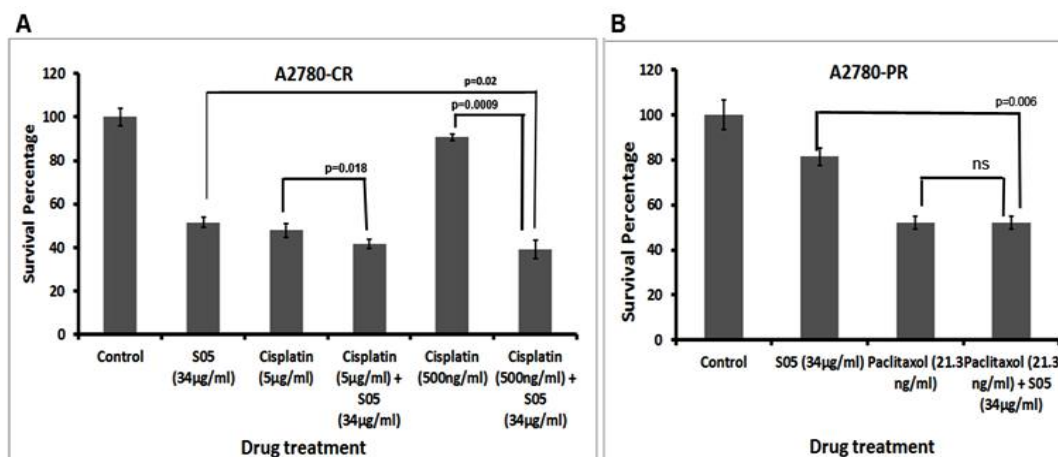
Fig. (9). Growth inhibitory effect of compound **S05** as a combinatorial treatment on (A) A2780-CR (B) A2780-PR cell lines.

evaluated the efficacy of compound **S05** against chemoresistant cellular model for cisplatin and paclitaxel. Interestingly, when tested against cisplatin resistant cells, compound **S05** significantly decreased the viability with IC_{50} value determined at 34µg/ml. However, in paclitaxel resistant cells decreased viability was only observed at very high concentration indicating that level of IGFR/EGFR probably varies with drug dependent resistance which in turn determines the effect of these compounds.

Further, we assessed the influence of compound **S05** as a combinatorial drug with platinum or taxane based drugs. We observed that compound **S05** is more effective cytotoxic agent in combination with chemotherapeutic drugs than alone in both sensitive and resistant model. The compound **S05** makes cisplatin treatment even more effective against resistant cellular models, indicating a synergistic effect. In fact, even at lower dosage of cisplatin, compound **S05** was found to be more effective than cisplatin or **S05** alone. Combinatorial treatment of compound **S05** with paclitaxel was effective only in sensitive model but no significant effect was observed in resistance model, indicating the least influence of EGFR-driven pathways in paclitaxel resistance.

3.5. Inhibition of EGFR Tyrosine Kinase Phosphorylation

The *in silico* studies and anti-proliferative assay suggested that synthesized benzothiazole derivatives bind to EGFR-TK and showed significant cytotoxicity. Concomitantly, we carried out immunoblotting by using specific antibody of phosphorylated EGFR to unravel the mechanism of targeted inhibition. The synthesized Schiff base derivatives **S01-S20** were evaluated for their ability to inhibit the autophosphorylation of EGFR-TK. EGFR

is a 170 kDa transmembrane glycoprotein, contains an external membrane binding and intracellular tyrosine kinase domain. Gefitinib was employed as the positive control which mimics the ATP competitive binding regions of EGFR tyrosine kinase. Densitometric analysis of the western blots was quantified in order to translate biochemical results into statistical values. Fig. (**10**) shows the results of immunoblotting for phosphorylated EGFR after exposure to compounds **S11, S13, S02**, **S05** and gefitinib for 48 hours. Gefitinib completely inhibits phosphorylated EGFR (~100% inhibition) and exhibited lethal effects at a single dose (10 µM) against the EGFR expressing cell lines SKOV3, A2780-S and A2780-CR. The results are summarized in Table **6**. It was observed that Schiff base-benzothiazole hybrid **S05** containing dihydroxy substituents showed fairly good inhibitory activity against EGFR-TK with percentage enzyme inhibition value of 69.71, 67.80 and 75.36 against SKOV3, A2780-S and A2780-CR respectively, as compared to that of gefitinib. Subsequently, SAR studies were performed by modification of the parent compound to determine how the different substituents of the subunits affect the EGFR inhibitory activity. The introduction of more electron releasing substituents in phenyl ring resulted in dramatic decrease in activity. For instance, compound **S13** bearing hydroxy and methoxy substituents, demonstrated only 10.52, 11.07 and 25.37 percentage EGFR inhibition against SKOV3, A2780-S and A2780-CR respectively, in comparison to gefitinib. Compound **S02** with electronegative group 'Cl' in phenyl ring demonstrated favorable inhibitory activity with 33.66 and 46.93 percentage EGFR inhibition against SKOV3 and A2780-S, respectively. However, compound **S11** possessing electron withdrawing ($-$ NO_2) group showed 40.63 and 12.48 percentage EGFR inhibition on SKOV3

Table 6. Percentage EGFR-TK inhibitory activity of synthesized Schiff bases S01-S20.

Compound Code	% EGFR-TK Inhibition of SKOV3[a]	% EGFR-TK Inhibition of A2780-S[a]	% EGFR-TK Inhibition of A2780-CR[a]
S01	-	-	-
S02	33.66± 0.52	46.93± 0.12	-
S03	-	-	-
S04	-	-	-
S05	69.71± 0.07	67.80± 0.16	75.36± 0.15
S06	-	-	-
S07	-	-	-
S08	-	-	-
S09	-	-	-
S10	-	-	-
S11	40.63± 0.22	12.48± 0.68	-
S12	-	-	-
S13	10.52± 0.10	11.07± 0.17	25.37± 0.34
S14	-	-	-
S15	-	-	-
S16	-	-	-
S17	-	-	-
S18	-	-	-
S19	-	-	-
S20	-	-	-
Gefitinib	~100*	~100*	~100*

[a] The data were means from at least three independent experiments at a single dose of 100 µM.
[b] Gefitinib was used as a reference compound tested at 10 µM concentration.
*Absence of immunoblot in Lane 6 of SKOV3 and A2780 and in Lane 4 of A2780-CR, showed complete inhibition of EGFR phosphorylation.
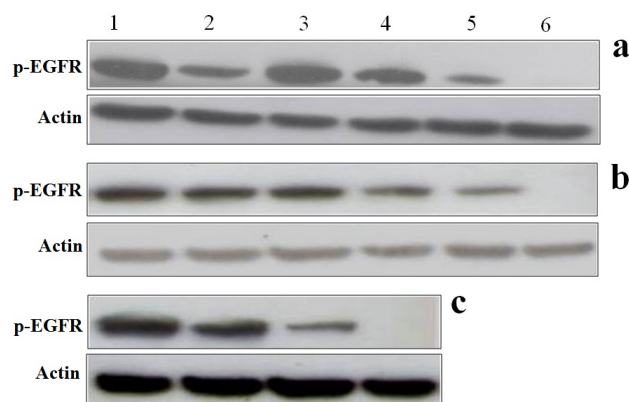
Fig. (10). Immunoblot analysis of the EGFR in ovarian cancer cell lines. The (**a**) SKOV3 and (**b**) A2780-S ovarian cancer cell lysates were prepared from cells treated for 48 hr without chemical treatment, Lane 1: phosphorylated EGFR and with chemical treatment, Lane 2: **S11**, Lane 3: **S13,** Lane 4: **S02**, Lane 5: **S05**, Lane 6: **Gefitinib**, in normal growth medium. The (**c**) A2780-CR ovarian cancer cell lysates was prepared from cells treated for 48 hr without chemical treatment, Lane 1: phosphorylated EGFR and with chemical treatment, Lane 2: **S13**, Lane 3: **S05**, Lane 4: Gefitinib, in normal growth medium. EGFR was immunoprecipitated and probed with antiphosphotyrosine antibodies, as described in Material and Methods. Another blot represents the Actin to ensure equal loading in all the cell lines described in the figure.

and A2780-S, respectively. Overall, this indicated that less bulky electron releasing moiety suitably adapted the hydrophobic and hydrophilic pocket of EGFR kinase domain. Thus, four compounds **S02**, **S05**, **S11** and **S13** exhibited EGFR tyrosine kinase inhibition, while rest of the compounds of the S-series were not active to this target. In cisplatin resistant cells *i.e.* A2780-CR**,** phosphorylated EGFR expression was decreased significantly for compounds **S05** and **S13**, suggesting that the maximum inhibition of overexpression was in resistant cells. The high selectivity of compound **S05** towards EGFR tyrosine kinase might be attributed to difference in the geometry of the binding pocket of this enzyme which enables its fitting and interaction.

4. CONCLUSION

The results of *in-vitro* antiproliferative screening of synthesized compounds revealed that compounds containing electron releasing 'hydroxy' groups and electronegative 'Cl' group, respectively in phenyl ring, have significant cytotoxicity against the human ovarian cancer cell lines. Compound containing dihydroxy substituents was further evaluated for cytotoxicity against normal ovarian cell line (IOSE 364) and exhibited selective killing of cancer cells as compared to normal cells. Compound, N-(2, 4-dihydroxybenzyl-idene)-4-(benzo[d]thiazol-2-yl)benzenamine with IC_{50} value of 102.02 µM against A2780-S, 101.89 µM against A2780-CR and 102.90 µM against SKOV3 cancer cell lines (supplementary Table **S1**) proved to be the most active member in this study. Molecular

docking studies revealed that compound containing dihydroxy substituents has minimum binding and docking energy on EGFR-TK. The findings of docking and inhibition of EGFR tyrosine kinase phosphorylation studies support the postulation that the designed active compounds act on the same target enzyme where the known EGFR-TK inhibitor (gefitinib) acts. Furthermore, compound containing dihydroxy substituents is more effective cytotoxic agent in combination with chemotherapeutic drugs (cisplatin and paclitaxel) than alone in both the sensitive (A2780, SKOV3) as well as in A2780-CR resistant models. Our findings of biological screenings hold promise for excellent framework towards the search for potent antitumor agents. Further, on the basis of *in silico* ADME studies, compound containing dihydroxy substituents can be further exploited for the development of more effective anticancer agent. In conclusion, a highly potent, safe and selective antitumor agent as well as EGFR tyrosine kinase inhibitor *i.e.*, compound containing dihydroxy substituents was synthesized which holds promise for lead as new selective inhibitor of EGFR tyrosine kinase.

CONFLICT OF INTEREST

The authors confirm that this article content has no conflict of interest.

SUPPLEMENTARY MATERIAL

Supplementary material is available on the publisher's web site along with the published article.

LIST OF ABBREVIATIONS

EGFR	=	Epidermal growth factor receptor
EGFR-TK	=	Epidermal growth factor receptor-Tyrosine kinase
IGFR	=	Insulin growth factor receptor
MTT	=	3-(4, 5-dimethylthiazol-2-yl)-2, 5-diphenyltetrazolium bromide
SAR	=	Structure-activity relationship
A2780-S	=	Sensitive cells of A2780
A2780-CR	=	Cisplatin resistant cells of A2780
A2780-PR	=	Paclitaxel resistant cells of A2780
DMSO	=	Dimethyl sulfoxide

REFERENCES

[1]   Beneteau, V.; Besson, T.; Guillard, J.; Leonce, S.; Pfeiffer, B. Synthesis and *in vitro* antitumour evaluation of benzothiazole-2-carbonitrile derivative. Eur. J. Med. Chem., 1999, 34, 1053-1060.

[2]   Mortimer, C.G.; Wells, G.; Crochard, J.P.; Stone, E.L.; Bradshaw, T.D.; Stevens, M.F.G.; Westwell, A.D. Antitumor Benzothiazoles 26. 2-(3,4-Dimethoxyphenyl)-5-fluorobenzothiazole (GW610,NSC 721648), a Simple Fluorinated 2-Arylbenzothiazole, Shows Potent and Selective Inhibitory Activity against Lung, Colon, and Breast Cancer Cell Lines, J. Med. Chem., 2006, 49, 179-185.

[3]   Shi, D.; Bradshaw, T.D.; Chua, M.; Westwell, A.D.; Stevens, M.F.G. Antitumour benzothiazoles. Part 15:1 The synthesis and physico-chemical properties of 2-(4-aminophenyl) benzothiazole sulfamate salt derivatives. Bioorg. & Med. Chem., 2001, 11, 1093-1105.

[4]   Hutchinson, I.; Bradshaw, T.D.; Matthews, C.S.; Stevens, M.F.G.; Westwell, A.D. Antitumour benzothiazoles. Part 20: 3'-cyano and 3'-alkynyl- substituted 2-(4-'aminophenyl) benzothiazole as new potent and selective analogues. Bioorg. Med. Chem. Lett., 2003, 13, 471-474.

[5]   Yalcin, I.; Oren, I.; Sener, E.; Akin, A.; Ucarturk, N. The synthesis and the structure-activity relationships of some substituted benzoxazoles, oxazolo(4,5-*b*)pyridines, benzothiazoles and benzimidazoles as antimicrobial agents. Eur. J. Med. Chem., 1992, 27, 401-406.

[6]   Latrofa, A.; Franco, M.; Lopedota, A.; Rosato, A.; Carone, D.; Vitali, C. Structural modifications and antimicrobial activity of *N*-cycloalkenyl-2-acylalkylidene-2,3-dihydro-1,3-benzothiazoles. IL Farmaco., 2005, 60, 291-297.

[7]   Patel, N.B.; Khan, I.H.; Rajani, S.D. Antimycobacterial and antimicrobial study of new 1,2,4-triazoles with benzothiazoles, Arch. Pharm. Chem. Life Sci., 2010, 10, 692-699.

[8]   Burger, A.; Sawhney, S.N. Antimalarials. III. Benzothiazole amino alcohols. J. Med. Chem., 1968, 11, 270-273.

[9]   Amnerkar, N.D.; Bhusari, K.P. Synthesis, anticonvulsant activity and 3D-QSAR study of some prop-2-eneamido and 1-acetyl-pyrazolin derivatives of aminobenzothiazole. Eur. J. Med. Chem., 2010, 45, 149-159.

[10]   Chakole, R.D.; Amnerkar, N.D.; Khedekar, P.B.; Bhusari, K.P. Synthesis of substituted benzothiazole derivatives of thioquinazoline as anticovulsant agents. Indian J. Heterocyclic Chem., 2005, 15, 27-30.

[11]   Amnerkar, N.D.; Bhusari, K.P. Synthesis of some thiazolyl aminobenzothiazole derivatives as potential antibacterial, antifungal and anthelmintic agents. J. Enzyme Inhib. Med. Chem., 2011, 26, 22-28.

[12]   Siddiqui, N.; Alam, M.; Siddiqui, A.A. Synthesis and analgesic activity of some 2-[{4-(Alkyl thioureido) phenyl}sulphonamido]-6-substituted benzothiazoles. Asian J. Chem., 2004, 16, 1005-1008.

[13]   Kaur, H.; Kumar, S.; Singh, I.; Saxena, K.K.; Kumar, A. Synthesis, Characterization and Biological activity of various substituted Benzothiazole derivatives. Digest J. Nano. Bio. str., 2010, 5, 67-76.

[14]   Navarrete-Vazquez, G.; Paoli, P.; León-Rivera, I.; Villalobos-Molina, R.; Medina-Franco, J.L.; Ortiz-Andrade, R.; Estrada-Soto, S.; Camici, G.; Diaz-Coutiño, D.; Gallardo-Ortiz, I.; Martinez-Mayorga, M.; Moreno-Díaz, H. Synthesis, *in vitro* and computational studies of protein tyrosine phosphatase1B inhibition of a small library of 2-arylsulfonylaminobenzothiazoles with anti hyperglycemic activity. Bioorg. & Med. Chem., 2009, 17, 3332-3341.

[15]   Bozec, L.L.; Moody, C.J. Naturally Occurring Nitrogen-Sulfur Compounds. Aust. J. Chem., 2009, 62, 639-647.

[16]   The Merck Index: An Encyclopedia of Chemicals, Drugs, and Biologicals, twelfth ed., Merck Research Laboratories, Division of MERCK & CO, Inc., New Jersey, 1996.

[17]   Wang, M.; Wang, L.F.; Li, Y.Z.; Li, Q.X.; Xu, Z.D.; Qu, D.M. Antitumour activity of transition metal complexes with the thiosemicarbazone derived from 3-acetylumbelliferone. Trans. Met. Chem., 2001, 26, 307-310.

[18]   Yadav, L.D.S.; Singh, S. Synthesis of antiviral acyclic C-nucleosides incorporating thiazolo-1,3,4-oxa(thia) diazole or thiazolo-1,2,4-triazole structure as a nucleobase. Indian J. Chem., 2001, 40B, 440-442.

[19]   Bradshaw, T.D.; Bibby, M.C.; Double, J.A.; Fichtner, I.; Cooper, P.A.; Alley, M.C.; Donohue, S.; Stinson, S.F.; Tomaszewjski, J.E.; Sausville, E.A.; Stevens, M.F.G. Preclinical evaluation of amino acid prodrugs of novel 2-(4-amino-3-methylphenyl)benzothiazoles. Mol. Cancer. Ther., 2002, 45, 239-246.

[20]   Bradshaw, T.D.; Chua, M.S.; Browne, H.L.; Trapani, V.; Sausville, E.A.; Stevens, M.F.G. *In vitro* evaluation of amino acid prodrugs of

novel antitumour 2-(4-amino-3-methylphenyl)benzothiazoles. Brit. J. Cancer., 2002, 86, 1348-1354.

[21]   Reddy, P.; Lin, Y.; Chang, H. Synthesis of novel benzothiazole compounds with an extended conjugated system. Arkivoc, 2007, xvi, 113-122.

[22]   Heo, Y.; Song, Y.; Kim, B.; Heo, J. A highly regioselective synthesis of 2-aryl-6-chlorobenzothiazoles employing microwave-promoted Suzuki-Miyaura coupling reaction. Tetrahedron Lett., 2006, 47, 3091-3094.

[23]   Piscitelli, F.; Ballatore, C.; Smith, A. Solid Phase synthesis of 2-aminobenzothiazoles. Bioorg. Med. Chem. Lett., 2010, 20, 644-648.

[24]   Murthi, Y.; Pathak, D. Synthesis and Antimicrobial screening of Substituted 2-Mercaptobenzothiazoles. J. Pharm. Res., 2008, 7, 153-155.

[25]   Rajeeva, B.; Srinivasulu, N.; Shantakumar, S. Synthesis and Antimicrobial activity of some new 2-substituted benzothiazole derivatives. E-J. Chem., 2009, 6, 775-779.

[26]   Maharan, M.; William, S.; Ramzy, F.; Sembel, A. Synthesis and *in vitro* Evaluation of new benzothiazole derivaties as schistosomicidal agents. Molecules. 2007, 12, 622-633.

[27]   Singh, M.; Singh, S.K. Benzothiazoles: How Relevant in Cancer Drug Design Strategy? Anticancer Agents Med. Chem., 2014, 14, 127-146.

[28]   Vicini, P.; Geronikaki, A.; Incerti, M.; Busonera, M.; Poni, G.; Cabrasc, C.A.; Collac, P.L. Synthesis and Biological Evaluation of Benzo[d]isothiazole, Benzothiazole and Thiazole Schiff Bases. Bioorg. & Med. Chem., 2003, 11, 4785-4789.

[29]   Berchuck, A.; Rodriguez, G.C.; Kamel, A.; Dodge, R.K.; Soper, J.T.; Clarke-Pearson, D.L.; Bast, R.C. Epidermal growth factor-receptor expression in normal ovarian epithelium and ovarian cancer. I. Correlation of receptor expression with prognostic factors in patients with ovarian cancer. Am. J. Obstet. Gynecol., 1991, 164, 669 - 674.

[30]   Bartlett, J.M.S.; Langdon, S.P.; Simpson, B.J.B.; Stewart, M.; Katsaros, D.; Sismondi, P.; Love, S.; Scott, W.N.; Williams, A.R.W.; Lessells, A.M.; Macleod, K.G.; Smyth, J.F.; Miller, W.R. The prognostic value of epidermal growth factor receptor mRNA expression in primary ovarian cancer. Brit. J. Cancer 1996, 73, 301-306.

[31]   Bridges, A. Inhibitors of protein kinases. J. Chem. Rev., 2001, 101, 2541-2572.

[32]   Grünwald, V.; Hidalgo, M.; Developing inhibitors of the epidermal growth factor receptor for cancer treatment. J. Natl. Cancer Inst., 2003, 95, 851-867.

[33]   Sewell, J.M.; Macleod, K.G.; Ritchie, A.; Smyth, J.F.; Langdon, S.P. Targeting the EGF receptor in ovarian cancer with the tyrosine kinase inhibitor ZD 1839 ('Iressa'). Brit. J. Cancer. 2002, 86, 456-462.

[34]   Smith, J. Erlotinib: small-molecule targeted therapy in the treatment of non-small cell lung cancer. Clin. Ther., 2005, 27, 1513-1534.

[35]   Singh, M.; Singh, S.K.; Gangwar, M.; Nath, G.; Singh, S.K. Design, Synthesis and mode of action of some benzothiazole derivatives bearing amide moiety as antibacterial agents. RSC Adv., 2014, 4, 19013-19023.

[36]   Singh, M.; Gangwar, M.; Nath, G.; Singh, S.K. Synthesis, DNA Cleavage and Antimicrobial activity of 4-Thiazolidinones-Benzothiazole Conjugates. Indian J. Exp. Bio., 2014, 52, 1062-1070.

[37]   Singh, M.; Singh, S.K.; Gangwar, M.; Sellamuthu, S.K.; Nath, G.; Singh, S.K. Design, Synthesis and Mode of action of some new 2-(4′-aminophenyl)benzothiazole derivatives as potent antimicrobial agents. Lett. Drug Des. Discov., 2015, DOI: 10.2174/1570180812666150821003220.

[38]   Singh, M.; Singh, S.K.; Gangwar, M.; Nath, G.; Singh, S.K. Design, synthesis and mode of action of novel 2-(4-aminophenyl) benzothiazole derivatives bearing semicarbazone and thiosemicarbazone moiety as potent antimicrobial agents. Med. Chem. Res., 2015, 25(2), 263-282

[39]   Bhuva, H.A.; Kini, S.G. Synthesis, anticancer activity and docking of some substituted benzothiazoles as tyrosine kinase inhibitors. J. Mol. Graph Model., 2010, 29, 32-37.

[40]   Noolvi, M.N.; Patel, H.M.; Kaur, M. Benzothiazoles: Search for anticancer agents. Eur. J. Med. Chem., 2012, 54, 447-462.

[41]   Perin, D.D.; Armargo, W.L.; Perin, D.R. Purification of Laboratory Chemicals, Pergamon, London, 1966.

[42]   Shi, D-F.; Bradshaw, T.D.; Wrigley, S.; McCall, C.J.; Lelieveld, P.; Fichtner, I.; Stevens, M.F.G. Antitumor Benzothiazoles. 3.1 Synthesis of 2-(4-Aminophenyl)benzothiazoles and Evaluation of Their Activities against Breast Cancer Cell Lines *in Vitro* and *in Vivo*. J. Med. Chem., 1996, 39, 3375-3384.

[43]   Casewit, C.J.; Colwell, K.S.; Rappe, A.K. "Application of a Universal Force Field to Organic Molecules". J. Am. Chem. Soc., 1992, 114, 10035-10046.

[44]   Clark, D.E. In silico prediction of blood-brain barrier permeation. Drug Discov. Today. 2003, 8, 927-933.

[45]   Didziapetris, R.; Japertas, P.; Avdeef, A.; Petrauskas, A.J. Classification analysis of P-glycoprotein substrate specificity. Drug Target. 2003, 11, 391-406.

[46]   Johnson, A.C.; Murphy, B.A.; Matelis, C.M.; Rubinstein, Y.; Piebenga, E.C.; Akers, L.M.; Neta, G.; Vinson, C.; Birrer, M.; Activator Protein-1 Mediates Induced but not Basal Epidermal Growth Factor Receptor Gene Expression. Mol. Medicine. 2000, 6, 17-27.

[47]   Mendelsohn, J.; Baselga, J. The EGF receptor family as targets for cancer therapy. Oncogene. 2000, 19, 6550-6565.

[48]   Noble, M.E.M.; Endicott, J.A.; Johnson, L.N. Protein kinase inhibitors: insights into drug design from structure. Science. 2004, 303, 1800-1805.

[49]   Traxler, P.; Bold, G.; Buchdunger, E.; Caravatti, G.; Furet, P.; Manley, P.; Reilly, T.O.; Wood, J.; Zimmermann, J. Tyrosine kinase inhibitors: from rational design to clinical trials. Med. Res. Rev., 2001, 21 499-512.

[50]   Yates, P.C.; McCall, C.J.; Stevens, M.F.G. Structural studies on benzothiazoles. Crystal and molecular structure of 5,6-dimethoxy-2-(4-methoxyphenyl)-benzothiazole and molecular orbital calculations on related compounds. Tetrahedron. 1991, 47, 6493-6502.

[51]   Fabbro, D.; Ruetz, S.; Buchdunger, E.; Cowan-Jacob, S.W.; Fendrich, G.; Liebetanz, J.; Reilley, T.O.; Traxler, P.; Chaudhari, B.; Fretz, H.; Zimmermann, J.; Meyer, T.; Carvatti, G.; Furet, P.; Manley, P.W. Protein kinases as targets for anticancer agents: from inhibitors to useful drugs. Pharmacol. Ther., 2002, 93, 79-98.

[52]   Moorthy, N.S.H.N.; Karthikeyan, C.; Trivedi, P. Cytotoxic evaluation and in silico pharmacokinetic prediction of some benzo[a]phenazine-5-sulfonic acid derivatives. Med. Chem., 2009, 5, 549-557.

Molecular Imaging of Therapeutic Potential of Reporter Probes

Bhushan Thakur, Subhoshree Chatterjee, Smrita Chaudhury and Pritha Ray[*]

Advanced Centre for Treatment, Research and Education in Cancer (ACTREC), Tata Memorial Centre, Navi Mumbai, Maharashtra, India
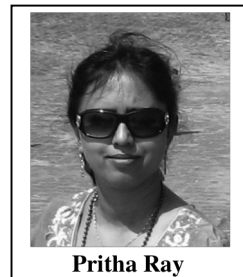
Pritha Ray

Abstract: Success of medical treatments for any pathological disorders majorly depends on the efficacy of the therapeutic molecules and their delivery to the target sites. Non-invasive molecular imaging technologies have emerged as prime methods for validating both these aspects ranging from preclinical level to clinical application. Reporter genes and the respective reporter probes are essential components of molecular functional imaging that gained wide popularity throughout the world due to easy adaptation, user friendly software and cost-effective experiments. However, to monitor the therapeutic effects, reporter gene-reporter probes (RG-RP) are often combined with separate introductions of therapeutics whose delivery at target sites are not appropriately measured. A small group of reporter genes is associated with probes that behave like a signature as well as a therapeutic molecule thereby having theranostic properties. This Reporter Gene-Therapeutic Reporter Probe (RG-TRP) system bears additional advantages over RG-RP system and holds the promise of direct translational applications in humans. This short review focuses on describing the currently available and validated RG-TRP systems, delivery vehicles, associated imaging modalities, applications in various pathological conditions along with the merits and demerits. Identification of new RG-TRP system will open new direction in theranostic imaging with potential human applications.

Keywords: Imaging, reporter gene, reporter probe.

INTRODUCTION

A disease is a pathological state with specific symptoms that affect a part or whole system of an organism resulting from either hereditary defects or environmental factors including infectious agents. Since birth, human body suffers from various types of diseases such as infectious diseases, cardiovascular disorders, cancer, and neurodegenerative disorders. The intensity of such diseases differs from individual to individual due to differences in their physical-immune characteristics as well as their response to treatments. The concept of remedial system was introduced in ancient time to combat such biochemical and genetic disorders responsible for the disease. Origin of such medical practice is quite debatable. However, the traditional Ayurveda system from the Indian subcontinent is probably the most ancient medicinal practice since 5000 BC [1]. The knowledge about medicinal preparations and surgical practice for treatment of sick people was compiled into the *Suśrutha Samhitā* [2] and the *Charaka Samhitā* [3]. Perhaps, these two are the oldest compiled medicinal scripts where detailed methods about prevention and cure of ailments with simple examination and natural herbs were enlisted. The perception of diagnosis, health surveillance and medication for better prognosis of diseases were mentioned in these books and thus they possible were the first documentations

of systematic medicines. This concept of medical surveillance was further advanced by ancient Greeks and Egyptians who also developed the concept of medical ethics [4, 5]. These and many other distinct pioneering efforts by the ancient civilizations gradually shaped the current concept of our medical system.

The presently available medical system comprises of prognosis, diagnosis, and therapy followed by medical care. Therapy is an integral part of medicinal system, which takes account of administrating diverse composites to patients for prevention, cure or/and alleviating pain. These therapeutic compounds consist of small molecules for direct intervention and, genetic modifiers to accomplish gene therapy or cell replacement therapy which is also termed as stem cell therapy. Developing effective therapeutics against multifactorial diseases has been an ever challenging task. One of the currently used strategies involves identification and development of small molecules from either chemically synthesised libraries or natural libraries based on their characteristics modulatory effects on the trait. Other strategies include gene therapy and cell replacement therapy. Gene therapy involves the use of DNA/RNA as therapeutics to correct the function of the non-functional or mutated gene. X-linked SCID [6], Adrenoleudystropy [7], Hemophilia [8, 9], Parkinson disease [10], Acute lymphocytic leukemia [11] etc., are few examples where gene therapy is approved as a treatment modality. Some of the systemic disorders such as neurodegenerative diseases are more complex and involve loss of functional cells. Such disorders can be treated with cell replacement therapies by administering either stem cells or specially engineered cells.

*Address correspondence to this author at the Advanced Centre for Treatment, Research and Education in Cancer (ACTREC), Tata Memorial Centre, Navi Mumbai, Maharashtra, India, 410210; Tel: +91-22-2740 5119; Fax: +91-22-2740 5085; E-mail: pray@actrec.gov.in

Major problems associated with these therapeutics are limited efficacy and off target effects. Thus the thrust in current pharmacological research is to address these limitations by developing efficient therapeutics and targeted therapy. First approach involves identification of drugable targets and development of potential drugs against them. Discovery of efficient modulators against these targets may lead to better prognosis of a disease. These modulators may be bioactive compounds identified from different chemical or natural libraries by various assays commonly known as 'Drug Screening'. The course of discovery and development of such bioactive molecules into successful therapeutics is an ever-challenging task with very poor success rates. By and large this process can be summarized as screening of various libraries, validation of target activity and pharmacokinetics in small animal models followed by clinical trials [12]. These bioactive molecules are finally approved as marketed drugs only after successful completion of phase I to phase III clinical trials. However, these last steps experience challenges not only for the validation of new therapeutics, but also for their delivery to target sites.

Ongoing research in the field of drug delivery is constantly attempting to improve the efficacy and to reduce the side-effects of currently available drugs. However, even after developing improved targeted drug moieties, many of them show poor pharmacokinetics and inappropriate biodistribution, thus limiting their use. Conventional methods of biodistribution are based on monitoring drug levels in body fluid and/or invasive methods to study organ specific accumulation [13-16]. However, obtaining evidence for drug adsorption, distribution, metabolism and excretion (ADME) properties are not possible for all candidate drugs. Assessment of such ADME and other pharmacological properties during pre-clinical and clinical studies are crucial for authorisation of therapeutics. Evaluations of these aspects using conventional methods in small animal models are inadequate and limit the scope for their improvement. Even differential or individualistic response and dynamic drug efficacies are often overlooked. Therefore, dynamic assessment of these criteria in living subjects in repetitive and non-invasive manner is critical for proper evaluation of therapeutic molecules. Non-invasive imaging modalities can be used for such assessment to support and improve various aspects of drug delivery.

The concept of *in vivo* imaging is well known for a few decades and was initially applied for gross anatomical imaging. Information obtained from various imaging modalities, for instance, X-ray scan, radionucleotide imaging, and ultrasound was used to diagnose asymptomatic diseases. Information obtained from anatomical abnormalities was used to monitor therapy outcome. Subsequent advancement in technologies and probe labelling chemistry aided to exponentially increase their sensitivity as well as specificity. However, it is still a challenge to label every drug with an appropriate signature molecule and achieve enough binding or trapping of the probe molecule endogenously that could be imaged above the background signal. Often the evaluation of real time biodistribution of a candidate molecule by imaging is not possible. Interestingly, scientists circumvent these problems using an indirect reporter gene-reporter probe strategy where a drug molecule can act as the reporter probe.

This reporter gene-therapeutic reporter probe (RG-TRP) strategy often uses an endogenous physiologically relevant gene to avoid elicitation of immunological response. This method imparts certain merits over conventional imaging of physiological distribution of labelled drug molecules to monitor the efficacy, bioavailability and off target effects. These are:

1. Development of generalized methods for assessing therapeutic effects of different pathological conditions such as cancer or neurological or infectious diseases

2. The same strategy can be used for both diagnosis and therapy

3. No or minimal immunological response

4. Immediate scope of being translated in human patients

However, examples of these reporter gene-therapeutic reporter probes are few since it is difficult to identify these naturally occurring gene-substrate combinations. As illustrated in Fig. (**1**), this short review is focused on describing the currently available Reporter gene-Therapeutic reporter probe strategies (RG-TRP) for various pathological conditions and the merits and demerits of these systems. Detailed review on how reporter gene-reporter probe strategy associated with different imaging modalities assist drug discovery and development can be found in another review [12].

VEHICLES USED FOR DELIVERING REPORTER GENE

An important component of the RG-TRP strategy is the choice of delivery vehicles since in majority of the cases the gene requires to be introduced exogenously. These delivery vehicles could be of non-targeted type (for proof of concept validation) or of targeted in nature (for monitoring the therapeutic efficacy). Recent advancement in genetic engineering and manipulations has helped in designing sophisticated vectors and the concept of gene therapy has been initialized and practiced. The same strategy can be used effectively to monitor drug delivery and drug validation using the RG-TRP strategy. Various non-hazardous viral vectors developed from an infectious virus system are used for targeted gene delivery. Though viral based vectors are the first choice for gene delivery, many other non-viral vector based delivery vehicles have also been developed.

Some of the most widely used delivery systems for gene therapy include:

Biological or Viral Vectors

1. Retroviral and Lentiviral systems [17-21]

2. Adenovirus and Adenovirus associated viruses [9, 22-36]

3. Herpes virus vectors [24, 37-40]

4. Vaccinia virus vectors [41-43]

Chemical Vectors

1. Liposomes [44-50]

2. Dendrimers [51, 52]

3. Drug-polymer composites [53-55]
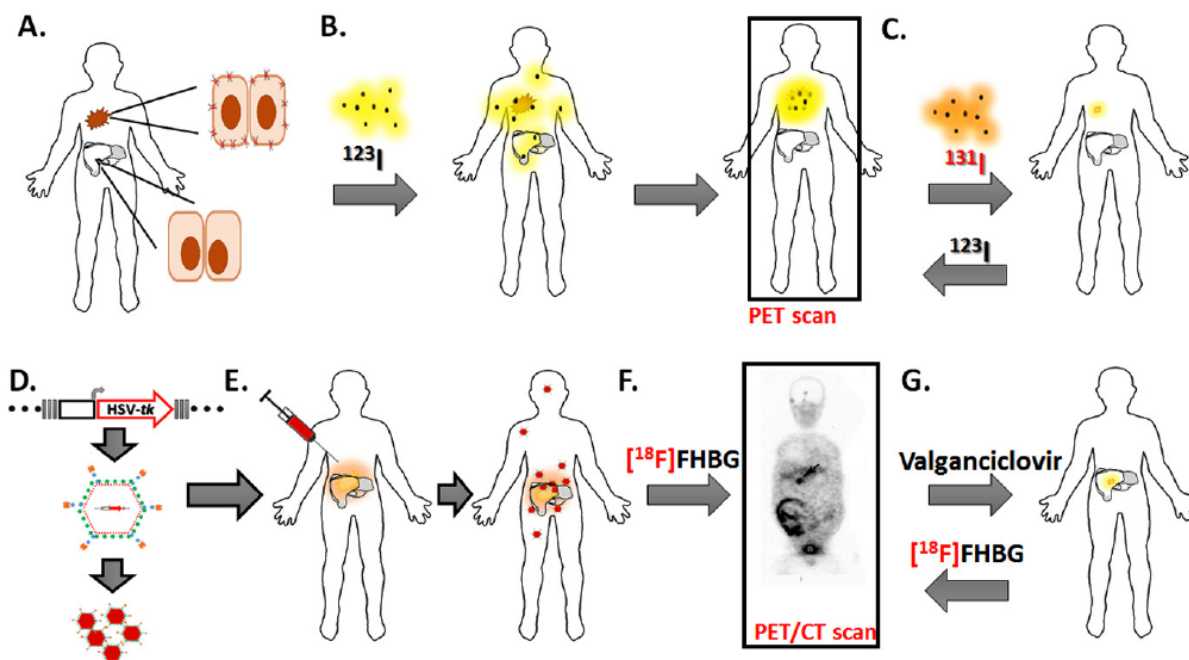
Fig. (1). Schematic diagram describing the strategies of Reporter gene-therapeutic reporter probe (RG-TRP) imaging using either endogenous (**A-C**) or targeted exogenous (**D-G**) reporter gene. Schematics of endogenous RG-TRP (**A-C**): Endogenous reporter genes such as Sodium Iodide Symporter (NIS) when overexpressed on tumor cells in comparison to normal cells selectively help in accumulation of iodine (Fig. **1A**). These reporter genes can be used to visualise tumor growth via PET imaging modality after administration of ^{123}I as a reporter probe (Fig. **1B**). Selective accumulation of iodine in NIS expressing cells furthermore provides scope for targeted radiotherapy via ^{131}I administration (Fig. **1C**). The efficacy of this therapy can be monitored via PET after administration of ^{123}I as reporter probe. Schematics of exogenous RG-TRP (**D-G**): Exogenous reporter genes such as HSV1-*tk* can be administered using recombinant viral vectors for targeted delivery to specific sites (Fig. **1D**). HSV1-TK phosphorylates the reporter probes such as [^{18}F]-FHBG or [^{124}I]-FIAU resulting in accumulation of phosphorylated probes in target cells. These accumulated probes can be monitored using PET imaging modalities (Fig. **1F**, adopted from Penuelas *et al.*, 2005[50]). The same HSV1-TK can convert prodrug (which is also a substrate of HSV1-TK) such as Valganciclovir into its active tri phosphorylate form resulting in cell death and regression in tumor size. Further efficacy of these treatments can be monitored via PET after administration of [^{18}F]-FHBG as reporter probe.

4. Nanomaterials (Further classified as Nanoparticles, Nanocapsules and Nanoimulsions) [12].

Based on their origin, these delivery vehicles can be categorized into two groups – biologically derived and chemically synthesized. Biologically derived vehicles include non-hazardous viral vectors developed from infectious viruses and attenuated bacterial delivery systems. Non-replicating DNA viral vectors (i.e. adenovirus [56], herpes simplex virus [57], adenovirus associated virus [58], etc.) are most widely used because of their ability to infect different cell types producing transient but higher gene expression. Initially viral vectors gained prominence as gene therapy vehicles in animal models, but they showed very less gene transfer rates in clinical trials [59]. This may be due to insufficient expression of surface receptor like Coxsackie and adenoviral receptor (CAR) on target cells (in case of adenovirus) [59]. Retroviral based systems provide better transduction efficacy and stable expression, but their infectivity is restricted to proliferative cells [60]. Recently attenuated strains of *Salmonella* [61, 62], *Shigella* [63] and *Lactococcus* [64], as well as *Escherichia coli* [65] were employed as gene delivery vectors. For some of these bacterial systems, mechanisms of gene delivery to mammalian cells are still not well understood. Currently 2076 gene therapy clinical trials

have been reported worldwide. Among them, 22.8% clinical trials used adenoviral based systems followed by retroviral (19.1%) and naked/plasmid DNA (17.7%). Also, direct physical administration (via gene gun or electroporation) and the bacteria based system were used in 2% and 1.6% of these trials respectively.

In recent times, chemically synthesized delivery vehicles are gaining popularity due to their special features like biocompatibility and controlled release of therapeutic molecules. These vehicles are broadly classified into liposomes, dendrimers, drug-polymer conjugate (polyamino acids, dendrimers etc.) and nanocomposites. Nanocomposites are further subclassified as metallic nanoparticles, nanoemulsion, and nanocapsule [12]. Among them, the polymeric delivery vehicles such as liposomes, dendrimers, polylysine, etc., are used to deliver reporter genes in RG-TRP systems [44-52], whereas nanocomposites are mostly used to deliver therapeutic and/or reporter probes [12, 53-55]. All these properties of reporter gene delivery systems are summarized in Table **1**.

Though modified drug delivery systems improve distribution of intact therapeutics and its efficacy, they lack specific targeting. Non-viral vectors provide a better rate of gene transfer (up to 60%) [44-50] over viral vectors (10-50%) [9, 22-36]. Variability in transfer rates and site-specific

Table 1. **Properties of reporter gene delivery systems.**

Properties / System	Insert Size	Viral Titer	Integration	Sustained Expression	Transduction Efficiency	References
Biological delivery system						
Adenovirus	8 kb	10^{11}	NO	Transient	10-50%	[22-31]
Retrovirus	8 kb	10^{7-10}	YES	Variable	0.9-14.5%	[17-21]
Herpes Simplex Virus (HSV)	>20 kb	10^8	NO	Transient	80%	[24, 37-40]
Adenovirus-Associated Virus (AAV)	<4 kb	10^9	NO	Transient	64%	[9, 32-36]
Physical and chemical delivery systems						
Plasmid + Electroporation	>20 kb	N/A	NO	Only in muscles	3-8%	[66, 143-146]
Liposomes	>20 kb	N/A	NO	Transient	40-50%	[44-50]

gene transfer limits the use of non-viral vectors during clinical trials [59]. Viral vectors such as adenoviral ones provides a promising approach for distant gene transfer, but many times lack specificity in targeting [66]. To improve the specificity of viral based systems numerous strategies such as the development of recombinant targeted vectors, use of tissue specific promoter to drive gene expression, etc., have been adopted. Till date adenoviruses are the preferred choice for gene delivery because they can be produced at high titres. Infectivity of these adenoviral vectors depend on the presence of CAR- receptor on cell surface which makes them very effective against hepatocellular carcinomas and colon cancer [67, 68]. This CAR-receptor dependency limits the use of adenoviral vectors since majority of the primary tumors lack CAR and also results in toxicity to normal liver especially to liver parenchyma [66]. To overcome such shortcomings, these vectors were genetically modified to target alternative receptor selectively expressed on the target cell surface. One such strategy uses the insertion of an Arg-Gly-Asp (RGD) motif into the HI loop of the adenoviral knob, thus increasing its affinity towards integrins, leading to targeting pancreatic cells in CAR-independent manner [69]. Another strategy comprises of adenovirus fibre knob conjugation with other target specific moieties such as antigen targeting peptide, DNA or RNA aptamers, monoclonal antibodies and their derivatives, which assists in homing to defined tissue or organ. A typical example of such a strategy includes targeting EpCAM, a surface antigen, which is over expressed in majority of adenocarcinomas. In this strategy EpCAM-targeted adenoviral vector was developed by conjugating bispecific antibodies against EpCAM with the fibre knob (antiEpCAM/antiknob) to target adenocarcinomas [70]. Other receptors such as α-folate receptor [71] and epidermal growth factor receptor (EGFR) [72] were also targeted using a similar approach.

Another way of achieving target specificity for these RG systems is the use of tissue specific promoter. In such cases, reporter gene is expressed under tissue specific promoter to achieve transcriptional selectivity. This strategy has been shown to be effective in many cases such as α-fetoprotein

(AFP) promoter to target hepatocellular carcinoma [73], prostate specific antigen (PSA) to target prostate cancer [74, 75], Willebrandt factor to target endothelial cells [76, 77], JC virus promoter and myelin-based promoter to target glioma cells [78], prs-9 promoter to target rabdomyosarcoma cells [79], c-erbB2 promoter to target breast [80], pancreatic and non-small cell lung cancer (NSCLC) cells, and the osteocalcin promoter to target osteosarcoma [81, 82].

Further specificity of such system can be improved by using two or more therapeutic/reporter genes. In this approach simultaneous use of two suicidal genes, e.g., cytochrome P450 (CYP) along with cytosine deaminase (CD) [83] or thymidine kinase and cytosine deaminase [84] proved to be more effective compared to the single gene system. In addition, multiple genes were transfected together to enhance drug activation, since prodrug activation requires a metabolic cascade involving several enzymes. In case of ganciclovir (GCV), simultaneous transfection of three kinases such as HSV-TK, guanylate kinase, and nucleoside diphosphate kinase improved its activation rates to >90% [85]. Similarly, simultaneous transfection of cytochrome P450 and the P450-reductase increase conversion of cyclophosphamide (CP) to cytotoxic drug 4-hydroxy cyclophosphamide [86].

Non-invasive molecular imaging, the method for assessing RG-TRP system *in vivo*, is broadly classified into five categories, namely: Optical Imaging (Fluorescence and Bioluminescence), Radionuclide Imaging (SPECT and PET), Magnetic Resonance Imaging (MRI), Computed Tomography (CT) and Ultrasound imaging. The RG-TRP concept is mainly associated with Radionuclide and MR imaging since they can adapt endogenous genes as reporters and generate the functional aspects of the probe validation [87].

FUNCTIONAL IMAGING MODALITIES ASSOCIATED WITH RG-TRP

Radionuclide Imaging

Radionuclide imaging primarily utilizes various radioisotopes as signal generating molecules and is broadly classified into Positron Emission Tomography (PET) and Single Pho-

ton Emission Computed Tomography (SPECT) imaging. Both gamma emitting and positron emitting radioisotopes are used for these modalities. PET records high energy gamma rays emitted after an eventual annihilation of a positron and an electron while SPECT detects low energy gamma rays emitted from ^{99m}Tc, ^{111}In, ^{123}I, ^{131}I and other isotopes. PET technology involves simultaneous and coincident detection of two gamma rays 180^0 away from each other by the detectors which imparts ten times higher sensitivity than SPECT. They require a cyclotron to produce positron and gamma emitting radioisotopes. For example, PET requires high end cyclotron to generate positron emitting radionuclides like ^{11}C, ^{18}F, ^{64}Cu. As SPECT aids in the detection of a single gamma ray at a time, it suffers from significant background noise and requires application of collimators or lead blocks that reduce the ultimate detection level [88].

Gene Systems Used in Radionucleotide Imaging

Till date, several reporter gene-therapeutic reporter probe systems have been validated by radionuclide imaging. Herpes Simplex Virus 1-thymidine kinase (HSV1-*tk*) is one of the most commonly used radionuclide based reporter gene system which can easily convert a prodrug into a therapeutic agent. Though thymidine kinase (TK) is a crucial enzyme required for DNA replication and present in every cell (prokaryotes to eukaryotes), the one mostly utilized for imaging is adapted from Herpes Simplex Virus. Thymidine kinase catalyses the phosphorylation of deoxythimidine resulting in the formation of an ester and the phosphorylation of deoxythymidine-5'-monophosphate gives rise to an anhydride that gets trapped inside the cell [89]. The substrates for HSV1-tk can be classified into two categories, namely, pyrimidine nucleoside derivatives like $[^{124}I/^{18}F]$-29-fluoro-29-deoxy-1-b-D-arabinofuranosyl-5-iodouracil (FIAU) and 2'-deoxy-2'-$[^{18}F]$-fluoro-5-ethyl-1-β-D-arabinofuranosyluracil ($[^{18}F]$-FEAU) and acycloguanosine derivatives like, acyclovir, ganciclovir (GCV), pencyclovir (PCV) and fluorine-18-labeled acycloguanosine derivative substrate for herpes simplex virus type-1 thymidine kinase (HSV1-TK) (FHBG). In comparison to mammalian *tk*, HSV1-*tk* has lesser substrate specificity. Thus along with thymidine, it can phosphorylate other nucleotide substrates. Pyrimidine derivatives having a structure similar to thymidine are more efficient and suitable for imaging as compared to the acycloderivatives. However, owing to their excessive toxicity towards mitochondria they cannot be used for therapy along with imaging. As wild type HSV1-*tk* shows less specificity towards various substrates, groups around the world have tried mutating the gene to enhance its specificity for the acycloderivatives in order to enable successful imaging along with therapy. One such mutant is HSVI-sr39*tk* which shows increased specificity for acycloderivatives [87] and hence can be imaged using ^{18}F and ^{124}I radiolabeled acycloguanosine and pyrimidine derivatives [90]. Likar *et al.* (2008) reported a mutant HSV1-A167Ysr39TK which could readily phosphorylate ^{3}H-GCV and also showed enhanced activity with ^{3}H-PCV *in vitro* and $[^{18}F]$-FHBG *in vivo* [91]. Ponomarev *et al.* (2007) discussed the utility of the non-immunogenic human derived mitochondrial thymidine kinase type 2 (*hmtk*2) reporter gene and assessed its specificity with a series of radiotracers and prodrugs like $[^{124}I]$-FIAU, $[^{18}F]$-FIAU or $[^{18}F]$-FEAU [92].

Dopamine receptors, another example of TRG-TRP system, are G-Protein Coupled Receptors (GPCR) expressed on the surface of the neuronal cells. The greatest advantage of using dopamine 2 receptor is that the non-mutated form of the gene is not immunogenic. This gene system uses $[^{18}F]$-Fluoroethyl spiperone (FESP) as substrate which has good pharmacokinetics and can easily cross the blood brain barrier. On the contrary, HSV1-*tk* and its probes fail to cross the blood brain barrier. However, there are a few disadvantages as well. High background in pituitary and striatum and long clearance time of the probe impose difficulties on clinical trials. Apart from [3-(2'-$[^{18}F]$-fluroethyl)-spiperone] (FESP) the most common substrate, $[^{11}C]$-Raclopride and $[^{11}C]$N-methylspiperone are also considered to be potential probes for D_2R [87].

Within the category of radionuclide reporters, the thyroidal Sodium Iodide Symporter (*NIS*) has emerged as one of the most promising for preclinical and translational research. Sodium iodide symporter gene attains a special status by utilizing various radioisotopes and ^{99m}Tc directly as probes. Easy availability of these probes (for PET and SPECT imaging as well as therapy) and lack of immune reaction also makes *hNIS* one of the widely used reporter systems for radionuclide imaging. *NIS* is a membrane glycoprotein with 13 transmembrane domains found to be naturally expressed in thyroid, salivary gland, mammary gland, stomach and sometimes in breast cells (during lactation) [93]. The most important function of *NIS* is to mediate the passage of iodine to the follicular cells of the thyroid and also the extrathyroidal tissues. The symporter transports two sodium ions along with one iodide ion thus, creating a transmembrane concentration gradient which ultimately favours the uptake of iodine. Commonly used substrates for *hNIS* are ^{123}I and ^{99m}Tc which are used in diagnosis as they are exclusively gamma emitters. Similarly, ^{124}I and ^{18}F tetrafluroborate are also used in diagnosis as positron and gamma emitters. On the other hand, ^{131}I, ^{186}Re, ^{188}Re being gamma and beta emitters are used in therapy. ^{211}At is the only radionuclide used for *NIS*, which is an alpha and X-Ray emitter. *NIS* has been incorporated into a remarkable variety of viral and non-viral vectors in which its functionality is conveniently determined by *in vitro* iodide uptake assays prior to live animal imaging. However, post translational modifications associated with this protein may impose certain challenges [87], [93-95].

Somatostatin receptor (*SSTr*) is a G-protein coupled receptor and is composed of seven transmembrane segments. This reporter system uses radiolabeled octreotide as a ligand like, ^{111}In labelled DTPA-D-Phe-octreotides. *SStr2* has been mutated like D_2R so that it can efficiently bind to its radiolabelled probe without producing any physiological lethality [87].

The human norepinephrin transporter (*hNET*), a very small gene system is used to image myocardial sympathetic innervations and neural crest tumors using various radioisotope labelled MIBG (metaiodobenzylguanidine). Similar to *hNIS*, MIBG can be labelled with ^{131}I and used for therapy [96].

Magnetic Resonance Imaging

Magnetic resonance imaging is another non-invasive functional imaging technique which in principle relies on the

altered alignment of magnetic dipoles. The radiofrequency pulse and the strong magnetic field enable a change in the alignment of the spins which immediately return to the baseline after withdrawal of the pulse. The rate of change of the oscillatory alignment of the dipoles gets translated into an MR signal [88].

MRI is associated with T1 contrast and T2 contrast images. The T1-weighted MR images are helpful in identifying tissues with varying viscosities that cause the water molecules inside the tissue to have different rotational tumbling motion. So, minor differences inside a particular tissue can also be detected by the T1 weighted image. On the other hand the T2-weighted MR images are useful in identifying biological tissues with varying air-tissue interfaces. In other words, tissue homogeneities are easily detected in this T2-weighted MR images [87]. The reporter gene systems used in MRI can be classified into the following categories [97]:

- Enzyme Based

- Spectroscopy Based

- Iron Based

- Chemical Exchange Saturation Transfer Based (CEST)

The commonly used MR reporter systems are transferrin receptor, β-galactosidase, tyrosinase, ferritin, cytosine deaminase and lysine rich-protein (LRP). However, only transferrin receptor and cytosine deaminase have the potential to be developed as an RG-TRP system [98].

Among the enzyme based MR reporter category, cytosine deaminase is relatively more significant as it enables imaging and also converts prodrug into a toxic compound. The gene encodes an enzyme that catalyzes the conversion of the prodrug 5-flurocytosine into 5-flurouracil in tumor cells which can be monitored by magnetic resonance spectroscopy. Flurouracil and flurocytosine being anions cannot cross the membrane and remain trapped in the cells, thereby exerting production of toxic metabolites which eventually kill the tumor cells [97].

Transferrin receptors are known to efficiently deliver iron oxide into the cells. They bind to transferrin molecules containing two paramagnetic iron atoms. Iron gets released into the cell via acidic endosome thereby, resulting in an improved T2-weighted image. In the recent days Doxorubicin has been conjugated with transferrin to improve bioavailability, toxicity and specific targeting to cells over expressing transferring receptors. However, non-invasive imaging of this transferrin-drug conjugate is yet to be achieved [99].

APPLICATION OF RG-TRP IN VARIOUS PATHOLOGICAL DISEASES

Cancer

Unlike other life threatening pathological diseases like neurodegenerative disease, cardiovascular disease, cancer is endowed by the tremendous amount of heterogeneity. This multifactorial lethal disease initiates with neoplasm due to the uncontrolled proliferation of cells and is often associated with distant metastasis. Such malignancy can arise due to genetic (somatic or hereditary) or environmental factor(s) [100, 101]. Though various treatment modalities such as

cytotoxic chemotherapy, radiotherapy and surgery are available, poor prognosis is observed majorly due to non-targeted effects, relapse and metastasis. To overcome such limitations, Molten in 1989, pioneered the concept of suicide gene therapy against solid tumors [102]. This therapy is also known as Gene directed enzyme-prodrug therapy that comprises of targeted expression of an enzymatic gene which converts prodrug into an active cytotoxic drug. Developing suicidal gene therapy is advantageous over conventional therapy as it improves the therapeutic index due to target selectivity and bystander effect [103]. RG-TRP is used along with various imaging modalities and it plays a crucial role in optimising delivery and the distribution of therapeutic transgenes *in vivo.*

HSV1-TK that was discussed earlier as an example of TRG-TRP system can also act as a suicidal gene with significant bystander effect. The anti-tumor activity of HSV-TK along with ganciclovir was assessed in various tumors, including lymphoma [104], prostate cancer [105], leukaemia [106], lung cancer [107], melanoma [108] and glioma [105]. HSV-TK converts ganciclovir (GCV) into ganciclovir triphosphate, which inhibit DNA replication leading to apoptosis. Due to bystander effect through gap junctions, GCV-triphosphate also kills neighbouring tumor cells, making therapy more efficient [109, 110]. This also emphasises that administration of the therapeutic gene to all tumor cells is not obligatory and complete tumor regression can be obtained with as less as 10% transduced cells. Off-target effects, and low expression levels impose certain limitations to HSV1-*tk* gene therapy which could be improved using targeted delivery, cell/tissue specific expression, creating mutations and other strategies.

Maron *et al.* (1995) studied the cytotoxic effect of the GCV-*tk* system in orthotopic tumor mouse model developed from HSV-*tk* transfected C6 rat glioma cells followed by ganciclovir treatment and MR imaging [111]. The treated group showed complete regression of tumor as assessed by MRI and improved survival rates (60% treated *vs* 30% in control) up to 12 months. Puntuck *et al.* (2002), demonstrated that sr39tk variant of HSV-TK has improved killing efficiency compared to its wild type counterpart [112]. To exercise target specific delivery monoclonal antibodies, peptides, etc., are often incorporated into delivery systems. Also, in many instances the conventional CMV promoter is replaced with cell type/tissue specific promoter. Conventional HSV-*tk* therapy in case of hepatocellular carcinoma is limited due to toxicity experienced by surrounding healthy liver parenchymal cells. To overcome these limitations a-fetoprotein promoter driven HSV1-*tk* was administered for targeting HCC cells, leaving the healthy parenchymal cells [73]. Similarly hTERT promoter was used for treating non-small cell lung squamous carcinoma (NSCLC) due to elevated hTERT expression found in NSCLC [113].

NIS is already being used in the clinic for thyroid cancer where ^{131}I is administered to expedite selective ablation of residual tumor cells after thyroidectomy and further monitored by ^{123}I imaging [114]. Other than thyroid tissue, elevated NIS expression can be exploited in the use of radioactive substrate for diagnosis and therapeutic purpose. Such elevated expression was seen in the case of many primary

cancers, including breast cancer [115-117], colon cancer [118], lung cancer [118] and urological malignancies [118] as well as in liver [119] and brain metastasis [120]. For successful therapy via NIS, membrane localization is equally a crucial factor as that of its expression. In case of breast cancer, despite of positive NIS expression, the majority of cases shows low levels of iodine uptake due to lower expression or lack of membrane localization of the protein and thus limits therapeutic applications [121]. To overcome such limitations various strategies were adapted where compounds such as retinoic acid, AGN190168, theophylline, LBH589, etc., were administered to improve NIS expression and in turn efficiency of radiotherapy [122]. Also an exogenous expression of the NIS gene via targeted delivery can be used as RG-TRP for number of malignancies. These include delivery of exogenous NIS to neuroblastoma, gliomas, colorectal cancer, hepatoma, pancreatic cancer, etc., via various viral delivery systems [122]. One such strategy, with measles virus encoding thyroidal sodium symporter is currently in clinical trial for breast cancer [123].

Further, various novel strategies such as a combination of two genes and use of fusion gene are being introduced to increase efficacy or reduce side effects of gene therapy. For example, use of E-cadherin along with HSV-TK [124], fusion of VP22 with HSV-TK [125], nitroreducatse (NTR) fused with HSV-TK [126] has been validated. E-cadherin and VP22 increases bystander effect on tumor cells, whereas HSV-TK-NTR helps to reduce toxicity. Similarly, utilization of two or more reporters/therapeutic genes improves efficacy of therapy such as a CD+UPRT/5-FC system in prostate cancer xenografts or HSV1-*tk*/CD system for cervical cancer xenografts with GCV and 5-FC as a prodrug [83, 84].

Infectious Disease Models

The RG-TRP system is now being introduced and utilized for diseases caused by various infectious agents like Mycobacterium tuberculosis and influenza virus. Davis *et al.* (2009) first time attempted to monitor the response of tuberculosis treatment by infecting BALB/c and C3HeB/FeJ with the bacterium followed by [^{18}F]-FDG imaging. Two and six weeks post infection, BALB/c and C3HeB/FeJ mice were either administered with bactericidal or bacteriostatic TB drug combinations. The efficiency of drug delivery along with the extent of drug action was monitored using [^{18}F]-FDG. In this study, PET imaging could not only detect relapse of the disease, but it could also clearly distinguish the two forms of treatments [127]. Another study by the same group in 2009 used M.tuberculosis engineered with tk gene driven by a strong hsp60 promoter. The engineered bacterial cells were used in thigh inoculation and low dose aerosol infection in BALB/c and C3HeB/FeJ mice respectively. [^{125}I]-FIAU uptake, antimicrobial susceptibility and growth characteristics were studied. Three to twelve hours, post thigh inoculation and six to eight weeks post low dose aerosol infection, mice were administered with 1mCi [^{125}I]-FIAU and imaged with SPECT, which helped to determine the localization of the bacteria non-invasively [128].

Research on the pathogenesis and therapy of influenza virus has also increased in recent years. Bray *et al.* (2011) discussed the use of drugs like acyclovir for an antiviral therapy and also an imaging tool using HSV1-tk gene system. Drugs like oseltamivir and zanamivir are commonly used for treatment to inhibit influenza viral replication. The same drugs after being labelled with radioisotopes can be used to image the site of delivery and to determine the efficacy of the drugs [129].

PROS AND CONS OF RG-TRP SYSTEM

Reporter genes are extensively used to elucidate numerous biological phenomena such as cell migration, localization, protein-protein interactions, monitoring pharmacokinetics-pharmacodynamics of drugs, elucidating drug delivery in real-time *in vitro* (cells) and *in vivo* (small animals) in various disease models. The flexibility to genetically manipulate the cDNA expression cassette in order to incorporate the reporter gene of interest facilitates versatility in non-invasive reporter gene imaging. The cDNA cassette that contains a therapeutic marker gene may be placed under the control of the promoter or enhancer elements. Under the influence of constitutively expressed promoters (e.g.: cytomegalovirus, Rous Sarcoma Viral promoters) or inducible promoters (induced by transcriptional factors, drugs, tissue-specific expression) imaging of reporter genes can gather information on route of migration, localization of delivery vectors and monitor the efficiency of therapeutic genes.

Reporter gene imaging is a sensitive, cost effective, non-invasive imaging method that is easily quantified by enzymatic assays and by extent of probe binding and obtain spatial and temporal information *via* live imaging of the cells and small animals [12, 130-132]. This robust imaging modality provides the advantage of monitoring cause and consequence of biological phenomena systematically. The ubiquitous expression and shorter time needed for the formation of the reporter gene protein can directly facilitate tracking of molecules *in vivo* and *in vitro* precisely thereby expedite the appraisal of the biological event lucidly [130].

One of the key advantages of imaging through reporter genes is that it enables longitudinal study in xenograft of human disease models. Preclinical studies carried out in small animals that bear xenograft tumors containing a reporter gene can be repeatedly administrated with drugs or theranostic molecules and the effect can be monitored without having the need to sacrifice the animal at regular intervals. This limits sacrificing numerous small animals to analyse single event and minimizes experimental error.

Currently there are numerous reporter genes that may be either non-mammalian in origin (HSV1-*tk*, HSV1-ser39*tk*) or mammalian in origin (*htk2, hNIS, hNET, hD₂R*). Reporter genes such as HSV1-*tk* and its mutant HSV1-ser39*tk* may have the disadvantage of being slightly immunogenic to humans but its property of flexible substrate specificity and higher competence to phosphorylate compounds like acyclovir, ganciclovir has catapulted them as reporter genes than mammalian thymidine kinases (htk1). However, the immunogenic potential of the viral thymidine kinase may be overcome by using the human mitochondrial thymidine kinase (*hmtk2*) that has potential equivalent to HSV1-*tk*. Enzyme-based reporter genes like HSV1-*tk* and its variants are found to accumulate within the cell, thereby causing higher noise to signal ratio, disruption of signal emitted as well as decreased

uptake of the reporter probe at specific sites. Reporter genes such as human dopamine D2 receptor (*hD$_2$R*), human soma-tostain receptor subtype 2 (*hSSTr2*), human sodium iodide symporter (*hNIS*) are localized to specific parts of the human brain and thyroid respectively, and encode for receptors that facilitate the transportation of specific probe thereby demon-strating their capacity to be useful reporter genes. The bene-fit of a reporter gene of mammalian origin includes absence of immunogenic potential, organ-specific expression of the reporter gene, and may act as suicide-therapeutic gene [133]. *In vivo* introduction and subsequent appraisal of reporter genes and therapeutic genes may be facilitated by biological vectors such as adenoviral vectors, adenoviral-associated vectors or retroviral vectors. Advantages of these biological vehicles include elevated transgene expression, capacity of holding ~8 Kb of heterologous DNA and ability to transduce dividing and quiescent cells. However, the limitations of these vectors may result from activation of the immune sys-tem, causing anaphylactic shock *in vivo* and incidental inser-tion in critical regions of the genome causing mutation [134]. Thus, there is a dearth of optimal delivery vectors to intro-duce the reporter-therapeutic gene, which acts as a parapet against the translation of reporter gene imaging in clinical set up [135].

Assessment of the reporter gene is possible only if the re-porter protein interacts with the specific reporter probe lead-ing to emission of a signal that is captured through various imaging modalities. A reporter probe has specific prerequi-sites that include stable and site-specific accumulation in liv-ing subjects, absence of toxicity of the reporter probe or its metabolites *in vivo*, optimal pharmacokinetics of the probe. The probe should be unlimited by biological barriers (blood-brain barrier) and it should not get metabolised before reach-ing the target [136]. The most frequently used probe for PET imaging in pre-clinical and clinical application is [^{18}F] FDG, a glucose analogue. It is phosphorylated by hexokinase-2 and gets accumulated within the cells as it is unable to enter the glycolytic cycle. The accumulation of radioactive probe aids in visualization of the metabolic activity in that specific site. However, since inflammatory cells also have an affinity to [^{18}F]-FDG, probes such as [^{18}F]-FHBG, [^{18}F]-thymidine, [^{11}C]-thymidine, [^{11}C]-methionine, [^{124}I]-NaI have also been attempted to PET imaging for information. HSV1-TK has the ability to act on radiolabelled thymidine substrates like [^{18}F]-FIAU, [^{18}F]-FEAU and acycloguanosine derivatives such as ganciclovir, pencyclovir, FHBG [98, 133]. The mutant ver-sions of HSV1-tk such as HSV1-A167Ysr39*tk*, HSV1-R176Q*tk* can also be imaged with [^{18}F]-FHBG. In presence of acycloguanosine compounds these mutants can act as thera-peutic suicide genes [133]. [^{18}F]-FMAU can be used as a probe for the mutant version of the human mitochondrial thymidine kinase (hTK2-N93D/L109F) Other reporter probes include ^{131}I-iodide, ^{11}C-ephedrine, [^{18}F]-FESP and [^{111}In]-DOTA-BASS that aid in PET imaging of reporter genes *hNIS, hNET, D$_2$R* and *hSSTr2* respectively [133].

In the past ten to fifteen years, RG-RP imaging brought a new dimension to biomedical research [110, 137-139]. Advancement at several fronts in RG-RP research led to quick adaptation and popularity across the world. The RG-TRP, however, are less popular due to certain limitations such as need of expensive instrumentation, production of

isotopes and highly trained professional while disadvantage of MRI based reporter gene imaging includes large size of reporters or contrast agents that hinders delivery *in vivo* [140]. Prerequisite factors that may limit RG-TRP applica-tion are endogenous or mammalian origin of reporter genes, high noise to signal ratio and specific physiological uptake at sites of endogenous gene expression. Similarly, deiodination of radio-labelled iodine probes, higher clear-ance rate and short imaging window for some radionucleo-tides are limitations for specific systems.

A major advantage of RG-TRP system over RG-RP sys-tem is the scope of translation to human studies since the probe can generate dual information- imaging and therapeu-tic effects. Of course the non-mammalian RG might suffer from immunogenic responses. Reporter gene imaging has predominantly been explored in small animals; however, in recent years, researchers have extended the same to detect the reporter gene expression and efficacy of drugs *via* clini-cal trials in humans.

ADAPTATION OF RG-TRP IMAGING IN CLINICAL TRIALS

Even though there are limitations immense endeavours are being undertaken to translate reporter gene imaging from small animals to clinical trials to expedite translation of can-didate drugs from bench to bedside, and monitor the efficacy of drugs in various diseases. Among the prevalent imaging modalities reporter gene imaging in humans through PET imaging has been most successful due to greater penetrating power of gamma rays, and higher sensitivity.

Jacobs *et al.* (2001) for the first time demonstrated the feasibility of monitoring liposome complex containing HSV1 thymidine kinase (LIPO-HSV1-*tk*) gene administered intratumourally in five patients diagnosed with recurrent glioblastoma by PET and MRI. In this study patients were injected with a cationic liposomal vector DAC-30 encapsu-lating a plasmid containing the HSV1-*tk* gene through a catheter. Four days after intratumoural infusion, patients were administered with ganciclovir and the treatment re-sponse was investigated through MRI, ^{18}FDG-PET, carbon-11-labeled methionine (MET-PET), and [^{124}I] FIAU-PET. In one patient, intratumoural infusion of HSV1-*tk* containing vector led to an enhanced accumulation of [^{124}I]-FIAU within the tumour as opposed to the absence of FIAU accu-mulation before vector infusion. Also, a gradual increase in the ratio of radioactivity between tissue and plasma level was noted. Upon ganciclovir treatment necrosis was observed in the tumour region which was transfected with HSV1-*tk* and had entrapped FIAU. The ganciclovir treated necrotic tu-mour was imaged by MET-PET and ^{18}FDG-PET thus indica-tive of therapeutic response facilitated by HSV1-*tk*. This study demonstrated the successful transfection of HSV1-*tk* gene into gliomablastoma tumours and enhanced treatment efficacy of ganciclovir through PET imaging. However, limi-tations of the study include PET imaging of accumulation of [^{124}I]-FIAU only in one of the five glioblastoma patients and long half-life of ^{124}I due to which serial PET imaging of the tumours was not possible [141].

In another study Penuelas *et al.* (2005) used PET imag-ing to elucidate expression of HSV1-TK in a pilot clinical

trial. In order to monitor expression of HSV1-*tk*, seven hepatocellular carcinoma (HCC) patients were administered with increasing doses of recombinant adenoviral vector encoding herpes simplex thymidine kinase enzyme (AdCMV*TK*). After intratumoural infusion the tumours were imaged on the second day by [^{18}F]-FHBG-PET and [^{18}F]-FHBG-PET/CT followed by treating the patients with 900 mg of vanganciclovir for a fortnight to induce tumour regression. This study confirmed accumulation and localization of [^{18}F]-FHBG specifically in tumour nodules of patients that received an intratumoural infusion of 10^{12} viral particles (vp) and vanciclovir. Patients who received more than 10^{12} vp were found to have an arrest in tumour progression on the 30th day from start of treatment as opposed to those who received less than 10^{12} viral particles. The novelty of this study includes two aspects that PET imaging may be used to assess reporter gene transduction mediated by viral vectors in human HCC tumours, and direct infusion of adenoviral vector into tumour poses no risk to bystander normal hepatocytes thereby favouring safety in human clinical trials. However, this study showed patients treated with a higher dose (2×10^{12} vp) of AdCMV*tk* did not positively correlate with higher accumulation of [^{18}F]-FHBG, which may be attributive to inter-tumoural variability from patient-to-patient, inability to re-infect tumours the second time with adenoviral vectors, and/or impaired expression of HSV1*tk* when tumour cells are infected in excess. These limitations may be dispelled or affirmed through clinical trial of a larger cohort [67].

Sangro *et al.* (2010), in a phase I clinical trial that included ten patients diagnosed with advanced stage hepatocellular carcinoma, administered three doses of adenoviral-vector (intratumourally with 10^{10} to 2×10^{12} viral particles) containing HSV1-*tk* reporter gene along with ganciclovir treatment. PET imaging demonstrated transgene expression in 100% cases and intratumour necrosis in two patients while for one patient overall survival was enhanced till 26 months [142].

While these studies illustrate heartening results, translation of RG-TRP imaging in different phases of clinical trials as a modus operandi to advance treatment in various disease models still warrants tremendous research and efforts.

FUTURE DIRECTIONS

In order to fight any disease, we need efficient therapeutic molecules that will aid in combating the disease. The various modes of delivery system prevalent for targeted transfer of drugs may be assessed for efficacy noninvasively by reporter gene imaging. Although, reporter gene imaging has a tremendous role in non-invasive assessment of various biological processes *in vivo*; however, this mode has been predominantly limited to small animals for investigating pharmacokinetics and pharmacodynamics of drugs. The translation of reporter gene imaging of small animals to human clinical trials is as yet rigged with numerous unanswered questions that include extent of biodistribution of reporter cum suicide gene; extent of gene expression of transduced or transfected cells into diseased tissue and the optimal time to initiate prodrug treatment in prodrug-gene therapy cases. In this context reporter gene-therapeutic re-

porter probe systems open up the scope of translatability by utilizing the probes as therapeutic molecules. The plausibility of identifying more novel reporter genes that may act as therapeutic or suicide genes with minimal immunogenic potential, higher sensitivity, and an enhanced signal to noise ratio, decreased clearance rate and longer imaging window would certainly be the future of this arena of research. The newly identified reporter gene associated reporter probes will further aid in decreasing the time frame of identifying the therapeutic potential of candidate drugs.

Another critical area of future research involves development of targeted delivery strategies. Both biological and abiological vectors/entities must be distributed at specific disease sites which is quite challenging, but will be the key to success of RG-TRP research.

In spite of several examples of the use of RG-TRP system in human patients, we are yet to exploit the full potential in majority if not all pathological conditions. Development of reporter probes to facilitate the action of reporter-suicide genes in disease models such as autoimmune diseases (rheumatoid arthritis, bloom's syndrome), neurodegenerative disorders (Alzheimer's diseases) and infectious diseases is as yet warranted. Available radiotracer diversity heralds the necessity to engineer probes that can effectively convert novel prodrugs to its lethal metabolites, thereby, achieve necrosis or apoptosis of host and neighbouring cells.

In conclusion, reporter gene imaging will not only aid in optimizing threshold of gene expression, deciphering optimal time point to initiate prodrug treatment, but also determines the efficacy of prodrug-gene therapy protocols in various disease models. The time taken for validating the potential of a candidate drug takes numerous years. Thus, endeavours on synthesizing novel reporter gene-therapeutic reporter probes have the potential to harbinger translation of novel prodrugs from bench-to-bedside and propel human health care towards the era of personalized medicine.

CONFLICT OF INTEREST

ACKNOWLEDGEMENTS

REFERENCES

[1]   Metri K, Bhargav H, Chowdhury P, Koka PS. Ayurveda for chemo-radiotherapy induced side effects in cancer patients. J Stem Cells 2013; 8(2): 115-29.

[2]   Skandhan KP, Rajahariprasad A, Sumangala B. Support for human estrus: documentation in Ayurveda. J Sex Med 2012; 9(1): 322-5.

[3]   Vishwakarma R, Goswami PK. A review through Charaka Uttara-Tantra. Ayu 2013; 34(1): 17-20.

[4]   Gurib-Fakim A. Medicinal plants: traditions of yesterday and drugs of tomorrow. Mol Aspects Med 2006; 27(1): 1-93.

[5]   Subbarayappa BV. The roots of ancient medicine: an historical outline. J Biosci 2001; 26(2): 135-43.

[6]   Fischer A, Hacein-Bey-Abina S, Cavazzana-Calvo M. 20 years of gene therapy for SCID. Nat Immunol. 2010; 11(6): 457-60.

[7]   Cartier N, Aubourg P. Hematopoietic stem cell transplantation and hematopoietic stem cell gene therapy in X-linked adrenoleukodystrophy. Brain Pathol 2010; 20(4): 857-62.

[8]   Xu Z, Ye J, Zhang A, *et al.* Gene Therapy for Hemophilia B with liver-specific element mediated by Rep-RBE site-specific integration system. J Cardiovasc Pharmacol 2014.

[9]   Nathwani AC, Tuddenham EG, Rangarajan S, *et al.* Adenovirus-associated virus vector-mediated gene transfer in hemophilia B. N Engl J Med 2011; 365(25): 2357-65.

[10]   LeWitt PA, Rezai AR, Leehey MA, *et al.* AAV2-GAD gene therapy for advanced Parkinson's disease: a double-blind, sham-surgery controlled, randomised trial. Lancet Neurol 2011; 10(4): 309-19.

[11]   Liu T, Kishton RJ, Macintyre AN, *et al.* Glucose transporter 1-mediated glucose uptake is limiting for B-cell acute lymphoblastic leukemia anabolic metabolism and resistance to apoptosis. Cell Death Dis 2014; 5: e1470.

[12]   Chaudhury S TB, Chateerjee S. Molecular Imaging Aided Improvement in Drug Discovery and Development , 2014. Current Biotechnology 2014; 3(3): 218-37(20).

[13]   Liu H, Delgado MR. Therapeutic drug concentration monitoring using saliva samples. Focus on anticonvulsants. Clin Pharmacokinet 1999; 36(6): 453-70.

[14]   Drummer OH. Drug testing in oral fluid. Clin Biochem Rev. 2006; 27(3): 147-59.

[15]   Kapur BM. Drug-testing methods and clinical interpretations of test results. Bull Narc 1993; 45(2): 115-54.

[16]   Kiang TK, Schmitt V, Ensom MH, Chua B, Hafeli UO. Therapeutic drug monitoring in interstitial fluid: a feasibility study using a comprehensive panel of drugs. J Pharm Sci 2012; 101(12): 4642-52.

[17]   Mavria G, Porter CD. Reduced growth in response to ganciclovir treatment of subcutaneous xenografts expressing HSV-tk in the vascular compartment. Gene Ther 2001; 8(12): 913-20.

[18]   Walling HW, Swarthout JT, Culver KW. Bystander-mediated regression of osteosarcoma via retroviral transfer of the herpes simplex virus thymidine kinase and human interleukin-2 genes. Cancer Gene Ther 2000; 7(2): 187-96.

[19]   Hamstra DA, Page M, Maybaum J, Rehemtulla A. Expression of endogenously activated secreted or cell surface carboxypeptidase A sensitizes tumor cells to methotrexate-alpha-peptide prodrugs. Cancer Res 2000; 60(3): 657-65.

[20]   Rivas C, Chandler P, Melo JV, Simpson E, Apperley JF. Absence of *in vitro* or *in vivo* bystander effects in a thymidine kinase-transduced murine T lymphoma. Cancer Gene Ther 2000; 7(6): 954-62.

[21]   Steffens S, Frank S, Fischer U, *et al.* Enhanced green fluorescent protein fusion proteins of herpes simplex virus type 1 thymidine kinase and cytochrome P450 4B1: applications for prodrug-activating gene therapy. Cancer Gene Ther 2000; 7(5): 806-12.

[22]   McKay TR, MacVinish LJ, Carpenter B, *et al.* Selective *in vivo* transfection of murine biliary epithelia using polycation-enhanced adenovirus. Gene Ther 2000; 7(8): 644-52.

[23]   Tanaka M, Fraizer GC, De La Cerda J, *et al.* Connexin 26 enhances the bystander effect in HSVtk/GCV gene therapy for human bladder cancer by adenovirus/PLL/DNA gene delivery. Gene Ther 2001; 8(2): 139-48.

[24]   Majumdar AS, Zolotorev A, Samuel S, *et al.* Efficacy of herpes simplex virus thymidine kinase in combination with cytokine gene therapy in an experimental metastatic breast cancer model. Cancer Gene Ther 2000; 7(7): 1086-99.

[25]   Nishino K, Osaki T, Kumagai T, *et al.* Adenovirus-mediated gene therapy specific for small cell lung cancer cells using a Myc-Max binding motif. Int J Cancer 2001; 91(6): 851-6.

[26]   Peng XY, Won JH, Rutherford T, *et al.* The use of the L-plastin promoter for adenoviral-mediated, tumor-specific gene expression in ovarian and bladder cancer cell lines. Cancer Res 2001; 61(11): 4405-13.

[27]   Watanabe T, Shinohara N, Sazawa A, *et al.* Adenovirus-mediated gene therapy for bladder cancer in an orthotopic model using a dominant negative H-ras mutant. Int J Cancer 2001; 92(5): 712-7.

[28]   Bilbao R, Gerolami R, Bralet MP, *et al.* Transduction efficacy, antitumoral effect, and toxicity of adenovirus-mediated herpes simplex virus thymidine kinase/ ganciclovir therapy of hepatocellular carcinoma: the woodchuck animal model. Cancer Gene Ther 2000; 7(5): 657-62.

[29]   Adachi Y, Reynolds PN, Yamamoto M, *et al.* Midkine promoter-based adenoviral vector gene delivery for pediatric solid tumors. Cancer Res 2000; 60(16): 4305-10.

[30]   Brust D, Feden J, Farnsworth J, *et al.* Radiosensitization of rat glioma with bromodeoxycytidine and adenovirus expressing herpes simplex virus-thymidine kinase delivered by slow, rate-controlled positive pressure infusion. Cancer Gene Ther 2000; 7(5): 778-88.

[31]   Erbs P, Regulier E, Kintz J, *et al. In vivo* cancer gene therapy by adenovirus-mediated transfer of a bifunctional yeast cytosine deaminase/uracil phosphoribosyltransferase fusion gene. Cancer Res 2000; 60(14): 3813-22.

[32]   Kanazawa T, Urabe M, Mizukami H, *et al.* Gamma-rays enhance rAAV-mediated transgene expression and cytocidal effect of AAV-HSVtk/ganciclovir on cancer cells. Cancer Gene Ther 2001; 8(2): 99-106.

[33]   Montenegro-Miranda PS, Pichard V, Aubert D, *et al.* In the rat liver, Adenoviral gene transfer efficiency is comparable to AAV. Gene Ther 2014; 21(2): 168-74.

[34]   Joo CH. Recombinant adeno-associated virus expressing a modified transcription factor triggered by the hepatitis C viral protease NS3/4a. Bioeng Bugs 2011; 2(3): 168-73.

[35]   Yiang GT, Harn HJ, Yu YL, *et al.* Immunotherapy: rAAV2 expressing interleukin-15 inhibits HeLa cell tumor growth in mice. J Biomed Sci 2009; 16: 47.

[36]   Li XP, Li CY, Li X, *et al.* Inhibition of human nasopharyngeal carcinoma growth and metastasis in mice by adenovirus-associated virus-mediated expression of human endostatin. Mol Cancer Ther 2006; 5(5): 1290-8.

[37]   Zheng W, Huang W, Liu S, *et al.* Interleukin 10 mediated by herpes simplex virus vectors suppresses neuropathic pain induced by human immunodeficiency virus gp120 in rats. Anesth Analg 2014; 119(3): 693-701.

[38]   Zheng W, Huang W, Liu S, *et al.* IL-10 mediated by herpes simplex virus vector reduces neuropathic pain induced by HIV gp120 combined with ddC in rats. Mol Pain 2014; 10: 49.

[39]   Guedon JM, Zhang M, Glorioso JC, Goins WF, Kinchington PR. Relief of pain induced by varicella-zoster virus in a rat model of post-herpetic neuralgia using a herpes simplex virus vector expressing enkephalin. Gene Ther 2014; 21(7): 694-702.

[40]   Goins WF, Huang S, Cohen JB, Glorioso JC. Engineering HSV-1 vectors for gene therapy. Methods Mol Biol 2014; 1144: 63-79.

[41]   Autio K, Knuuttila A, Kipar A, *et al.* Anti-tumour activity of oncolytic Western Reserve vaccinia viruses in canine tumour cell lines, xenografts, and fresh tumour biopsies. Vet Comp Oncol 2014.

[42]   Stritzker J, Huppertz S, Zhang Q, *et al.* Inducible gene expression in tumors colonized by modified oncolytic vaccinia virus strains. J Virol 2014; 88(19): 11556-67.

[43]   Ady JW, Heffner J, Mojica K, *et al.* Oncolytic immunotherapy using recombinant vaccinia virus GLV-1h68 kills sorafenib-resistant hepatocellular carcinoma efficiently. Surgery 2014; 156(2): 263-9.

[44]   Xu L, Pirollo KF, Tang WH, Rait A, Chang EH. Transferrin-liposome-mediated systemic p53 gene therapy in combination with radiation results in regression of human head and neck cancer xenografts. Hum Gene Ther 1999; 10(18): 2941-52.

[45]   Schatzlein AG. Non-viral vectors in cancer gene therapy: principles and progress. Anticancer Drugs 2001; 12(4): 275-304.

[46]   Hasegawa H, Shimada M, Yonemitsu Y, *et al.* Preclinical and therapeutic utility of HVJ liposomes as a gene transfer vector for hepatocellular carcinoma using herpes simplex virus thymidine kinase. Cancer Gene Ther 2001; 8(4): 252-8.

[47]   Bentires-Alj M, Hellin AC, Lechanteur C, *et al.* Cytosine deaminase suicide gene therapy for peritoneal carcinomatosis. Cancer Gene Ther 2000; 7(1): 20-6.

[48]   Greco O, Folkes LK, Wardman P, Tozer GM, Dachs GU. Development of a novel enzyme/prodrug combination for gene therapy of cancer: horseradish peroxidase/indole-3-acetic acid. Cancer Gene Ther 2000; 7(11): 1414-20.

[49]   Harada Y, Iwai M, Tanaka S, *et al.* Highly efficient suicide gene expression in hepatocellular carcinoma cells by epstein-barr virus-based plasmid vectors combined with polyamidoamine dendrimer. Cancer Gene Ther 2000; 7(1): 27-36.

[50] Hagihara Y, Saitoh Y, Kaneda Y, Kohmura E, Yoshimine T. Widespread gene transfection into the central nervous system of primates. Gene Ther 2000; 7(9): 759-63.

[51] Somani S, Dufes C. Applications of dendrimers for brain delivery and cancer therapy. Nanomedicine (Lond) 2014; 9(15): 2403-14.

[52] Wong PT, Tang K, Coulter A, *et al.* Multivalent dendrimer vectors with DNA intercalation motifs for gene delivery. Biomacromolecules 2014; 15(11): 4134-45.

[53] Dong DW, Tong SW, Qi XR. Comparative studies of polyethylenimine-doxorubicin conjugates with pH-sensitive and pH-insensitive linkers. J Biomed Mater Res A 2013; 101(5): 1336-44.

[54] Abioye AO, Kola-Mustapha A, Chi GT, Ilya S. Quantification of in situ granulation-induced changes in pre-compression, solubility, dose distribution and intrinsic *in vitro* release characteristics of ibuprofen-cationic dextran conjugate crystanules. Int J Pharm 2014; 471(1-2): 453-77.

[55] Mastorakos P, Kambhampati SP, Mishra MK, *et al.* Hydroxyl PAMAM dendrimer-based gene vectors for transgene delivery to human retinal pigment epithelial cells. Nanoscale 2014.

[56] Douglas JT. Adenovirus-mediated gene delivery: an overview. Methods Mol Biol. 2004; 246: 3-14.

[57] Burton EA, Fink DJ, Glorioso JC. Gene delivery using herpes simplex virus vectors. DNA Cell Biol 2002; 21(12): 915-36.

[58] Wang AY, Peng PD, Ehrhardt A, Storm TA, Kay MA. Comparison of adenoviral and adeno-associated viral vectors for pancreatic gene delivery *in vivo*. Hum Gene Ther 2004; 15(4): 405-13.

[59] Curiel DT, Gerritsen WR, Krul MR. Progress in cancer gene therapy. Cancer Gene Ther 2000; 7(8): 1197-9.

[60] Miller DG, Adam MA, Miller AD. Gene transfer by retrovirus vectors occurs only in cells that are actively replicating at the time of infection. Mol Cell Biol 1990; 10(8): 4239-42.

[61] Pawelek JM, Low KB, Bermudes D. Tumor-targeted Salmonella as a novel anticancer vector. Cancer Res 1997; 57(20): 4537-44.

[62] Low KB, Ittensohn M, Le T, *et al.* Lipid A mutant Salmonella with suppressed virulence and TNFalpha induction retain tumor-targeting *in vivo*. Nat Biotechnol 1999; 17(1): 37-41.

[63] Sizemore DR, Branstrom AA, Sadoff JC. Attenuated Shigella as a DNA delivery vehicle for DNA-mediated immunization. Science 1995; 270(5234): 299-302.

[64] Bahey-El-Din M, Gahan CG, Griffin BT. Lactococcus lactis as a cell factory for delivery of therapeutic proteins. Curr Gene Ther 2010; 10(1): 34-45.

[65] Castagliuolo I, Beggiao E, Brun P, *et al.* Engineered E. coli delivers therapeutic genes to the colonic mucosa. Gene Ther 2005; 12(13): 1070-8.

[66] Emr BM, Roy S, Kollisch-Singule M, *et al.* Electroporation Mediated Gene Delivery of Na+,K+-ATPase and ENaC Subunits to the Lung Attenuates Acute Respiratory Distress Syndrome in a Two-Hit Porcine Model Shock 2014.

[67] Penuelas I, Mazzolini G, Boan JF, *et al.* Positron emission tomography imaging of adenoviral-mediated transgene expression in liver cancer patients. Gastroenterology 2005; 128(7): 1787-95.

[68] Zhang Y, Chen X, Qiao M, *et al.* Bone morphogenetic protein 2 inhibits the proliferation and growth of human colorectal cancer cells. Oncol Rep 2014; 32(3): 1013-20.

[69] Wesseling JG, Bosma PJ, Krasnykh V, *et al.* Improved gene transfer efficiency to primary and established human pancreatic carcinoma target cells via epidermal growth factor receptor and integrin-targeted adenoviral vectors. Gene Ther 2001; 8(13): 969-76.

[70] Heideman DA, Snijders PJ, Craanen ME, *et al.* Selective gene delivery toward gastric and esophageal adenocarcinoma cells via EpCAM-targeted adenoviral vectors. Cancer Gene Ther 2001; 8(5): 342-51.

[71] Reddy JA, Clapp DW, Low PS. Retargeting of viral vectors to the folate receptor endocytic pathway. J Control Release 2001; 74(1-3): 77-82.

[72] Grunwald GK, Vetter A, Klutz K, *et al.* EGFR-Targeted Adenovirus Dendrimer Coating for Improved Systemic Delivery of the Theranostic NIS Gene. Mol Ther Nucleic Acids 2013; 2: e131.

[73] Su H, Lu R, Chang JC, Kan YW. Tissue-specific expression of herpes simplex virus thymidine kinase gene delivered by adeno-associated virus inhibits the growth of human hepatocellular carci-

[74] noma in athymic mice. Proc Natl Acad Sci USA 1997; 94(25): 13891-6.

[74] Yu D, Chen D, Chiu C, *et al.* Prostate-specific targeting using PSA promoter-based lentiviral vectors. Cancer Gene Ther 2001; 8(9): 628-35.

[75] Furuhata S, Ide H, Miura Y, Yoshida T, Aoki K. Development of a prostate-specific promoter for gene therapy against androgen-independent prostate cancer. Mol Ther 2003; 7(3): 366-74.

[76] Romani de Wit T, de Leeuw HP, Rondaij MG, *et al.* Von Willebrand factor targets IL-8 to Weibel-Palade bodies in an endothelial cell line. Exp Cell Res 2003; 286(1): 67-74.

[77] Jahroudi N, Schmaier A, Srikanth S, *et al.* Von Willebrand factor promoter targets the expression of amyloid beta protein precursor to brain vascular endothelial cells of transgenic mice. J Alzheimers Dis 2003; 5(2): 149-58.

[78] Devireddy LR, Kumar KU, Pater MM, Pater A. Evidence for a mechanism of demyelination by human JC virus: negative transcriptional regulation of RNA and protein levels from myelin basic protein gene by large tumor antigen in human glioblastoma cells. J Med Virol 1996; 49(3): 205-11.

[79] Massuda ES, Dunphy EJ, Redman RA, *et al.* Regulated expression of the diphtheria toxin A chain by a tumor-specific chimeric transcription factor results in selective toxicity for alveolar rhabdomyosarcoma cells. Proc Natl Acad Sci USA 1997; 94(26): 14701-6.

[80] Lanteri M, Ollier L, Giordanengo V, Lefebvre JC. Designing a HER2/neu promoter to drive alpha1,3galactosyltransferase expression for targeted anti-alphaGal antibody-mediated tumor cell killing. Breast Cancer Res 2005; 7(4): R487-94.

[81] Haviv YS, Curiel DT. Conditional gene targeting for cancer gene therapy. Adv Drug Deliv Rev 2001; 53(2): 135-54.

[82] Dachs GU, Dougherty GJ, Stratford IJ, Chaplin DJ. Targeting gene therapy to cancer: a review. Oncol Res 1997; 9(6-7): 313-25.

[83] Kammertoens T, Gelbmann W, Karle P, *et al.* Combined chemotherapy of murine mammary tumors by local activation of the prodrugs ifosfamide and 5-fluorocytosine. Cancer Gene Ther 2000; 7(4): 629-36.

[84] Rogulski KR, Wing MS, Paielli DL, *et al.* Double suicide gene therapy augments the antitumor activity of a replication-competent lytic adenovirus through enhanced cytotoxicity and radiosensitization. Hum Gene Ther 2000; 11(1): 67-76.

[85] Blanche F, Cameron, B., Couder, M., and Crouzet, J, inventorEnzymes Combinations for destroying Proliferative Cells,1997.

[86] Chen L, Yu LJ, Waxman DJ. Potentiation of cytochrome P450/cyclophosphamide-based cancer gene therapy by coexpression of the P450 reductase gene. Cancer Res 1997; 57(21): 4830-7.

[87] Yaghoubi SSGaSS. Molecular Imaging With Reporter Genes: Cambridge University Press; 2010. 321 p.

[88] Massoud TF, Gambhir SS. Molecular imaging in living subjects: seeing fundamental biological processes in a new light. Genes Dev 2003; 17(5): 545-80.

[89] Wild K, Bohner T, Folkers G, Schulz GE. The structures of thymidine kinase from herpes simplex virus type 1 in complex with substrates and a substrate analogue. Protein Sci 1997; 6(10): 2097-106.

[90] Yaghoubi SS, Gambhir SS. PET imaging of herpes simplex virus type 1 thymidine kinase (HSV1-tk) or mutant HSV1-sr39tk reporter gene expression in mice and humans using [18F]FHBG. Nat Protoc 2006; 1(6): 3069-75.

[91] Likar Y, Dobrenkov K, Olszewska M, *et al.* A new acycloguanosine-specific supermutant of herpes simplex virus type 1 thymidine kinase suitable for PET imaging and suicide gene therapy for potential use in patients treated with pyrimidine-based cytotoxic drugs. J Nucl Med 2008; 49(5): 713-20.

[92] Ponomarev V, Doubrovin M, Shavrin A, *et al.* A human-derived reporter gene for noninvasive imaging in humans: mitochondrial thymidine kinase type 2. J Nucl Med 2007; 48(5): 819-26.

[93] Yaghoubi SS, Campbell DO, Radu CG, Czernin J. Positron emission tomography reporter genes and reporter probes: gene and cell therapy applications. Theranostics 2012; 2(4): 374-91.

[94] Gambhir SS, Barrio JR, Herschman HR, Phelps ME. Assays for noninvasive imaging of reporter gene expression. Nucl Med Biol 1999; 26(5): 481-90.

[95] Ahn BC. Sodium iodide symporter for nuclear molecular imaging and gene therapy: from bedside to bench and back. Theranostics 2012; 2(4): 392-402.

[96] Giammarile F, Chiti A, Lassmann M, Brans B, Flux G. EANM procedure guidelines for 131I-meta-iodobenzylguanidine (131I-mIBG) therapy. Eur J Nucl Med Mol Imaging 2008; 35(5): 1039-47.

[97] Lee SW, Lee SH, Biswal S. Magnetic resonance reporter gene imaging. Theranostics 2012; 2(4): 403-12.

[98] Kang JH, Chung JK. Molecular-genetic imaging based on reporter gene expression. J Nucl Med 2008; 49 Suppl 2: 164S-79S.

[99] Lubgan D, Jozwiak Z, Grabenbauer GG, Distel LV. Doxorubicin-transferrin conjugate selectively overcomes multidrug resistance in leukaemia cells. Cell Mol Biol Lett 2009; 14(1): 113-27.

[100] Kushi LH, Doyle C, McCullough M, et al. American Cancer Society Guidelines on nutrition and physical activity for cancer prevention: reducing the risk of cancer with healthy food choices and physical activity. CA Cancer J Clin 2012; 62(1): 30-67.

[101] Hanahan D, Weinberg RA. The hallmarks of cancer. Cell 2000; 100(1): 57-70.

[102] Moolten FL. Tumor chemosensitivity conferred by inserted herpes thymidine kinase genes: paradigm for a prospective cancer control strategy. Cancer Res 1986; 46(10): 5276-81.

[103] Toossi MT, Mohebbi S, Samani RK, Soleymanifard S. MRC5 and QU-DB bystander cells can produce bystander factors and induce radiation bystander effect. J Med Phys 2014; 39(3): 192-6.

[104] Moolten FL, Wells JM, Heyman RA, Evans RM. Lymphoma regression induced by ganciclovir in mice bearing a herpes thymidine kinase transgene. Hum Gene Ther 1990; 1(2): 125-34.

[105] Miletic H, Fischer YH, Giroglou T, et al. Normal brain cells contribute to the bystander effect in suicide gene therapy of malignant glioma. Clin Cancer Res 2007; 13(22 Pt 1): 6761-8.

[106] Blumenthal M, Skelton D, Pepper KA, et al. Effective suicide gene therapy for leukemia in a model of insertional oncogenesis in mice. Mol Ther 2007; 15(1): 183-92.

[107] Maatta AM, Tenhunen A, Pasanen T, et al. Non-small cell lung cancer as a target disease for herpes simplex type 1 thymidine kinase-ganciclovir gene therapy. Int J Oncol 2004; 24(4): 943-9.

[108] Yarovoi SV, Mouawad R, Colbere-Garapin F, et al. In vitro sensitization of the B16 murine melanoma cells to ganciclovir by different RNA and plasmid DNA constructions encoding HSVtk. Gene Ther 1996; 3(10): 913-8.

[109] Hayashi K, Lee JB, Maitani Y, et al. The role of a HSV thymidine kinase stimulating substance, scopadulciol, in improving the efficacy of cancer gene therapy. J Gene Med 2006; 8(8): 1056-67.

[110] Fillat C, Carrio M, Cascante A, Sangro B. Suicide gene therapy mediated by the Herpes Simplex virus thymidine kinase gene/Ganciclovir system: fifteen years of application. Curr Gene Ther 2003; 3(1): 13-26.

[111] Maron A, Gustin T, Mottet I, Demeure R, Octave JN. Ganciclovir mediated regression of rat brain tumors expressing the herpes simplex virus thymidine kinase imaged by magnetic resonance. J Neurooncol 1995; 24(3): 259-65.

[112] Pantuck AJ, Matherly J, Zisman A, et al. Optimizing prostate cancer suicide gene therapy using herpes simplex virus thymidine kinase active site variants. Hum Gene Ther 2002; 13(7): 777-89.

[113] Zhang JF, Wei F, Wang HP, et al. Potent anti-tumor activity of telomerase-dependent and HSV-TK armed oncolytic adenovirus for non-small cell lung cancer in vitro and in vivo. J Exp Clin Cancer Res 2010; 29: 52.

[114] Arturi F, Russo D, Giuffrida D, Schlumberger M, Filetti S. Sodium-iodide symporter (NIS) gene expression in lymph-node metastases of papillary thyroid carcinomas. Eur J Endocrinol 2000; 143(5): 623-7.

[115] Wapnir IL, Goris M, Yudd A, et al. The Na+/I- symporter mediates iodide uptake in breast cancer metastases and can be selectively down-regulated in the thyroid. Clin Cancer Res 2004; 10(13): 4294-302.

[116] Rudnicka L, Sinczak A, Szybinski P, Huszno B, Stachura J. Expression of the Na(+)/I(-) symporter in invasive ductal breast cancer. Folia Histochem Cytobiol 2003; 41(1): 37-40.

[117] Tandon A, Shrivastava A, Kumar A, et al. Sodium iodide symporter, estrogen receptor, and progesterone receptor expression in carcinoma breast--an immunohistochemical analysis. Indian J Pathol Microbiol 2011; 54(4): 745-51.

[118] Wapnir IL, van de Rijn M, Nowels K, et al. Immunohistochemical profile of the sodium/iodide symporter in thyroid, breast, and other carcinomas using high density tissue microarrays and conventional sections. J Clin Endocrinol Metab 2003; 88(4): 1880-8.

[119] Lacoste C, Herve J, Bou Nader M, et al. Iodide transporter NIS regulates cancer cell motility and invasiveness by interacting with the Rho guanine nucleotide exchange factor LARG. Cancer Res 2012; 72(21): 5505-15.

[120] Renier C, Vogel H, Offor O, Yao C, Wapnir I. Breast cancer brain metastases express the sodium iodide symporter. J Neurooncol 2010; 96(3): 331-6.

[121] Peyrottes I, Navarro V, Ondo-Mendez A, et al. Immunoanalysis indicates that the sodium iodide symporter is not overexpressed in intracellular compartments in thyroid and breast cancers. Eur J Endocrinol 2009; 160(2): 215-25.

[122] Micali S, Bulotta S, Puppin C, et al. Sodium iodide symporter (NIS) in extrathyroidal malignancies: focus on breast and urological cancer. BMC Cancer 2014; 14: 303.

[123] Li H, Peng KW, Russell SJ. Oncolytic measles virus encoding thyroidal sodium iodide symporter for squamous cell cancer of the head and neck radiovirotherapy. Hum Gene Ther 2012; 23(3): 295-301.

[124] Garcia-Rodriguez L, Abate-Daga D, Rojas A, Gonzalez JR, Fillat C. E-cadherin contributes to the bystander effect of TK/GCV suicide therapy and enhances its antitumoral activity in pancreatic cancer models. Gene Ther 2011; 18(1): 73-81.

[125] Dilber MS, Phelan A, Aints A, et al. Intercellular delivery of thymidine kinase prodrug activating enzyme by the herpes simplex virus protein, VP22. Gene Ther 1999; 6(1): 12-21.

[126] Sekar TV, Foygel K, Willmann JK, Paulmurugan R. Dual-therapeutic reporter genes fusion for enhanced cancer gene therapy and imaging. Gene Ther 2013; 20(5): 529-37.

[127] Davis SL, Nuermberger EL, Um PK, et al. Noninvasive pulmonary [18F]-2-fluoro-deoxy-D-glucose positron emission tomography correlates with bactericidal activity of tuberculosis drug treatment. Antimicrob Agents Chemother 2009; 53(11): 4879-84.

[128] Davis SL, Be NA, Lamichhane G, et al. Bacterial thymidine kinase as a non-invasive imaging reporter for Mycobacterium tuberculosis in live animals. PLoS One 2009; 4(7): e6297.

[129] Bray M, Lawler J, Paragas J, Jahrling PB, Mollura DJ. Molecular imaging of influenza and other emerging respiratory viral infections. J Infect Dis 2011; 203(10): 1348-59.

[130] Ottobrini L, Ciana P, Biserni A, Lucignani G, Maggi A. Molecular imaging: a new way to study molecular processes in vivo. Mol Cell Endocrinol 2006; 246(1-2): 69-75.

[131] Massoud TF, Gambhir SS. Integrating noninvasive molecular imaging into molecular medicine: an evolving paradigm. Trends Mol Med 2007; 13(5): 183-91.

[132] Naylor LH. Reporter gene technology: the future looks bright. Biochem Pharmacol 1999; 58(5): 749-57.

[133] Serganova I PV, Blasberg R,. Radionuclide-based reporter gene imaging: pre-clinical and clinical implementation and application. Nuclear Medicine 2012; 15((suppl C): C20–C36).

[134] Vannucci L, Lai M, Chiuppesi F, Ceccherini-Nelli L, Pistello M. Viral vectors: a look back and ahead on gene transfer technology. New Microbiol 2013; 36(1): 1-22.

[135] Serganova I, Blasberg R. Reporter gene imaging: potential impact on therapy. Nucl Med Biol 2005; 32(7): 763-80.

[136] <Joseph P. Hornak-Encyclopedia of Imaging Science & Technology 2 volume set. Volume 2-Wiley-Interscience (2002).pdf>.

[137] Yaghoubi SS, Barrio JR, Namavari M, et al. Imaging progress of herpes simplex virus type 1 thymidine kinase suicide gene therapy in living subjects with positron emission tomography. Cancer Gene Ther 2005; 12(3): 329-39.

[138] Iyer M, Barrio JR, Namavari M, et al. 8-[18F]Fluoropenciclovir: an improved reporter probe for imaging HSV1-tk reporter gene expression in vivo using PET. J Nucl Med 2001; 42(1): 96-105.

[139] Qin C, Cheng K, Chen K, et al. Tyrosinase as a multifunctional reporter gene for Photoacoustic/MRI/PET triple modality molecular imaging. Sci Rep 2013; 3: 1490.

[140]   Glunde K, Pathak AP, Bhujwalla ZM. Molecular-functional imaging of cancer: to image and imagine. Trends Mol Med 2007; 13(7): 287-97.

[141]   Jacobs A, Voges J, Reszka R, *et al.* Positron-emission tomography of vector-mediated gene expression in gene therapy for gliomas. Lancet 2001; 358(9283): 727-9.

[142]   Sangro B, Mazzolini G, Ruiz M, *et al.* A phase I clinical trial of thymidine kinase-based gene therapy in advanced hepatocellular carcinoma. Cancer Gene Ther 2010; 17(12): 837-43.

[143]   Bergamaschi C, Kulkarni V, Rosati M, *et al.* Intramuscular delivery of heterodimeric IL-15 DNA in macaques produces systemic levels of bioactive cytokine inducing proliferation of NK and T cells. Gene Ther 2014.

[144]   Hou S, Gao Y, Wang Y, *et al.* [Construction and application of plasmid pVAX-HBVE harboring hepatitis B surface antibody targeted interferon and interleukin 12 genes]. Xi Bao Yu Fen Zi Mian Yi Xue Za Zhi 2014; 30(9): 921-4.

[145]   Abdul Halim NS, Fakiruddin KS, Ali SA, Yahaya BH. A comparative study of non-viral gene delivery techniques to human adipose-derived mesenchymal stem cell. Int J Mol Sci 2014; 15(9): 15044-60.

[146]   Garcia PA, Davalos RV, Miklavcic D. A numerical investigation of the electric and thermal cell kill distributions in electroporation-based therapies in tissue. PLoS One 2014; 9(8): e103083.

Molecular Imaging Aided Improvement in Drug Discovery and Development

Smrita Chaudhury, Bhushan Thakur, Subhoshree Chatterjee and Pritha Ray[*]

Advanced Centre for Treatment, Research and Education in Cancer (ACTREC), Tata Memorial Centre, Navi Mumbai, Maharashtra, India

Abstract: The current drug discovery and development platform is rapidly expanding with new classes of pharmaceuticals and novel biological information. The drug discovery and development process relies on the utilization of relevant and robust tools, methods, and models that are predictive of clinical effects in terms of diagnosis, prevention, therapy and prognosis. One of the methods that have gained prominence over the years is Molecular Functional Imaging that optimizes and ensures delivery, measures efficacy and toxicity of the therapeutic agents to the target cell or site in pre-clinical setting. Currently three different imaging modalities that include Radionuclide Imaging (Positron Emission Tomography or PET and Single Photon Emitted Computed Tomography or SPECT), Magnetic Resonance Imaging (MRI) and Optical Imaging (Bioluminescence and Florescence) are being extensively used in preclinical models to assess the pharmacokinetics, functional alteration of target and other sites and efficacy of treatment. These real time monitoring modalities are promoting development of novel and sophisticated molecular technologies to identify modulators of protein-protein interactions, apoptosis, protease actions and various other physiological responses. In parallel, significant paradigm shift is occurring at drug discovery and development landscape through emergence of several drug delivery systems like hydrogels, polymers, liposomes and nanoparticles. These innovative delivery vehicles are the future of modern personalized medicine which is still in experimental phases. Molecular Imaging techniques are again the final validation tools for determining the safety, efficacy and need of further improvement of these delivery vehicles. In this review we discuss the current and evolving state of drug discovery and development aided by functional molecular imaging techniques.

Keywords: Drug delivery and nanoparticle, drug discovery, high throughput screening, molecular functional imaging, protein-protein interaction.

INTRODUCTION

The human body can be subjected to various genetic and biochemical manipulation and infection with numerous pathological agents causing a wide range of aliments and need for therapeutic molecules. The startling observation by Alexander Flemming that *Penicillium rubens* when grown on particular substrate exudes a substance with antibiotic properties named penicillin heralded the era of antibiotic discovery and with time establishment of numerous pharmaceutical companies. The goal to achieve novel therapeutic drugs against diseases is dependent on two aspects namely Discovery and Development. The discovery phase consists of identifying cellular targets (enzymes or receptors specific to the disease), analysing drug-target interaction *in vitro* and *in vivo* analysis in biological models (transgenic animals like mice, rabbit, monkeys) and deciphering the pharmacokinetics and pharmacodynamic of the drugs. While the development phase determines analysing levels of toxicities, safety and efficacy of novel drug molecules through various phases of clinical trials in human volunteers [1].

The whole process of discovery and development of new drugs against specific disease is lengthy and requires significant amount of financial investment [2]. The final selection of candidate drugs depends on selective and specific action on cellular targets, bioavailability and biodistribution, metabolism *in vivo* and pharmacodynamics of drugs. In order to ascertain these aspects numerous small animals that model human diseases are used as host. Advantages of using small animals for evaluating candidate drugs include easy accessibility and maintenance, short phases of reproductive cycles, and feasibility of genetic manipulations. However, often large sets of animals are required in order to achieve the time kinetics of pharmacokinetic and pharmacodynamic data of the drug molecules. This practice does not truly mimic the pharmacological effect of drugs in individual patient. Hence, in order to understand individual response and to prevent sacrificing of large number of animals, Molecular Imaging has found application to image and decipher pharmacokinetics and pharmacodynamics of candidate drugs. Molecular imaging aids in real-time monitoring of drug-target interactions under physiologic conditions replicating clinical condition of the disease in the same animal. It acts as a bridge in extrapolating data between *in vitro* and *in vivo* set-ups and can hasten drug discovery and development [3].

*Address correspondence to this author at the Advanced Centre for Treatment, Research and Education in Cancer (ACTREC), Tata Memorial Centre, Navi Mumbai, Maharashtra, 410210, India; Tel: +91-22-27405119; Fax: +91-22-27495085; E-mail: pray@actrec.gov.in

Non-invasive detection and diagnosis of diseases in living subjects is crucial for the field of medicine. Imaging strategies are broadly classified into Anatomical imaging and Functional imaging. Anatomical imaging expedites visualization of structural aberration in organs and it is facilitated by Computer Tomography (CT) scan (Fig. **1A**, **G**), Magnetic Resonance Imaging (Fig. **1B**, **H**) and Ultrasound Imaging (US) (Fig. **1F**, **K**). While functional imaging involves non-invasive detection of molecular and metabolic factors in the living subject *via* probes which is made possible by radionuclide imaging (Positron Emission Tomography or PET (Fig. **1C**, **I**), Single Photon Emission Computed tomography or SPECT (Fig. **1D**, **J**), Magnetic Resonance Imaging (MRI), optical imaging (bioluminescence imaging (Fig. **1E1**) and fluorescence imaging (Fig. **1E2**) and photoacoustic imaging (Fig. **2**).

Over the past decades a paradigm shift in imaging strategy has occurred with the dawn of Molecular Functional Imaging (MFI). In contrast to traditional imaging techniques that detect either anatomical aberrations or erroneous physiological factors, MFI aims to classify and quantify biological processes at the cellular and subcellular levels in a non-invasive manner in living subjects [4] and aids in characterizing disease progression [4, 5].

Molecular probes are an essential component to successful molecular functional imaging. The structure of these probes are divided into 3 parts i.e., (A) a molecule that recognizes the target of interest, (B) a molecule that provides signal or acts as a signalling agent, (C) and a linker in between these two molecules [6]. An optimal molecular probe must have characteristics that include higher specificity and affinity to target, superior sensitivity, higher stability and signal to noise ratio, low toxicity and production costs. Molecular probes are varied and it may be cytokines, radiolabelled ligands, antibody, aptamers, peptides, and engineered proteins [6, 7].

MFI may be achieved in two ways namely Direct imaging and Indirect imaging. Direct imaging involves molecular probes that can directly act/bind upon indigenous biomolecules (either receptors or intracellular enzymes) and aid in detecting them [8]. The intensity of signal obtained during direct imaging correlates directly to the interaction between target and target-specific-probe [9]. Direct labelling strategy therefore can significantly aid in drug evaluation process. Direct labelling being the most preferred strategy for clinical application is difficult to achieve since it is nearly impossible to develop imaging probes against each and every biomolecules [4]. Examples of direct labelling include enzyme-mediated entrapment of ^{18}F-deoxyglucose (FDG) that directly correlates with presence of cancer cells in various malignancies [10].

Indirect imaging can also aid in facilitating drug development and discovery. Indirect imaging relies on introduction of an exogenous reporter gene either through implanted cells (*ex vivo* labelled) or biological vectors (plasmid, viruses) that upon interacting with a reporter probe would generate signals to be captured by an imaging modality. This reporter gene/reporter probe can aid in monitoring the effects of plausible candidate therapeutic molecules. Expression of reporter genes would mimic either promoter activity when placed downstream of specific promoters or target genes when fused or joined through an IRES (internal ribosomal entry sequence) segment with them [9]. There are various types of reporter genes that include bioluminescence reporter genes (e.g., firefly luciferase, *Renilla* luciferase, Gaussia luciferase, Metridia luciferase), fluorescence reporter genes (e.g., green/red/yellow/blue fluorescent proteins) [11], colorimetric reporter genes (beta-galactosidase), and magnetic resonance reporter genes (e.g., creatine kinase, tyrosinase, ferritin, bacterial iron transporter from *A. Magnetotacticum* called Mag A) [12].

Though drug discovery platform benefits significant improvement through the existing MFI approaches, development of newer strategies to identify intricate relationship between biomolecules is in progress. Efficient delivery of drug molecules at target sites is often impeded by solubility and bioavailability factors and is an important arena of drug discovery research. MFI can significantly aid in validation of these delivery vehicles. In this review we aim to briefly highlight various avant-garde molecular imaging strategies and then discuss the emerging role of MFI in drug development, innovative strategies involved in discovery of drugs and role of nanoparticles in drug delivery.

CURRENTLY USED IMAGING MODALITIES

Molecular functional imaging techniques useful for drug discovery include radionuclide imaging, optical imaging and magnetic resonance imaging (MRI). Molecular functional imaging modalities provide visualization of metabolic factors which aid to identify diseased sites from normal tissues. Radionuclide imaging uses radionuclide labelled molecular probes administered orally or intravenously into the living subject which after localization in specific sites provides cellular and physiological information of the diseased organs. Radionuclide imaging modalities comprise of Single photon emitted computed tomography (SPECT) and Positron emission tomography (PET) that use either gamma-emitting radionuclide (^{99m}Tc, ^{111}In and ^{123}I) or positron- emitting radionuclide (^{18}F, ^{124}I, ^{11}C, ^{64}Cu) tracers. In SPECT, multiple images of single gamma ray emission event is recorded by a rotating camera around the subject which is later reconstructed to form a three dimensional tomographic image. In PET, administration of positron-emitting radionuclide in living subjects undergoes positron emission decay followed by annihilation with a neighbouring electron and generates two high energy (511 kev) gamma rays. The camera simultaneously detects both the gamma rays that move in opposite direction followed by reconstructions of three dimensional tomographic images. SPECT is cost-effective than PET due to readily available radioisotopes with higher shelf-life [13] but a log order less sensitive in detection. Till date six isotopes for SPECT [gallium-67 (^{67}Ga), iodine-123 (^{123}I), iodine-125 (^{125}I), indium-111 (^{111}In), lutetium-177 (^{177}Lu), and technetium-99m (^{99m}Tc)] and four isotopes [copper-64 (^{64}Cu), fluorine-18 (^{18}F), gallium-68 (^{68}Ga), and iodine-124 (^{124}I)] for PET imaging are routinely used in clinic [14].

Magnetic resonance imaging (MRI) is a non-invasive radiological technique that uses magnetic field and radio waves to form images of the organs. MRI images are formed
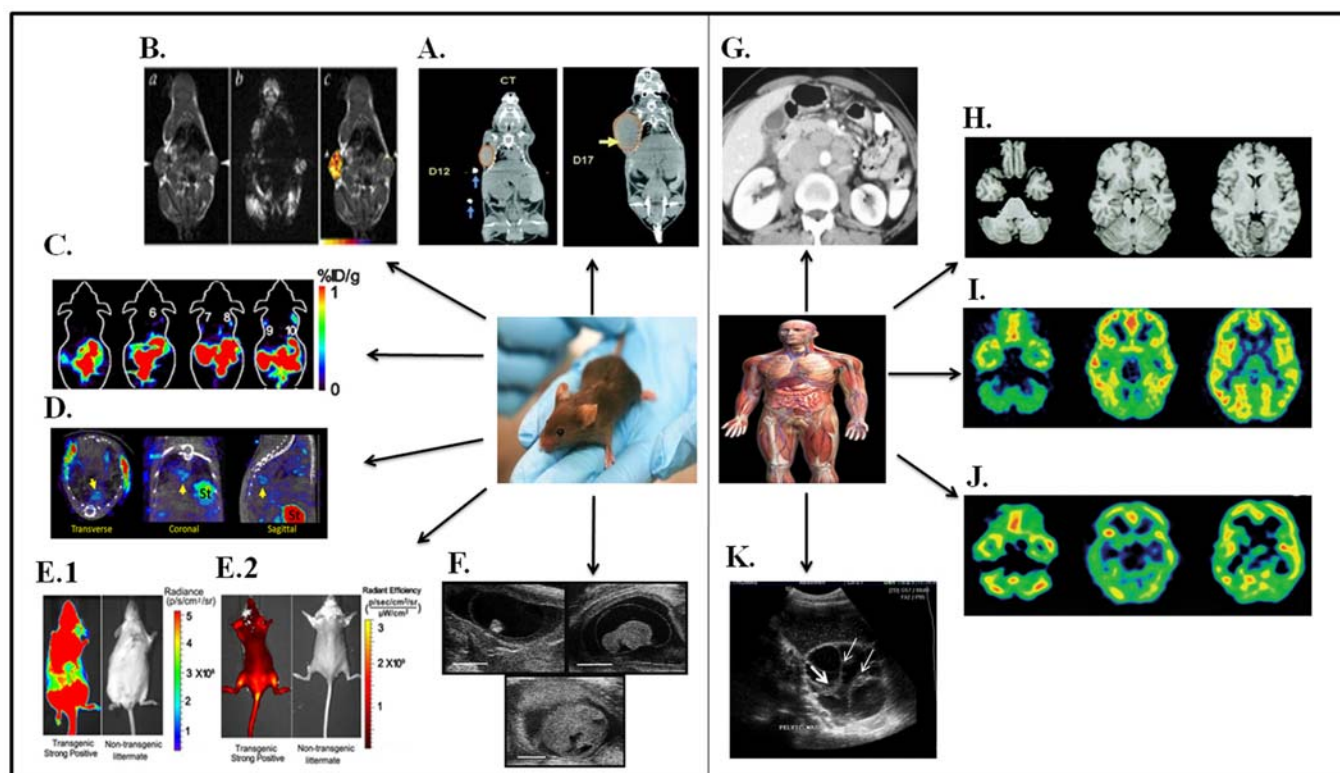
Fig. (1). *In vivo* **Imaging modalities for small animals and human**. **Images A to F and images G to K illustrate examples of the various imaging modalities applicable in small-animal imaging and human imaging respectively**. **A**. **Computer Tomography (CT) imaging:** Evolution of xenograft growth at days 12 and 17 after inoculation of 0.5x10^6 C6 cells in nude mouse as seen on CT. Tumor ROIs are outlined in orange. (Adapted from: Deroose *et al*. (2007) [141]) **B**. **Magnetic Resonance Imaging (MRI):** *In vivo* MR imaging of a single mouse with ETR+ (left arrow heads) and ETR- (right arrowheads) flank tumors. *a*,T1-weighted coronal SE image. ETR- and ETR+ tumors have similar signal intensities. *b*, T2-weighted gradient-echo image corresponding to the image is showing substantial differences between ETR- and ETR+ tumors. As expected, ETR-mediated cellular accumulation of the supramagnetic probe decreases signal intensity. These differences in MR signal intensity were more pronounced using T2 and T2*-weighted imaging pulse sequences, consistent with the increased transverse relaxation rate (R2) after cellular internalization. *c,* Composite image of a T1-weighted spin-echo image obtained for anatomic detail with superimposed R2 changes after Tf-MION administration, as a color map. *,* differences in R2 changes between the ETR+ and ETR- tumours. Scale bar (bottom left) represents 10nm, n=1 (Adapted from: Weisleder *et al*. (2000) [142] with permission.) **C**. **Positron Emission Tomography (PET):** PET imaging of a nude mouse injected with P4 mesenchymal stem cells (MSCs) isolated from the transgenic mice constitutively expressing a tri-fusion (combination of a bioluminescence, a fluorescence and a PET reporter protein) reporter. The mouse was imaged in microPET using FHBG. The PET signal was found in the mouse injected with 2.5x10^5 or more MSCs. (Adapted from: Yan *et al*. (2013) [143]) **D**. **Single-Photon Emission Computed Tomography (SPECT):** SPECT imaging of *Mycobacterium tuberculosis* P$_{hsp60}$TK shows its localization to a tuberculosis (TB) granuloma (arrows) in C3Heb/FeJ mice imaged 8-weeks after infection. (Adapted from: Davis *et al*. (2009)[144]) **E**. **Bioluminescence and Fluorescence Imaging:** E1 and E2: "Tri-Modality Reporter Mouse" system was used to image for bioluminescent (*fluc2*) and fluorescent (tdTomato) reporter expression. Strong bioluminescence and fluorescence signals were found in tri-fusion transgenic mice, but not in non-transgenic littermates. (Adapted from: Yan *et al*. (2013) [143]) **F**. **Ultrasonography:** Stages of embryonic resorption on 36th day before parturition in naked mole rat (*Heterocephalusglaber*) using ultrasound biomicroscopy. (Adapted from: Roellig *et al*. (2011) [145]) **G**. **Computer Tomography (CT) imaging:** Contrast enhanced CT scans in advanced ovarian disease showing multiple enhancing metastatic retroperitoneal nodes in a human patient. (Adapted from: Chaudhury *et al*. (2014) [146]) **H**. **Magnetic Resonance Imaging (MRI):** MRI image of the brain of a normal human at different anatomic levels. (Adapted from: Millet *et al*. (2000) [147] with permission) **I**. **Positron Emission Tomography (PET):** PET image of the brain of the same normal subject at different anatomic levels injected intravenously with 4mCi ^{11}C-Flumazenil (FMZ). (Adapted from: Millet *et al*. (2000) [147] with permission) **J**. **Single-Photon Emission Computed Tomography (SPECT):** SPECT image of the brain of the same normal subject at different anatomic levels injected intravenously with 3 mCi [^{123}I] iomazenil. (Adapted from: Millet *et al*. (2000) [147] with permission) **K**. **Ultrasonography:** Transabdominal ultrasonography showing a multicystic adnexal mass with thickened walls, thick septations (solid arrows) and solid areas in the centre (dotted arrow) in an ovarian cancer patient. (Adapted from: Chaudhury *et al*. (2014) [146]).

as an outcome of alteration in alignment of the hydrogen atoms in the living subject placed in a strong magnetic field that results in release of weak radio waves which is detected and captured by the scanner and recorded on the monitor. Advantages of MRI include non-invasive detection with enhanced spatial and temporal resolution in both smaller animals and in human. However, limitation of MRI includes expensive instrumentation [15].

Optical imaging uses the region of visible to infrared range in the electromagnetic spectrum to obtain images of tissues and is predominantly used in smaller animals. Optical
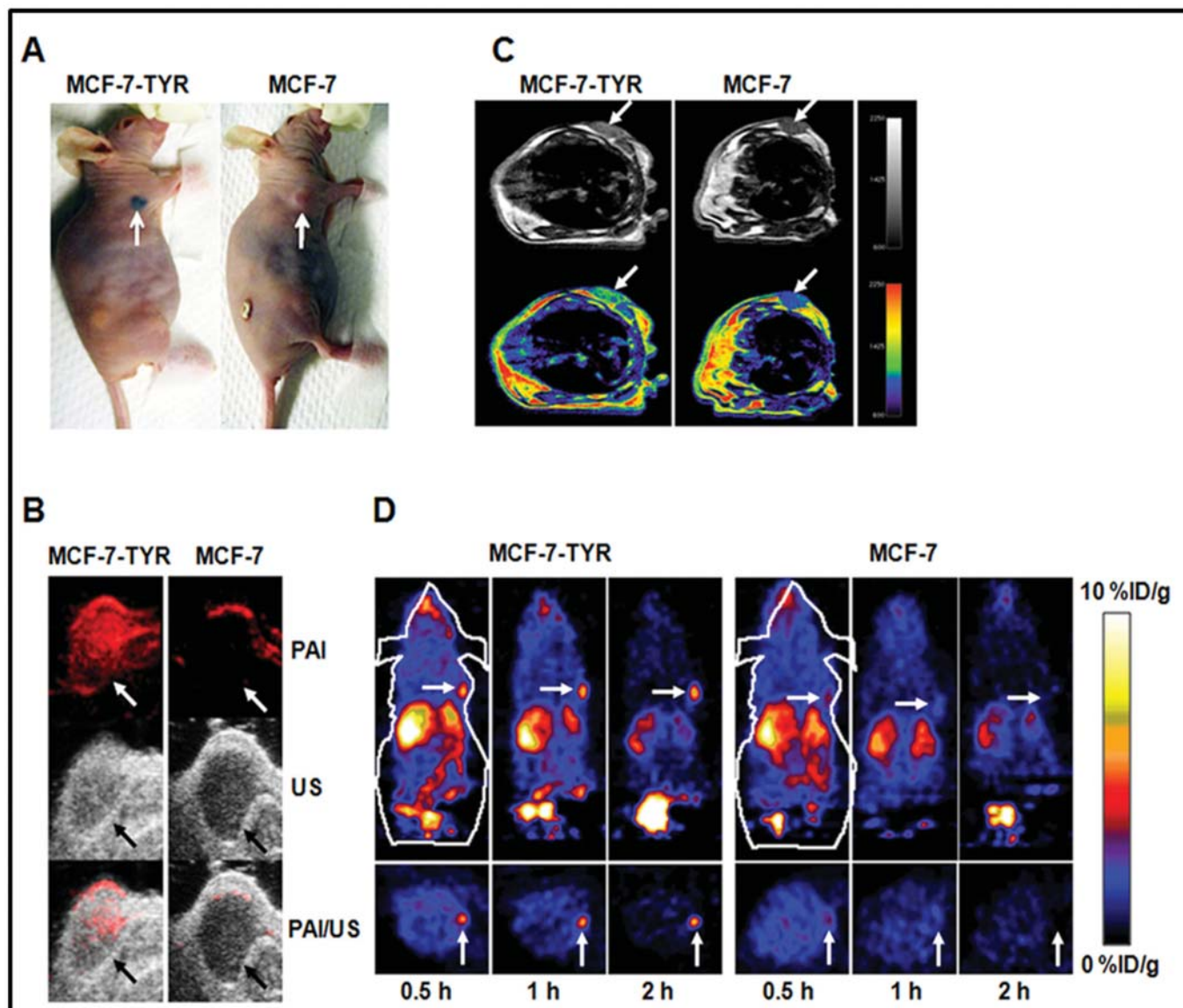
Fig. (2). *In vivo* **multimodality imaging of Tyrosinase (TYR) gene as a multifunctional reporter gene using magnetic resonance imaging (MRI), photoacoustic imaging (PAI), ultrasound (US) and positron emission tomography (PET) from living mice.** Mice bearing MCF-7 (breast cancer cell line) tumor xenografts as control or stably expressing Tyrosinase gene (MCF-7-TYR) were imaged with various imaging modalities. (**A**) Photographic images of tumor bearing mice (left: MCF-7-TYR tumor; right: MCF-7 tumor). (**B**) PAI (top), ultrasound (middle), and PAI/US images (bottom) of the tumor bearing mice (left: MCF-7-TYR; right: MCF-7). (**C**) MRI images of MCF-7-TYR (left) and MCF-7 (right) tumors. Top row shows black and white images, and bottom row shows the pseudo-colored images. (**D**) Representative decay-corrected coronal (top) and transaxial (bottom) small animal PET images of MCF-7-TYR (left three images) and MCF-7 (right three images) tumors acquired at 0.5, 1 and 2 h after tail vein injection of ^{18}F-P3BZA. In all three imaging modalities, MCF-7-TYR tumor shows higher contrast than that of MCF-7 tumor. (Adapted and modified from: Qin *et al.* (2013) [148]).

imaging strategies include bioluminescent imaging (BLI) and fluorescent imaging (FLI). In BLI administered substrate (luciferin or coelenterazine) on interaction with luciferase proteins synthesised in engineered cells emits light. While in FLI specific fluorescing proteins or agents after excitation emit light at particular wavelength. Advantages demonstrated in FLI and BLI include cost effectiveness and semi-quantitative measurement of signal in living subjects however BLI shows higher signal-to-background ratio than FLI [9, 13].

Apart from molecular functional imaging, imaging modalities that provide structure-oriented information are expedited primarily by CT, ultrasound tomography, and MRI. Anatomical scans provide information on size, shape and position of aberration in the organs [16]. Recently apart from obtaining diagnostic information, ultrasonography along with microbubbles is being used to assess efficacy of drug delivery *in vivo*. Microbubbles are tiny microspheres (< 1 millimetre) filled with air or perfluorocarbon. They do not cause immune reaction *in vivo* and on application of

ultrasound waves it is able to oscillate and reflect the ultrasound waves. Thus microbubble has found utility as contrast agents in ultrasonography [17]. Ultrasonography uses non-focused transducers to analyze ultrasound enhanced trans-dermal delivery or sonophoresis of drugs [18] while high intensity focused ultrasound (HIFU) in association with photoacoustic imaging may be used in tumor ablation through targeted delivery of drugs [19]. Amalgamation of MFI with anatomical imaging either using a hybrid scanner (PET/SPECT-CT) or by coregistering images (MRI-PET) produces the ultimate functional information with location.

MOLECULAR IMAGING AND DRUG DISCOVERY

In recent years imaging modalities are not being restricted to diagnosis and monitoring of disease but also incorporated into clinical trials to ascertain early outcome of drug activity. Pharmaceutical companies are undertaking humongous efforts to formulate drugs against numerous diseases. The route taken for a drug to translate from bench-to- bedside is a long drawn process and involves tremendous amount of financial investment. Ideally the process of drug discovery includes identifying specific molecular targets, formulating chemically synthesized products against molecule of interest, assessment of tolerability of the formulations, followed by appraisal of long term safety, side-effects and efficacy of the drugs *via* clinical trials. In recent years imaging modalities has shown tremendous potential to hasten drug discovery by increasing target confidence, characterizing pharmacokinetics and pharmacodynamics of drugs, elucidating effects of the drug on target tissue with emphasis on primary and downstream effects and improving success rates of drug discovery thus achieving therapeutic endpoint [20].

Identification of molecular factors or target molecules *in vivo* is the first step to drug discovery. At this stage it is pertinent to understand whether expression of target molecule is organ-specific or whether it is getting distorted during patho-physiology [21]. Magnetic resonance imaging (MRI) uses MR reporter genes and contrast agents in order to facilitate discovery and development of candidate molecules. Creatine kinase (ck) the first identified MR reporter gene functions by converting ATP to ADP, releases phosphocreatine (PCr) that is detected by phosphorous-31 magnetic resonance spectroscopy (^{31}P MRS). Li *et al.* (2005) used creatine kinase as a reporter gene to scrutinize insertion of low-density lipoprotein receptor (LDLr) gene in mice deficient of LDLr gene that is a model of familial hypercholesterolemia. This study used ^{31}P-MRS to detect presence of phosphocreatine in the liver and demonstrated that ck gene may be useful in determining expression of therapeutic gene like LDLr genes in future [22].

In vivo analysis of drugs through MRI may be enhanced on using iron oxide particles, superparamagnetic iron oxide particles (SPIO) and MR contrast agents such as gadoterate meglumin (Gd-DOTA and Gd-DTPA) [23]. MRI has been used in imaging action of formulated drugs in various diseases including stroke, rheumatoid arthritis, cancer, and cardiovascular diseases. Sauter *et al.* (1988) used MRI to evaluate action of dihydropyridine calcium antagonist isradipine on brain infarcts in spontaneously hypertensive rats (SHR). This study concluded a positive correlation of

use of isradipine with normalising levels of dopamine, noradrenaline and improved neurological scores in spontaneously hypertensive rats [24]. MRI has been used in murine model for human embolic stroke to assess the cytoprotective efficiency of anti-ischemic drugs while in rheumatoid arthritis patients gadolinium-enhanced MRI has been actively used to assess synovitis [23].

In a study by Mueggler *et al.* (2002) had used functional MRI on APP23 transgenic mice that overexpressed human amyloid precursor protein (APP$_{751}$) to study functional status of brain. Through fMRI they were able to identify decreased cerebral hemodynamic on use of GABA$_{A}$ antagonists bicuculline in aged APP23 mice than control population thus emphasizing role of fMRI in characterising disease phenotype in transgenic models [25]. In a randomised placebo controlled study for Metoprolol CR/XL Randomized Intervention Trial in Heart Failure (MERIT-HF), MRI was used to analyse effect of beta-1 blockade on left ventricular (LV) size and function in a cohort of 41 patients suffering from chronic heart failure. Imaging through MRI showed decrease in LV end volume diastolic and systolic index in chronic heart patients. The MERIT-HF trial concludes that beta-1 blocker can aid as an anti-remodelling agent on left ventricular of patients and help decrease mortality [26].

Radiotracer drug imaging PET and SPECT also plays an important role in accelerating drug development. These non-invasive imaging modalities use positron emitting radiotracer to aid in understanding absorption, distribution, metabolism and elimination of drugs along with cytotoxic effect of drug on target. The possibility of monitoring tumor growth and DNA synthesis has propelled numerous investigations on DNA precursors. PET has been used to correlate incorporation of 2-[11C] thymidine into DNA, that in turn provides real time monitoring of DNA proliferation *in vivo* [27]. However, initial studies of using labelled ^{11}C-Thymidine to monitor DNA synthesis through PET fell through due to rapid biodegradation of ^{11}C-Thymidine. In 1957, Dr Charles Heidelberg undertook the task of identifying analogues of thymidine in order to prevent DNA synthesis thus resulted in synthesis of 5-fluorouracil, 5-iododeoxyuridine, 5-bromodeoxyuridine. However, pitfall of these thymidine analogues is swift degradation [28]. 18F labelled glucose (^{18}F-FDG) molecule is considered as a gold standard while evaluating new tracers. ^{18}F-FDG is the most successful and abundant probe to monitor tumor growth and drug efficacy by PET imaging [29]. Apart from these, FMAU (1-(2-deoxy-2-fluoro-D-arabinofurano-syl) thymine) and FBAU (1-(2-deoxy-2-fluoro-D-arabinofuranosyl)-5-bromouracil) labelled with ^{18}F, ^{11}C and ^{76}Br have also been evaluated as tracers for PET imaging [28] and recently ^{18}F-FLT (a 18F labelled thymidine) succeeded as an optimal tracer in PET imaging and is now being used in clinic to monitor proliferating tumor cells. PET imaging has also aided in elucidating pharmacokinetics and pharmacodynamic of fluorouracil (5-FU) using ^{18}F radioisotope attributive to easy synthesis of 18F-fluouracil. For instance Eniluracil (an inhibitor of dihydropyrimidine dehydrogenase) has been used to evaluate metabolism of ^{18}F labelled 5-FU through PET. This study showed higher radioactivity of 5-[^{18}F] FU in normal liver than liver metastases in subjects not treated with Eniluracil. In contrast subjects administered with Eniluracil showed decreased 5-[^{18}F] FU radioactivity in normal liver

than those with liver metastases. This study highlights utility of PET imaging in evaluation of pharmacodynamics of ^{18}F-labelled fluorouracil using biomodulator like Eniluracil [29].

Many potential drug targets are evaluated by PET imaging. Cai *et al.* (2006) showed increased uptake of ^{64}Cu-DOTA-VEGF$_{121}$ in human glioblastoma (U87MG) tumors implanted in mice thereby demonstrating affinity of it to VEGF receptors [30]. Kamath *et al.* (2012) used PET to evaluate kinetics of human recombinant IgG1 antibody targeted against oxidized Low Density Lipoprotein (anti-oxLDL) and distribution of anti-oxLDL in tissues on cynomolgus monkey. This study demonstrated predominant distribution of ^{64}Cu-anti-oxLDL complex conjugated to DOTA in blood pool in heart, trunk and limbs with faint signal from liver, spleen, and kidney and clearance rate of anti-oxLDL (8-17 ml/day/Kg) was found increased over IgG1 antibodies in the subjects [31]. Spencer *et al.* (2010) had designed two different oral delivery systems of methylephenidate (MPH), a commonly used drug to treat attention deficit hyperactivity disorder (ADHD). In brain striatal dopamine transporter (DAT) is the target of MPH hence interaction of DAT with MPH is thought to elucidate pharmacokinetics of MPH. Two formulations i.e., diffucaps bead-delivery system (DBDS-MPH) and osmotically controlled oral release delivery system (OCOR-MPH) with shelf-life for 8 and 12 hours respectively were injected in 21 healthy individuals who were already administered with ^{11}C-Altropane and then assessed by PET imaging before and after administration of oral doses of DBDS-MPH and OCOR-MPH. Despite similar dosing of DBDS-MPH and OROS-MPH formulation, the latter was found at higher concentration in plasma as well as DAT occupancy. This study emphasises on the role of PET imaging in accurately predicting pharmacokinetic profiling of drugs [32].

SPECT imaging has also gained prominence in drug development. Chen *et al.* (2010) have demonstrated use of SPECT imaging to assess bio distribution and pharmacokinetics of ^{188}Re-liposome and ^{188}Re-DXR-liposome compared to ^{188}Re-BMEDA in nude mice bearing xenografts of human HT-29 colorectal carcinoma cells. Both ^{188}Re-liposome and ^{188}Re-DXR-liposome show higher accumulation in tumors than ^{188}Re-BMEDA. Also SPECT images highlighted prolonged circulation and decreased clearance of ^{188}Re-DXR-liposome in blood [33]. Cheng *et al.* (2012) have used SPECT to demonstrate affinity of [(99m)Tc]BAT-Bp-2 in identifying beta-amyloid plaques in Tg2576 transgenic mice. This study demonstrates [(99m)Tc]BAT-Bp-2 as a prospective SPECT probe to recognize beta-amyloid plaques that may be helpful in early diagnosis of Alzheimer's disease in future [34]. Imaging of lymph nodes noninvasively is also gaining prominence by lymphoscintigraphy that aids in evaluating lymph drainage on injection of macromolecules attached to gamma-emitting radionuclide or colloidal particles into tissue. Agents such as ^{99m}Tc-sulphur-colloidal, ^{99m}Tc-dextran, ^{99m}Tc-dextran-acetate have been used in numerous studies to elucidate transport of drug delivery and biodistribution in small animals [35].

Optical imaging modalities that include BLI and FLI are being used to assess drug delivery in animals that model human disease conditions. Fluorescent labelled probes can be tagged to specific drugs which then may be monitored in real time throughout the animal in a continuous and non-invasive manner. Jin *et al.* (2007) subcutaneously transplanted human embryonic kidney cells HEK293($\alpha_v\beta$3) and HEK293($\alpha_v\beta$1) in mice and used optical imaging to demonstrate that in comparison to monomeric cRGD analogue, Cy5-RAFT-c(-RGDfK-)4 showed superior uptake and long-lasting circulation of it in mice that modelled HEK293($\alpha_v\beta$3) subcutaneous tumors than mice bearing HEK293($\alpha_v\beta$1) subcutaneous tumors. This study highlights Cy5-RAFT-c(-RGDfK-)4 binds to $\alpha_v\beta_3$ integrin thus increasing plausibility of its use in tumor targeted drug-delivery [36]. Hulper *et al.* (2011) studied localization of anti-TGF-β antibody in mice that were modelled to bear gliomas. These were administered with AF680-labeled 1D11 intravenously and the biodistribution was analysed through fluorescence imaging [37]. Detection of monoclonal antibodies (mAbs) specific to a disease conjugated to fluorescent dyes and imaged by optical imaging is called as photoimmunodetection (PID). This method facilitates real-time and high resolution images of diseased condition *in vivo*. In a study by Cohen *et al.* (2011) used PID to assess biodistribution of mAbs cetuximab and bevacizumab labelled with zirconium-89 (^{89}Zr) and conjugated with varying quantity of IRDye800CW in nude mice bearing A431 and FaDu tumor xenografts respectively. This study demonstrated that 24-72 hours after injection of ^{89}Zr-cetuximab conjugated with two molecules of IRDye800CW dye showed elevated uptake of mAb in liver but decreased uptake in the tumor and enhanced blood clearance. Whereas ^{89}Zr-bevacizumab conjugated to two molecules of IRDye800CW showed impaired biodistribution of mAb; however blood clearance rate, uptake of mAb in liver and tumor in mice with FaDu tumors was similar to mice treated with ^{89}Zr-cetuximab-IRDye800CW. Whereas 24-48 hours postinjection of ^{89}Zr-cetuximab and ^{89}Zr-bevacizumab conjugated with one molecule of IRDye800CW showed no significant alteration of biodistribution in mice with A431 tumors and FaDu tumors respectively [38]. This study concludes that difference in conjugation of molecules of IRdye800CW to mAbs affects the biodistribution *in vivo*. Aforementioned studies demonstrate FLI has substantial role in elucidating pharmacokinetics of fluorescent-labelled molecules *in vivo*. BLI can be used to track cell trafficking, tumor growth, metastases and response to therapy, real-time monitoring of infections and protein-protein interaction that expedites development of novel drugs [11]. Luker *et al.* (2002) have used BLI to monitor titre of luciferase-expressing herpes virus simplex type-I (HSV-I) injected in cornea of mice. This study demonstrated a positive correlation of increase in viral titre with increase in bioluminescence. The same group also used BLI to monitor reduction of HSV-1 corneal infection by treating mice with increased concentrations of nucleoside analogue valacyclovir. Their investigation showed a correlation between decrease in bioluminescence with valacyclovir treatment as compared to vehicle control indicating reduction in viral titre with treatment [39]. Thus, elucidating potential of BLI in monitoring antiviral therapy, facilitating information on drug-target interaction, regulation of doses leading to production of new therapeutic molecules. Zhang *et al.* (2009) showed bioluminescence imaging can aid in screening of ABCG2 inhibitors by a BLI based assay on

HEK293 cells (genetically manipulated to express ABCG2 and fLuc) panned against drugs in Hopkins Drug Library containing Food and Drug Administration (FDA) approved drugs and drugs at phase I clinical trial. This study screened 3273 candidate compounds out of which 219 compounds were attributed as ABCG2 inhibitors such as glafenine, harmonin, gefitinib, and prazosin. This study endorses BLI as a potential tool in screening for novel molecules drug libraries that will propel candidate molecules towards clinical trials [40]. Mezzanotte *et al.* (2014) recently investigated efficacy of plant derived compounds (curcumin, celastrol, resveratrol, sulphoraphane) on NF-kB signalling pathway and apoptosis in MDA-MB-231 breast cancer cell line by developing for the first time a multicolour bioluminescent imaging modality. In this study different bioluminescent reporters were used to monitor several phenomena simultaneously after lentiviral-transduction i.e., cell vitality by click beetle green luciferase (CBG99), NF-kB promoter activity by red mutant of firefly luciferase (PpyRE9) and caspase3 and caspase 7 activation by luciferase pro-substrate Z-DEVD-aminoluciferin *in vitro* and *in vivo*. This study highlights potential of multicolour bioluminescence imaging in elucidating efficacy of drugs on NF-kB promoter activity in a dose-dependent way, as well as monitoring development of tumor and state of apoptotic factors in murine model of human breast cancer [41]. In our lab Gaikward *et al.* (2013) used BLI to elucidate effect of cisplatin on PIK3CA promoter in ovarian cancer cells (PA-1, A2780 and SKOV3) *in vitro* and *in vivo* by constructing a PIK3CA-*fluc-Tdt* sensor. The PIK3CA sensor was comprised of a mutant red fluorescent protein (tdTomato/tdt) fused with a mutant firefly luciferase (fluc2). This study showed cisplatin induced p53 activity and in turn downregulated expression of PIK3CA sensor in PA-1 and A2780 cells, however no such effect was seen in SKOV3 cells (a p53 null cell line). *In vivo* imaging of mice with PA-1, A2780 and SKOV3 tumor xenografts containing PIK3CA sensor demonstrated that cisplatin attenuated activity of PIK3CA sensor in PA-1 and A2780 xenografts with an absence of such effect in SKOV3 xenografts [42]. All these studies elucidate the important role of BLI in screening of novel theranostic molecules.

NOVEL STRATEGIES IN MFI AND DRUG DEVELOPMENT

Advancement in understanding biology of multifactorial diseases acquainted us with novel drugable targets. These drug targets can be enzymes, non-enzyme metabolites, receptors, ion channels, transport proteins, DNA/RNA and ribosome and other types of biomolecules [43]. Majority of the existing drugs target protein-protein interactions (PPI) that take place in normal cellular milieu. In addition, targeting specific proteins involved in various physiological and cellular processes often serve as tools for drug development. Combination of current information of PPI and other biological processes, screening of various chemical libraries followed by identifying probable candidates and their systematic validation in small animals and human clinical trials propelled development of existing drugs. However several limitations of these pre-existing drugs such as severe cytotoxicity and adverse effects on patient health,

differential response in disease subtypes and ineffectiveness in case of drug resistance compels development of new therapeutic molecules. In addition, better understanding of disease biology through high throughput technologies and discovery of new targets propel development of new drugs. Thus increased magnitude of target identification necessitates efficient tools and innovative strategies for high throughput drug development.

Non-conventional target based drug development strategies include mechanism based screening (e.g., enzyme activity modulator), physiology based assays (e.g., osmotically active compound screening) and functional assays (e.g., metabolism modulator screening, antagonist for angiogenesis screening). One such non-conventional approach comprises of reporter gene based strategy that provides essential spatiotemporal resolution in cells and animals to characterize phenotype and elucidate molecular events supporting validation of drug efficacy. Reporter gene/reporter protein (RG/RP) based system has several advantages over conventional approaches like ELISA [44], coimmunoprecipitation [45], gel filtration chromatography [46] which are routinely used for drug discovery. The greatest advantage of RG/RP system is reporting of time dependent functional alteration of biomolecules by drugs in live cells and in living animals. Recent development of novel strategies to identify disruption in nuclear PPI, cytoplasmic PPI, apoptotic pathway, promoter activity by candidate drug molecules using non-invasive reporters permits more robust and sophisticated drug development which are further aided by preclinical imaging in small animals. A comprehensive detail of these reporter gene based high throughput drug screening strategies is mentioned in Table **1** with some important ones discussed in detail in next few sections.

Yeast Two Hybrid System

Yeast two hybrid technique (Y2H) to measure the physical interaction between two proteins was first described by Fields and Song in 1989 in yeast and was developed following the principle of eukaryotic transcriptional initiation mechanism [47]. Interaction between two target proteins (prey and bait) expressed as fusion partners with a DNA binding domain (BD) and an activation domain (AD) of a transcription factor results in activation of a reporter gene brought by the binding of BD and AD onto an upstream activating sequence (UAS) driving the reporter. Field and Song demonstrated the interaction between AMP-activated serine/threonine protein kinase (SNF1) and activating gamma subunit of the AMP-activated Snf1p kinase (SNF4) using Gal4/UAS Y2H system through blue coloration of yeast colonies due to expression of β-galactosidase reporter. This original Y2H assay was subsequently modified into various types of two hybrid assays like forward assay [48-50], reverse assay [51-54] and forward duplex [55] assay to accommodate different biological responses.

Yeast Three Hybrid Assay

Yeast three hybrid assay, as the name suggests attempt to identify modulators for interaction of three protein partners. Y3H, a variation of classical Y2H system, was first described by Licitra and colleagues (1996) for identification of FKBP12 as a target for FK506 [56]. In this assay,

Table 1.   Novel molecular functional imaging strategies used for monitoring protein-protein interaction and drug development.

Strategy	Principle	Applications	Ref.
Yeast two hybrid (Y2H)	Reporter expression as a result of interaction between a DNA binding domain and a transcription activator domain of a transcription factor	Inhibitors of interaction between Myc/max, Ras-MAPK, inhibitors of G-protein signaling, modulators of neurotransmitter release/ stroke, traumas, potassium transporter and sodium transporter etc.	[47]
Forward Y2H	A modified Y2H strategy where interaction results in cell viability		[48-50]
Reverse Y2H	A modified Y2H strategy where interaction results into cell growth inhibition		[51-54]
Forward duplex Y2H	A modified Y2H strategy where second forward Y2H assay used as a control to reduce off target effect or toxicity along with target interactor Y2H system.		[55]
Yeast three hybrid	Interaction of DNA binding domain and activation domain occurs only in presence of an intermediate molecule thus recognizing interaction between three proteins	Identification of Purvalanol B as an inhibitor for casein kinase, ERK1 and ERK2, (R)-Roscovitine as an inhibitor for CDK 1, 2 and 5. Indenopyrazoles as an inhibitor for CDK 1, 2 and 4.	[56-59]
Membrane yeast two hybrid	Interaction of proteins localized in membrane results in reporter activation	Identified three new interactors for epidermal growth factor (ErbB3), Screening of modulators of GPCRs	[60, 61]
Cytoplasmic yeast two hybrid	Interaction between two cytoplasmic protein results in reporter activation	Identified interacting partners for uncharacterized yeast protein Uri1p, identification of interacting partners for untraceable non-segmented negative strand RNA viral proteins.	[62, 63]
Protein complementation assay/ Split reporter assay	Complementation of two inactive halves in a functional reporter protein brought by interaction of two proteins	Identification of inhibitors for TCF7/β-catenin interaction.	[75, 79, 80]
Split tobacco etch virus (TEV) proteases	Proteolytic activation of reporter by the complementation of split TEV proteases	Monitoring receptor activation such as G-protein activation, Erb2/Erb4 receptor heterodimerization induced by neuregulin.	[149]
Tango assay	Receptor cleavage from receptor due to TEV protease recruitment	Monitoring activation of GPCRs, receptor tyrosine kinases and steroid hormone receptors	[150]
Mammalian protein-protein interaction trap (MAPPIT)	STAT transcription factor based system in which PPI results into activation of reporter due to STAT transcription activity.	Identification of interactors of a phosphotyrosine-binding motif in the erythropoietin receptor.	[151, 152]
Bimolecular fragment complementation assay (BiFC)	Complementation between two halves of a fluorescent protein used as reporter	Identification of inhibitors for HIV-1 nef dimerization,	[153]
Split luciferase reporter	Restored luciferase activity due to complementation of two halves brought by interaction of two proteins	Monitoring estrogen receptor dimerization, identification of inhibitors of c-Myc activation, modulators of Hsp90α/p23 and Hsp90β/p23 interaction, monitoring AKT activation.	[77, 78, 82-84]
Fluorescence resonance energy transfer (FRET)	Resonance energy transfer due to physical interaction of two fluorescent proteins brought by two interacting proteins	Identification of modulators of calmodulin (CaM) and a CaM-binding peptide (M13) interaction, FRET based caspase 3 activity detection assay.	[88-90]
Bioluminescence resonance energy transfer (BRET)	Resonance energy transfer due to physical interaction of a bioluminescence and a fluorescent protein brought by two interacting proteins	Identification of inhibitors of agonist-induced β-arrestin2 recruitment to CCR5.	[91]
Apoptotic sensors (Caspase 3 sensor)	Cleavage at DEVD sequence activates reporter	Screening of anticancer drugs	[96, 97]
Protease sensor (molecular beacons)	Cleavage at protease target sequence separates quencher from fluorophore results in increased signal	Monitoring protease activity, screening of protease inhibitors	[99-101]

simultaneous interaction of three proteins are targeted which is analogous to the interaction between a hook and fish facilitated/modulated by a third bait molecule and a disruption of this interaction help to identify the inhibitor. This assay also potentiates in screening of a genome wide novel protein interactors molecule of small molecule. Using this approach, various inhibitors such as Purvalanol B (against casein kinase, ERK1 and ERK2 interaction) [57]

Indenopyrazoles (against CDK1, CDK2 and CDK4 interaction) [58] were identified. Roscovitine, an inhibitor of cyclin-dependent kinases that has antitumor activity was identified by Y3H approach and currently in phase II clinical trial [59].

Although, Y2H and Y3H systems are powerful techniques and are constantly being used for high throughput drug screening, they suffer certain limitations such as:

a) False positivity upon self-activation of reporter genes

b) Assay system is mainly optimized in lower eukaryotes, hence it may lack contextual specificity

c) Not all proteins show flexibility to construct fusion hybrid protein which will demonstrate proper activation

d) Not all proteins show sufficient affinity to trigger transcription in two/three hybrid conformation

e) Restricted to nucleus and thus not possible to screen for interactions for cytoplasmic proteins

To overcome some of the limitations, certain strategic modification such as replacement of classical transcription activator with various split reporters (enzymes or optical reporters) that will show a much greater flexibility to act as fusion partners and will not demonstrate self-activation and can be used to report cytoplasmic or membrane PPI are being developed.

Membrane Yeast Two Hybrid System (MYTH)

To study interactions of protein partners embedded or localized in plasma membrane, split ubiquitin (in place of classical Gal4) attached to target membrane proteins (pray and bait) was utilized. Membrane embedded target proteins fused with two inactive halves of ubiquitin and one of these halves fused with the transcription factor. Interaction between the two membrane embedded target proteins fused with two inactive halves of ubiquitin produces an active ubiquitin by complementation which then acts as a signal to cleave off the transcription factor. The released transcription factor after localizing to nucleus activates the target reporter gene. This assay was used to screen for new interactors for epidermal growth factor receptor ErbB3 [60] and modulators of G-protein-coupled receptors (GPCRs) [61].

Cytoplasmic Yeast Two Hybrid System (CYTH)

This is a variant of MYTH system where cytoplasmic proteins act as prey and bait. This system has been applied to find new interacting partners of Uri1p, an uncharacterized yeast protein [62]. Moerdyk-Schauwecker *et al.* (2011) used Sos recruiting system (SRS) based CYTH for monitoring interaction between proteins from vesicular stomatitis virus (VSV), a prototypic non-segmented negative strand RNA (NNS) virus. In this system, target cDNA library constructed as a fusion with myristoylation signal (myr), causing its cytoplasmic membrane localization. Interaction between Sos-viral protein and myr-target partner recruits SRS to cytoplasmic membrane consequences into cell growth in CDC25 temperature sensitive strain. They identified SFRS18, a cellular protein as a potential interactor for VSV nucleocaspid protein from a human cDNA library using CYTH system. This system can easily be adopted to monitor interaction of other less tractable NNS viruses with cytoplasmic proteins [63]. Understanding such interaction will help to find probable drug target/s against these untraceable virus infections.

Till today, all the above mentioned strategies are predominantly restricted in lower eukaryotes and thus do not predict an accurate PPI in mammalian cells and small animals. Thus to improve and create more robust drug screening approach, the Y2H system has recently been adapted to mammalian system by use of multiple copies of Gal4-UAS in promoter region and replacing conventional yeast reporters with optical reporters. Li *et al.* (2011) used mammalian two hybrid system to screen a library of 3840 small molecules to identify an inhibitor for p53/MDM2 interaction in HEK293, U2OS, and MDA-MB-435 cell lines. Here they used two luciferases as reporters where firefly luciferase acted as a p53/MDM2 interaction reporter while renilla luciferase as an internal control [64]. Similarly Zhao *et al.* (2004) identified AG1478 as an inhibitor of EGFR/PI3K-p85 interaction using an *in vitro* mammalian two hybrid system [65]. The mammalian two hybrid system has added advantage of implementation of non-invasive *in vivo* imaging strategy that can directly test the drug in small animals. Both bioluminescent (luciferase) and PET reporters (thymidine kinase or TK) as complete or split proteins have been used to monitor the PPI *in vivo*.

To adopt Y2H for *in vivo* studies, DNA binding domain of Gal4 transcription factor from Yeast and activation domain of VP16 from Herpes Simplex Virus 1(HSV1) fused with the interacting partners are introduced in the system along with a reporter gene driven by multiple Gal4 binding elements (Gal4-UAS). Interactions between these two chimeric proteins in mammalian cells can bring the Gal4 activation domain and the DNA binding domain together and reconstitute the Gal4 transcription-activation function which in turn binds to Gal4-UAS and activates reporter gene expression. This MYTH system is further modified to be conditionally inducible for studying the kinetics of interaction as well as the interactions between lethal proteins which is otherwise not possible. As a proof of principle, Luker *et al.* (2003) used doxycycline inducible Gal4-BD-p53/VP16-TAg construct to monitor p53/TAg interaction *in vivo via* expression of a green fluorescent protein and a PET reporter thymidine kinase (GFP-TK) dual fusion reporter. The time and doxycycline dose dependent increase in p53/TAg interaction were measured from live cells and living animals by fluorescence microscopy and microPET [66]. Using a similar strategy, Ray *et al.* (2002) studied the TNF α inducible MyoD and ID interaction where they used Gal4-ID and VP16-MyoD fusion proteins both driven by Nf-κB promoter. Interaction between ID-MyoD brought the Gal4-VP16 trans-activating domains in close proximity which in turn activated a firefly luciferase reporter driven by Gal4 binding sites. Using 293T cells expressing all three constructs and implanted in mice, they were able to image the TNFα induced protein-protein interaction for 30 hrs [67]. Thus adaptation of yeast two hybrid strategy to mammalian system and its extension to small animals allow us to measure pharmacokinetics and validation of drug candidates in real time.

Protein Complementation Assay/Split Reporter System

Protein complementation assay (PCA) or Split reporter system is another important strategy for drug screening where two inactive halves of the reporter protein fused to target proteins is utilized. Under proper stimulation, interaction between target protein results into restoration of reporter activity due to complementation. Various types of

reporter proteins have been used to develop split complementation assay which include enzymes (such as adenylate cyclase [68], anthranilateisomerase [69], lactamase [70], dihydroforate reductase [71], galactosidase [72], proteases such as (ubiquitin [73], optical reporters such as fluorescent proteins [74, 75] and luciferases [76-78]. Unlike classical yeast two hybrid system, this system can easily be adopted in mammalian system as the protein-protein interaction takes place in cytoplasmic milieu. Like Y2H, several variants of PCA have been developed which are Split TEV assay, tango assay, Mammalian protein-protein interaction trap (MAPPIT) and Mammalian small molecule protein interaction trap (MASPIT), Bimolecular fragment complementation assay (BiFC) assay.

PCA is applicable for both *in vitro* and *in vivo* drug screening. Hashimoto *et al.* (2009) used monomeric Kusabira-Green fluorescence protein (mKG) based PCA to screen a natural library containing 123,599 compounds to identify inhibitors of TCF7/β-catenin interaction, PAC1/PAC2 interaction, and PAC3 homodimerinteraction [75]. Filonov *et al.* (2013) developed BiFC based on infrared red fluorescent protein (iRFP), since mammalian tissue is most transparent at near-infrared region. As a proof of principle, they monitored FRB and FKBP protein interaction in presence of rapamycin in MTLn3 tumor xenograft using split iRFP system [79]. Massoud *et al.* (2010) developed split Herpes simplex virus type 1 thymidine kinase (HSV1-TK), a PET reporter protein to image modulation in FRB and FKBP12 interaction induced by rapamycin from tumor xenografts, for interaction between hypoxia-inducible factor 1α (Hif1α) and von Hippel-Lindau tumor suppressor, and for estrogen receptor intramolecular protein folding [80].

Split luciferase reporter strategies have been used more extensively for visualization of interaction of various types of proteins and evaluation of several potential therapeutic molecules *in vivo*. Paulmurugan *et al.* (2011) studied dimerization kinetics of estrogen receptor α and β mediated by ER subtype-selective and non-selective ligands, and selective ER modulators (SERM) by bioluminescence imaging [77]. Fan-Minoque *et al.* (2010) developed split firefly luciferase based strategy to assess phosphorylation driven GSK-β and c-Myc interaction which allowed them to monitor the kinetics of activation of c-Myc in normal and malignant cells and tumors (Fig. **3A1**) [78, 81]. Further using this sensor, they conducted a quantitative high throughput screening of 5,000 bioactive compounds and identified nitazoxanide as a potent inhibitor of c-Myc activity (Fig. **3A2**). Finally they could successfully image the inhibition of c-Myc activity by nitazoxanide in breast cancer cell line as well as tumor xenografts bearing nude mice (Figs. **3A3**, **4A**)[82]. Similarly, Chan *et al.* (2012) demonstrated drug dependent modulation in Hsp90α/p23 and Hsp90β/p23 interaction using split renilla luciferase as reporter and screened a small molecule compound library (30,176 compounds) to identify potential inhibitor/s of HSP90, an important chaperone protein. This screening led to identification of *N*-(5-methylisoxazol-3-yl)-2-[4-(thiophen-2-yl)-6-(trifluoromethyl) pyrimidin-2-ylthio]acetamide (CP9) as an inhibitor of Hsp90 whose efficacy was further validated by non-invasive bioluminescence imaging [83]. All

these exemplary studies reflect the rapid development in drug screening and validation processes using unique functional imaging strategies.

Split luciferase strategy was also used to develop phospho-AKT sensor to measure phosphorylation of AKT [84], and caspase sensor [85]. Using both these sensors, Wang *et al.* (2013) simultaneously monitored the modulation of AKT activation and caspase activity induced by therapeutic drugs in two different myeloid (W25) tumor xenografts in same mice [86]. This strategy allowed them to assess efficacy of various drugs to find most effective therapeutic molecule for treating chemoresistant tumors. Bhojani *et al.* (2011) also used this similar strategy in UMSCC-1 (head and neck cancer cells) tumor xenografts to assess combinatorial response of cetuximab and gemcitabine [87]. These studies revealed the potency of non-invasive imaging in determining drug responsiveness.

Though high throughput screening and *in vivo* applicability are two important advantages of protein complementation assay/split reporter based assays, they often suffer from lower sensitivity and less activity due to suboptimal complementation of reporters. To overcome these limitations, a very different and specialized strategy involving fully active reporters and resonance energy transfer (RET) phenomenon has been developed. This RET technology depends upon the close/physical association (<10nm) of a donor and an acceptor protein brought by the interacting partners. Upon appropriate induction (either a substrate or an excitation light), the energy in the form of photons generated from donor molecule can excite the acceptor and the emitted light at a specific wavelength is captured by a sensitive camera. The ratiometric measure of signals emitted by donor protein with signals emitted by acceptor protein determines the strength and physical association of the interacting partners. RET technology is gaining prominence and is divided in two types based on the nature of reporter proteins.

Fluorescent Resonance Energy Transfer (FRET)

In FRET which is based on resonance energy transfer between two fluorescent proteins with overlapping spectra, the emission spectrum of donor fluorescent protein acts as the excitation spectra for acceptor once they come in close proximity. Various FRET pairs were developed for monitoring protein-protein interaction such as eCFP-Venus, eGFP-mCherry, mTfp1-mOrange from live cells. Tian *et al.* (2007) described FRET based caspase specific CFP-DEVD-YFP sensor for screening of anticancer drugs where decrease in FRET ratio indicated activation of caspase 3 and cell death in HeLa cell line [88]. Similarly Honarnejad *et al.* (2013) developed FRET-based calcium imaging tool for high throughput screening of drug molecules against Alzheimer's disease. This sensor is based on calcium dependent interaction between calmodulin (CaM)-CFP fusion and a CaM-binding peptide (M13)-YFP fusion which in presence of calcium generates FRET signal. After screening a library of 20,000 compounds, the authors identified Bepridil and four more compounds as calcium channel antagonist [89, 90].
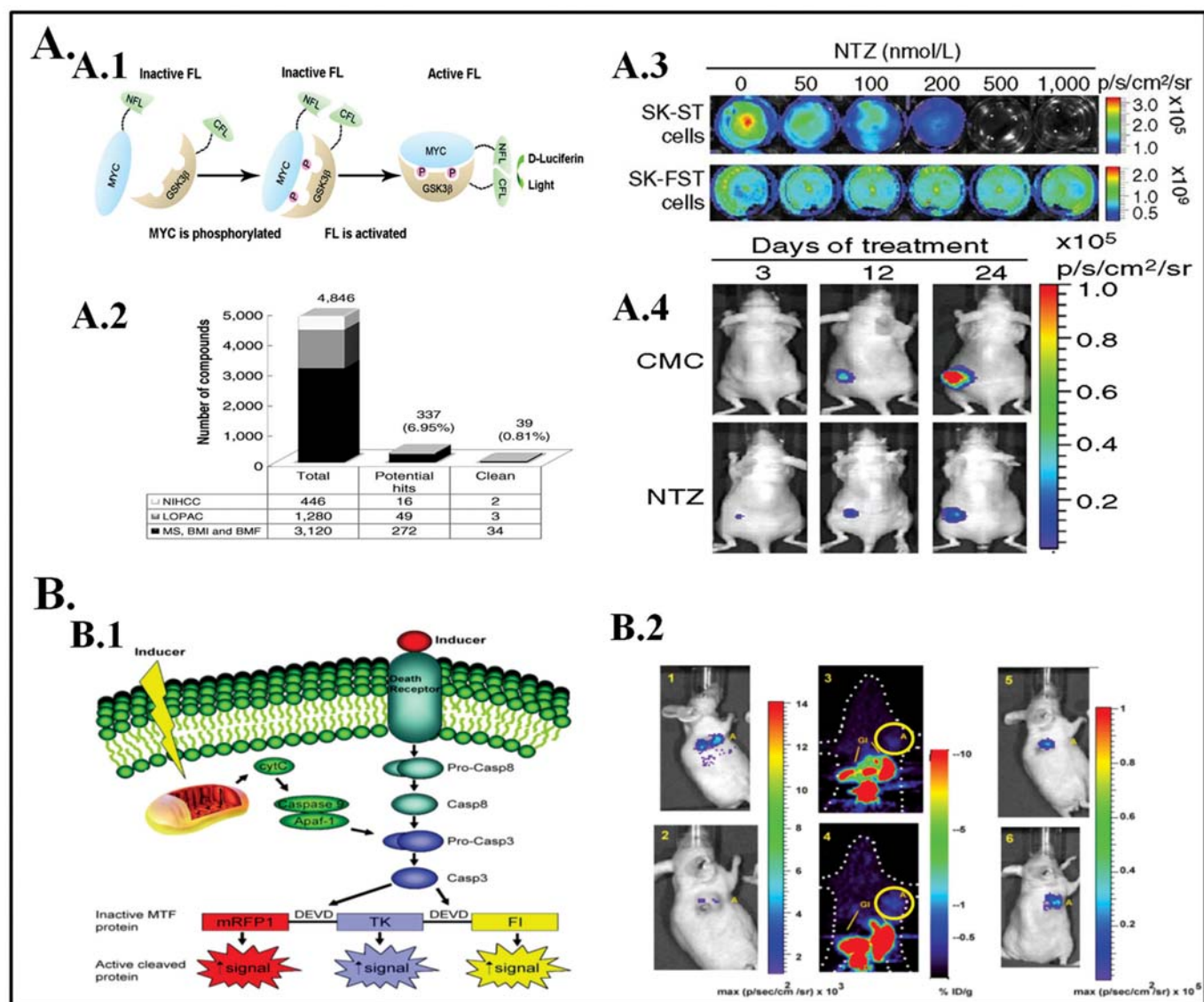
Fig. (3). *In vitro* **and** *in vivo* **validation of drug efficacy using novel non invasive strategies**. **A**. **Validation of a novel c-Myc phosphorylation sensor**. **A**.**1**, Schematic representation of c-Myc phosphorylation sensor. The N and C-termini of split firefly luciferase (FL) were fused to the phospho regulated domain of MYC and the corresponding domain of GSK3β, respectively. Phosphorylation of the MYC peptide results restoration of FL enzyme and its activity. (Adapted from: Cao *et al*. (2011) [81]) **A.2**, Graphical representation of the screening of three libraries comprising 5,000 bioactive compounds for identification of inhibitor/s of c-Myc activation. The contribution of each library to the total screened compounds, the potential hits, and the clean hits are listed in the table. The total number of all libraries in each column is plotted above the table. The percentage of potential hits and clean hits is in the parenthesis. The potential hits are screened compounds that have a minimum of 30% inhibitory effect at 10 μmol/L and the clean hits are those potential hits that are not cytotoxic or luciferase inhibitors. **A.3**, Efficacy of nitazoxanide (NTZ), a candidate drug obtained from above mentioned screening in cell culture. SK-ST (c-Myc phospho sensor) and SK-FST (control luciferase expressing cell line) stable cells were treated with nitazoxanide at indicated concentrations and subjected to bioluminescence imaging. **A.4**, Efficacy of nitazoxanide (NTZ) in a breast cancer xenograft mouse model. SK-ST stable cells were subcutaneously implanted and treated with CMC (control) or nitazoxanide (treated). Decrease in luciferase activity due to NTZ represents decrease in c-Myc activation in tumor xenografts. (A2-4 partly adapted from: Fan-Minogue *et al*. (2013) [82]) **B**. **A novel multimodality caspase sensor**. **B**.**1**, Schematic representation of caspase-3–mediated cleavage of the multimodal fusion protein resulting increased reporter activities. **B.2**, Bioluminescence and microPET imaging of a living mouse implanted with *B16F10-mtf-hrl* tumors before and 24 h after the intratumoral injection of staurosporine, a protein kinase C inhibitor. Upper panel represents control group while lower panel represents staurosporine treated group. Left side bioluminescence images represent RL activity corresponds to cell viability, while middle microPET images represent TK activity using [18F]FHBG and right side bioluminescence represent FL activity corresponds to caspase activation. Increased intensity of signal from TK (yellow circles) and FL activity represents caspase activation in tumor xenografts due to staurosporine treatment. (Adopted from: Ray *et al.* (2008) [97]).

Unfortunately FRET is exclusively limited to cell based screening and has failed to be adapted to *in vivo* imaging due to auto fluorescence by biomolecules that creates significant noise in measurement. To overcome this limitation, another resonance energy transfer approach has recently been developed to study PPI *in vivo.*

Bioluminescence Resonance Energy Transfer (BRET)

In BRET strategy, a bioluminescent reporter (luciferase) is used as donor molecule while a fluorescent protein serves as an acceptor molecule. Upon induction of PPI and administration of luciferase substrate (D-luciferin or coelenterazine), luciferase emits the light from where energy at appropriate wavelength excites the acceptor florescence protein partner. Reduced signal to noise ratio and almost no background interference allows BRET to be successfully adapted from cellular imaging to small animal imaging. Like FRET, BRET is applicable for *in vitro* cellular assays as shown by Hamdan *et al.* (2005) who used BRET 1- β-arrestin2 translocation HTS assay to screen a library of 26,000 compounds and found 12 potent inhibitors of agonist-induced β-arrestin2 recruitment to CCR5 in HEK293 cell line [91]. Later De *et al.* (2005), for the first time demonstrated application of BRET to image and monitor kinetics of protein-protein interaction non-invasively in mouse model [92]. The BRET technology has seen significant improvement in terms of signal generation and BRET ratio by introducing mutant luciferases (Rluc 8 and Rluc 8.6) mutant red fluorescent proteins and alternate substrates [93] in the system. Dragulescu-Andrasi *et al.* (2011) used variants of renilla luciferase (Rluc 8 and 8.6) as donor and red fluorescent proteins (TagRFP and TurboFP635) as acceptor molecules to study *in vivo*

modulation of FKBP12 (FK506 binding protein 12- a rapamycin induced protein) with FRB (FKBP12 rapamycin binding domain) interaction by rapamycin [94].

Current approach for drug development focused on developing magic bullet against multifactorial diseases i.e. therapeutic molecule with multiple specific targets. For identification of such drugs, modulations in either specific pathways or overall changes in cellular physiology such as cell death, angiogenesis, receptor modulation, neurotransmission are considered as criteria for screening rather than investigating changes in specific PPI. Various smart probes developed for accessing these pathways or physiological effects are as follows:

Apoptosis

Dysregulation of programmed cell death (PCD) is a characteristic feature of many disorders including cancer, stroke etc. and modulators of these PCD had proven to be effective therapeutics for these diseases. Various strategies such as measuring ATP consumption, autophagic flux and quantification, caspase activation, tetrazolium salt (MTT, XTT, MTS, WST) conversion by mitochondrial oxidoreductase enzymes are used for high throughput screening of drugs involved in cellular death [95]. Few of such apoptotic sensors have been translated to small animal studies which can be used to evaluate drug efficacy and pharmacokinetics. Two such reports using similar strategy but different protein candidates are described by Laxman *et al.* (2002) and Ray *et al.* (2008) for monitoring *in vivo* caspase activation. Laxman *et al.* (2002) described hybrid luciferase reporter containing estrogen receptor regulatory domain (ER) fused with firefly luciferase through a small caspase 3 clevage specific amino acid (DEVD) linker. In this
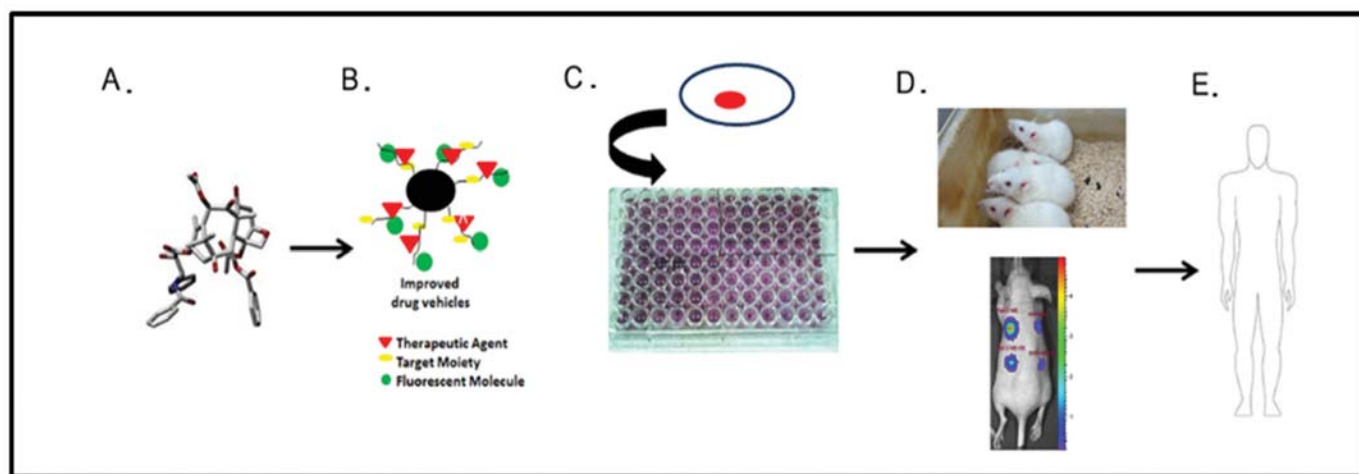
Fig. (4). Development of carrier molecules to favour efficient drug delivery: A. Schematic structure of a pure drug molecule which often exhibits poor bioavailability, low retention, and non-specific targeting. **B**. Encapsulation of nanosized vehicles with drug cargo, labelled with target moiety and fluorescent probes or radionucleotides enhance target specificity, drug efficacy and allow controlled drug release over a period of time. **C**. Schematic diagram of *in vitro* testing of vehicle conjugated drugs using mammalian cells. Cells seeded in 96 well plate are treated with drugs for various concentrations and different time points. Finally, the endpoint result is measured by cell viability assays. **D**. The lead compounds derived from *in vitro* testing are subjected to pre-clinical validation on small animal models. Optical imaging, one of the most preferred techniques is used to determine bioavailability and pattern of drug accumulation in various organs of the animal body. (Adapted from Gaikwad *et al.* (2013) [42]) **E**. Finally, clinical studies are performed on human subjects so that the drug could be made available for end users.

construct, activated caspase 3 cleaves off the reporter at DEVD sequence and releases an active luciferase protein from the ER-luciferase fusion protein. Thus activation of caspase 3 results in increased luciferase activity that can be measured by bioluminescence imaging [96]. Ray *et al.* (2008) similarly developed a multimodality caspase sensor comprising of a fluorescence reporter (mRFP), a luminescence reporter (firefly luciferase) and a PET reporter (thymidine kinase) protein linked through the caspase 3 target sequence DEVD (mRFP-DEVD-TK-DEVD-Fluc). Caspase 3 activation due to induced apoptosis separates all the three reporters from fusion background thus resulting in increased reporter activities which can be measured using three different imaging modalities from the same subject (Fig. **3B**) [97]. These caspase sensors are powerful vectors to identify molecules capable of inducing apoptosis in live cells as well as in small animals.

Protease Imaging

Elevated extracellular protease activity play crucial role in various diseases such as cancer, arthritis, atherosclerosis and myocardial infarction [98]. Classically modulators of these protease activity screened with gene expression analysis, zymography, immunochemical assays, and hydrogel degradation assay which are time consuming and laborious. To overcome these hindrances and to speed up the screening process variety of probes known as "molecular beacons" are developed. Structurally these probes consist of a reporter (fluorophore) and a signal masking agent (quencher molecule) linked through a protease target sequence. Increased signal due to cleavage of the probe indicates presence of an active protease. Various probes suitable for different imaging modalities have been developed for monitoring protease activity such as poly-L-lysin and methoxy-polyethylene glycol (PEG) succinate bound to near-infrared fluorescent (NIFR) fluorophore for fluorescence imaging of cathepsin [99], N-terminus hybrid of MMP-2 cleavage peptide and paramagnetic gadolinium chelate (Gd-DOTA) as contrast agent for MRI imaging of MMP-2[100], CTT MMP-2/9 inhibitory peptide conjugated with DOTA and labeled with ^{64}Cu for PET imaging of MMP expression [101].

In spite of developing novel and clever strategies to screen, validate and real time measurement of pharmacokinetics and efficacy of drug molecules at cellular and organism level, efficient treatment gets hindered by poor delivery of drugs at target sites. Many of the existing drugs are turned out to be poorly biocompatible (hydrophobic in nature), exhibit degradation in blood and therefore reach target site with less efficiency. Thus there is a growing need for developing vehicles that would ensure efficient drug delivery to target sites with minimum hindrance. Significant efforts are going on at research and industrial level for designing novel vehicles. The next section will describe some of those potent vehicles and their application.

STRATEGIES FOR IMPROVED DRUG DELIVERY

Development of smart and unique drug delivery vehicles is a major thrust area for pharmaceutical science. Among many such experimental vehicles, nanomaterials have taken the lead due to several advantages over conventional ones. The recent years have witnessed an unprecedented growth in the field of nanotechnology and nanomedicine as seen in Fig. (**4**). Nanoparticles (NPs) have gained a lot of significance as both therapeutic and diagnostic agents due to properties like lesser toxicity, increased drug efficacy, targeted delivery, formulation stability, controlled release, tunable retention time in plasma and cost of synthesis. Particles loaded with specific contrast agents have made these vehicles compatible to various imaging modalities that can enable a real time monitoring of drug specificity and kinetics.

Briefly, nanoparticle can be defined as small sized particle with an ability to behave as an independent unit with respect to stability and transport. However, the multifunctional feature of nanoparticles of incorporating target moiety, therapeutic drug and contrast agents have made them suitable for therapy and detection of diseases without increasing the burden of the side-effects.

Property of controlled drug release is considered to be one of the key parameters used to evaluate and optimize formulations. The mechanism mostly depends on either endogenous or exogenous stimulus. The former includes stimulus from the microenvironment of the surrounding medium and the latter includes properties like, temperature change, magnetic field, ultrasound and electric field. Feng *et al.* (2013) synthesised a pH responsive mesoporous silica nanoparticles loaded with doxorubicin and demonstrated an accelerated drug release with decrease of pH. A time point based study was performed *in vivo* that illustrated low toxicity and comparatively enhanced retention time of these particles in blood plasma. Meng *et al.* (2010) reported the synthesis of a novel mesoporous silica nanoparticle based on the function of beta-cyclodextrin nanovalves that were also responsive to the acidic conditions [102]. Hydrogels, a product of polymer science are smart molecules that perceive change in stimuli. Absorption of water and simultaneous desorption of drug *via* a swelling controlled mechanism facilitate drug release. Many pH responsive hydrogel networks have been designed such as, pH sensitive hydrogels loaded with a saturated solution of insulin and immobilized with enzymes like glucose oxidase and catalase. Diffusion of glucose into these structures and simultaneous conversion of glucose to gluconic acid by enzymes cause reduction of pH which in turn changes the mesh size of the polymeric network thereby increasing the rate of insulin release. Thus, in the recent years hydrogels have emerged as a promising option as a tool for controlled drug release [103].

NPs are composed of either natural materials of biological origin like phospholipid, lipids, dextran and chitosan or chemicals like polymers, carbon, silica and metals [104]. Based on the particle nature commonly used in drug delivery and imaging, NPs can be broadly classified as follows:

1.   Drug Conjugates

2.   Dendrimer

3.   Vesicle

4.   Micelle

5.   Core Shell Nanoparticle

6.   Microbubble

7.   Carbon Tubes

DRUG CONJUGATES

Drug conjugates, the most widely used class of nanoparticles are composed of protein and polymers and are synthesized by either complexation or covalent conjugations. One of the most remarkable examples of protein conjugated theranostic nanoparticles (TNPs) already in clinical use is Abraxane which is a formulation of paclitaxel reversibly bound to 130-150nm human albumin *via* high pressure homoginization [105]. Paclitaxel is a member of taxane family of microtubule disrupting agents and greatly used as an anticancer agent. Though paclitaxel has numerous clinical advantages but the effect is limited due to solvent based delivery system of polyethoxylated castor oil and ethanol which is not compatible with body fluid. Abraxane was able to receive FDA approval due to its conjugation with human albumin, a natural protein with non-covalent and reversible binding characteristics that facilitates endothelial transcytosis through the formation of transcytotic vesicle referred to as cavadae [105, 106]. In a similar way doxorubicin, another DNA damaging drug was conjugated to NPs which had significantly less toxicity to normal tissues and enhanced retention as compared to the therapeutic agent alone. Moreover, the inherent fluorescence property of doxorubicin may allow optical imaging after coupled with contrast agents [105]. Many clinical studies have been conducted using protein and peptide drug conjugates. Some, of the recent ongoing trials are listed below in Table **2**.

Apart from proteins and peptides, polymers like N-(2-hydroxypropyl)methacrylamide (HPMA) can be used as drug conjugates. The two step process for labelling of HPMA copolymer and their drug conjugates with imaging probes include use of a drug molecule with an intrinsic fluorescence and subsequent linking the drug and contrast agents either by copolymerization or by conjugation [105, 107]. Efficient localization of different drugs and agents in association with HPMA and a target moiety in various cells have been studied. In one of such studies, enhanced cytotoxicity was found in OVCAR-3 cells and tumors treated with Fab fragment as target attached to Mce_6 drug conjugate HPMA copolymer as compared to the Mce_6 conjugate-HPMA copolymer alone [105, 107]. Various imaging modalities like gamma-ray scintigraphy, SPECT, PET, MRI and CT have been used for monitoring HPMA copolymer conjugated drug delivery in preclinical and clinical studies. In one such clinical trial, 36 patients with mean age of 58.3 years were infused with 2-320mg/m^2 of ^{131}I labeled pHPMA-Gly.Phe.Leu.Gly-Doxorubicin conjugate (PK1). Imaging study suggested an efficient uptake of drug by tumor and also no polymer related toxicity. The study was extended to the phase II level with a dose of 280mg/m^2 PK1 administered to patients along with ^{123}I imaging analogue. Imaging of 16 patients showed tumor accumulation of drug [107-109]. Report by Lammers *et al.* (2009) showed the delivery, specificity and cytotoxicity of doxorubicin and gemcitabine were significantly enhanced when conjugated with proteolytic HPMA copolymer [110]. Further, HPMA copolymer and cyclic RGD conjugate was also shown to inhibit $\alpha5\beta3$ mediated adhesion to human umbilical vein endothelial Cells using scintigraphy [111].

However, protein or peptide NPs still suffer from lower drug loading, complexity, reliability and increased production cost. Thus polymeric drug conjugates with improved pharmacokinetics and increased therapeutic index are gaining popularity for drug delivery [105].

DENDRIMERS

Dendrimers are a unique class of nanoparticles considered to be a versatile nanodevice. These are complex structures of 1 to 10nm in diameter with hyperbranched subunits and end groups diverging from the central core [112]. The most common form of dendrimer used in drug delivery is PAMAM which is a poly (amidoamine) spherical dendrimer tagged with ethylene diamine. Folate and FITC labelled PAMAM was successfully imaged in KB cells by confocal microscopy. A time dependant biodistribution study

Table 2.   **Clinical trials with the use of nanoparticles (source: www.clinicaltrials.gov).**

Types of Nanoparticles	Clinical Trials
Drug Conjugate	
Nab-Paclitaxel or Abraxane	NCT01583426, NCT00691054, NCT01336062, NCT00583349, NCT02033538, NCT01463072, NCT01746225
Abraxane in combination with pure drugs	NCT01493310, NCT02041819, NCT01847326, NCT01730833, NCT00934895
Cremophor Free Paclitaxel nanoparticle	NCT00915369
CRLX101	NCT01652079
Metal Nanoparticle	
Silver nanoparticle gel (SilvaSorb)	NCT00659204
Plasmonic Nanoparticles	NCT01270139
Liposomal Drug Delivery	
Anti-EGFR immunoliposomes	NCT01702129, NCT00734682
Microbubbles	
Microbubbles	NCT00837369, NCT01240356, NCT01270139, NCT01949961, NCT01105364, NCT02086331

was performed on immunodeficient mice bearing tumor xenografts administered with either tritiated dendrimer or tritiated dendrimer tagged with folic acid. The clearance rate of non-targeted dendrimer was higher as compared to the targeted. Moreover, confocal images of mouse KB cell tumor harvested 15 hours post injection with the targeted and non-targeted dendrimers demonstrated a significant uptake of folic acid targeted material by the tumor [113]. Choi *et al.* (2010) highlighted the utility of PAMAM as a carrier for doxorubicin to enable photocaging (process which refers to temporary inactivation of a biologically active molecule using protective photocleavable groups) [114]. Shi *et al.* (2011) showed the use of scanning microscopy to image paclitaxel loaded thiol modified telodendrimer micelle [115]. Thus, dendrimers have a great potential as carriers because of their biocompatibility, biodistribution and pharmacokinetics. However, very little pre-clinical data is available to enable us classify dendrimers as 'safe' or 'toxic'.

VESICLES

Vesicles can be classified as liposomal vesicles and polymer based vesicle or polymerosomes [105] Liposomes are made up of phospholipids while, the polymerosomes are mostly composed of polylactic acid (PLA), polyglycolic acid (PGA), polyethelene glycol (PEG), chitosan and polylactic-co-glycolic acid [116]. One of the most prominent examples of vesicle based therapeutic agent currently in clinical use is Doxil, a formulation containing doxorubicin bound to Polyethylene Glycol (PEG) [105, 117]. Hypothermia mediated therapy with temperature sensitive liposome containing doxorubicin has also been reported by Pounc AM *et al.* (2006) [118]. These liposomal formulations are highly stable and hence, can be loaded with quantum dots, radionucleotides or inert gas for being used as imaging probes for different imaging modalities [105]. Among all contrast agents used in MRI, liposomes draw a special attention because of their properties and pharmacological characteristics. They are regularly used as contrast agents when combined with polylysine based polychelating amphilic polymer (PAP), heavy metal like gadolinium and target moiety [119]. Viglianti *et al.* (2004) monitored delivery of $MnSO_4$ and doxorubicin conjugated liposome in tumor xenografts by MRI with precise location of drug unloading and with high spatial and temporal resolution [120].

Polymerosomes are mesoscopic polymer vesicles with a large hydrophilic reservoir and a thick hydrophobic lamellar membrane that have been used extensively to deliver hydrophobic drugs and also to perform imaging [116]. Polymerosomes are considered to be more stable and robust than liposomes. Sanson *et al.* (2009) reported the synthesis of biodegradable polymerosomes composed of Poly (trimethylene carbonate)-b-poly(L-glutamic acid) (PTMC-b-PGA) whose function could be fine-tuned or manipulated with changes in pH and ionic concentration and showed efficient targeted delivery in Ehrlich acsitic tumor bearing mice [112, 121]. Most importantly, these liposomal and polymersomal vesicles are able to hold structurally different therapeutic drug and contrast agents together in the same structure.

MICELLES

Unlike vesicles, micelles are uniform structures which do not have an aqueous core and are composed of a wide range of materials like chitosan, PEG, methacrylic acid, 2-hydroxyethyl methocrylate [105]. These structures composed of a hydrophobic core and the hydrophilic corona are useful for localized drug delivery [112]. Polychelating amphiphilic polymers (PAP) that possess multiple side groups for chelation can be anchored to the micellar surface. Different combinations of chelators and hydrophobic anchors have been tested in the preparation of ^{111}In, ^{99m}Tc and Gd conjugated liposomes. Due to ease of formation and higher stability, these structures are popular for monitoring drug delivery though pre-clinical imaging [105]. Xiao *et al.* (2012) reported enhanced tumor uptake of micelles loaded with doxorubicin in U87MG tumor bearing mice by PET imaging. Similarly another form of micelle loaded with doxorubicin was shown to localize in 4T1 tumor bearing mice by PET imaging [122, 123].

CORE SHELLS

Core shells nanoparticles have properties intermediate between those of small, individual NPs and those of bulky, crystalline semiconductors and mostly include quantum dots, metal and metal oxides and superparamagnetic iron oxide nanoparticles (SPIONS). These nanocrystals are composed of a quantum dot semiconducting core material and a shell of a distinct semiconducting material stabilized by ionic or covalent bonds. Various kinds of drugs, genes and contrast agents can be loaded onto them. The size of fluorescent quantum dots range between 2 to 10nm with a broad absorption and narrow emission spectrum in the visible and the infra-red region. Depending upon the utility quantum dots are modified in a number of ways, for example silica coat on the quantum dots ensure biocompatibility and increased shelf life even at low pH [112]. Gao *et al.* (2004) demonstrated the use of quantum dots conjugated to monoclonal antibody specific to prostate specific membrane antigen to trace prostate cancer cells by confocal fluorescence microscopy. Cai *et al.* (2007) used arginine-glycine-aspartic acid (RGD) peptide-conjugated quantum dots to determine the expression of α5β3 integrins in tumor bearing mice and this study was also able to distinguish the tumor bed from a normal tissue by optical imaging [124-126].

Another class of core shells include SPIONS whose inherent and unique magnetic property make them attractive material for drug delivery based applications using MRI as an imaging modality. SPIONS are often used for thermal therapy as they can convert external electromagnetic field into heat thereby killing the tumor cells. In a phase I clinical trial performed by Johannesen M, *et al.* (2007), ten prostate cancer patients were administered with an intraprostatic injection of nanoparticles and thermal therapy was given for 60 minutes over a weekly interval. A drastic decrease in blood PSA levels were observed in 8 out of 10 patients indicating the effectiveness of the SPION nanoparticle based therapy [112, 127]. Taylor and Sillerud (2012) have shown that introduction of SPIONS mixed with paclitaxel embedded in pegylated fluorescent biotin functionalized

phospholipid could exert significant anti-tumor activity in prostrate tumor xenografts [112, 128]. Other than drug delivery, SPION (such as FDA approved Faraheme) can be used for intravascular imaging as well as treating anaemia [105]. The core shell NPs are often formed with metal bearing core such as gold or silver with unique absorption and scattering features [112]. Cheng *et al.* (2013) demonstrated the benefit of using folic acid coated gold nanoparticle loaded with cytotoxic drug like doxorubicin to overcome multi drug resistance by efficient cellular entry and enhanced toxicity [129]. Gold nanorods can absorb and scatter in near infrared region. Nanorods tagged with anti-epidermal growth factor monoclonal antibody bind to the membrane of malignant cells and emit red light in dark background thereby enabling selection of malignant cells. In a similar way gold nanoparticles tagged with anti-EGFR antibody showed enhanced accumulation in liver cancer cells. These when activated with non-invasive radiofrequency waves generated heat which eventually killed the tumor cells [112, 130-132]. Unfortunately, in spite of so many advantages these metal nanoshells have a compromised rapid clearance rate and impart some toxicity.

MICROBUBBLES

Another powerful vehicle that uses ultrasound mediated drug delivery is microbubbles. These particles are less than 10μm in diameter and have a spherical space filled with a gas and a shell made up of proteins and polymers. The most common gases used in microbubble formation include perflurocarbons such as octofluropropane, decaflurobutane and sulfur hexafluoride. For better visualization in imaging, contrast agents can also be loaded in these microbubbles. Angiogenesis, tumor vasculature and inflammation at the tumor site can be easily treated using microbubbles and ultrasonography. The strategy involves introduction of drug/antibody conjugated microbubbles in circulation followed by a rapid pulse of sound waves resulting in bursting of the bubbles and releasing the drug. Recently, Gao *et al.* (2008) used perfluorocarbon nanodrops stabilized by biodegradable block polymer loaded with doxorubicin to produce microbubble or nanobubble. They infused a dose of these nanobubbles and demonstrated tumor uptake by imaging in murine model [105, 133]. Lukianova-Hleb *et al.* (2010) showed the generation of tunable plasmonic nanobubbles (PNBs) from gold nanoparticles which were used in diagnostics and therapy. PNBs when stimulated by laser probe generate a transient state that would scatter light from laser thereby aiding diagnosis and also produce a therapeutic action by a localized mechanical impact [105, 134]. Thus, like the other forms of nanoparticles, microbubbles and nanobubbles have been also proved extremely versatile in the field of drug delivery and imaging.

CARBON NANOTUBES

Carbon nanotubes based drug delivery holds great promise for cancer therapy. They are cylindrical structures predominantly made of carbon and are broadly classified into two categories namely, single walled carbon nano tubes (SWCNTs) and multi walled carbon nano tubes (MWCNTs). SWCNTs are proven to be superior to MWCNTs due to their

one dimensional structure and efficient drug loading capability [135]. Recent reports showed that amine functionalized SWCNTs conjugated with cisplatin and folic acid through amide linkage outperformed the administration of pure cisplatin in terms of tumor accumulation and efficacy [136]. Bhirde *et al.* (2009) discussed the utility of EGF-cisplatin attached to SWCNTs in targeting head and neck squamous carcinoma cells *in vitro*. They did extensive imaging using qdot fluorescence and confocal microscopy. Two photon intravital video imaging was used for *in vivo* study to show selective uptake of targeted cisplatin loaded SWNTs by the HNSCC derived tumors as compared to the non-targed cisplatin loaded SWNTs [137]. As SWCNTs show strong optical absorbance in the near infrared region, Kam *et al.* (2005) used SWCNTs wrapped with Cy3 labelled oligonucleotides and folate moiety to cause light induced cell death of malignant cells overexpressing folate receptor [138]. However certain degree of toxicity confers limitations to extensive use of these nanotubes. This toxicity issue can be tackled by using alternative approaches like synthesis of fluorescent nanoparticle by carbohydrate carbonization [139].

Application of nanotechnology in medicine has brought momentous advances in the fight against a range of diseases. The versatile nature of NPs, size modulation, surface area, shape, ability to hold drug molecules and targeted moiety, stability, ability to gradually release drugs in circulation have revolutionized the drug delivery system. Two families of therapeutic nanocarriers - liposomes and albumin NPs are already in clinical practice worldwide and many are in the preclinical phases of development. However, the initial excitement with nanomedicine has slowed down after discovering their innate toxicity shown by the naked quantum dots (hemolysis), cationic gold and polysterene NPs (blood clotting), SWCNTs and MWCNTS (ROS generation, lipid peroxidation, oxidative stress, platelet aggregation etc.) that complicated patience compliance. Thus integration of nanomaterials into drug delivery systems still requires a greater understanding of both surface chemistry and interaction chemistry of these NPs with biological systems. Future of nanoparticles in medicine lies in better engineering of their properties specific to biomedical application which can only be achieved through collaborative efforts among scientists in different disciplines. Understanding the risks and benefits of these new particles will thus be essential for successful implementation of new drug delivery technologies and decision making for drug developers [104, 140].

DRUG DISCOVERY: WHAT THE FUTURE HOLDS

In recent years, even after remarkable scientific advancements and a significant increase in pharmaceutical research and development, very few new drugs are reaching markets and many drugs are frequently withdrawn from markets. This is primarily due to their side effects or toxicities, off-target effects, poor biocompatibility and stability and incomplete validation in living subjects. Thus new paradigms for assisting drug discovery system are highly desirable. Presently molecular functional imaging technologies are significantly aiding in improvement in drug discovery and validation process by real time monitoring of efficacy and pharmacokinetics of newly discovered

therapeutic molecules. Application of these technologies are not only limited in validating existing drugs but also extends to advancement of newer strategies for multi-targeting activities, selectivity, overcoming drug resistance, bio availability and assessing physiological responses for new drug candidates. Systemic integration of these data derived from different imaging modalities, from cell based assays to animal experiments produce in depth validation of each molecule in pre-clinical setting. These imaging technologies are also essential part of development of the drug delivery system. Hence future success of next generation therapeutic agents lies in stringent practice of molecular functional imaging techniques as the final validation step.

CONFLICT OF INTEREST

The authors confirm that this article content has no conflict of interest.

ACKNOWLEDGEMENTS

REFERENCES

[1] Lin JH, Lu AY. Role of pharmacokinetics and metabolism in drug discovery and development. Pharmacol Rev 1997; 49(4): 403-49.

[2] Khanna I. Drug discovery in pharmaceutical industry: productivity challenges and trends. Drug discov today 2012; 17(19-20): 1088-102.

[3] Pomper MG, Lee JS. Small animal imaging in drug development. Curr Pharm Des 2005; 11(25): 3247-72.

[4] Massoud TF, Gambhir SS. Integrating noninvasive molecular imaging into molecular medicine: an evolving paradigm. Trends Mol Med 2007; 13(5): 183-91.

[5] Hoffman JM, Gambhir SS. Molecular imaging: the vision and opportunity for radiology in the future. Radiology 2007; 244(1): 39-47.

[6] Weissleder R, Ross BD, Rehemtulla A, Gambhir SS. Molecular Imaging Principles and Practice. 1st ed. People's Medical Publishing House: Shelton 2010.

[7] Hildebrandt IJ, Gambhir SS. Molecular imaging applications for immunology. Clin Immunol 2004; 111(2): 210-24.

[8] Rollo FD. Molecular imaging: an overview and clinical applications. Radiol Manage 2003; 25(3): 28-32.

[9] Youn H, Hong KJ. *In vivo* Noninvasive Small Animal Molecular Imaging. Osong Public Health Res Perspect 2012; 3(1): 48-59.

[10] Kostakoglu L, Agress H, Goldsmith SJ. Clinical role of FDG PET in evaluation of cancer patients. Radiographics 2003; 23(2): 315-40.

[11] Close DM, Xu T, Sayler GS, Ripp S. *In vivo* bioluminescent imaging (BLI): noninvasive visualization and interrogation of biological processes in living animals. Sensors (Basel) 2011; 11(1): 180-206.

[12] Gilad AA, Winnard PT, van Zijl PC, Bulte JW. Developing MR reporter genes: promises and pitfalls. NMR Biomed 2007; 20(3): 275-90.

[13] Gu E, Chen WY, Gu J, Burridge P, Wu JC. Molecular imaging of stem cells: tracking survival, biodistribution, tumorigenicity, and immunogenicity. Theranostics 2012; 2(4): 335-45.

[14] Hoppin J, Orcutt KD, Hesterman JY, *et al*. Assessing antibody pharmacokinetics in mice with *in vivo* imaging. J Pharmacol Exp Ther 2011; 337(2): 350-8.

[15] Gross S, Piwnica-Worms D. Molecular imaging strategies for drug discovery and development. Curr Opin Chem Biol 2006; 10(4): 334-42.

[16] Eckelman WC, Reba RC, Kelloff GJ. Targeted imaging: an important biomarker for understanding disease progression in the era of personalized medicine. Drug discov today 2008; 13(17-18): 748-59.

[17] Dijkmans PA, Juffermans LJ, Musters RJ, *et al*. Microbubbles and ultrasound: from diagnosis to therapy. Eur J Echocardiogr 2004; 5(4): 245-56.

[18] Frenkel V. Ultrasound mediated delivery of drugs and genes to solid tumors. Adv Drug Deliv Rev 2008; 60(10): 1193-208.

[19] Rajian JR, Fabiilli ML, Fowlkes JB, Carson PL, Wang X. Drug delivery monitoring by photoacoustic tomography with an ICG encapsulated double emulsion. Opt Express 2011; 19(15): 14335-47.

[20] Ricketts SA, Hockings PD, Waterton JC. Small Animal Imaging: Basics and Practical Guide. Springer: Germany 2011.

[21] Rudin M. Noninvasive structural, functional, and molecular imaging in drug development. Curr Opin Chem Biol 2009; 13(3): 360-71.

[22] Li Z, Qiao H, Lebherz C, *et al*. Creatine kinase, a magnetic resonance-detectable marker gene for quantification of liver-directed gene transfer. Hum Gene Ther 2005; 16(12): 1429-38.

[23] Beckmann N, Laurent D, Tigani B, Panizzutti R, Rudin M. Magnetic resonance imaging in drug discovery: lessons from disease areas. Drug discovery today 2004; 9(1): 35-42.

[24] Sauter A, Rudin M, Wiederhold KH. Reduction of neural damage in irreversible cerebral ischemia by calcium antagonists. Neurochemical pathology 1988; 9: 211-36.

[25] Mueggler T, Sturchler-Pierrat C, Baumann D, *et al*. Compromised hemodynamic response in amyloid precursor protein transgenic mice. J Neurosci 2002; 22(16): 7218-24.

[26] Groenning BA, Nilsson JC, Sondergaard L, *et al*. Antiremodeling effects on the left ventricle during beta-blockade with metoprolol in the treatment of chronic heart failure. J Am Coll Cardiol 2000; 36(7): 2072-80.

[27] Gupta N, Price PM, Aboagye EO. PET for *in vivo* pharmacokinetic and pharmacodynamic measurements. Eur J Cancer 2002; 38(16): 2094-107.

[28] Shields AF. PET imaging with 18F-FLT and thymidine analogs: promise and pitfalls. J Nucl Med 2003; 44(9): 1432-4.

[29] Saleem A, Aboagye EO, Price PM. *In vivo* monitoring of drugs using radiotracer techniques. Adv Drug Deliv Rev 2000; 41(1): 21-39.

[30] Cai W, Rao J, Gambhir SS, Chen X. How molecular imaging is speeding up antiangiogenic drug development. Mol cancer ther 2006; 5(11): 2624-33.

[31] Kamath AV, Williams SP, Bullens S, *et al*. Pharmacokinetics and biodistribution of a human monoclonal antibody to oxidized LDL in cynomolgus monkey using PET imaging. PLoS One 2012; 7(9): e45116.

[32] Spencer TJ, Bonab AA, Dougherty DD, *et al*. A PET study examining pharmacokinetics and dopamine transporter occupancy of two long-acting formulations of methylphenidate in adults. Int J Mol Med 2010; 25(2): 261-5.

[33] Chen MH, Chang CH, Chang YJ, *et al*. MicroSPECT/CT imaging and pharmacokinetics of 188Re-(DXR)-liposome in human colorectal adenocarcinoma-bearing mice. Anticancer Res 2010; 30(1): 65-72.

[34] Cheng Y, Ono M, Kimura H, Ueda M, Saji H. Technetium-99m labeled pyridyl benzofuran derivatives as single photon emission computed tomography imaging probes for beta-amyloid plaques in Alzheimer's brains. J Med Chem 2012; 55(5): 2279-86.

[35] Zhang F, Niu G, Lu G, Chen X. Preclinical lymphatic imaging. Mol Imaging Biol 2011; 13(4): 599-612.

[36] Jin ZH, Josserand V, Foillard S, *et al*. *In vivo* optical imaging of integrin alphaV-beta3 in mice using multivalent or monovalent cRGD targeting vectors. Mol Cancer 2007; 6: 41.

[37] Hulper P, Schulz-Schaeffer W, Dullin C, *et al*. Tumor localization of an anti-TGF-beta antibody and its effects on gliomas. Int J Oncol 2011; 38(1): 51-9.

[38] Cohen R, Stammes MA, de Roos IH, *et al*. Inert coupling of IRDye800CW to monoclonal antibodies for clinical optical imaging of tumor targets. EJNMMI Res 2011; 1(1): 31.

[39] Luker KE, Luker GD. Applications of bioluminescence imaging to antiviral research and therapy: multiple luciferase enzymes and quantitation. Antiviral Res 2008; 78(3): 179-87.

[40] Zhang Y, Byun Y, Ren YR, *et al*. Identification of inhibitors of ABCG2 by a bioluminescence imaging-based high-throughput assay. Cancer Res 2009; 69(14): 5867-75.

[41] Mezzanotte L, An N, Mol IM, Lowik CW, Kaijzel EL. A new multicolor bioluminescence imaging platform to investigate NF-

kappaB activity and apoptosis in human breast cancer cells. PLoS One. 2014; 9(1): e85550.

[42]   Gaikwad SM, Gunjal L, Junutula AR, *et al*. Non-invasive imaging of phosphoinositide-3-kinase-catalytic-subunit-alpha (PIK3CA) promoter modulation in small animal models. PloS one 2013; 8(2): e55971.

[43]   Imming P, Sinning C, Meyer A. Drugs, their targets and the nature and number of drug targets. Nat Rev Drug Discov 2006; 5(10): 821-34.

[44]   Rediger A, Tarnow P, Bickenbach A, *et al*. Heterodimerization of hypothalamic G-protein-coupled receptors involved in weight regulation. Obes Facts 2009; 2(2): 80-6.

[45]   Selbach M, Mann M. Protein interaction screening by quantitative immunoprecipitation combined with knockdown (QUICK). Nat Methods 2006; 3(12): 981-3.

[46]   Phizicky EM, Fields S. Protein-protein interactions: methods for detection and analysis. Microbiol Rev 1995; 59(1): 94-123.

[47]   Fields S, Song O. A novel genetic system to detect protein-protein interactions. Nature 1989; 340(6230): 245-6.

[48]   Kato-Stankiewicz J, Hakimi I, Zhi G, *et al*. Inhibitors of Ras/Raf-1 interaction identified by two-hybrid screening revert Ras-dependent transformation phenotypes in human cancer cells. Proc Natl Acad Sci 2002; 99(22): 14398-403.

[49]   deCarvalho AC, Ndi CP, Tsopmo A, *et al*. A novel natural product compound enhances cAMP-regulated chloride conductance of cells expressing CFTR[delta]F508. Mol Med 2002; 8(2): 75-87.

[50]   Yin X, Giap C, Lazo JS, Prochownik EV. Low molecular weight inhibitors of Myc-Max interaction and function. Oncogene 2003; 22(40): 6151-9.

[51]   Young K, Lin S, Sun L, *et al*. Identification of a calcium channel modulator using a high throughput yeast two-hybrid screen. Nat Biotechnol 1998; 16(10): 946-50.

[52]   Gunde T, Tanner S, Auf der Maur A, Petrascheck M, Barberis A. Quenching accumulation of toxic galactose-1-phosphate as a system to select disruption of protein-protein interactions *in vivo*. Biotechniques 2004; 37(5): 844-52.

[53]   Lu Q, Peevey J, Jow F, *et al*. Disruption of Kv1.1 N-type inactivation by novel small molecule inhibitors (disinactivators). Bioorg Med Chem 2008; 16(6): 3067-75.

[54]   Bowlby MR, Chanda P, Edris W, *et al*. Identification and characterization of small molecule modulators of KChIP/Kv4 function. Bioorg Med Chem 2005; 13(22): 6112-9.

[55]   Nieuwenhuijsen BW, Huang Y, Wang Y, *et al*. A dual luciferase multiplexed high-throughput screening platform for protein-protein interactions. J Biomol Screen 2003; 8(6): 676-84.

[56]   Licitra EJ, Liu JO. A three-hybrid system for detecting small ligand-protein receptor interactions. Proc Natl Acad Sci 1996; 93(23): 12817-21.

[57]   Knockaert M, Lenormand P, Gray N, *et al*. p42/p44 MAPKs are intracellular targets of the CDK inhibitor purvalanol. Oncogene 2002; 21(42): 6413-24.

[58]   Nugiel DA, Etzkorn AM, Vidwans A, *et al*. Indenopyrazoles as novel cyclin dependent kinase (CDK) inhibitors. J Med Chem 2001; 44(9): 1334-6.

[59]   Fischer PM, Gianella-Borradori A. CDK inhibitors in clinical development for the treatment of cancer. Expert Opin Invest Drugs 2003; 12(6): 955-70.

[60]   Thaminy S, Auerbach D, Arnoldo A, Stagljar I. Identification of novel ErbB3-interacting factors using the split-ubiquitin membrane yeast two-hybrid system. Genome Res 2003; 13(7): 1744-53.

[61]   Suter B, Kittanakom S, Stagljar I. Interactive proteomics: what lies ahead? Biotechniques 2008; 44(5): 681-91.

[62]   Mockli N, Deplazes A, Hassa PO, *et al*. Yeast split-ubiquitin-based cytosolic screening system to detect interactions between transcriptionally active proteins. Biotechniques. 2007; 42(6): 725-30.

[63]   Moerdyk-Schauwecker M, Destephanis D, Hastie E, Grdzelishvili VZ. Detecting protein-protein interactions in vesicular stomatitis virus using a cytoplasmic yeast two hybrid system. J Virol Methods 2011; 173(2): 203-12.

[64]   Li J, Zhang S, Gao L, Chen Y, Xie X. A cell-based high-throughput assay for the screening of small-molecule inhibitors of p53-MDM2 interaction. J Biomol Screen 2011; 16(4): 450-6.

[65]   Zhao HF, Kiyota T, Chowdhury S, *et al*. A mammalian genetic system to screen for small molecules capable of disrupting protein-protein interactions. Anal Chem 2004; 76(10): 2922-7.

[66]   Luker GD, Sharma V, Pica CM, *et al*. Molecular imaging of protein-protein interactions: controlled expression of p53 and large T-antigen fusion proteins *in vivo*. Cancer Res 2003; 63(8): 1780-8.

[67]   Ray P, Pimenta H, Paulmurugan R, *et al*. Noninvasive quantitative imaging of protein-protein interactions in living subjects. Proc Natl Acad Sci 2002; 99(5): 3105-10.

[68]   Karimova G, Pidoux J, Ullmann A, Ladant D. A bacterial two-hybrid system based on a reconstituted signal transduction pathway. Proc Natl Acad Sci 1998; 95(10): 5752-6.

[69]   Tafelmeyer P, Johnsson N, Johnsson K. Transforming a (beta/alpha)8--barrel enzyme into a split-protein sensor through directed evolution. Chem Biol 2004; 11(5): 681-9.

[70]   Galarneau A, Primeau M, Trudeau LE, Michnick SW. Beta-lactamase protein fragment complementation assays as *in vivo* and *in vitro* sensors of protein protein interactions. Nat Biotechnol 2002; 20(6): 619-22.

[71]   Remy I, Michnick SW. Clonal selection and *in vivo* quantitation of protein interactions with protein-fragment complementation assays. Proc Natl Acad Sci 1999; 96(10): 5394-9.

[72]   Rossi F, Charlton CA, Blau HM. Monitoring protein-protein interactions in intact eukaryotic cells by beta-galactosidase complementation. Proc Natl Acad Sci 1997; 94(16): 8405-10.

[73]   Stagljar I, Korostensky C, Johnsson N, te Heesen S. A genetic system based on split-ubiquitin for the analysis of interactions between membrane proteins *in vivo*. Proc Natl Acad Sci 1998; 95(9): 5187-92.

[74]   Chun W, Waldo GS, Johnson GV. Split GFP complementation assay for quantitative measurement of tau aggregation in situ. Methods Mol Biol 2011; 670: 109-23.

[75]   Hashimoto J, Watanabe T, Seki T, *et al*. Novel *in vitro* protein fragment complementation assay applicable to high-throughput screening in a 1536-well format. J Biomol Screen 2009; 14(8): 970-9.

[76]   Chan CT, Paulmurugan R, Gheysens OS, *et al*. Molecular imaging of the efficacy of heat shock protein 90 inhibitors in living subjects. Cancer Res 2008; 68(1): 216-26.

[77]   Paulmurugan R, Tamrazi A, Massoud TF, Katzenellenbogen JA, Gambhir SS. *In vitro* and *in vivo* molecular imaging of estrogen receptor alpha and beta homo- and heterodimerization: exploration of new modes of receptor regulation. Mol Endocrinol 2011; 25(12): 2029-40.

[78]   Fan-Minogue H, Cao Z, Paulmurugan R, *et al*. Noninvasive molecular imaging of c-Myc activation in living mice. Proc Natl Acad Sci 2010; 107(36): 15892-7.

[79]   Filonov GS, Verkhusha VV. A near-infrared BiFC reporter for *in vivo* imaging of protein-protein interactions. Chem Biol 2013; 20(8): 1078-86.

[80]   Massoud TF, Paulmurugan R, Gambhir SS. A molecularly engineered split reporter for imaging protein-protein interactions with positron emission tomography. Nat Med 2010; 16(8): 921-6.

[81]   Cao Z, Fan-Minogue H, Bellovin DI, *et al*. MYC phosphorylation, activation, and tumorigenic potential in hepatocellular carcinoma are regulated by HMG-CoA reductase. Cancer Res 2011; 71(6): 2286-97.

[82]   Fan-Minogue H, Bodapati S, Solow-Cordero D, *et al*. A c-Myc activation sensor-based high-throughput drug screening identifies an antineoplastic effect of nitazoxanide. Mol Cancer Ther 2013; 12(9): 1896-905.

[83]   Chan CT, Reeves RE, Geller R, *et al*. Discovery and validation of small-molecule heat-shock protein 90 inhibitors through multimodality molecular imaging in living subjects. Proc Natl Acad Sci 2012; 109(37): E2476-85.

[84]   Zhang L, Lee KC, Bhojani MS, *et al*. Molecular imaging of Akt kinase activity. Nat Med 2007; 13(9): 1114-9.

[85]   Coppola JM, Ross BD, Rehemtulla A. Noninvasive imaging of apoptosis and its application in cancer therapeutics. Clin Cancer Res 2008; 14(8): 2492-501.

[86]   Wang H, Galban S, Wu R, *et al*. Molecular imaging reveals a role for AKT in resistance to cisplatin for ovarian endometrioid adenocarcinoma. Clin Cancer Res 2013; 19(1): 158-69.

[87]   Bhojani MS, Nyati MK, Zhao L, *et al*. Molecular imaging of akt enables early prediction of response to molecular targeted therapy. Transl Oncol 2011; 4(3): 122-5.

[88]   Tian H, Ip L, Luo H, Chang DC, Luo KQ. A high throughput drug screen based on fluorescence resonance energy transfer (FRET) for

anticancer activity of compounds from herbal medicine. Br J Pharmacol 2007; 150(3): 321-34.

[89]   Honarnejad K, Kirsch AK, Daschner A, *et al*. FRET-based calcium imaging: a tool for high-throughput/content phenotypic drug screening in Alzheimer disease. J Biomol Screen 2013; 18(10): 1309-20.

[90]   Honarnejad K, Daschner A, Giese A, *et al*. Development and implementation of a high-throughput compound screening assay for targeting disrupted ER calcium homeostasis in Alzheimer's disease. PLoS One 2013; 8(11): e80645.

[91]   Hamdan FF, Audet M, Garneau P, Pelletier J, Bouvier M. High-throughput screening of G protein-coupled receptor antagonists using a bioluminescence resonance energy transfer 1-based beta-arrestin2 recruitment assay. J Biomol Screen 2005; 10(5): 463-75.

[92]   De A, Gambhir SS. Noninvasive imaging of protein-protein interactions from live cells and living subjects using bioluminescence resonance energy transfer. FASEB J 2005; 19(14): 2017-9.

[93]   De A, Jasani A, Arora R, Gambhir SS. Evolution of BRET Biosensors from Live Cell to Tissue-Scale Imaging. Front Endocrinol (Lausanne) 2013; 4: 131.

[94]   Dragulescu-Andrasi A, Chan CT, De A, Massoud TF, Gambhir SS. Bioluminescence resonance energy transfer (BRET) imaging of protein-protein interactions within deep tissues of living subjects. Proc Natl Acad Sci 2011; 108(29): 12060-5.

[95]   Kepp O, Galluzzi L, Lipinski M, Yuan J, Kroemer G. Cell death assays for drug discovery. Nat Rev Drug Discov 2011; 10(3): 221-37.

[96]   Laxman B, Hall DE, Bhojani MS, *et al*. Noninvasive real-time imaging of apoptosis. Proc Natl Acad Sci 2002; 99(26): 16551-5.

[97]   Ray P, De A, Patel M, Gambhir SS. Monitoring caspase-3 activation with a multimodality imaging sensor in living subjects. Clin Cancer Res 2008; 14(18): 5801-9.

[98]   Yang Y, Hong H, Zhang Y, Cai W. Molecular Imaging of Proteases in Cancer. Cancer Growth Metastasis 2009; 2: 13-27.

[99]   Weissleder R, Tung CH, Mahmood U, Bogdanov A. *In vivo* imaging of tumors with protease-activated near-infrared fluorescent probes. Nat Biotechnol 1999; 17(4): 375-8.

[100] Jastrzebska B, Lebel R, Therriault H, *et al*. New enzyme-activated solubility-switchable contrast agent for magnetic resonance imaging: from synthesis to *in vivo* imaging. J Med Chem 2009; 52(6): 1576-81.

[101] Sprague JE, Li WP, Liang K, Achilefu S, Anderson CJ. *In vitro* and *in vivo* investigation of matrix metalloproteinase expression in metastatic tumor models. Nucl Med Biol 2006; 33(2): 227-37.

[102] Yang KN, Zhang CQ, Wang W, *et al*. pH-responsive mesoporous silica nanoparticles employed in controlled drug delivery systems for cancer treatment. Cancer Biol Med 2014; 11(1): 34-43.

[103] Gupta P, Vermani K, Garg S. Hydrogels: from controlled release to pH-responsive drug delivery. Drug Discov Today 2002; 7(10): 569-79.

[104] De Jong WH, Borm PJ. Drug delivery and nanoparticles: applications and hazards. Int J Nanomed 2008; 3(2): 133-49.

[105] Janib SM, Moses AS, MacKay JA. Imaging and drug delivery using theranostic nanoparticles. Adv Drug Deliv Rev 2010; 62(11): 1052-63.

[106] Hawkins MJ, Soon-Shiong P, Desai N. Protein nanoparticles as drug carriers in clinical medicine. Adv Drug Deliv Rev 2008; 60(8): 876-85.

[107] Lu ZR. Molecular imaging of HPMA copolymers: visualizing drug delivery in cell, mouse and man. Adv Drug Deliv Rev 2010; 62(2): 246-57.

[108] Vasey PA, Kaye SB, Morrison R, *et al*. Phase I clinical and pharmacokinetic study of PK1 [N-(2-hydroxypropyl)methacrylamide copolymer doxorubicin]: first member of a new class of chemotherapeutic agents-drug-polymer conjugates. Cancer Research Campaign Phase I/II Committee. Clin Cancer Res 1999; 5(1): 83-94.

[109] Seymour LW, Ferry DR, Kerr DJ, *et al*. Phase II studies of polymer-doxorubicin (PK1, FCE28068) in the treatment of breast, lung and colorectal cancer. Int J Oncol 2009; 34(6): 1629-36.

[110] Lammers T, Subr V, Ulbrich K, *et al*. Simultaneous delivery of doxorubicin and gemcitabine to tumors *in vivo* using prototypic polymeric drug carriers. Biomaterials 2009; 30(20): 3466-75.

[111] Pike DB, Ghandehari H. HPMA copolymer-cyclic RGD conjugates for tumor targeting. Adv Drug Deliv Rev 2010; 62(2): 167-83.

[112] Nazir S, Hussain T, Ayub A, Rashid U, MacRobert AJ. Nanomaterials in combating cancer: therapeutic applications and developments. Nanomedicine 2014; 10(1): 19-34.

[113] Baker JR. Dendrimer-based nanoparticles for cancer therapy. Hematology Am Soc Hematol Educ Program 2009: 708-19.

[114] Choi SK, Thomas T, Li MH, *et al*. Light-controlled release of caged doxorubicin from folate receptor-targeting PAMAM dendrimer nanoconjugate. Chem Commun (Camb) 2010; 46(15): 2632-4.

[115] Shi L, Fleming CJ, Riechers SL, *et al*. High-Resolution Imaging of Dendrimers Used in Drug Delivery *via* Scanning Probe Microscopy. J Drug Deliv 2011; 254095.

[116] Levine DH, Ghoroghchian PP, Freudenberg J, *et al*. Polymersomes: a new multi-functional tool for cancer diagnosis and therapy. Methods 2008; 46(1): 25-32.

[117] Gaitanis A, Staal S. Liposomal doxorubicin and nab-paclitaxel: nanoparticle cancer chemotherapy in current clinical use. Methods Mol Biol 2010; 624: 385-92.

[118] Ponce AM, Vujaskovic Z, Yuan F, Needham D, Dewhirst MW. Hyperthermia mediated liposomal drug delivery. Int J Hyperthermia 2006; 22(3): 205-13.

[119] Erdogan S, Torchilin VP. Gadolinium-loaded polychelating polymer-containing tumor-targeted liposomes. Methods Mol Biol 2010; 605: 321-34.

[120] Viglianti BL, Abraham SA, Michelich CR, *et al*. *In vivo* monitoring of tissue pharmacokinetics of liposome/drug using MRI: illustration of targeted delivery. Magn Reson Med 2004; 51(6): 1153-62.

[121] Sanson C, Schatz C, Le Meins JF, *et al*. Biocompatible and biodegradable poly(trimethylene carbonate)-b-poly(L-glutamic acid) polymersomes: size control and stability. Langmuir 2010; 26(4): 2751-60.

[122] Xiao Y, Hong H, Javadi A, *et al*. Multifunctional unimolecular micelles for cancer-targeted drug delivery and positron emission tomography imaging. Biomaterials 2012; 33(11): 3071-82.

[123] Guo J, Hong H, Chen G, *et al*. Image-guided and tumor-targeted drug delivery with radiolabeled unimolecular micelles. Biomaterials 2013; 34(33): 8323-32.

[124] Bentolila LA, Ebenstein Y, Weiss S. Quantum dots for *in vivo* small-animal imaging. J Nucl Med 2009; 50(4): 493-6.

[125] Gao X, Cui Y, Levenson RM, Chung LW, Nie S. *In vivo* cancer targeting and imaging with semiconductor quantum dots. Nat Biotechnol 2004; 22(8): 969-76.

[126] Cai W, Chen K, Li ZB, Gambhir SS, Chen X. Dual-function probe for PET and near-infrared fluorescence imaging of tumor vasculature. J Nucl Med 2007; 48(11): 1862-70.

[127] Johannsen M, Gneveckow U, Taymoorian K, *et al*. Morbidity and quality of life during thermotherapy using magnetic nanoparticles in locally recurrent prostate cancer: results of a prospective phase I trial. Int J Hyperthermia 2007; 23(3): 315-23.

[128] Taylor RM, Sillerud LO. Paclitaxel-loaded iron platinum stealth immunomicelles are potent MRI imaging agents that prevent prostate cancer growth in a PSMA-dependent manner. Int J Nanomed 2012; 7: 4341-52.

[129] Cheng J, Gu YJ, Cheng SH, Wong WT. Surface functionalized gold nanoparticles for drug delivery. J Biomed Nanotechnol 2013; 9(8): 1362-9.

[130] Dreaden EC, El-Sayed MA. Detecting and destroying cancer cells in more than one way with noble metals and different confinement properties on the nanoscale. Acc Chem Res 2012; 45(11): 1854-65.

[131] Huang X, El-Sayed IH, Qian W, El-Sayed MA. Cancer cell imaging and photothermal therapy in the near-infrared region by using gold nanorods. J Am Chem Soc 2006; 128(6): 2115-20.

[132] Raoof M, Corr SJ, Kaluarachchi WD, *et al*. Stability of antibody-conjugated gold nanoparticles in the endolysosomal nanoenvironment: implications for noninvasive radiofrequency-based cancer therapy. Nanomedicine 2012; 8(7): 1096-105.

[133] Gao Z, Kennedy AM, Christensen DA, Rapoport NY. Drug-loaded nano/microbubbles for combining ultrasonography and targeted chemotherapy. Ultrasonics 2008; 48(4): 260-70.

[134] Lukianova-Hleb EY, Hanna EY, Hafner JH, Lapotko DO. Tunable plasmonic nanobubbles for cell theranostics. Nanotechnology 2010; 21(8): 85102.

[135] Madani SY, Naderi N, Dissanayake O, Tan A, Seifalian AM. A new era of cancer treatment: carbon nanotubes as drug delivery tools. Int J Nanomedicine 2011; 6: 2963-79.

[136] Dhar S, Liu Z, Thomale J, Dai H, Lippard SJ. Targeted single-wall carbon nanotube-mediated Pt(IV) prodrug delivery using folate as a homing device. J Am Chem Soc 2008; 130(34): 11467-76.

[137] Bhirde AA, Patel V, Gavard J, *et al*. Targeted killing of cancer cells *in vivo* and *in vitro* with EGF-directed carbon nanotube-based drug delivery. ACS Nano 2009; 3(2): 307-16.

[138] Kam NW, O'Connell M, Wisdom JA, Dai H. Carbon nanotubes as multifunctional biological transporters and near-infrared agents for selective cancer cell destruction. Proc Natl Acad Sci 2005; 102(33): 11600-5.

[139] Bhunia SK, Saha A, Maity AR, Ray SC, Jana NR. Carbon nanoparticle-based fluorescent bioimaging probes. Sci Rep 2013; 3: 1473.

[140] Aillon KL, Xie Y, El-Gendy N, Berkland CJ, Forrest ML. Effects of nanomaterial physicochemical properties on *in vivo* toxicity. Adv Drug Deliv Rev 2009; 61(6): 457-66.

[141] Deroose CM, De A, Loening AM, *et al*. Multimodality imaging of tumor xenografts and metastases in mice with combined small-animal PET, small-animal CT, and bioluminescence imaging. J Nucl Med 2007; 48(2): 295-303.

[142] Weissleder R, Moore A, Mahmood U, *et al*. *In vivo* magnetic resonance imaging of transgene expression. Nat Med 2000; 6(3): 351-5.

[143] Yan X, Ray P, Paulmurugan R, *et al*. A transgenic tri-modality reporter mouse. PLoS One 2013; 8(8): e73580.

[144] Davis SL, Be NA, Lamichhane G, *et al*. Bacterial thymidine kinase as a non-invasive imaging reporter for Mycobacterium tuberculosis in live animals. PLoS One 2009; 4(7): e6297.

[145] Roellig K, Drews B, Goeritz F, Hildebrandt TB. The long gestation of the small naked mole-rat (Heterocephalus glaber Ruppell, 1842) studied with ultrasound biomicroscopy and 3D-ultrasonography. PLoS One 2011; 6(3): e17744.

[146] Chaudhury S, Maheshwari APR. Ovarian Cancer: An ever challenging malady. Biomed Res J 2014; 1(1): 34-55.

[147] Millet P, Graf C, Buck A, *et al*. Similarity and robustness of PET and SPECT binding parameters for benzodiazepine receptors. J Cereb Blood Flow Metab 2000; 20(11): 1587-603.

[148] Qin C, Cheng K, Chen K, *et al*. Tyrosinase as a multifunctional reporter gene for Photoacoustic/MRI/PET triple modality molecular imaging. Sci Rep 2013; 3: 1490.

[149] Wehr MC, Laage R, Bolz U, *et al*. Monitoring regulated protein-protein interactions using split TEV. Nat Methods 2006; 3(12): 985-93.

[150] Deng Y, Gam J, French JB, *et al*. Mapping protein-protein proximity in the purinosome. J Biol Chem 2012; 287(43): 36201-7.

[151] Eyckerman S, Lemmens I, Catteeuw D, *et al*. Reverse MAPPIT: screening for protein-protein interaction modifiers in mammalian cells. Nat Methods 2005; 2(6): 427-33.

[152] Baker SJ, Rane SG, Reddy EP. Hematopoietic cytokine receptor signaling. Oncogene 2007; 26(47): 6724-37.

[153] Poe JA, Vollmer L, Vogt A, Smithgall TE. Development and validation of a high-content bimolecular fluorescence complementation assay for small-molecule inhibitors of HIV-1 Nef dimerization. J Biomol Screen 2014; 19(4): 556-65.